Loughborough University Institutional Repository

Pulse electroplating of copper for printed circuit technology

This item was submitted to Loughborough University's Institutional Repository by the/an author.

Additional Information:

- A Doctoral Thesis. Submitted in partial fulfillment of the requirements for the award of Doctor of Philosophy of Loughborough University.

Metadata Record: https://dspace.lboro.ac.uk/2134/7417

Publisher: © Mehrdad R-Kalantary

Please cite the published version.

Loughborough University

This item is held in Loughborough University's Institutional Repository (https://dspace.lboro.ac.uk/) and was harvested from the British Library's EThOS service (http://www.ethos.bl.uk/). It is made available under the following Creative Commons Licence conditions.

creative commons

COMMONS DEED

Attribution-NonCommercial-NoDerivs 2.5

You are free:

- to copy, distribute, display, and perform the work

Under the following conditions:

Attribution. You must attribute the work in the manner specified by the author or licensor.

Noncommercial. You may not use this work for commercial purposes.

No Derivative Works. You may not alter, transform, or build upon this work.

- For any reuse or distribution, you must make clear to others the license terms of this work.
- Any of these conditions can be waived if you get permission from the copyright holder.

Your fair use and other rights are in no way affected by the above.

This is a human-readable summary of the Legal Code (the full license).

Disclaimer

For the full text of this licence, please go to:
http://creativecommons.org/licenses/by-nc-nd/2.5/

PULSE ELECTROPLATING OF COPPER FOR PRINTED CIRCUIT BOARD TECHNOLOGY

by

MEHRDAD REZAI-KALANTARY
P.G. Diploma (Brunel), M.Sc. (Loughborough), M.I.Corr.S.

A thesis submitted in partial fulfilment of the requirement
for the award of degree of
Doctor of Philosophy
of the Loughborough University of Technology

October 1990

Supervisors: Dr. D.R. Gabe(Academic)
Dr. M.R. Goodenough(Industrial)

© Mehrdad R-Kalantary 1990

SYNOPSIS

This thesis is concerned with the study of square wave unipolar pulse and bipolar pulse reverse electroplating of copper for printed circuit board(PCB) production. The aim of this research programme was to develop an acid copper electrolyte, preferably with additives under certain pulse conditions for electroplating of PCBs having hole diameters as small as 0.3mm. The aim was to obtain a surface to hole thickness ratio of 1:1. The use of additives in the electrolyte is preferred for commercial purposes.

The literature review comprises an examination of the technology of copper electroplating, comparison between different electrolytes and their uses in PCB industries, study of the theoretical aspects of pulse current and its effectiveness in comparison to direct current(DC) and also an up-to-date bibliographical literature survey on pulse electroplating of metals and alloys with particular emphasis on copper.

The experimental work was concerned with studying and understanding of the pulse unit behaviour, substrate pre-treatments, effect of chloride ion concentration, comparisons between different electrolytes under DC, unipolar pulse and bipolar pulse reverse using polarisation curves (potential–current density curves). Furthermore, comparisons between unipolar pulse, bipolar pulse reverse and DC in terms of hardness, tensile strength, efficiency, morphology and surface topography have been made.

A systematic behaviour was observed using a pulse unit and power supply as a means of power source unlike the results obtained with a pulse unit and a potentiostat. The examination of the behaviour was made by polarisation studies. They indicated that the electronics within the pulse unit and potentiostat causes an inconsistant or surge in polarisation curves.

The polarisation studies of DC, unipolar pulse and bipolar pulse reverse were carried out by a step-wise method using a power supply for DC and unipolar pulse and two power supplies for bipolar pulse reverse. To compare different pulse conditions, the Tafel region from the calculated polarisation curves, potential-logarithmic converted current density curves, were used to obtain the Wagner number and from that an enhanced Wagner number ratio(RWa), which is the ratio of pulse Wagner number to DC Wagner number, was derived. It was found that the electrolyte containing no additives, 'electrolyte I', gave the highest RWa values and the deposits had long columnar structures. The electrolyte containing all the additives, 'electrolyte V', provided higher RWa than DC but 23% and 47% lower RWa than electrolyte I for unipolar pulse and bipolar pulse reverse, respectively, were obtained.

A cathodic/anodic on-time ratio of 10ms/0.2ms and peak cathodic/anodic ratio of 1/4 produced the best coating thickness distributions under bipolar pulse reverse for electrolyte V at an average current denisty of $3.0Adm^{-2}$. The surface apearance obtained was lustrous being similar to that of DC.

The electrolyte V produced a finer grain deposit structure than electrolyte I and hence it is more appropriate for use on PCBs since it permits the deposit to survive the solder float test and also provides an efficient electrical continuity. The optimum chloride ion concentration was found to be 50ppm for both DC and unipolar pulse conditions.

The hardness, roughness, tensile strength and morphology were found to vary depending upon the pulse conditions employed for both unipolar pulse and bipolar pulse reverse. The surface appearances obtained under unipolar pulse were similar to that of DC for the electrolytes mentioned above but for bipolar pulse revese, the surface appearance varied depending upon the pulse parameters used.

ACKNOWLEDGEMENTS

It gives me pleasure to express my sincere gratitude to my supervisors, Dr. D.R. Gabe and Dr. M.R. Goodenough for their considerable help and discussions, encouragement and inspiration throughout the course of this research work.

I wish to thank LeaRonal(UK) for the grant and also the facilities provided throughout the research programme.

Thanks also to Professor I.A. Menzies my director of research, Mr. J.S. Bate and Mr. M.F. Page for their help for STEM and SEM, Dr. D.H. Ross for his valuable discussions, Mr. T.J. Atkinson, Miss M.J. Pollard and all the staff in the IPTME department, who have helped me.

My gratitude also extends to Messrs. D. Brookes and J. Elvyn for their assistance and cooperation during my stay and visits at LeaRonal(UK).

Last, but not least, I wish to thank my brother Majid for his moral support and useful discussions, and Dr. A. Afshar, Dr. G.D. Wilcox, Mr. A. Jamani and Mr. S.A. Amadi for their charm and humour in the laboratory during my research.

To my parents ...

Notation

a	Anodic
c	Cathodic
C_O	Concentration of the species at the electrode surface pertaining to species O in $O+ne \leftrightarrow R$(mol cm^{-3})
$C_O(x=0)$	Concentration at the electrode surface(mol cm^{-3})
C_O^*	Concentration of the species of the bulk pertaining to species O in $O+ne \leftrightarrow R$(mol cm^{-3})
C_R	Concentration of the species at the electrode surface pertaining to species R in $O+ne \leftrightarrow R$(mol cm^{-3})
$C_R(x=0)$	Bulk concentration at the electrode surface(mol cm^{-3})
C_R^*	Concentration of the species of the bulk pertaining to species O in $O+ne \leftrightarrow R$(mol cm^{-3})
d	Deposit thickness(μm)
E	Potential(V)
E.F.	Enhancement factor[$=i_L$ of agitated mode/i_L of still mode](--)
i_b	Off-time current density or base line(Adm^{-2})
j^*	Reaction rate for through-hole(--)
i_C	Cathodic current density(Adm^{-2})
i, i_m, i_P	Mean, peak current density (Adm^{-2})
i_L	Limiting current density for DC(Adm^{-2})
i_p	Peak current density(Adm^{-2})
i_{Pl}	Pulse limiting current density
j_m, i_{av}	Mean, average current density(Adm^{-2})
L	Characteristic length of the plating system(cm)
R, R_a	Roughness average(μm)
R_{tm}	Mean or peak-to peak roughness average(μm)
R_O	Radius of the plated through-hole[PTH](cm)
t	time(s)
t_B	Board thickness(cm)
t_f	Full time(s)

t_H	Plated copper thickness in PTH centre(cm)
t_r	Rise time(s)
t_p	Plated copper thickness at PTH entrance or exit(cm)
t_p/t_H	Throwing power(--)
t_{on}	On-time(s)
t_{off}	Off-time(s)
n,F	Number of electron, Faraday constant($Asmol^{-1}$)
x	Distance(cm)
R,T	Gas constant($J\ K\ mol^{-1}$), temperature(K)
RWa	Wagner Number enhancement ratio[$=Wa_p/Wa_{DC}$]
V_b	Velocity of bulk(cm/s)
V_h	Velocity of hole(cm/s)
V_t	Velocity of translating board(cm/s)
Wa	Wagner number[$=\{\kappa(d\eta/di)\}/L$] (--)
Wa_p	Pulse Wagner number(--)
Wa_{DC}	DC Wagner number(--)
$d\eta/di$	Slope of the polarization curve of Tafel slope(V/A)
%	Efficiency[$=M_p/M_{DC}$]

<u>Greek letters</u>

η	Cathode overpotential(V)
τ	Transition time(s)
ξ	Reaction parameters for through-hole(--)
ϕ	Duty cycle [$=(t_{on}/t_{on}+t_{off}) \times 100$](%)
κ	Electrolyte conductivity(Scm^{-1})

Contents

	Page number
Synopsis	i
Acknowledgement	ii
Dedication	iii
Notation	iv
1.0 INTRODUCTION	1
2.0 COPPER ELECTROPLATING	4
2.1 Critique of Electrolytes and their Variables	4
2.1.1 Polarization and current distribution	5
2.1.2 Relationship between the Tafel slope and Wagner number	6
2.1.3 Wagner number	8
2.2 Uses in P.C.B. Technology	9
2.3 Through-hole Plating	10
2.3.1 Modelling/designing through-holes	11
2.3.2 Throwing power and mass transfer in holes	13
3.0 PULSE PLATING THEORY	16
3.1 Pulse Plating Equipment - Definitions, Behaviour and Irregularities	16
3.2 Pulse Plating Parameters	18
3.2.1 Current and voltage regimes	19
3.2.2 Benefits of pulse reverse	20
3.3 Comparison between Direct Current(DC) and Pulse Electroplating	20
3.3.1 Advantages and disadvantages of unipolar pulse(P) and bipolar pulse reverse(PR) to DC electroplating	22
3.4 Effect of Pulse Current in Electroplating	22
3.4.1 Crystallisation	24
3.5 Capacitance Effects	24
3.6 Mass Transfer Effects	25
3.7 Current Distribution	26
3.7.1 Primary current distribution	27
3.7.2 Secondary current distribution	27

3.7.3 Tertiary current distribution 28
3.8 Current Efficiency 29
3.9 Effect of Pulse Current on Morphology 29

4.0 LITERATURE SURVEY OF PULSE PLATING 31
4.1 Pulse Plating of Copper 31
4.2 Bibliographical Survey of Pulse Plating Technology 35

5.0 EXPERIMENTAL WORK 53
5.1 Equipment 53
5.2 Conductivity Measurements 55
5.3 Pretreatment Assessments 55
5.4 Hull Cell Measurements 57
5.5 Cathode Size 58
5.6 Anode Size 59
5.7 Electrolytes 60
5.8 Use of Agitation 60
5.9 Pulse Electronic Behaviour 62
5.9.1 Comparative study of different power sources 63
5.9.2 Establishing standard parameters using a pulse unit and a power supply 63
5.9.3 Behaviour of pulse parameters 64
5.10 Polarization, Tafel and Wagner NumberStudies 65
5.10.1 Direct current 66
5.10.2 Unipolar pulse 67
5.10.3 Bipolar pulse reverse 68
5.10.4 Optimisation of Chloride Ions under DC and Pulsing 69
5.10.5 Metallurgical Studies of PCBs 70
5.11 Assessment of Pulse Plated Electrodeposits 70
5.11.1 Efficiency of deposition 71
5.11.2 Micro-hardness 72
5.11.3 Roughness 73
5.11.4 Tensile strength and elongation 74
5.11.5 Coating thickness distribution 75
5.11.6 Surface appearance 76
5.11.7 Morphological study of the deposits 76

6.0 RESULTS 78
6.1 Standardisation 78
6.1.1 Solution conductivity 78
6.1.2 Pretreatment assessments 78
6.1.3 Hull cell results 79
6.1.4 Effects of agitation 80
6.1.5 Pulse electronic behaviour 80
6.1.6 Comparative study of different power sources 81
6.1.7 Establishing standard parameters using a pulse unit and a power supply 81
6.1.8 Behaviour of pulse parameters 82
6.2 Polarisation, Tafel and Wagner Number Studies 82
6.2.1 Direct current 82
6.2.2 Unipolar pulse 83
6.2.3 Bipolar pulse reverse 84
6.2.4 Optimisation of chloride ions under DC and pulsing 85
6.2.5 Assessments of unipolar pulse and bipolar pulse reverse 85
6.3 Assessment of Pulse Plated Electrodeposits 88

7.0 DISCUSSION 91
7.1 Standardisation 91
7.1.1 Solution conductivity 91
7.1.2 Pretreatment assessments 92
7.1.3 Hull cell results 93
7.1.4 Effects of agitation 94
7.1.5 Pulse electronic behaviour 95
7.1.6 Comparative study of different power sources 98
7.1.7 Behaviour of pulse parameters 98
7.2 Polarisation, Tafel and Wagner Number Studies 99
7.2.1 Direct current 100
7.2.2 Unipolar pulse 101
7.2.3 Bipolar pulse reverse 104
7.2.4 Optimisation of chloride ions under DC and pulsing 106
7.2.5 Assessments of plated PCBs under unipolar pulse and bipolar pulse reverse to DC 107
7.2.6 Behaviour of the additives 112
7.3 Assessment of Pulse Plated Electrodeposits 113
7.3.1 Efficiency of deposition 114

7.3.2 Micro-hardness 115
7.3.3 Roughness 116
7.3.4 Tensile strength and elongation 117
7.3.5 Coating thickness distribution 118
7.3.6 Surface appearance 119
7.3.7 Morphological study of the deposits 120

8.0 CONCLUSIONS 123
8.1 Standardisation of Solutions 123
8.2 Polarisation, Tafel and Wagner Number Studies 123
8.3 Assessment of Pulse Plated Electrodeposits 125

9.0 FURTHER WORK 127

References
Tables
Figures
Appendix 1: Electrolyte Constituents and Conductivities
Appendix 2: Additive constituents
Appendix 3: 2-D and 3-D maps of the results obtained under unipolar pulse conditions for electrolytes I-IX.
Appendix 4: Papers published prior to submission of thesis.
Vibratory Agitation for Electrodeposition:
I Characterisation of Agitations (47).
II Enhancement of Deposition Rate (47).
III Electrodeposition of Composite (48).
Vibratory agitation to enhance mass transfer in electrodeposition (49).
Appendix 5: Conference paper for "Asia Pacific Interfinish 90" at Singapore, November 1990.
Pulse Plating for Printed Circuit Board Technology (133).

CHAPTER 1

1.0 INTRODUCTION

The examination of the effects of applying pulse currents to an electroplating process dates back to the early 1960's, with the first commercial pulse plater becoming available in 1965. Thus in practice, the technique is relatively new although earlier indications of the idea can be found in textbooks and papers.

From these earlier studies, it has become usual to think of a pulse as approximately <1s in duration. Larger polarity changes are often referred to as periodic reverse changes and when up to 20s duration have been used, successfully, to improve levelling in electrowinning processes.

Since that time there have been many published papers and articles on the subject, now running into several thousands worldwide. The most extensive publication on pulse plating has been carried out by Puippe et al (1). The method has been applied to virtually all metals which it is possible to electrodeposit - from aqueous, non-aqueous and molten salt electrolytes. Many variants on the basic pulse principle have been developed, including the periodic reverse or pulse reverse method.

However, although the technique has been applied to a variety of commercial applications, the method of selecting the pulse parameters remains largely an 'ad hoc' choice. For each application, therefore, a trial-and-error method is usually the approach used to optimise the conditions. The parameters devised for one system (metal, electrolyte, current density, cell design, etc.) seem largely unrelated to those eventually evolved for another. For this reason there is a tendency in practice to lose patience and attempt to achieve a compromise using direct current conditions. The reputation of pulse plating equipment is that it is a luxury, perhaps purchased out of curiosity or to complete a specific plating task. They are then largely ignored until another seemingly insoluble problem emerges and pulsing is tried as a last resort!

The object of pulsing is to provide an enhanced plating rate and performance

without loss of properties which might be caused by the otherwise excessive current employed. Thus a high forward (cathodic) current can be interrupted by reverse pulses (either anodic or low cathodic) which perhaps causes levelling, anodic polishing or relaxing of the diffusion layers. Consequently, the average or nett forward must be employed to define overall rates and the pulse character to define any effects achieved.

In practice, the use of pulse plating is restricted mainly by a lack of fundamental knowledge of its effects on the properties of the deposit concerned. More variables are involved in pulse plating than with direct current and consequently it may appear easier to produce an adverse effect than the beneficial one sought! The majority of basic work has been done worldwide but the efforts do not appear coordinated with the result that a variety of sometimes conflicting and/or confusing conclusions have been reached. Nevertheless, Pearson and Dennis [2] recent work on pulse electroplating of copper on printed circuit boards and also the pulse plating effects on additives have been researched in detail. Similarly, work in the U.S.A. by Alkire et al [3] and Chin et al [4] has been directed at the through-hole problem specifically.

During the last ten years, pulse plating has been recognised and reported [5,6] as being useful in certain specific applications, in particular instances of throwing power where activation polarisation and solution conductivity may be the controlling factors. This is especially true for through-holes in printed circuit boards.

The aim of this research programme was to study the square wave unipolar pulse and bipolar pulse reverse electroplating of copper for printed circuit board production. The main part of the research was to develop an acid copper electrolyte, preferably with additives, using a pulse unit under certain pulse conditions for electroplating of printed circuit boards, having hole diameters as low as 0.3mm. The intention was to obtain a surface to hole thickness ratio of 1:1. The reason for using acid copper electrolyte lies with the fact that firstly, it is simple to understand its behaviour, secondly, it is commercially used in plating industries for printed circuit boards, and thirdly, with the current technology in the surface mount industry, holes are becoming smaller and the coating thickness distribution and also the deposit continuity becomes important for printed circuit board technology. Also, the use of additives is important for commercial purposes. It was found that bipolar pulse reverse produces a better coating thickness distribution than unipolar pulse and better than conventional plating and the critical factors are the pulse parameters and the electrolyte constituents.

Further research work was carried out on the properties of the coating deposited

under unipolar pulse and bipolar pulse reverse such as cathode efficiency, hardness, roughness, tensile strength, elongation, coating surface distribution, surface appearance and also grain structure. It was found that a major improvement in the properties of the coating can be expected under both unipolar pulse and bipolar pulse reverse, but the main factors remain to be the pulse conditions and the electrolyte constituents.

CHAPTER 2

2.0 COPPER ELECTROPLATING

Copper electrodeposition has a variety of applications in metal finishing but the primary uses are as follows:

- An undercoat for surface finishes such as nickel-chromium electrodeposits on steel, aluminium and zinc-based die-castings.
- Electroforming of precision components and moulds for polymeric materials.
- Thick deposits for the restoration or build-up of worn or damaged surfaces not subject to heavy mechanical loading.
- Thick deposits applied to steel as a stop-off coating in case-hardening processes such carburising and nitriding.
- In the production of electronic printed circuits, and of electrotypes and printing surfaces.
- As a base for oxidised or coloured finishes on steel and other metals.
- For metallisation of plastics and protection for silvered mirrors.

2.1 Critique of Electrolytes and their Variables

Copper can be electrodeposited from a variety of solutions although the main baths are the acid sulphate, cyanide, pyrophosphate and fluoborate (Tables 1 and 2)[7,8]. However, the choice of electrolytes should be carefully considered (Table 3)[7].

The simplest copper electrodeposition solution is the acid copper sulphate bath based on copper sulphate and sulphuric acid. It is cheap and easy to operate but has

relatively poor throwing power compared to pyrophosphate and cyanide electrolytes. Deposits are normally soft and matt in appearance with a tendency to nodular growth. However, they can be brightened and hardened with additives.

The alkaline cyanide solution is widely used as a 'strike' bath for plating on steel or zinc and its highly complex nature causes a shift in deposition potential which provides an excellent throwing power for complex shapes of objects. However, although it is simplest to operate and relatively cheap it is toxic and causes additional problems for effluent treatment. Furthermore, its efficiency is low (60–80%) and, having a low concentration of copper, cannot be operated at a very high current density. It is little used in the electronic field.

The pyrophosphate solution has been an important development offering some of the advantages of a complexed solution without serious problems of toxicity and gives deposits which are harder but more susceptible to soldering difficulties. It has good throwing power and solubility and being almost neutral in pH is not very corrosive. It is widely used for electroforming and electrotyping where high current densities are advantageous.

The acid fluoborate solution is less commonly used because of its corrosivity and cost but can offer advantages, through its higher current densities and smoother deposits, in the field of electroforming.

All of these copper solutions are well-established and understood[7,9,10,11], they can all be alternatives to each other to some extent. Table 3 shows the comparisons of copper plating solutions and the choice depends entirely upon the requirements of the process.

2.1.1 Polarization and current distribution

The criteria for satisfactory electrodeposition include appearance, metal distribution and flexibility with respect to the primary variables of solution composition, temperature, current density, etc. These criteria can be monitored by a number of tests in order to measure the variation which may occur.

Provided the cathode current efficiency is constant the metal distribution over a surface is a consequence of the current distribution which is affected by IR-drop effects in solution between the electrodes and polarization at the cathode-electrolyte interface.

The current distribution is therefore affected in two ways:

- Primary current distribution due purely to IR effects in solution. This is determined by the geometrical shape of the anode, cathode, electrolysis cell and their distance from the cell walls, and in the case of the electrodes, each other. This type of current distribution may be calculated from potential theory [12], may be measured using potential probes [13,14] and is the basis of the Hull Cell test [15];
- Secondary current distribution (or electrical and electrochemical factors) due to the superimposition of polarization upon IR effects. These electrochemical factors which include polarization ie. shape of polarization curve, electrical conductivity of the solution, the factors which influence these, such as current density, metal ion concentration, temperature, pH, viscosity of the electrolyte, contamination, etc. The relative influence of each being measured using Wagner's [16] ratio:

$$Wa = \frac{\kappa}{L}\left(\frac{d\eta}{di}\right)$$

where L is the distance between cathode-anode or cathode-reference electrodes or electrode diameter, κ is the electrolyte conductivity and $d\eta/di$ is the slope of polarization curve(also see section 2.1.3).

The ability of a solution to deposit evenly on an uneven cathode surface is measured by its throwing power (see section 2.3.2). If the surface irregularities are macroscopic a Haring-Blum cell [17] may be used to examine throwing power. However, if the irregularities are microscopic a scratched surface or record matrix may be used to examine performance.

2.1.2 Relationship between the Tafel slope and Wagner number

The Tafel slope can be calculated in two ways:

- use of E-logi curve [18]
- use of E-log converted current density(E-$\log i_c$) curve

Both methods have been well established and the Tafel slope can be calculated by means of gradient of the activation polarisation region (Figure 1). As for E-$\log i_c$ the converted current densities are calculated using the average current density values for each overpotentials (see section 2.1.3). However, for an acid copper electrolyte, the Tafel slope lies in the region of 30-200mV. As for this research work, the E-$\log i_c$ method is used.

The Wagner number can be related to the Tafel slope and throwing power [19,20,21]. It can be calculated using the Tafel slope of a polarization curve. The relation between the Wagner number and throwing power is such that the higher the Wagner number the higher the throwing power and hence the high Tafel slope value.

The current-overpotential derivation for obtaining the Tafel slope is given by:

$$i = i_o \left\{ \frac{C_o(0,t)}{C_o^*} \exp\left[\frac{-\alpha nF\eta}{RT}\right] - \frac{C_R(0,t)}{C_R^*} \exp\left[\frac{(1-\alpha)nF\eta}{RT}\right] \right\} \quad (1)$$

The first term below describes the cathodic component current at any potential and the second term gives the anodic contribution.

$$\frac{C_o(x=0)}{C_o^*} = 1 - \frac{i}{i_{LC}} \quad \& \quad \frac{C_R(x=0)}{C_R^*} = 1 - \frac{i}{i_{LA}} \quad (2)$$

For the cathodic reaction

$$\frac{i}{i_o} = \left(1 - \frac{i}{i_L}\right) \exp \frac{-\alpha nF\eta}{RT} \quad (3)$$

rearranging equation (3) then:

$$\exp\left(-\frac{\alpha nF\eta}{RT}\right) = \frac{i_o}{i}\left(\frac{i_L - i}{i_L}\right) \quad (4)$$

taking logrithms of a product, ie. equation (4) can be written as:

$$-\frac{\alpha nF\eta}{RT} = \ln(i_o) + \ln\left(\frac{i_L - i}{i_L i}\right) \quad (5)$$

integrate with respect to i and also multiply both sides by minus then:

$$\frac{\alpha nF\eta}{RT} = -\ln\left(\frac{1}{i} - \frac{1}{i_L}\right) - \text{constant} \quad (6)$$

equation (6) may be written as:

$$\ln\left[i_C\right] = -\frac{\alpha n\eta F}{RT} + \text{constant} \quad (7)$$

Hence the converted current density can be calculated using the limiting current density (i_L) and the average current density(i) at a particular overpotential.

The slope of the Tafel region is given by:

$$\frac{d\eta}{di} = -\frac{RT}{\alpha nFi} \tag{8}$$

It is known that:

$$\frac{d(\ln i)}{di} = \frac{1}{i}, \text{ therefore } d(\ln i) = \frac{di}{i} \tag{9}$$

therefore

$$\frac{di}{i} = 2.303\ d(\log i) \tag{10}$$

hence equation (8) takes the form of:

$$\frac{d\eta}{d(\log i)} = 2.303\ \frac{RT}{-\alpha nF} \tag{11}$$

equating (8) and (11) the Wagner number can be derived as:

$$Wa = \left(\frac{d\eta}{di} x \frac{1}{2.303\ i}\right)\frac{\kappa}{L} \tag{12}$$

and in literature the equation (12) is defined as:

$$Wa = \frac{\kappa}{L}\left(\frac{d\eta}{di}\right) \tag{13}$$

where κ is the electrolyte conductivity (Scm^{-1} or $\Omega^{-1}cm^{-1}$)

L is the characteristic length of the deposition process (cm)

$\left(\frac{d\eta}{di}\right)$ is the slope of the polarization curve and calculated at an average current density ($VA^{-1}cm^2$)

2.1.3 Wagner number

As explained earlier in section 2.1.1, current distribution is a matter of mass transfer and charge transfer. It can be deduced that the main factors influencing the distribution of current over an electrode surface are:

a) the geometry of the system;
b) the conductivities of the electrolyte;
c) the kinetics of the electrode reaction, ie. the type and extent of polarization prevailing under the conditions considered. The main kinds of polarization usually taken into account are those due to mass transport and to the charge transfer reaction. (ie. concentration and activation)

If a plating current efficiency of 100 percent is assumed, the characteristic of metal distribution can be described by the current distribution at the cathode. In the potential

theory, the important quantity that characterises the uniformity of current distribution is the value of a dimensionless group called the Wagner number such that:

$$Wa = \frac{\kappa}{L}\left(\frac{d\eta}{di}\right)$$

where κ is the electrolyte conductivity (Scm^{-1} or $\Omega^{-1}cm^{-1}$)

L is the characteristic length of the deposition process (cm)

$\left(\frac{d\eta}{di}\right)$ is the slope of the polarization curve and calculated at an average current density ($VA^{-1}cm^2$)

The larger the Wagner number the more uniform the current distribution, whereas when $Wa \rightarrow 0$, this corresponds to primary current distribution. It can be concluded[21,22] that the higher the Tafel slope, the larger the Wagner number, as Figure 1 shows.

2.2 Uses in PCB Technology

Copper is plated on the surface and also on the hole walls of printed circuit boards to form conductive paths for electrical connections. A typical plating sequence is shown in Table 4 showing the various stages of cleaning, etching, plating and rinsing involved[23].

At present most printed circuits are plated with acid copper sulphate for speed and relative cheapness. Other types of solutions are available and those based on fluoboric acid and potassium pyrophosphate (section 2.1) have been, and still are, used successfully, but are more difficult to control than acid sulphate solutions.

The copper sulphate based solutions which are widely used today have a typical formulation of:

Copper sulphate	75 - 100g/l
Sulphuric acid (SG 1.42)	100 - 120ml/l
Chloride ion as NaCl	50 - 60ppm
Additive	2 - 10ml/l
Current density	up to $8Adm^{-2}$ depending on solution and workpiece movement
Temperature	25 - 30°C

Normally, temperatures above 30°C promote additive degradation and therefore

additive consumption increases. These additives are used for grain-refinement. Mechanical properties of deposits can deteriorate as the contamination from degraded additives increases in concentration over long periods of operation at elevated temperatures.

Typical mechanical properties of deposits produced from the acid sulphate solution are as follows[23]:

	As plated	After heat treatment After 1 hour at 120 °C
Ductility (Elongation)	6 - 15%	9 - 20%
Internal stress (KPa/mm^2)	1.0 tensile	-
Ultimate tensile strength(KPa/mm^2)	60	40
Hardness	210 VPN	85 - 120 VPN

Of these properties ductility is considered to be the most important and this must be at least 6% elongation if deposits are not to fail the thermal shock tests demanded by relevant specifications. Hardness is reported [23] to be of little significance although its reduction with storage at 120 °C for 1 hour or approximately 3 days at room temperature indicates that the elongation and thermal shock resistance have improved.

2.3 Through-hole Plating

The characteristics of electroplated metals in plated-through holes have been determined experimentally [9]. Also the effect of different electrolytes on through-holes of varying aspect ratios have been studied by Jawitz [8] and Dini [24]. A systematic study of the effect of additives on through-hole plating has also been carried out by Goodenough and Whitlaw[21].

Basically, in the economic evaluation of printed circuit board fabrication, three characteristics of the plating of through-holes should be considered, they are:

1) deposit thickness distribution [25-31]
   a) surface-to-hole ratio;
   b) hole length-to-hole diameter ratio or aspect ratio;
2) metallurgical structure of the deposit, ie. to produce plated through-holes which would have the ability to resist and barrel cracking during the solder float [25];
3) speed of the plating process which in effect relates to process parameters and agitation(s) [32,33].

An extensive set of experiments with several plating baths by Rothschild[25] has shown that the plated thickness distribution becomes more nonuniform as the ratio of the board thickness (t_B) to the hole radius (R_o) increases. For each plating bath Rothschild found the resulting plated thickness on the board surface for a specific minimum thickness in a hole was a function only of t_B/R_o.

As for metallurgical structure, the development of additives have greatly improved the properties of the deposit required to meet the industrial standards, hence efforts are now focussed on the current distribution and plating thickness distribution (section 2.3.2).

2.3.1 Modelling/designing through-holes

In general, through-holes are studied by cross-sectioning PCBs having different hole diameters and aspect ratios. The coating thickness distributions of the cross-sectioned PCBs provide S/H ratio results.

In order to understand the main parameters affecting the current distribution in the bath, various authors have devised modelling techniques such as:

a) mathematical modelling [29,34-39,40];
b) computational modelling [41,42];
c) bath, cell or PCB design [28,31,33,43,44,45].

It is noted that in some cases the authors have used two or more modelling methods to confirm their theory. As far as this thesis is concerned, the mathematical and computational modelling is of minor interest but the bath design and cell, probe and PCB design will be discussed with emphasis on the importance of the design itself taking into account the geometrical and hydrodynamic parameters influencing the overall mass transfer in the through-holes.

The simplest method of studying the behaviour of an electrolyte is the technique used by Barringer et al [43] known as "2^3 factorial design" or the "Box-Behnken(box) method" as shown in Figure 2. Although this technique allows access in obtaining results at various positions within the cell, realistically it is not a good comparative method to that of the PCB in terms of hole diameter and aspect ratio. However, it is an ideal method for speedy data collection and optimisation of electrolytes.

Perakh [44] has used slot-type field-shaping cell as shown in Figure 3. Although,

this cell is not directly related to a PCB it certainly can be used as an indication of the throwing power of the solution in which the position of the partition and slot size can be adjusted.

Olsen et al [31] have patented a method and an apparatus for plating large length to diameter ratio holes in a substrate. Figures 4a and 4b show the design of a tapered hole and the plating apparatus with a cross-section of the cell in situ. Basically, this design is ideal for tapered holes which are formed by electron beam or laser drilling or by forcing an appropriate etchant through a previously drilled hole. Although, this design can be used for obtaining uniform hole diameter it is inappropriate on conventional PCBs where holes have 'uniform' diameters. A major disadvantage with tapered holes could be the method of producing holes and/or the cost of plating larger holes than necessary in comparison to that of conventional PCBs.

Yung and Romankiw [28] have used through-hole plating experiments using a gap cell and also a Plexiglas board, as shown in Figures 5 and 6. They have found that the gap cell provided good simulation of the plated through-hole system and allowed accurate and non-destructive profile analysis of the copper deposit. As for the Plexiglas, it is a simulation of a PCBs for which various aspect ratios(hole length/hole diameter) could be used to study the surface/hole thickness ratio.

The cell design has been used to study the effect of different agitation methods for through-holes. Haak et al [33] have used a fabricated test board for the evaluation of agitation within PCB through-holes. Figure 7 illustrates the fabricated test board and their dimensions noting that the test board consists of five layers of 0.15mm copper to form appropriate circuitry pattern separated by 0.15mm layer of epoxy glass fibre laminates. For the data acquisition a computer was used. The results obtained were found to be reproducible [33](see section 2.3.2).

The use of theoretical [3,27] and mathematical [40,45] modelling has been common, with many authors using them in combination to their system of interest. Lanzi et al [40] and Kessler et al [45] have used multi-layer board(MLB) cells in their studies, as shown in Figures 8 and 9, respectively. As for bath and cell design, Alkire et al [3] and Engelmaier et al [27] have used a forced-flow method on MLBs and impinging jet in their studies as shown in Figures 10 and 11, respectively.

As far as the choice of these models are concerned, it depends on the specific requirement but the author recommends the design devised by Yung et al [28] for studying MLBs.

2.3.2 Throwing power and mass tansfer in through-holes

In printed circuit boards, throwing power (ie. the ability of a solution to deposit uniformly on an uneven surface) and mass transfer are related to each other. For example, for high throwing power acid copper plating solutions, the throwing power is inversely proportional to the current density and proportional to the degree of agitation through holes.

The traditional method for measuring throwing power is with the use of the Haring-Blum Cell [17]. Such throwing power results are calculated using the Field formula derived to produce percentage throwing power numbers. Luke [23] has used an alternative formula [46], which is a modified Field formula for the Haring Cell. He considered the importance of throwing power for printed circuits and in particular multi-layer circuits such that:

$$\text{Throwing Power} = \frac{L - M}{L + M - 1} \times 100$$

Where $L = \frac{L_2}{L_1}$ and $M = \frac{M_1}{M_2}$, where L is the ratio of distances of far(2) and near(1) cathodes from the anode and M is the ratio of increase in mass of the near : far cathodes(figure 12).

Luke[23] has found that using acid copper solutions throwing power improves with:

1) decrease of current density;
2) decrease of solution temperature;
3) increase of solution agitation through holes;
4) absence of organic contamination;
5) increase of additive (to a nominal level above which, throwing power decreases).

Solution agitation is one of the major factors for holes of small diameter, such that they will transport ions to the critical areas and hence the deposition will take place. The methods of agitation could be carried out by air sparging[33], reciprocating[33], forced-flow [27], vibratory [47-49], jetting [3], etc. The importance of throwing power and mass-transport using air sparging and forced flow agitation has been stressed by Engelmaier et al [27] and Kessler et al [45]. Figures 10[27] and 8[45] show the typical arrangement used, using a forced-flow electroplating system and also an electroplating cell, respectively.

Engelmaier et al[27] have derived a new formulation for throwing power such that:

$$\text{Throwing power} = \frac{t_p}{t_H}$$

where t_p = plated copper thickness at plated through hole(PTH) entrance or exit

and t_H = plated copper thickness in PTH centre.

Figure 13 [27] shows the sketch of plated through hole in cross section. Figure 14 illustrates an schematic diagram of a PCB in cross-section indicating different throwing power in holes.

The metallographic cross-sections of plated through-holes using an additive-free acid copper sulphate [27] showed that increasing the agitation velocity in PTH and decreasing the PTH electrical resistance will lead to a lower surface to hole ratio(t_S/t_H=2.0) at constant current density. Also, decreasing the current density and decreasing the electrical resistance(=0) at a constant velocity will lead to a lower surface to hole ratio(t_S/t_H = 0.99).

Furthermore, increasing the levels of agitation improves the deposit quality dramatically up to the point of eliminating ion concentration gradients causing mass transport-limited plating conditions. Further increases in the level of agitation, however, provide no further improvement in the PTH copper deposit. To prevent mass transport-limited plating conditions, agitation requirements increase rapidly with increasing current density and decreasing cupric ion concentration.

The effect of an impinging fluid jet on mass transfer and current distribution in a circular through hole has been studied by Alkire et al [3]. Figure 11 shows the design used. Using ferro-cyanide, Alkire et al [3] has found that:

a) the limiting current density depended strongly upon the through-hole diameter and aspect ratio;
b) fluid flow pattern was relatively insensitive to whether the external jet was submerged or unsubmerged;
c) the limiting current distribution was relatively insensitive as to whether the convective flow pattern lies in the entrance or the well developed regime;
d) uniform deposits may be anticipated when both reaction parameters, 'relative' exchange current density(ξ), for through-hole and local reaction rate(j^*) have values which are less than unity, noting that both are defined as dimensionless numbers;
e) for ensuring adequate supply of reactants, the value of the average limiting

current density(N), as a dimensionless number, should be about 5 times of value of local reaction rate(j*), ie. the stirring condition should be less than 20% of the mass-transfer limiting current;

f) the flow configuration studied provided the greatest level of mass-transfer enhancement.

Similar results have been obtained by Haak et al [33] using air sparging and reciprocating agitation. They have concluded that:

a) mass transport rate generally increases with sparging rate and noted that the design of the agitator is important;
b) uniformity of mass transport tends to decrease with increase in air sparging rate, but the relationship is not monotonic, especially for the board outer surfaces;
c) perpendicular board motion has little effect on the overall air flow rates, but significantly improves the uniformity of agitation provided by air sparging;
d) hole size is apparently important, ie., mass transport is significantly restricted for diameters less than about 1.5mm;
e) mass transport to positively etched back regions within the through-hole is significantly reduced.

Finally, it can be summarised that the choice of electrolytes with a high throwing power and a good agitation method is necessary to obtain a high mass transfer rate to take place for through holes.

CHAPTER 3

3.0 PULSE PLATING THEORY

3.1 Pulse Plating Equipment - Definitions, Behaviour and Irregularities

Electroplating has evolved as a process depending on the supply of a flow of direct electrical current through an electrolytic cell (vat or tank). Conventional power supplies are based on the transformation/rectification of mains (alternating current) electricity, most direct current (DC) is produced as an average value, about which there is a varying amount of so called alternating current (AC) ripple (Figure 15) [50]. For most purposes the amplitude of this ripple should be within 5% of the average direct current for satisfactory results. Thus it can be concluded that electroplating rarely takes place under conditions of a constant, unvarying current.

The general definition of a pulsed supply is, that in which a constant current is switched from one level to another. The simplest case is that of the alternate switching on and off of a DC supply.

Two common pulse power supplies are square-wave and the modified sine wave, Figure 16[1] shows a theoretical representation of various pulse waveforms.

The most commonly applied wave shapes include the sine-wave, the half-wave pulse delayed, the full-wave phase delayed, the skip-sine, the unipolar pulses (pulse reverse) with or without off-time between the cathodic and anodic cycle, the pulsed pulse reverse, the pulse-on-pulse and duplex pulses.

In the plating industry, various methods of defining a current or voltage pulse have been used. A pulse requires time for the excursion from one amplitude to another amplitude. The exact beginning and ending of this excursion is usually difficult to locate on a waveform obtained on an oscilloscope. This is due to the inductance and capacitance of the power source and the external load effecting the wave shape. Therefore, the pulse rise time (t_r) and the fall time (t_f) are specified at the 10 percent and

90 percent points of the pulse amplitude (Figure 17) [1]. Pulse duration (t_{on}) is specified at the 50 percent point of the pulse amplitude.

The most commonly used waveform for precious metals are the square-wave. This fast rise and fall time allow them to be used at frequencies exceeding 10KHz. Precious metal is often plated at pulse frequencies in the range of 500Hz to 5KHz. The pulse frequency is determined by an internal frequency generator which is independent of, and usually much higher than, the power line frequency [1].

This research work is mainly based on square-wave current pulses, therefore, this discussion will be confined to them.

In practice, it is difficult to produce an idealised, geometrically square waveform as illustrated in Figure 16. Normally, the shape of the pulse as shown in Figure 18 [50] are seen when an oscilloscope is used to measure the output of a pulse plating unit. The irregularities are normally due to the non-ideal nature of the switching circuitry, leading to oscillation over the first few milliseconds or less.

Another factor affecting the pulse pattern is due to the external circuit producing inductance and/or capacitance. The inductance effect can be minimised by adding capacitance between the anode and cathode bus wires. Figure 19 [1] shows an example of such a behaviour and the method to overcome this. Also, it is recommended [1] that the power supply to be located as close to the plating bath as practical; this will help to reduce the inductance effect of the bus system.

Final consideration should be given to the amperage capacity or current rating of the anode and the cathode wires to minimise voltage drops. Therefore, the wire must be sized properly, firstly to minimise voltage drop and secondly, to allow for the RMS heating affect of the peak current. Pulse currents generate greater heat than the average current [1]. For example:

100 amps. peak, 25% duty cycle

Average current 25 amps.

RMS current $\sqrt{\text{peak x average}}$

Conductor rating 50 amps.

3.2 Pulse Plating Parameters

In general, pulse techniques permit deposition of coatings with excellent properties, pulse currents also reduce or eliminate the effects of hydrogen uptake and subsequent embrittlement due to the cathode inefficiency during plating. In addition, it has been reported[51-53] that pulsing techniques permit the deposition of alloy compositions that can not be obtained by conventional direct current deposition. Coating compositions can be controlled by adjusting the pulse plating parameters.

There are four variables that are of primary importance in unipolar pulse plating. These are:

1) peak current density (i_p);

2) off-time current density or base line (i_b);

3) on-time (t_{on});

4) off-time (t_{off}).

The sum of on-time and off-time constitutes one pulsing cycle (Figure 20) and (Figure 21) [1]. The duty cycle is defined as the ratio of the on-time to the sum of the on-time and off-time, in other words the pulsing cycle is defined as:

$$\text{Duty cycle } (\phi) = \frac{t_{on}}{t_{on} + t_{off}} \times 100\%$$

The on-time and off-time are usually in the millisecond range. A duty cycle of 100% corresponds to conventional, DC, plating because there is no off-time, Figure 20.

In the application of pulse plating, it is possible to use an average pulse current density equal to the current density normally used in conventional plating. The average current density (i_{av}) under pulse condition is defined as:

$$i_{av} = i_p \times \phi$$

where i_p= peak current density and i_{av} and i_p are in Adm^{-2}.

In practice, a duty cycle of 5% or greater has been reported to be appropriate [54].

In bipolar pulse reverse (Figure 22) the average current density is defined by the following equation:

$$i_{av} = \frac{i_{p(c)} \times t_{on(c)} + i_{p(a)} \times t_{on(a)}}{t_{on(c)} + t_{on(a)}}$$

where $i_{p(c)}$= cathodic peak current density(Adm^{-2})
$i_{p(a)}$= anodic peak current density(Adm^{-2})

$t_{on(c)}$= cathodic on-time(s)
$t_{on(a)}$= anodic on-time(s)

It should be noted that the peak current densities are of opposite sign and also the characterisation of the bipolar pulse reverse current wave form requires at least four known parameters.

3.2.1 Current and voltage regimes

Electrolysis can be controlled by regulation of either current or voltage. In voltage regulation mode, the driving force for the reaction is kept constant and the reaction rate varies as a function of time. This can be carried out by either using a power supply or using a potentiostat. In the current regulation mode, the reaction rate is kept constant and the potential varies as a function of time. This can also be carried out by either a power supply or using a galvanostat.

In a pulse current regime, the average deposition rate can be derived from the following equation (see section 3.2):

Average current density = Peak current density x Duty cycle

$$\text{where} \quad \text{duty cycle} = \frac{\text{on–time}}{\text{on–time + off–time}} \times 100\%$$

While in pulse voltage regulation, the average deposition rate can be predicted only from computations of a speculative nature. The main advantage of voltage regulation is that a better control of the current efficiency and of alloy composition can be acheived. Also, high overpotentials resulting from excessive concentration depletion can be avoided.

In order to achieve the pulse voltage in pulse voltage regulation mode, a third electrode, a reference electrode should be added to the system. Moreover, to get instantaneously a given potential at the electrode, the current should start theoretically from an infinite value, which is obviously not possible because of apparatus limitations. On the other hand, at the end of the pulse, for instantaneous reestablishment of the starting potential (which might be the rest potential of the system), some metal should be redissolved; hence a constant voltage pulse requires a short inversion of current at the end of the pulse, which is not generally desirable [1]. It is to be noted that the above remarks apply to a generated cathodic potential and not to the voltage between the negative and positive poles of the power generator or supply.

It has been reported by many investigators [50] that current regulation is preferred especially for very high currents. There are also other methods of regulations such as constant current density, current/voltage cross-over and ramped-start [51]. In the literature studied, the use of regulating techniques in pulse plating were limited to voltage and current regulation, which were discussed earlier.

3.2.2 Benefits of bipolar pulse reverse(PR)

Among the different modes of current modulation, (Figure 20), bipolar pulse reverse is a very early one and is very common. The main purpose of inverting the current(Figure 22) from cathodic to anodic during a short fraction of the total period is to remove metal preferentially from areas that tend to overplate during the cathodic part of the cycle. It is thus possible to considerably retard the development of dendritic formation or to improve the plating thickness distribution over complicated shapes. It has been reported by many authors [1,55] that changes in deposit structure, mainly grain size, can also be achieved because of forced nucleation at each new cathodic pulse. This is believed to be due to adsorption as well as recrystallisation phenomena, and has been reported to be quite different from those in unipolar pulse plating.

However, pulse plating can be of great help in equalising the plating thickness distribution. For example in printed circuit board industries where areas exposed to concentrations of current density are preferentially plated in the cathodic cycle, but for the same reason, metal is preferentially removed in the anodic cycle.

To take advantage of the bipolar pulse reverse, the anodic current density should be adjusted independently of the cathodic current density. The reason for this is to increase the dissolution rate of peaks by applying very high anodic peak current densities, but for short durations. It is obvious that the balance of the charges over a total period should remain cathodic.

3.3 Comparisons between Direct Current (DC) and Unipolar Pulse(P) Electroplating

In many electrodeposition processes, the main factor is the rate at which the metal ions can be transported to the cathode interface where they are discharged electrolytically to provide the coating or structure. The rate of deposition by pulse

plating is controlled by many factors (section 3.1.1).

During conventional electrodeposition, cations are discharged at the cathode, and the concentration of the metal ion is reduced. As deposition continues a 'diffusion layer' is formed in which the metal ion concentration is reduced below the metal concentration in the bulk of the electrolyte. As deposition continues, an equilibrium is attained wherein the metal ions pass through the diffusion layer at the same rate as that at which they are discharged at the cathode. The thickness of this diffusion layer is an important variable in determining the rate of the electrodeposition process. Agitation is one of the most effective ways of reducing the thickness of the diffusion layer and allows deposition to proceed at higher current densities.

In pulse plating, three parameters can independently be varied and influence the properties of the electrodeposit. These parameters are the on-time, the off-time and the peak current density. During the on-time the concentration of the metal ions to be deposited is reduced within a certain distance from the cathode surface. This so-called diffusion layer pulsates with the same frequency as the applied, pulsed current. Its thickness is also related to the peak current density, but reaches a limiting value governed primarily by the diffusion coefficient of the metal ions. During the 'off-time', the concentration of the metal ions builds up again by diffusion from the bulk electrolyte if enough time is allowed. However, a general comparison cited by many authors [1,28] claims that:

a) a higher instantaneous cathode current density can be applied to the pulse plating system because of a higher concentration of metal ion in the diffusion layer. Applying pulsed current does not increase the overall plating rate but raises the limiting current density;
b) in pulse plating, raising the current density, there is a possibility of improving the physical properties through structural modifications of the electrodeposit. More fine grained electrodeposits are usually obtained;
c) with direct current plating, only voltage or current can be controlled. However, with pulse plating, three parameters, time-on, time-off and the peak current density can independently be varied (for the same average current density) such that (a) mass transport situations (b) electrocrystallisation conditions, and (c) adsorption and desorption phenomena have to be taken into account.

3.3.1 Advantages and disadvantages of unipolar pulse and bipolar pulse reverse to DC electroplating

The expected advantages of pulse plating can be enumerated:

a) possibility of improving the physical properties of the deposit; finer, purer and smoother deposit;
b) by applying pulse current it is possible to raise the limiting current density hence increase the plating speed;
c) better adhesion of deposit to substrate;
d) improve plating distribution.

Furthermore, uniform distribution is possible on complex shapes using pulse reverse[1].

The disadvantages of pulse plating are based upon the theoretical considerations such that the current distribution in pulse is poorer than DC[1]. The deterioration of current density in pulse plating is due to:

a) higher ohmic drops in solution leading to higher current density differences between peaks and recesses of the substrate profile;
b) decrease in activation overpotential with increasing current distribution[50,56].

The deterioration of current distribution with pulse plating occurs if the pulse current density is substantially increased when compared to the normal DC density. If the pulse current density is the same as the usual DC density, pulse plating could improve the current distribution.

Finally, it can be concluded that a pulse condition which provides certain characteristic deposit for one system will not necessarily provide similar deposits for another system.

3.4 Effect of Pulse Current in Electroplating

In order to understand the effects of pulse plating on the physical properties of the deposit, it is necessary to review the electrochemical mechanisms involved in the cathodic deposition.

Academic studies [50] of the process to date, with few exceptions, have tended to concentrate either on the electrode kinetics of the electron transfer reaction(s) or on the micrographic study of crystal formation. Although, these effects are worthy of study,

both tend to neglect the effects of mass transfer to the electrode surface, ie. diffusion, convection, etc. In practice, the rate of most plating processes, and those of many other commercial applications of electrochemistry, are controlled by the rate of diffusion of ions to and from the cathode surface, particularly where high speeds are involved.

The sequence of processes occurring during the transformation of an ion in the bulk of solution to its appearance as a metal atom in the plated deposit is illustrated in Figure 23[50]. The hydrated cation (assuming the plating ion is not contained in an ionic complex) moves towards the cathode under the influence of convection and subsequently by diffusion until it enters the field of the double layer which exists at the electrode surface. The exact sequence of events at this point will vary from one constituent to the next but involves gradual removal of the 'hydration sheath' around the cation, and any other complexing ions or molecules, adsorption on the cathode surface, electron transfer (from cathode to the cation) and surface migration to an energetically favourable growth point. The point on the surface at which the adatoms or adion becomes incorporated into a growing layer depends on many factors, including the nature of the solution, flow conditions, current density, nature of the surface, temperature, etc. The site may be one at which two dimensional(layer) or three dimensional growth occurs, or it may be the initial atom at a particular site, resulting in so-called nucleation of a new growth point. The predominant process will influence the appearance and general nature of the electroplating surface.

The beneficial effects noticed in the literature [50] when the optimum pulse parameters are applied, can be related to the nucleation and growth processes. More even, dense deposits result from an increase in the occurrence of the former as result of switching 'on' after a brief 'off' period. During the passage of a direct current, nucleation and growth processes compete for the available deposit adatoms or adions. Nucleation and growth are retarded temporarily during the 'off' period, such that when the current is switched 'on' there will be a tendency to form new nuclei. This may be associated with the adsorption of organic solution additives, such as brighteners and levellers, preferentially on to growth points or the substrate itself. The former will prevent further deposition of metal atoms at that point and the latter will block surface migration of atoms towards existing growth points.

Finally, it must be noted that pulsed current does not always lead to improvements, sometimes quite the reverse. This indicates the importance of the 'on' and 'off' times and the current density to the application.

3.4.1 Crystallisation

Crystallisation is a process by which the adatoms or adions are incorporated in the crystal lattice(see section 3.4). Crystallisation occurs either by the build-up of the old crystals or by the formation and growth of new ones, Figure 24 [1]. These two processes are in competition and can be influenced by different factors. High surface diffusion rates, low population of adatoms and low overpotentials are factors enhancing the build-up of the old crystals, while conversely low surface diffusion rate, high population of adatoms, and high overpotentials on the surface enhance the creation of new nuclei.

In pulse plating, the pulse current density is usually higher than the corresponding DC density [57], the population of adatoms on the surface during pulse deposition is higher than DC deposition, resulting in an increased nucleation rate and therefore in a finer grain structure. An increased nucleation rate is also expected from the high potential corresponding to the increased pulse current density when compared to DC.

The off-time is not a dead time for the crystallisation. Small grains are thermodynamically less stable than large ones because of high surface energy and tend to recrystallise if no inhibition occurs.

Finally, it has been reported [57] that in pulse plating with very high pulse current densities, the concentration of the adatoms at the interface is so high during the pulse that there is no time for ordering them into a crystal lattice, resulting in similar effects, as in rapid thermal quenching.

3.5 Capacitance Effects

The electrical double layer at any electrode/solution interface can be approximated to a parallel plate capacitor with an interplate distance of a few angstroms and therefore with a high capacitance. Typically, the value of the double layer capacitance for such a system is of the order of $50\mu Fcm^{-2}$.

Basically, a double layer must be charged in order to raise its potential to the value required for metal deposition at the rate corresponding to the applied current pulse. The electrode behaves like a capacitor with a resistor connected in parallel to it (Figure 25) where the latter is the charge transfer for the electrode reaction occurring at the applied

potential [58].

However, the charging of the double layer requires a certain time which depends on the current density and the physio-chemical parameters of the system. For practical purposes, the charging time should be shorter than the pulse duration/length, otherwise the faradic current pulse is strongly distorted as shown in Figure 26[55]. As for unipolar pulses, it is important that the off-time to be longer than the discharge time for the double layer and as for the bipolar pulses, both cathodic and anodic pulse times should be longer than the charge times.

Furthermore, in an extreme case, where the charging and discharging times of the double layer are much longer than the on-time and off-time of the pulse, respectively, the pulse current is virtually a DC and the potential benefit of pulse current in terms of changes in electrodeposition is lost [1]. However, the current used to charge the double layer is not lost but is recovered at the end of a pulse during the double layer discharge as shown in Figure 27[58]. Thus it has been found that the efficiency of metal deposition with pulse current is generally similar to DC in electrolytes where only one reaction occurs; except in copper cyanide, where discharge of hydrogen and copper in cyanide copper electrolyte takes place and the relative efficiency of the electrode process may be altered.

Finally, it has been reported[1,58] that due to the design of the pulse generator, the electroplating bath is left in an open circuit at the end of each pulse because plating occurs by discharging of the stored double layer through the charge transfer resistance. Otherwise, under closed circuit condition, the double layer can discharge through the pulse generator rather than the charge transfer resistance. This is believed to cause a major reduction in the apparent cathode efficiency of an electrolyte.

3.6 Mass Transfer Effects

The limitations of the useful range of pulse conditions due to mass transfer effects arise from the depletion of cations in the diffusion layer [1]. In pulse plating, with short pulse durations, two distinct cathodic diffusion layers can be defined instead of one as in DC [55], as shown in Figure 28. In the immediate vicinity of the cathode the concentration pulsates with the frequency of the pulsating current, decreasing during the pulses and relaxing in the interval between them. For relaxation of the pulsating diffusion layer metal ions are transported from the bulk of the solution, building up a

concentration gradient into the bulk of the electrolyte. The thickness of this diffusion layer corresponds essentially to that which would be established under the same hydrodynamic conditions in DC electrolysis.

In terms of the 'double' diffusion layer model, the two layers are related to two kinds of limitations [57]. The depletion of the cationic concentration in the pulsating diffusion layer limits the pulse current density and the depletion of the cationic concentration in the outer diffusion layer limits the average current density.

However, there is a quantitative relationship between the maximum pulse length as far as current efficiency and the pulse current density are concerned. This maximum pulse length is called transition time. A pulse current density with a pulse length corresponding to the transition time represents the maximum deposition rate without significant loss in current efficiency [57]. This pulse current density is known as pulse limiting current density or peak limiting current density. Mathematical approaches have been carried out by Chin [4], Ibl [51] and Cheh [59] and a review on mass transport in pulse plating has been described by Landolt [1].

Finally, it has been pointed out by Cheh [59] that the practical average current density, which is below the diffusion limiting current density, can sometimes be increased in pulse plating as compared to DC while keeping a constant deposit quality. The increase, however, is only modest and does not represent the main advantage of the pulse plating technique but rather relates to the improvement of the deposit properties and hence deposit structure.

3.7 Current Distribution

In applied electrochemistry, potential and current distribution are of major importance. They are governed by phenomena related to charge transfer at the electrodes and mass transport in the electrolytes. They can be related to problems such as current efficiency, product selectivity and utilisation of an electrolysis cell [1].

In metal deposition, the current distribution determines the variation of the deposit thickness along the cathode surface and it can have an effect on the roughness of the coating. Current distribution can be said to be closely associated with concepts of practical importance such as throwing power and levelling(see section 2.1.3).

Basically, the distribution of the current is attributed substantially to:

a) the geometry of the system;

b) the conductivity of the electrolyte ;

c) the kinetics or polarisation prevailing during electrodeposition.

These factors are directly related to the primary and secondary current distribution while tertiary distribution is related to the surface characteristics such as irregularities or roughness or even pretreatment.

3.7.1 Primary current distribution

The primary current distribution, as explained above, depends solely upon the geometry of the system. This can be either the shape of the electrodes and/or the distance between the electrodes. As far as the shape of the electrodes are concerned, it is well known that the current efficiency is usually higher on protruding parts or edges, while the anode to cathode distance affects the throwing power distribution of the metal. Because the primary current distribution is dependent solely upon the cell geometry and is independent of current density, it is therefore expected that the primary current distribution should be the same for pulse plating as in DC [60].

3.7.2 Secondary current distribution

The secondary current distribution is related to the conductivity of the electrolyte and also the activation overpotential of the system for which they can be related and expressed as a dimensionless Wagner number, see section 2.1.3, such that:

$$Wa = \frac{\kappa}{L}\left(\frac{d\eta}{di}\right)$$

where κ is the electrolyte conductivity (Scm^{-1} or $\Omega^{-1}cm^{-1}$)

L is the characteristic length of the deposition process (cm)

$\left(\frac{d\eta}{di}\right)$ is the slope of the polarization curve and calculated at an average current density ($VA^{-1}cm^{2}$)

In general, the greater the rate of change of potential with increasing current density, the more the overall current distribution tends towards a secondary current distribution and, excluding mass transfer effects, produces a more even metal distribution[61]. As current density is increased, the charge transfer resistance falls so

the rate of change of potential with current density also becomes less. Thus as current density is increased, so the current distribution and throwing power deteriorates.

However, in pulse plating, whether unipolar or bipolar pulse, in order to maintain the same rate of deposition as for DC, the cathodic current density during the cathodic pulse must be higher than the equivalent direct current density. This means that the overall current density distribution tends towards a primary distribution when pulse plating is employed [51,62]. Consequently, the deposit distribution would be expected to be less uniform using pulsed current than with DC.

Solution additives also play an important role in the distribution of current as described by Pearson and Dennis [2] and have shown some of the benefits of pulse reverse in their study with regard to the deposition rate and its uniformity.

3.7.3 Tertiary current distribution

The tertiary current distribution is related to microprofiles and macroprofiles, influenced by the diffusion layer thickness. As shown in Figure 29 [1], microprofile is described when a surface profile whose characteristic height, h is smaller than the thickness of the diffusion layer. The crests are privileged from the view point of diffusion and as a consequence of geometrical effect or primary distribution, the irregularities of the surface are amplified in the course of deposition. The effect is important as it affects the appearance and the properties of the deposit. On the other hand, in macroprofile, the characteristics height, h is larger than the thickness of the diffusion layer. In general, the thickness of the diffusion layer is considered to be constant, that is, each point on the surface is equally accessible for diffusion, which is not affected by geometrical factors.

It has been described[1,63] that the tertiary current distribution is usually highly irregular under DC as opposed to pulse conditions because the situation of microprofile occurs; in other words, during the relaxation or off-time some replenishment of metal ion takes place and hence the severity of the profile reduces from diffusion view point. Therefore, it can be summerised that the thickness of the pulsating a diffusion layer is dependent on the pulse length. Thus, if pulse parameters are chosen correctly in terms of pulse length and average current density, the above findings could be true. Hence, an improvement on microthrowing power can be expected. But it has been reported[51,63] that the macrothrowing power can be expected to become worse under

pulse conditions when compared to DC.

As far as pulse reverse is concerned, significant improvement can be expected. For example a better coating thickness distribution can be expected compared to DC. This is due the fact that after every cathodic and anodic cycles, the deposits at high current density areas will dissolve back into the electrolyte.

3.8 Current Efficiency

In pulse plating, the electrodeposition can be considerably increased during the on-time as compared to DC. The kinetics of competitive reactions will therefore play a relevant role on the relative rate of possible competitive reactions in plating with hydrogen codeposition or in alloy plating [1].

Basically, the current efficiency is effected by the pulse parameters. This is due to desorption of hydrogen from the cathode during the off-time. As for copper, it has been reported[57] that the current efficiency decreases. This has been explained in terms of transition electrode potential that pulse current lead to a readjustment of the partial currents causing Cu^{2+}/Cu^{+} and $Cu^{+}/Cu^{\bullet}$ reactions to occur and hence effect the current efficiency of the plating process[64].

From the literature it is understood that current efficiency can either increase or decrease depending upon the electrolyte and its characteristics, additives, pH, etc. For this reason, there is scope for research using pulse plating.

3.9 Effects of Pulse Current on Morphology

In pulse plating, the morphology can be expected to vary with the pulse parameters. These parameters play an important role in the purity, grain size and the deposit structure.

The morphological studies reported[1] have shown that the structure of an electrodeposit in pulse plating is also much affected by factors other than mass transport. The phenomena of nucleation and crystal growth, of desorption and adsorption play an essential role. They can take place both during the on-time and off-time, thus the variation of both parameters can affect the properties of an

electrodeposit. In general, pulse length or on-time, off-time, peak current density and average current density are the major factor effecting the deposit structure which can cause grain changes and hence affect the hardness.

It has been reported [1,55] that additives can have either a positive or negative effect on the morphology of the deposit with pulse plating when compared to normal DC, see section 4.0.

Finally, it can be concluded that the pulse current can be used to obtain properties which are not normally possible under DC. But as far as bipolar pulse reverse is concerned the changes in morphology are more pronounced [1].

CHAPTER 4

4.0 LITERATURE SURVEY OF PULSE PLATING

Originally, a literature survey was carried out in order to obtain a general view on pulse plating behaviour with respect to pulse parameters and their effects on morphology, hardness, tensile strength, grain size, etc. Consequently, the whole range of pulse plating technologies has been surveyed. This (section 4.2) although not comprehensive, does report the trends apparent in the literature. Section 4.1 indicated literature reported for copper and, because of the importance of this metal, to the author's investigations, is essentially of more a detailed nature.

4.1 Pulse Plating of Copper

Amongst many metals, the pulse plating of copper has been under study for many years due to its characteristics and simplicity, however, only a few studies have been 'in depth'.

It has been known and confirmed[1] that the most important factors affecting the copper deposition are the pulse parameters. These parameters include pulse length or on-time, off-time, peak current density, average current density and the direction of the pulse either positive and/or negative. Therefore, the morphology of the deposits are dependent on the pulse parameters. Furthermore, any effects on the morphology will lead to changes in tensile strength, elongation, hardness, grain size, roughness, etc.

An extensive study of pulse parameters has been carried out by Puippe et al [1] and Chene et al [65] using acid copper sulphate electrolytes. Table 5 shows the bath constituents and the conditions used. These authors have studied the influence of mass transport on surface morphology and the uniformity of the deposit. Figure 30 shows the effect of peak current density for different average current densities of $1.6Acm^{-2}$ and $34.8Acm^{-2}$ at t_{on}=0.3ms and t_{off}=100ms. It can be seen that the structural changes in the deposit are very small. Figure 31 shows the effect of on-time on the deposit morphology. The peak current density and off-times were kept constant at

$3Acm^{-2}$ and 100ms, respectively, for on-times of 0.1, 10, 30ms. The deposits changed from a fine granular structure to a cauliflower-type structure. However, an increase in peak current density at constant on-time and constant average current density affect the grain size, Figures 32 and 33. It can be inferred that with an increase in peak current density, the off-time is also increased provided average current density remains constant and it therefore influences the crystallisation. The latter has been investigated[1] further by increasing the pulse current density while keeping both the average current density and the number of coulombs per pulse constant, Figure 34. Figure 35 shows this off-time effect to be extensive in terms of changes in grains causing growth. The most plausible explanation is said to be due to a crystallisation process occuring during the off-time. The bigger grains are thermodynamically more stable and, if enough time is allowed to the system, the most stable configuration will be reached[1].

The study carried out by Hayashi et al [66,67], using a platinum rotating disc electrode in 0.8M $CuSO_4$ and 0.5M H_2SO_4, found that the surface morphology during the off-time was of major importance. Figure 36 shows that the change of surface morphology of the copper deposit on the copper single crystal plane(111) with the various pulse off-times at the same pulse current density and on-time. With increasing pulse off-time, the small pyramidal growth ceased gradually and layer growth then predominates.

Figure 37 [67] shows the effect of the pulsed current density on the morphology at constant average current density. The distinct layer growth is observed even at the high average current density of $75mAdm^{-2}$ and the well-defined spiral growth was also noticed. This transformation in growth forms would be brought about by the dissolution and reconfiguration of unstable copper atoms on the copper electrode during the pulse off-time. The current efficiency of the electrodeposition of copper with pulsing has also been reported to decrease with decreasing average current density and with a longer pulse off-time under the pulse current electrolysis.

In direct current plating dendritic or powdery deposits are obtained if deposition is carried out at or near the limiting current density [1]. This is due to the fact that asperities on a surface are more accessible than recesses from a mass transport point of view. The applied current density in DC plating, therefore, usually does not exceed 10-20 percent of the value of the limiting current density value. The situation in pulse plating is somewhat different because smooth deposits may be obtained even at the limiting current, provided the pulsating diffusion layer thickness is extremely small [68].

Ibl et al verified this behaviour for copper [69]. If the pulsating diffusion layer is smaller than the original surface roughness, it follows the surface profile rendering all points equally accessible [68]. Despic et al [70], Maksimovic et al [71] and Popov et al[72], using the same reasoning, were able to explain the observed influence of pulse frequency on deposit smoothness. Dendrites can grow only when under low frequency condition and pulsating diffusion layers can diverge from the surface profile[70]. As in DC plating, the average current in pulse plating should stay well below the DC limiting current density (i_L) if dendrite and powder formation is to be avoided [73]. This is illustrated for the case of copper deposition from a copper sulphate/sulphuric acid electrolyte in Figure 38 [65,74]. On the ordinate is shown the ratio of pulse current/pulse current density of limiting current pulse (i_p/i_{pl}) and on the abscissa, the ratio of average current density/limiting current density for DC (i_{av}/i_L). Figure 38 shows that when $i_{av}/i_L \leq 0.5$, the deposits form a granular shape but when $i_{av}/i_L \geq 0.5$, a powdery non-compact nodular deposits are formed. The same deposit shape has been observed under DC. This indicates that the form of the deposit, under pulse, can be related to its thickness which is partially or entirely limited by the thickness of the diffusion layer.

Mass transport may affect current density as in DC plating, and the current efficiency for metal deposition drops as the limiting current density is exceeded. The same behaviour is to be expected in pulse plating while with pure metals one will usually stay below the limiting current. However, in pulse alloy plating this is not the case such that one metal will behave at an expense of the other(s). This is due to the fact that one component deposits under diffusion control and the other under activation control[65].

Studies on pulsating current copper deposition in a Haring Blum type cell have also been carried out as reported by Dossenbach [75]. The pulse duration varied between 50μs and 100ms; the other pulse parameters were chosen so as to avoid mass transfer effects. Figure 39 represents a plot of the throwing power(s) versus the applied overall pulse current density. The results show that the current distribution is mainly a function of pulse current density. The pulse duration has relatively little influence. The throwing power becomes comparable to the DC values if the pulse and the DC current density become equal, with a corresponding decrease of the average current density of the pulses. It has been reported that the results presented above confirm that in secondary current distribution the uniformity depends mainly on the actual metal deposition current density rather than on the average one and also on a theoretical

basis[75], a secondary current distribution with a pulsating current is normally less uniform than with DC.

Studies of surface roughness of electrodeposit and diffusion layer thickness as a function of the ratio of on-time/transition time (t_{on}/τ) for copper, silver and cadmium have been reported [75], Figure 40. The pulses were much longer than the transition time so that the discharge of the metal ions was controlled by their transport through the pulsating diffusion layer and took place under limiting current conditions during the major part of the pulse. The thicknesses of the pulsating diffusion layer were less than half a micrometer. They were executed by very short pulses; t_{on} was always below 50μs. Peak current densities as high as 25000Adm^{-2} were used in order to make the transition time (τ) small. The roughness (R) of the deposit were found to be very small although they were obtained at current densities, 1000 to 10000 times higher than under usual DC conditions. However, the studies carried out by Chene et al [65] found a strong increase in the value of average roughness(R_a) when the condition i_{av}/i_L is approached. Figure 41[65] shows the influence of pulse parameters on the roughness average of deposits obtained and compared to DC. It can be seen that the roughness average is smaller under pulse when compared to DC. In a general comparison, the roughness values for $i_p>i_{pl}$ (peak current denisty>peak limiting current density) are higher than $i_p<i_{pl}$ which indicates that as peak limiting current is reached more powdery deposits are formed reaching the peak limiting current of DC, also it must must be pointed out that the off-time can provide a wide range of roughness values for different i_{av}/i_L, as shown in Figure 41.

The thickness of the diffusion layer, Figure 40, was reported[75] to be small enough as to have macroprofiles with constant diffusion layer thicknesses in all cases, and the roughness decreased with increasing t_{on}/τ. ie., with increasing mass transport influence. For each metal, the highest roughness values were observed for pulse durations which were lower than the transition time. In these cases secondary current distribution was predominant and therefore the equalising action of mass transport on the current distribution was not effective.

Figure 42 [1] shows for copper deposition that under mass transport controlled conditions (t_{on}/τ = 9.1), the roughness is independent of the deposit thickness, in contrast to the observation in DC [65]. The results also show that a good throwing power on a microscopic scale can be obtained if the diffusion layer is thin as compared

to the dimensions of the surface irregularities (macroprofile) and if simultaneously t_{on}/τ has a sufficient high value (diffusion control). However, it can be concluded that in practical applications the current distribution is not clearly primary, secondary or tertiary but usually lies between a secondary and a tertiary one [1].

The deposit appearances have been studied by Hall and Challdhuri [76] by plating copper foils under pulse using a standard copper sulphate electrolyte and have indicated that the foils colours ranged from orange to brown as the limiting region is reached.

It is well known that additives can play an important role in DC plating but in pulse plating their effect can be somewhat indecisive. Major studies using polarisation curves on additives such as polyether and sulphide base have been carried out by Pearson and Dennis [2]. It has been reported that the additives used caused a shift in the Tafel slope compared to the electrolytes without additives and an improvement in throwing power can be expected. Another important constituents in the bath reported [2,77] is chloride ion. It has been indicated that the presence of Chloride ion is important in adsoption mechanisms and also in the case of some additives such as polyethylene glycol this additive has little influence alone on the cathode efficiency compared to DC.

The importance of pulse reverse plating of copper and also on printed circuit boards have been reported [2,5,6] and have indicated that an improvement in plating distribution, surface coverage and throwing power is possible compared to P and DC. Further accounts of the findings have also been reported in section 4.2.

Finally, it can be concluded that pulse plating of copper can be beneficial depending upon the requirements such as improvement in metallurgical properties, the surface uniformity, etc. It is due to these positive factors that pulse plating has led to increased research in this field.

4.2 Bibliographical Survey of Pulse Plating Technology

This section provides a brief summary of some of the work and also theories on pulse plating. It outlines the name of the author, metal or alloy and bath constituent used, type of substrate used and its usage, the authors' remarks and the reference number. This section was originally compiled in order to understand the benefits of pulse plating. Hence, it is incorporated in this section for possible future use and in some cases as a comparison to this research work.

Author (s) Company	Metal/alloy Bath constituent	Substrate Usage	Remarks	Reference Number
J. Cl. Puippe F. Leaman	Cu, Cd, Ag Au, Zn, Pd Ni, Cr, and other metals & alloys		Survey information on Cu and see section 4.1, otherwise reference 1,Chapters 7-12.	1
T. Pearson J.K. Dennis	Cu 75g/l $CuSO_4$ 114ml/l H_2SO_4 60ppm Cl^- 75ppm Polyether [OX], M.W. 50000 40ppm Mercapto -propaneSulphonic acid, sodium salt[MPS] 40ppm 3-Sulphopropyl (disulphide-disodium salt) [SSP] 22°C, 3Adm^{-2}, PR $t_{on(c)}/t_{on(a)}$=10ms/0.5ms Peak c.d. ratio= 3:1 Air agitation	Copper	PR: Tafel Slopes are similar to DC for electrolytes without additives, improvement in throwing power not expected. More even metal distribution can be produced at low c.d. under PR compared to DC. Polarisation studies under PR for: OX only –the deposition potentials for a given c.d. are higher than the corresponding deposition potential in absence of this additive; due to the surface blocking caused by the adsorption of the polyether on the cathode surface. Polyether causes a shift in E_{rest} to more negative value and a reduction in i_o. SSP only– the deposition potentials for a given c.d. are less negative than the corresponding deposition potentials without this additive present; due to catalytic effect of the active sulphur containing group. Any addition causes a shift in E_{rest} to less negative value and an increase in the i_o. Cl^- is important in adsorption mechanisms; increase in Cl^- concentration causes the E_{rest} to become more negative. In additive free solution and either OX or SSP under PR and DC, Straight line behaviour obtained on E/logi curves which implies that: a) system is under activation control neglecting concentration polarisation b) the system obeyed the Tafel kinetics. The E_{rest} and i_o for OX and MPS are close to SSP. Pulse current causes desorption of SSP at higher c.d. and this shifts the polarisation potential to more negative values owing to desorption of the polyether.	2

Author (s) / Company	Metal/alloy / Bath constituent	Substrate / Usage	Remarks	Reference Number
			Optimum concentration of additives in the bath for PR are: 75ppm-1g/l OX(M.W.50000), 10-45ppm MPS and 100-200 Cl^-.	
D.T. Chin	Cu Acid sulphate 0.75M $CuSO_4$ 0.75M H_2SO_4	Cu rotating disc	By mathematical modelling shown that mass transfer rate is 100-1000 times greater than DC. Pulse current reduces the overpotential required for the electrode reaction and eliminates the Tafel region from the polarization curves. With PR, pulse current shifted the apparent rest potential in the negative direction.	4
A. Montgomery	Cu Acid copper sulphate	PCB	Improved throwing power. Improved covering power. Better copper distribution at low c.d. compared to DC. Plated isolated pads at 30asf gave even deposition with no burning under pulse compared to DC at 10asf. Complex shapes can be plated at higher c.d. than DC.	5
J.C.T. Controls	Cu, Au Acid copper sulphate 125LX* Plating cond. Cu: PR Au: P * LeaRonal proprietory	Cu: isolated pads Au: multiple image pattern	Cu: Improvement in plating distribution. Best condition for all round performance: +ve pulse 10ms peak c.d.=35asf -ve pulse 0.5ms peak c.d.=100asf (i_{av}=5asf). Optimum conditions must be maintained and c.d. to be controlled within ±10% of recommended pulse conditions. Additives must be kept within the suppliers recommendations. Au: 70% improvement in uniformity compared to DC. Additives may have adverse effect such as arsenic.	6
N.R.K. Vilambi D.T. Chin	0.75M $CuSO_4$ 0.75M H_2SO_4 25°C Bubbling nitrogen Polished cathodes PR i_p= 0.05Acm^{-2}	Brass	Thicker deposit in the centre of cathode under pulse compared to DC and thickness increases with ϕ. Compact crystalline deposits of 1-2μm at c.d.= 0.1Acm^{-2} and crystalline deposits increased in size to 8-10μm at c.d.= 0.5Acm^{-2}.	22

Author (s) / Company	Metal/alloy / Bath constituent	Substrate / Usage	Remarks	Reference Number
	ϕ=1-100% t_{on}= 1-100ms i_{av}= 0.05-0.5Acm^{-2}		Brighter deposits– brightness increased by increasing peak c.d. and decreasing ϕ. At peak c.d.>2-4Acm^{-2}, (ϕ=5% and t_{on}=10ms), a secondary nucleation observed– deposit changed from crystalline to nodular-type growth. Polarisation studies– pulse current behaved as depolariser and reduced the average overpotential required for the plating process. Overpotential reduction increased by decreasing ϕ. Pulse current reduces the Tafel slope and shifts them to a more horizontal position, thus for a given current density $(Wa)_P<(Wa)_{DC}$, ∴ current distribution is less uniform. Localised deposit can be obtained with Pulse current.	
G. Bulman et al	Pd, Ag Pure Au Hard Au	Socket and pin, contacts reel-to-reel plating	Pulse/Jet used. Low c.d. with low agitation, smaller t_{on} and larger t_{off}. High c.d. with high agitation larger t_{on} and smaller t_{off}. Ag: produces dull silver deposit than DC. Pure Au: With pulse the contamination in solution has no effect on plating. Hard Au: With pulse physical properties eg. wear, hardness changes.	50
N.Ibl	Cu, Cd, Ag	Electronic components	Damping of the faradic current does not decrease the current efficiency for metal deposition during the t_{off}, (also ref. 1, chapter 4, section 4). Fine grain structure, low electrical resistance, high purity.	51
A. Ishihama T. Hayashi	Cr-Ni-Fe alloy 0.6M $CrCl_3$, 0.05M $NiCl_2$, 0.2M $FeCl_2$, 0.6–1.8M HCOONa, 0.2–0.7M NH_2CH_2COOH, 0.15M NH_4Br, 1M NH_4Cl, 0.6M H_3BO_3, 30°C, pH= 2.8 No agitation	Platinum	Higher hardness compared to DC Cr content in the alloy deposits increased with increase in i_p but Ni and Fe contents in deposit decreased. Decrease in duty cycle, increased the Fe content. Finer structure compared to DC. Higher current efficiency compared to DC.	52

Author (s) / Company	Metal/alloy / Bath constituent	Substrate / Usage	Remarks	Reference Number
D.S. Lashmore et al			Fine grain structure, low electrical resistance, high purity.	53
M.F. El-Shazley et al	Co-Ni alloy Fluoborate solution 1000Hz 10%, 30%, 80%ϕ	Bearings	Pulse/high speed deposition. Smooth appearance with increase in pulse frequency for a particular i_{av}. Also smooth appearance with decrease in f at a particular pulse frequency Current efficiency 90-100% for i_{av}= 25-15Ain^{-2}. Below 1Ain^{-2} independent of pulse frequency and ϕ, stress cracks occurred. Columnar texture band increases with increase in f.	54
J.Cl. Puippe N. Ibl	Cd, Cu, Ag, Au 0.75M $CdSO_4$, 1M H_2SO_4, 20°C 0.23M Cd, 170g/l NaCN 18g/l NaOH+ additives, 20°C $[Pd(NH_3)_4]Cl_2$, 1M NH_4Cl, 20°C 0.75M $CuSO_4$, 1M H_2SO_4, 20°C 15g/l $KAu(CN)_2$ 80g/l citric acid 0.1g/l base metal Co pH= 3.7 adjusted by KOH, 27°C	Electronic components	Cd: With increase in t_{off} the deposit becomes finer at a constant i_p and pulse t_{on}. With increase in t_{on} at a fixed t_{off} and i_p the deposit becomes coarser. Pd: Finer deposit with pulse than DC Cu: Finer deposit with increase in i_p. Coarser deposit with increase in t_{off} at a constant i_p and t_{on}. Au: Coarser deposit with increase in t_{off} at a constant i_p and t_{on}.	55
T.Pearson J.K. Dennis	Cu, Ni, Cr Cu: Acid copper sulphate, Ni: Watts bath, Cr: Sulphate bath Mach 1* Chromfast * * Proprietory		Cu: Organic additives such as polyeter and sulphides improve the throwing power. Grain size effect is less compared to the effects of organic additives. Ni: An increase in tensile strength with decreasing ϕ at f=100Hz and 5KHz is obtained. The effect is more linear at lower f than higher f. Tensile strength is less using PR. Cr: Reduction in tensile strength with increasing thickness observed under unipolar pulse compared to DC. Hardness value of 1000HV is possible at high f.	61

Author (s) Company	Metal/alloy Bath constituent	Substrate Usage	Remarks	Reference Number
M. Datta D. Landolt	0.25M Cu SO_4 1M H_2SO_4 (1)Mechanically Polished (2)Pre-deposition 0.05M $CuSO_4$ 1M H_2SO_4 1000 rev/min 2mAcm^{-2} 5 mins Polarization Studies Sweeping 6mV/sec	Cu rotating hemispheri-cal electrode	Use of simplified models gave an adequate description of transport rates. For most practical pulse-plating applications high pulsed c.d. can be applied due to thinner diffusion layerwith no powder formation at the limiting current. Fine grain structure.	62
M. Yokoi T. Hayashi	Cu		Epitaxial growth of Cu resulting from pulse becomes wider with increasing pulsed current density, therefore pulse c.d. magnitude is insignificant to the crystallisation. Pulse off-time is important. Double layer has a buffering effect against the pulsed current. Tafel relationship from i-η curve $\eta(mV)=226+92\log[i(A)]$.	66
T. Hayashi M. Yokoi	Cu 0.8M $CuSO_4$ 0.5M H_2SO_4 30°C	pt rotating ring-disc electrode	In Ar atmosphere: Current efficiency decreases with an increase in pulse current density. In atmosphere of saturated air: Current efficiency (C.E.) decreases further more which may be due to the oxidation of Cu deposit or cuprous ion by oxygen. Tafel slope line is about 60mV/decade. C.E. decreases with decrease in i_{av} and with longer t_{off} under the pulsed current electrolysis. Change in surface morphology in plane(111) from pyramidal growth to the layer forms. Off-time is important. Dissolution of Cu in $CuSO_4$ composed of the reaction $Cu^{2+}+e^- \rightarrow Cu^+$ and $Cu \rightarrow Cu^+ + e^-$	67
N. Ibl J.Cl. Puippe N. Angerer	Cd, Cu, Ag, Au Au-Co Cd: Acid Sulphate bath	Electronic components	"Review"; Fine grain structure, low electrical resistance, high purity. High pulse c.d. of 250Acm^{-2} can be applied due to thin diffusion layer,	68

Author (s) / Company	Metal/alloy / Bath constituent	Substrate / Usage	Remarks	Reference Number
	Au-Co: Acid bath from citric acid - cyanide with Co addition		no powder formation at the limiting current. Cu:surface coverage better than Cd. Cd: Increase in pulse c.d., decreases grain size. Increase in t_{off}, decreases grain size. Increase in pulse length, increases the crystal size. Au: Increase in t_{off}, decreases current efficiency and carbon content.	
M.D. Maksimovic et al	0.1M $CuSO_4$ 0.5M H_2SO_4 Pause:pulse = 1:1, 1:3, 1:10 $t_{on}=10^{-4}$ -10s $i_{av} = 0.6i_L$ $i_{av} = 0.9i_L$ (10-500Hz)	1.0mm dia. Cu wire	Increase in i_{av} and increase in pause-to-pulse ratio leads to decrease in the frequency range and decrease in the appearance of deposit can be achieved. Average overpotential dependent on the frequency of pulsation, ie. the optimum frequency range corresponds to the minimum value of average overpotential.	71
K.I. Popov et al	0.5M $CuSO_4$ 1M H_2SO_4 Pause:pulse 1:1, 1:9 $t_{on}=10^{-4}$-10s Limiting diffusion Current= 0.06Acm^{-2} deposition rate= 0.18hr/cm^2	Pt for η-i Cu wire for plating and deposit assessment	ditto (71) An increase in the current amplitude leads to a decrease in critical pulse duration.	72
	0.471M Ni SO_4 0.069M Ni Cl_2 0.485M H_3BO_3 t_{on}=10-2s Pause:pulse= 1:1, 4:1 deposition c.d.= 10 mAcm^{-2} coating thickness= 7.5μm porosity test using feroxyl test Adhesion test by cracking	Steel	Ni: For a given average deposit thickness, the same deposition time, the same average current density and the same initial surface roughness, a decrease in porosity with increasing pause-to-pulse ratio obtained.	
D. Towne	Au		Better macro-throwing power.	74

Author (s) Company	Metal/alloy Bath constituent	Substrate Usage	Remarks	Reference Number
W.F. Hall A.R. Cha dhuri	Cu Acid copper sulphate Pulsed pulse reverse (PPR) 1ms off intervals between cathodic and anodic pulses Cathodic ϕ= 30-90% Anodic ϕ= 20-75%	Satinless steel 4.5" x 7" PCBs with holes dia.= .01", .011", .012", .013", .0156" and .018" Board thick. =.062", .093" and .125"	Copper foil colours ranged from brown to orange. 27% and 30% elongation with and without heat treatment, respectively, obtained with matt coloured foils. Some conditions produced even higher % of elongation. Microhardness ranged from 68-84 $kgmm^{-2}$, for a relatively soft copper. In comparison, no voids in PPR deposit to 5-58% in DC. X-ray diffraction: DC foil has random planes but PPR show preference for the <111> and <220>. Finer grain under PR for the same i_{av} as DC, more ductile. Avoids deposit build-up at the hole mouth on small holes. S/H ratio is smaller under PPR compared to DC. Plating rate can be doubled.	76
J.R. White	0.31M $CuSO_4$ 1 M H_2SO_4 0.86M Cl^- 0.1% PEG $i_{p(c)}$= 17mA or 50mAcm^{-2} $i_{p(a)}$= 0, 4.25, 8.5 or 17.5mA $t_{on(c\&a)}$= 1, 10ms	Pt ring/disc	The CE for PR is lower than P and DC. Presence of Cl^- and PEG alone has little influence on the CE compared to DC.	77
A.J. Avila	Gold	Panel pins, battery caps	Saving gold by 20-50%. Better macro-throwing power.	78
A. Knowles	Au - Co Acid gold potassium Cyanide solution		Higher hardness than DC. Reduction in C, O, H, N than DC. Reduction in carbon content with increase in t_{off}. Less tensile strength, less bright. Fine grain structure, high purity. Crack-free Cr and Rhodium is possible.	79
A.J. Avila, M.J. Brown	Hard Au	Au Integrated Circuits	Fine grain, high purity, lower volume resistivity. Reduction in additives eg. brighteners, levellers and anti-pitting agents.	80
T. Hayashi et al	Ag Ag ammonia		ditto (80)	81

Author (s) / Company	Metal/alloy / Bath constituent	Substrate / Usage	Remarks	Reference Number
	and cyanide bath			
L. Missel et al	Au Sulphite complex Au Citrate-phosphate & Au aurocyanide	Round ceramic or glass wafer metallized	Dense, less porous deposit.	82
P.F. Mentone		Semi-conductors	ditto (82)	83
J. Cl. Puippe et al	Au		Reduction in Au plating while retaining the physical and electrical properties. Reduction in carbon content with increase in t_{off}. Lower current efficiency.	84
M. Branik et al	Au-Co Au 12g/l Co 100ppm i_{av}= 1Adm^{-2} t_{on}= 8.5-7.5ms t_{off}=1.70ms		Co content in Au deposit increases with increase in t_{off}. Reduction in carbon and potassium content with increase in t_{off}. Fine grain structure, high purity, low electrical resistance.	85
C.J. Raub et al	Au - Co		Increase in Co percentage at higher c.d.	86
F. Leaman et al	Au-Co	Ni	Increase in Co content at higher c.d. Reduction in porosity of Au-Co layer by half.	87
G. Perger et al	Au, Ag, Cu, Co		"Review"; Improvement in macro-throwing power for complex and large area samples.	88
E. Robert			Better at higher c.d. Improvement in wear resistance.	89
J. Ehrhardt et al	Ag 8, 16, 24, 32g/l i_{av}= 2, 4, 10, 15, 20, 25Adm^{-2} 50°C, 70°C, 80°C f = 0, 250, 1000, 2250, 4000Hz	Connectors	ditto (89)	90

Author (s) / Company	Metal/alloy / Bath constituent	Substrate / Usage	Remarks	Reference Number
B. Inglot et al	Au–Co Au–Ni		ditto (89)	91
C.J. Raub et al	Au		Fine grain structure, low electrical resistance, high purity.	92
W.S. Miu Y.S. Fung	Rhodium Sulphate solution 1-3g/l Rh 50-150ml/l H_2SO_4	Flat brass or 3mm dia. rods	Crack-free deposit. Best condition with t_{on}/t_{off} ratio of 0.1ms/0.9ms. Reduction in porosity and contact resistance with pulse.	93
N.M. Osero	Ni, Au, Cu, Pb Sn-Pb, Rh, Ag		"Review" on different pulse shapes for electronic, electroforming, electroetching and electrocleaning industry. Fine grain structure, low electrical resistance, high purity.	94
D.L. Rehrig			Less porous than DC.	95
J. Lendray C.J. Raub	Hard Au		Increase in tensile strength by 25%. Decrease in elongation by two fold Improvement in ductility.	96
A.R. Despic K.I. Popov	Cu, Zn Sulphate bath		At high frequencies, surface smoothness maintained. Smoother & denser deposits than DC.	97
C.J. Stimetz	Hard Au Proprietary Au +Co hardening agent 46°C, pH=3.5 0.32-1.3 Adm^{-2} ϕ=1, 33, 50% Au sulphate electrolyte + Arsenite brightener Soft $Au(CN)_2^-$ with phosphate or citrate buffer Ni bath	Brass Electrical contact	With decrease in ϕ, cobalt weight increased at a fixed c.d. High current or high voltage may cause contamination by degradation. High voltage in pulse may oxidise the arsenite. Hardened Au-Co: low ϕ, electrodeposits were dull. Soft Au: microhardness grain structure and surface morphology changed very little compared to DC. Ni: No significant differences between pulse and DC for solutions of sulphamate chloride. Ni Watts: 35% increase in yield strength. 25% increase in microhardness. Preferred orientation are affected. Fine grain size ranges from 0.4-2.5µm and surface morphology is less pyramidal.	98

Author (s) / Company	Metal/alloy / Bath constituent	Substrate / Usage	Remarks	Reference Number
C.C. Wan et al	Cu		Decrease in current efficiency.	99
V.V. Romanov	Zn, Cu Sulphate bath Zn Alkaline bath		Sulphate bath: Dendritic formation is less. Deposits are smoother and denser. Alkaline Zn: Similar dendritic appearance as DC at low f=500Hz. Increase pause-to-pulse ratio leads to a decrease in surface roughness of metal deposits.	100
M. Viswanathan et al	Au-Ni Alkaline cyanide		Fine grained deposit.	101
W. Sullivan	Co		Fine grained deposit, higher ductility.	102
K.I. Popov et al	Cu	Steel	Decreases porosity. In powder formation, the particle size increase with increase frequency and off-time at constant pulse length.	103
K.I. Popov et al			ditto (103)	104
M.J. Leland	Cr		Increase in hardness in upper layers of deposit.	105
K. Hosokawa Y. Tsuru	Ag Cyanide, Iodide Thiocyanate Ethylenediamine Ammonia, Thiourea Perchlorate Nitrate bath		Better deposit for thiocyanate, ethylenediamine and ammonia baths. Similar deposit for the rest of the baths. Ammonia: Increase granular size with increase t_{off}. i_p=5Acm^{-2} Fine deposit with t_{on}=10μs increase in pulse length at constant i_p and ϕ. Fine grain at higher overpotential. Thiocyanate: Increase granular size with increase t_{off}. i_p=5Acm^{-2} Off-time very important. ϕ =1/1000 Ethylenediamine: Surface deposit changes very little with increase in pulse period. Large grain size with increase in pulse length t_{off} was not so effective. Cyanide: Larger granular size of deposit with increase in toff at	106

Author (s) / Company	Metal/alloy / Bath constituent	Substrate / Usage	Remarks	Reference Number
			constant i_p and ϕ. Overpotential was constant with pulse period of 5-50ms. Off-time very important. Morphology similar to DC.	
B. Sutter et al	Ni Sulphate, Chloride & Sulphamate bath	Cu Alloy Electrical Connectors	Ni: At 100Hz, the use of pulse current leads to a sensible decrease in porosity can modify deposit hardness by adjusting f and i_p, grain size is smaller compared to DC. Au: During off-time, potential falls to initial value. Deposit is less porous than DC. Pulse improve some properties with no increase in deposition rate.	107
Gemdata Group & Techno Instrument Ltd	Au, Ag, Cu Ag: Silver Cyanide 6 - 70g/l Na cyanide 140-180g/l Na carbonate 1g/l Na Hydroxide 1-2g/l c.d.= 2-10Adm^{-2} Cathode & anode cycle time of 50 & 5ms Cu: Cyanide Cu Alkaline Cu Acid Cu High concentration Cu $CuSO_4$ 200-240g/l 98% H_2SO_4 80-90g/l Low concentration Cu $CuSO_4$ 70-80g/l 98% H_2SO_4 180-200g/l		Au: At elevated frequency (ie. low on/off time of pulse and forward and reverse cycles), produces reduction in porosity, improvement in hardness and distribution, utilisation of densities of current between 1-4Adm^{-2} and they are dependent on distance of anode-cathode, circulation of solution, height of form of the bath, solution and its 'complexants' which reduces the efficiency. Ag: Advantagous to work without additives/brilliants or very weak concentrations. Hardness 140-280HV, good deposit, recommended f=10KHz. Cu: Fine grain and low internal stress for alkaline Cu compared to cyanide and acid Cu. Alkaline Cu: best result at high f. Acid Cu: low f compared to alkaline Cu. Better penetration with low Cu concentrations, not possible to increase c.d. without the risk of burning. Utilization of pulse current with concentration solution permits. improvement of penetration & also to work at high c.d.	108

Author (s) / Company	Metal/alloy / Bath constituent	Substrate / Usage	Remarks	Reference Number
K.I. Popov M.D. Maksimovic et al	Cu $CuSO_4$ 200g/l 98% H_2SO_4 50g/l i_{av}= 0.9i_L Pause:Pulse=2:1 f = 50Hz Plating time=1-3hrs	Ni plated Cu wire	Smoother deposit at same i_{av} and deposition time than DC. From mathematical formulations it is concluded that an increase in Pause-to-pulse ratio, for the same average current density leads to deposition of smoother deposit.	109
W. Kim R. Weil	Ni		Yield and tensile strength of deposit increased by factor of 3 by periodic imposition of anodic pulses which leads to better tribological properties.	110
R.J. Kendrick	Ni		Presence of Cl^- prevents passivation during the anodic portion of the cycle in periodic reversal plating; such passivation of Ni surface leads to poor adhesion of Ni beneath the surface layer & hence improvement in tribological property may be achieved.	111
R.D. Grim D. Landolt	$Pd(NH_3)_3Cl_3$ 16g/l Pd Ethylene-diamine complexant 2mol/mol	Pd rotating Hemispherical electrode	With pulse reverse current crack-free deposit obtained. Current efficiency of Pd decreased with increasing anodic to cathodic charge ratio.	112
Nenov et al	Pd Ethylenediamine based electrolyte		Cracking could be suppressed.	113
A.R. Despic et al	Cu		The capacitance current of periodic charging and discharging of the layer at frequencies which the effect of the double layer cannot be neglected produces a smearing of faradic current wave, hence, as f increases, the faradic wave flattens and approaches DC.	114
L.G. Holmbom B.E. Jacobson	Au 10g/l Citric acid 115g/l pH=4.6 Electrolyte flow 2 cm/sec ϕ = 20% f = 0-2KHz Anode = Pt/Nb	PCB, Cu anodic degreasing in metasilicate base alkaline solution electropolish at 350Acm^{-2},	At 40°C, smooth, bright gold deposit without brightener and fine grain structure was obtained. Dull, rough, coarse-grained deposits at room temperature. The current efficiency increased with temperature and frequency. At f≥200Hz, the efficiency was equivalent compared to DC.	115

Author (s) / Company	Metal/alloy / Bath constituent	Substrate / Usage	Remarks	Reference Number
		1 min. in Orthophos -phoric, Propylene glycol mixture an 30sec in 10% H_2SO_4	A flake-like morphology is & frequency when the Au concentraton in the vicinity of cathode is low and the Au adatoms on the surface is high enough to allow long range diffusion.	
J. Locket	Au reel-reel selective gold plating	Semi-conductors	With larger ϕ, more carbon (or polymer) found in the deposit At t_{on}=0.1ms & t_{off}=0.3ms, an slightly better distribution, a more consistent and reproducible gold structure and slightly lower average voltage is obtained than t_{on}=1ms and t_{off}=3ms; ∴ can be said, with short t_{on}, the cathode layer is less depleted of Au ions than longer t_{on}, ∴ more uniform resulting deposit. Gold flash is important using silicone -gold eutectic and monitored closely. Wetting is important.	116
T. Pearson J.K. Dennis	Cr 250g/l Chromic acid 2.5g/l H_2SO_4 (hard Cr) 54°C Mach 1* Chromfast C* 40Adm^{-2} 100 & 2500Hz ϕ= 50, 70% * Proprietory		With ϕ= 50%, possible to produce crack-free deposits from a sulphate or silicofluoborate catalysed solution with similar deposit hardness obtained under direct current. At high frequencies 0.2-3KHz the hardest deposit was obtained. Also, with proprietary solution, cracked deposits obtained at f down to below 1000Hz, and cracked-free deposits produced at f≤500Hz with hardness value of <600HV. In general, hardness increased with f; pulse hardness lower than DC. Deposit appearance varied from dull to bright with no systematic relation to f, except, with Mach 1 where the deposits were bright at f≥1KHz. Reduction in C.E. at f=16-500Hz using sulphate and fluoborate solutions. At f=16-500Hz, no cracking was observed using proprietory, fluoride-free bath –soft deposit. At high f, crack were obseved.	117

Author (s) Company	Metal/alloy Bath constituent	Substrate Usage	Remarks	Reference Number
M. Cherkaoui E. Chassaing K.V. Quang	Ni-Mo alloy 0.2M $NiSO_4$ 0.015M NaMo 0.025M Tri -sodium citrate pH= 9.5, 40°C 25μm Ni anode Corrosion test in 3wt% NaCl at pH=2	Armco Steel sheet ($4cm^2$)	Molybdenum content influenced by t_{on} and t_{off} and also current efficiency is reduced. The morphology becomes disordered with nodules of irregular shapes and also an enhanced nucleation is observed with large t_{off}. X-ray diffraction study: with increasing t_{off}, the intensity of the x-ray lines decreases, d-spacing increases markedly. Deposit hardness is 800-900 Vickers for ϕ>4%. Low corrosion resistance due to disturbed morphology, ie. large surface area and increased porosity.	118
K.I. Popov D.N. Keca et al	Cu 0.1M $CuSO_4$ 0.5M H_2SO_4 20°C Cu anode Cu reference electrodes Rectangular, sinusoidal and triangular pulsing	Pt electrode	Experimental and mathematical and digital simulation are in agreement with each other – no differences in polarisation curves is observed for different frequencies, except at low i_{av} for rectangular pulse and the same value for average overpotential going from rectangular to triangular pulsating overpotential. Effective limiting diffusion c.d. is at 200mV. Increasing f leads to smaller values of i_L. C.E. is near 100% in all experiments. Smoother Cu deposit possible using rectangular pulsing at 1000Hz and η_{av}=116mV than with constant overpotential for the same c.d. It is possible to lower the energy consumption for electrodeposition at the same c.d. and hence the same or better quality of metal deposits could be obtained – ideal for metal refining and plating.	119
K.I. Popov B.J. Lazarevic M. Kostic	0.005M $CuSO_4$ with 0.05M Na_2SO_4 as supporting electrolyte 25°C Cu anode	Nickel Sheet	Experimental and theoretical predicted results overlap up to third pulse – descrpencies due to simplifications on the mathematical model of the system. Possible to electrodeposit thin layers with currents higher than the limiting diffusion current without process becoming diffusion controlled. The	120

Author (s) / Company	Metal/alloy / Bath constituent	Substrate / Usage	Remarks	Reference Number
			times for electrolysis exceeds the transition times for corresponding effective DC current densities.	
K.I. Popov M.D. Maksimovic S.S. Djokic	Cd, Cu Cd: 0.1M $CdSO_4$ 0.5M H_2SO_4 Cu: 0.1M $CuSO_4$ 0.5M H_2SO_4 and 0.5M $CuSO_4$ 0.5M H_2SO_4 21°C, f= 50Hz I_{av}= $0.9i_L$, $0.6i_L$ and $0.45i_L$ Cylindrical anode	Cu wire Pt	Smoother deposits under the same deposition conditions and thickness to DC and also at higher c.d. In electrolytes with good throwing power, smooth deposits can be obtained on smooth substrate at i_{av}< limiting diffusion current density, ie. the pulse current deposition at i_{av}= $0.9i_L$, pause-to pulse=1, f=50Hz and plating time of 165mins. smoother deposit is produced that i_{DC}= $0.45i_L$ and plating time of 330mins.	121
K.I Popov M.D. Maksimovic V.M. Nakic M.D. Spasojevic	Cu 0.075M $CuSO_4$ 0.5M H_2SO_4 30°C, f=10Hz i_p= 2.5mAcm^{-2} i_{av}= 0.5mAcm^{-2} pause-to-pulse=4 Cu anode and reference electrode	Pt wire	Results show that the Tafel slope and i_o for: a) steady state potenstiatatic is 120mV and 1.6mAcm^{-2}, b) galvanostatic single pulses is 120mV and 1.4mAcm^{-2} and c) the mathematical model is 120mV and 4.5mAcm^{-2} in the same solution, indicating the validity of the mathematical formulation.	122
K.I. Popov M.D. Maksimovic S.K. Zecevic M.R. Stojic	Cu 0.2M $CuSO_4$ 0.5M H_2SO_4 21°C Cu anode and reference electrode	Cu wire	The deposits obtained by square wave with pause-to pulse of 1 and 5000Hz are similar to the triangular wave – due to the double layer capacitace effect. The dendritic growth in square wave is slower than triangular wave due to the faradic current resulting from the shape of the input overpotential. Increasing the f leads to a decrease in the average deposition current density especially in triangular wave and sinusoidal wave.	123
K.I. Popov M.G. Pavalovic et al	Cu 0.1M $CuSO_4$ 0.5M H_2SO_4 21°C 20mAhcm^{-2}	Copper sheet	Deposits obtained in pulsating overpotential electrodeposition are different in structure and less course than deposits obtained in the constant overpotential regimes.	124

Author (s) / Company	Metal/alloy / Bath constituent	Substrate / Usage	Remarks	Reference Number
	Cu anode and reference electrode Deposition at overpotential of 70, 90, 140 and 210mV. t_{on}= 10ms pause-to-pulse of 1 and 3			
J. Mann	Cu High and low concentration of copper sulphate low and high concentration of sulphuric acid, respectively f= 10Hz-10KHz PR		PR: very high pulse c.d. can be produced without adversely affecting the deposition quality. The effective c.d. can be increased by about 40% but current efficiency drops. Improvement in throwing power. Deposition quality depends on the pulse parameter. Possible to improve one characteristic at the expense of other, such as throwing power, surface quality and plating speed.	125
O. Chene D. Landolt	Cu 0.1M $CuSO_4$ 1M H_2SO_4 25°C Argon bubbling c.d.=3.2mAcm^{-2} 15h Cathode rotation speed= 1000rpm Cu plated anode	Cu plated Rotating hemispherical electrode 10mm dia. (1.75cm^2)	Compact granular deposits formed for pulse current densities smaller than pulse limiting c.d., $i_p>i_{pl}$ dendritic deposit results. Shapes and sizes of dendrites and their microstructure depend on the pulse parameters and the total amount of metal deposited. C.E. for a given set of pulse parameters is affected by the uniformity of the current distribution and the apparent surface area, which may vary with the deposit thickness.	126
G.W. Jernstedt	Cu PR		"Review"; PR works better with some electrolytes than other. It may be possible to expect: a) an increase in plating rate; b) an increase in the density of the metal deposited; c) an improvement in the brightness of the surface; d) greater smoothness than the base metal; e) to obtain heavier deposits; f) a reduction in porosity; g) a better metal distribution.	127

Author (s) Company	Metal/alloy Bath constituent	Substrate Usage	Remarks	Reference Number
J.R. White R.T. Galasco	Cu 76.6g/l $CuSO_4.5H_2O$ 200g/l H_2SO_4 50ppm Cl^- 1% additive Plating thick. = 35.6μm Phosphorised Cu anode Anode-Cathode distance= 12cm 1h, P and PR	Lined pattern Copper foil 7.6 x7.6cm	'Surface height' uniformity on circuit lines degrades as i_{av} increased. Enhanced metallurgical properties. With no additive electrolyte: distributed columnar structure, increase in ductility, improved microlevelling is obtained. Electrolytes with additives did not function under pulse as expected under DC.	128
G. Holmbom B.E. Jacobson	Cu 'High throw' Cu 25g/l Copper 120ml/l H_2SO_4 60mg/l Cl^- 15g/l Brightener* 50μmh^{-1} f=1, 10, 100, 1000, 10000Hz PR: $i_{p(c)}$:$i_{p(a)}$= 1:1 or 1:9 $t_{on(a)}$:$t_{on(c)}$= 1:9 or 1:1 respecectively. P: $i_{p(c)}$= 106mAcm^{-2} ϕ= 35% *Enplate CU-944	PCB 0.3mm dia. holes Board thick. 1.5mm	P: thicknesss distribution ratio at f= 1Hz-10KHz increased from 28-68%to that of 60% under DC. Off-time improves metal distribution. PR: Through-hole capability is as good as that of DC and high frequency of P plating. Deposits are dull due to desorption of brighteners during the anodic pulses. Cl^- consumption takes place at the cathode during the anodic part of the plating cycle. Cl^- gas evolution is possible resulting from high overpotential in which oxidisation of Cl^- occurs.	129
V.A. Lamb	Cu 250g/l $CuSO_4.5H_2O$ 75g/l H_2SO_4 25°C Agitation flow = 3mmin^{-1}	Cu 1 x 1cm	For pulse time of 0.1-50μs and c.d.≤10Acm^{-2}, the microstructure and hardness are similar to DC. Decrease in C.E. with decrease in c.d. and t_{on}.	130

CHAPTER 5

5.0 EXPERIMENTAL WORK

The experimental work was carried out using different copper electrolytes. The research work can briefly be described to consist of three parts:

- Standardisation and methodology - this is important in terms of reproducibility of data, therefore various studies such as equipment types and their behaviour under pulse electrodeposition were examined. Other aspects such as pretreatment(s), effect of chloride ions, conductivity, agitation, etc were also studied.
- Pulse plating - this involved studying square wave unipolar pulse and bipolar pulse reverse electroplating for printed circuit board production. The aim was to develop an acid copper electrolyte, preferably with additives, using a pulse unit and certain pulse conditions, for printed circuit boards with board thickness/hole diameter(aspect ratio) of ≤ 8:1 and hole diameters as low as 0.3mm. The aim is to obtain a surface/hole coating thickness ratio of 1:1.
- Morphological, property and surface topographical studies of copper deposits under pulse conditions with a comparison to DC. The morphological studies describe the structural changes, ie. grain refinement. Property study involves tensile strength, hardness and elongation measurements. The surface topography relates to surface coverage and surface appearances of the deposits.

5.1 Equipment

Pulse Plating Unit - J.C.T. Model PDM 2015 (15A, 40V)

The electronic facilities within allow programming of up to 9 channels. The programmes consist of four parameters:

Frequency	range 16Hz - 4999Hz
Duty cycle	range 1% - 99%
Direction	forward and reverse
Time duration	0.0001sec - 99.9999sec

Potentiostat - Model E-series (18A, 12V)

The 'Thompson' potentiostat was used as both a potentiostat or galvanostat.

Power Supplies - Farnell Model L12-10C (10A, 12V), Farnell H30/100 (30V, 100A) and Farnell AP30-80 (30V, 80A).

The power supplies can be set to work as both constant voltage or constant current sources.

Oscilloscope - Advanced Bryan Model DS-1526

The digital oscilloscope was used to study the pulse parameters patterns. Also a differential amplifier, Model DA-1000V, was used for floating system.

Resistors -1Ω

The resistors used were a 1ΩRS (50W) and a high heat dissipating home-made resistor. This was made out of AISI 304 stainless steel machined out to length equivalent to 1Ω.

Chart Recorder

A Servoscribe Y-t recorder was used for polarization studies and pulse pattern studies.

Digital Multimeters - Thandar

The digital multimeters were used as voltmeters or ammeters where necessary.

Conductivity Meter and Electrode - Phillips Models PW9501 and PW9517 respectively.

The glass electrode had a measuring range of 1-1000 $M\Omega^{-1}\ cm^{-1}$ ($MS\ cm^{-1}$)

Reciprocating Cathode Agitator - RS Model 336-450

The reciprocating cathode agitator had a forward and reverse movement of 20rev./min. The reciprocation distance was 60cm/minute.

Air Pump Agitator - Wisper Model W1000

The air pump agitator had a capability of pumping air at a rate of up to 8 litres/min. and up to a maximum tank depth of 1.70 metres.

Magnetic Stirrer - Chem Lab SS3H (240V, 50Hz)

The stirrer was used as both a heater and magnetic stirrer.

Plating Tanks

The plating tanks used were either a 2 litre beaker having 14cm diameter and 19cm height or a 20 litre propylene tank having a 28.5cm width, 23.8cm length and 35cm height. For polarisation studies, a 2 litre beaker was used, but for all electroplating a 20 litre propylene tank was used.

5.2 Conductivity Measurements

Conductivity was measured using a Phillips glass electrode. The conductivity meter was calibrated against water as a reference. Then the conductivity of the electrolytes were measured, with various concentrations of sulphuric acid and different molarities of cupric sulphate. The conductivity is known to be important in affecting the secondary current distribution, and hence the throwing power of the electrolyte. In general, the conductivity increased with increase in acid concentration.

Furthermore, conductivity of all the electrolytes, that is, solutions used throughout this research work, were measured in the same manner for throwing power studies.

5.3 Pretreatment Assessments

In order to be able to reproduce a result, it is necessary that the surface preparation or surface cleanliness to be taken into account. It is believed that any 'irregularities' such as dirt, oxide, etc can have a detrimental effect on surface appearance and also on the life of a material in an environment. For this reason, the effect of different pretreatment solutions and subsequently electroplating were examined by polarisation studies (E-i curves) and also Hull cell tests. The pretreatment solutions consists of the following constituents:

Pretreatment 1

Nitric acid (SG 1.42)	50%V/V	1min.
Water rinse		1min.

Pretreatment 2

Nitric acid (SG 1.42)	50%V/V	1min.
Water rinse		1min.
98% H_2SO_4 (SG 1.84)		
and 30% H_2O_2 dip.	10%V/V	1min.

Pretreatment 3

Nitric acid (SG 1.42)	50%V/V	1min.	
Water rinse		1min.	
98% H_2SO_4 (SG 1.84) etch	10%V/V	2secs.	
Electrodeposited Cu*, no agitations		2mins.	$0.6Adm^{-2}$

* 0.3M $CuSO_4$, 2.25M H_2SO_4, 50ppm Cl^-

Pretreatment 4

Alkaline soak cleaning*		50g/l	80°C	2mins.
Electrolytic alkaline cleaning*	50g/l	80°C	2mins.	$3Adm^{-2}$
Water rinse			1min.	

* Lea Ronal proprietary alkaline cleaner - Ronaclean GP-300

Pretreatment 5

Alkaline soak cleaning*		50g/l	80°C	2mins.
Electrolytic alkaline cleaning*	50g/l	80°C	2mins.	$3Adm^{-2}$
Water rinse			1min.	
Water rinse			1min.	
98% H_2SO_4+ 30% H_2O_2 etch	10%V/V		1min.	

* Lea Ronal proprietary alkaline cleaner - Ronaclean GP-300

Pretreatment 6

Diamond paste (Buehler)	1μm		
Methanol cleaning (Ultrasonically)		15mins.	
98% H_2SO_4 (SG 1.84) etch	10%V/V	1min.	

Pretreatment 7

Diamond paste (Buehler)	1μm		
Methanol cleaning (Ultrasonically)		15mins.	
Electropolish in			
Orthophosphoric acid (SG 1.69)	70%V/V	2mins.	$7Adm^{-2}$
Water rinse		2mins.	
98% H_2SO_4 (SG 1.84) etch	10%V/V	1min.	

Pretreatment 8

Acetone clean (wipe)			
Electropolish in			
Orthophosphoric acid (SG 1.69)	70%V/V	2mins.	$7Adm^{-2}$
98% H_2SO_4 (SG 1.84) etch	10%V/V	1min.	

The examination of the effect of pretreatments was carried out by polarisation

studies and Hull cell methods using electrolyte I (0.3M $CuSO_4$, 2.25M H_2SO_4, 50ppm Cl^-).

For polarisation studies the cathodes were copper (Goodfellow, 99.9%) with an exposed surface area of $30cm^2$ having a width of 1.5cm and length of 10cm, the plating was carried out on both sides.

The Hull cell tests were carried out on copper sheets (Goodfellow, 99.9%) with a surface area of $75cm^2$ having a width x length of 7.5cm x 10cm, respectively. The two anodes used were phosphorus deoxidised copper with an area of $180cm^2$ each. Note: for both polarisation and Hull cell studies no agitation was used.

The results indicated that pretreatments 4 and 5 are the best. Therefore it was decided that pretreatment 5 was to be used throughout the study, unless otherwise stated.

The pretreatment of stainless steel was also studied for producing foils for tensile strength and elongation measurements. This can be carried out in many ways, such as electropolishing, grinding and polishing, etc. The grinding and polishing was favoured in this research programme. The stainless steel sheets were firstly ground to 1200grit size (Buehlers grinding strips) and then polished to a mirror finish using 6μm and 3μm diamond paste. It was found that polishing down to 1μm, causes a reduction in adherence of the deposits after 5-10 hours of plating. It is to be noted that the grinding must be carried out by hand otherwise the scratches resulting from grinding by machine could be deep and hence affect the tensile strength and elongation values. Also for morphological studies, this could cause an uneven deposit making the structural studies meaningless.

5.4 Hull Cell Measurements

The Hull cell studies were carried out in order to study the surface appearance at different current densities for different electrolytes; 0.3M $CuSO_4$ and 2.25M H_2SO_4 remained constant for all tests. The electrolyte constituents are detailed below:

I- 0.3M $CuSO_4$, 2.25M 98%H_2SO_4, 50ppm Cl^-; R.T.

II- 0.3M $CuSO_4$, 2.25M 98%H_2SO_4, 50ppm Cl^-, 1g/l C140; R.T.

III- 0.3M $CuSO_4$, 2.25M 98%H_2SO_4, 50ppm Cl^-, 1g/l C140, 6.25mg/l N1; R.T.

IV- 0.3M $CuSO_4$, 2.25M 98%H_2SO_4, 50ppm Cl^-, 1g/l C140, 0.625mg/l DS4; R.T.

V- 0.3M $CuSO_4$, 2.25M 98%H_2SO_4, 50ppm Cl^-, 1g/l C140, 0.625mg/l DS4, 6.25mg/l N1; R.T.

VI- 0.3M $CuSO_4$, 2.25M 98%H_2SO_4, 50ppm Cl^-, 0.1g/l C140; R.T.

VII- 0.3M $CuSO_4$, 2.25M 98%H_2SO_4, 50ppm Cl^-, 10g/l C140; R.T.

VIII- 0.3M $CuSO_4$, 2.25M 98%H_2SO_4, 0ppm Cl^-; R.T.

IX- 0.3M $CuSO_4$, 2.25M 98%H_2SO_4, 0ppm Cl^-, 1g/l C140; R.T.

The Hull cell tests were carried out with and without agitation, the former as air sparging. The cathodes were copper and brass panels for without and with agitations, respectively. The cathode surface area was 75cm^2 for both types of panels using pretreatment 5 for sample preparation. The anode was a pure copper sheet. For Hull cell studies, the procedure used is similar to that of Cannings handbook[131].

5.5 Cathode Size

The cathode sizes used in this research work are described under four categories:

- For agitation studies, the cathodes used were AISI 304 stainless steel with an exposed surface area of 300cm^2 having a width and length of 5cm and 30cm, respectively. The plating was carried out on both sides of the cathodes.
- For pulse plating behaviour studies, the cathodes used were brass sheet (Goodfellow, Cu/Zn of 63/37 composition, half hard tempered, 0.25mm thick) with an exposed surface area of 12.5cm^2 having a width and length of 2.5cm. The plating was carried out on both sides of the cathodes. Each of the brass electrodes were suspended in the bath with a copper wire. The copper wire was fed through a glass tubing, Figure 46. The contacts were sealed using a red lacquer in order to obtain the correct surface area.
- For polarisation studies, the cathodes used were copper sheets (Goodfellow, 99.9%, half hard tempered, 0.25mm thick) with an exposed surface area of 30cm^2 having a width of 1.5cm and length of 10cm. The plating was carried out on both sides of the cathodes.
- For morphological and property studies such as hardness, roughness and also cathode efficiency under DC and unipolar pulse, the cathodes used were copper sheets (Goodfellow, 99.9%, half hard tempered, 0.25mm thick) with an exposed surface area of 70cm^2 having a width of 3.5cm and length of 10cm. The plating was carried out on both sides of the cathodes. But for the study of tensile strength and elongation plated under DC, unipolar pulse and bipolar pulse reverse conditions, the plating were carried out on AISI 304 stainless steel with an exposed surface area of 150cm^2 having a width of 5cm and length of 15cm. The plating was carried out on both sides of the cathodes. The

preparation of stainless steel has been described in section 5.3. The use of stainless steel was preferred because of poor deposit adhesion allowing production of foils.

The dimensions described above were used for the tests mentioned unless otherwise stated.

5.6 Anode Size

The anodes used throughout this research work were phosphorised copper having width x length and exposed height of 5cm x 1cm x 15cm, respectively. The grade of anodes(Cu-DHP according to BS 6017: 1981) were phosphorus deoxidised copper - high residual phosphorus. This type of anode is used commonly in the electroplating industry and it is known to reduce the deposit roughness of the coatings. For all polarisation studies and plating experiments two anodes were used unless otherwise stated.

5.7 Electrolytes

In this research work, a whole combination of electrolytes with and without additives were used in order to elucidate the effect(s) of pulsing. Also, studies on concentrations of additives and temperatures were carried out. The constituents of electrolytes and temperature used are listed below:

I- 0.3M $CuSO_4$, 2.25M 98%H_2SO_4, 50ppm Cl^-; R.T.

II- 0.3M $CuSO_4$, 2.25M 98%H_2SO_4, 50ppm Cl^-, 1g/l C140; R.T.

III- 0.3M $CuSO_4$, 2.25M 98%H_2SO_4, 50ppm Cl^-, 1g/l C140, 6.25mg/l N1; R.T.

IV- 0.3M CuSO4, 2.25M 98%H_2SO_4, 50ppm Cl^-, 1g/l C140, 0.625mg/l DS4; R.T.

V- 0.3M $CuSO_4$, 2.25M 98%H_2SO_4, 50ppm Cl^-, 1g/l C140, 0.625mg/l DS4, 6.25mg/l N1; R.T.

VI- 0.3M $CuSO_4$, 2.25M 98%H_2SO_4, 50ppm Cl^-, 0.1g/l C140; R.T.

VII- 0.3M $CuSO_4$, 2.25M 98%H_2SO_4, 50ppm Cl^-, 10g/l C140; R.T.

VIII- 0.3M $CuSO_4$, 2.25M 98%H_2SO_4, 0ppm Cl^-; R.T.

IX- 0.3M $CuSO_4$, 2.25M 98%H_2SO_4, 0ppm Cl^-, 1g/l C140; R.T.

X- 0.3M $CuSO_4$, 2.25M 98%H_2SO_4, 50ppm Cl^-, 1g/l C140, 0.625mg/l DS4, 6.25mg/l N1; 35°C

XI- 0.14M $CuSO_4$, 3.375M 98%H_2SO_4, 50ppm Cl^-, 1g/l C140, 0.625mg/l DS4, 6.25mg/l N1; R.T.

XII- 0.14M $CuSO_4$, 3.375M 98%H_2SO_4, 50ppm Cl^-, 1g/l C140, 0.625mg/l DS4, 6.25mg/l N1; 35°C

XIII- 0.3M $CuSO_4$, 2.25M 98%H_2SO_4, 50ppm Cl^-, 1g/l C140, 0.625mg/l DS4, 6.25mg/l N1; 10°C

For studies at low temperature (10°C), liquid nitrogen was used to cool the electrolytes and for higher temperature(35°C), a water bath was used to heat up the electrolytes.

Electrolyte I was used for agitation and pulse electronic behaviour studies.

For polarisation or throwing power studies under DC and uniploar pulse all electrolytes were examined. However, for polarisation studies under bipolar pulse reverse the electrolytes used were limited to I and V.

For morphological and also property studies only electrolytes I, III and V were used.

The proprietary additives (Lea Ronal proprietary) used in this research are described as C140, DS4 and N1. Basically, they can be described in Appendix 2 in detail.

5.8 Use of Agitation

The use of agitation can have a beneficial effect in electroplating. For example, in terms of morphology, it can cause grain refinement which can increase the hardness and tensile strength. In the printed circuit board industries agitation is used to transport metal ions into the holes of the PCBs in order to plate uniformly. Therefore, the importance of agitation can be significant in electroplating.

However, as an exercise various agitation methods were examined using different electrolytes and temperatures. The electrolyte solutions were:

Solution A: 0.3M $CuSO_4$, 2.25M 98%H_2SO_4, 50ppm Cl^-

Solution B: 0.015M $CuSO_4$, 0.5M 98%H_2SO_4

and the temperatures used were 21°C and 50°C.

The agitation methods were reciprocating cathode agitation, slight air agitation (pumping rate of 3 litres/min.), extensive air agitation (pumping rate of 8 litres/min.), magnetic stirring agitation at various rotation speeds of 5-8. These rotation speeds are related to the magnetic stirrer settings model specified in section 5.1. Furthermore, reciprocating agitation was used in conjunction with all other agitation methods. For comparison purposes, polarisation studies were carried out. The polarisation curves (E-i curves) were obtained using copper sheets having an exposed area of $3cm^2$. The tests were carried out in a 2 litre beaker having a diameter and height of 14cm and 19cm, respectively. The reference electrode used for polarisation studies was mercury/mercury sulphate. From the polarisation curves the limiting current density values were obtained at an overpotential of -0.40V and -0.37V for solutions A and B, respectively. Also, the limiting current densities were compared to those of DC. The enhancement factor(E.F.), was calculated such that:

$$E.F. = \frac{\text{Limiting current density of agitated mode}}{\text{Limiting current density of still mode}} = \frac{i_{L(A)}}{i_{L(0)}}$$

As for printed circuit boards, the use of magnetic agitation is not viable since it is believed that it does not have a significant effect, compared to air sparging, in transporting metal ions in small through-holes, therefore, air agitation was studied at different sparging rates. Figure 47a shows the caliberation curves obtained for half and full pumping rates but the latter was used throughout the experiments. The air sparging rates were varied in 'settings' ranged from 2-6; 2- being slight(4.5 litre/min.) and 6- being extensive (8.0 litre/min.) agitation rates. Also, reciprocating agitation was used in conjunction with different air sparging rates. For comparative purposes, the agitation rates were compared by plating on AISI 304 stainless steel strips having an exposed surface area of $300cm^2$, with width of 5cm and length of 30cm. The area of anode to cathode ratio used was 1.2:1. The cathode length was important in order to study the coating thickness distribution resulting from different agitation rates since the best uniformity is dependent upon an adequate agitation condition. The coating thicknesses obtained were measured by x-ray fluorescence (Fisher XRF) technique at intervals of 3cm, relative, and comparable to the height of the tank. Note: the tank dimensions were 28.5cm x 23.8cm x 30cm, width x length x height, respectively. Figure 48 shows the air agitation 'rig' designed for use in plating.

5.9 Pulse Electronic Behaviour

In order to distinguish the effects of different pulse conditions, it was decided that polarisation studies should be carried out and the Tafel slopes to be calculated, section 5.10. For this reason, a potentiostat was used in either galvanostatic or potentiostatic mode.

The 'switching' modes were examined by polarisation study that is, the pulse unit and/or the potentiostat were either switched on separately or together. Figure 49a shows the experimental arrangement used.

The polarisation studies were carried out using electrolyte I without any agitation. The cathodes were brass sheets (Goodfellow, Cu/Zn of 63/37 composition, half hard tempered, 0.25mm thick) with an exposed surface area of 12.5cm^2 having a width and length of 2.5cm. Each brass electrode was suspended in the bath with a copper wire. The copper wire was fed through a glass tubing, Figure 46. The contacts were sealed using a red lacquer in order to obtain the correct surface area. The exposed phosphorus deoxidised copper anode area was 360cm^2. The reference electrode was mercury/ mercury sulphate.

The polarisation curves obtained showed some features caused by the electronics in the pulse unit and also the potentiostat. Figure 49b shows a polarisation curve obtained under unipolar pulse setting of 100% duty cycle, 50Hz and an on-time of 99.9999sec which in effect is DC. Also, the polarisation studies were carried out under pulsing conditions, that is with a duty cycle of 50%. In general term, 50% duty cycle means that for every cycle the on-time is only half of that of DC but the peak current is higher than that of DC. However, the polarisation studies were obtained by switching on the pulse unit or the potentiostat either separately (with a switching gap of one second) or together. This 'switching' did not promote a reproducible result. Therefore, it was concluded that the potentiostat is not feasible for pulse polarisation studies.

Further polarisation studies were carried out by using pulse unit and different methods of sweeping, that is, using the potentiostat in step-wise fashion and/or using it in conjunction with a power supply at either constant current-step or constant potential-step, Figures 50-53; these studies were based upon the manufacturer of the pulse unit since it was claimed that the potentiostat can be used in conjunction with the pulse unit for polarisation studies. However, the polarisation studies which were carried out can be described as:

- using the potentiostat either in potential-step or current-step fashion, Figure 50.

- using the potentiostat and power supply (constant voltage or constant potential), both connected to the same anode, Figure 51.
- using the potentiostat and power supply (constant voltage or constant potential), each connected to a separate anode, Figure 52.
- using a power supply in step-wise fashion, that is, either at constant potential or constant current, Figure 53.

The polarisation studies showed that the use of potentiostat in any mode described above is not feasible since it does not give a reproducible result.

However, the use of the pulse unit with a power supply in either constant current or constant potential modes produced meaningful and reproducible results comparable to a DC condition, Figure 55. This arrangement was used throughout the experimental work for both unipolar pulse and bipolar pulse reverse conditions.

5.9.1 Comparative study of different power sources

In order to prove that different power sources are reliable and can produce a similar result, various sweeping methods were examined under DC.

The polarisation curves carried out using a potentiostat, potentiodynamically and galvanodynamically, and a power supply at constant current and constant potential. The results showed that considering all conditions (such as cathode size, electrolyte, etc) being equal, the polarisation curves were similar. Therefore, it can be concluded that the power supply can be as good as the potentiostat for polarisation studies.

5.9.2 Establishing standard parameters using a pulse unit and a power supply

The pulse parameters available from the J.C.T. unit are wide in terms of frequency and the duty cycle or the on-time, therefore, it was originally decided to study different frequencies and duty cycles. The frequencies studied were 20, 500, 1000, 2000 and 5000Hz and duty cycles were 5, 25, 50, 75 and 99%. Noting that 99% duty cycle is similar to DC. This was necessary in order to compare different pulsing conditions to that of DC using standard electrolyte (I) with no agitation.

The polarisation curves were used as a means for comparison. The studies were

carried out using standard electrolyte (I) with no agitation. The cathodes used were copper sheet (Goodfellow, 99.9%) with an exposed area of $30cm^2$. The two anodes used were phosphorus deoxidised copper with an exposed area of $180cm^2$ each. The reference electrode was mercury/mercury sulphate.

It was found that at low duty cycles (5%) and low frequencies (20Hz), the Tafel slopes decreased significantly compared to other conditions, indicating poor throwing power. But from an industrial point of view, low duty cycles are not really advisable since they incur a further cost in terms of running of the plant as the output will be reduced.

Therefore, further research work was based on frequency ranges of 20, 500, 1000, 2000 and 5000Hz (as they provided a wide range of pulsing conditions) and duty cycles of 25, 50 and 75%. Also, in further studies different agitation modes such as natural convection(still solution), reciprocating cathode agitation and reciprocating cathode and air sparging agitations combined, were examined under DC for comparison with different pulsing conditions. The combined agitation is believed to be important in simulating the 'type' of plating conditions of industrial printed circuit board plating production.

5.9.3 Behaviour of pulse parameters

This study was concerned with the effect of average current density, peak current density, potential and duty cycle.

The measurements were carried out at an initial input current equivalent to direct current of 1A for the study of average current density and potential for different duty cycles. Further measurements were undertaken at a constant input current of 1A for the study of peak current density and potential for different duty cycles. The agitations used were air sparging combined with cathode reciprocation using electrolyte V. The trend obtained was as expected, indicating further that the power supply is compatible with the pulse unit under the conditions examined.

5.10 Polarisation, Tafel and Wagner Number Studies

As explained in the previous section, the polarisation studies were carried out using different electrolytes. The polarisation curves were used to calculate the Tafel slopes for different pulse conditions. The method used for calculating the Tafel slope values has been long established and was discussed in sections 2.1.2 and in recent years Goodenough and Whitlaw [21] have used the Tafel theory in their studies and found it to be useful in determining the throwing power of a solution under specific conditions. The throwing power of the electrolyte can be related to the Tafel slope. Wagner [16] has derived a formulation to determine the throwing power, taking into account the Tafel slope, conductivity of the solution and a characteristic length which could be the dimension(s) of the cathode or the distance between the cathode and anode electrodes or even the distance between the cathode and reference electrodes.

For this research programme, the polarisation curves (E-i curves) were obtained by a current-step technique and they were plotted and then the current densities for each of the conditions were converted to new current densities taking into account the average limiting current density for each electrolyte, as suggested by Goodenough and Whitlaw[21], see section 2.1.2. The potential was plotted against converted current density and the Tafel slopes were calculated in mV/decade. The Tafel slopes obtained were used to calculate the Wagner number for different current densities, then the current density was plotted against the Wagner number. The Wagner number is derived to be:

$$Wa = \frac{\kappa}{L}\left(\frac{d\eta}{di}\right)$$

where

κ is the electrolyte conductivity (Scm^{-1} or $\Omega^{-1}cm^{-1}$)

L is the characteristic length of the deposition process (cm)

$\left(\frac{d\eta}{di}\right)$ is the slope of the polarization curve and calculated at an average current density ($VA^{-1}cm^{2}$)

In order to differentiate and also to characterise the changes in Wagner Number, an enhancement ratio (RWa) was defined such that:

$$R_{Wa} = \frac{\text{Pulse Wagner Number } (Wa_p)}{\text{DC Wagner Number } (Wa_{DC})}$$

The RWa values obtained for each pulsing condition were found to have a

systematic relationship to that of Wagner number.

5.10.1 Direct current

The polarisation studies were carried out under DC using all electrolytes (I-XIII), described in section 5.7. The agitation modes used were reciprocating cathode and also reciprocating cathode combined with air sparging. This was compared to still or natural convection. The cathodes used were copper sheets having an exposed area of $30cm^2$ with an anode to cathode ratio of 12:1. The anodes were phosphorus deoxidised copper. Figure 54a shows the experimental arrangement used.

Once the polarisation curves were carried out and the Wagner number values were calculated for DC and pulse conditions, see next section, then the best electrolytes under unipolar pulse were chosen for plating of PCBs under DC. The optimum electrolytes were I, III and V. The electroplating was carried out at an average current density of $3.0Adm^{-2}$ using air and cathode reciprocation combined. The electroplating was carried out on printed circuit boards with hole diameters of 1.5mm and 0.8mm having a board thickness of 2.5mm and also hole diameters of 0.8mm and 0.3mm with a board thickness of 2.4mm.

Basically, the conditions used in plating PCBs under DC are described below:

Electrolyte	Hole diameter (mm)	Board thickness (mm)	C.D. Adm^{-2}	Condition
I	1.5,0.8	2.5	3	DC
I	0.8,0.3	2.4	3	DC
III	1.5,0.8	2.5	3	DC
V	1.5,0.8	2.5	3	DC
V	0.8,0.3	2.4	3	DC

The plated samples were mounted and the coating thickness distributions were measured at ten points on the cross-section of the holes. The metallurgical examination is described in section 5.10.5. The comparative studies were made upon the surface(S) to hole(H) thickness ratios obtained, that is, the closer the S/H ratio to 1, the better the coating distribution for printed circuit board manufacture.

5.10.2 Unipolar pulse

The polarisation studies were carried out under unipolar pulse condition with frequencies of 20Hz, 500Hz, 1000Hz, 2000Hz and 5000Hz and duty cycles of 25%, 50% and 75%, as explained in section 5.9.2. For comparative purposes standard electrolyte (I) was used and also electrolytes containing additives. the effect of different temperatures(10°C and 35°C) was also examined. All the electrolyte (I-XIII) constituents have been described in section 5.7. Pretreatment 5 was used for the polarisation studies. The exposed area of cathode was $30cm^2$ and an anode to cathode ratio of 12:1. The form of agitation used was reciprocating cathode combined with air sparging. Figure 55 shows the experimental arrangement used.

Once the polarisation curves were obtained then the RWa values were calculated, as explained above. The best(B1) and/or second(B2) best and worst(W) pulse conditions were used to electroplate printed circuit boards. The list below shows the conditions used:

Electrolyte	Hole diameter (mm)	Board thickness (mm)	C.D. Adm^{-2}	Pulse conditions
I	1.5,0.8	2.5	4,3,1,0.5	5000Hz,50%ϕ:B1
I	1.5,0.8	2.5	3,1,0.5	20Hz,25%ϕ:W
I	0.8,0.3	2.4	3	5000Hz,50%ϕ:B1
I	0.8,0.3	2.4	3	20Hz,25%ϕ:W
III	1.5,0.8	2.5	4,3,1,0.5	1000Hz,75%ϕ:B1
III	1.5,0.8	2.5	3,1,0.5	20Hz,25%ϕ:W
III	1.5,0.8	1.6	3	1000Hz,75%ϕ:B1
III	1.5,0.8	1.6	3	20Hz,25%ϕ:W
III	0.8,0.3	2.4	3	1000Hz,75%ϕ:B1
III	0.8,0.3	2.4	3	5000Hz,25%ϕ:B2
III	0.8,0.3	2.4	3	20Hz,25%ϕ:W
V	1.5,0.8	2.5	3	1000Hz,75%ϕ:B1
V	1.5,0.8	2.5	3	20Hz,25%ϕ:W
V	1.5,0.8	1.6	3	1000Hz,75%ϕ:B1
V	0.8,0.3	2.4	3	1000Hz,75%ϕ:B1
V	0.8,0.3	2.5	3	5000Hz,25%ϕ:B2
V	0.8,0.3	2.5	3	20Hz,25%ϕ:W
XIII	0.8,0.3	2.5	3	500Hz,75%ϕ:B1

Amongst the electrolytes used only three were found to be appropriate, ie. electrolytes I, III and V. The electroplating was carried out on printed circuit boards with hole diameters of 1.5mm and 0.8mm having board thicknesses of 2.5mm and 1.6mm and also hole diameters of 0.8mm and 0.3mm with board thickness of 2.4mm.

The plated samples were mounted and the coating thickness distributions were measured at ten points on the cross-section of the holes. The metallurgical examination is described in section 5.10.5. Comparative studies were then made upon the surface(S) to hole(H) thickness ratios obtained.

5.10.3 Bipolar pulse reverse

The polarisation studies were carried out using electrolytes I and V. The electrolyte I was used as a base for comparison to V. Pretreatment 5 was used for the polarisation studies. The exposed area of cathode was $30cm^2$ with anode to cathode ratio of 12:1. The form of agitation used was reciprocating cathode combined with air sparging. The experimental arrangment can be seen in Figure 55.

The bipolar pulse reverse conditions used for the working electrode were systematic with cathodic/anodic peak current density ratios($i_{p(c)}/i_{p(a)}$) of 1/1, 1/2, 1/3 and 1/4 and cathodic/anodic on-time ratios($t_{on(c)}/t_{on(a)}$) of 10/0.2, 10/0.5, 10/1, 10/2 plus 20/0.5 for only $i_{p(c)}/i_{p(a)}$ of 1/1 plus 20/1 for only $i_{p(c)}/i_{p(a)}$ of 1/1 and 1/2. The limit on the choice of the conditions chosen was dependent upon the polarisation curves obtained and also the voltage which the power source could supply. (Note: on-times are in milliseconds).

From the polarisation curves obtained, the limiting current densities were calculated and an average current density of each pulse reverse was used in order to calculate the Tafel slope and hence the Wagner number. The Wagner number enhancement ratio(RWa) defined to be:

$$R_{Wa} = \frac{\text{Pulse reverse Wagner number}(Wa_{PR})}{\text{DC Wagner number}(Wa_{DC})}$$

Once the RWa was obtained the best(B1), middle(M) and worst(W) range conditions were used to electroplate printed circuit boards. The electroplating was carried out at an average current density of $3.0Adm^{-2}$ using printed circuit boards with hole diameters of 0.8mm and 0.3mm having board thickness of 2.4mm and the results

were compared to DC.

The list below shows the conditions used:

Electrolyte	Hole diameter (mm)	Board thickness (mm)	C.D. Adm^{-2}	Pulse reverse conditions $i_{p(c)}/i_{p(a)}$, $t_{on(c)}/t_{on(a)}$
I	0.8,0.3	2.4	3	1/1, 10/0.2:B1
I	0.8,0.3	2.4	3	1/3, 10/0.5:M
I	0.8,0.3	2.4	3	1/3, 10/2:W
V	0.8,0.3	2.4	3	1/1, 10/0.2:B1
V	0.8,0.3	2.4	3	1/2, 10/0.2:M
V	0.8,0.3	2.4	3	1/3, 10/0.2:M
V	0.8,0.3	2.4	3	1/4, 10/0.2:M
V	0.8,0.3	2.4	3	1/3, 10/2:W
V	0.8,0.3	2.4	3	1/8, 10/0.2

The plated samples were mounted and the coating thickness distributions were measured at ten points on the cross-section of the holes. The metallurgical examination is described in section 5.10.5. The comparative studies were made upon the surface(S) to hole(H) thickness ratios obtained.

5.10.4 Optimisation of Chloride Ions under DC and Pulsing

In this study, different concentrations of chloride ion were examined. The base electrolyte used was 0.3M $CuSO_4$, 2.25M H_2SO_4. The chloride ion concentrations ranged form 0, 25, 50, 75, 100, 150 and 200ppm. The cathodes used were copper sheets with an exposed area of $30cm^2$ having an anode to cathode ratio of 12:1. The pretreatment 5 was used for cleaning the cathodes. The polarisation curves were obtained under DC and unipolar pulse conditions of 100Hz and 50%ϕ at room temperature. The pulse condition was chosen arbitrarily. The agitation used was reciprocating cathode and air sparging combined. Figures 54a and 55 show the experimental arrangements used under DC and unipolar pulse conditions, respectively.

The polarisation studies were carried out as described in section 5.10 and Wagner numbers were obtained. It was found that the optimum chloride ion concentration was 50ppm.

5.10.5 Metallurgical Studies of PCBs

The mounting of the PCBs was carried out (by the sponsoring company - LeaRonal) by jigging each set of samples using the PCB mounting jig and then cutting each set to a correct dimension. The jigged samples were mounted in an Araldite type resin. Once the resin cured, grinding was carried out on 1200grit and then polished using diamond pastes of 6μm and 1μm, respectively.

The examination of the coating in through-holes was aided using either of the two etching solutions listed below:

1) AMMONIUM PERSULPHATE SOLUTION –Micro-etching

Ammonium persulphate	2g
Water	50ml
10% Ammonia (SG 0.88)	50ml

2) ACID FERRIC CHLORIDE SOLUTION – Macro-etching

Ferric chloride	5g
Hydrochloric acid (SG 1.18)	50ml
Water	100ml

As far as this research is concerned, the difference between the two etching solution lies in the speed of the etching. For (1) the etching time is 1-2 seconds, but for (2) the etching time is 4-9seconds. The majority of the etching was carried out using etchant (1). The etching was carried out by wiping each surface with cotton wool.

The plated coating thickness measurements were carried out on an optical microscope (Reichert-Jung Model MeF 3) equipped with a graticule.

5.11 Assessment of Pulse Plated Electrodeposits

This section examines the variations observed under pulsing compared to DC. The assessment of pulsing whether unipolar pulse or bipolar pulse reverse was carried out by electroplating two different samples with various aspect ratios.

For unipolar pulse the efficiency, hardness, average roughness, peak roughness to trough measurements and also for morphological studies of the samples, procedure A was followed. As for tensile strength, elongation, coating thickness distribution and surface appearance and STEM studies procedure B was followed for both unipolar pulse and bipolar pulse reverse conditions.

Procedure A

- The agitation mode was reciprocating cathode combined with air sparging. The cathodes used were copper sheet (Goodfellow, 99.9%, half hard tempered, 0.25mm thick) having an exposed area of $70cm^2$ with an anode to cathode ratio of 5.2:1. The two anodes used were phosphorus deoxidised copper with an exposed area of $180cm^2$ each. The electrolytes I, VIII and V were used for the study. Also pretreatment 5 was favoured, as in previous studies.

Procedure B

- The agitation mode was reciprocating cathode combined with air sparging. The cathode used was a AISI 304 stainless steel sheet having an exposed area of $150cm^2$ with an anode to cathode ratio of 2.4:1. The two anodes used were phosphorus deoxidised copper with an exposed area of $180cm^2$ each. Stainless steel was effective because of poor deposit adhesion allowing production of foils, therefore, making the tensile strength and elongation studies straight forward. As for pretreatment, grinding was carried out using a 1200grit grinding paper and then followed by polishing with a 6μm and a 3μm diamond paste, respectively. Electrolytes I and V were used for the study.

The plating for unipolar pulse and DC was carried out at an average current density of $3Adm^{-2}$. The unipolar pulse plating conditions were at frequencies of 20, 100, 500, 1000, 2000, 3000, 4000 and 5000Hz and at duty cycles of 25, 50 and 75%.

The plating for bipolar pulse reverse was carried out at an average current density of $3Adm^{-2}$. The unipolar pulse reverse plating conditions were at cathodic/anodic peak current density ratios($i_{p(c)}/i_{p(a)}$) of 1/1, 1/2, 1/3 and 1/4 and cathodic/anodic on-time ratio($t_{on(c)}/t_{on(a)}$) of 10/0.2 and also at $i_{p(c)}/i_{p(a)}$ of 1/3 and $t_{on(c)}/t_{on(a)}$ of 10/0.5. (Note: on-times are in milliseconds).

For the examination of cathode efficiency, roughness and micro-hardness, the calculated average plating thickness was 25μm and for tensile strength, elongation and surface coverage examinations, the calculated average plating thickness was 50μm, (Tables 19 and 20).

5.11.1 Efficiency of deposition

The cathode efficiency was calculated by weight gain measurement. Each cathode was weighed before and after plating and then the weight gain of the pulsed coatings

were measured as a comparison to DC. The efficiencies were calculated by the following equation:

$$\text{Efficiency (\%)} = \frac{\text{Weight gain under pulse } (M_P)}{\text{Weight gain under DC } (M_{DC})}$$

The efficiency values were only calculated for unipolar pulse. The procedure A described earlier was followed.

5.11.2 Micro-hardness

The micro-hardness measurements were carried out using a Vickers micro-hardness tester on the Reichert MeF 2 microscope, see Table 19. The measurements were taken only for unipolar pulse conditions, and procedure A was followed.

The Vickers micro-hardness was arranged according to the instruction manual. The plated samples were mounted in cross-section in bakelite and then ground with 1200grit and then mirror polished to 6μm followed by 3μm using Buehler diamond pastes. For this study several different loads were chosen in order to find a common weight for all the micro-hardness measurements. The weights ranged from 5-100g and the most suitable weights were 20g and 50g; 20g being used in the majority of the measurements. Once the indentation number was read then the micro-hardness number was calculated from the equation:

$$\text{Hardness value(HV)} = 1854.4 \frac{P}{d^2} \qquad \text{Kgmm}^{-2}$$

where P= load in grams(=20g)

d= ocular reading x 0.157 μm

This procedure was repeated five times on each sample and an average of the five values is reported.

Furthermore, for comparative purposes, a copper foil (Goodfellow, 99.9%, half hard tempered, 0.25mm thick) was chosen and the foil was rolled giving reductions of 0, 5, 25, 50 and 75%. The hardness values were obtained following the same micro-hardness measuring procedures described above.

5.11.3 Roughness

This provides information relating to the smoothness of the coating of a deposit relative to the surface texture. The basic components of the instrument (Rank Taylor-Hobson, model: Talysurf 10) are a stylus, pick-up, transverse unit, amplifier, processor and outputs. The stylus can be positioned to travel across the surface and the pick-up converts its vertical movements (caused through surface irregularities) into an electrical signal. This signal is amplified and processed to give various parameters such as mean peak-to peak roughness(R_{tm}) and roughness average(R_a), and the results are fed to a visual display by an analogue meter or printout device. The measurements were repeated four times and the average of the four values was taken in μm for comparative purposes. The distance travelled by the stylus for each sample measurements was about 0.8mm.

However, the roughness measurements were carried out only for unipolar pulse conditions and DC conditions for electrolytes I, VIII and V. Procedure A was followed for each plated sample.

The roughness values were obtained by two types of measurements for comparative reasons. The first roughness measurements is called mean roughness (R_{tm}) and the second roughness is known as average roughness(R_a). The R_{tm} is the measurements from peak to trough of a coating, and the R_a is the average area measurements of a coating, as shown below:

A typical mean roughness(R_{tm}) measurement profile.

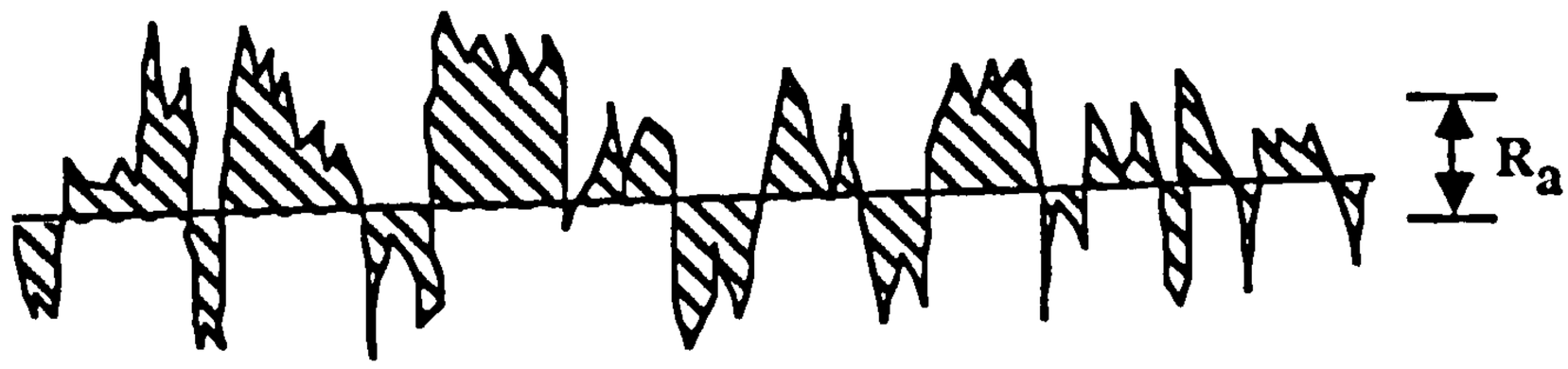

A typical roughness average (R_a) measurement profile

For comparative purposes, the unipolar pulse results were compared to DC as literature in this area is very limited. The surface of the substrates were not taken into account as they were rolled copper sheets (Goodfellow, 99.9%, half hard tempered) obtained form the manufacturer and were believed to have a standard or constant smoothness.

5.11.4 Tensile strength and elongation

For tensile strength and elongation studies a stainless steel substrate was used to aid foil preparation since the properties of the electrodeposit were required separate to those of the substrate. For this reason, the procedure B of section 5.13 was used. The tensile studies were carried out under unipolar pulse, bipolar pulse reverse and also under DC using electrolytes I and V.

However, in order to compare the results of the electroplated samples to rolled sheets, a copper (Goodfellow, 99.9%, half hard tempered, 0.25mm thick.) sheet was chosen and was rolled to reduction in thickness of 0, 5, 25, 50 and 75%.

Tensile specimens were prepared from copper foils under the conditions mentioned above and uniaxial tensile properties evaluated using a J.J. Lloyd testing machine (T5002) fitted with a 500N load cell and an X-Y chart recorder, according to ASTM: D 638: (1972). The tensile specimens were stamped out to form dumb-bell test pieces. The electroplated foils were blanked out on a press with their major axis parallel to the direction of the grinding and polishing of the substrate, (stainless steel). The rolled copper sheets were blanked in the direction of rolling. The cutting of the specimens were carried out by a press die and the test pieces conformed to dimensions of type BS 903: part A2: (1971). A typical test specimen profile is shown below:

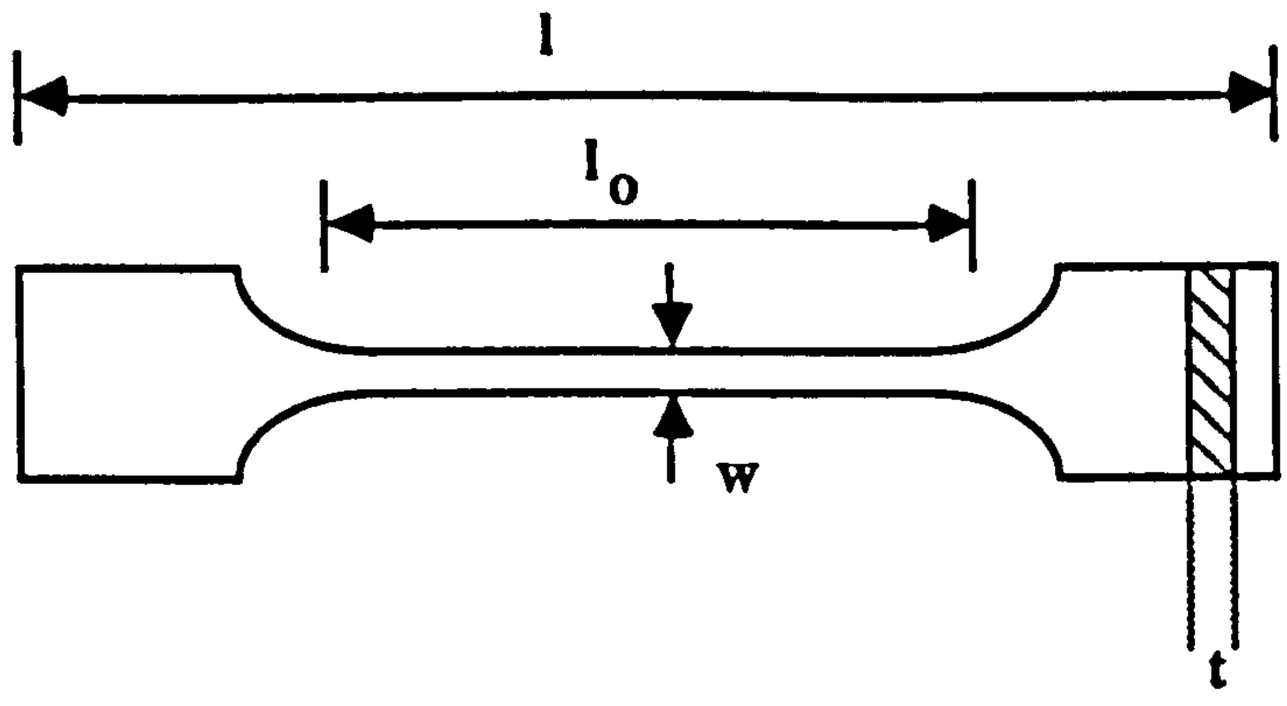

Where	l = overall length	75mm
	l_o= length of narrow parallel portion	30mm
	w= width of narrow parallel portion	4mm
	t= thickness	0.05mm

All the samples were carefully examined for any tear or imperfections left from cutting or punching. Four test pieces were tested for each pulsing or DC condition at room temperature and at a cross-head speed of 10mm/min. From the force-crosshead displacement curves obtained, the values of tensile stress at fracture were calculated from the following equation:

$$\sigma = \frac{F}{A}$$

where σ = tensile strength at fracture (MPa)

F = force at fracture (N)

A = initial mean cross-sectional area (mm^2)

and the percentage elongation was calculated at fracture in relation to the initial gauge length from the following equation:

$$\text{Elongation (\%)} = \frac{l_b - l_o}{l_o} \times 100$$

where l_o= length of narrow parallel portion (mm)

l_b= displacement at fracture (mm)

5.11.5 Coating thickness distribution

The coating thickness distribution or surface coverage of the metal deposit is believed to be important in order to study the metal distribution on a surface resulting from different types of electrolytes (I and V) and also different pulse conditions (unipolar pulse or bipolar pulse reverse) compared to DC. The electroplating was

carried out according to the procedure B of section 5.11.

The coating thicknesses were carried out using a flat, 'contact faces', Micrometer and for more detailed measurements a point Micrometer was also used. The areas measured for each Micrometer is shown below:

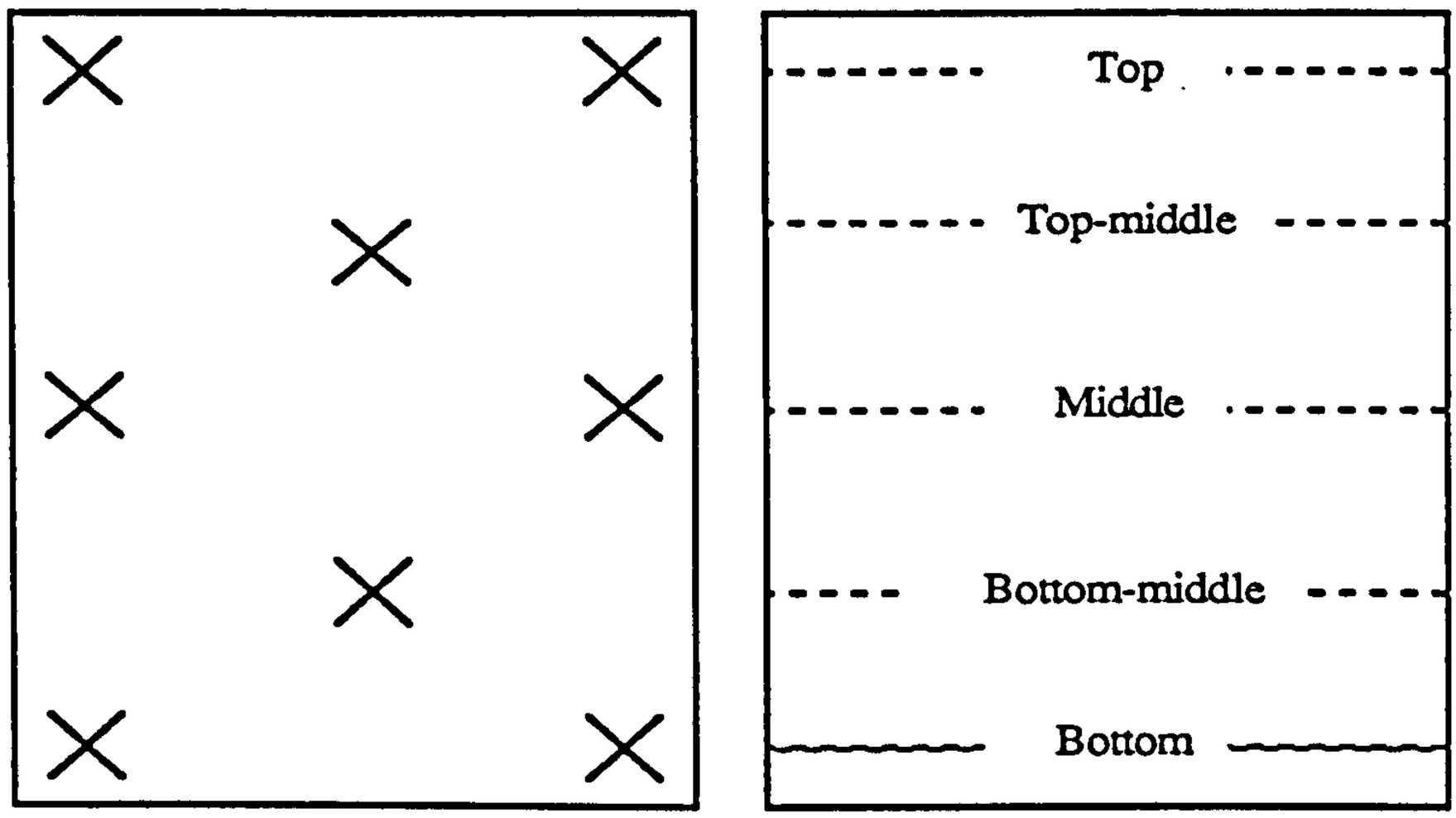

Flat Micrometer **Point Micrometer**

5.11.6 Surface appearance

Basically, the surface appearance or coating finish describes the types of coating finishes obtained using electrolytes I and V under all pulsing conditions studied in this section, 5.11. The finishes are described as lustrous, semi-lustrous, dull, matt and burnt. The terminologies can be defined to be: lustrous for a shiny finish, semi-lustrous for a deposit in between dull and lustrous, dull for an orange coloured deposit, matt for a red coloured deposit and burnt for a brown coloured deposit.

5.11.7 Morphological study of the deposits

The morphological assessment of the deposited coatings were carried out using scanning electron microscope(SEM), model: Cambridge Stereoscan 360, and transmission electron microscope(TEM), model: JEOL 100CX STEMMA.

The deposits obtained have been produced according to procedures A and B using electrolyte I and V under unipolar pulse, bipolar pulse reverse and DC. The

morphological studies are mainly based upon the changes in electrodeposit structure resulting from different pulsing conditions and their comparison to DC.

The metallurgical examination of the coating using electrolyte V under bipolar pulse reverse was carried using the etching solution described below:

AMMONIUM PERSULPHATE AND HYDROGEN PEROXIDE SOLUTION

	– Micro-etching
Ammonia (SG 0.88) 35% W/W	20ml
Water	20ml
30% hydrogen peroxide	1-2ml

This etchant was important in the study of the grain size of the deposits produced when using electrolyte V and hence it made the morphological study of the pulse reverse easier for comparison. The etching time was 5seconds. It is to be noted that the etchant mentioned, was only used when the deposits were lustrous or shiny otherwise, it was not necessary.

CHAPTER 6

6.0 RESULTS

This gives the results obtained for the examination of pulsing techniques and their comparison to direct current. This chapter is described under three categories: a) standardisation: this includes parameters such as conductivity, pretreatment, agitation and pulse behaviour; b) polarisation curves, Tafel slope and Wagner number: this includes the coating distribution and metallurgical studies of PCBs; and c) assessment of pulsed electrodeposits: this includes the morphological aspects, properties and surface appearances.

6.1 Standardisation

6.1.1 Solution conductivity

The conductivity measurements obtained for different acid concentrations and different copper sulphate concentrations are shown in Table 6. Figure 43 also shows the graphical picture of the results illustrating the relationship between conductivity for different sulphuric acid concentrations (25, 50, 75, 100, 125, 150, 175, 200, 225 and 250 mll^{-1}) in differing molarities of copper sulphate solution. The conductivity is described as Scm^{-1} or $\Omega^{-1}cm^{-1}$.

6.1.2 Pretreatment assessments

The pretreatment assessments were carried out by polarisation studies (E-i curves) and also Hull cell techniques using 0.3M $CuSO_4$, 2.25M H_2SO_4 and 50ppm Cl^-. The eight pretreatments studied are explained in section 5.3. Figure 44a shows the potential against average current density for different pretreatments. Figure 44b shows the Hull cell results as a bar chart in which surface appearances obtained for different pretreatments are plotted against current density. The surface appearances obtained by the Hull cell technique are described as; good deposit indicating orange coloured

deposits, light burnt indicating red coloured deposits and heavy burnt indicating brown coloured deposits.

6.1.3 Hull cell results

As for the study of additives, the Hull cell studies were carried out using nine electrolytes(I-IX), described in section 5.4. The surface appearances obtained for electrolytes examined were plotted against the current density for without and with air agitation, (Figures 45a and 45b, respectively). The surface appearances obtained are described as bright finish indicating shiny or lustrous deposits, semi-bright finish indicating a finish in between shiny gold to orange coloured deposits, matt deposit indicating orange coloured deposits, light burnt indicating red coloured deposits and heavy burnt indicating brown coloured deposits.

6.1.4 Effects of agitation

The study of different modes of agitation have produced some interesting results. Table 7a shows the agitation types and the limiting current densities obtained from the polarisation curves. The agitation types were reciprocating cathode, slight and extensive air and also different magnetic rotation speeds; for comparison natural convection was also studied. For all the agitations, cathode reciprocation was also combined in order to study the superimposed agitation as further comparison. The study involved using two different types of electrolytes and also two different temperatures. Electrolyte A had constituents of 0.3M $CuSO_4$, 2.25M H_2SO_4 and 50ppm Cl^- and electrolyte B had constituents of 0.015M $CuSO_4$ and 0.5M H_2SO_4, the temperatures studied were 21°C and 50°C. The limiting current density values reported also include the surge values obtained from polarisation curves, for example, a limiting current density of 5.67± 0.17 Adm^{-2} means the value could be in the range of 5.5-5.84 Adm^{-2}. For comparative studies, an enhancement factor was defined indicating the ratio of the limiting current density of agitated mode to that of natural convection. Table 7b shows the enhancement factors for different solution concentrations and temperatures for different agitation modes.

For polarisation studies and also the plating of the PCBs, different agitation rates were studied in order to obtain the best types of conditions for uniformity of deposits within the tank. The assessment of the agitation were carried out by electroplating substrates and measuring the thickness by x-ray fluorescence. Figure 47a shows the

air pump flow rate against different pump setting positions and Figure 47b shows the coating thickness against the cathode position in the tank for different agitation rates and their combination with reciprocating cathode. It was found that air sparging with an air flow rate of 4.5litres/min. combined with reciprocating cathode provides the best linear result within the tank.

6.1.5 Pulse electronic behaviour

The pulse electronic behaviour studied showed that the electronics within the pulse unit and potentiostat have an effect on the results, for this reason various switching techniques were studied. Figure 49a shows the experimental arrangement used for the study in which a sweep unit was connected to a potentiostat and the cell via a pulse unit. The Figures 49b-49f show the systematic studies carried out:

- Figure 49b shows the polarisation curve obtained using a pulse unit and a potentiostat. The polarisation curves were carried out potentiodynamically using electrolyte I (0.3M $CuSO_4$, 2.25M H_2SO_4 and 50ppm Cl^-) without agitation and the pulse unit was set at a frequency of 50Hz and a duty cycle of 99%, which in effect is DC. The sweep rate used was 150mV/minute.
- Figure 49c shows the polarisation curve obtained using a pulse unit and a potentiostat arranged to run potentiodynamically. The potentiostat was switched on with a second gap to that of pulse unit. The electrolyte, sweep unit and the chart recorder conditions remained the same as above, except the duty cycle was reduced to 50%.
- Figure 49d shows the polarisation curve obtained when both potentiostat and pulse unit were switched on together. The conditions remained the same as Figure 49c.
- Figure 49e shows the results obtained under the same conditions as 49d, in order to check the reproducibility of the curve.
- Figure 49f shows the polarisation curve obtained when the pulse unit was switched on a second later to that of the potentiostat. The conditions remain the same as Figure 49c.

The switching study did not promote reproducible results indicating that the potentiostat is not suitable for polarisation studies when pulsing.

Further studies also confirmed the same point. These studies involved using a pulse unit and different methods of sweeping, that is, using a potentiostat in step-wise fashion and/or using it in conjunction with a power supply at either constant current or

potential mode, Figures 50-53. In other words, the studies carried out are:

- using the potentiostat either potential-step or current-step, Figure 50.
- using the potentiostat and a power supply (constant current or constant potential), both connected to the same anode, Figure 51.
- using the potentiostat and a power supply (constant current or constant potential), each connected to a separate anode, Figure 52.
- using a power supply in step-wise fashion, that is, either at constant potential or constant current, Figure 53.

The polarisation studies showed that using the potentiostat in any mode is not feasible as it did not promote reproducible results. However, the use of the pulse unit with a power supply in either constant current or constant potential mode produced meaningful and reproducible results comparable to a DC condition. Therefore, the polarisation studies were carried out using this arrangement throughout the experimental work, whether using DC or a pulsing technique, ie. unipolar pulse or bipolar pulse reverse.

6.1.6 Comparative study of different power sources

A comparative study using different power sources was also carried out under DC. The power sources were a potentiostat, which was operated potentiodynamically and also galvanodynamically, and a power supply which was operated at constant potential and also at a constant current mode. Figure 54a shows the experimental arrangement used. The polarisation curves were obtained using 0.3M $CuSO_4$, 2.25M H_2SO_4 and 50ppm Cl^-. Figures 54b and 54c show the polarisation curves obtained under conditions specified above and plotted as both linear and logarithmic, respectively. The curves were obtained in a still solution. As expected, the results obtained indicated a good correlation between the four polarising techniques.

6.1.7 Establishing standard parameters using a pulse unit and a power supply

In order to establish a standard range of tests, a combination of polarisation studies was carried out. Figures 56a-e show the polarisation curves obtained using a pulse unit and a power supply. The frequencies studied were 20, 500, 1000, 2000 and 5000Hz and the common duty cycles were 5, 25, 50, 75 and 99%. The studies were carried out using a standard electrolyte(I) with no agitation and an exposed cathode area of $30cm^2$.

The potentials were measured against a mercury/mercury sulphate reference electrode. It was found that the best conditions for further studies are at frequencies of 20, 500, 1000, 2000 and 5000Hz and at duty cycles of 25, 50 and 75% since they provide a wide range of combinations.

6.1.8 Behaviour of pulse parameters

The effects of pulsing were also examined in this research programme, using a cathode size of $1dm^{-2}$. The measurements were carried out at an initial input current equivalent to direct current of 1A for the study of average current density and potential for different duty cycles. Figure 57a shows the effect of average current density and its relative potential for different duty cycles. Further measurements were undertaken at a constant input current of 1A for the study of peak current density and potential for different duty cycles. Figure 57b shows the effect of peak current density and potential against duty cycle. The agitations used were air sparging combined with cathode reciprocation using electrolyte V. It can be seen that the average current density values decrease linearly as the duty cycles increase, but the cell potentials increase linearly with peak current density values decreasing exponentially. This indicates that the power supply is compatible with the pulse unit under the conditions examined.

6.2 Polarisation, Tafel and Wagner Number Studies

The polarisation, Tafel and Wagner number studies have been calculated for all the electrolytes(I-XIII), section 5.7. The limiting current densities were used to calculate the Tafel slope values and also the Wagner numbers, section 5.10. Furthermore, the Wagner enhancement ratio was also calculated for each pulse and electrolyte conditions. The conductivity of each electrolyte and also any other important parameters have been specified in Appendix 1.

6.2.1 Direct current

Figures 58a-70a are the potential versus average current density plots for different electrolytes under DC conditions; the potentials were measured against a mercury/ mercury sulphate reference electrode. Each Figure relates to the electrolyte used, for example 58a relates to electrolyte I and Figure 70a relates to electrolyte XIII. The polarisation studies were carried out under DC as a comparison to that of the pulsing

conditions. For the study, three agitation modes were examined; natural convection, reciprocating cathode and also reciprocating cathode combined with air sparging and the limiting current density value was calculated for each of the agitation modes and electrolytes, Table 8a.

Figures 58b-70b show the potential-logarithmic converted current density graph for all the agitation modes. The Tafel slope values were calculated as shown in Table 9a. Also, Table 10a shows the Tafel slope values and also the agitation modes in order of best to worst.

Figures 58c-70c show the current density-Wagner number. The Wagner numbers were calculated, Table 11a, using the Tafel slope, electrolyte conductivity and the characteristic length, see section 5.10 for more detail.

For comparative purposes, plating was carried out using reciprocating cathode and air sparging. The results and conditions used are explained in section 6.2.5.

6.2.2 Unipolar pulse

Figures 71a-83a are the potential versus average current density plots under unipolar pulse conditions for different electrolytes under DC conditions. The potentials were measured against mercury/mercury sulphate reference electrode. Each figure relates to the electrolyte used, ie. Figure 71a relates to electrolyte I and Figure 83a to electrolyte XIII. The polarisation studies were obtained under unipolar pulse using reciprocating cathode combined with air sparging as a means of agitation. The limiting current density for each condition and electrolyte was calculated, Table 8b.

Figures 71b-83b show the potential-logarithmic converted current density graphs. The Tafel slope values were calculated as shown in Table 9b. Also, Table 10b shows the three best and one worst Tafel slopes and the unipolar pulse conditions utilised.

Figures 71c-83c show the current density-Wagner number plots. The Wagner numbers were calculated using the Tafel slope, electrolyte conductivity and the characteristic length, see section 5.10 for detail. The Wagner number values are listed in Table 11b.

For comparative purposes, an enhancement Wagner ratio(RWa) was used. The

RWa values under unipolar pulse were calculated relative to the DC condition. The results obtained are listed in Tables 12a and 12b. Furthermore, a graphical representation of the results can be seen in Figure 84, showing RWa against different electrolyte constituents indicating the three best and two worst pulse conditions. The RWa=1 indicates a pulsing condition equivalent to DC and RWa<1 indicates a pulsing condition worse than DC.

To examine the unipolar pulse conditions, the calculated RWa values were used to electroplate PCBs. The results are explained in section 6.2.5.

6.2.3 Bipolar pulse reverse

Figures 85a-90a are the potential versus average current density using electrolyte I and Figures 95a-100a are also the potential versus average current density plots using electrolyte V for bipolar pulse reverse conditions. The potentials were measured against mercury/mercury sulphate reference electrode. The polarisation studies were obtained under bipolar pulse reverse using a reciprocating cathode combined with air sparging as a means of agitation. The bipolar pulse reverse conditions used were systematic with cathodic/anodic peak current density ratios($i_{p(c)}/i_{p(a)}$) of 1/1, 1/2, 1/3 and 1/4 and cathodic/anodic on-time ratios($t_{on(c)}/t_{on(a)}$) of 10/0.2, 10/0.5, 10/1, 10/2 plus 20/0.5 for only $i_{p(c)}/i_{p(a)}$ of 1/1 plus 20/1 for only $i_{p(c)}/i_{p(a)}$ of 1/1 and 1/2. The limit on conditions chosen were dependent upon the polarisation curves obtained, and the voltage which the power source could supply. (Note: on-times are in milliseconds).

The limiting current density of each unipolar pulse reverse condition for the two electrolytes was calculated as shown in Table 13.

Figures 85b-90b and 95b-100b show the potential-logarithmic converted current density graphs for all pulse conditions specified above and the Tafel slope values were calculated as shown in Table 14.

Figures 91-94 show the current density-Wagner number curves for electrolyte I and Figures 101-104 show similar plots for electrolyte V. The Wagner numbers were calculated, Table 15, using the Tafel slope, electrolyte conductivity and the characteristic length, see section 5.10 for more detail.

To examine the bipolar pulse reverse conditions, the RWa values were calculated, Table 16, and used to electroplate actual PCBs. The results are explained in section 6.2.5.

6.2.4 Optimisation of chloride ions under DC and pulsing

The chloride ion concentrations were examined using electrolyte VIII. Figures 105a and 106a show the polarisation curves obtained under DC and pulse conditions(100Hz, 50%ϕ), respectively, for 0, 25, 50, 75, 100, 125, 150 and 200ppm of chloride ion. The limiting current density values were obtained, (Table 17a) to calculate the logarithmic converted current density.

Figures 105b and 106b show the potential-logarithmic converted current density. Table 17b shows the Tafel slope values obtained.

Figures 105c and 106c show the current density-Wagner number. The Wagner number values obtained are shown in Table 17c.

It can be concluded from the Wagner number values that the best concentration of chloride ion is 50ppm under both DC and unipolar pulse conditions.

6.2.5 Assessment of unipolar pulse and bipolar pulse reverse

To assess the results obtained for both unipolar pulse and bipolar pulse reverse, the plating of PCBs was carried out under DC and also different unipolar pulse and bipolar pulse reverse conditions. Electroplated PCBs were used as a means for comparison. Figures 107 and 108 show the thickness distribution of the plated PCBs for the best electrolytes and pulse conditions (best(B1), second best(B2), middle(M) and worst(W) relative to RWa values).

The Tables below show the summary of the electrolytes, hole diameters, board thicknesses, current densities and conditions examined:

- DC

Electrolyte [Figure No.]	Hole diameter (mm)	Board thickness (mm)	C.D. Adm^{-2}	Condition
I [85]	1.5,0.8	2.5	3	DC
I [86]	0.8,0.3	2.4	3	DC
III [85]	1.5,0.8	2.5	3	DC
V [85]	1.5,0.8	2.5	3	DC
V [86]	0.8,0.3	2.4	3	DC

- Unipolar Pulse

Electrolyte [Figure No.]	Hole diameter (mm)	Board thickness (mm)	C.D. Adm^{-2}	Unipolar Pulse conditions
I [85]	1.5,0.8	2.5	4,3,1,0.5	5000Hz,50%ϕ:B1
I [85]	1.5,0.8	2.5	3,1,0.5	20Hz,25%ϕ:W
I [86]	0.8,0.3	2.4	3	5000Hz,50%ϕ:B1
I [86]	0.8,0.3	2.4	3	20Hz,25%ϕ:W
III [85]	1.5,0.8	2.5	4,3,1,0.5	1000Hz,75%ϕ:B1
III [85]	1.5,0.8	2.5	3,1,0.5	20Hz,25%ϕ:W
III [85]	1.5,0.8	1.6	3	1000Hz,75%ϕ:B1
III [85]	1.5,0.8	1.6	3	20Hz,25%ϕ:W
III [86]	0.8,0.3	2.4	3	1000Hz,75%ϕ:B1
III [86]	0.8,0.3	2.4	3	5000Hz,25%ϕ:B2
III [86]	0.8,0.3	2.4	3	20Hz,25%ϕ:W
V [85]	1.5,0.8	2.5	3	1000Hz,75%ϕ:B1
V [85]	1.5,0.8	2.5	3	20Hz,25%ϕ:W
V [85]	1.5,0.8	1.6	3	1000Hz,75%ϕ:B1
V [86]	0.8,0.3	2.4	3	1000Hz,75%ϕ:B1
V [85]	0.8,0.3	2.5	3	5000Hz,25%ϕ:B2
V [85]	0.8,0.3	2.5	3	20Hz,25%ϕ:W
XIII[85]	0.8,0.3	2.5	3	500Hz,75%ϕ:B1

- Bipolar Pulse Reverse

Electrolyte [Figure No.]	Hole diameter (mm)	Board thickness (mm)	C.D. Adm^{-2}	Pulse reverse conditions $i_{p(c)}/i_{p(a)}$, $t_{on(c)}/t_{on(a)}$
I [86]	0.8,0.3	2.4	3	1/1, 10/0.2:B1
I [86]	0.8,0.3	2.4	3	1/3, 10/0.5:M
I [86]	0.8,0.3	2.4	3	1/3, 10/2:W
V [85]	1.5,0.8	2.5	3	1/3, 10/0.5:M
V [86]	0.8,0.3	2.4	3	1/1, 10/0.2:B1
V [86]	0.8,0.3	2.4	3	1/2, 10/0.2:M
V [86]	0.8,0.3	2.4	3	1/3, 10/0.2:M
V [86]	0.8,0.3	2.4	3	1/4, 10/0.2:M
V [86]	0.8,0.3	2.4	3	1/3, 10/2:W
V [86]	0.8,0.3	2.4	3	1/8, 10/0.2

Figure 109a shows the surface(S) to hole(H) ratio against hole diameter for electrolytes III and V using a board thickness of 1.6mm.

Figure 109b shows the S/H ratio versus different aspect ratios for electrolytes I, III and V for best and worst pulsing conditions using a board thickness of 2.5mm..

Figure 109c shows the S/H ratio versus average current density for electrolytes I and III under DC and also best pulse conditions using different hole sizes. The board thickness being 2.5mm.

Table 18 shows the S/H ratio for different conditions such as DC, unipolar pulse and bipolar pulse reverse using various holes and board thicknesses.

The optical micrographs of PCBs in cross-section can be seen in Figures 122, 123 and 124 for electrolytes I, III and V, respectively, showing the coating thickness distributions under DC and best unipolar pulse conditions for a board thickness of 2.5mm and hole diameter of 0.8mm.

As an alternative method for looking at the results, the Wagner number, duty cycle and frequecy values obtained for electrolytes I-IX were used in a computer modelling excercise in order to see whether these results can be interpreted differently and the unipolar pulse conditions optimised. The examination was carried out graphically, using Gino-surf on the mainframe computer, as a contour map or 2-D profile and also

as a 3-D profile. The 2-D profiles show the duty cycle against frequecncy for different Wagner number values and the 3-D profiles show the Wagner number, duty cycle and frequency against each other for electrolytes I-IX, see Appendix 3. The representation gave a good indication of optimum conditions for pulse plating. Unfortunately, the very limited plating tests carried out using these optimised conditions were inconclusive.

6.3 Assessment of Pulse Plated Electrodeposits

The pulse electrodeposits were assessed by morphological, property and surface coverage studies. For comparative purposes direct current was also examined. Tables 19 and 20 show the conditions for which the electroplating was carried out and also the results obtained.

The study of cathode efficiency for electrolytes I, VIII and V under DC and unipolar pulse conditions can be seen in Table 19.

Figures 110a and 110b show the hardness value versus frequency for different duty cycles and also under DC using electrolyte I and V, respectively. Figure 110c shows the hardness value against duty cycle for electrolyte I, VIII and V and also under DC. In general, they show that the hardness values decrease under pulse compared to DC using electrolytes I or V but increase for electrolyte(VIII) containing no chloride ion or additives.

Figures 111a and 111b show the roughness average(R_a) and also peak-to-peak roughness average(R_{tm}) against frequency and also under DC using electrolyte I and V, respectively. Figure 111c shows the roughness average and also peak-to-peak roughness average against duty cycles for electrolyte I, VIII and V and also under DC. The roughness values obtained under unipolar pulse tend to remain about the same as DC using electrolyte I, but the roughness is dependent on frequency and also duty cycle when using electrolyte VIII and V.

Figures 112a, 112b and 112c show the hardness value, tensile strength and elongation to fracture against the percentage of the original specimen thickness of cold rolled copper, (manufacturers product, see section 5.11 for details). This test is believed to be useful as a means for further comparison for DC, unipolar pulse and also bipolar pulse reverse regimes.

Figures 113a and 113b show the tensile strength against frequency for different duty cycles and also DC using electrolytes I and V, respectively. Figure 113c shows the combined figures mentioned above. They show that depending upon the frequency and duty cycle, the tensile strength can be higher, compared to DC, by using electrolytes V and I.

Figures 114a and 114b show the elongation against frequency for different duty cycles and also DC using electrolytes I and V, respectively. Figure 113c shows the combined figures mentioned above. The findings are similar to those of tensile strength.

Figures 115 and 116 show the tensile strength and elongation against different bipolar pulse reverse conditions, respectively, using electrolytes I and V. The conditions studied were at peak current density of cathodic/anodic ratios of 1/1, 1/2, 1/3 and 1/4 and cathodic/anodic on-time ratio of 10ms/0.2ms plus peak current density of cathodic/anodic ratio of 1/3 and cathodic/anodic on-time ratio of 10ms/0.5ms, as a means for comparison.

Figures 117 and 118 show the coating distribution of foils plated at $3.0Adm^{-2}$ for 37minutes under DC, unipolar pulse and bipolar pulse reverse using electrolytes I and V, respectively. The measurements were carried out using a 'flat' Micrometer. The unipolar pulse conditions were at frequencies of 20, 100, 500, 1000, 2000, 3000, 4000 and 5000Hz and also duty cycles of 25, 50 and 75%. The bipolar pulse reverse conditions were at peak current density of cathodic/anodic ratio of 1/1, 1/2, 1/3 and 1/4 and also cathodic/anodic on-time ratio of 10ms/0.2ms. Also for comparison, peak current density of cathodic/anodic ratio of 1/3 and cathodic/anodic on-time ratio of 10ms/0.5ms were studied.

The examination of coating thickness distribution was also carried out using a point Micrometer, see illustration in section 5.11.5. Figure 119 shows the coating thickness across the cathode width at top, middle, bottom, half way top-middle and half way bottom-middle areas of the copper foils under DC, unipolar pulse and bipolar pulse reverse using electrolyte I. Figure 120 shows the thickness distribution of the coating across the cathode width of copper foils under DC, unipolar pulse and bipolar pulse reverse using electrolyte V. The unipolar pulse examined was at a frequency of 2000Hz and a duty cycle of 75% and the bipolar pulse reverse examined was at a peak current density of cathodic/anodic ratio of 1/4 and cathodic/anodic on-time ratio of 10ms/0.2ms.

Figure 121 shows the surface appearance of the foils under bipolar pulse reverse in which the peak current density of cathode/anode ratio is plotted against cathodic/anodic on-time ratio. The peak current density of cathodic/anodic ratio and cathodic/anodic on time ratio examined were 1/1, 1/2, 1/3 and 1/4 and 10ms/0.2ms, 10ms/0.5ms, 10ms/1ms, 10ms/2mss, 20ms/0.5ms and 20ms/1ms, respectively. The appearance is described as lustrous indicating shiny deposits, semi-lustrous indicating a finish between shiny and matt coloured deposits, matt indicating orange coloured deposits, dull indicating red coloured deposits and burnt indicating brown coloured deposits.

Figures 125, 126 and 127 show the morphology of the plated deposits obtained under DC and different P conditions using electrolytes I, V and VIII, respectively. The micorgraphs under unipolar pulse conditions for electrolyte I are at frequencies of 20, 100, 500, 1000, 2000, 3000, 4000 and 5000Hz at duty cycles of 25, 50 and 75% and for electrolyte V are at a frequency of 20Hz and duty cycle of 25%. The micrographs under unipolar pulse conditions for electrolyte VIII are at a frequency of 100Hz and duty cycles of 25, 50 and 75%. The micrographs under DC conditions are for electrolytes I, V and VIII.

Figures 128 and 129 show the morphology of the electroplated deposits obtained under bipolar pulse reverse conditions using electrolytes I and V, respectively. The bipolar pulse reverse conditions examined are as follows:

Cathodic/anodic on-time ratio (ms/ms)	Peak current density of Cathodic/anodic on-time	Electrolyte [Figure No.]
10/0.5	1/3	I [126]
10/0.2	1/1,1/2,1/3,1/4	I [126]
10/0.5	1/1,1/2,1/3,1/4	V [127]
10/0.2	1/1,1/2,1/4	V [127]
10/1	1/1,1/2	V [127]
10/2	1/1,1/2	V [127]
20/0.5	1/2,1/3,1/4	V [127]
20/1	1/1,1/2,1/3	V [127]

CHAPTER 7

7.0 DISCUSSION

This chapter is described under three categories:

- standardisation: this includes the parameters such as conductivity, pretreatment, agitation and pulse behaviour.
- polarisation curves, Tafel slope and Wagner number: this includes the coating thickness distribution and metallurgical studies of PCBs.
- assessments of pulsed electrodeposits: this includes the morphological aspects, properties and surface appearances.

7.1 Standardisation

As explained earlier, the standardisation describes the conductivity, pretreatment, agitation methods and pulse behaviour. These were necessary in order to provide a reproducible and comparable result. However, though the literature on the above factors is limited, nevertheless, some comparative reasoning has been made where appropriate.

7.1.1 Solution conductivity

Solution conductivity is believed to be important in affecting the secondary current distribution which can be related to the throwing power of the electrolytes. The initial part of this research work was mainly concerned with examining the conductivity of different molarities of copper sulphate at various molarities of sulphuric acid.

The conductivity measurements obtained for different acid concentrations and different copper sulphate concentrations are shown in Table 6. Figure 43 also shows the graphical picture of the results such that the relationship between conductivity for different quantities of sulphuric acid concentrations (25, 50, 75, 100, 125, 150, 175, 200, 225 and 250 mll^{-1}) for different molarities of copper sulphate solution are plotted.

The conductivity is described as Scm^{-1} or $\Omega^{-1}cm^{-1}$. The curves obtained were parabolic such that as the concentration of the acid increased and the concentration of the copper sulphate decreased, the conductivity values increased sharply up to $150mll^{-1}$ of acid concentration, and then the profile increased and in some instances decreased very gradually.

As for the use of conductivity values for the study of throwing power in the following research work for different electrolytes and pulsing and direct current conditions, the same measuring techniques were used and will be explained in section 7.2.

7.1.2 Pretreatment assessments

In order to standardise and use the best pretreatment methods throughout the study, different pretreatments were used and assessed qualitatively. The eight pretreatments examined ranged from the use of standard nitric acid dip to alkaline cleaning and hand polishing. Full detail of these pretreatments are given in section 5.3. For the assessment, two different methods were used:

- use of polarisation curves(E-i curves);
- use of Hull cell technique; relative surface appearance or surface quality.

The electrolyte used for the examination was 0.3M $CuSO_4$, 2.25M H_2SO_4 and 50ppm Cl^-. For the polarisation studies, the potential was plotted against average current density showing the region of Tafel and limiting current density for different pretreatments, Figure 44a. For Hull cell examination, the pretreatments were plotted against the plating current density, Figure 44b. The surface appearances obtained by the Hull cell technique are described as; good deposit, indicating orange coloured deposits; Light burnt, indicating red coloured deposits, and heavy burnt, indicating brown coloured deposits.

However, amongst the pretreatments used, the polarisation curves and Hull cell studies showed that pretreatment 4 with alkaline cleaner and pretreatment 5 with alkaline cleaner, sulphuric acid and hydrogen peroxide are the best methods of sample preparation. This can be described by polarisation curves as the region of Tafel that the higher the Tafel slope the higher the throwing power[21] and by Hull cell technique as the best pretreatment provides a better range of good deposit. Pretreatment 5 was used throughout the study unless otherwise stated.

Another pretreatment method studied was on a stainless steel for producing foils for tensile strength and elongation measurements. This can be carried out in many ways, such as electropolishing, grinding and polishing, etc. Electropolishing of stainless steel can involve special and somewhat expensive types of solutions, therefore, grinding and polishing was favoured. The stainless steels were firstly ground to 1200grit size (Buehlers grinding strips) and then polished to a mirror finish with 6μm and 3μm diamond paste (Buehlers polishing paste). It was found that polishing down to 1μm causes a reduction in adherence of the deposit after 5-10 hours of plating. It is to be noted that the grinding must be carried out by hand otherwise the scratches resulting from grinding by machine could be deep, and hence affect the tensile strength and also the elongation values. For morphological studies, this could cause an uneven deposit making the structural studies meaningless.

7.1.3 Hull cell results

The Hull cell studies were undertaken in order to examine the surface appearances resulting from different additives. The electrolyte constituents used are described in detail in section 5.4. The electrolytes studied were plotted against the plating current density for without and with air agitation, Figures 45a and 45b, respectively. The surface appearances obtained are described as bright finish indicating shiny deposits, semi-bright finish indicating a finish in between shiny gold to orange coloured deposits, matt deposit indicating orange coloured deposits, light burnt indicating red coloured deposits and heavy burnt indicating brown coloured deposits.

This study was necessary for comparative studies, in order to see whether the additives produce a bright or lustrous deposit such that in an ideal situation it would be an achievement to obtain such deposit appearances under pulse plating especially for printed circuit boards.

However, amongst the electrolytes used, the electrolyte V with constituents of 0.3M $CuSO_4$, 2.25M H_2SO_4, 50ppm Cl^-, 1g/l C140, 0.625mg/l DS4 and 6.25mg/l N1 produced a fully bright deposit with air agitation but without air sparging, the region of bright deposit is extremely small. Comparatively other electrolytes produce matt deposits with agitation, but without any agitation, they are somewhat variable in deposit appearance ranging from semi-bright to heavy burnt, Figures 45a and 45b.

7.1.4 Effects of agitation

As explained in section 5.8, agitation can have beneficial effects in plating industries. For example, in printed circuit board industries, agitation is used to transport metal ions into the holes of the PCBs in order to plate uniformly. Also, for good electrical continuity small grains are preferred, which from a morphological point of view, can lead to an increase in hardness and hence tensile strength.

There are many different agitation techniques which are available but very little is published to date. The effects of agitation are described extensively, in section 2.3.2, in terms of its importance and mass transfer behaviour, a common example being the improvement in throwing power in recesses[49].

However, studies by Haak et al [33] on air agitation is the only known published work available for PCBs and the importance of air sparging and the design of pipe work is clearly stressed. However, other forms of agitations such as forced-flow [27], jetting [3], reciprocating [33] and vibratory [47-49] are also known and used in many industrial applications. But reciprocating and air agitation combined have commonly been used for plating of PCBs. Nevertheless, vibratory agitation has been under study for many years at Loughborough by Johal, Kalantary, Amadi and Gabe [47-49], see Appendix 4, and the most recent unpublished work by Amadi [132] confirms the importance and benefits of vibratory and/or air agitation for PCB industries and its improvements in terms of throwing power in through-holes has been described in detail. Therefore, the importance of agitation can be significant in electroplating.

However, various agitation methods were used with different electrolytes and also under different temperatures. The electrolyte solutions were:

Solution A: 0.3M $CuSO_4$, 2.25M 98%H_2SO_4, 50ppm Cl^-

Solution B: 0.015M $CuSO_4$, 0.5M 98%H_2SO_4

and the temperatures used were 21°C and 50°C.

The study of different modes of agitation have provided some interesting results. Table 7a shows the agitation types and the limiting current densities obtained from the polarisation curves is reported. The agitation types were reciprocating cathode agitation, slight air agitation (pumping rates of 3litres/min.), extensive air agitation (pumping rate of 8litres/min.), magnetic stirring agitation at various rotation speeds of 5-8 (arbitrary units). Furthermore, reciprocating agitation was used in conjunction with all other agitation modes. For comparison of agitation modes, polarisation studies

were carried out. From the polarisation curves the limiting current density values were obtained at an overpotential of -0.40V and -0.37V for solutions A and B, respectively. Also, the limiting current densities were compared to that of DC. From that the enhancement factors(E.F.) were calculated, Table 7b.

The results, Table 7a, show that with increasing temperature from 21°C to 50°C the limiting current densities increased, but the limiting current densities decreased with decreasing electrolyte concentration. The increase in temperature has an inconsistent effect on E.F. values using electrolyte A, Table 7b. The effect is even more extensive at lower electrolyte(B) concentration.

However, as for printed circuit boards, the use of magnetic stirrer agitation is not viable since it is believed that it does not have a significant effect, comparable to air sparging, in transporting metal ions in small through-holes, therefore, air agitation was studied at different sparging rates. The air sparging rates were varied in settings, ranging from 2-6, Figure 47a; 2- being slight (4.5 litres/min.) and 6- being extensive (8.0 litres/min.) agitation rates. Also, reciprocating agitation was used in conjunction with different air sparging rates. For comparative purposes, the agitation rates were compared by plating on AISI 304 stainless steel strips having width x length of 5cm x 30cm. The cathode length was important in order to study the coating thickness distribution resulting from different agitation rates since the best uniformity is dependent upon the adequate agitation conditions. Figure 48 shows the air agitation 'rig' designed for use in this research work. However, the coating thicknesses obtained were measured by x-ray fluorescence(XRF) technique at intervals of 3cm, relative, and comparable to the height of the tank, Figure 47b.

It was found that air sparging with an air flow rate of 4.5 litres/min. combined with reciprocating cathode provides the best uniformity of plating within the tank compared to other agitation conditions examined, Figure 47b.

7.1.5 Pulse electronic behaviour

In order to distinguish the effects of different pulse conditions, it was decided that polarisation studies should be carried out and the Tafel slopes for different electrolytes should be calculated, section 5.10. For this reason, a potentiostat was originally used in either galvanostatic or potentiostatic mode. Polarisation studies were carried out using a pulse unit and a potentiostat which were switched on separately or together.

The polarisation studies were carried out using the electrolyte I (0.3M $CuSO_4$, 2.25M H_2SO_4 and 50ppm Cl^-) without any agitation mode.

The pulse electronic behaviour studied showed that the electronics within the pulse unit and the potentiostat have an effect on the result. Figure 49a shows the experimental arrangement used for the study in which a sweep unit was connected to a potentiostat and the cell via a pulse unit. The Figure below describe the systematic studies carried out:

- Figure 49b shows the polarisation curve obtained using a pulse unit and a potentiostat. The polarisation curve was carried out potentiodynamically and the pulse unit was set at a frequency of 50Hz and a duty cycle of 99%, which in effect is DC. The sweep rate used was 150mV/minute.
- Figure 49c shows the polarisation curve obtained using a pulse unit and a potentiostat arranged to run potentiodynamically. The potentiostat was switched on with a second gap to that of pulse unit. The electrolyte, sweep unit and the chart recorder conditions remained the same as above, except the duty cycle was reduced to 50%.
- Figure 49d shows the polarisation curve obtained when both potentiostat and pulse unit were switched on together. The conditions remained the same as Figure 49c.
- Figure 49e shows the results obtained under the same conditions as 49d, in order to check the reproducibility of the curve.
- Figure 49f shows the polarisation curve obtained when the pulse unit was switched on a second later to that of potentiostat. The conditions remain the same as Figure 49c.

From the polarisation curves produced it can be seen that the pulse unit and the potentiostat function as expected, when set to DC, Figure 49b, but as the pulsing conditions is set to duty cycle of 50%, Figure 49c, the polarisation curves became very irregular indicating that the potentiostat is not appropriate for this study. It was found that the polarisation curves are not even reproducible when tests are repeated, Figures 49d and 49e. It was understood that this peculiarity is due to incompatibility of both the pulse unit and the potentiostat in terms of circuitry and the electronics within the units.

To explain this further by taking an example; Figure 49f shows when the pulse unit was switched on a few seconds after the potentiostat and then sweeped. The curve obtained gave a clear indication that the electronics possibly in the pulse unit are

affected. It can be noted that because the sweeping is carried out potentiodynamically, the switching off within the pulse unit causes spikes to be generated. This spike is generated as a surge of the potentiostat which formed on the polarisation curves. The so-called surge is due to the fact that the potentiostat is not designed for such pulsing conditions and hence tries to adjust the potential of the system to the correct level. Furthermore, the use of potentiostat in galvanostatic mode produced the same sort of patterns. Therefore, it can be concluded that it is not feasible to use a Thomson ministat potentiostat with this type of experimental arrangement.

Further studies also confirmed the same point. These studies involved using a pulse unit and different methods of sweeping, that is, using a potentiostat in step-wise fashion and/or using it in conjunction with a power supply at either constant current or potential mode, Figures 50-53. In other words, the studies carried out were:

- using the potentiostat either step-potential or step-current, Figure 50.
- using the potentiostat and a power supply (constant voltage or constant potential), both connected to the same anode, Figure 51.
- using the potentiostat and a power supply (constant voltage or constant potential), each connected to a separate anode, Figure 52.
- using a power supply in step-wise fashion, that is, either at constant potential or constant current, Figure 53.

The polarization curves obtained using the pulse unit, the power supply and the potentiostat showed very peculiar patterns. As has already been mentioned, using a potentiostat (Figure 49a) as a means of power source with the pulse unit has its own problems. Results obtained using the potentiostat (step-wise method), Figure 51 also indicated some meaningless results as before. Use of potentiostat and power supply connected to the same anodes (Figure 52) or each to a separate anode (Figure 53) indicated the same effects. The tests were repeated many times but the patterns were mostly peculiar, even the oscilloscope gave no sensible patterns. It was noted that the potentiostat became hot due to overloading.

The polarisation studies showed that using the potentiostat in any mode is not feasible since it did not produce a reproducible result. However, the use of pulse unit with a power supply in either constant current or constant potential mode produced meaningful and reproducible results comparable to DC conditions. The oscilloscope pulse wave patterns using a power supply and the pulse unit were also shown to be very clear unlike the potentiostat and pulse unit patterns. The oscilloscope patterns were similar to the patterns obtained by other authors [1,67]. Therefore, the polarisation

studies were carried out using this arrangement, Figure 53, throughout the experimental work for both unipolar pulse and bipolar pulse reverse.

7.1.6 Comparative study of different power sources

In order to prove that different modes are reliable and can provide a similar result, various sweeping methods were examined under DC conditions. The power sources were a potentiostat, which was operated potentiodynamically and also galvanodynamically, and a power supply which was operated at a constant potential and also in a constant current mode. Figure 54a shows the experimental arrangement used. The polarisation curves were obtained using 0.3M $CuSO_4$, 2.25M H_2SO_4 and 50ppm Cl^-. Figures 54b and 54c show the polarisation curves obtained under the conditions specified above and plotted as both linear and logarithmic, respectively. The curves were obtained in a still solution. The results obtained showed that the limiting current density values are almost unchanged, indicating a good correlation between the four polarising techniques, as expected. Therefore, for pulsing techniques it can be said that the use of power supply is as good as sweeping with a potentiostat, in an ideal situation.

7.1.7 Behaviour of pulse parameters

The effects of pulsing were also examined in this research programme, using a cathode size of $1dm^{-2}$. The measurements were carried out at an initial input current equivalent to direct current of 1A for the study of average current density and potential for different duty cycles. Figure 57a shows the effect of average current density and its relative potential for different duty cycles. Further measurements were undertaken at a constant input current of 1A for the study of peak current density and potential for different duty cycles. Figure 57b shows the effect of peak current density and its relative potential against duty cycle. The agitations used were air sparging combined with cathode reciprocation using electrolyte V. It can be seen that the average current density values decrease linearly as the duty cycles increase, but the cell potentials increase linearly with peak current density values decreasing exponentially. The results are as expected following the formulation for average current density such that:

$$i_{av} = i_p \times \phi$$

where i_{av}= average current density, Adm^{-2}

i_p= peak current density, Adm^{-2}

ϕ= duty cycle, %

This trend also indicates further that the power supply is compatible to be used in conjunction with the pulse unit. Furthermore, the profile remains the same for different input currents and cathode size.

7.2 Polarisation, Tafel and Wagner Number Studies

The use of polarisation curves in pulse plating of copper has not been studied as extensively as in this research work, with the exception of Pearson and Dennis [2]. They have studied the effect of additives using bipolar pulse reverse. Nevertheless, the combination of unipolar pulse (P) conditions and also bipolar pulse reverse (PR) conditions are more extensive than any previously reported research work. A current example of unpublished research work can also be seen in Appendix 5 [133].

However, polarisation studies for unipolar pulse were carried out using thirteen electrolytes(I-XIII), each having different additive constituents and also some at different temperatures, see Appendix 1. The pulse frequencies used are 20, 500, 1000, 2000 and 5000Hz with duty cycles of 25, 50 and 75%. The choice of these conditions has been explained in section 5.9. The agitation modes used were air sparging and cathode reciprocation combined. These pulse conditions have been compared to direct current using the electrolytes I-XIII for different agitation modes of still or natural convection, reciprocating cathode and air sparging combined with reciprocating cathode.

The polarisation curves(E-i) were used to calculate potential against logrithmic converted current density. From that the Tafel slopes were calculated using Goodenough and Whitlaw's [21] theory. It was found that this method was useful in determining the throwing power of the electrolytes under specific conditions. The Tafel slope values were used to calculate the Wagner number and from that an enhancement Wagner ratio was derived for each pulsing conditions, see section 5.10.

As for bipolar pulse reverse the same method was applied using different combinations of conditions but limiting the number of electrolytes to only two(I and V). The important parameters were changed systematically with cathodic/anodic peak current density ratios($i_{p(c)}/i_{p(a)}$) of 1/1, 1/2, 1/3 and 1/4 and cathodic/anodic on-time

ratios($t_{on(c)}/t_{on(a)}$) of 10/0.2, 10/0.5, 10/1, 10/2 plus 20/0.5 for only $i_{p(c)}/i_{p(a)}$ of 1/1 plus 20/1 for only $i_{p(c)}/i_{p(a)}$ of 1/1 and 1/2. The limit on the choice of the conditions were dependent upon the polarisation curves obtained and also the voltage which the power source could supply. (Note: on-times are in milliseconds).

7.2.1 Direct current

For examination and assessment, the results obtained from the Figures 58a-70a were tabulated. Table 8a shows the limiting current densities(i_L) obtained for electrolytes I-XIII. The i_L values simply give an indication, where the rate of deposition is limited by the diffusion of metal ion, that is, where the mass transfer is obeyed. In plating industries, electroplating is carried out at about 1/3 to 1/4 of i_L values. It can be seen clearly, Table 8a, that the limiting current density values increased as the agitation becomes more extensive. For example, using electrolyte I and comparing still solution to that of air sparging and reciprocating cathode(A&R) combined, the limiting current density increased from 1.5Adm^{-2} to 8.25Adm^{-2}. This clearly indicates that the A&R is the ideal agitation to be used for the polarisation studies, as explained in section 7.1.4. However, comparing the results for different electrolytes it can be seen that depending upon the additives and temperatures, the i_L values increase or decrease. The range of i_L value is 4.39Adm^{-2} for electrolyte XI and 9.34Adm^{-2} for electrolyte X. The polarisation curves show this mass transfer behaviour clearly, Figures 58a-70a.

The Tafel slope values obtained from the potential-logarithmic converted current density values also show that the change in slope values for different types of agitation are quite dramatic and do not follow the i_L values obtained, Table 9a. These variations depend upon the electrolyte, temperature and also agitation type. Figures 58b-70b show the changes graphically for each individual electrolytes. To differentiate these changes, Table 10a shows the Tafel slope values for the three agitation modes and different electrolyte. The best to worst slope values are also defined. It can be seen that the Tafel slope values under A&R agitation modes are less in comparison to other modes. This could be explained by the fact that under natural convection and also reciprocating cathode action, the mass transfer does not fully take place because the agitation rate is small in comparison to that of air sparging and cathode reciprocation combined. However, it is an area which has been very little researched and reported up to now; nevertheless, it is a good comparison for initial studies. It can be further added

that probably, the best comparison to A&R agitation would be the use of other agitation modes such as vibratory, jetting, rotating discs, etc which are believed to have a more uniform mass transfer behaviour.

The Wagner number values were calculated using the Tafel slope values for different current densities, taking into account the conductivity of each electrolyte and the characteristic length of the cathode to reference electrodes. The relationship between Tafel slope and Wagner number values for each electrolyte is proportional but in comparison to other electrolytes is not the same because the conductivity of the electrolytes differed slightly during each make up. It could be said that the Wagner number values give a better indication of throwing power than Tafel slope.

The calculated Wagner number values obtained at $2.0Adm^{-2}$ are shown in Table 11a. The Wagner Number values under A&R agitation modes were used for comparative studies to that of unipolar pulse and bipolar pulse reverse conditions. The Wagner number values obtained under A&R ranged from 0.203-0.333. As explained previously, this agitation mode was used throughout the study because it provides a better electrolyte mixing for through-hole plating. The current density-Wagner number curves obtained can be seen in Figures 58c-70c. The Wagner number values were calculated from $0.5\text{-}3.0Adm^{-2}$ and it can be seen that the Wagner number values are higher at lower current densities indicating a better throwing power, ideal for recesses. But it must be noted that in electroplating industries cost is very important and, therefore, the lower current densities are not always preferred. In other words, a current density of $3.0Adm^{-2}$ is normal but it is known that a current density of $0.5Adm^{-2}$ is used for plating of small through-holes under DC conditions.

7.2.2 Unipolar pulse

The unipolar pulse conditions were used at different frequencies of 20, 500, 1000, 2000 and 5000Hz and also at various duty cycles of 25, 50 and 75%. The electrolytes and temperatures used are specified in Appendix 1. The agitation mode was A&R.

The polarisation curves obtained and the limiting current densities(i_L) were calculated similarly to that of DC conditions. Table 8b shows the i_L values obtained for different pulse conditions and also electrolyte constituents, except in some cases the i_L values were obtained at a arbitrary pulse condition and used as an average i_L for the

calculation of the logarithmic converted current densities. It can be seen that the i_L values under pulse condition, Table 8b, can either increase or decrease compared to DC, Table 8a, but in the majority of instances an increase in i_L values are observed. This is clearly an indication that pulsing can have a beneficial effect on electroplating processes whereby, plating can be carried out at higher current density under unipolar pulse condition to that of DC in order to obtain the same deposition thickness in lesser time.

The average i_L values ranged from 3.93 to 12.02Adm^{-2}. Figures 71a-83a show the polarisation curves obtained and the scatter of the results can be seen clearly on each figure. All the data obtained is plotted in order to observe the scatter of the results produced under various pulsing conditions for each particular electrolyte. It is to be noted that these results are also reproducible under conditions specified in this research programme.

The Tafel slope values were calculated in the same manner as for DC. Table 9b shows the Tafel slope values for different unipolar pulse conditions and different electrolytes. For comparative purposes, Table 10b shows the worst and three best pulse conditions obtained for each electrolyte. It can be seen that the worst and best Tafel slope value in the majority of cases is 20Hz, 25% and 5000Hz, 50% or 75%, respectively. In other words, the worst conditions are at low frequencies and low duty cycles and the best conditions are at high frequencies and high duty cycles. Figures 71b-83b show the potential-logarithmic converted current density curves obtained for different electrolytes. As in DC, the changes in slopes can be seen very clearly. Once again, the scatter of the results is shown for information only.

The calculated Wagner number values for different current densities were also calculated using the standard method described earlier, section 7.2.1. Figures 71c-83c show the current density against Wagner number for different electrolytes. It can be stated that the best throwing power is when the Wagner number value is high. For example, Figure 71c shows current density versus Wagner number; the further the exponential curves move to the right the better is the throwing power at a particular current density of 2.0Adm^{-2}, the best pulsing condition can be seen to be 5000Hz, 50%ϕ and the worst pulsing condition is 20Hz, 25%ϕ. These best and worst Tafel slopes can also be seen in Figure 71b.

However, Table 11b shows the tabulated results obtained at 2.0Adm^{-2} for different unipolar pulse conditions and various electrolytes. Since the number of experiments

carried out were vast and comparability is difficult, an enhancement Wagner number ratio (RWa) was defined such that:

$$R_{Wa} = \frac{\text{Pulse Wagner Number } (Wa_p)}{\text{DC Wagner Number } (Wa_{DC})}$$

That is, if RWa=1, then the pulse condition is similar to that of DC but if RWa<1 then the pulse condition is worse than DC. If RWa>1, then the pulse condition is better than DC. Furthermore, the higher the RWa, the better the throwing power.

The results obtained using RWa<1 and RWa >1 can be seen in Tables 12a and 12b, respectively. As already explained the RWa provides the same information as Wagner number since they are related to each other, but it makes the differentiation between good and bad pulse conditions easier. The RWa obtained under pulse condition for worst and best conditions ranges from 0.372-1.79 indicating that pulsing can produce an enhancement ratio of 0.37 times worse or 1.79 times better 'throwing power' than DC.

The results obtained were used to plot RWa against different electrolytes, Figure 84. The information in the graph was used to define conditions for plating of printed circuit boards with different aspect ratios.

The electrolytes found to be most favourable were I, III and V and XIII. The electrolyte I was used as a base for comparison since no additives were present and also RWa was found to be high. Electrolyte III contained only two additives of C140 and N1, see Appendix 2, and also provided the highest RWa at certain pulse conditions. The electrolyte V was also studied because it contained all the additives and has been recommended by the manufacturer-LeaRonal. Furthermore, the RWa values were fairly high under certain pulse conditions. The electrolyte XIII was used because it provided the third highest RWa under specific pulse condition and low temperature (10°C).

The conditions used for plating have been explained in detail in sections 5.10.2 and 6.2.2 and Table 18 shows the conditions used very clearly. A discussion on the assessment of the plated printed circuit boards can be seen in section 7.2.5.

7.2.3 Bipolar pulse reverse

The polarisation studies for bipolar pulse reverse were carried out using electrolytes I and V. The electrolyte I being chosen as a base comparison to that of V which contained all additives of C140, DS4 and N1, see Appendix 1 and 2.

The parameters studied have been altered systematically as explained in section 7.3, for different cathodic/anodic peak current density ratios($i_{p(c)}/i_{p(a)}$) and also various cathodic/anodic on-time ratios($t_{on(c)}/t_{on(a)}$). The polarisation curves were carried out until the limiting regions were reached, except in some cases where the power source could not supply sufficient volts during the reverse pulse (or negative cycle). Figures 85a-90a and 95a-100a show the potential-average current density curves obtained for electrolytes I and V, respectively, under the bipolar pulse reverse conditions specified. The limit on the pulse conditions were dependent on two factors:

- the capability of power sources
- the cost effectiveness of producing pulses for industrial uses

These are important since on an industrial scale large power supplies are expensive and the cost effectiveness of using pulse to that of DC would be very little as can be seen later from the results obtained.

However, Table 13 shows the limiting current density values for the two electrolytes. In order to be systematic in calculating the logarithmic converted current densities, an average current density for each on-time ratio was calculated. It can be seen that the limiting current density value for electrolyte I is higher than electrolyte V containing all additives. Pearson and Dennis[2] explained this behaviour in their study in which C140, a polyethylene glycol additive, caused the deposition potentials to increase for a given current density compared to the corresponding deposition potential in the absence of this additive; this is explained to be due to the surface blocking caused by the adsorption of the polyethylene on the cathode surface. Furthermore, C140 causes a shift in rest potential to a more negative value and also causes the exchange current density to reduce. Effects of other additives have also been explained in sections 4.2 and 7.2.6 in more detail.

Figures 85b-90b and 95b-100b show the potential-logarithmic converted current density curves obtained for electrolytes I and V, respectively, under the pulse conditions specified. Table 14 shows the Tafel slope values obtained for both electrolytes. The Tafel slope values obtained for electrolytes V are smaller than electrolyte I. This was expected as explained earlier, due to the shift in potential

resulting from the additives. The manufacturers of the additive (LeaRonal) have also pointed out that under bipolar pulse reverse the additive replenishment may need to be increased, because during plating some of the additives plate out or become absorbed in the deposits and during the negative cycle some may be decomposed and will dissolve back into the electrolyte and lose their effect. However, no evidence of that has been observed.

The Wagner number values were also calculated, Table 15, in the manner explained earlier using the Tafel slope values, conductivity of the electrolytes and characteristic length. Figures 91-94 show the current density-Wagner number for electrolyte I and Figures 101-104 show the current density-Wagner number for electrolyte V. The results obtained under pulse reverse have been shown to be systematic such that the cathodic/anodic on-times are the controlling factors in Wagner number values for each sets of cathodic/anodic peak current densities. For example, Figure 91 shows the current density-Wagner number for electrolyte I and cathodic/anodic peak current density of 1/1; the Wagner number increases from low to high gradually at a particular current density relative to the cathodic/anodic on-times of 10/2, 10/1, 20/1, 10/0.5, 20/0.5 and 10/0.2. This applies for almost all the peak current density ratios. The explanation for this lies with the on-time ratios such that as the cathodic on-time increases relative to the anodic on-time or anodic on-time decreases relative to cathodic on-time then the condition becomes almost similar to that of bipolar pulse and it was found that the Wagner number value increases. It can also be seen that the smaller the anodic on-time the higher the Wagner value, ie. 10/0.2 (Wa=0.609) and 10/0.5 (Wa=0.461) for electrolyte I and cathodic/ anodic peak current density of 1/1.

The other aspect is the effect of cathodic/anodic peak current density ratios; these have a major effect on the Wagner number values and from the results obtained no easy and systematic conclusions can be made on their effects compared to on-time ratios but it can be deduced from Table 15 that peak current density plays a key role on the Wagner number values or the throwing power. However, in comparison, it can be seen that the relative position of different peak current densities are affected depending upon the electrolyte constituents (Table 15).

For further comparison of the changes, the enhancement Wagner number ratio was defined as:

$$R_{Wa} = \frac{\text{Pulse reverse Wagner number}(Wa_{PR})}{\text{DC Wagner number}(Wa_{DC})}$$

Table 16 shows RWa values for different cathodic peak current density and on-time

ratios for both electrolytes. As Wagner number values indicate, the RWa for electrolyte I is higher than electrolyte V and also the RWa for electrolyte I is >1 or >DC in all the bipolar pulse reverse conditions used. But for electrolyte V two bands were obtained, indicating that using electrolytes with additives can also produce results worse than that of DC. This has again been explained earlier and is not surprising. Comparing the results obtained for unipolar pulse to that of bipolar pulse reverse for electrolyte I, Tables 12 and 16, it can be seen that pulse reverse can produce a better Wagner number or throwing power under certain conditions. For example, for unipolar pulse the maximum RWa= 1.79 at 5000Hz,50%ϕ and for bipolar pulse reverse the maximum RWa= 2.83 at cathodic/anodic on-time and peak current density of 10/0.2 and 1/1, respectively. However, the deposit structures are nodular-like under pulse reverse compared to long columnar growth of DC. In comparison to that of electrolyte V, the increase in throwing power is not as pronounced, see Tables 12 and 16.

The RWa was used to differentiate the changes and the plating was carried out on PCBs under different conditions, see sections 5.10.3 and 6.2.3 for more detail. Table 18 shows the pulse reverse conditions and also aspect ratios used in more detail. A discussion on the assessment of the plated printed circuit boards can be seen in section 7.2.5.

7.2.4 Optimisation of chloride ions under DC and pulsing

In this study, different concentrations of chloride ion were examined. The base electrolyte used was 0.3M $CuSO_4$, 2.25M H_2SO_4. The chloride ion concentrations ranged from 0, 25, 50, 75, 100, 150 to 200ppm. The polarisation curves were obtained under DC and unipolar pulse conditions of 100Hz and 50%ϕ at room temperature. The pulse condition used was chosen arbitrarily. The agitations used were reciprocating cathode and air sparging combined. The experimental arrangement used can be seen in Figures 54a for DC and 55 for unipolar pulse.

The polarisation measurements obtained for both DC and unipolar pulse were carried out exactly as explained in sections 7.2.1 and 7.2.2, respectively. Figures 105a and 106a show the potential-average current density curves obtained for different concentrations of chloride ions(Cl^-). They show that in the absence of Cl^-, the limiting current density is highest for both DC and unipolar pulse conditions, Table 17a, but the limiting current densities increases or decreases depending upon the Cl^- concentration

with fairly systematic changes under DC and also unipolar pulse conditions. This was described by Goodenough and Whitlaw [21] that Cl^- cause the potential to polarise or depolarise under relavent conditions used.

However, the limiting current density values were used to calculate the logarithmic converted current density. Figures 105b and 106b show potential-logarithmic converted current density curves. The Tafel slope values obtained from the curves can be seen in Table 17b. The slope values obtained are low for electrolytes without additives indicating that the Cl^- causes the slope of the Tafel to polarise for a particular potential. This finding has also been observed by Pearson and Dennis [2]. The highest Tafel slope value was found to be at a Cl^- concentration of 50ppm for both DC and unipolar pulse conditions.

The Tafel slope values were also used to calculate the Wagner number values for different current densities. Figures 105c and 106c show the current density-Wagner number curves. They also confirm that the best Wagner number is obtained when the Cl^- concentration is at 50ppm, Table 17c. However, the limit of Cl^- concentrations satisfies the information given by LeaRonal that the best concentration for use in additive electrolytes is also 50ppm. Nevertheless, the finding by Pearson and Dennis[2] confirms the use of the same concentrations in their studies and further indicated that the optimum concentration of Cl^- is 60ppm for bipolar pulse reverse. In this research programme, the concentration of Cl^- in some of the electrolytes used was 50ppm. Finally, it can be summed up that Cl^- is necessary in the electrolyte solutions, also see section 7.2.6, especially when certain types of additive are present.

7.2.5 Assessment of plated PCBs under unipolar pulse and bipolar pulse reverse to DC

The assessment of different pulse conditions whether unipolar pulse(P) or bipolar pulse reverse(PR) was carried out using printed circuit boards with various aspect ratios.

The plating of PCBs were carried out under several different conditions. For P, the best and worst conditions were chosen relative to the RWa values for electrolytes I, III, V and XIII. For PR, best(B1), second best(B2), middle(M) and worst(W) conditions were chosen relative to the RWa values for electrolytes I and V. For further comparison, DC plating was also carried out on PCBs with different aspect ratios and

current densities using electrolytes I, III and V. A detailed account of these conditions can be seen in section 6.2.5.

In order to assess the coating thickness distribution of each plated PCB for the chosen electrolytes and pulse conditions, the results were drawn pictorially, Figures 107 and 108. Originally, the plating was carried out on two different board thicknesses of 2.5mm and 1.6mm with hole diameters of 1.5mm, 0.8mm for electrolytes I, III and V. The results obtained, Figure 107, have shown that using electrolyte I under best P condition of 5000Hz and 50%ϕ at 4.0Adm^{-2}, the thickness distribution of deposited copper is more uniform to that of DC at 3.0Adm^{-2} and furthermore, the thickness distribution becomes better as the plating current density decreases. The results show that the surface(S)/hole(H) ratio of DC to that of P have changed from 1.47:1 to 0.99:1 and from 1.51:1 to 1.08:1 for hole diameters of 1.5mm and 0.8mm, respectively, for the same board thickness of 2.5mm. However, comparing DC to that of worst P condition(20Hz,25%ϕ), the results were better depending upon the current density used. The best result for worst P condition was found to be at a current density of 0.5Adm^{-2}.

Using electrolyte III, containing C140 and N1 additives, the S/H ratio under DC was better than electrolyte I. Under P condition the S/H ratio of electrolyte III is worst at higher current densities compared to electrolyte I, Figure 107.

Use of electrolyte V, containing all additives of C140, DS4 and N1, shows that under DC conditions the S/H ratio is better than that of electrolyte I but the S/H ratios obtained under P condition(1000Hz,75%ϕ) are worse than that of DC for the electrolyte V. The S/H ratios obtained for P for hole diameters of 1.5mm and 0.8mm and board thickness of 2.5mm are 1.36:1 and 1.78:1, respectively, compared to DC of 1.30:1 and 1.42:1, respectively, Figure 107. The results become better as the aspect ratios decrease, for example S/H ratios were 1:1 for both 1.5mm and 0.8mm diameter hole with board thickness of 1.6mm at P condition of 1000Hz,75%ϕ. However, under worst unipolar pulse condition(20Hz,25%), the S/H ratio is better than DC. It can therefore be stated that unipolar pulse can be better than DC under certain conditions.

The optical micrographs relating to some of the results can be seen in Figures 122, 123 and 124 for electrolytes I, III and V, respectively, showing the coating thickness distributions under DC and best and worst P conditions for a board thickness of 2.5mm and hole diameter of 0.8mm. These micrographs show the behaviour of pulsing to be the same. However, optical micrographs are used here as a representation and proof,

indicating the presence of the coatings and its uniformity; Figure 107 shows a more detailed account of the coating thickness distributions.

For further comparisons, S/H ratio was plotted against different hole diameters, Figure 109a, and it can be seen that electrolyte V is better than electrolyte III under best P conditions. In comparison to electrolyte I, S/H ratio was plotted against aspect ratio, Figure 109b, under best and worst P conditions, it can be seen that the S/H ratio for electrolyte I is better than III is better than V under best P conditions and S/H ratio for electrolyte V is better than I and better than III under worst P conditions for a particular aspect ratio. The results follow almost the same trend as the aspect ratio increases, Figure 109b. In order to compare the results obtained for electrolyte I and III under P to DC for the same electrolytes, Figure 109c, S/H ratio was plotted against average current density and it can be seen that in all cases the P provides a better S/H ratio to that of DC. Furthermore, the S/H ratio improved as the current density decreased.

It should be borne in mind that despite the fact that electrolyte I provides a better result than that of DC in printed circuit through-holes, a good continuity of deposit with small grain is the best. It is understood from the sponsoring company (LeaRonal) that electrolyte V produces a much finer grain to that of I, this has also been proved and shown in section 7.3.7. For this reason, electrolyte V is more preferable to any of the other electrolytes mentioned in this section, nevertheless, it is the pulsing condition which is the most critical part of this study, and further studies have shown the improvements and further confirmations on the reproducibility of the findings.

Figure 108 shows the cross-section of the PCBs obtained using electrolyte I, III, V and XIII for board thickness of 2.4mm and hole diameters of 0.8mm and 0.3mm. The electroplating was carried out at an average current density of $3.0Adm^{-2}$. The conditions and coating thickness distribution are shown clearly. It must be noted that the plating was carried out for 37minutes in order to obtain an overall coating thickness of 20μm. The results are interesting in terms of uniformity of the coatings, such that electrolytes containing additives, ie. V and XIII, the coating thickness distributions are closer to 25μm to that of electrolyte I. This clearly indicates that electrolyte I may provide a better S/H ratio compared to others but the amount of deposit in the holes is less than on the surface of the PCBs, indicating that the majority of the deposition takes place on the surface of the cathodes. From an economical point of view, electrolyte I can be ignored. However, this was expected since the sponsored company has pointed this out, also the results obtained for the Wagner number or throwing power studies were carried out on flat sheets. Therefore, design of electrode ought to be considered

but this is clearly another research project.

However, the electrolyte I can still be used for comparison with other conditions and electrolytes. It can be seen that under best P condition(5000Hz,50%ϕ), the S/H ratio becomes better for electrolyte I, and also under the worst P condition (20Hz,25%ϕ), the S/H ratio is best at higher aspect ratio compared to DC, confirming the earlier results mentioned above, Figure 108. The results of PR for electrolyte I have shown that the S/H ratio can become much better than DC and P; for example at $t_{on(c)}/t_{on(a)}$ and $i_{p(c)}/i_{p(a)}$ of 10/0.2 and 1/3, respectively, the S/H ratio for hole diameters of 0.8mm and 0.3mm, with board thickness of 2.4mm, are 1.03:1 and 1.09:1, respectively, compared to 1.31:1 and 1.35:1, respectively, for DC condition. The explanation lies with the fact that during the negative cycle the coating at the edges will dissolve in the electrolyte and allow the metal ion replenishment in and around the hole to take place, this concept has been known theoretically (1) and also practically (2,76,129).

The results obtained for electrolyte III were examined for two best P conditions (B1:1000Hz,75%ϕ and B2:5000Hz,25%ϕ) and one worst condition (20Hz,25%ϕ). It was found, as explained earlier, that the S/H ratio for B1 was not as good as DC but the S/H ratio of B2 is much better than DC and for the worst conditions the S/H ratio remains worst of all for these aspect ratio. It indicated that the right choice of P can produce better S/H ratio than DC. The electrolyte III is better than I due to the fact that it contains a suppressing agent which causes less edge build-up in and around the holes.

The coating thickness distributions obtained for electrolyte V were examined for two best P conditions (B1:1000Hz,75%ϕ and B2:5000Hz,25%ϕ) and one worst condition (20Hz,25%ϕ). It was found that at highest RWa, ie. B1, the S/H ratio is the best compared to other P conditions but similar to that of DC, indicating that using additives does not improve the S/H ratio very much. However, under PR conditions it was found that the S/H ratio has improved very much to that of DC or even P conditions. The best PR conditions compared to DC amongst the plated PCBs from good to best S/H ratio for $t_{on(c)}/t_{on(a)}$ and $i_{p(c)}/i_{p(a)}$ are 10/0.5 and 1/3, 10/0.2 and 1/2, 10/0.2 and 1/3, 10/0.2 and 1/4 plus 10/0.2 and 1/8 for aspect ratios of 3:1 and 8:1 for board thickness of 2.4mm. It must be pointed out that the improvements were also observed relative to the surface appearances since it is preferred that the deposits have a lustrous finish. The study has shown three conclusions:

- low duration of anodic cycle can be used to obtain better S/H ratio compared to

DC, ie. cathodic/anodic on-time ratios of 10/0.2 was the best;

- as $i_{p(a)}$ increases, the coating thickness distribution for a particular on-time ratio improves.
- lustrous or shiny finish can be obtained under PR compared to DC, also see section 7.3.6.

In other words, it was found that PCBs plated using PR for cathodic/anodic on-time ratios of 10/0.2 were lustrous and S/H ratios were better than DC and at higher $i_{p(c)}/i_{p(a)}$ of 1/8, the S/H was the best with semi-lustrous surface appearance. However, under the worst PR conditions for electrolyte V, the S/H ratio was extremely disappointing, Fig. 107/108, as expected.

Also, for electrolyte XIII, under best P condition(5000Hz,75%ϕ), the S/H ratio was not as good as expected, Fig. 107/108. This is understandable because as before, the additives are affected by the temperature(10°C) used and makes the replenishment of ions in the holes difficult; no direct evidence on this is available.

Table 18 shows the summary of the results in a tabulated form obtained for different electrolytes, hole diameters, board thicknesses, aspect ratio, average current densities and conditions(DC, P and PR).

Finally, it can be concluded that electrolyte V containing all the additives is the best and provides lustrous to semi-lustrous coatings under PR conditions (at $t_{on(c)}/t_{on(a)}$ and $i_{p(c)}/i_{p(a)}$ of 10/0.2 and 1/3, 10/0.2 and 1/4, 10/0.2 and 1/8) at room temperature. Comparing these results to the work carried out by Pearson and Dennis [2], they found that at $t_{on(c)}/t_{on(a)}$ and $i_{p(c)}/i_{p(a)}$ of 10/0.5 and 1/3, respectively, the S/H ratio obtained was 1:1 with a matt deposit,but no evidence of S/H ratio of 1:1 was observed in the coated deposits but the matt finish was observed in the present work. Nevertheless, it was found that this condition was better than DC in this research programme. Also, other studies carried out by CR Circuit [134] indicates that PR plating can be beneficial in plating of PCBs. It has been concluded that the results of the production trial demonstrated several major benefits including:

- boards with 9:1 aspect ratios could be plated at a normal plating rate without any loss of quality, ie. 25μm achieved in 45 minutes with improved distribution.
- small holes 0.3mm could be plated to a much higher quality, which is beneficial for surface mount production.
- The improvement in copper covering power was a major assistance in overcoming solder-masking problems associated with over-plating of isolated

tracks.

The above findings are in agreement with the results obtained in this research programme.

7.2.6 Behaviour of the additives

The use of additives and their concentrations in electrolytes are believed to be important in electroplating in obtaining properties such as good levelling, fine grains, bright finish, etc. For this reason the behaviour of such additives has been under study by many authors[2,24].

Goodenough and Whitlaw [24] have examined some of the additives used in this research work under DC with respect to different temperatures, electrolyte concentrations, chloride ion concentrations and current densities for high aspect ratio printed circuit boards. They have found that electrolytes containing low copper sulphate(0.14M) and high acid concentration(3.3M) with additives (PEG and MPSA - LeaRonal proprietary) provide a better throwing power at lower current density ($0.3Adm^{-2}$) but at higher current density ($3Adm^{-2}$) the throwing power is about the same for higher concentrations of copper (0.3M) and lower concentration of sulphuric acid (2.2M). The effect of increasing temperature is the same. The effect of chloride ion concentration is optimum at 50ppm. However, the electrolyte containing 0.2M copper sulphate and 3.3M sulphuric acid with additives (125L- LeaRonal proprietary) showed the best S/H ratio at $3Adm^{-2}$ and also electrolytes with additives (PEG and mercapto-propane sulphonic acid, sodium salt, (MPSA)- LeaRonal proprietaries) provided the best S/H ratio at 25°C for current densities of up to $3Adm^{-2}$.

Pearson and Dennis[2] have used polarisation curves in their study using polyether and sulphide based additives. They have reported that these additives cause a shift in the Tafel slope up compared to the electrolytes without additives and an improvement in throwing power is expected. Another important constituents in the bath reported[2,77] is chloride ion. It has been indicated that the presence of chloride ion is important in adsorption mechanisms and in the case of some additives such as polyethylene glycol this additive has little influence alone on the cathode efficiency for DC or any pulse conditions. These findings have been explained in this research work in terms of process conditions.

The additives used in this research work have been described in detail in Appendix

2. These proprietary additives known as C140, N1 and DS4. These additives are similar to the ones studied by Goodenough et al [21] . The additives can be assumed to have the following functions in the plating:

C140	has a structure related to non-ionic surfactants and alkyd resins. It suppresses the deposition process. Cl^- is essential for it to work.
N1	has a brightener property especially at low current densities.
DS4	has little effect on its own. It reactivates the surface and also affects the crystal structure. It is also a brightening agent with effects similar to that of thiourea.

The additives used in this research work and were provided by the sponsoring company, LeaRonal, who believed they were an optimum combination for use in plating under DC as well as pulse conditions.

7.3 Assessment of Pulse Plated Electrodeposits

The assessments of plated electrodeposits were carried out for both unipolar pulse(P) and bipolar pulse reverse(PR) and compared to DC.

The plating for unipolar pulse and DC was carried out at an average current density of $3Adm^{-2}$. The unipolar pulse plating conditions were at frequencies of 20, 100, 500, 1000, 2000, 3000, 4000 and 5000Hz and at duty cycles of 25%, 50%and 75%.

The plating for bipolar pulse reverse was carried out at an average current density of $3Adm^{-2}$. The unipolar pulse reverse plating conditions were at cathodic/anodic peak current density ratios($i_{p(c)}/i_{p(a)}$) of 1/1, 1/2, 1/3 and 1/4 and cathodic/anodic on-time ratio($t_{on(c)}/t_{on(a)}$) of 10/0.2 and also at $i_{p(c)}/i_{p(a)}$ of 1/3 and $t_{on(c)}/t_{on(a)}$ of 10/0.5. (Note: on-times are in milliseconds).

The methods and conditions used have been explained in sections 5.11 and 6.3. These assessments are based upon the cathode efficiency, micro-hardness, roughness, tensile strength and elongation, coating surface distribution, surface appearance and morphological studies. The electrolytes used for these studies were VIII, I and V for P conditions and electrolytes I and V for PR conditions, see Appendix 1.

7.3.1 Efficiency of deposition

The efficiency of deposition, better known as cathode efficiency, was examined for only unipolar pulse. The examinations were based upon the coated deposits for a particular plating time of 37 minutes to obtain a coating thickness of 25μm; it was expected to obtain a weight increase of 1.563g at 100% efficiency on these sample sizes.

The efficiency was calculated by weight gain measurements. Each cathode was weighed before and after plating and then the weight gain of the pulsed coatings were measured as a comparison to DC. The efficiency was calculated by the following equation:

$$\text{Efficiency (\%)} = \frac{\text{Weight gain under pulse } (M_P)}{\text{Weight gain under DC } (M_{DC})}$$

The results obtained using electrolyte VIII, Table 19, showed that the cathode efficiency of pulse plating is a little less than DC but the electrolyte I showed a bigger difference in cathode efficiency of pulse to that of DC. It was also noted that under DC the weight gain is 1.8006g: the reason for this increase is not really known but it could be due to an error which may have be made during measurements. However, if it is assumed that the weight gain during DC for electrolyte I is similar to that of electrolyte VIII, ie. 1.5696g, then it could be said that the cathode efficiency of pulse can be higher or lower than 100%, depending upon the P condition used. The results of the electrolyte V, Table 18, confirms that cathode efficiency is dependent upon the pulse conditions and also electrolytes used assuming all other conditions such as pretreatments, etc remain equal. It must be said that the cathode efficiency cannot exceed 100% in real terms but it is assumed to be 100% under DC as expected by calculation such as:

$$Wg = \frac{zIt}{nF}$$

where Wg= weight gain(g)
z= atomic weight
I= current(A)
n= number of electrons
F= Faradaic constant(=96500Asmol^{-1})

The classical example of this can be seen in Table 19 for electrolyte V whereby the weight gain is 1.5193g for DC and the calculated weight gain is 1.563g which indicated that in real terms plating process is inefficient. However, it can be said from the pulse

results that the cathode efficiency can be expected to be higher than DC depending upon the pulse conditions, similar to the findings by Popov et al [119].

7.3.2 Micro-hardness

The micro-hardness studies have been carried out for P and the results were compared to DC, Table 19, and cold rolled copper, Table 20, see section 5.11.2.

It was found that the hardness values of the plated samples for electrolytes I, V and VIII under DC condition are 142HV, 130HV and 92HV, respectively, see Table 19. The hardness values obtained for electrolyte I and V under P conditions are always less than DC, Figures 110a and 110b. For electrolyte VIII, the hardness values for P conditions were higher than equivalent DC plated samples, Figure 110c.

It was also found that for electrolyte I, Figure 110a, the hardness value at low frequency of 100Hz and duty cycle of 75% to be the highest. But for electrolyte V, this was not the case, such that the highest hardness value was obtained at a frequency of 1000Hz and duty cycle of 50%, Figure 110b. However, for electrolyte VIII it was found that the hardness values increased as the duty cycles increased at a frequency of 100Hz. The increase at 100Hz for electrolyte VIII is similar to that of electrolyte I, Figures 110c.

The hardness value obtained for 'as received' or 'hard tempered' 0.25mm thick copper, is 90HV, Table 20 and Figure 112a. In comparison to P plated samples the hardness values for electrolytes I, V and VIII are higher.

With respect to the cold rolled copper, the hardness values increased from 100HV to 123HV as the percentage of original/specimen thickness increased from 5% to 50% but then decreased to 113HV as cold rolling increased to 75%, Figure 112a; this indicates some work softening due to partial recrystallisation during rolling. The hardness values of electrolyte I, V and VIII can be compared to rolled sheet. This indicated that not only electroplating copper can produce a higher hardness than standard copper sheet or foil but it can be as good as cold rolled copper presumably because of the absence of work softening behaviour. Even further, it is possible to achieve a coating similar or higher in hardness than cold rolled copper depending upon the pulse condition.

It can be summed up that electrolyte VIII contains no chloride ions and the hardness values under DC are lower than that of electrolyte I, indicating that chloride ion plays an important role. With regard to electrolyte V, it can be seen that even under DC the hardness values are affected, indicating again that the choice of additives play an important role. Comparatively, electrolyte V produces more even hardness values and its dependence to pulse conditions is somewhat less than electrolytes I and VIII, Figures 110a, 110b and 110c. Finally, from the results it can be deduced that the hardness values are dependent upon the pulse conditions and also electrolyte constituents.

7.3.3 Roughness

The surface texture of the coated deposits was examined by measuring the roughness. Two methods were used for comparative purposes, firstly the roughness average(R_a) and secondly, the mean peak-to-peak roughness average(R_{tm}), see section 5.11.3, for electrolytes I, V and VIII, Table 19.

It was found that electrolyte I is rougher, in terms of R_a and R_{tm}, than electrolyte V under P conditions. This was expected since electrolyte V contains levelling additives and hence causes a reduction in surface roughness. In comparison, the roughness (R_a and R_{tm}) values of the deposits under P conditions for electrolyte I is somewhat similar to DC and the roughness values are less dependent on frequency and duty cycle for R_{tm} than R_a, Figure 111a. However, the roughness (R_a and R_{tm}) values of the deposits under P conditions for electrolyte V are higher than DC and the roughness (R_a and R_{tm}) values are dependent on frequency and duty cycle, Figure 111b. For electrolyte VIII, the results obtained are similar to that of electrolyte I, indicating that electrolytes containing no additives can cause an increase in roughness, Figure 111c.

The results obtained are comparable with the findings by Chene et al [65], that using electrolyte I the roughness average is around 1μm for DC and for pulse condition it is dependent on the pulse conditions.

It can be concluded that an electrolyte with additives(V) is better for both DC and P conditions.

7.3.4 Tensile strength and elongation

The tensile strength and also elongation values were obtained for P, PR, DC and cold rolled copper, Table 20, for electrolytes I and V.

The tensile strength values obtained for electrolyte I under DC produced almost the highest value of 312.6Nmm^{-2}, but for P plated samples the tensile strength values were the lowest at low frequency and duty cycle and increased as the frequency increased, Figure 113a. The highest tensile strength was obtained under P at a frequency of 4000Hz and a duty cycle of 75% (348.1Nmm^{-2}) compared to DC.

The tensile strength values obtained for electrolyte V were dependent upon the P conditions used when compared to DC, Figure 113b. The tensile strength values were at their lowest at a frequency of 20Hz irrespective of the duty cycle but it can be expected to obtain tensile strength values higher than DC, for example the highest tensile strength values were 338.2Nmm^{-2} at P condition of 1000Hz and 75%ϕ compared to 301.1Nmm^{-2} for DC.

However, comparing the electrolytes I and V, Figure 113c, it can be seen that in the majority of P conditions the tensile strength for electrolyte V was higher than electrolyte I. This is surprising since under DC, the tensile strength value for electrolyte V is less than electrolyte I indicating that P can increase the tensile strength.

The tensile strength value obtained for 'as received' or 'hard tempered' 0.25mm thick copper, is 235.9Nmm^{-2}, Table 20 and Figure 112b. In comparison to P the tensile strength values for electrolytes I can be expected to be higher or lower depending upon the frequency and/or duty cycle, but for electrolyte V the tensile strength is higher than 'hard tempered' or 'as received' copper sheet.

With respect to the cold rolled copper, the tensile strength values decreased between 5 and 25 percent of original/specimen thickness but, at 75% the tensile strength increased to be as high as 771.2Nmm^{-2}, Figure 112b. The tensile strength of both electrolytes was greater than 5 and 25% samples and 'as received' material, Table 20.

The elongation values obtained, Table 20, under P are similar in terms of overall pattern to that of tensile strength, such that for electrolyte I the elongation value is higher under DC condition compared to the majority of the P conditions studied and is at its lowest at low frequency and low duty cycle, Figure 114a. The elongation can be

expected to increase or decrease depending upon the frequency and duty cycle used. As for electrolyte V, the elongation is at its lowest for DC compared to P. Figure 114b shows the combined results for the two electrolytes, Figure 114c, indicates that the elongation for electrolyte V is lower than electrolyte I under DC but it is possible to expect a higher tensile strength under P with electrolyte V. There appear to be a general trend that samples produced at higher frequencies have greater alongation.

The elongation values obtained for samples produced in both electrolytes are lower than 'as received' copper sheet but in comparison to cold rolled copper, Figure 112c and Table 20, the elongation values under DC are higher than 5%-75% cold rolled copper. It was found that pulsed plated samples in general had somewhat higher elongation values than the cold rolled material.

However, it can be said that tensile strength and elongation values under P and DC are comparable to not only a standard tempered copper sheet of 0.25mm thick but also to cold rolled copper. The results are promising, indicating the advantages which P does have in obtaining useful properties.

As for PR, the conditions used are limited for this type of assessment but since the conditions used were chosen at random, it probably makes a good comparative examination. However, in general it is possible to expect to obtain a tensile strength and also elongation value equal or higher under PR to that of DC, P and cold rolled, Table 20. The tensile strength values obtained under PR for electrolyte I was higher under certain pulse conditions than electrolyte V, Figure 115, but the elongation values for electrolyte V was higher under certain pulse conditions than electrolyte I, Figure 116.

Finally it can be summed up that P and PR are comparable to cold rolled copper and in terms of industrial usage they certainly can produce better properties than DC.

7.3.5 Coating thickness distribution

In order to study the coating thickness distributions, the thickness of the deposit was measured by flat Micrometer and point Micrometers. The findings obtained indicated a very interesting result with respect to the surface roughness. The coating thicknesses obtained using a flat Micrometers showed that the the build-up of the deposits at the edges was greater under P and PR conditions than DC for electrolyte I,

Figure 117.

The coating thicknesses obtained from electrolytes V using a flat Micrometer showed that it is possible to obtain coating thickness uniformity similar at the edges under P and PR to DC, Figure 118. It can also be seen that the overall uniformity under both P and PR is better than DC for electrolyte V. The improvement of the coating thickness distribution is very much dependent upon the P or PR conditions and also the choice of electrolyte.

The point Micrometer was used to measure the coating thickness distributions for three conditions of DC, P: 2000Hz,75%ϕ and PR: $t_{on(c)}/t_{on(a)}$, $i_{p(c)}/i_{p(a)}$ of 10/0.2,1/4 for electrolytes I and V. The choice of both P and PR conditions were arbitrary. The profiles obtained for DC, P and PR were similar to that obtained from the flat Micrometer for both electrolytes, Figures 119 and 120, except that the thickness distribution at the edges which was discussed earlier were less pronounced. For example, the thicknesses obtained under P: 2000Hz,75%ϕ at the bottom edges of the foils are 77µm and 78µm when a flat Micrometer was used but with point Micrometer the thicknesses were 53µm and 45µm. The results show the 'nodular' nature of the surface.

Finally, it can be concluded that under both P and PR, it is possible to achieve a better coating thickness uniformity than DC but it is dependent upon the P and PR conditions and also the electrolyte constituents. Similar trends have been reported by Montgomery [5] and J.C.T. Controls[6].

7.3.6 Surface appearance

In general, it is preferred that copper plated coatings should have a lustrous finish but it is believed that many factors affect the surface appearance, such as current density, electrolyte constituents and additives, agitation, etc.

It was found that the coated deposits obtained from the electrolytes studied under DC, P and PR depended upon the electrolyte constituents and the conditions used. The electroplating was carried out at 3.0Adm^{-2}, with air and reciprocating agitations combined. The surface appearances were studied only for electrolytes I and V.

The results obtained using electrolyte I under both DC and P conditions produced

matt or orange coloured finishes, but with electrolyte V the finishes were lustrous or shiny.

The results of PR were rather different than expected. For electrolyte I, the finishes were from matt to burnt(orange to brown colour). But using the electrolyte V have shown that it is possible to obtain different finishes depending upon the pulse conditions. Figure 121 shows the cathodic/anodic peak current density ratio against cathodic/anodic on-time ratio, indicating different finishes obtained using electrolyte V and under PR. It was found that at low anodic on-times, it is possible to obtain a lustrous finish but other finishes can also be obtained ranging from semi-lustrous, matt, dull to burnt finishes. In copper or decorative plating industries, it is preferred to obtain a lustrous finish.

Therefore, it can be concluded that it is possible to obtain a lustrous finish under P and PR similar to DC under specific conditions of electrodeposition.

7.3.7 Morphological study of the deposits

The morphological study of the plated deposits was carried out for electrolytes I, V and VIII for unipolar pulse and compared to DC. Also, electrolytes I and V were used under PR conditions.

Figure 125 shows the structures obtained using scanning electron microscopy (SEM) under DC and P conditions for electrolyte I. It can be seen that at a particular frequency of say 20Hz and duty cycle of 25%, the crystal structures are long and columnar and they reduce in size as the duty cycle increases to 75%. The growth size of crystal structures are generally systematic up to a frequency of 500Hz but as the frequencies are increased from 1000Hz to 5000Hz at a duty cycle of 25%, the structures change gradually and their size becomes similar to that of DC. Also, the increase in duty cycle causes a reduction in size of the crystal structures to more compact nodular type crystals. It can be said that as the duty cycle and or frequency increases, the structures change from long columnar to nodular crystal structures similar, or rather smaller in size to that of DC condition. Puippe and Ibl [55] found the same effect that deposits become finer with increase in peak current density, and coarser grains with increase in off-time at a constant peak current density and on-time.

The structures obtained under P and DC conditions for electrolyte V showed that

the grains are very similar, Figure 126. This was expected as the electrolyte V contains additives which can cause grain refinement and therefore, similarity in structure of the deposit is not surprising.

The study of the deposits structure for electrolyte VIII was only examined at a frequency of 20Hz and duty cycles of 25, 50 and 75%. For comparison, DC plating was also carried out. The findings were similar to electrolyte I, such that the crystal structures were long columnar grains and as the duty cycles increased the grain size were reduced, Figure 127. It was found that under DC, the crystal structures were smaller for electrolyte VIII than I under DC and also under the corresponding P conditions. This effect is believed to be due to the absence of chloride ion in the electrolyte VIII.

The morphological studies carried out under PR using electrolyte I were limited to only two cathodic/anodic on-times of 10/0.5 and 10/0.2. It was found that at $t_{on(c)}/t_{on(a)}$ of 10/0.5 and $i_{p(c)}/i_{p(a)}$ of 1/3, the structures are plate-like and at $t_{on(c)}/t_{on(a)}$ of 10/0.2 and $i_{p(c)}/i_{p(a)}$ for 1/1, the structures are ball-like or nodular-like. Figure 128 shows the structures obtained under scanning transmission electron microscope(STEM). It was also found that as the cathodic/anodic peak current density increased for $t_{on(c)}/t_{on(a)}$ of 10/0.2, more smaller grains appeared. The examination of the structures showed that the shape of the plated grains are long columnar, somewhat similar to P, but as a result of negative cycle the structures take a new form, Figure 128.

The morphological examination of the PR conditions using electrolyte V were systematic taking into account various $t_{on(c)}/t_{on(a)}$ and $i_{p(c)}/i_{p(a)}$ ratios, Figure 129. The best way of explaining the structure obtained under PR for electrolyte V can be related to the surface appearance, Figure 121. The foils with lustrous appearance showed very little information on grain structure under STEM. For this reason, the plated samples were etched in order to be compared to DC and the others were examined without any etching.

Under all PR conditions, where the surface appearance was lustrous or shiny, the grain structures were very small when etched, Figure 129, similar to that of P and DC in surface topography. The differences in structure between the shiny finishes are very small or none under PR. But as far as other finishes are concerned, it can be seen that the number of grains are the main difference between different PR conditions. As

before, the surface appearance can be used to explain the changes, such that when the deposit finish is semi-lustrous, the number of grains are lesser in extent than matt and dull finish and that when the deposits are burnt, the number of grains are very much higher. The shape of each grain is either in a form of plate-like and/or leaf-like structure, Figure 129, and the deposit growth is similar to the build-up of an iceberg.

Finally, it can be concluded that the morphological structures of the P can be related to DC and under PR can be related to surface appearance. They are dependent on pulse parameter and also the electrolyte [126]. In terms of usage, both P and PR conditions can provide a deposit comparable to that of DC.

CHAPTER 8

8.0 CONCLUSIONS

8.1 Standarisation of Solutions

1. A parabolic relationship was obtained for the conductivity of solution as the concentration of sulphuric acid increased for various concentration of copper sulphate.

2. The best pretreatment for copper or brass for subsequent electroplating was found to be the pretreatment 5 consisting of alkaline cleaner, sulphuric acid and hydrogen peroxide pickling.

3. The best agitation technique was found to be reciprocating cathode and air sparging, at a rate of 4.5 litre/minute, combined.

4. The use of a potentiostat or a galvanostat was not suitable for polarization studies under pulse conditions as it is neither capable nor designed for this purpose due to the electronic basis of the system. Therefore, a compatible system such as a fast response stabilised power supply was found to be ideal.

8.2 Polarisation, Tafel and Wagner Number Studies

5. Amongst the electrolytes used, the best unipolar pulse conditions for subsequent PCB electroplating were found to be at high frequencies and high duty cycles, ie. 5000Hz and 50 or 75% and the worst unipolar pulse conditions were at low frequencies and low duty cycles, ie. 20Hz and 25%. These conditions are dependent upon the electrolyte constituents.

6. The limiting current density studies showed that plating at higher current density is possible under unipolar pulse compared to DC, which in effect is more beneficial

for the plating industries.

7. The enhancement Wagner number ratio was found to be useful in determining and differentiating the best to worst pulse conditions with respect to throwing power.

8. It was found that the limiting current density for electrolyte I was higher than electrolyte V under PR. The reason is believed to be that the polyethylene glycol(C140) additive, causes the deposition potentials to increase for a given current density than the corresponding deposition potential in absence of this additive and also due to the surface blocking caused by the adsorption of polyether on the cathode surface.

9. The results obtained under PR were found to be systematic such that the on-times are the controlling factors with respect to a particular cathodic/anodic peak current density using electrolyte I. That is, the Wagner number increased from low to high gradually with cathodic/anodic on-times of 10/2, 10/1, 20/1, 10/0.5, 20/0.5 and 10/0.2 for cathodic/anodic peak current density of 1/1. This occurrence is believed to be due to that fact that, as the anodic on-time decreases relative to cathodic on-time, the Wagner number or 'throwing power' becomes almost similar to that of unipolar pulse.

11. The peak current density ratio was also found to play a key role in determining throwing power and the enhancement Wagner number ratio is dependent upon the electrolyte constituent.

12. The systematic relationship obtained under bipolar pulse reverse for electrolyte I does not apply to electrolytes with additives such as electrolyte V. This gives a clear indication that additives play an important role in bipolar pulse reverse.

13. The results of the plated PCBs under unipolar pulse reverse showed that better S/H ratio can be obtained for electrolyte I than V but electrolyte V provides better properties such as improved surface coverage and smaller grains. Thus pulsing conditions are critical for obtaining a good S/H ratio. The coating thickness distribution improves as the plating current density is reduced.

14. The results of the plated PCBs showed that S/H ratio for PR can be better than DC and also unipolar pulse conditions for electrolyte I.

15. The results of the plated PCBs for electrolyte V under PR showed that:
    - low duration of anodic cycle can be used to obtain a better S/H ratio than DC, ie. cathodic/anodic on-time ratio of 10/0.2 was the best;
    - the best bipolar pulse reverse conditions obtained from good to best S/H ratio are for $t_{on(c)}/t_{on(a)}$ and $i_{p(c)}/i_{p(a)}$ ratios of 10/0.5 and 1/3, 10/0.2 and 1/3, 10/0.2 and 1/4 and 10/0.2 and 1/8 for aspect ratios as high as 8:1;
    - as $i_{p(a)}$ increases, the S/H ratio for a particular on-time ratio improves;
    - lustrous or shiny finish can be obtained under PR.

16. The electrolyte consisting of all the additives appeared to be ideal for PR plating as no apparent additional breakdown of additives compared to DC rates was observed when following the LeaRonal replenishment recommendations.

17. The optimum chloride ion concentration was found to be 50ppm.

8.3 Assessment of Pulse Plated Electrodeposition

18. The cathode efficiency increased under certain unipolar pulse conditions and it is dependent upon the electrolyte constituents.

19. The micro-hardness values showed that the presence of chloride ion is significant. However, the electrolyte V produced more even hardness values such that its dependence on pulse condition is less than electrolyte I and VIII.

20. The roughness average and peak-to-peak roughness average values for electrolyte I and VIII are higher than electrolyte V indicating that electrolyte V is producing a smooth surface texture.

21. The tensile strength and elongation values under unipolar pulse and DC are comparable to hard tempered copper and also to cold rolled copper. The results are promising, indicating the advantages which unipolar pulse does have in obtaining useful properties. Also, the tensile strength and elongation values under PR are comparable to cold rolled and in terms of industrial usage they certainly can produce better properties than DC.

22. The coating thickness distribution under unipolar pulse and bipolar pulse reverse

can produce a better coating thickness distribution to that of DC. The coating thickness distribution is dependent upon the electrolyte constituents.

22. The surface appearances obtained under DC and unipolar pulse for electrolyte I and V were matt and lustrous, respectively. But the surface finishes obtained under bipolar pulse reverse for electrolyte I ranged from matt to burnt and for electrolyte V ranged from lustrous to burnt.

23. The structures obtained for electrolytes I and III under unipolar pulse were similar to DC at low frequencies and high duty cycles (20Hz and 75%) having long columnar structures. At higher frequencies (>1000Hz) and high duty cycles structures changed gradually to nodular type crystals rather smaller in size than DC. The grains obtained under unipolar pulse and DC for electrolyte V were extremely small.

24. The bipolar pulse reverse structures obtained for electrolyte I are nodular-type. But the structure for electrolyte V is different and can be related to surface appearance such that the deposits with lustrous finish have fine grain structures. The deposits with semi-lustrous finish have fewer grains than matt and dull finish and when the deposit is burnt the number of grains is very high. The shape of each grain is either in the form of a plate-like and/or leaf-like structure and the deposit growth is similar to the build-up of an iceberg.

CHAPTER 9

9.0 FUTURE WORK

1. During this research programme, it was understood that electrode design is important especially for studying printed circuit board through-holes. Haak et al[33] have designed a cell which it seems is ideal for this type of study. But other designs can also be made using cells to simulate PCB through-holes. The cells could be made out of stainless steel which would be designed to open in two halves for direct thickness measurements.

2. Other than the studies carried out on properties of the copper electrodeposits and their improvements, there is still scope for research on solderability of the deposits produced under pulse conditions for PCBs.

3. A study of the additives with regard to their adsorption and/or desorption for unipolar pulse and bipolar pulse reverse would be useful.

4. The use of duty cycle or relaxation time may provide a better result than already obtained under bipolar pulse reverse and hence scope for research remains.

5. It is believed that by using computer modelling it is possible to predict the best bipolar pulse reverse conditions for copper plating of the printed circuit board for different aspect ratios from the results already obtained. The possibility lies with the fact that the results of bipolar pulse reverse are more systematic than those of unipolar pulse conditions.

References

1. Puippe, J.C. and Leaman, F., "Theory and Practice of Pulse Plating", Publ. AESFS, (1986).
2. Pearson, T. and Dennis, J.K., J. Applied Electrochemistry, 20 (1990) 196-208.
3. Alkire, R.C. and Ju, J.B., J. Electrochemical Society, 134(5) (1987) 1172.
4. Chin, D.T., J. Electrochemical Society, 130 (1983) 1657.
5. Montgomery, A., Circuit World, 15(2) (1989).
6. J.C.T. Trial Test Report, 23rd may (1989).
7. Gabe, D.R., Circuit World, 8 (1981) 58.
8. Jawitz, M.W., Metal Finishing, 71 (1972) 31.
9. Lowenheim, F.A., "Modern Electroplating", 3rd ed., J. Wiley - Interscience Publication, (1974) 165-223.
10. Craig, S.E., Harr, R.E. and Wu, S.Y., Plating, 60 (1973).
11. Horner, J., Plating and Surface Finishing, (1987) 34.
12. Kasper, C., J. Electrochemical Society, 77 (1940) 353&365; 78 (1940) 131&147; 82 (1942) 153.
13. Kinney, G.F. and Festing, J.W., Plating, 41 (1954) 380.
14. Neufeld, P. and Patel, D.V., Trans. I.M.F., 52 (1974) 71.
15. Nohse, W., The Hull Cell, Republished Draper , Teddington, (1966).
16. Wagner, C., J. Electrochemical Society, 98 (1951) 116; Plating, 48 (1961) 997; Advanced Electrochemical Engineering, 2 (1962).
17. Haring, H.E. and Blum, W., Trans. Electrochemical Society, 44 (1923).
18. Noninski, C.I., Veleva, L.P. and Noninski, V.C., Surface Technology, 25 (1985) 127.
19. Bard, A.J. and Faulkner, L.R., "Electrochemical Methods-Fundamental and Applications", J. Wiley Publications, (1980) 29-110.
20. Albery, W.J., "Electrode Kinetics", Oxford University Press, (1975) 78-81.
21. Goodenough, M. and Whitlaw, K.J., Trans. I.M.F., 67 (1989) 57.
22. Vilambi, N.R.K. and Chin, D.T., Plating and Surface Finishing, (1988) 67; (1989) 74-82.
23. Luke, D.A., "Electroplating of Copper for Printed Circuit Manufacturers", LeaRonal(UK) Ltd, Buxton.
24. Dini, J.W., Plating, 51 (1964) 119.
25. Rothschild, B.F., Plating, 53 (1966) 437.
26. Blurton, K.F. and Nuzzi, F.J., Plating and Surface Finishing, (1987) 62.
27. Engelmaier, W. and Kessler, T., J. Electrochemical Society, 125 (1978) 36.
28. Yung, E.K. and Romankiw, L.T., Proceedings of the Symposium on "Electroplating Technology, Theory and Practice", Ed. Romankiw, L.T. and

Turner, D.R., The Electrochemical Society, 87(17) (1987) 607; J. Electrochemical Society, 136(3) (1989) 756.

29. Yung, E.K., Romankiw, L.T. and Alkire, R.C., J. Electrochemical Society, 136(1) (1989) 206.
30. Poskanzer, A.M., Plating and Surface Finishing, 72(4) (1985) 12&51.
31. Olsen, J.D., Salem, S. and Romankiw, L.T., U.S. Patent number 3798136, (March 19, 1974).
32. Uceda, D.A. and O'Keefe, J. Electrochemical Society, 20 (1990) 327.
33. Haak, R., Ogden, C. and Tench, D., J. Electrochemical Society, 11 (1981) 771.
34. Irvine, T.H., Metal Finishing, 65 (1967) 85.
35. Pesco, A.M. and Cheh, H.Y., J. Electrochemical Society, 131(10) (1984) 2259; 136(2) (1989) 229&408.
36. Ng, H.K., Tseung, A.C.C. and Hibbert, D.B., J. Electrochemical Society, 127(5) (1980) 1034.
37. Lanzi, O., Landau, U., Reid, J.D. and Galasco, R.T., J. Electrochemical Society, 136(2) (1989) 368.
38. Sullivan, T. and Middleman, S., J. Electrochemical Society, 132(5) (1985) 1050.
39. Ben-Poret, M., Yahalom, J. and Rubin, E., J. Electrochemical Society, 130(3) (1983) 561.
40. Lanzi, O. and Landau, U., J. Electrochemical Society, 135(8) (1988) 1923.
41. Alkire, R. and Mirarefi, A.A., J. Electrochemical Society, 120(11) (1973) 1507.
42. Cabán, R. and Chapman, T.W., J. Electrochemical Society, 123(7) (1976) 1036.
43. Barringer, T. and Cavano, M., Plating and Surface Finishing, (1986) 36.
44. Perakh, M., Surface and Coating Technology, 31 (1987) 409.
45. Kessler, T. and Alkire, R., J. Electrochemical Society, 123(7) (1976) 990.
46. Luke, D.A., Trans. I.M.F., 61 (1983) 64.
47. Kalantary, Mehrdad.R. and Gabe, D.R., Trans. I.M.F., 67 (1989) 24&28.
48. Johal, C.P.S., Kalantary, Mehrdad.R. and Gabe, D.R., Trans. I.M.F., 67 (1989) 31.
49. Kalantary, Mehrdad.R., Amadi, S.A. and Gabe, D.R., Circuit World, 15(4) (1989) 24.
50. Bulman, G. and Shaw, M., Connectors '85', (1985).
51. Ibl, N., Surface Technology, 10 (1980) 81.
52. Ishihama, A. and Hayashi, T., Bull. Univ. Osaka Prefect, Ser. A, 29(2) (1980) 83.
53. Lashmore, D.S. and Weisshaus, J., Intefinish '84', Jerusalem, Israel.
54. El-Shazley, M.F., White, J.L. and Brooman, E.W., 3rd International Pulse Plating Symp., AESF (1986) 1-18; Plating and Surface Finishing, (1987) 136-142.
55. Puippe, J.C. and Ibl, N., Plating and Surface Finishing, 68(6) (1980) 68.
56. Ibl, N., "Comprehensive Treatise of Electrochemistry", Vol. VI, Chap. 4, ed.

Yeager, E., Bockris, J.O'M. Conway, B.E. and Sarangapani, S.

57. Puippe, J.C., 3rd International Pulse Plating Symp., AESF, (1986) 1-14.
58. Puippe, J.C., Ibl, N., Hosokawa, K. and Angerer, H., Proc. AESF, International Plating Symp., Boston, April 19-20 (1979).
59. Cheh, H.Y., J. Electrochemical Society, 118 (1971) 551.
60. Ibl, N., Proc. AESF, International Pulse Plating Symp., Rosemount, Illinois, October 6-7 (1981).
61. Pearson, T. and Dennis, J.K., Proc. I.M.F. Conference, York (1990); 12th World Congress, Interfinish '88', Paris, France; Plating and Surface Finishing, (1989) 64-69.
62. Datta, M. and Landolt, D., Surface technology, 25 (1985) 97.
63. Popov, K.I. and Maksimovic, M.D., Surface Technology, 22 (1984) 155.
64. Wan, C.C., Cheh, H.Y. and Linford, H.B., J. Chinese Institute of Chemical Engineering, 9 (1978) 69.
65. Chene, O., Datta, M. and Landolt, D., Oberfläche/Surface, 26(2) (1985) 45-49.
66. Yokoi, M. and Hayashi, T., Denki Kagaku, 46(4), (1978) 195-201.
67. Hayashi, T. and Yokoi, M., Denki Kagaku, 47(11) (1979) 654-660.
68. Ibl, N., Puippe, J. C. and Angerer, H., Surface Technology, 6 (1978) 287.
69. Ibl, N. and Braun, M., Chemie Ingenieur Technik, 45 (1973) 182.
70. Despic, A. and Popov, K.I., J. Applied Electrochemistry, 3 (1973) 161.
71. Maksimovic, M.D. and Dimitrijeric, Z.S., Surface Technology, 17 (1982) 3-9.
72. Popov, K.I., Maksimovic, M.D., Ocokoljic, B.M. and Lazareric, B.J., Surface Technology, 11 (1980) 99.
73. Landolt, D., Proc. 11th World Congress on Metal Finishing, Jerusalem, (1984).
74. Towne, D., 1st. International Pulse Plating Symposium, A.E.S., (1979).
75. Dossenbach, O., See Reference 1, Chapter 3.
76. Hall, W.F. and Chadhuri, A.R., Proc. AES, 10th Plating in Electronics Industry Symp., (1983) 1-7.
77. White, J.R., J. Applied Electrochemistry, 17 (1987) 977-982.
78. Avila, A., 1st. International Pulse Plating Symposium, A.E.S., (1979).
79. Knodler, A., 1st. International Pulse Plating Symposium, A.E.S., (1979).
80. Avila, A.J. and Brown, M.J., Plating, 57(11) (1970), 1105.
81. Hayashi, T., Kitanishi, H. and Fuhumoto, Y., 2nd. International Pulse Plating Symposium, A.E.S., (1981).
82. Missel, L., Duke, P. and Montelbano, T., Semiconductor International, Feb., (1980).
83. Mentone, P.F., Products Finishing, April (1973).
84. Puippe, J.C., Ibl, N., Hosokana, K. and Angerer, H., 2nd. International Pulse Plating Symposium, A.E.S., (1981).

85. Branik, M. and Schaabl, R., 1st. International Pulse Plating Symposium, A.E.S., (1979).
86. Raub, C.J. and Knodler, A., Gold Bulletin, 10(2) (1977) 38.
87. Leaman, F. and Kownacki, B., 1st. International Pulse Plating Symposium, A.E.S., (1979).
88. Perger, G. and Robinson, P.M., Metal Finishing, December (1979) 8-11.
89. Robert, E., Oberflache Surf., 24 (1983) 413.
90. Ehrhardt, J. and Nowack, H., Metalloberflache, 36 (1982) 405.
91. Inglot, B., Pezinski, A. and Socha, J., Powloki Ochr., 9(3) (1981) 31.
92. Raub, C.J. and Knodler, A., Plating and Surface Finishing, 65(9) (1978) 32-34.
93. Miu, W.S. and Fung, Y.S., Plating and Surface Finishing, 73(3) (1986) 58.
94. Osero, N.M., Plating and Surface Finishing, 73(3) (1986) 20.
95. Rehrig, D.L., Plating, 61(1) (1974) 43.
96. Lendver, J. and Raub, C.J., Metalloberflache, 29(4) (1975).
97. Despic, A.R. and Popov, K.I., J. Applied Electrochemistry, 1 (1971) 275.
98. Stimetz, C.J., Final Report, BDX-613-3179 O/NO DE 85007057 NTIS, 0 (1985) 1-47.
99. Wan, C.C., Cheh, H.Y. and Linford, H.B., J. of Chinese Institute of Chemical Eng., 9 (1975) 69.
100. Romanov, V.V., Zh. Prikl. Khim., 36(5) (1963) 1050, 36 (1963) 1057; 34 (1961) 2692.
101. Viswanathan, M. and Raub, Ch.J., Galvanotechnik, 66(4) (1975) 277.
102. Sullivan, W., Plating (East Orange, N.J.), 62 (1975) 139
103. Popov, K.I., Keca, D.N. and Vuksanovic, B.I., J. Applied Electrochem., 7 (1977) 185.
104. Popov, K.I., Maksimovic, M.D., Pavlovic, M.G. and Ostojic, G.R., J. Applied Electrochem., 7 (1977) 331.
105. Leland, M.J., Programmable Pulse Electroplating Process U.S., 3886053 (Cl.204-36;C23b)(1975), Appl. 411962 (1973).
106. Hosokawa, K., Tsuru, Y., Tanimura, K. and Matsunaga, M., Interfinish '84', 197-200.
107. Sutter, B., Mortier, F., Laroche, M.A., Reby, J. and Vasseur, G., Interfinish '84', 201-210.
108. Gemdata Group and Techno Instruments Ltd., "Plating by Pulse and Reverse Polarity", Finishing Industries, 1982, 19-22; 3(8) (1979) 28-29.
109. Popov, K.I., Maksimovic, M.D. and Totovski, D.C., J. Serb. Chem. Soc., 50(6) (1965) 319-325.
110. Kim, W. and Weil, R., Surface and Coating Technology, 31 (1987) 143-150.
111. Kendrick, R.J., Trans. I.M.F., 44 (1966) 78.

112. Grim, R.D. and Landolt, D., Surface and Coating Technology, 31 (1987) 151-161.
113. Nenov and Tebai, (see ref. 112).
114. Despic, A.R. and Popov, K.I., Modern Aspects of Electrochem., 7 (1972) 199.
115. Holmbom, L.G. and Jacobson, B.E., Plating and Surface Finishing, (1987) 74-79: AESF Symposium (1986) [E1] 1-8.
116. Lochet, J., AESF, 2nd Symposium, pulse plating, 0 (1981) 1-6.
117. Pearson, T. and Dennis, J.K., 12th World Congress, Interfinish '88', Paris, France, 407-416; Plating and Surface Finishing, (1989) 64-69.
118. Cherkaoui, M., Chassaing, E. and Quang, K.V., 12th World Congress, Interfinish '88', Paris, France.
119. Popov, K.I., Keca, D.N., Vidojkovic, S.I., Lazarevic, B.J. and Milojkovic, V.B., J. Applied Electrochemistry, 6 (1976) 365-370.
120. Popov, K.I., Lazarevic, B.J. and Kostic, M., J. Applied Electrochemistry, 3 (1973) 161-167.
121. Popov, K.I., Maksimovic, M.D. and Djokic, S.S., Surface Technology, 14 (1981) 323-333; 19 (1983) 173-180.
122. Popov, K.I., Maksimovic, M.D., Nakic, V.M. and Spasojevic, M.D., Surface Technology, 15 (1982) 161-165.
123. Popov, K.I., Maksimovic, M.D., Zecevic, S.K. and Stojic, G.R., Surface Technology, 27 (1986) 117-129.
124. Popov, K.I., Pavlovic, M.G., Pavlovic, L.J., Cekerevac, M.I. and Removic, G.Z., Surface and Coating Technology, 34 (1988) 355-363; 35 (1988) 39-45.
125. Mann, J., Trans. I.M.F., 56 (1978) 70-74.
126. Chene, O. and Landolt, D., J. Applied Electrochemistry, 19 (1989) 188-194.
127. Jernstedt, G.W., Metal Finishing, Feb. (1947) 68-72.
128. White, J.R. and Galasco, R.T., Plating and Surface Finishing, (1988) 122-126.
129. Holbom, G. and Jacobson, B.E., Surface and Coating Technology, 35 (1988) 333-341.
130. Lamb, V.A., Plating, 56 (1969) 909-913.
131. Cannings Handbook on Electroplating, Twentieth ed. (1966).
132. Amadi, S.A., Ph.D. Thesis, Loughborough (1990).
133. Kalantary, Mehrdad.R., Gabe, D.R. and Goodenough, M., Asia Pacific Interfinish 90, Singapore, November (1990).
134. CR Circuit, Trans. I.M.F., Bulletin, August, 4, (1989).

Solution	Composition	
Alkaline cyanide	CuCN	20-80g/l
	NaCN	20-80g/l
	NaOH	10-40g/l
	Rochelle salt	20-30g/l
Pyrophosphate	Cu pyro	50-200g/l
	K pyro	100-250g/l
	NH_4OH	1-2g/l
	K_3 Citrate	10-20g/l
Acid sulphate	$CuSO_4$	100-250g/l
	H_2SO_4	40-120g/l
	Levellers	1-10mg/l
Acid fluoborate	$Cu(BF_4)_2$	200-450g/l
	KBF_4	15-30g/l
	K_3BO_3	15-30g/l

Table 1[7,8] Electrolyte solution compositions for copper electrodeposition.

Solution Type (pH)	Copper Content (g/l)	Current Density (Adm^{-2})	Cathode Efficiency (%)	Throwing Power
Cyanide (9-12)	12-25	1-6	40-70	+70
Pyrophosphate (7-9)	20-40	1-8	95	+50
Sulphate (1)	40-75	2-10	>95	-20/+20
Fluoborate (<1)	60-120	7-55	>95	-20/+10

Table 2[7] Characteristics of copper electroplating solutions.

Solution Type	Acid Copper Sulphate	Fluoborate	Cyanide	Pyrophosphate
Valency	2	2	1	2
Polarization	low	low	high	high
Throwing power	low	low	high	high
Appearance	dull/matte	dark/matte	semi-bright	bright
Grain size	large-small	large-small	small	large
Strength	low	–	high	average
Hardness	low	–	high	average
Cost	low	high	moderately high	moderate
Cathode efficiency	>95	>95	40-70	95
Addition agent necessary?	yes	yes	perhaps	perhaps
Plate on complex shapes	no	no	yes	yes
Anode/cathode ratio	1:1-2:1	1:1-2:1	2:1	1:1-2:1
Toxicity	low	low	high	low

Table 3[7] Comparison of copper electroplating solutions.

Stage	Process	Material	Temperature	Time(mins.)
1	Soak clean	Acid cleaner	30-60°C	3-5
2	Rinse	Clean running water	Cold	1
3	Mild etch	Suitable chemical or electrochemical etch	20-30°C	10-120
4	Rinse	Clean running water	Cold	1
5	Acid dip	10% Sulphuric acid	20°C	1
6	Rinse	Clean running water	Cold	1
7	Copper plate	Suitable copper	20-35°C	as required
8	Rinse	Clean running water	Cold	1
9	Acid dip	Acid compatible with tin-lead process. Normally fluoboric for fuoborate based tin-lead process, or organo-sulphonic acid for non-fluoborate.	20°C	1
10	Rinse	Clean running water	Cold	1
11	Tin-lead plate at 1-4 Adm^{-2}	Suitable tin-lead	20-30°C	as required
12	Rinse	Clean running water	Cold	1
13	Dry	Warm air		

Table : 4[23] A typical electroplating sequence for PCB.

Author	Bath Constituents	Temperature (°C)	Remarks
Puippe et al	0.75M $CuSO_4$ 1M H_2SO_4	20	flow agitation
Chene et al	0.5M $CuSO_4$ 1M H_2SO_4	25	electrode rotation

Table 5 Shows the bath constituents and conditions used by Puippe et al[1] and Chene et al[65].

Acid(98%H_2SO_4) Concentration ml/l	Conductivity ($\Omega^{-1}cm^{-1}$ or Scm^{-1}) $CuSO_4.5H_2O$ (g/l)				
	3.745 (.015M)	35 (.14M)	50 (.2M)	75 (.3M)	100 (.4M)
0	.00156	.0107	.0166	.0156	.0152
25	.131	.167	.184	.156	.134
50	.301	.276	.267	.270	.249
75	.411	.381	.360	.358	.306
100	.511	.467	.451	.429	.381
125	.588	.549	.490	.499	.429
150	.625	.580	.547	.531	.462
175	.652	.592	.561	.558	.493
200	.658	.613	.573	.560	.515
225	.654	.609	.574	.555	.524
250	.642	.509	.519	.545	.529

Table 6 Conductivity measurement values for different molarities of copper sulphate and acid concentration.

Table 7a Shows the limiting current densities for different solution concentrations and temperatures for different agitation modes.

Agitation Type	Limiting current density, i_L/Adm^{-2}			
	Solution A		Solution B	
	21°C	50°C	21°C	50°C
Still(Natural Convection)	2.6	5.2	0.09	0.21
Reciprocating(R) cathode	5.67 ± 0.17	10.26 ± 0.34	0.32 ± 0.06	0.71 ± 0.06
Slight Air	10.5 ± 0.83	13.33 ± 0.72	0.88 ± 0.15	2.91 ± 0.29
Slight Air & Reciprocating(R) cathode	10.5 ± 2	23.06 ± 3.99	0.66 ± 0.32	2.82 ± 0.8
Extensive Air	10.95 ± 0.47	16 ± 1.43	0.62 ± 0.05	1.67 ± 0.19
Extensive Air Reciprocating(R) cathode	10.95 ± 0.57	16.48 ± 1.91	0.64 ± 0.05	1.75 ± 0.05
Magnetic (5)	11.67 ± 1.67	25 ± 1.67	0.81 ± 0.05	2.2 ± 0.55
Magnetic (5) & Reciprocating(R) cathode	9.91 ± 1.8	21.17 ± 2.5	0.6 ± .002	1.76 ± 0.02
Magnetic (6)	12.17 ± 1.17	21.35 ± 0.73	0.69 ± 0.04	2.13 ± 0.29
Magnetic (6) & Reciprocating(R) cathode	13.0 ± 2.83	26.44 ± 8.47	0.82 ± 0.16	2.93 ± 1.69
Magnetic (7)	18.67 ± 3.0	35.83 ± 5.04	1.18 ± 0.13	3.74 ± 1.89
Magnetic (7) & Reciprocating(R) cathode	17.5 ± 4.17	40.31 ± 10.83	1.07 ± 0.43	3.28 ± 3.33
Magnetic (8)	22.3 ± 3.67	41.75 ± 5.8	1.30 ± 0.15	5.34 ± 2.17
Magnetic (8) & Reciprocating(R) cathode	22.3 ± 4.5	54.51 ± 14.12	1.63 ±0.22	5.78 ±1.14

Solution A: 75g/l $CuSO_4.5H_2O$ + 120ml/l 98%H_2SO_4 +50ppm Cl^- (0.3M and 2.25M)

Solution B: 3.75g/l $CuSO_4.5H_2O$ + 26.6ml/l 98%H_2SO_4 (0.015M and 0.5M)

For electrolyte A the limiting current densities were obtained at η= -.400V

For electrolyte B the limiting current densities were obtained at η= -.370V

Table 7b Shows the enhancement factors for different solution concentrations and temperatures for different agitation modes.

Agitation Type	Enhancement Factors, E.F.			
	Solution A		Solution B	
	21°C	50°C	21°C	50°C
Still(Natural Convection)	1	1	1	1
Reciprocating(R) cathode	2.2	1.9	3.6	3.4
Slight Air	4	2.5	9.8	13.9
Slight Air & Reciprocating(R) cathode	4	4.4	7.3	13.4
Extensive Air	4.2	3	6.9	8
Extensive Air Reciprocating(R) cathode	4.2	3.1	7.1	8.3
Magnetic (5)	4.5	4.7	9	10.5
Magnetic (5) & Reciprocating(R) cathode	3.8	4	6.7	8.4
Magnetic (6)	4.7	4	7.7	10.1
Magnetic (6) & Reciprocating(R) cathode	5	5	9.1	14
Magnetic (7)	7.2	6.8	13.1	17.8
Magnetic (7) & Reciprocating(R) cathode	6.7	7.6	11.9	15.6
Magnetic (8)	8.6	7.9	14.4	25.4
Magnetic (8) & Reciprocating(R) cathode	8.6	10.3	18.1	27.5

Solution A: 75g/l $CuSO_4.5H_2O$ + 120ml/l 98%H_2SO_4 +50ppm Cl^- (0.3M and 2.25M)

Solution B: 3.75g/l $CuSO_4.5H_2O$ + 26.6ml/l 98%H_2SO_4 (0.015M and 0.5M)

$$E.F. = \frac{\text{Limiting current densiy of agitated mode}}{\text{Limiting current density of still mode}} = \frac{i_{L(A)}}{i_{L(0)}}$$

Table 8a

Limiting current density values for different electrolytes using different agitations.

Electrolyte	Limiting current density, i_L /Adm^{-2}		
	Still	Reciprocating	Air & Reciprocating
I	1.5	4.33	8.25
II	1.41	4.29	7.96
III	1.30	3.72	8.88
IV	1.64	3.96	7.82
V	1.53	4.52	8.45
VI	1.6	4.8	7.8
VII	1.32	4.73	8.34
VIII	1.57	4.41	8.32
IX	1.65	3.88	8.31
X	2.14	5.86	9.34
XI	.829	1.95	4.39
XII	.814	2.52	5.37
XIII	1.75	4.1	5.32

Table 8b

Limiting current density values for electrolytes at different pulse conditions using air and reciprocating agitations.

	Limiting current density, i_L /Adm^{-2}															
Pulse conditions (Hz,% ϕ)	20,75	20,50	20,25	500,75	500,50	500,25	1000,75	1000,50	1000,25	2000,75	2000,50	2000,25	5000,75	5000,50	5000,25	Average
I	11.68	9.43	8.73	9.56	9.28	8.08	9.17	9.42	8.79	9.73	9.48	9.89	7.66	7.55	9.0	9.16
II	9.18	8.13	7.76	9.07	8.86	8.15	8.87	8.42	8.12	8.4	7.69	7.99	8.8	8.3	7.99	8.38
III	10.6	8.85	8.35	8.71	8.07	7.97	10.2	8.65	8.35	9.12	8.67	8.66	9.21	8.88	8.18	8.83
IV	6.67	6.77	6.0	6.53	6.69	6.17	6.82	6.50	6.26	6.38	6.36	6.86	6.3	6.81	6.21	6.49
V	7.35	8.26	8.92	6.59	8.64	6.54	6.45	6.92	6.59	7.09	6.39	7.79	7.45	7.16	6.83	7.27
VI	–	–	–	–	–	–	–	–	–	–	–	–	8.51	–	–	8.51
VII	–	–	–	–	–	–	–	–	–	–	–	–	6.43	–	–	6.43
VIII	–	–	–	–	–	–	9.16	–	–	–	–	–	–	–	–	9.16
IX	9.8	–	–	–	–	–	–	–	–	–	–	–	–	–	–	9.8
X	10.64	13.20	11.22	11.24	12.28	12.75	10.92	12.92	11.46	11.98	13.57	11.98	10.74	12.36	13.01	12.02
XI	3.79	3.79	5.04	3.89	2.71	3.76	3.88	3.88	4.06	4.11	4.2	4.01	3.94	3.89	4.0	3.93
XII	5.17	6.42	7.5	5.02	5.19	5.60	5.23	6.33	5.23	6.49	5.88	5.98	5.58	5.75	5.89	5.82
XIII	4.77	4.93	4.11	5.18	4.95	4.87	4.77	5.17	5.06	4.83	4.83	5.01	5.46	5.20	5.54	4.98

Table 9a

Calculated Tafel slope values for different electrolytes using different agitation modes.

	Tafel slope (mV/decade)												
	I	II	III	IV	V	VI	VII	VIII	IX	X	XI	XII	XIII
Still	111.0	159.1	110.4	147.2	130.1	121.7	164.6	138.9	137.0	150.0	149.5	148.5	143.5
Reciprocating	104.9	162.3	120.8	187.5	173.2	184.3	151.4	141.7	139.1	166.7	144.3	171.1	133.9
Air & reciprocating	102.4	157.1	100.5	147.2	126.4	184.3	173.6	152.8	137.0	179.2	140.2	157.2	139.1

Table 9b

Calculated Tafel slope values under different pulse conditions using air and reciprocating agitations.

Pulse conditions (Hz,% ϕ)	Tafel slope (mV/decade)												
	I	II	III	IV	V	VI	VII	VIII	IX	X	XI	XII	XIII
20,75	106.9	112.5	133.3	152.8	150.7	152.6	136.1	145.8	135.7	145.1	126.1	135.4	148.2
20,50	82.3	125.0	116.7	116.0	110.4	147.4	118.8	181.3	108.7	118.1	91.7	106.9	134.7
20,25	41.7	76.4	61.1	76.4	84.7	94.2	70.1	100.7	58.3	62.5	52.2	61.8	144.0
500,75	120.1	144.4	177.1	133.3	119.4	158.9	159.7	174.0	130.4	166.7	142.2	157.6	191.7
500,50	93.8	105.6	104.2	86.1	95.8	205.3	139.6	133.7	131.3	145.8	132.6	145.8	186.9
500,25	76.4	76.4	102.8	104.9	95.1	117.9	118.1	125.7	115.2	106.3	114.8	134.0	166.1
1000,75	145.5	152.7	180.1	164.6	170.1	226.3	150.0	107.6	134.8	175.0	152.2	142.4	166.5
1000,50	83.0	109.7	152.1	164.6	138.2	196.3	160.4	95.5	140.0	144.4	144.3	118.1	122.6
1000,25	100.0	97.2	84.0	91.0	104.2	111.6	131.9	110.1	133.9	121.5	134.8	111.1	119.5
2000,75	135.4	109.7	173.6	132.6	139.6	200.0	177.1	176.4	144.8	176.4	150.5	176.5	164.0
2000,50	132.6	117.4	128.5	117.4	120.1	200.0	159.7	129.2	150.4	168.1	141.8	163.9	136.0
2000,25	104.2	111.1	125.0	114.6	86.8	126.3	138.9	140.6	142.6	140.3	136.6	151.7	120.7
5000,75	145.8	138.9	163.2	182.6	135.4	184.2	225.7	156.3	134.8	183.3	158.8	194.3	154.3
5000,50	180.2	109.0	163.2	138.9	116.0	173.7	197.9	180.2	160.0	169.4	152.1	175.3	157.8
5000,25	142.7	95.8	177.1	138.9	129.2	173.7	204.2	144.1	147.8	158.3	150.5	163.9	138.4

Table 10a

Shows the order of sequence from the best to worst throwing power using different electrolytes and agitations; S-still, R-reciprocating and A-air.

	Conditions and Tafel values (mV/decade)		
Conditions	Best →		Worst
I	(S) 111.0	(R) 104.9	(A&R) 102.9
II	(R) 162.3	(S) 159.1	(A&R) 157.1
III	(R) 120.8	(S) 110.4	(A&R) 100.5
IV	(R) 187.5	(S) 147.2	(A&R) 147.2
V	(R) 173.2	(S) 130.1	(A&R) 126.4
VI	(R) 184.3	(S) 184.3	(A&R) 121.7
VII	(A&R) 173.6	(S) 164.6	(R) 151.4
VIII	(A&R) 152.8	(R) 141.7	(S) 138.9
IX	(R) 139.1	(A&R) 137.0	(S) 137.0
X	(A&R) 179.2	(R) 166.7	(S) 150.0
XI	(S) 149.5	(R) 144.3	(A&R) 140.2
XII	(R) 171.1	(A&R) 157.2	(S) 148.5
XIII	(S) 143.5	(A&R) 139.1	(R) 133.9

Table 10b

Shows the order of sequence for the worst and three best Tafel slopes under different pulse conditions and different electrolytes using air and reciprocating agitations combined.

	Pulse conditions (Hz, %ϕ) and Tafel slopes (mV/decade)			
Conditions	Worst	Best (3)	Best (2)	Best (1)
I	20,25 (41.7)	1000,75 (145.5)	5000,75 (145.8)	5000,50 (180.2)
II	20&500,25 (76.4)	5000,75 (138.9)	500,75 (144.4)	1000,75 (152.7)
III	20,25 (61.1)	2000,75 (173.6)	500,75& 1000,25 (177.1)	1000,75 (180.1)
IV	20,25 (76.4)	20,75 (152.8)	1000,75&50 (164.6)	5000,75 (182.6)
V	20,25 (84.7)	2000,75 (139.6)	20,75 (150.7)	1000,75 (170.1)
VI	20,25 (94.2)	2000,75&50 (200.0)	500,50 (205.3)	1000,75 (226.3)
VII	20,25 (70.1)	5000,50 (197.9)	5000,25 (204.2)	5000,75 (225.7)
VIII	1000,50 (95.5)	2000,75 (176.4)	5000,50 (180.2)	20,50 (181.3)
IX	20,25 (58.3)	5000,25 (147.8)	2000,50 (150.4)	5000,50 (160.0)
X	20,25 (62.5)	1000,75 (175.0)	2000,75 (176.4)	5000,75 (183.3)
XI	20,25 (52.5)	5000,25& 2000,75 (150.5)	5000,50& 1000,75 (152.1)	5000,50 (158.8)
XII	20,25 (61.8)	5000,50 (175.3)	2000,75 (186.5)	5000,75 (194.3)
XIII	1000,25 (119.5)	1000,75 (166.5)	500,50 (186.9)	500,75 (191.7)

Table 11a
Shows the Wagner number at $2.0Adm^{-2}$ for different agitation modes.

	Wagner Number												
	I	II	III	IV	V	VI	VII	VIII	IX	X	XI	XII	XIII
Still	.233	.335	.223	.292	.260	.220	.296	.251	.248	.265	.247	.302	.298
Reciprocating	.221	.341	.244	.372	.346	.333	.273	.256	.252	.295	.238	.348	.278
Air & reciprocating	.215	.330	.203	.292	.253	.333	.313	.276	.248	.317	.231	.320	.290

Table 11b
Shows the Wagner number at 2.0Adm^{-2} using both air and reciprocating agitations combined.

Pulse conditions (Hz,% ϕ)	Wagner Number												
	I	II	III	IV	V	VI	VII	VIII	IX	X	XI	XII	XIII
20,75	.225	.237	.270	.303	.301	.275	.245	.263	.246	.257	.208	.276	.309
20,50	.173	.263	.236	.230	.221	.266	.214	.327	.197	.209	.151	.216	.280
20,25	.088	.161	.124	.152	.169	.170	.126	.182	.105	.111	.086	.126	.300
500,75	.253	.304	.358	.265	.239	.287	.287	.314	.236	.295	.235	.321	.400
500,50	.197	.222	.211	.171	.192	.371	.251	.241	.238	.258	.219	.297	.390
500,25	.161	.161	.208	.208	.190	.213	.213	.227	.208	.188	.190	.273	.346
1000,75	.306	.321	.364	.327	.340	.408	.270	.194	.244	.309	.251	.290	.347
1000,50	.175	.231	.308	.327	.276	.354	.289	.172	.253	.255	.238	.240	.256
1000,25	.210	.204	.170	.181	.208	.201	.237	.199	.242	.215	.223	.226	.249
2000,75	.285	.231	.351	.263	.279	.361	.319	.318	.262	.312	.248	.380	.342
2000,50	.279	.247	.260	.233	.240	.361	.287	.233	.272	.297	.234	.334	.284
2000,25	.219	.234	.253	.228	.174	.228	.250	.254	.258	.248	.226	.309	.252
5000,75	.307	.292	.330	.363	.271	.332	.406	.282	.244	.324	.262	.395	.322
5000,50	.379	.229	.330	.276	.232	.313	.356	.325	.289	.300	.251	.357	.329
5000,25	.300	.201	.358	.276	.258	.313	.368	.260	.267	.280	.248	.334	.289

Table 12a

Shows the Wagner number enhacement ratio (RWa) at 2.0Adm^{-2} using both air and reciprocating agitations(A&R) combined under unipolar pulse conditions; for RWa≤1 (numerical equivalent of figure 84).

$$R_{Wa} = \frac{\text{Pulse Wagner number}(Wa_p)}{\text{DC Wagner number}(Wa_{DC})}$$

Conditions Hz,%♦ (RWa)												
I	II	III	IV	V	VI	VII	VIII	IX	X	XI	XII	XIII
	20,25 (.488)											
	500,25 (.488)								20,25 (.350)			
	5000,25 (.609)								500,25 (.593)			
	1000,25 (.618)								20,50 (.659)			
	500,50 (.673)		20,25 (.521)			20,25 (.403)			1000,25 (.678)			
	5000,50 (.694)		500,50 (.586)		20,25 (.511)	500,25 (.681)	1000,50 (.623)		2000,25 (.782)			
	1000,50 (.700)		1000,25 (.620)	20,25 (.688)	1000,25 (.604)	20,50 (.684)	20,25 (.659)	20,25 (.423)	1000,50 (.804)		20,25 (.394)	
	2000,75 (.700)		500,25 (.712)	2000,25 (.688)	500,25 (.640)	1000,25 (.757)	1000,75 (.703)	20,50 (.794)	20,75 (.811)		20,50 (.681)	
	2000,25 (.709)		2000,25 (.781)	500,25 (.751)	2000,25 (.685)	20,75 (.783)	1000,25 (.721)	500,25 (.839)	500,50 (.814)	20,25 (.372)	1000,25 (.706)	
20,25 (.409)	20,75 (.718)		20,50 (.788)	500,50 (.759)	20,50 (.799)	2000,25 (.799)	500,25 (.822)	500,75 (.952)	5000,25 (.883)	20,50 (.654)	1000,50 (.750)	1000,25 (.859)
500,25 (.749)	2000,50 (.748)		2000,50 (.798)	1000,25 (.822)	20,75 (.826)	500,50 (.802)	2000,50 (.844)	500,50 (.960)	500,75 (.931)	500,50 (.823)	500,25 (.853)	2000,25 (.869)
20,50 (.805)	20,50 (.797)		2000,75 (.901)	20,50 (.874)	500,75 (.862)	1000,75 (.863)	500,50 (.873)	1000,25 (.976)	2000,50 (.937)	20,75 (.900)	20,75 (.863)	1000,50 (.883)
1000,50 (.814)	5000,75 (.885)		500,75 (.908)	5000,50 (.917)	5000,50 (.940)	500,75 (.917)	2000,25 (.920)	1000,75 (.984)	5000,50 (.946)	500,50 (.948)	1000,25 (.906)	20,50 (.966)
500,50 (.916)	500,75 (.921)	20,25 (.611)	5000,50 (.945)	500,75 (.945)	5000,25 (.940)	2000,75 (.917)	5000,25 (.942)	5000,75 (.984)	1000,75 (.975)	1000,25 (.965)	500,50 (.928)	2000,50 (.979)
1000,25 (.977)	1000,75 (.973)	1000,25 (.837)	5000,25 (.945)	2000,50 (.949)	5000,75 (.997)	1000,50 (.923)	20,75 (.953)	20,75 (.992)	2000,75 (.984)	2000,25 (.978)	2000,25 (.966)	5000,25 (.977)
A&R (1)	A&R (1)	A&R (1)	A&R (1)	A&R (1)	A&R (1)	A&R (1)	A&R (1)	A&R (1)	A&R (1)	A&R (1)	A&R (1)	A&R (1)

Table 12b

Shows the Wagner number enhacement ratio (RWa) at 2.0Adm^{-2} using both air and reciprocating agitations(A&R) combined under unipolar pulse conditions; for RWa≥1 (numerical equivalent of figure 84).

$$R_{Wa} = \frac{\text{Pulse Wagner number}(Wa_P)}{\text{DC Wagner number}(Wa_{DC})}$$

Conditions Hz,%ϕ (RWa)												
I	II	III	IV	V	VI	VII	VIII	IX	X	XI	XII	XIII
A&R (1)	A&R (1)	A&R (1)	A&R (1)	A&R (1)	A&R (1)	A&R (1)	A&R (1)	A&R (1)	A&R (1)	A&R (1)	A&R (1)	A&R (1)
2000,25 (1.02)	Wa no. of the	500,25 (1.02)	20,75 (1.04)	5000,25 (1.02)	1000,50 (1.06)	2000,75 (1.02)	5000,75 (1.02)	1000,50 (1.02)	5000,75 (1.02)	2000,50 (1.01)	500,25 (1)	20,25 (1.03)
20,75 (1.05)	pulse is lower	500,50 (1.04)	1000,75 (1.12)	5000,75 (1.07)	2000,75 (1.08)	5000,50 (1.14)	500,75 (1.14)	2000,25 (1.04)		500,75 (1.02)	2000,50 (1.04)	20,75 (1.07)
500,75 (1.18)	than the DC.	20,50 (1.16)	1000,50 (1.12)	1000,50 (1.09)	2000,50 (1.08)	5000,25 (1.18)	2000,75 (1.15)	2000,75 (1.06)		1000,50 (1.03)	5000,25 (1.04)	5000,75 (1.11)
2000,50 (1.30)		2000,25 (1.25)	5000,75 (1.24)	2000,75 (1.10)	500,50 (1.11)	5000,75 (1.30)	5000,50 (1.18)	5000,25 (1.08)		2000,75 (1.07)	5000,50 (1.12)	5000,50 (1.13)
2000,75 (1.33)		2000,50 (1.28)		20,75 (1.19)	1000,75 (1.23)		20,50 (1.18)	2000,50 (1.10)		5000,25 (1.07)	2000,75 (1.19)	2000,75 (1.18)
5000,25 (1.40)		20,75 (1.33)		1000,75 (1.34)				5000,50 (1.17)		1000,75 (1.09)	5000,75 (1.23)	500,25 (1.19)
1000,75 (1.42)		1000,50 (1.52)								5000,50 (1.09)		1000,75 (1.20)
5000,75 (1.43)		5000,75 (1.63)								5000,75 (1.13)		500,50 (1.34)
5000,50 (1.76)		5000,50 (1.63)										500,75 (1.38)
		2000,75 (1.73)										
		500,75 (1.76)										
		5000,25 (1.76)										
		1000,75 (1.79)										

Table 13

Limiting current density values under PR for different Peak current densities of cathodic(c)/anodic(a) and also different ton(c)/ton(a) ratios for electrolytes I and V;
* indicates that theVoltage(~30V used) on the negative side of the pulse is run out on the power supply hence the limiting current region was not reached..

Peak of c/a	Limiting current density, i_L /Adm^{-2}																							
	1/1						1/2					1/3				1/4				Average				
ton(c)/ton(a)	10/0.2	10/0.5	10/1	10/2	20/0.5	20/1	10/0.2	10/0.5	10/1	10/2	20/1	10/0.2	10/0.5	10/1	10/2	10/0.2	10/0.5	10/1	10/2	10/0.2	10/0.5	10/1	10/2	20/0.5	20/1
Electrolyte I	12.99	10.66	10.46	10.33	10.05	9.40	12.84	10.23	*	*	*	*	*	*	*	*	*	*	*	12.92	10.45	10.46	10.33	10.05	9.40
V	6.97	9.31	9.43	10.05	7.65	7.94	7.15	8.38	*	*	*	*	*	*	*	*	*	*	*	7.06	8.85	9.43	10.05	7.65	7.94

Table 14

Tafel slope values under PR for different Peak current densities of cathodic(c)/anodic(a) and also different ton(c)/ton(a) ratios for electrolytes I and V.

Peak CD of c/a	Tafel slope(mV/decade)																		
	1/1						1/2					1/3				1/4			
ton(c)/ton(a)	10/0.2	10/0.5	10/1	10/2	20/0.5	20/1	10/0.2	10/0.5	10/1	10/2	20/1	10/0.2	10/0.5	10/1	10/2	10/0.2	10/0.5	10/1	10/2
Electrolyte I	277.4	210.3	198.7	185.9	242.0	204.3	253.8	186.2	195.7	143.6	223.6	228.0	178.0	153.2	102.8	202.2	207.5	-	-
V	163.4	142.9	124.2	115.4	149.0	140.4	150.5	140.3	122.4	83.9	133.0	129.0	121.5	97.2	52.1	123.7	112.4	83.9	69.3

Table 15

Wagner number values from high to low under PR condition at $2.0Adm^{-2}$.

$t_{on(c)}/t_{on(a)}$, peak CD of c/a (Wa)	
I	V
10/0.2,1/1 (0.609)	10/0.2,1/1 (0.379)
10/0.2,1/2 (0.557)	10/0.2,1/2 (0.376)
20/0.5,1/1 (0.531)	20/0.5,1/1 (0.343)
10/0.2,1/3 (0.500)	10/0.5,1/1 (0.329)
20/1,1/2 (0.491)	20/1,1/1 & 10/0.5,1/2 (0.323)
10/0.5,1/1 (0.461)	20/1,1/2 (0.306)
10/0.5,1/4 (0.455)	10/0.2,1/3 (0.297)
20/1,1/1 (0.488)	10/1,1/1 (0.286)
10/0.2,1/4 (0.444)	10/0.2,1/4 (0.285)
10/1,1/1 (0.436)	10/1,1/2 (0.282)
10/1,1/2 (0.429)	10/0.5,1/3 (0.280)
10/2,1/1 & 10/0.5,1/2 (0.408)	10/2,1/1 (0.266)
10/0.5,1/3 (0.390)	10/0.5,1/4 (0.259)
10/1,1/3 (0.336)	10/1,1/3 (0.224)
10/2,1/2 (0.315)	10/1,1/4 (0.193)
10/2,1/3 (0.226)	10/2,1/2 (0.192)
	10/2,1/4 (0.160)
	10/2,1/3 (0.120)

Table 16

Wagner enhancement ratios from high to low under PR condition at $2.0Adm^{-2}$.

$t_{on(c)}/t_{on(a)}$, peak CD of c/a R_{Wa}	
I	V
10/0.2,1/1 (2.83)	10/0.2,1/1 (1.50)
10/0.2,1/2 (2.59)	10/0.2,1/2 (1.49)
20/0.5,1/1 (2.47)	20/0.5,1/1 (1.36)
10/0.2,1/3 (2.33)	10/0.5,1/1 (1.30)
20/1,1/2 (2.28)	20/1,1/1 & 10/0.5,1/2 (1.28)
10/0.5,1/1 (2.14)	20/1,1/2 (1.21)
10/0.5,1/4 (2.12)	10/0.2,1/3 (1.17)
20/1,1/1 (2.27)	10/1,1/1 (1.13)
10/0.2,1/4 (2.07)	10/0.2,1/4 (1.13)
10/1,1/1 (2.03)	10/1,1/2 (1.11)
10/1,1/2 (2.00)	10/0.5,1/3 (1.11)
10/2,1/1 & 10/0.5,1/2 (1.90)	10/2,1/1 (1.05)
10/0.5,1/3 (1.81)	10/0.5,1/4 (1.02)
10/1,1/3 (1.56)	A&R (1)
10/2,1/2 (1.47)	10/1,1/3 (0.885)
10/2,1/3 (1.05)	10/1,1/4 (0.763)
A&R (1)	10/2,1/2 (0.759)
	10/2,1/4 (0.632)
	10/2,1/3 (0.474)

Table 17a

Limiting current density values for different quantities of Cl– concentrations under DC and pulse conditions using electrolyte I and A & R agitations combined.

	Limiting current density, i_L/Adm^{-2}						
ppm Cl^-	0	25	50	75	100	150	200
Conditions DC	9.77	9.17	7.96	8.89	7.79	8.29	8.89
100Hz, 50%ϕ	9.90	9.52	9.38	8.50	7.62	8.46	8.92

Table 17b

Tafel slope values for different quantities of Cl– concentrations under DC and pulse conditions using electrolyte I and A & R agitations combined.

	Tafel slope (mV/decade)						
ppm Cl^-	0	25	50	75	100	150	200
Conditions DC	106.5	145.2	154.8	152.7	134.4	144.1	152.7
100Hz, 50%ϕ	90.0	97.5	112.5	100.0	108.9	111.1	105.6

Table 17c

Wagner number values for different quantities of Cl– concentrations under DC and pulse conditions at 2.0Adm^{-2} using electrolyte I and A & R agitations combined.

	Wagner number						
ppm Cl^-	0	25	50	75	100	150	200
Conditions DC	.211	.288	.307	.303	.266	.285	.303
100Hz, 50%ϕ	.178	.193	.223	.198	.216	.220	.209

Table 18 Showing the S/H ratio for different conditions such as DC, P and PR using different holes and board thicknesses.

Hole Size (mm)	Board Thickness (mm)	Aspect Ratio	DC or Pulse Conditions Hz, %ϕ	S/H Ratio C.D. (Adm^{-2}) 4	3	2	1	Electrolyte
1.5	2.5	1.67:1	DC		1.47:1			I
1.5	2.5	1.67:1	DC		1.30:1			III
1.5	2.5	1.67:1	DC		1.30:1			V
0.8	2.4	3:1	DC		1.31:1			I
0.8	2.4	3:1	DC		1.28:1			III
0.8	2.4	3:1	DC		1.50:1			V
0.8	2.5	3.125:1	DC		1.51:1			I
0.8	2.5	3.125:1	DC		1.46:1			III
0.8	2.5	3.125:1	DC		1.42:1			V
0.3	2.4	8:1	DC		1.35:1			I
0.3	2.4	8:1	DC		1.30:1			III
0.3	2.4	8:1	DC		1.63:1			V
1.5	2.5	1.67:1	5000,50	1.04:1	1.05:1	1.04:1	0.99:1	I
1.5	2.5	1.67:1	1000,75	1.33:1	1.32:1	0.96:1	1.02:1	III
1.5	2.5	1.67:1	1000,75		1.36:1			V
0.8	2.4	3:1	5000,50		1.35:1			I
0.8	2.4	3:1	1000,75		1.31:1			III
0.8	2.4	3:1	5000,25		1.13:1			III
0.8	2.4	3:1	1000,75		1.50:1			V
0.8	2.4	3:1	5000,25		1.36:1			V
0.8	2.4	3:1	5000,75		2.23:1			XIII
0.8	2.5	3.125:1	5000,50	1.06:1	0.98:1	1.06:1	1.08:1	I
0.8	2.5	3.125:1	1000,75	1.26:1	1.34:1	1.13:1	1.08:1	III
0.8	2.5	3.125:1	1000,75		1.76:1			V

Table 18 Continued ...

Hole Size (mm)	Board Thickness (mm)	Aspect Ratio	DC or Pulse Conditions Hz, %ϕ	S/H Ratio C.D. (Adm^{-2}) 4	3	2	1	Electrolyte
0.3	2.4	8:1	5000,50		1.06:1			I
0.3	2.4	8:1	1000,75		1.32:1			III
0.3	2.4	8:1	5000,25		1.13:1			III
0.3	2.4	8:1	1000,75		1.75:1			V
0.3	2.4	8:1	5000,25		1.90:1			V
0.3	2.4	8:1	5000,75		1.68:1			XIII
1.5	1.6	1.06:1	1000,75		1.14:1			III
1.5	1.6	1.06:1	20,25		1.15:1			III
1.5	1.6	1.06:1	1000,75		1:1			V
1.5	2.5	1.67:1	20,25		1.1:1	1.6:1	0.77:1	I
1.5	2.5	1.67:1	20,25		1.70:1	1.1:1	1.04:1	III
1.5	2.5	1.67:1	20,25		1.11:1			V
0.8	1.6	2:1	1000,75		1.13:1			III
0.8	1.6	2:1	20,25		1.1:1			III
0.8	1.6	2:1	1000,75		1:1			V
0.8	2.4	3:1	20,25		1.19:1			I
0.8	2.4	3:1	20,25		1.50:1			III
0.8	2.4	3:1	20,25		1.48:1			V
0.8	2.5	3.125:1	20,25		1.36:1	2.17:1	0.97:1	I
0.8	2.5	3.125:1	20,25		1.77:1	1.26:1	1.17:1	III
0.8	2.5	3.125:1	20,25		1.28:1			V
0.3	2.4	8:1	20,25		1.67:1			I
0.3	2.4	8:1	20,25		2.40:1			III
0.3	2.4	8:1	20,25		1.58:1			V

Table 18 Continued ...

Hole Size (mm)	Board Thickness (mm)	Aspect Ratio	DC or PR* $t_{on(c)}/t_{on(a)}$, c/a Peak C.D.	S/H Ratio C.D. (Adm^{-2}) 4 3 2 1	Electrolyte
1.5	2.5	1.67:1	10/0.5,1/3	1:1	V
0.8	2.4	3:1	10/0.2,1/1	1.21:1	I
0.8	2.4	3:1	10/0.2,1/3	1.03:1	I
0.8	2.4	3:1	10/2,1/3	1.51:1	I
0.8	2.4	3:1	10/0.5,1/3	1.47:1	V
0.8	2.4	3:1	10/0.2,1/1	1.51:1	V
0.8	2.4	3:1	10/0.2,1/2	1.47:1	V
0.8	2.4	3:1	10/0.2,1/3	1.07:1	V
0.8	2.4	3:1	10/0.2,1/4	1.04:1	V
0.8	2.4	3:1	10/0.2,1/8	1.13:1	V
0.8	2.4	3:1	10/2,1/3	2.02:1	V
0.8	2.5	3.125:1	10/0.5,1/3	1:1	V
0.3	2.4	8:1	10/0.2,1/1	1.58:1	I
0.3	2.4	8:1	10/0.2,1/3	1.09:1	I
0.3	2.4	8:1	10/2,1/3	2.03:1	I
0.3	2.4	8:1	10/0.5,1/3	1.54:1	V
0.3	2.4	8:1	10/0.2,1/1	2.03:1	V
0.3	2.4	8:1	10/0.2,1/2	1.53:1	V
0.3	2.4	8:1	10/0.2,1/3	1.31:1	V
0.3	2.4	8:1	10/0.2,1/4	1.34:1	V
0.3	2.4	8:1	10/0.2,1/8	1.27:1	V
0.3	2.4	8:1	10/2,1/3	2.70:1	V

* t is in ms and ϕ=100%

Table 19
MORPHOLOGY, EFFICIENCY, SURFACE ROUGHNESS, GRAIN SIZE AND HARDNESS STUDIES.

ELECTROPLATING OF COPPER FOR THE STUDY OF:

A) MORPHOLOGY / SEM X2000, X750, X500
B) EFFICIENCY / M_P/M_{DC}
C) SUFACE ROUGHNESS / RANK TAYLOR HOBSON TELLYSURF 10
D) MICRO-HARDNESS / MEF2, VICKERS MICROHARDNESS

Conditions:

COPPER CATHODE SUBSTRATE (10x3.5x2)= 70cm^2 =0.7dm^2
FARNELL POWER SUPPLY L12-10C
DURATION OF PLATING 00:37:40
PLATING THICKNESS 25µm
ELECTROLYTE VIII STANDARD SOLUTION WITHOUT Cl$^-$.

Sample Number	Condition DC/Hz,%ø	Weight g	Efficiency* M_P/M_{DC}	i Adm^{-2}	Ip A	I A	R_a µm	R_{tm} µm	H.V. Kgmm^{-2}
32	DC	1.5696	100	3	2.1	2.1	1.12	5.97	92.12
29	100,25	1.5592	99.34	3	8.4	2.1	.83	5.7	94.77
30	100,50	1.5523	98.90	3	4.2	2.1	.79	4.5	111.69
31	100,75	1.5549	99.06	3	2.8	2.1	.87	5.1	112.07

ELECTROLYTE I STANDARD SOLUTION.

Sample Number	Condition DC/Hz,%ø	Weight g	Efficiency* W_P/W_{DC}	i Adm^{-2}	Ip A	I A	R_a µm	R_{tm} µm	H.V. Kgmm^{-2}
35	DC	1.8006	100	3	2.1	2.1	1.13	5.97	142.10
36	20,25	1.5857	88.1	3	8.4	2.1	.81	4.6	101.51
37	20,50	1.2864	71.4	3	4.2	2.1	1.04	5.63	101.86
38	20,75	1.5058	83.6	3	2.8	2.1	1.13	6.03	115.41
39	100,25	1.4189	78.8	3	8.4	2.1	.88	5.1	97.16
40	100,50	1.4741	81.9	3	4.2	2.1	.93	5.5	105.11
41	100,75	1.5218	84.5	3	2.8	2.1	1.0	5.13	130.36
42	500,25	1.4073	78.2	3	8.4	2.1	1.0	5.7	107.00
43	500,50	1.5156	84.2	3	4.2	2.1	1.13	6.43	108.11
44	500,75	1.5361	85.3	3	2.8	2.1	1.1	6.37	112.69
45	1000,25	1.4478	80.4	3	8.4	2.1	1.12	6.2	97.35
47	1000,50	1.5065	83.7	3	4.2	2.1	1.02	5.53	105.31
53	1000,75	1.5585	86.6	3	2.8	2.1	1.17	6.27	123.02
54	2000,25	1.5539	86.3	3	8.4	2.1	1.08	6.0	103.98
55	2000,50	1.5669	87.0	3	4.2	2.1	1.17	6.0	108.65
56	2000,75	1.5556	86.4	3	2.8	2.1	1.1	5.67	108.21
57	3000,25	1.5788	87.7	3	8.4	2.1	1.12	6.63	103.87
58	3000,50	1.5701	87.2	3	4.2	2.1	1.13	5.8	103.15
59	3000,75	1.5661	87.0	3	2.8	2.1	1.07	5.53	102.50
60	4000,25	1.5824	87.9	3	8.4	2.1	1.13	5.67	109.40
61	4000,50	1.5722	87.3	3	4.2	2.1	1.12	5.93	102.32
62	4000,75	1.5688	87.1	3	2.8	2.1	1.05	5.57	108.65
63	5000,25	1.5953	88.6	3	8.4	2.1	1.03	5.77	101.86
64	5000,50	1.5787	87.7	3	4.2	2.1	1.0	5.33	115.41
65	5000,75	1.5652	86.9	3	2.8	2.1	1.05	5.87	120.84
65	COPPER SHEET						.26	1.43	90.15

Table 19 Continued ...

ELECTROLYTE V CONTAINING ALL THE ADDITIVES.

Sample Number	Condition DC/Hz,%ø	Weight g	Efficiency* M_P/M_{DC}	i Adm^{-2}	Ip A	I A	R_a µm	R_{tm} µm	H.V. $Kgmm^{-2}$
1	DC	1.5193	100	3	2.1	2.1	.397	2.1	130.44
2	20,25	1.5169	99.8	3	8.4	2.1	.185	1.07	93.29
3	20,50	1.5587	103	3	4.2	2.1	.303	1.5	99.47
4	20,75	1.5502	102	3	2.8	2.1	.37	1.77	97.55
5	100,25	1.5512	102	3	8.4	2.1	.323	1.55	107.11
6	100,50	1.5485	102	3	4.2	2.1	.312	1.57	106.69
7	100,75	1.5777	104	3	2.8	2.1	.323	1.67	106.43
8	500,25	1.5562	103	3	8.4	2.1	.153	.85	107.57
9	500,50	1.5515	102	3	4.2	2.1	.092	.53	109.54
10	500,75	1.5443	102	3	2.8	2.1	.268	1.5	98.86
11	1000,25	1.5378	101	3	8.4	2.1	.283	.963	108.18
12	1000,50	1.5444	102	3	4.2	2.1	.157	.087	117.70
13	1000,75	1.5495	102	3	2.8	2.1	.227	1.23	111.82
14	2000,25	1.5559	102	3	8.4	2.1	.18	1.18	109.30
15	2000,50	1.5541	102	3	4.2	2.1	.2	1.07	103.30
16	2000,75	1.5508	102	3	2.8	2.1	.273	1.45	106.62
17	3000,25	1.5582	103	3	8.4	2.1	.227	1.18	111.51
18	3000,50	1.5665	103	3	4.2	2.1	.295	1.47	109.32
19	3000,75	1.5489	102	3	2.8	2.1	.393	1.87	105.86
20	4000,25	1.5769	104	3	8.4	2.1	.268	1.65	111.43
21	4000,50	1.5643	103	3	4.2	2.1	.278	1.42	117.31
22	4000,75	1.5538	102	3	2.8	2.1	.253	1.32	113.15
23	5000,25	1.5708	103	3	8.4	2.1	.168	.9	111.75
24	5000,50	1.5610	103	3	4.2	2.1	.203	1.03	112.08
25	5000,75	1.5598	103	3	2.8	2.1	.253	1.38	115.20
25	COPPER SHEET ONLY						.08	.6	

* N.B. not conventional current efficiency, DC = 100%

Table 20
MORPHOLOGY, TENSILE STRENGTH AND ELONGATION STUDIES UNDER DC, UNIPOLAR PULSE AND BIPOLAR PULSE REVERSE AND ALSO COLD ROLLED COPPER.

ELECTROPLATING OF COPPER FOR THE STUDY OF:
A) MORPHOLOGY
B) ULTIMATE TENSILE STRENGTH
C) ELONGATION
D) SURFACE COVERAGE

Conditions:
STAINLESS STEEL CATHODE SUBSTRATE (15x5x2)= 150cm^2 = 1.5dm^2
FARNELL POWER SUPPLY AP30-80
DURATION OF PLATING 01:15:20
PLATING THICKNESS 50µm

ELECTROLYTE I STANDARD SOLUTION - UNIPOLAR PULSE

Sample Number	Conditions DC/Hz,%ø	C.D. Adm^{-2}	T.S. Nmm^{-2}	Elongation (%)
1	DC	3	312.6	7.1
2	20,25	3	196.9	7.78
3	20,50	3	174.6	3.34
4	20,75	3	169.4	2.89
5	100,25	3	169.1	5.34
6	100,50	3	203.3	6.22
7	100,75	3	235.3	4.84
8	500,25	3	195.8	5
9	500,50	3	230.1	6.67
10	500,75	3	204.7	3.67
11	1000,25	3	188.5	3.84
12	1000,50	3	196.7	3
13	1000,75	3	202.8	2.5
14	2000,25	3	242.3	6.17
15	2000,50	3	248.6	3.33
16	2000,75	3	269.7	5.11
17	3000,25	3	274.6	7.7
18	3000,50	3	271.6	5.33
19	3000,75	3	269.5	6
20	4000,25	3	269.0	6.96
21	4000,50	3	229.8	3.33
22	4000,75	3	348.1	9.84
23	5000,25	3	249.5	4
24	5000,50	3	252.0	6.77
25	5000,75	3	215.7	3

ELECTROLYTE I STANDARD SOLUTION - BIPOLAR PULSE REVERSE

Sample Number	Conditions $i_{p(c)}/i_{p(a)}$, $t_{on(c)}/t_{on(a)}$	C.D. Adm^{-2}	T.S. Nmm^{-2}	Elongation (%)
A	1/3,10/0.5	3	179.8	9.2
B	1/1,10/0.2	3	319.2	6.7
C1	1/2,10/0.2	3	281.8	7.9
C2	1/3,10/0.2	3	274.2	7.7
C3	1/4,10/0.2	3	284.8	5.3

Table 20 Continued ...

ELECTROLYTE V CONTAINING ALL THE ADDITIVES - UNIPOLAR PULSE

Sample Number	Conditions DC/Hz,%ø	C.D. Adm-2	T.S. Nmm-2	Elongation (%)
1	DC	3	301.1	6.67
2	20,25	3	264.7	4.33
3	20,50	3	267.6	7.78
4	20,75	3	301.3	8.11
5	100,25	3	284.3	5.78
6	100,50	3	330.9	7.66
7	100,75	3	304.2	6.67
8	500,25	3	315.9	8.33
9	500,50	3	314.6	5.78
10	500,75	3	318.9	5.67
11	1000,25	3	298.1	6.55
12	1000,50	3	330.1	5.44
13	1000,75	3	338.2	7.67
14	2000,25	3	321.4	8.11
15	2000,50	3	301.9	11.11
16	2000,75	3	285.2	10
17	3000,25	3	283.2	11.78
18	3000,50	3	312.2	1.34
19	3000,75	3	296.2	11.78
20	4000,25	3	285.0	5.56
21	4000,50	3	306.2	5.84
22	4000,75	3	313.8	9
23	5000,25	3	306.9	10
24	5000,50	3	320.7	9.33
25	5000,75	3	316.3	9

ELECTROLYTE V STANDARD SOLUTION - BIPOLAR PULSE REVERSE

Sample Number	Conditions $i_{p(c)}/i_{p(a)}$, $t_{on(c)}/t_{on(a)}$	C.D. Adm^{-2}	T.S. Nmm^{-2}	Elongation (%)
F	1/3,10/0.5	3	289.4	9.45
G	1/1,10/0.2	3	282.2	9.78
H	1/2,10/0.2	3	251.3	7
I	1/3,10/0.2	3	281.3	7
J	1/4,10/0.2	3	293.9	10

COLD ROLLED COPPER

Percentage Cold Rolled	Thickness µm	H.V. $Kgmm^{-2}$	T.S. Nmm^{-2}	Elongation (%)
0	250	89.77	235.9	12
5	237.5	99.64	238.8	5.78
25	187.5	111.07	211.2	1.17
50	125	123.49	441.0	2.44
75	62.5	113.64	771.2	1.33

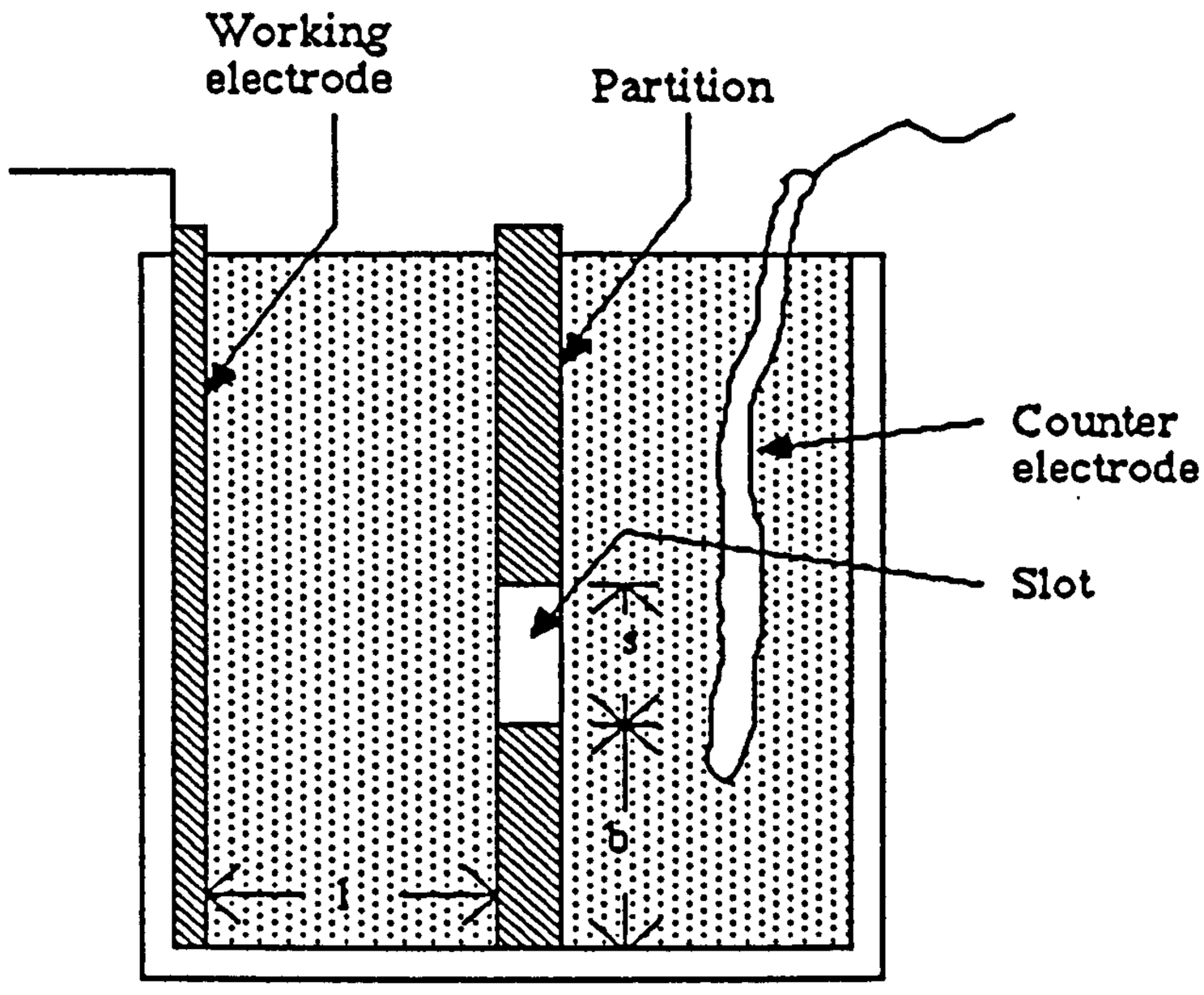

Figure 3[44] Schematic of slot-type field-shaping cell in which the position s, b and l can be adjusted.

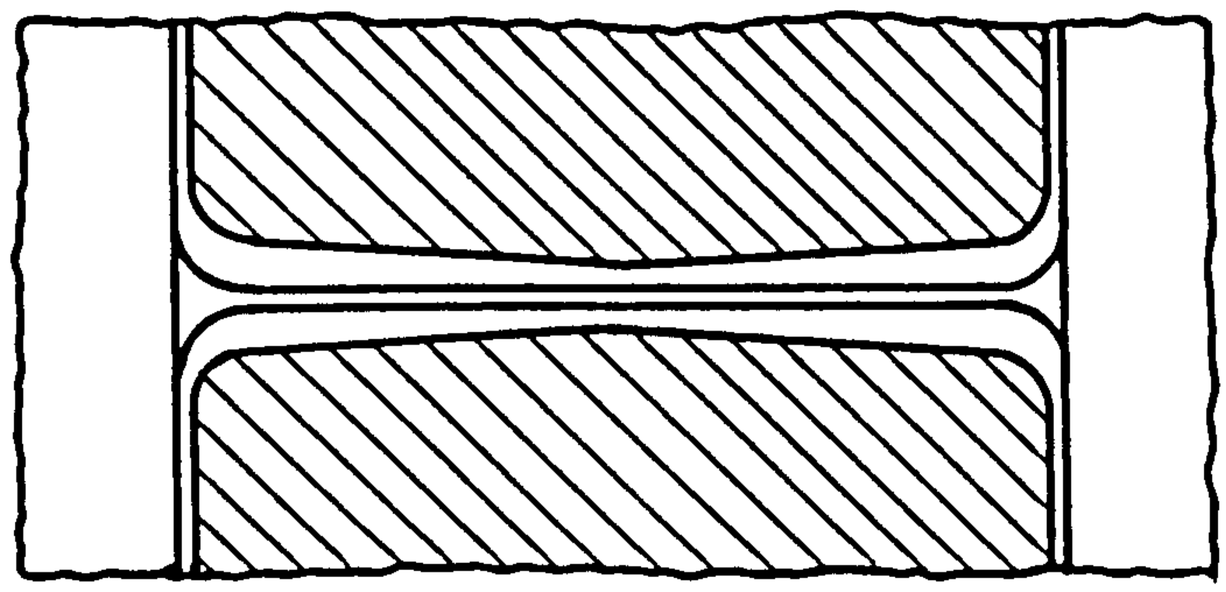

(a)

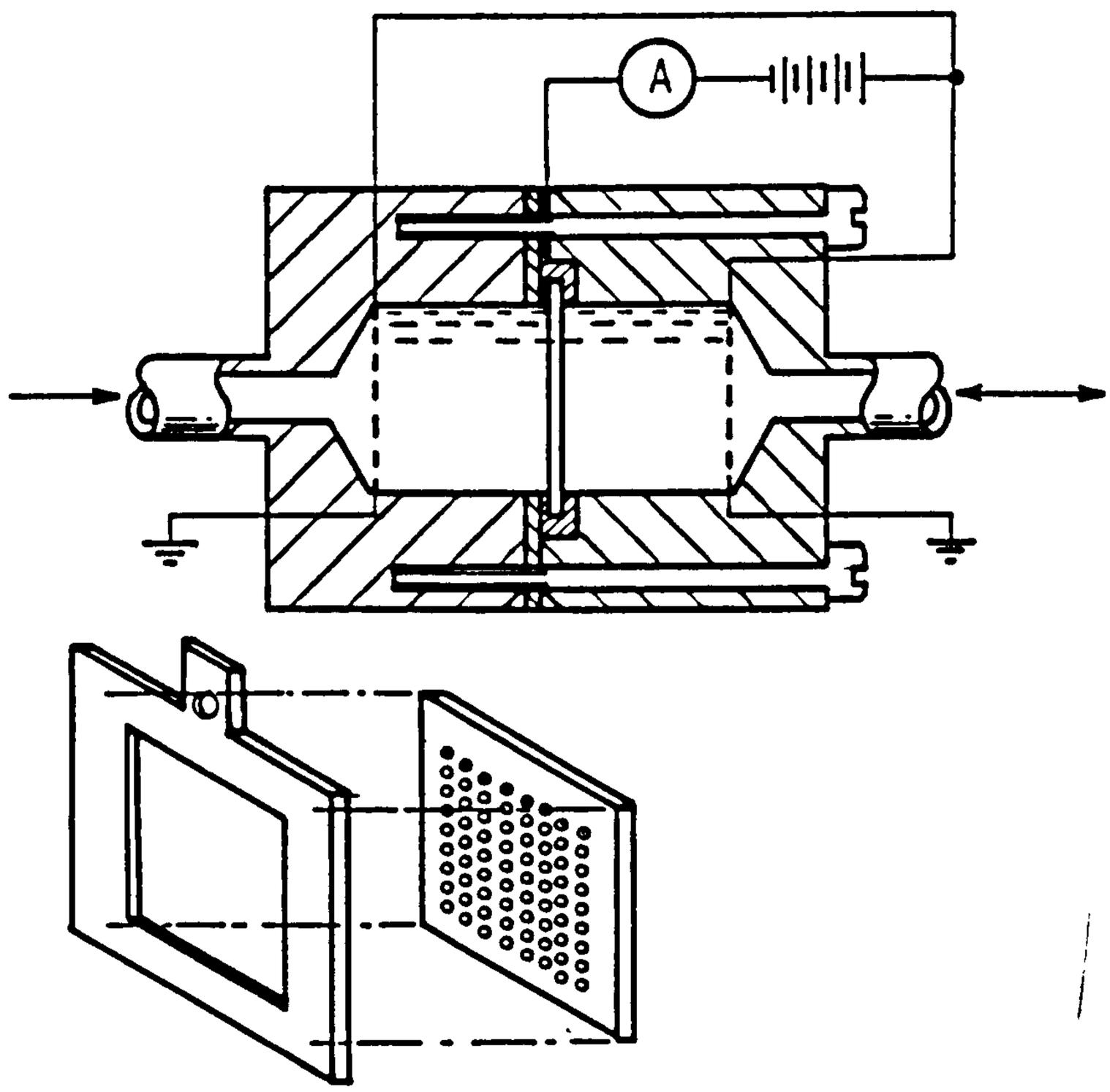

(b)

Figure 4[31] Schematic design of holes and a plating cell

a) enlarged tapered substrate

b) plating apparatus and cell cross-section in situ.

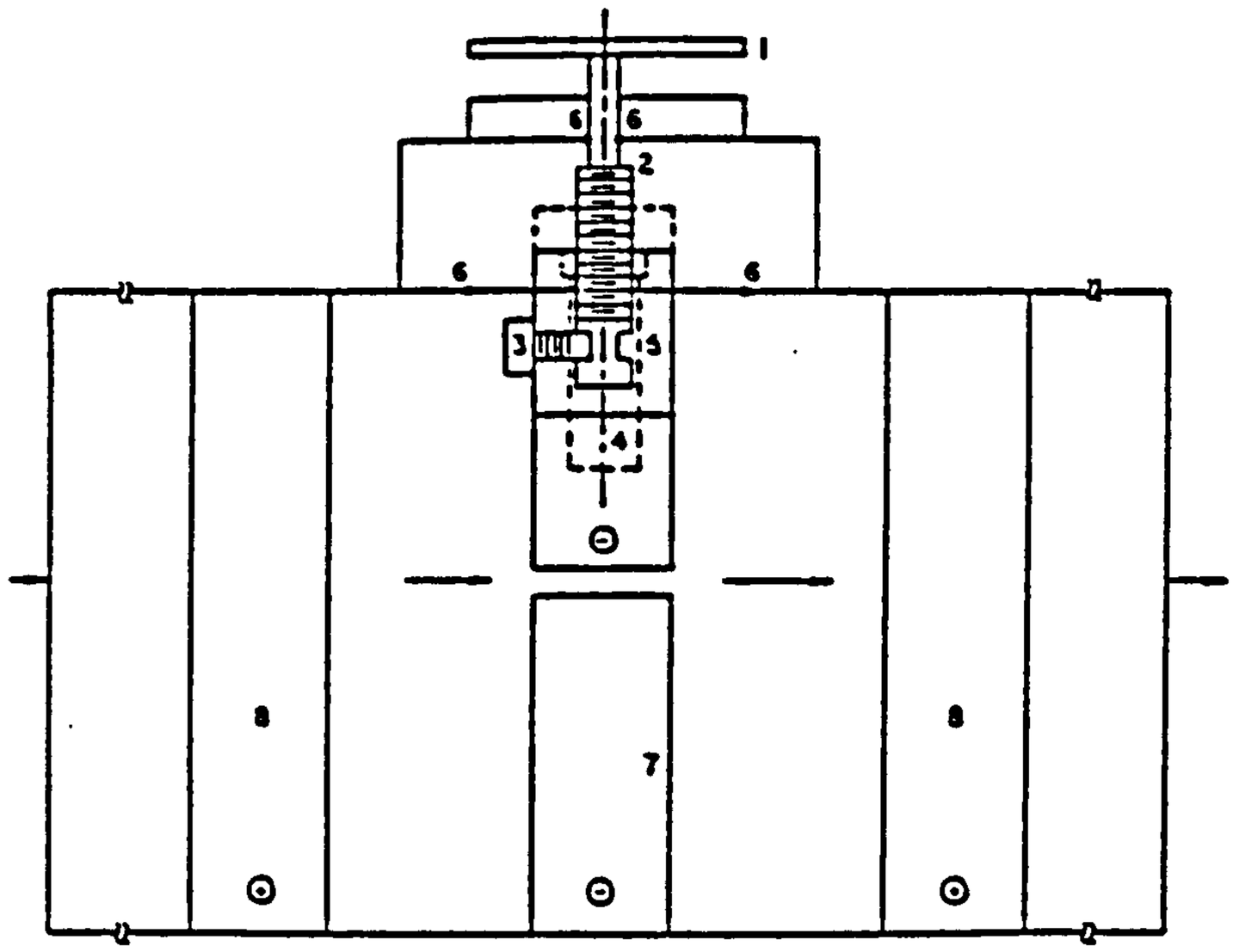

Figure 5[28] Schematic of the gap cell

1. dial 2. precision screw 3. set screw 4. bolt
5. upper cathode piece 6. O-ring 7. bottom cathode piece
8. anodes.

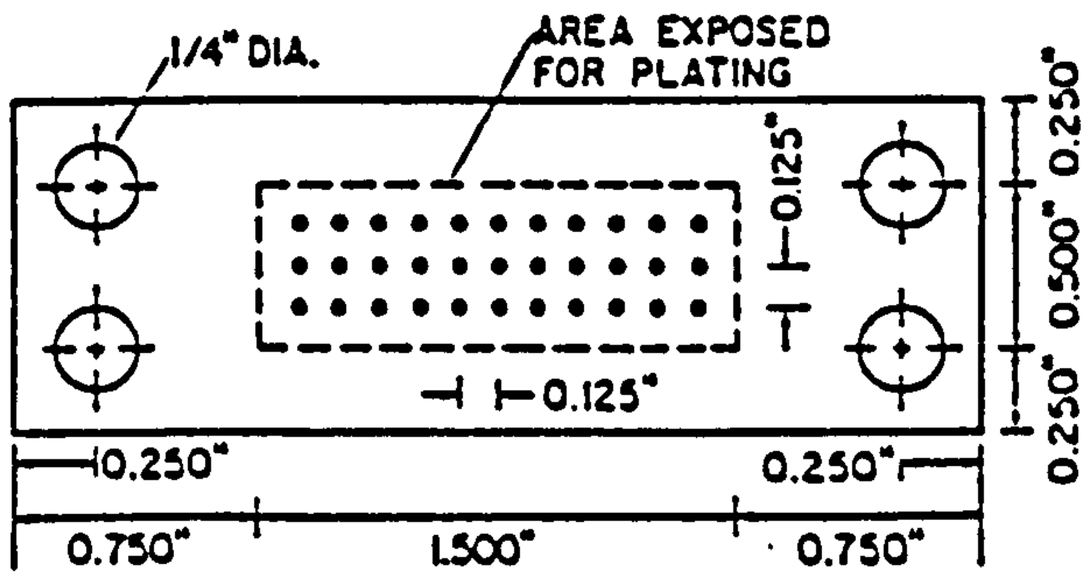

(a)

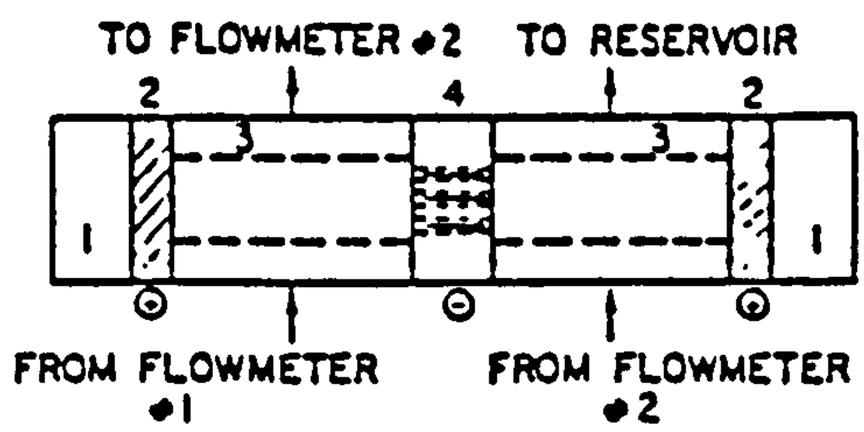

(b)

Figure 6[28] a) Layout of Plexiglas boards for PTH experiment b) cell design for PTH experiments

1. backing plates 2. anodes 3. spacers 4. cathodes(PTH sample boards).

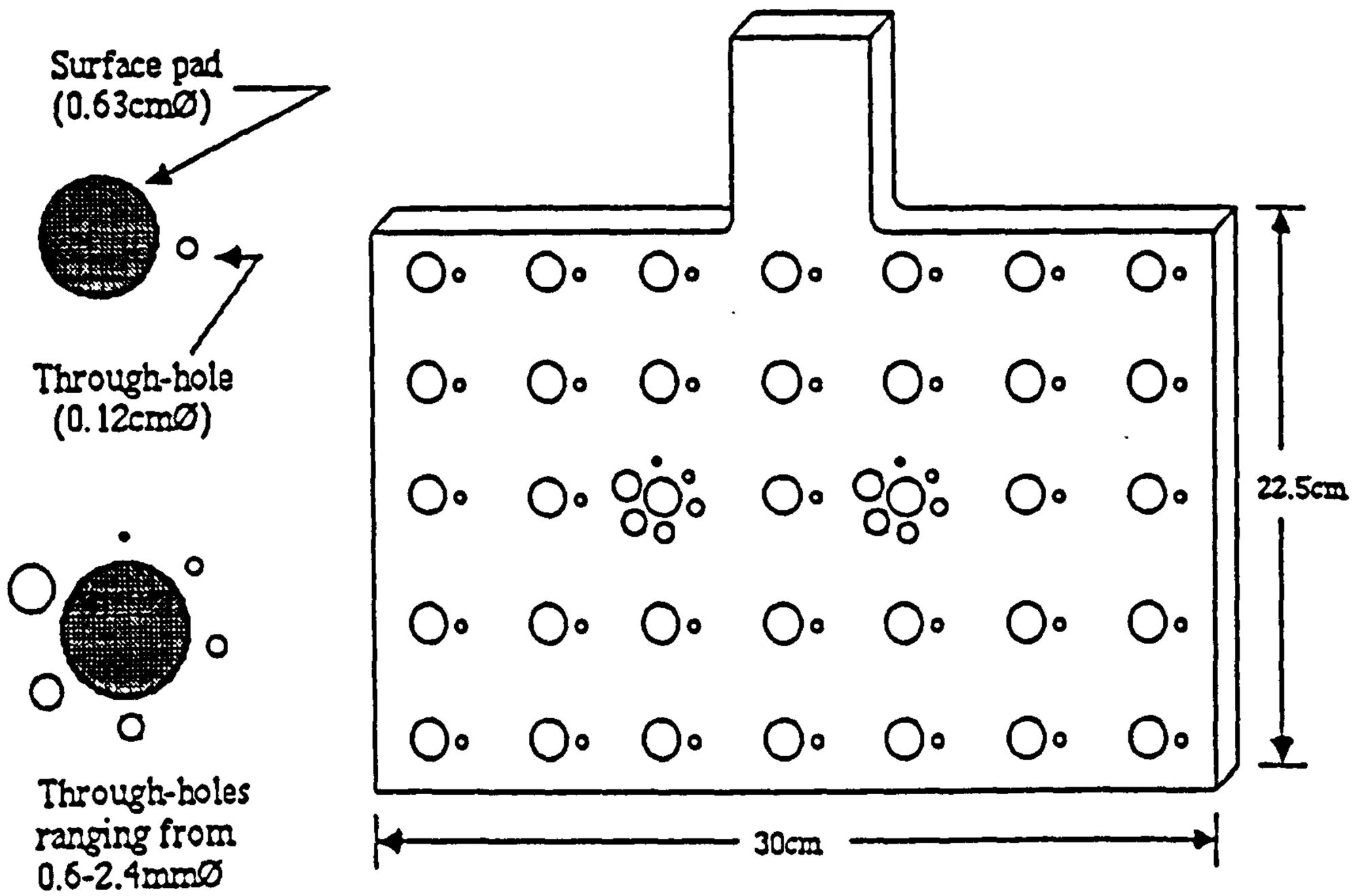

Figure 7[33] Illustration of the agitation test board used by Haak et al. Through-holes and surface pads are coated with gold.

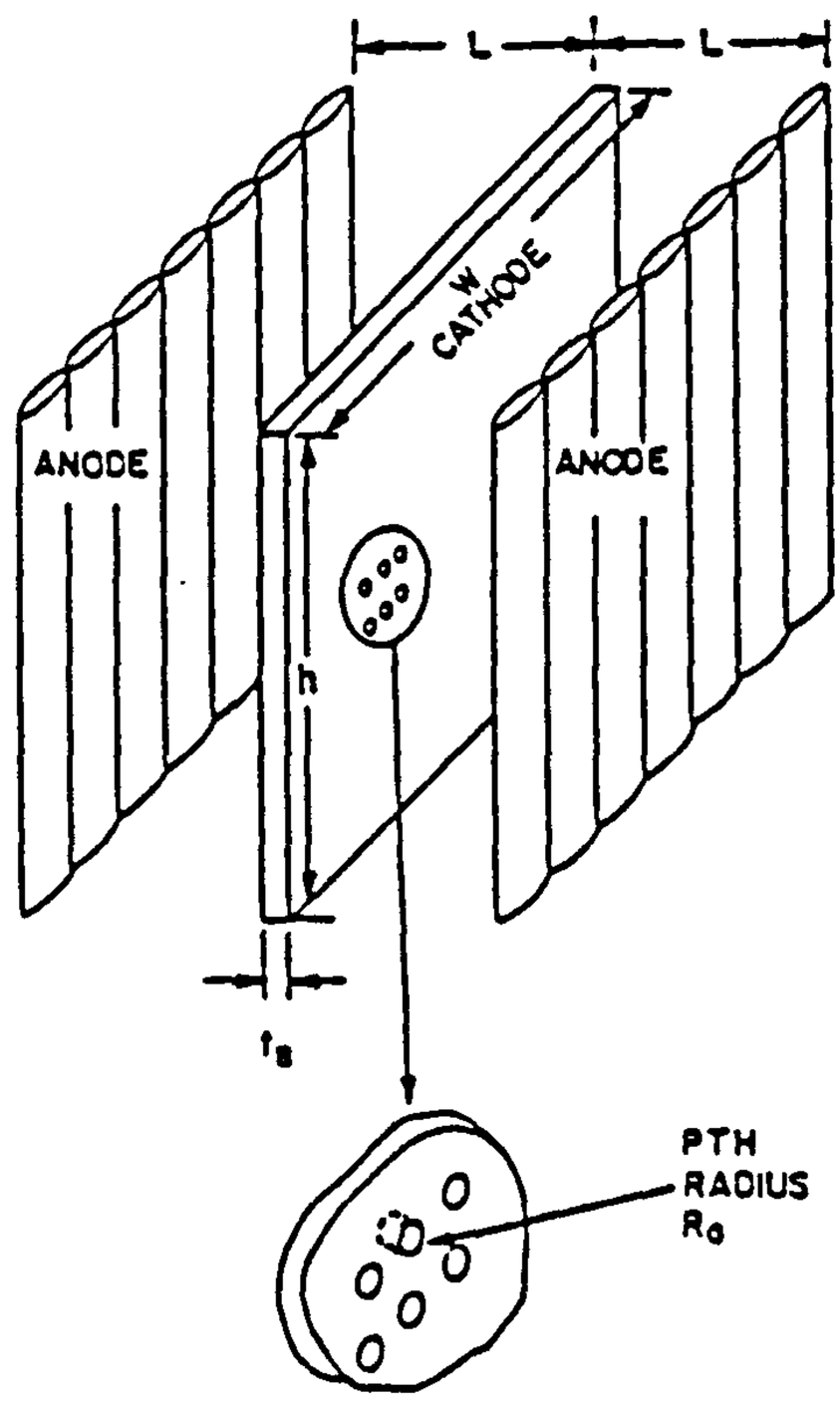

Figure 8[45] Schematic of a typical MLB electroplating cell.

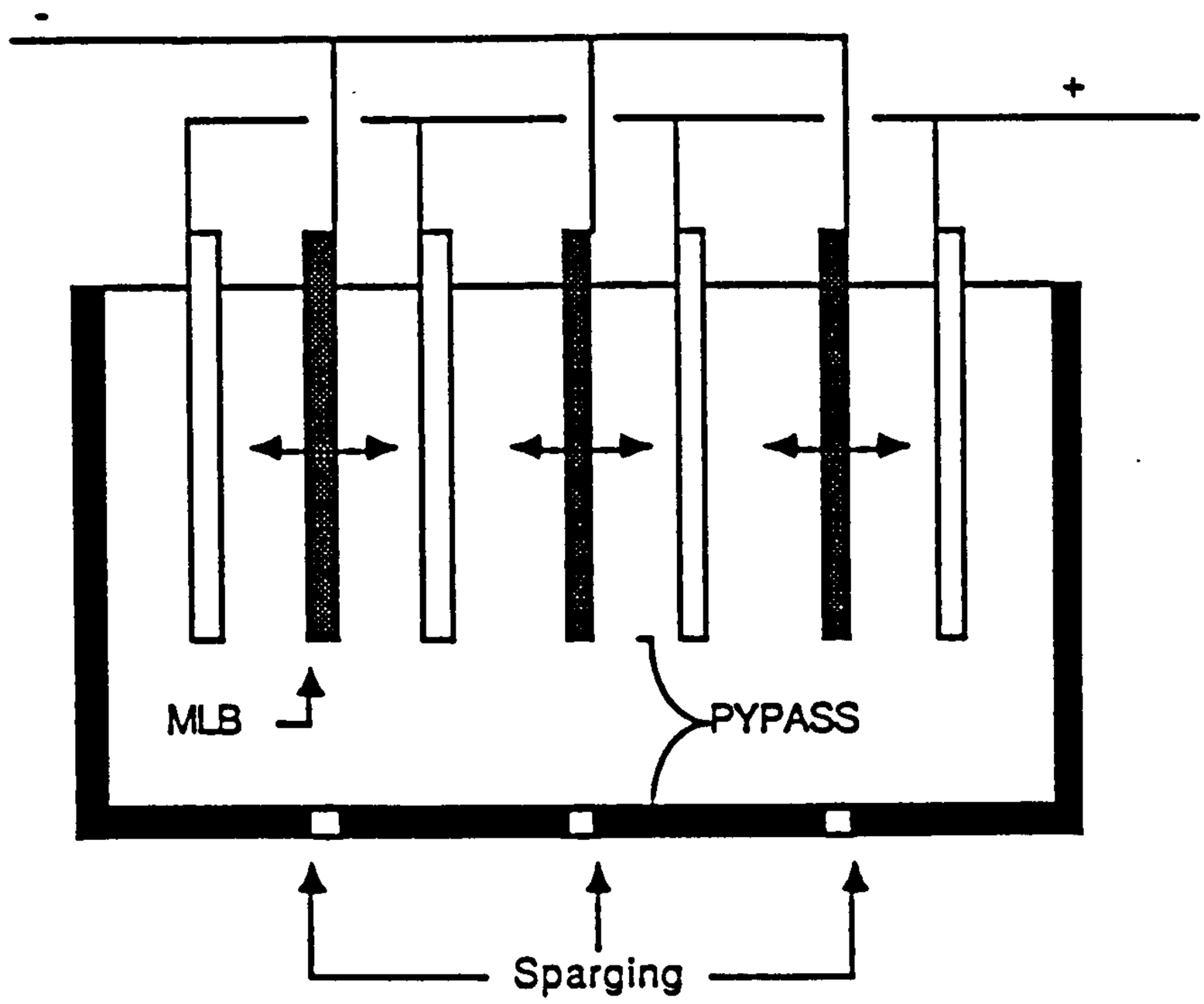

(a)

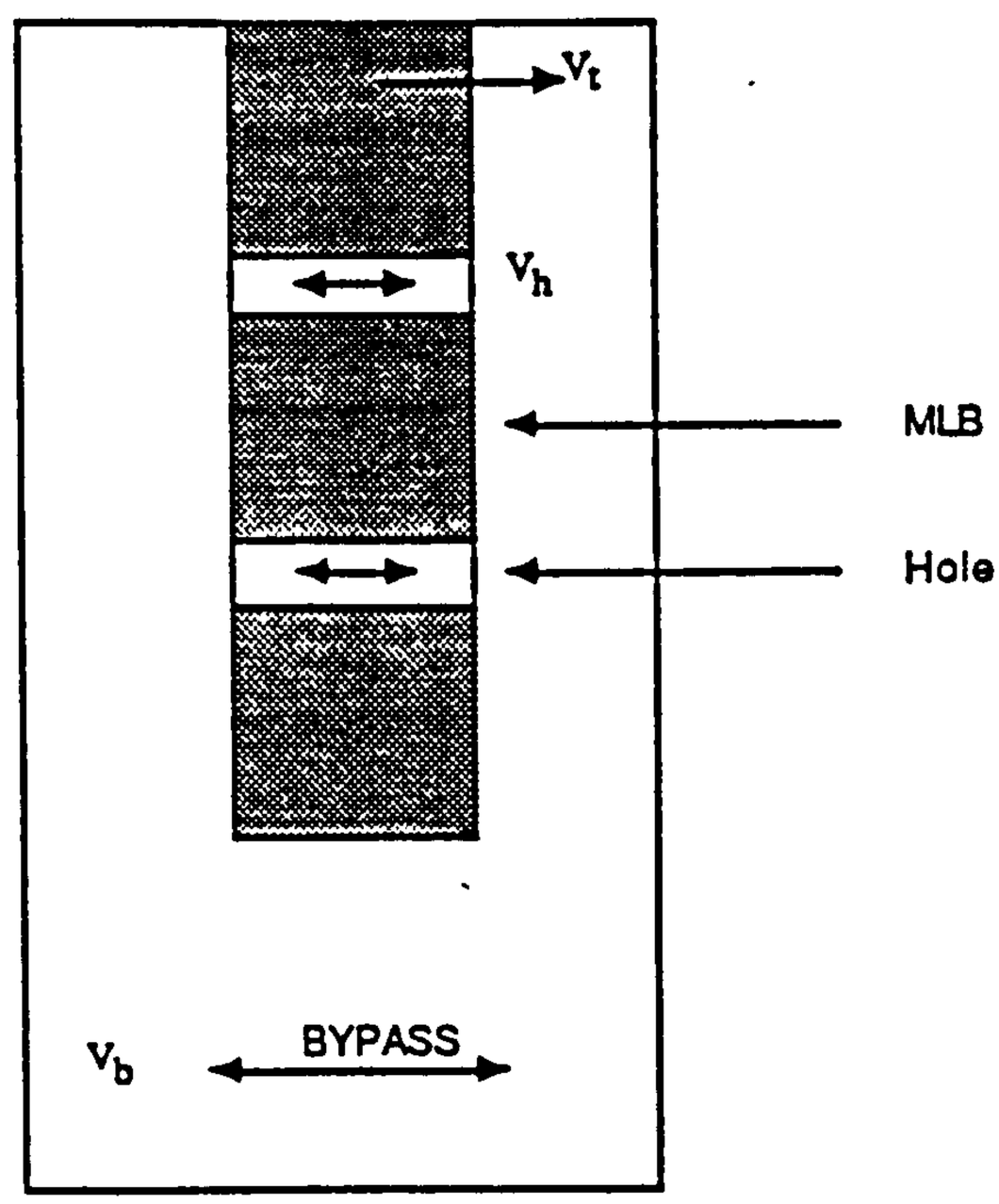

(b)

Figure 9[40] a) Schematic of a MLB cell

b) Diagram of a translating board and the resulting fluid flow; V_b, V_h and V_t indicate the velocities of the bulk, hole and translating board.

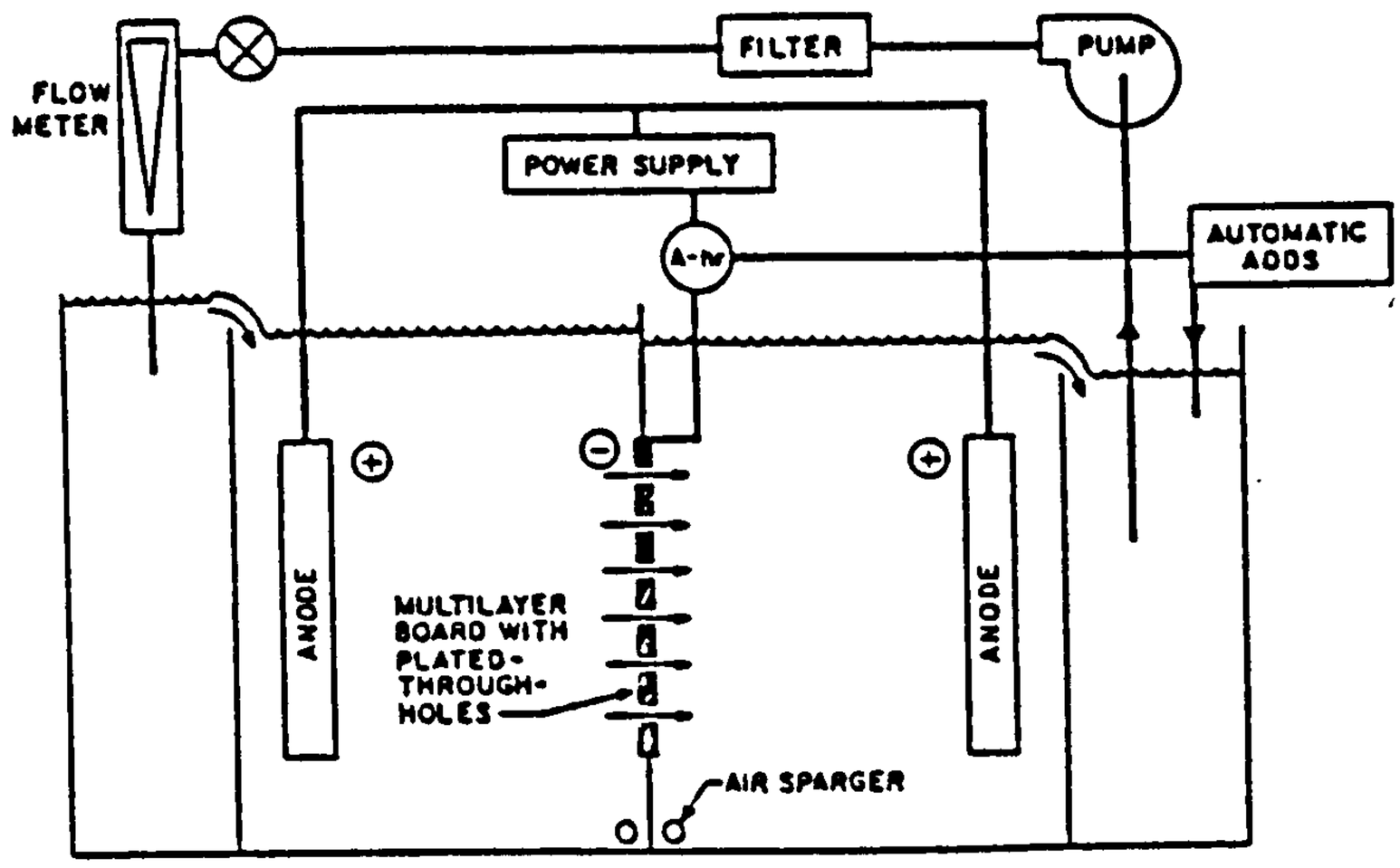

Figure 10[27] Schematic of a forced-flow electroplating system.

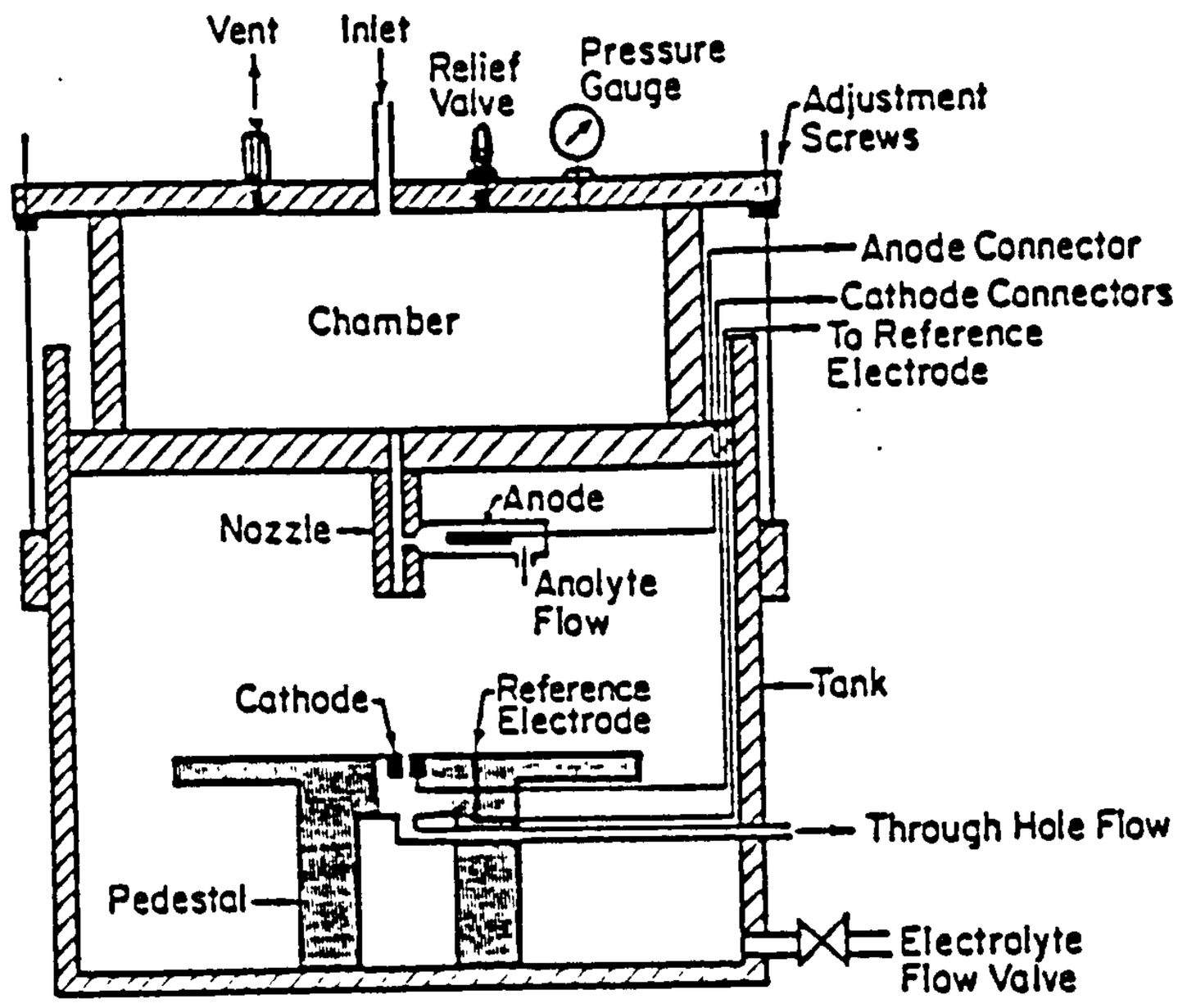

Figure 11[3] Schematic of an impinging jet electrochemical cell.

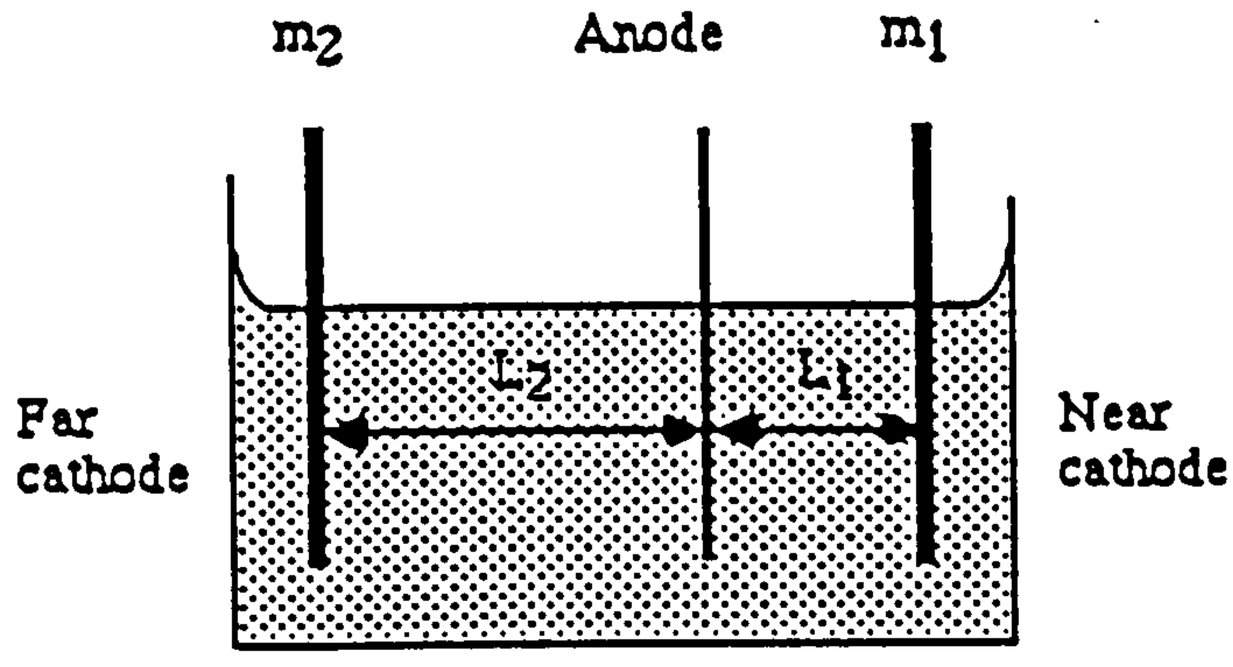

Figure 12 Shows the position of the electrodes in an Haring-Blum cell.

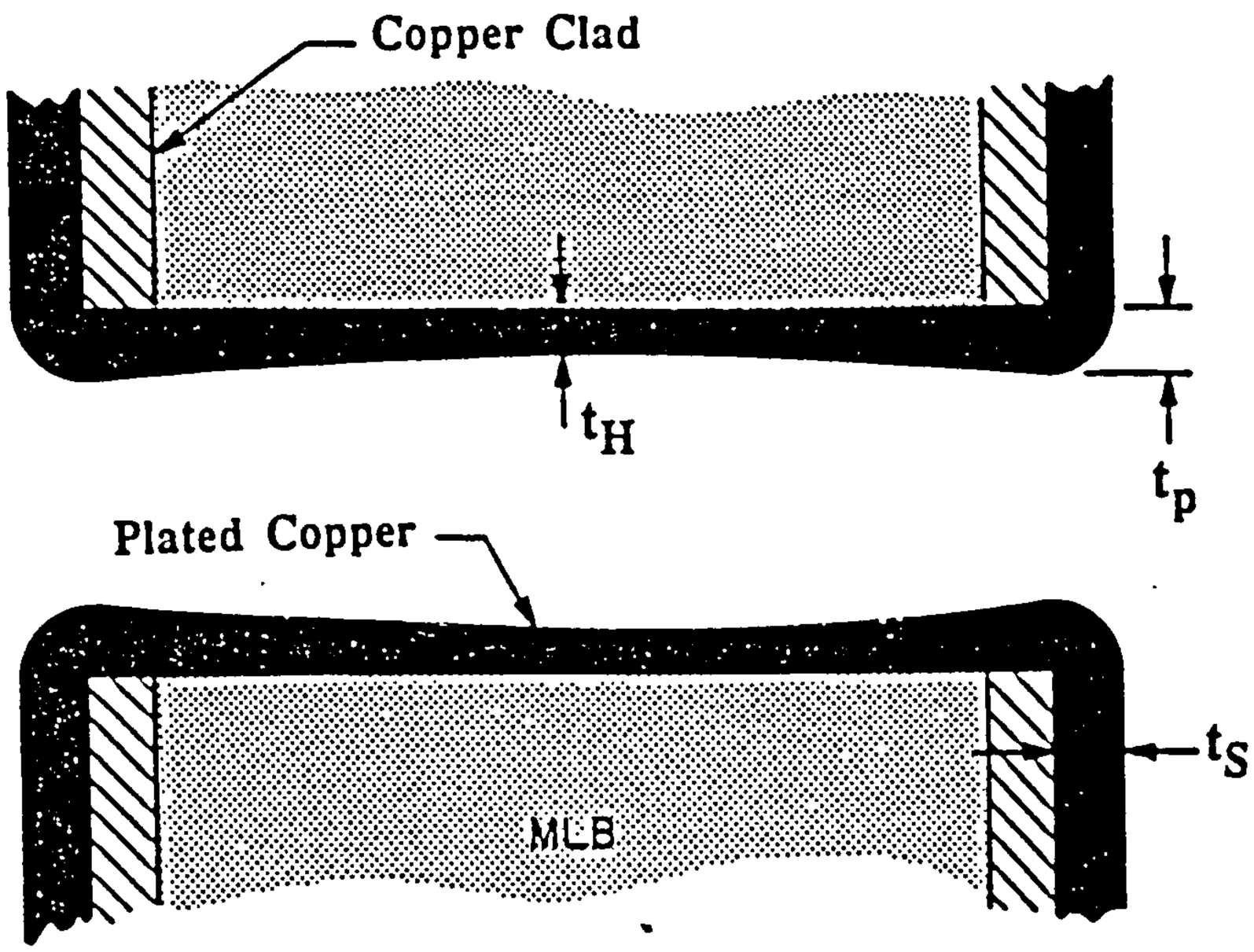

$$\text{Throwing Power} = \frac{t_P}{t_H}$$

Figure 13[27] Shows the sketch of plated through-hole in cross-section defining throwing power.

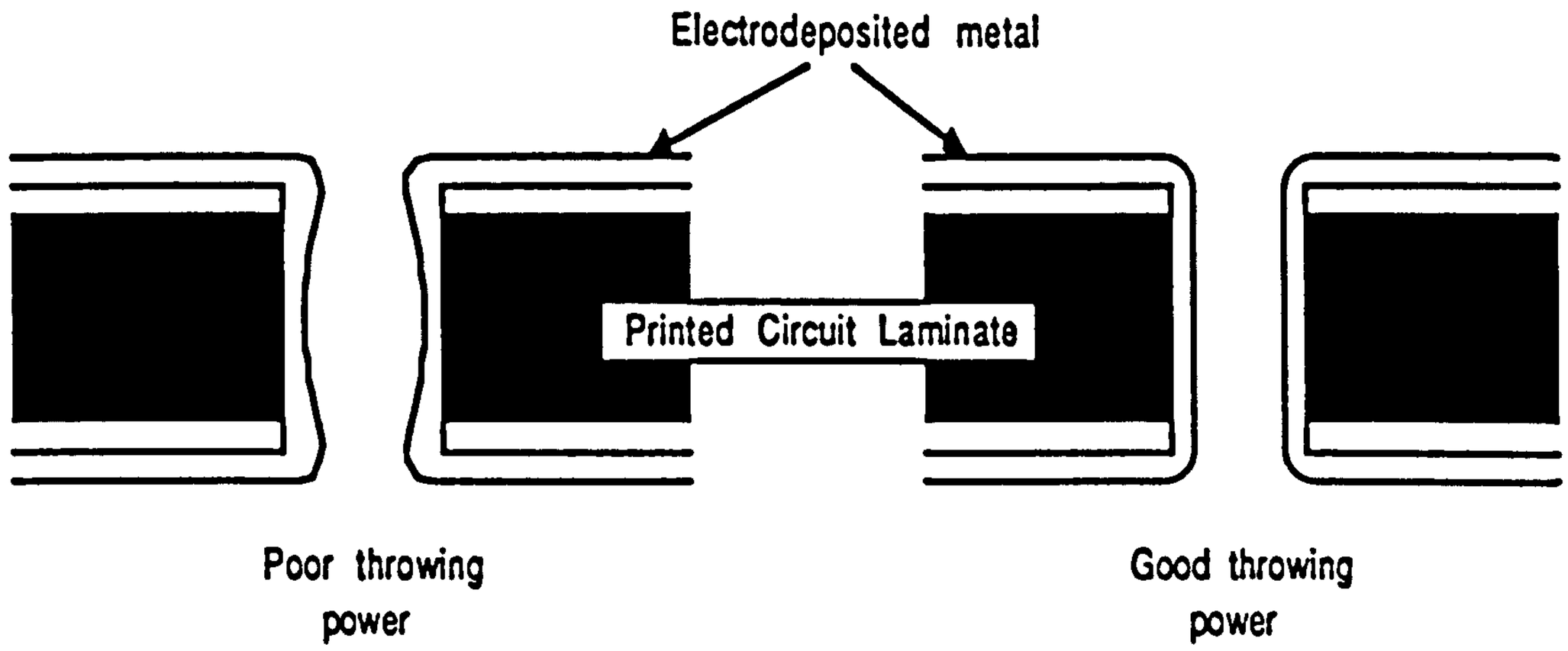

Figure 14 Schematic diagram of a PCB in cross-section indicating different throwing powers in the holes.

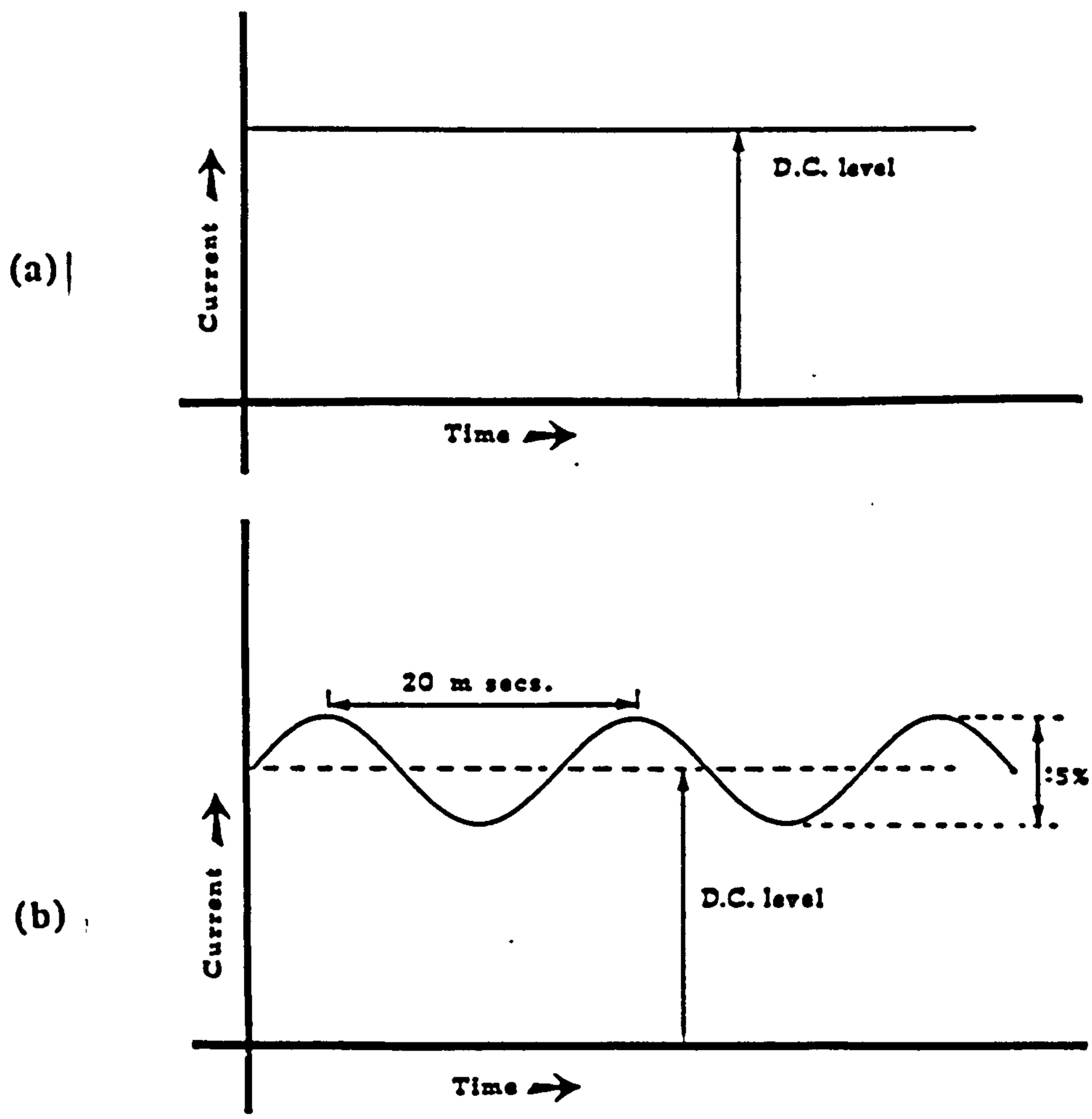

Figure 15[50] a) Theoretical DC
b) Practical DC

20ms ripple is a feature of all DC supplies derived from 50Hz mains.
Ripple amplitude of ±5% is typical but can be improved upon with more complex, and expensive, circuitry.

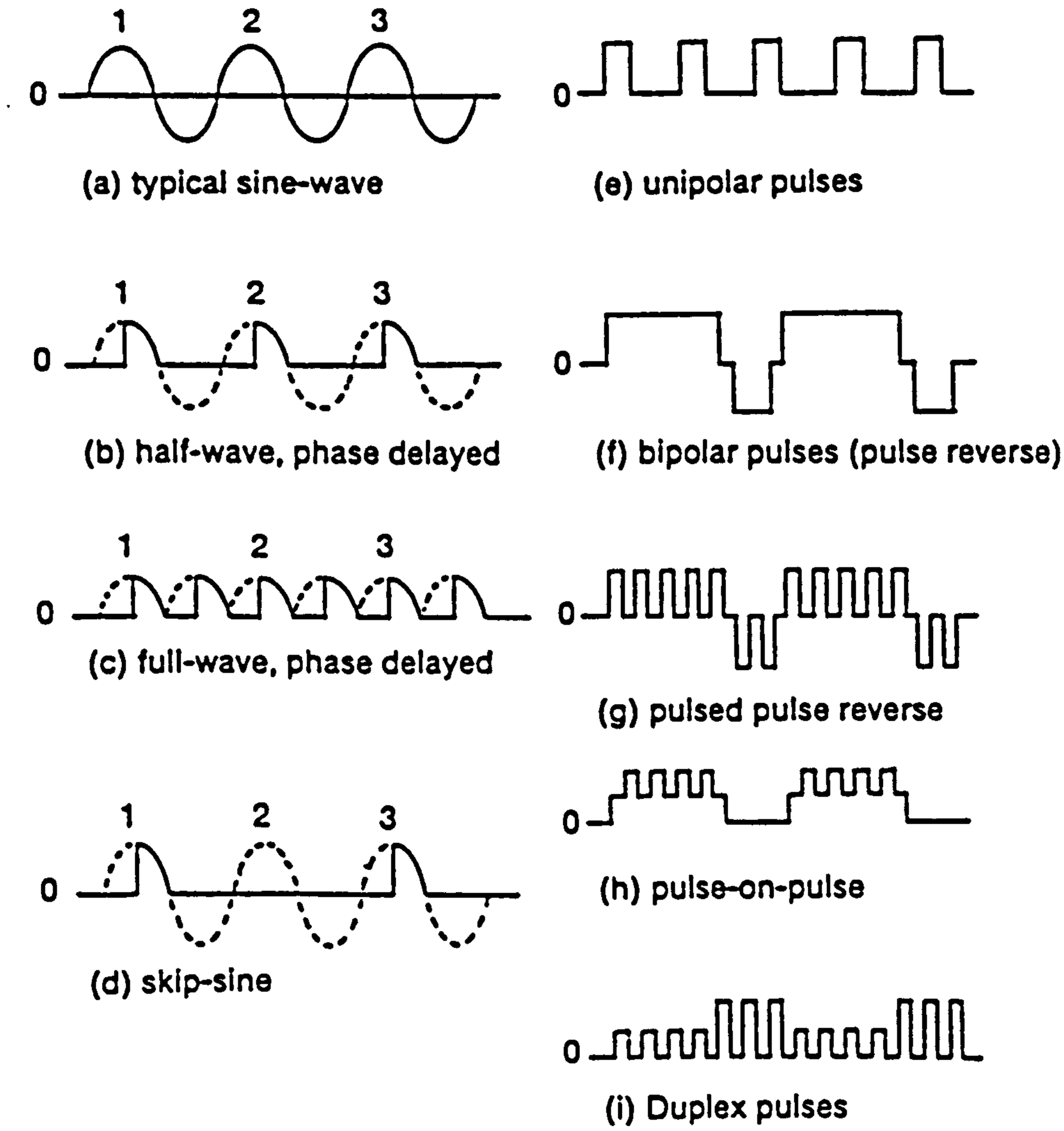

Figure 16[1] Examples of pulse waveforms.

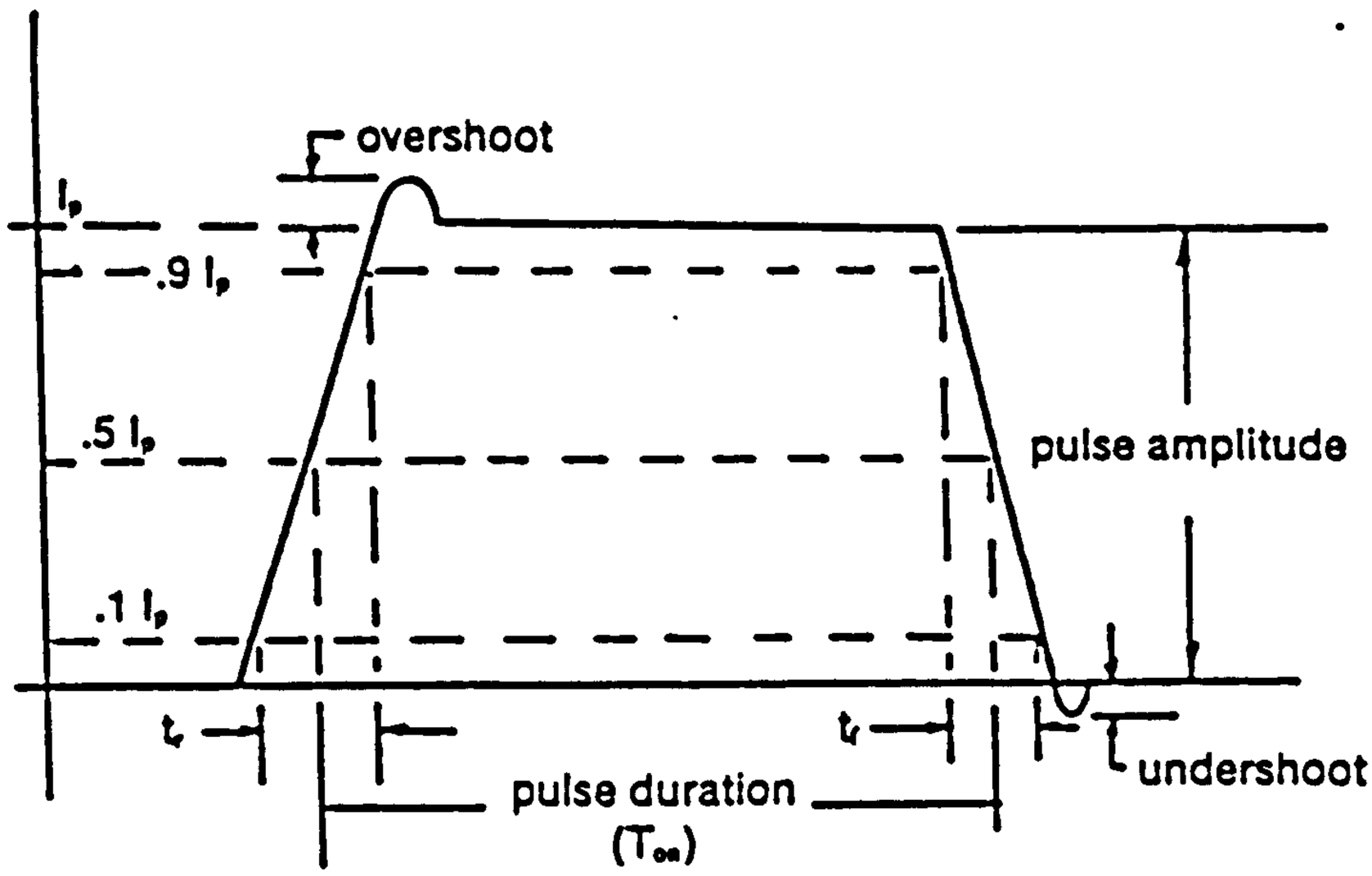

Figure 17[1] A typical standard pulse waveform obtained from an oscilloscope.

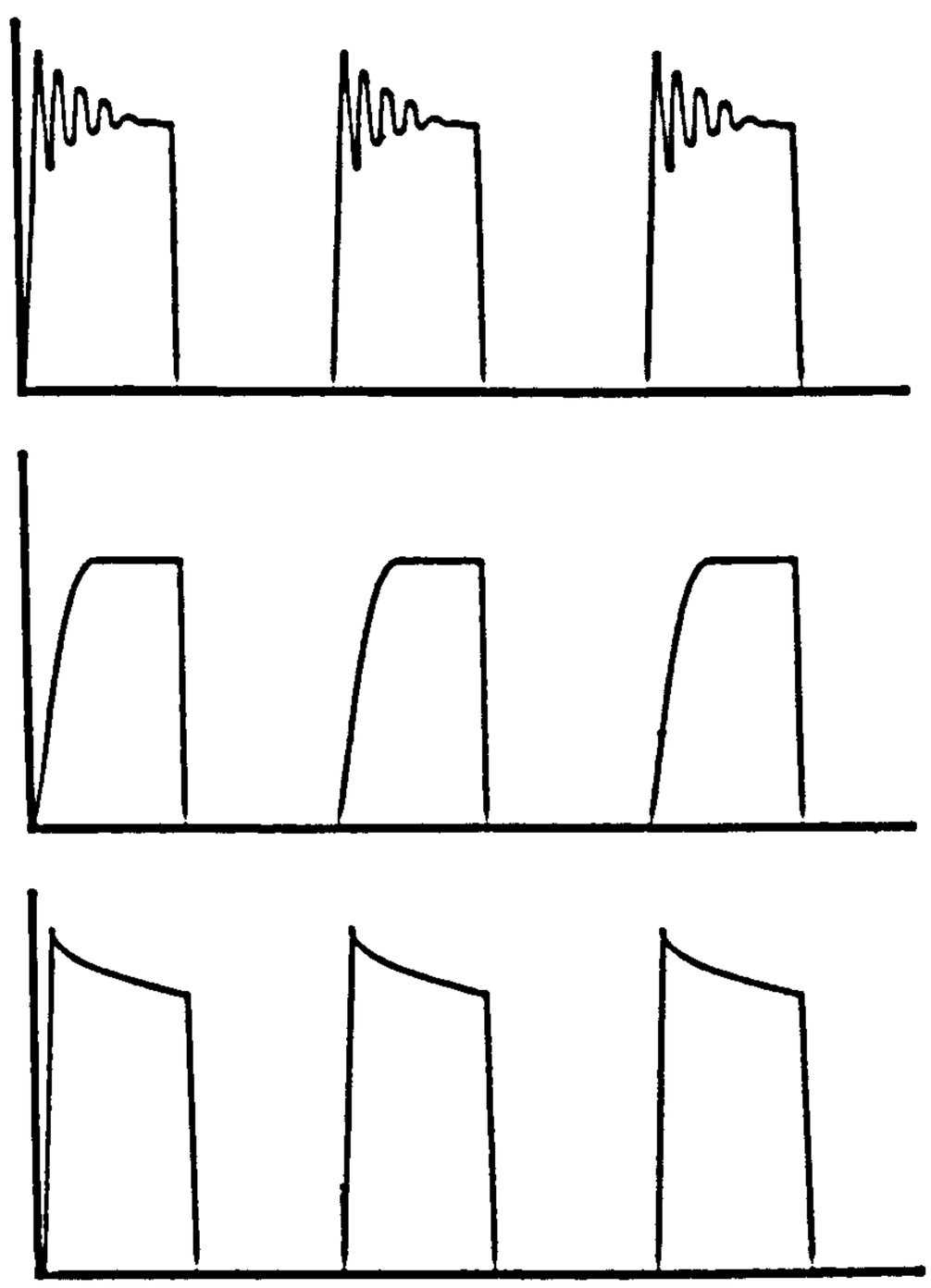

Figure 18[50] Actual waveform obtaines from an oscilloscope showing the irregularities of non-ideal nature of circuitry.

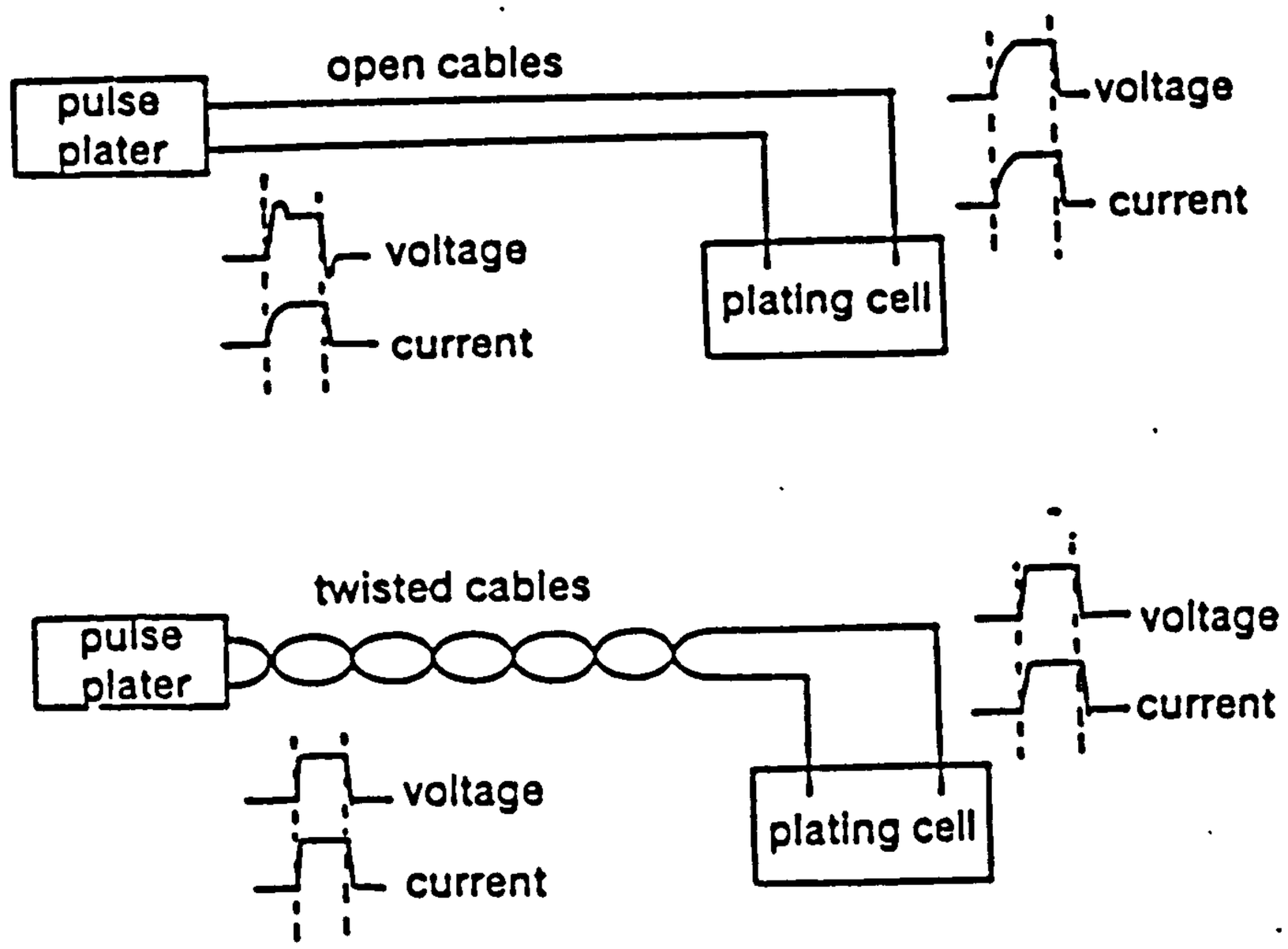

Figure 19[1] Typical oscilloscope waveforms for open cables and twisted pair cables.

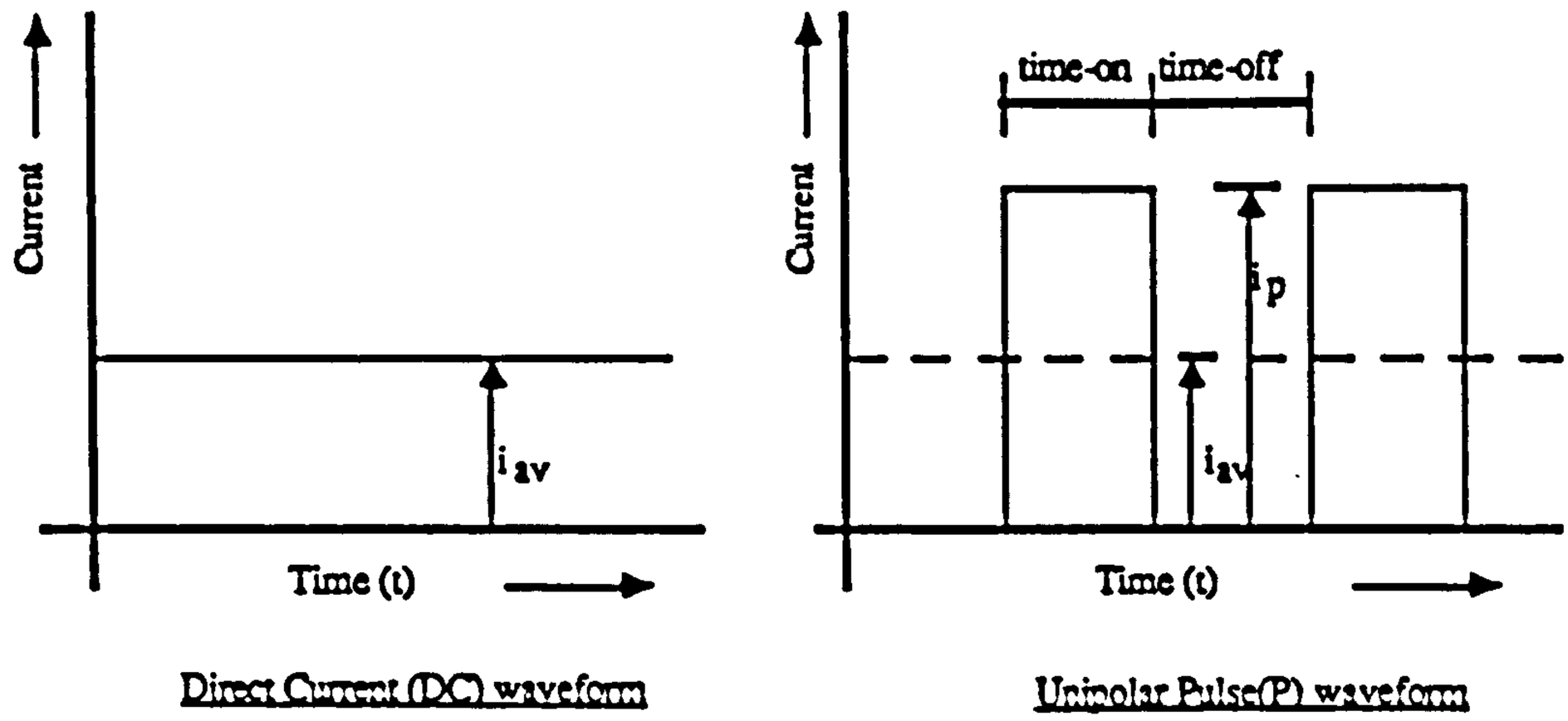

Figure 20 Schematic waveforms under DC and unipolar pulse showing the effective parameters. Average current density, i_{av} and peak current density, i_p.

Average current density = Peak current density x Duty cycle

$$\text{Duty cycle} = \frac{\text{on-time}}{\text{on-time} + \text{off-time}} \times 100\%$$

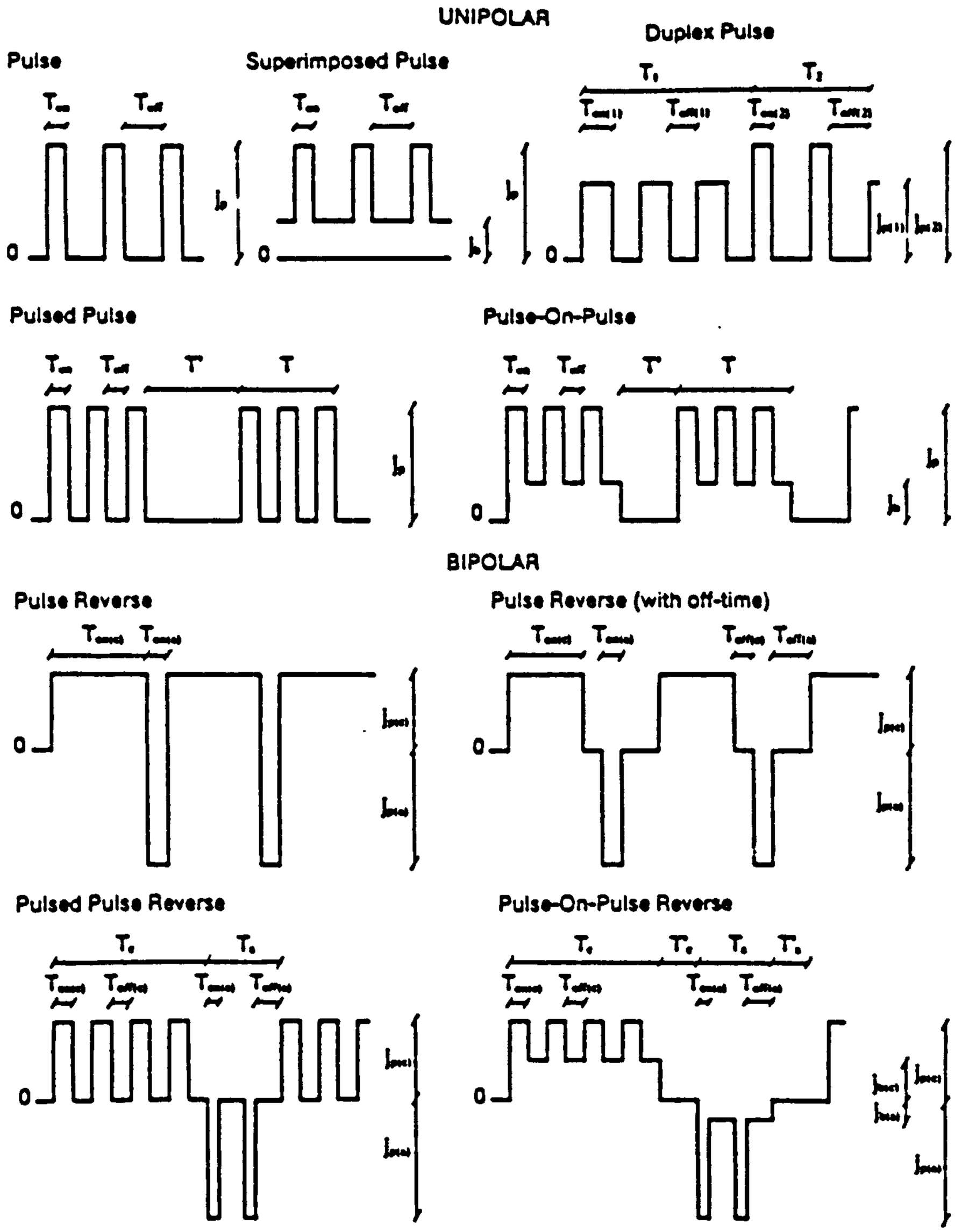

The parameters shown in this figure are independent. The average current density, j_m, dependent parameter, can be calculated from the above mentioned parameters. Pulse reverse is characterized by three different average current densities:

j_m, $j_{m(+)}$, $j_{m(-)}$, with $j_m = j_{m(+)} + j_{m(-)}$

Figure 21[1] Schematic representation and suggested nomenclature for some square-wave modulated current system, and definition of related parameters.

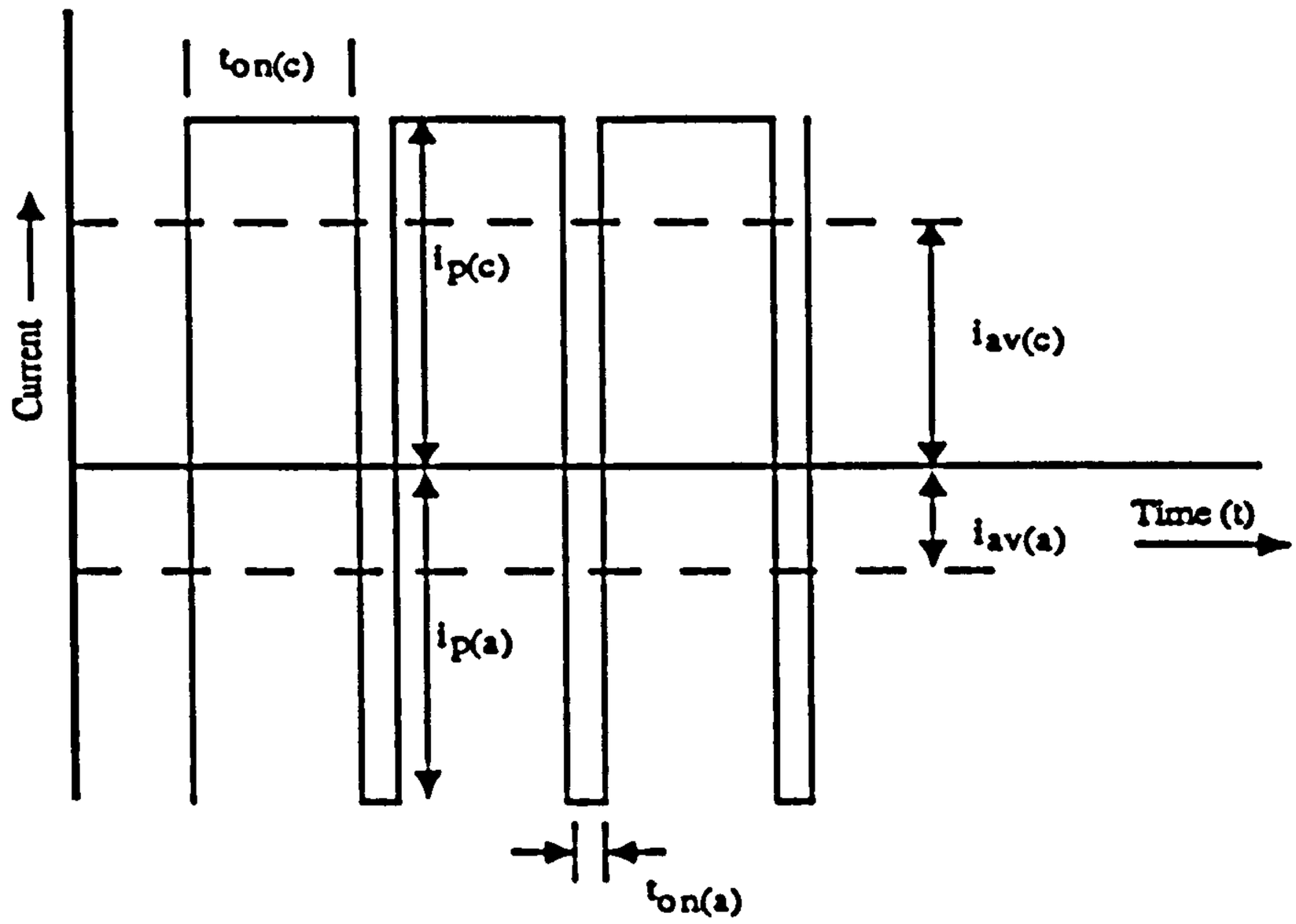

Pulse Reverse (PR) Waveform

Figure 22 Schematic diagram showing the pulse reverse parameters.

$$i_{av} = \frac{i_{p(c)} \times t_{on(c)} + i_{p(a)} \times t_{on(a)}}{t_{on(c)} + t_{on(a)}}$$

$$i_{av} = i_{av(c)} + i_{av(a)}$$

ELECTROCRYSTALLISATION

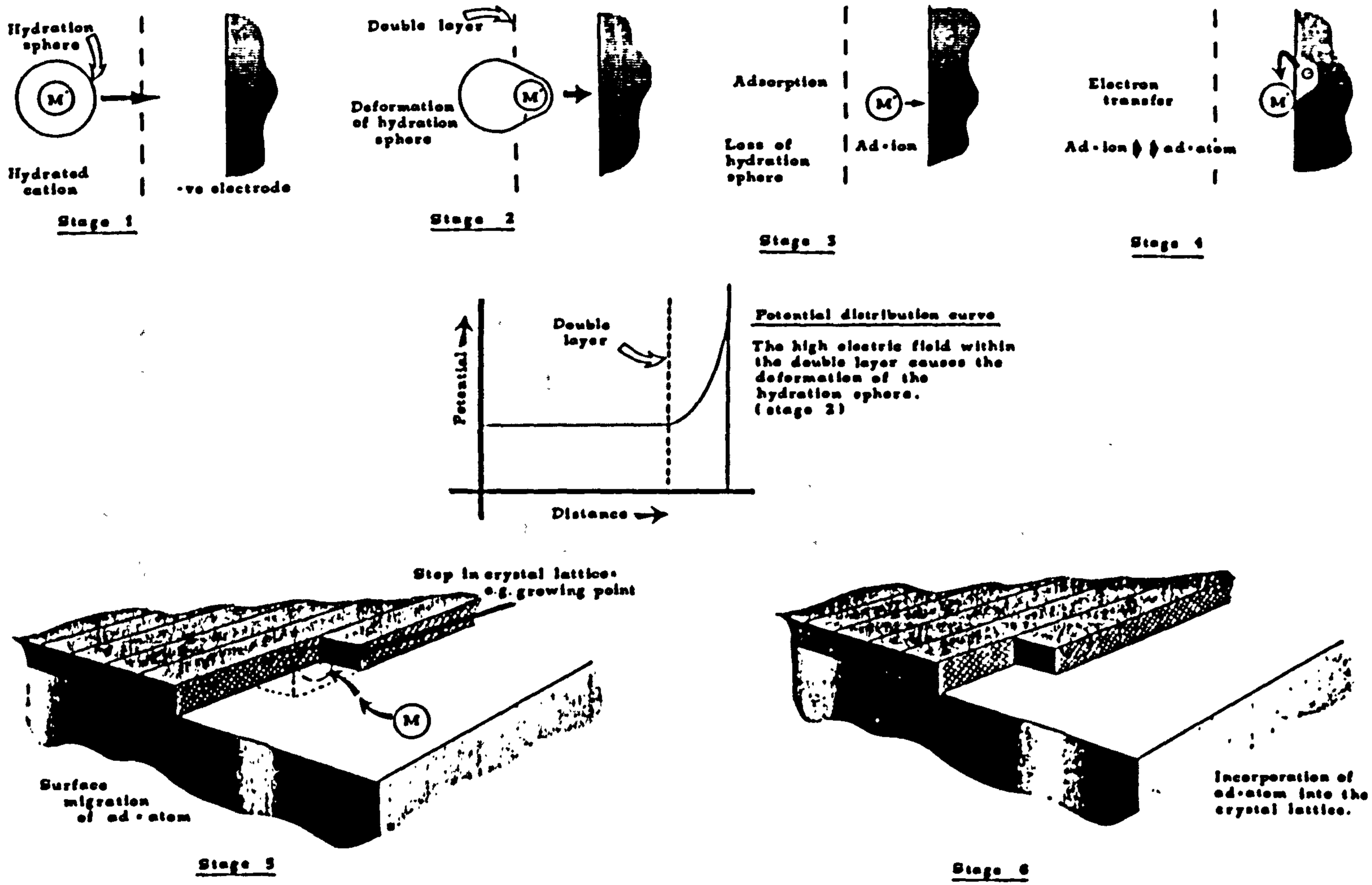

Figure 23[50] Illustration of processes showing the sequence of electrocrystallisation.

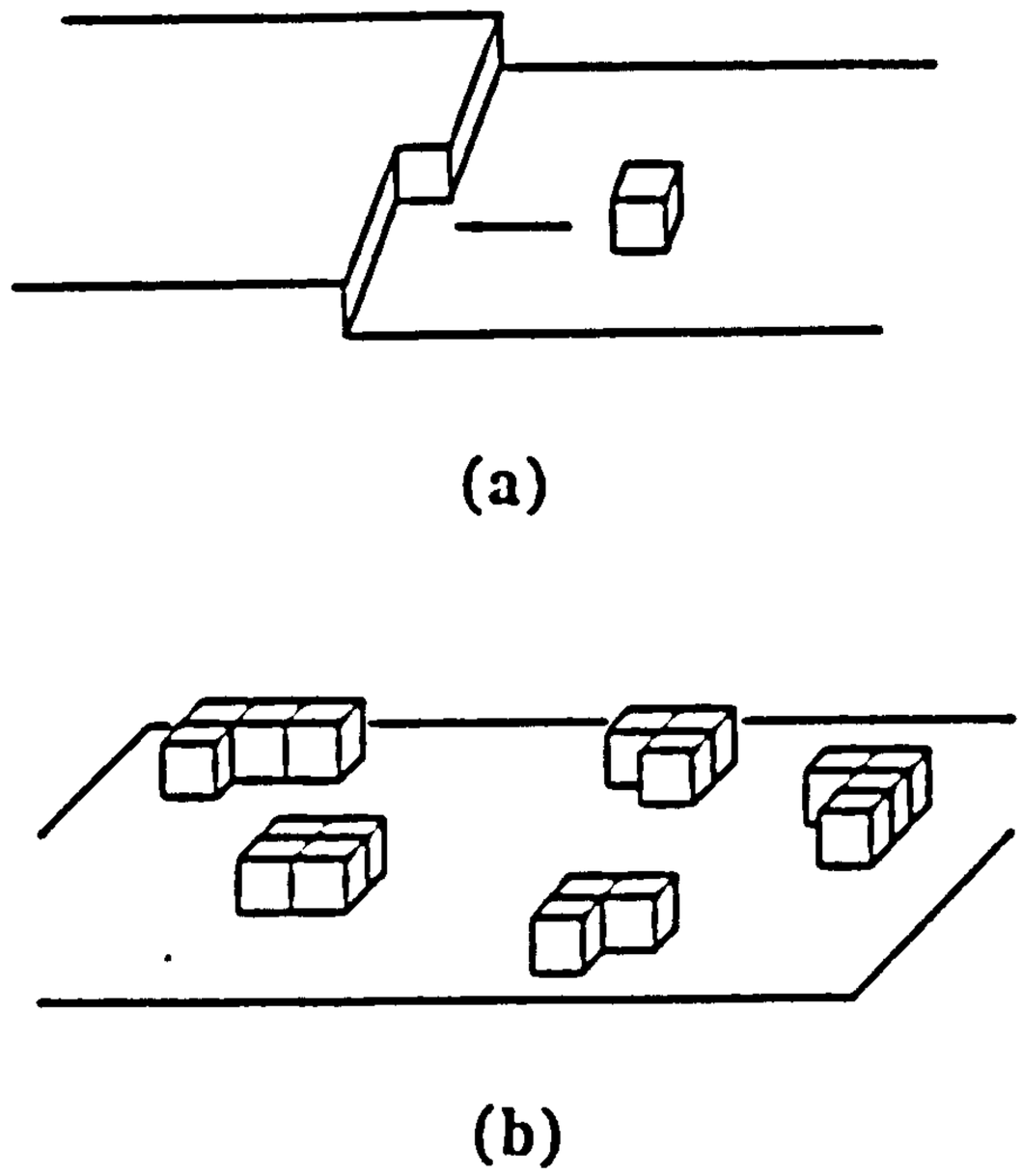

Figure 24[1] Crystallisation mechanisms
a) Build-up of existing crystals
b) Nucleation and formation of new crystals.

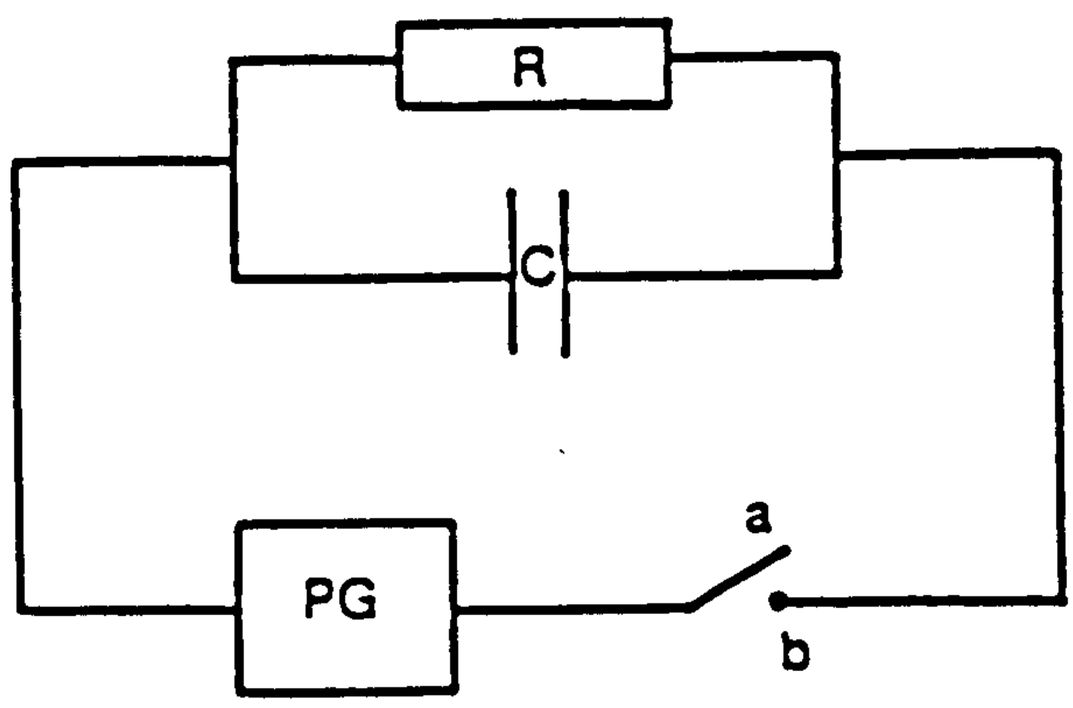

Figure 25[1] Schematic equivalent circuit of an electrode.
Position a: off-time, external circuit open.
Position b: on-time, external circuit closed.
PG, pulse generator; C, capacitance,
R, resistance.

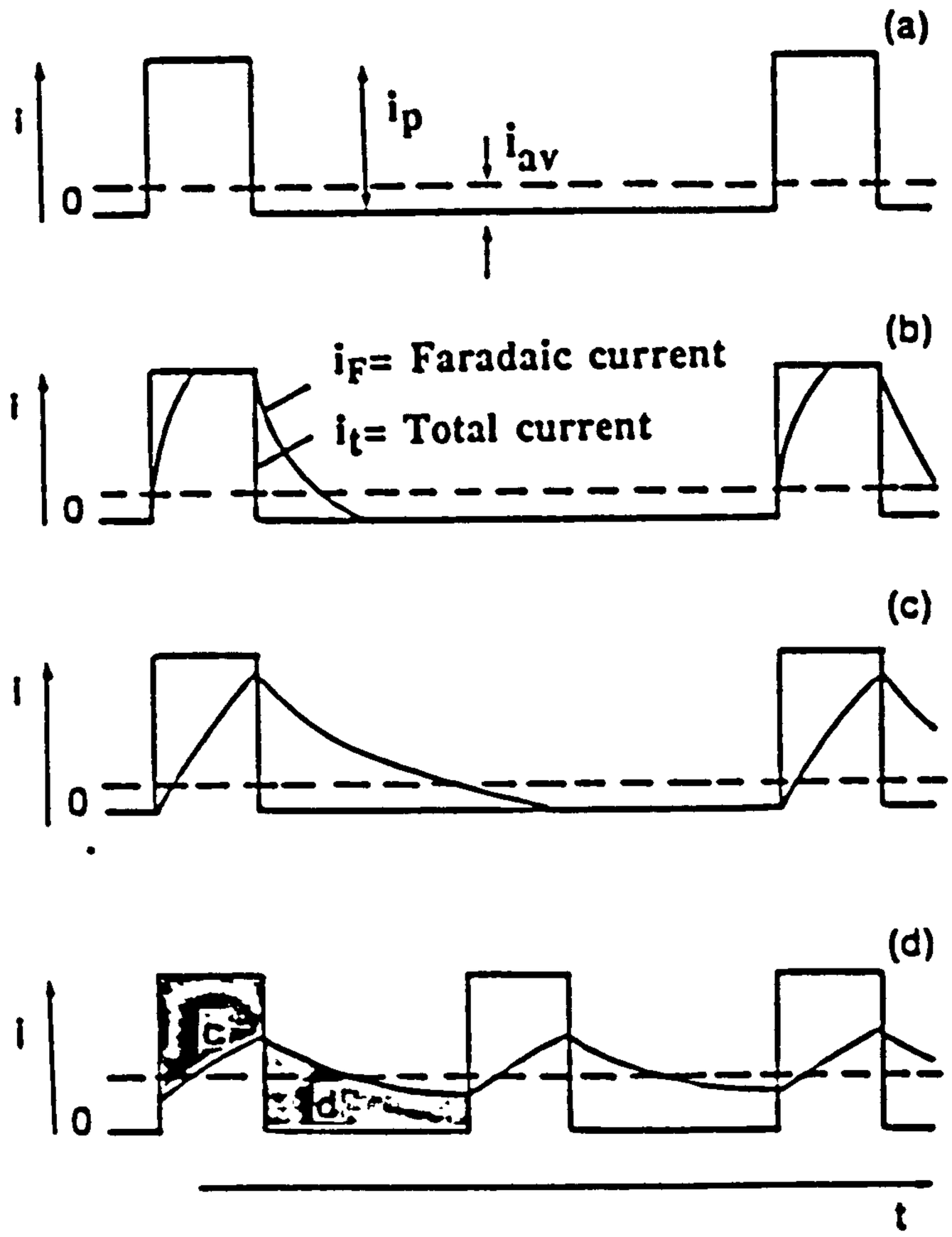

Figure 26[55] Damping of faradic current due to capacitance effects.
a) $t_c \leq t_{on}$; no damping ideal situation;
b) $t_c < t_{on}$; small damping;
c) $t_c > t_{on}$; madium damping;
d) $t_c \geq t_{on}$ and $t_d \geq t_{off}$; strong damping;
where t_c and t_d are charging and discharging times of the double layer, respectively.

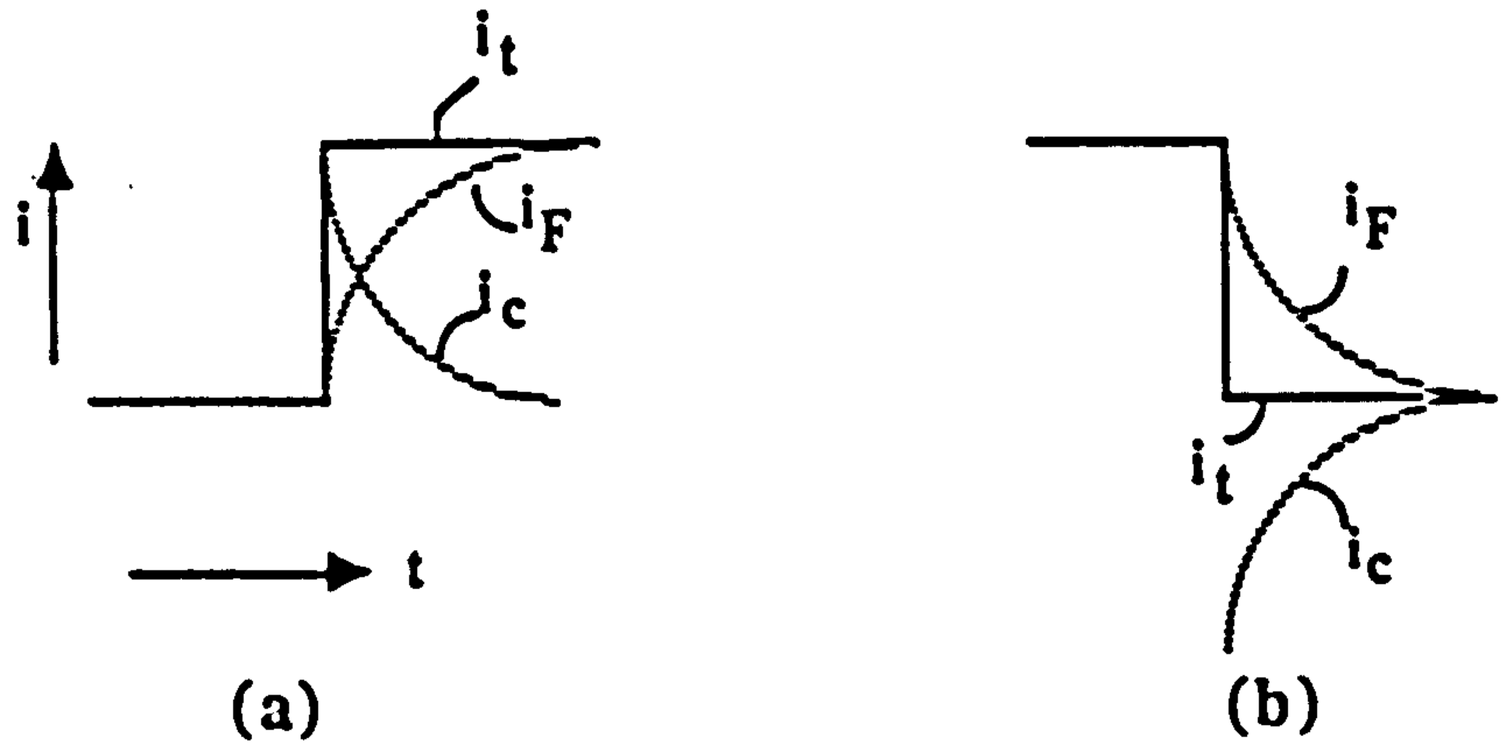

Figure 27[58] Schematic of current recovery of a pulse.
a) beginning of a pulse;
b) end of a pulse.
i_F, i_c and i_t are faradic, charge and total currents.

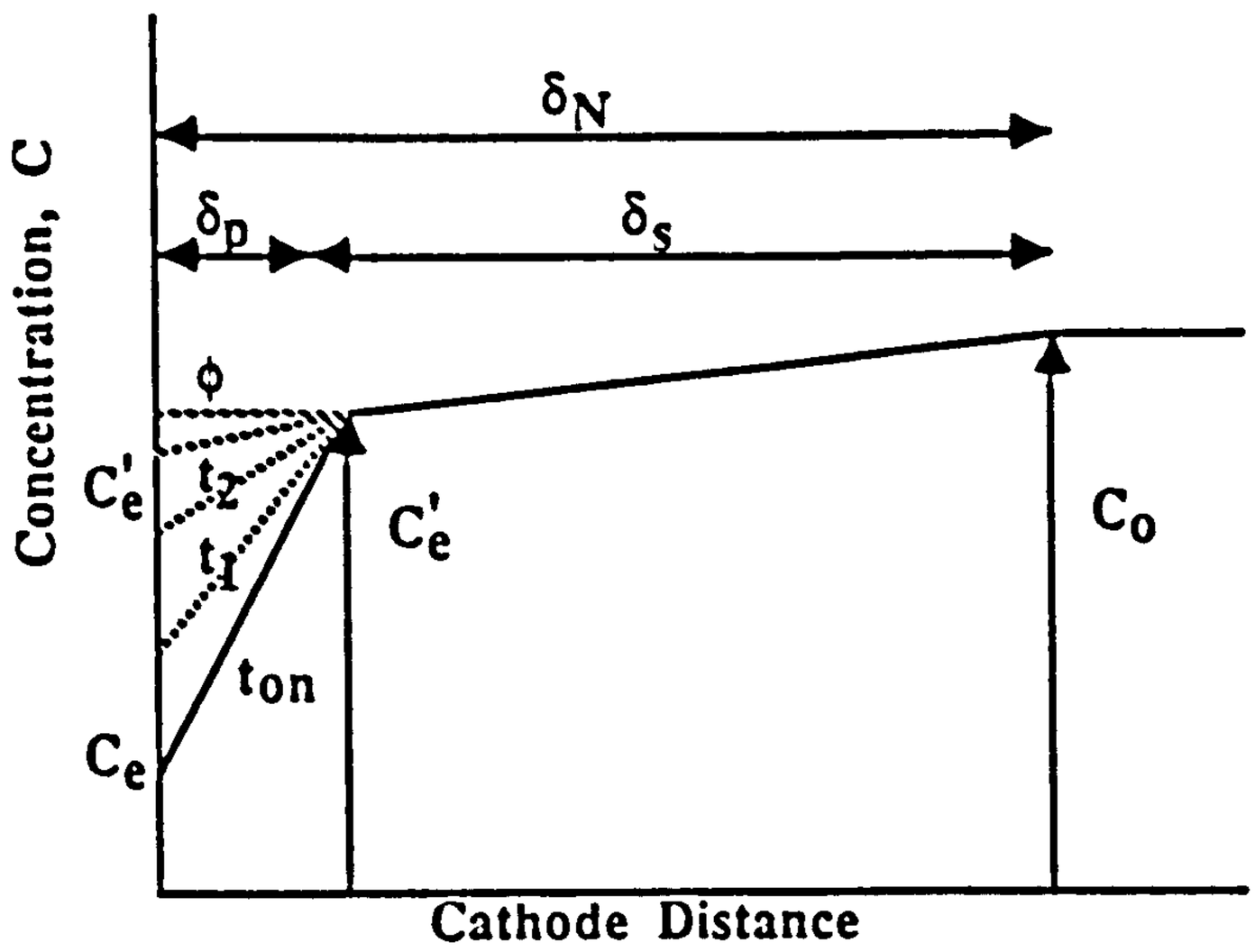

Figure 28[55] Concentration profiles of the two diffusion layer in pulse electrolysis at the end of a pulse. The broken lines (---) show the recovery of the concentration in the pulsating diffusion layer during the off-time ($t_{on}<t_1<t_2<\phi$).

δp: thickness of the pulsating diffusion layer

δ_S: thickness of the stationary diffusion layer

δ_N: thickness of the diffusion layer in DC electrolysis under the same hydrodynamic conditions as in pulse electrolysis.

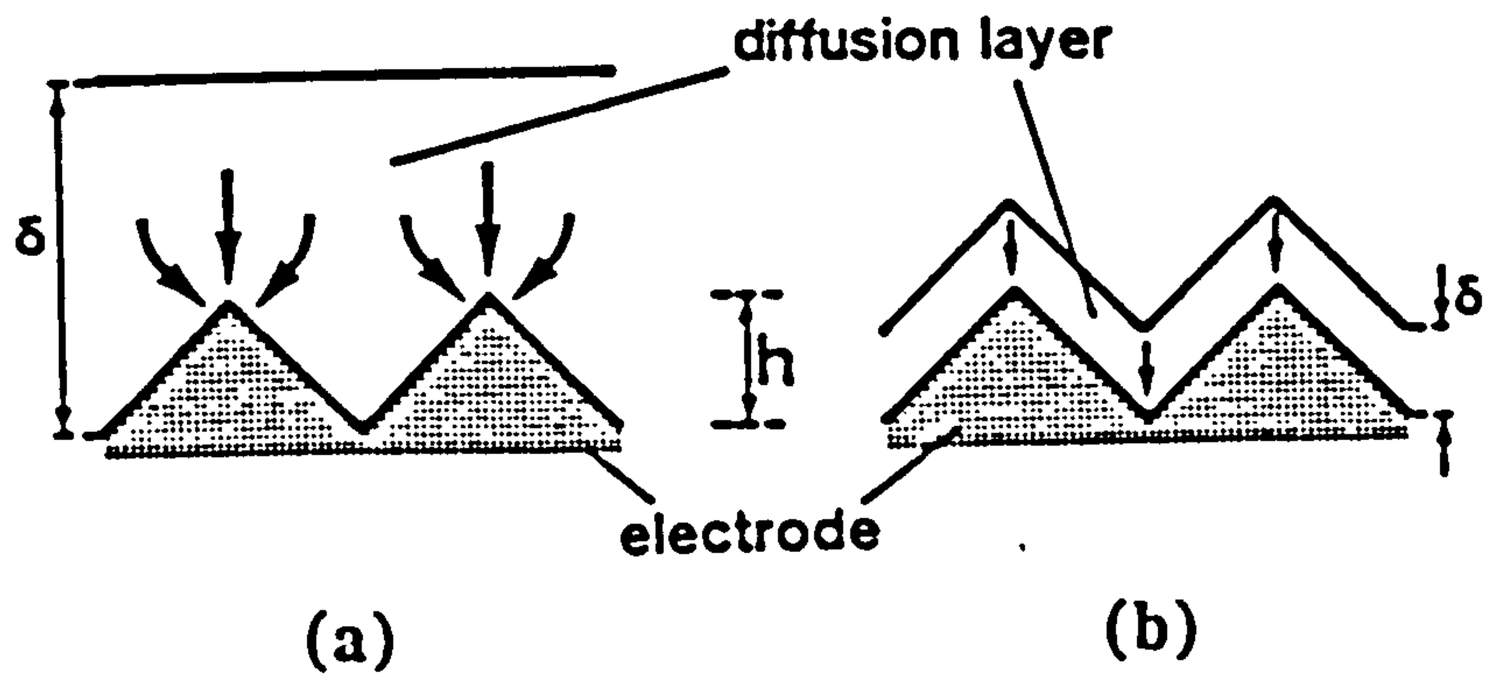

Figure 29[1] Influence of diffusion layer thickness on tertiary current distribution.
a) microprofile
b) macroprofile.

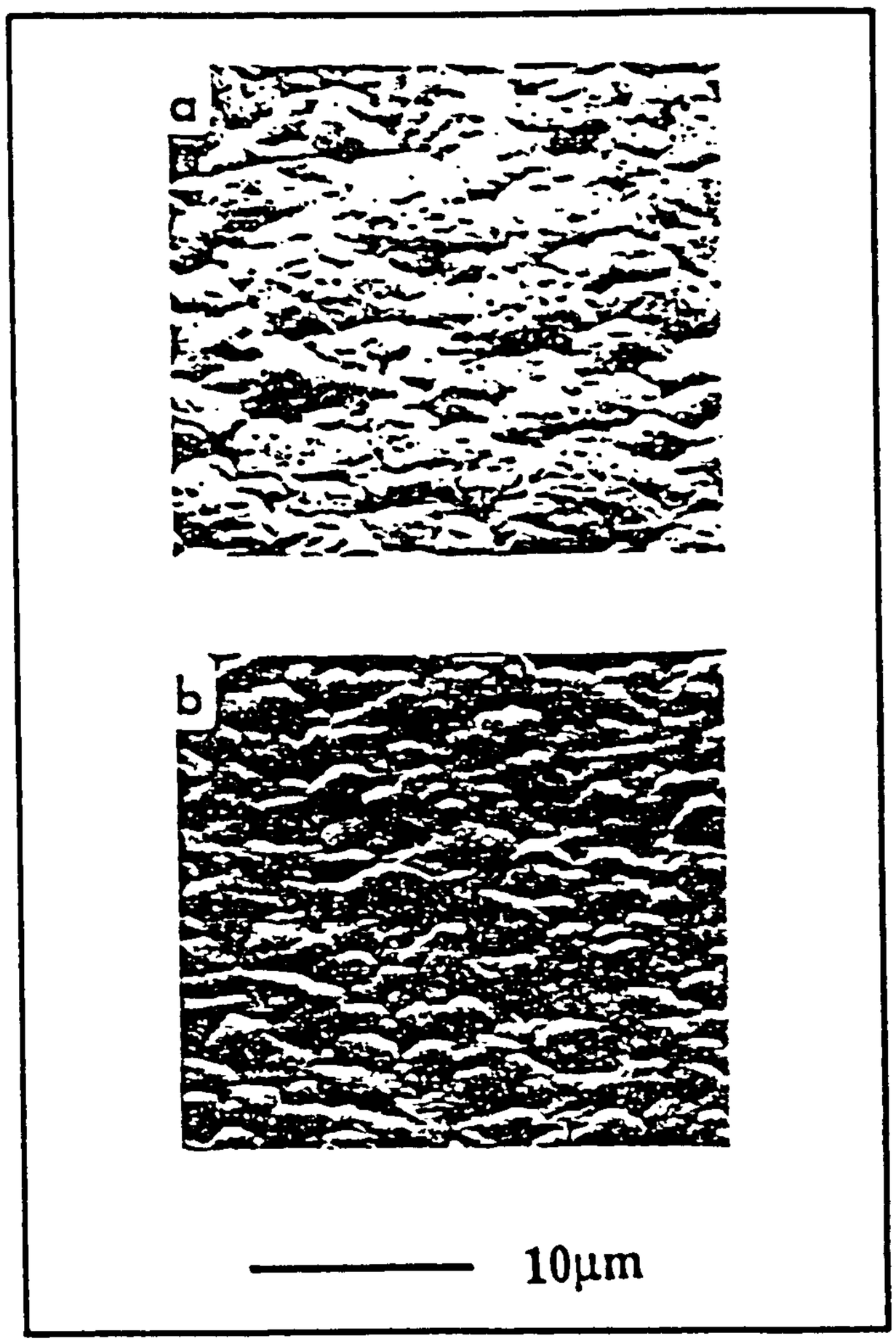

Figure 30[65] Influence of peak current density on surface morphology of deposit for different average current densities:
a) 1.6Acm^{-2} and b) 34.8Acm^{-2}
t_{on}= 0.3ms and t_{off}= 100ms.

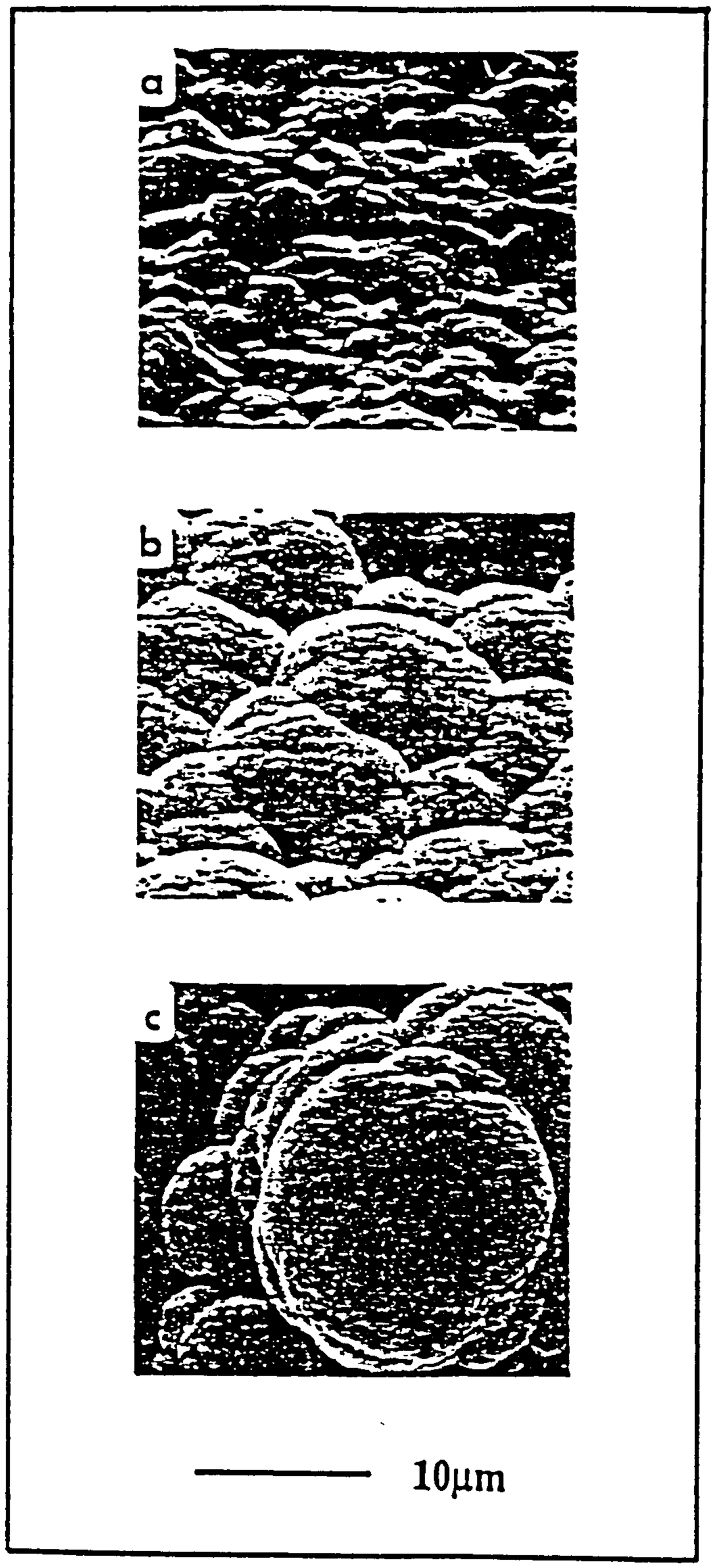

Figure 31[65] Influence of on-time on surface morphology of deposit:
a) t_{on} =0.1ms b) t_{on}=10ms and c) t_{on}=30ms
i_p= 3Acm^{-2} and t_{off}= 100ms.

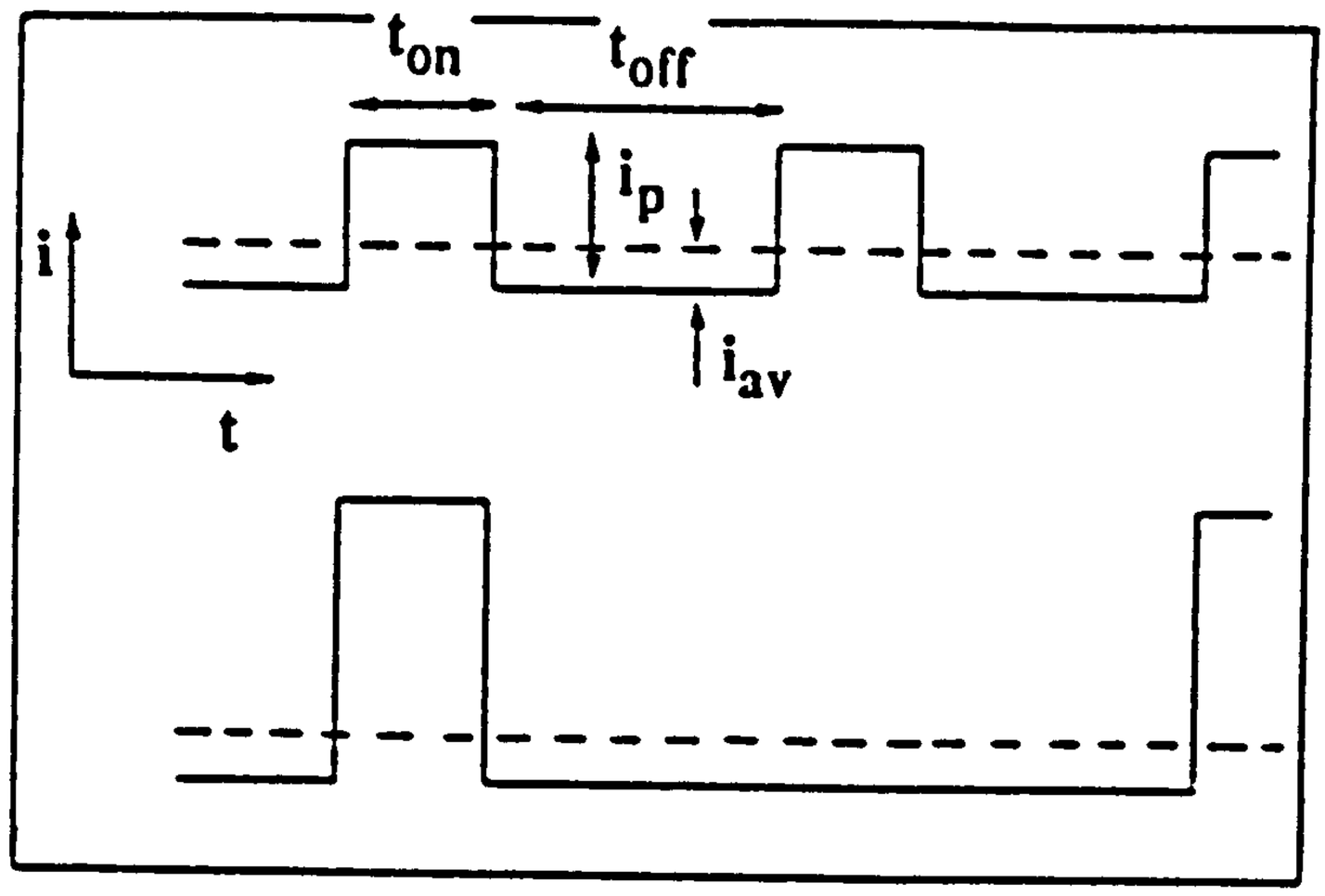

Figure 32[1] Scheme for investigating changes in peak current density with constant on-time and constant average current density.

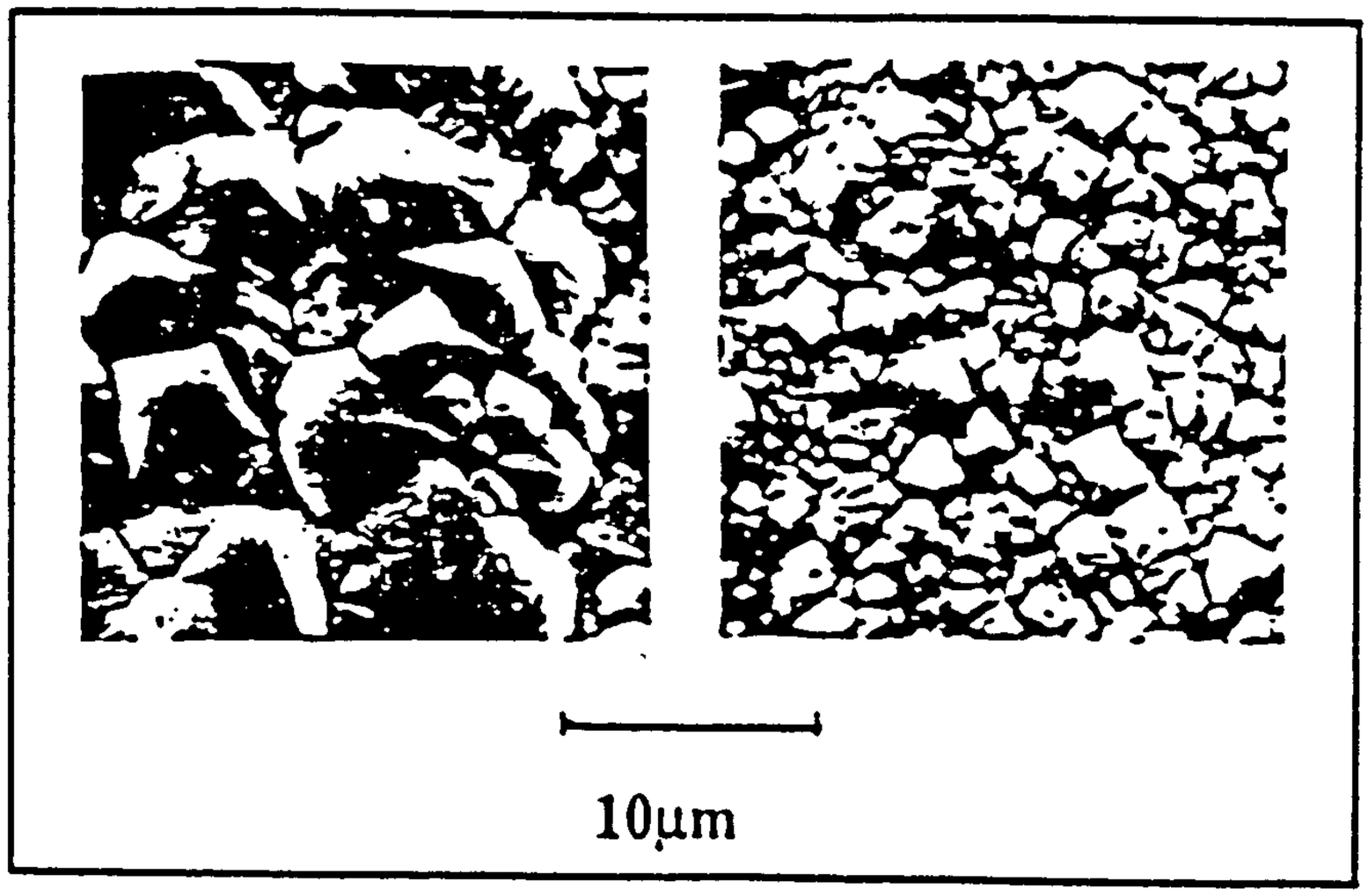

Figure 33[1] Influence of peak current density on the morphology of 10μm copper deposits with t_{on}= 30μs and an average current density of 37.5Adm^{-2}; from left to right: i_p=1000Adm^{-2}; i_p=4000Adm^{-2}.

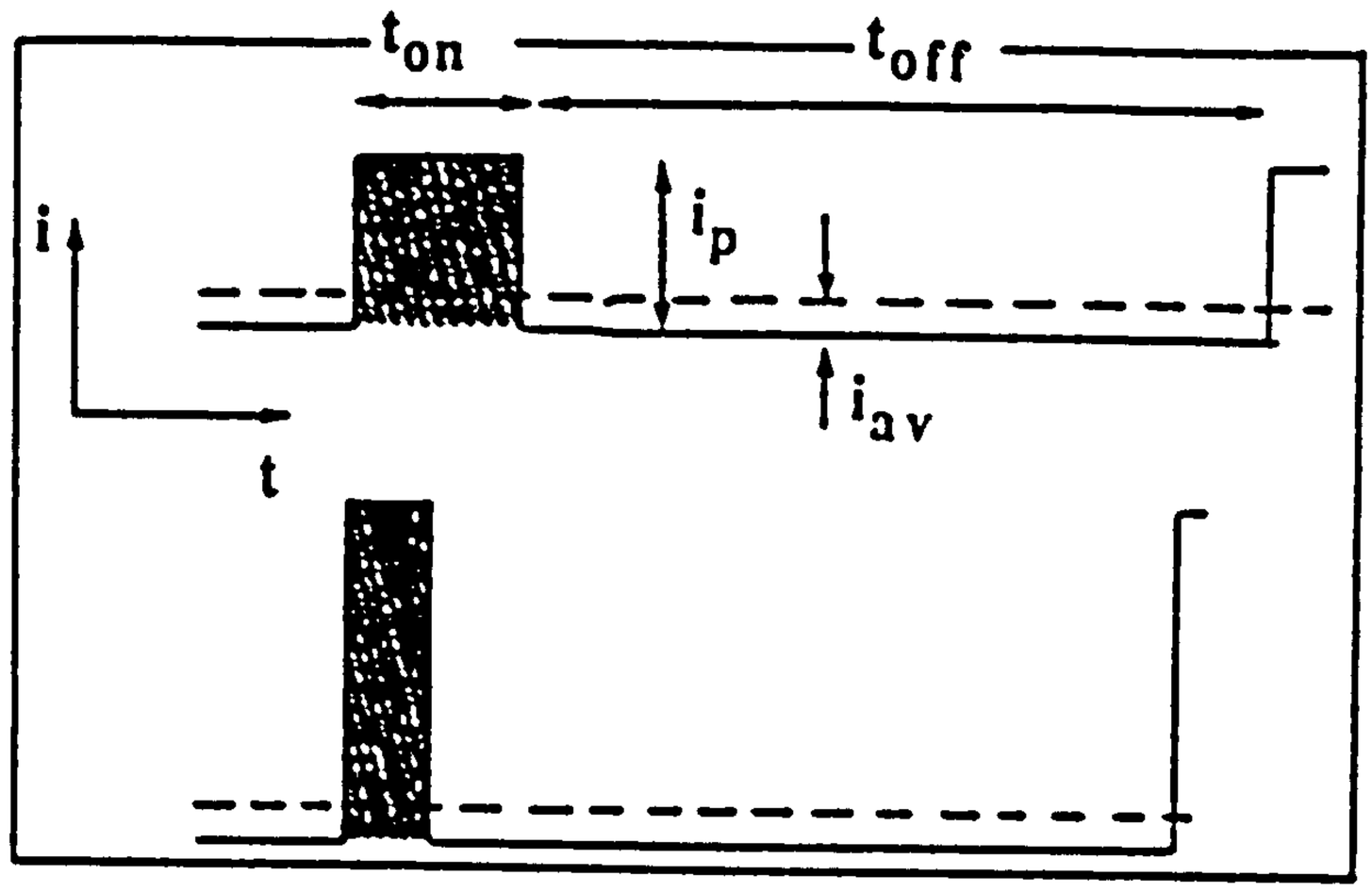

Figure 34[1] Scheme for investigating changes in peak current density with constant ($i_p t_{on}$) and t_{off}. (If t_{off} is much greater than t_{on}, i_{av} remains nearly constant at increasing i_p.) The shaded areas are equal.

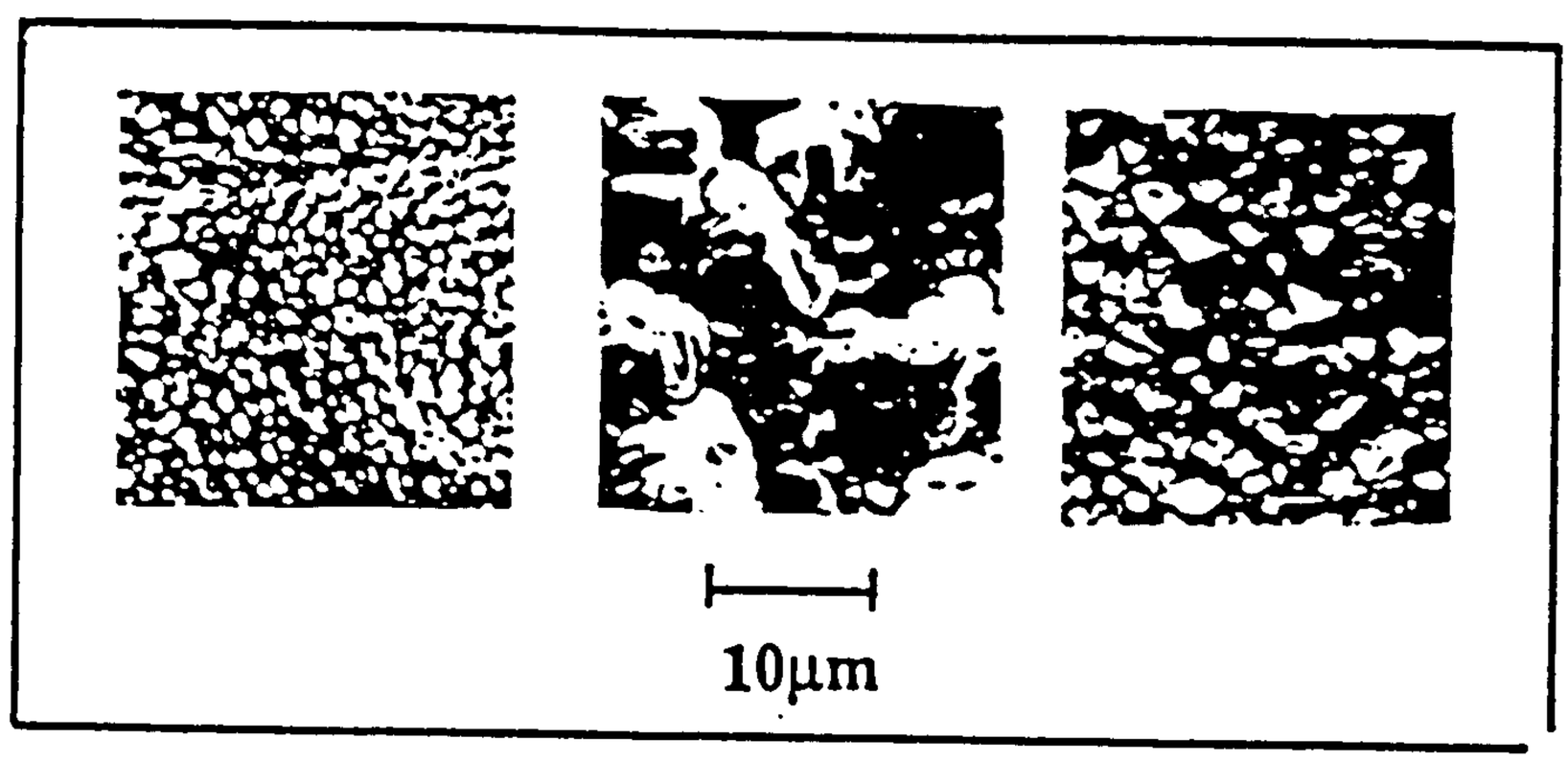

Figure 35[1] Influence of off-time on the morphology of 10μm copper deposits with t_{on}=30μs and i_p=4000Adm^{-2}; from left to right: t_{off}=3.2ms; t_{off}=80ms; t_{off}=400ms

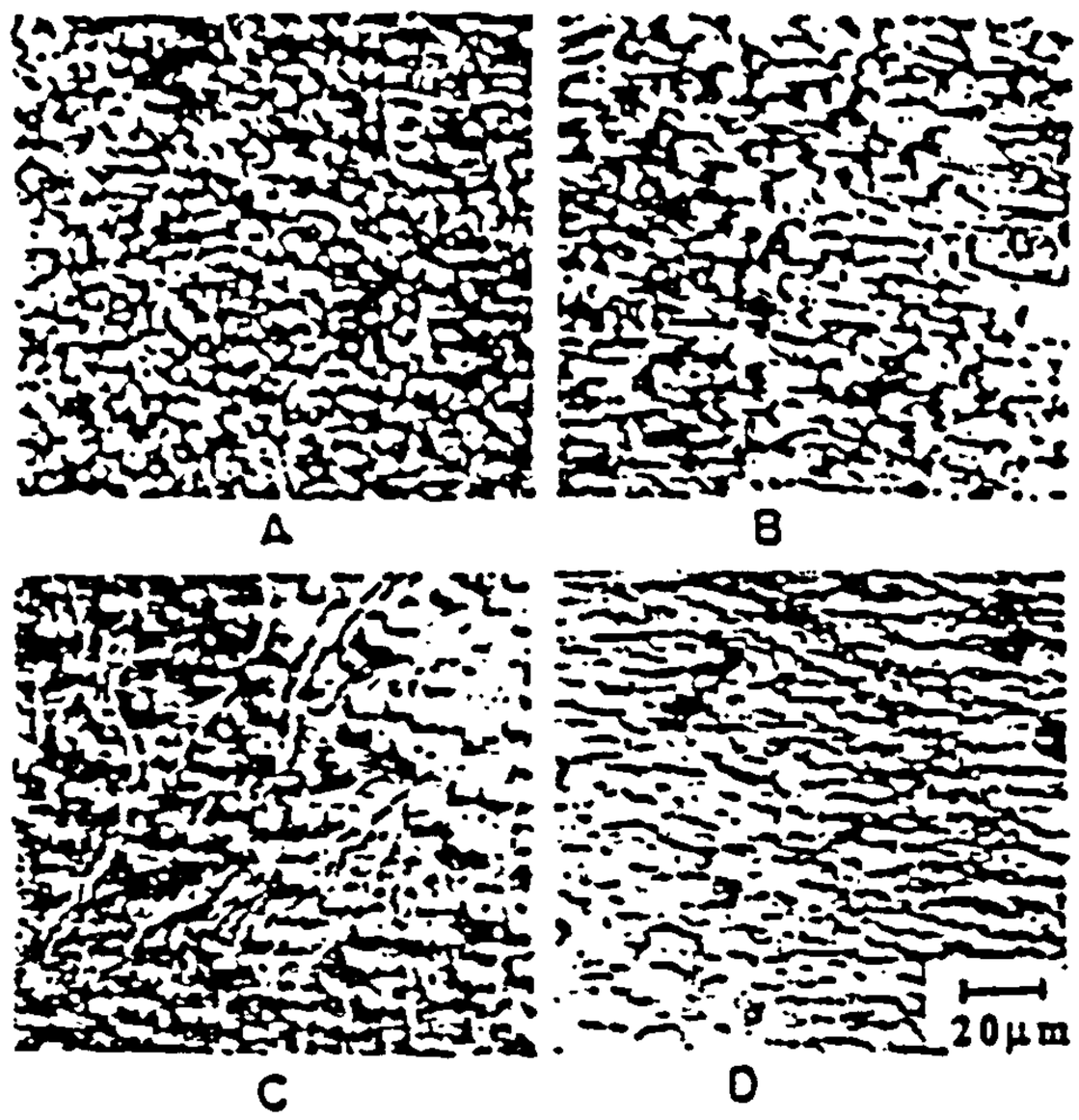

Figure 36[66] Surface structure of copper deposits obtained at the peak current density of 100mAdm^{-2}.

	on-time (ms)	Duty cycle (%)	Average current density (mAdm^{-2})
A	1	67	67
B	1	50	50
C	1	10	10
D	1	5	5

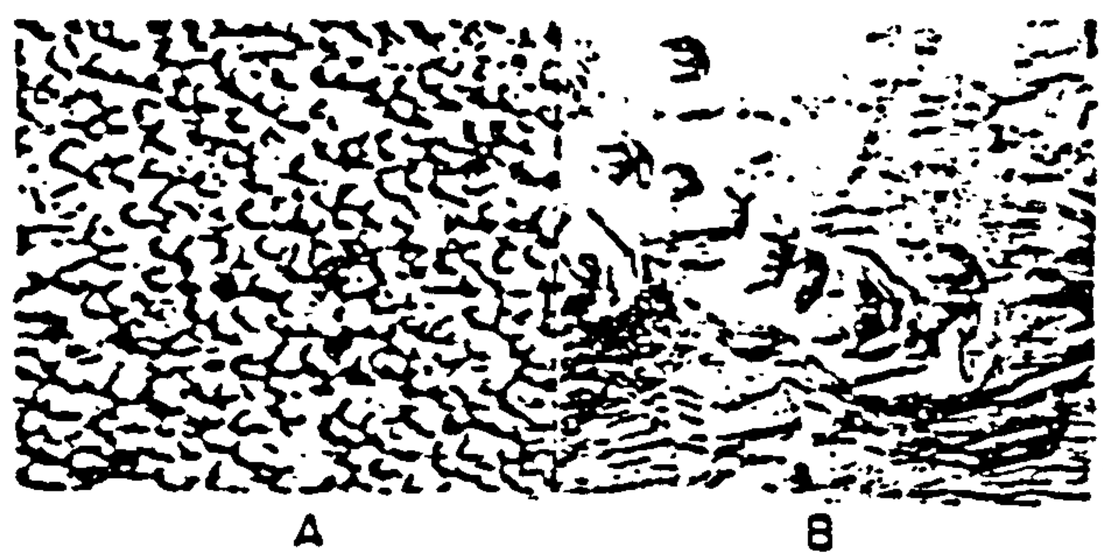

Figure 37[67] Surface structure of copper deposit obtained at the average current density of 75mAdm^{-2}.

	Peak current density (mAdm^{-2})	on-time (ms)	Duty cycle (%)
A	75	–	100
B	750	1	10

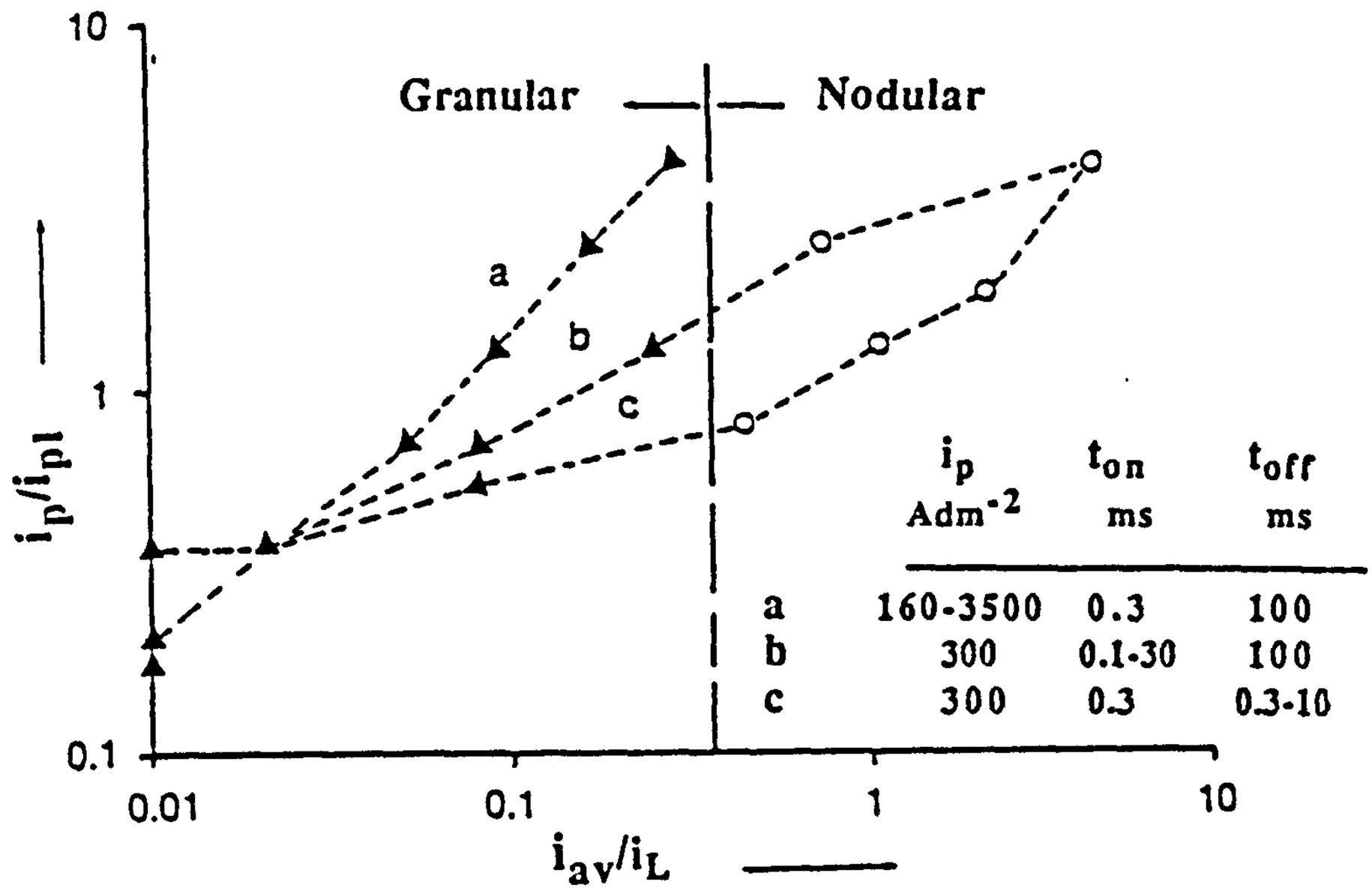

Figure 38[65] Influence of pulse parameters on deposit morphology for copper deposition from a copper sulphate/sulphuric acid electrolyte.

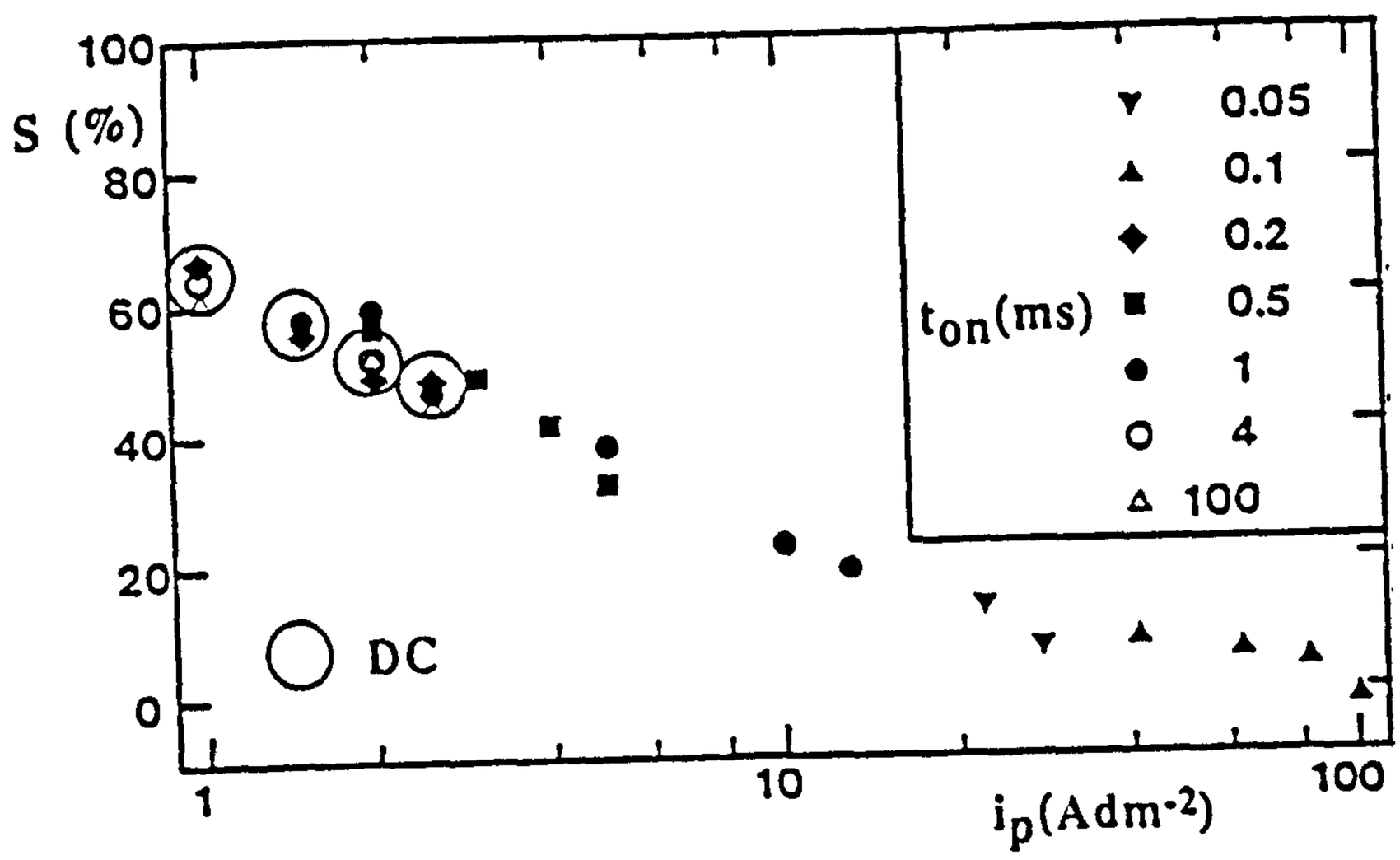

Figure 39[75] Secondary current distribution in a Haring-Blum cell as a function of peak current density, i_{av} varied from 1 and 2.5Adm^{-2}. Large circles: DC experiments the i values of which can be read on the abscissa.

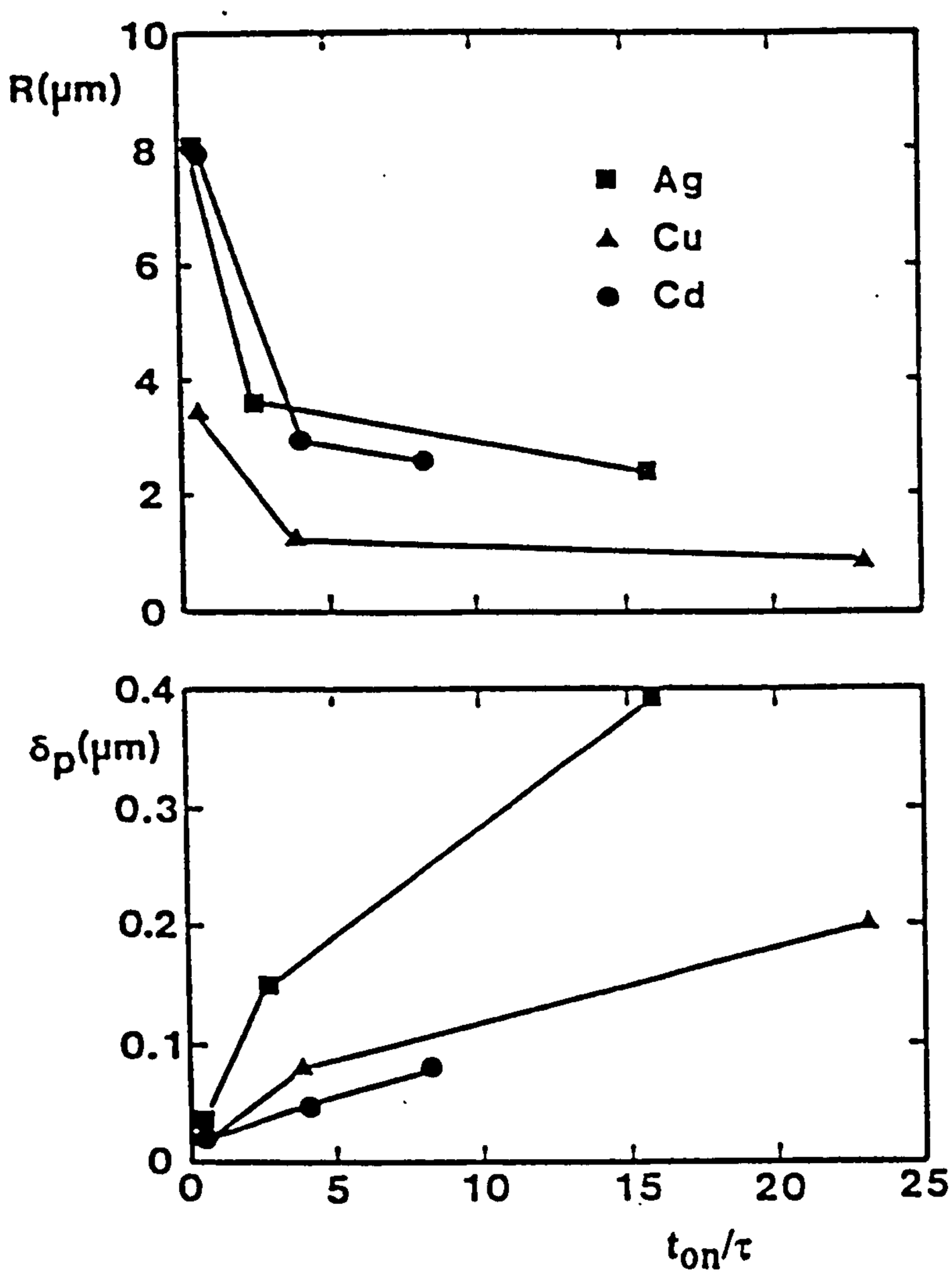

Figure 40[75] Roughness of electrodeposit on small scale profiles and corresponding diffusion layer thickness as a function of the ratio ton/τ for copper, silver and cadmium. τ=transition time.

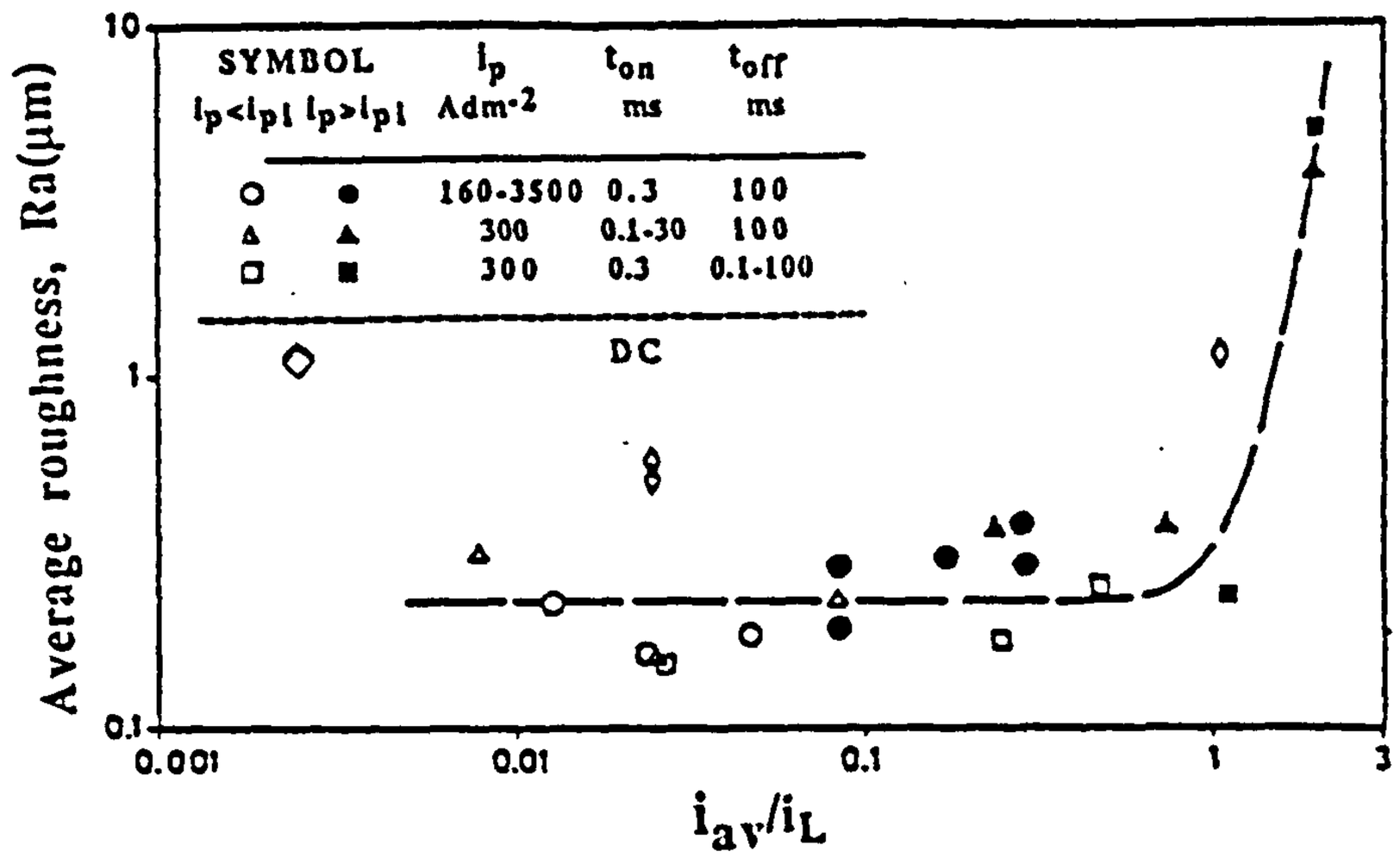

Figure 41[65] Shows the influence of pulse parameters on roughness average of deposit under different pulse conditions and DC.

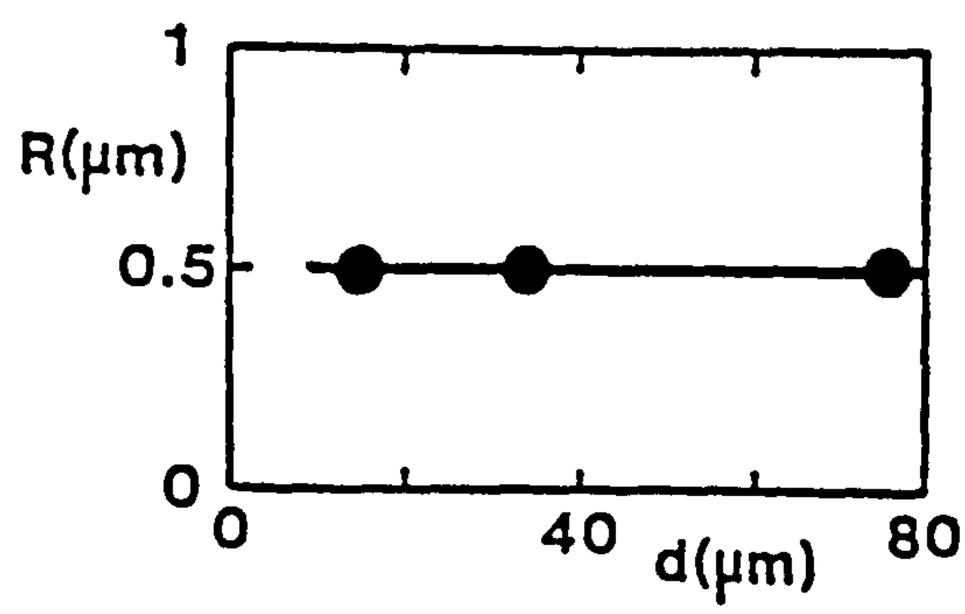

Figure 42[1] Tertiary current distribution in pulse plating on small profiles as a function of deposit thickness: no roughness amplification effect.

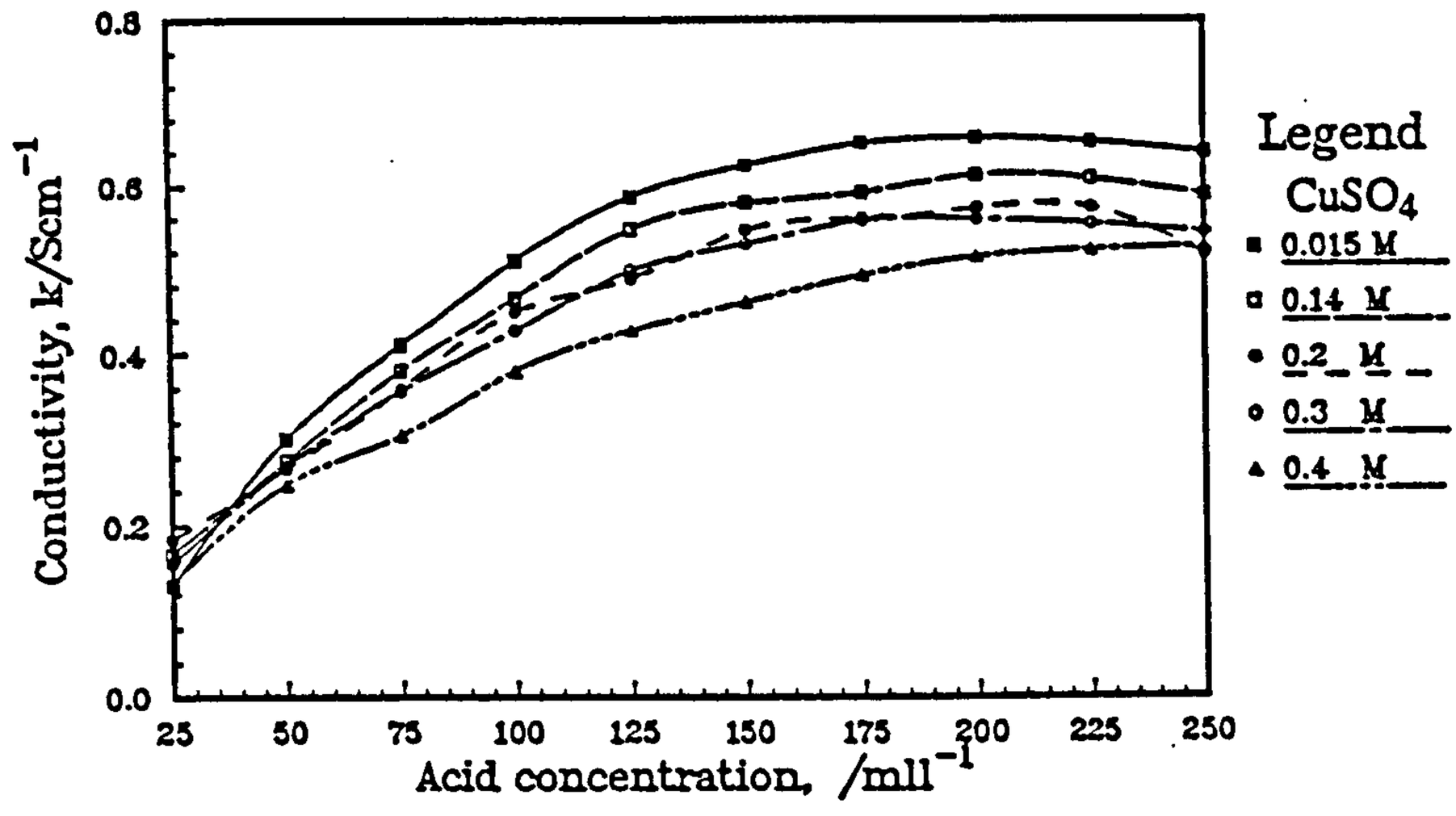

Figure 43 Relationship between conductivity and sulphuric acid concentrations in different molarities(M) of copper sulphate solutions.

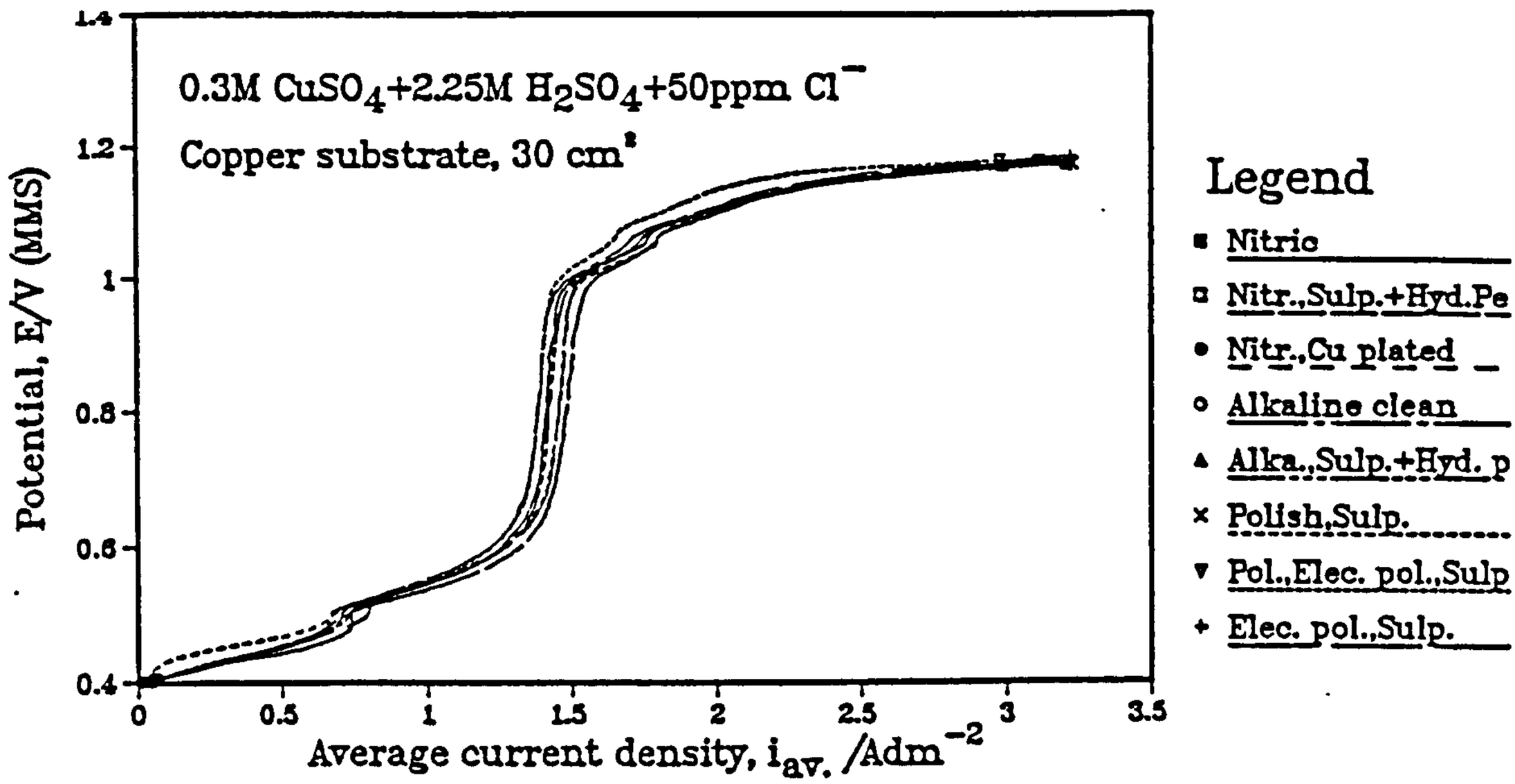

Figure 44a Pretreatment assesment of samples by polarisation study and the Tafel bahaviour under DC.

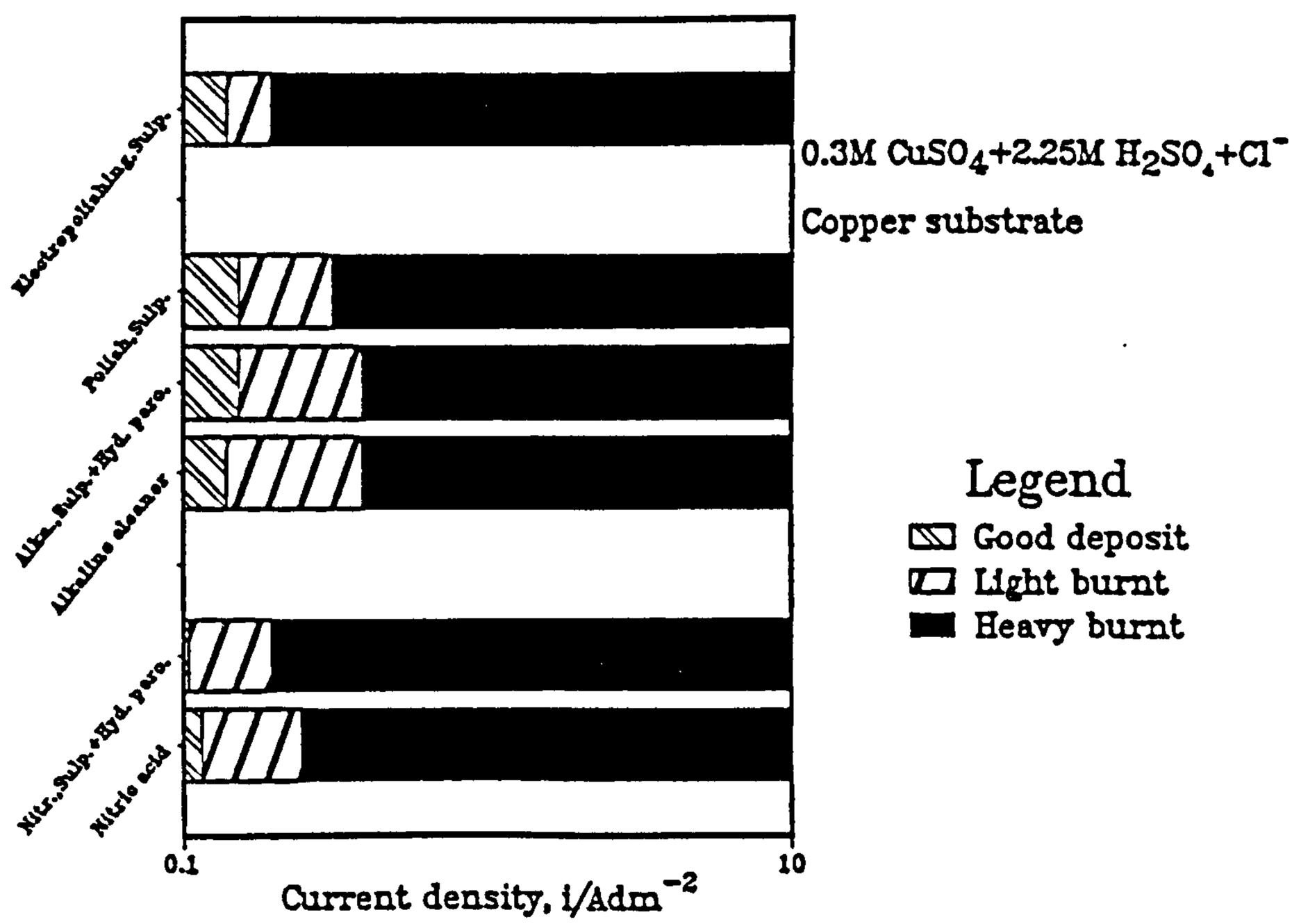

Figure 44b Hull cell data obtained using different pretreatments under DC.

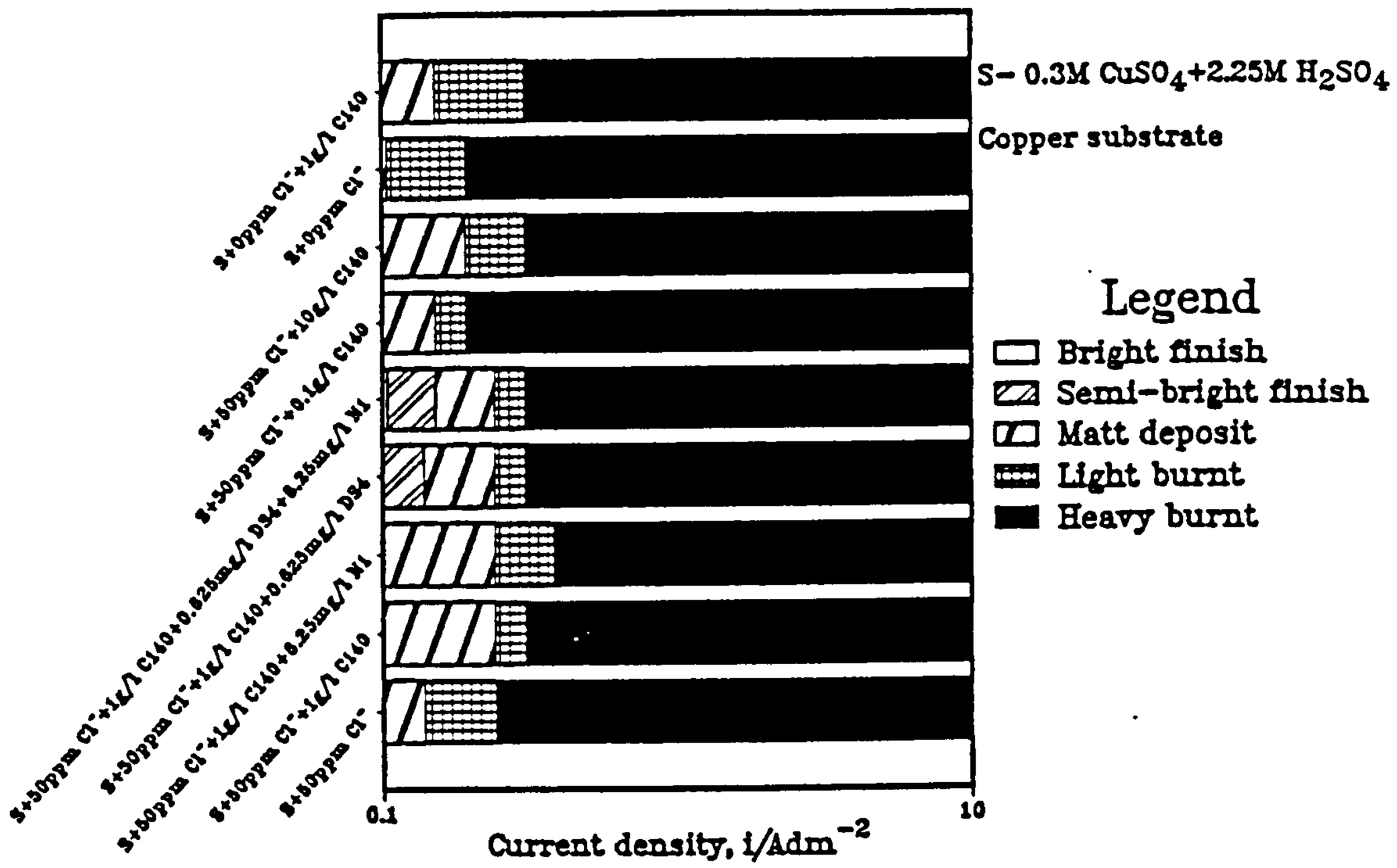

Figure 45a Hull cell data obtained using different electrolyte solutions; no agitation.

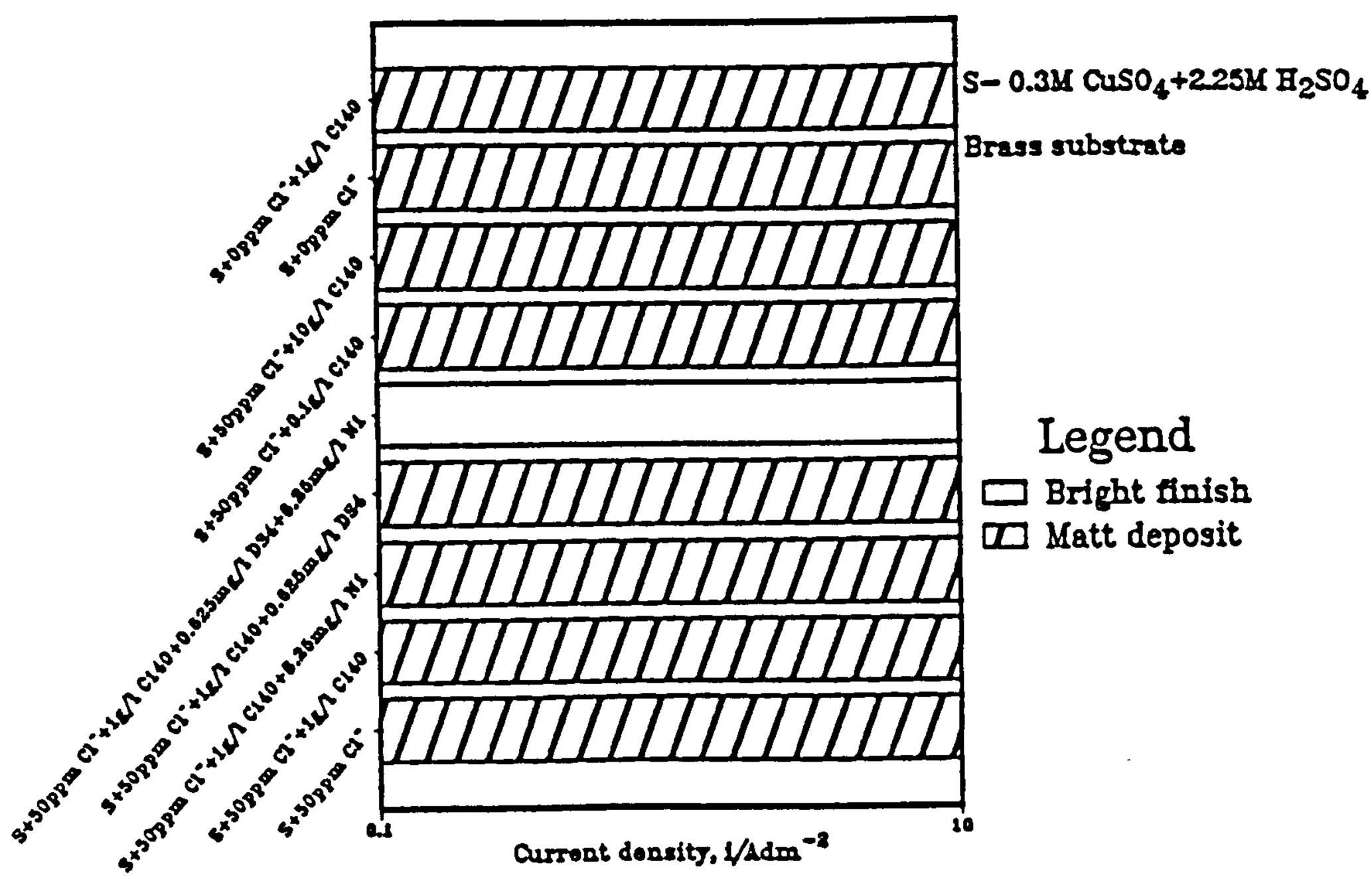

Figure 45b Hull cell data obtained using different electrolyte solutions; air agitation.

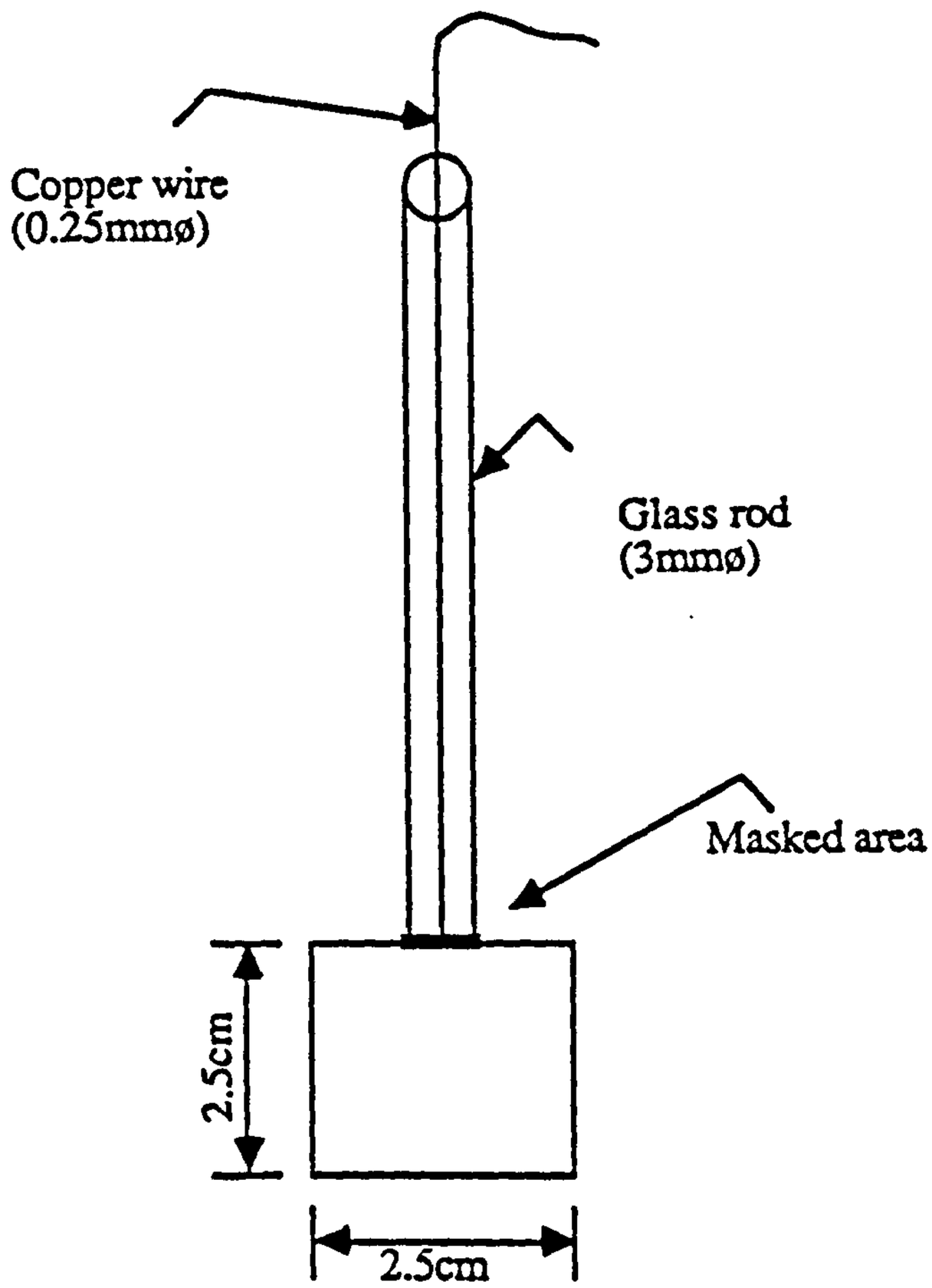

Figure 46 Shows the design of the electrode used for polarisation study of pulse electronic behaviour.

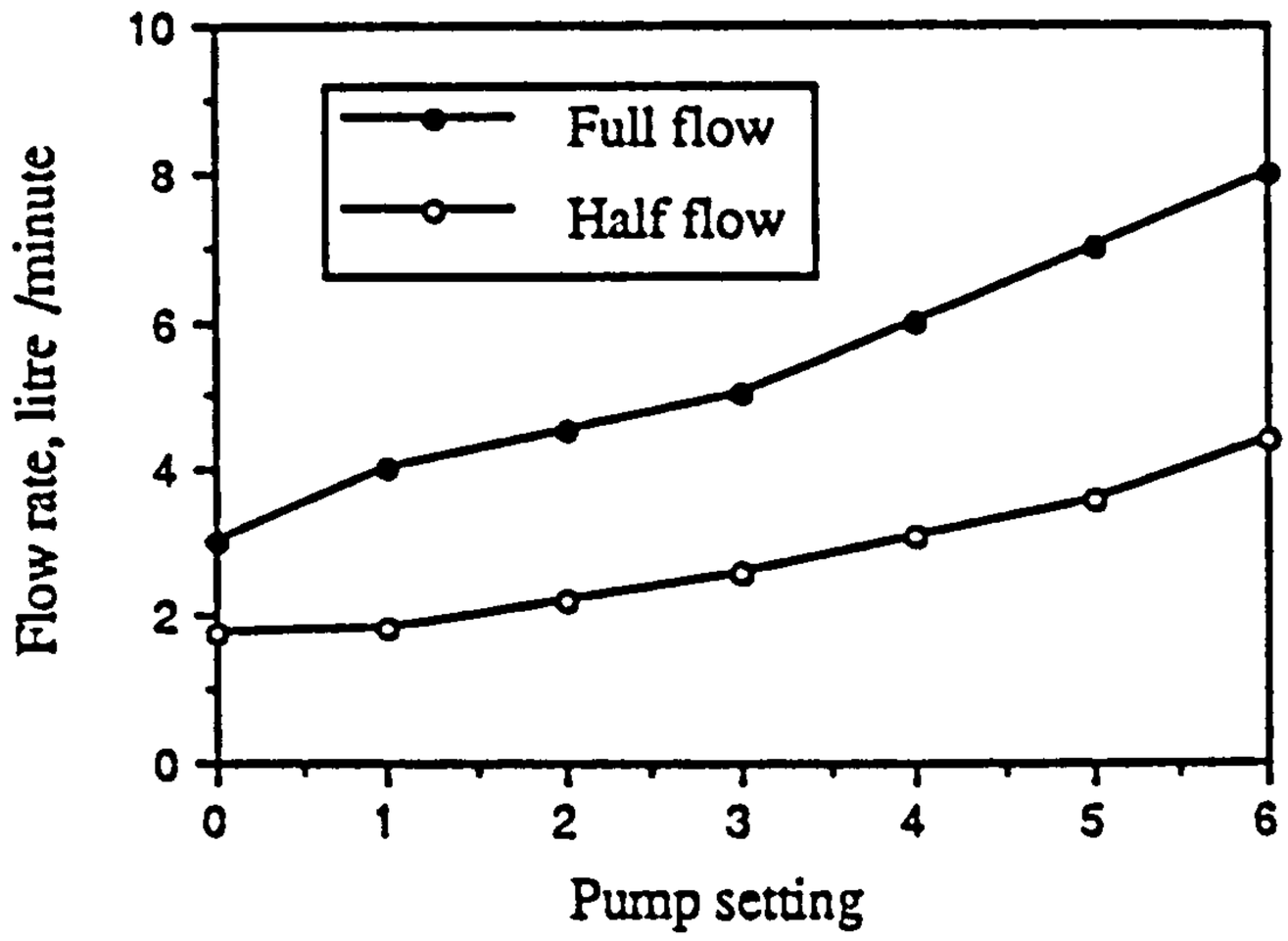

Figure 47a Shows the pump flow rate against pump setting with six divisions each having 10 sub-divisions; full fow rate indicates the maximum air rate which can be pumped at one time per settings.

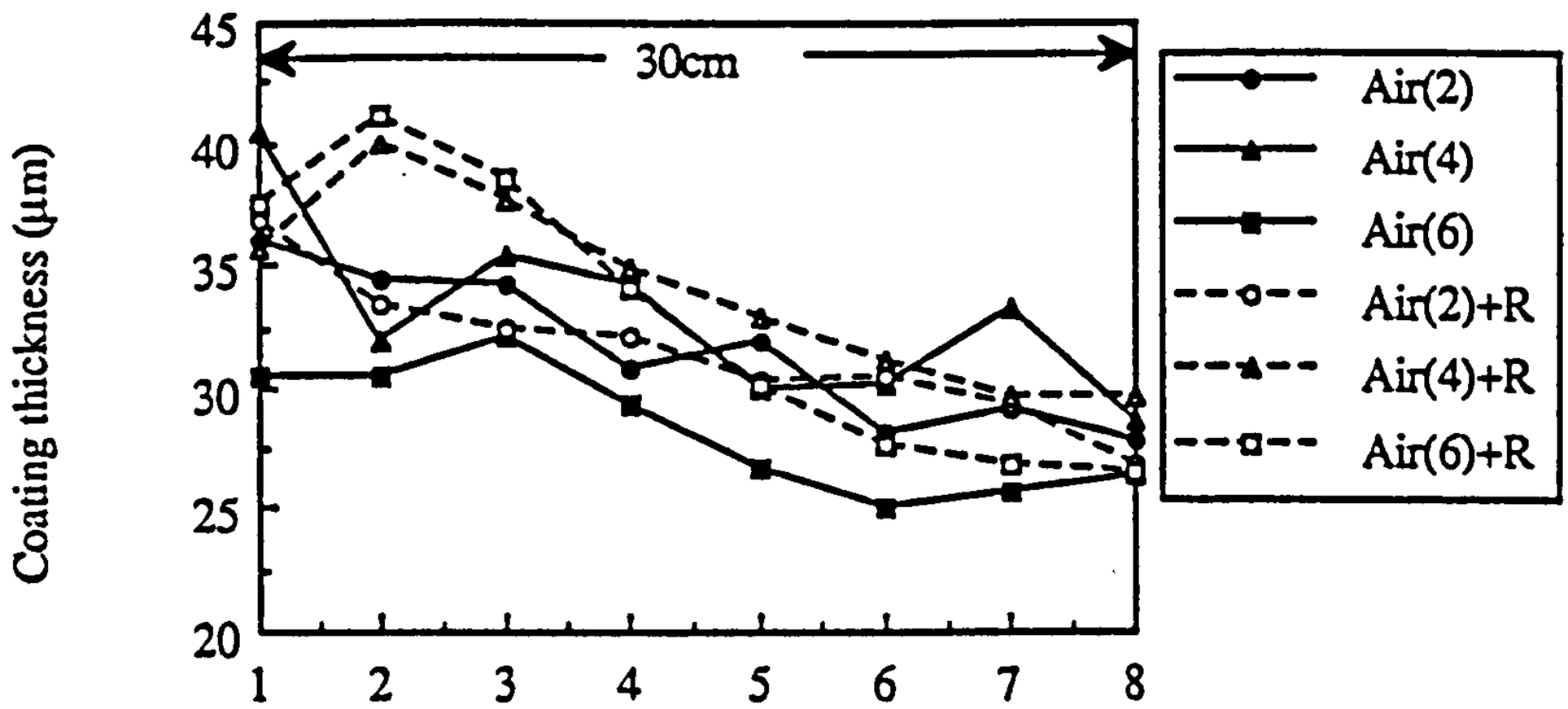

Figure 47b Coating thickness against position of the cathode in the tank for the height of 30cm; 1- bottom and 8- top of the tank, R- reciprocating agitation plating time of 37minutes.

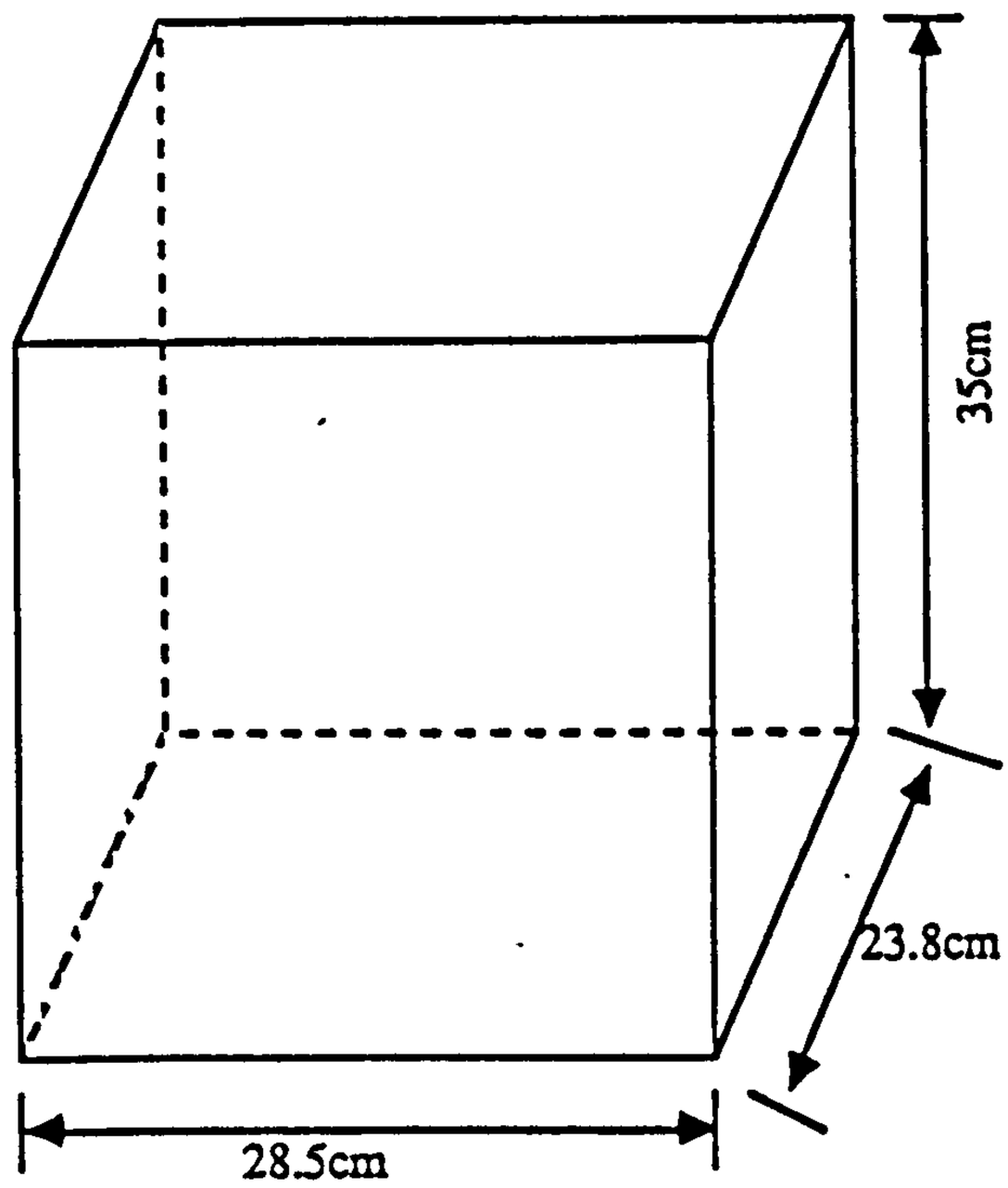

(a)

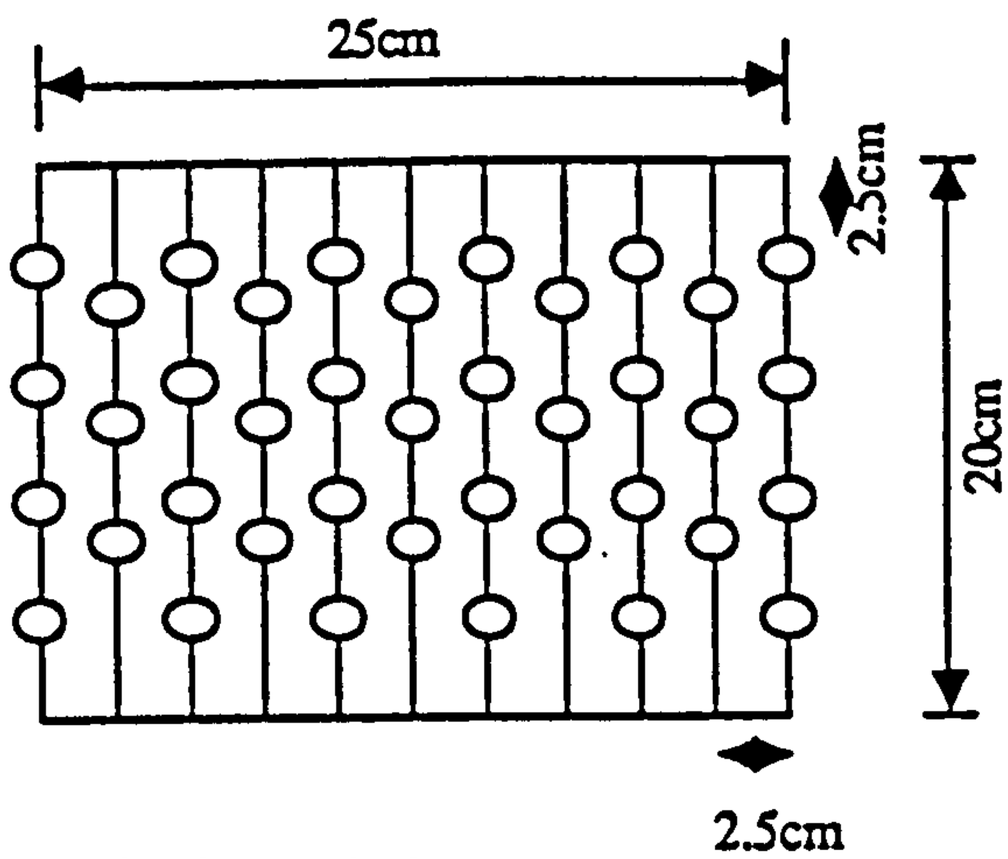

indicates hole

(b)

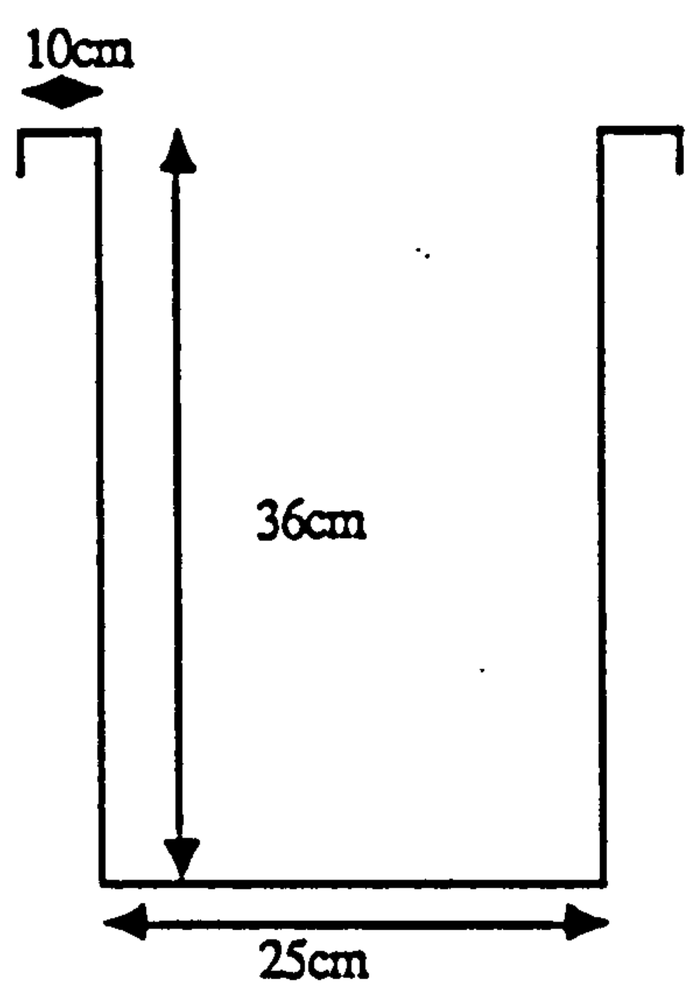

(c)

Figure 48 Shows the bath and the air sparging design using PVC pipes; 3mmø inside and 6mmø outside.
a) profile of the bath and its dimensions
b) plan view of the air agitation rig
c) side view of the air agitation rig.

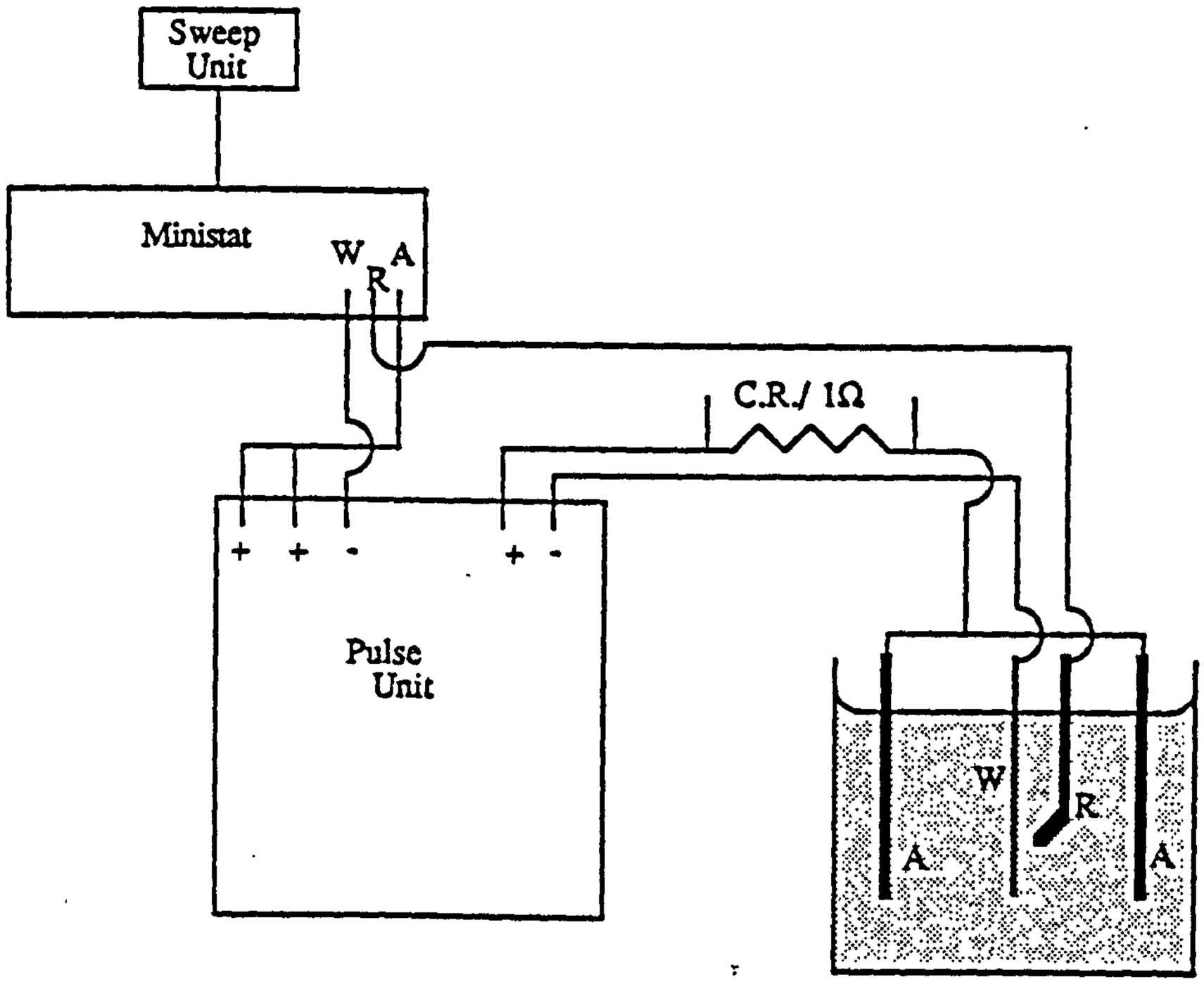

Figure 49a Shows a sweep unit connected to a potentiostat and the cell via pulse unit - potentiodynamically or galvanodynamically.

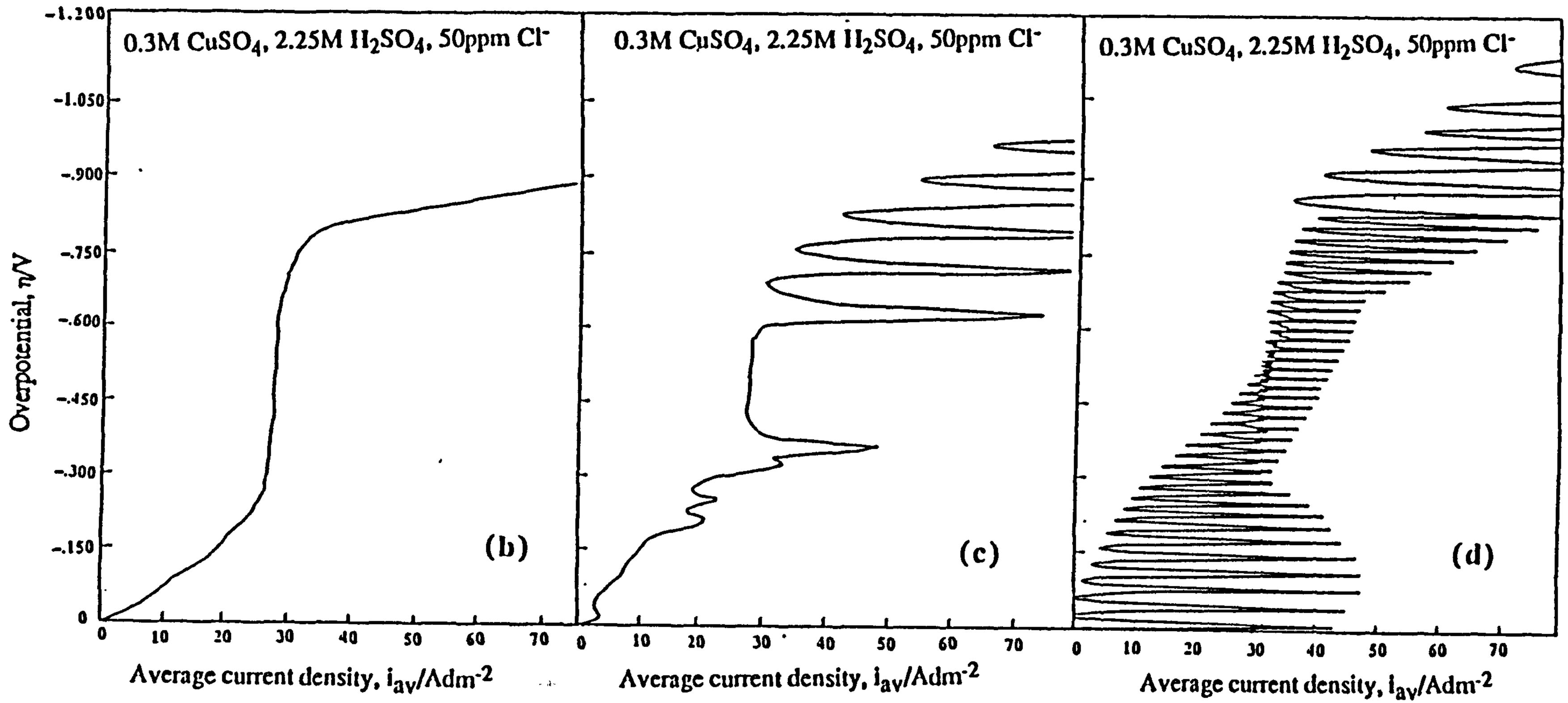

Figure 49b-f Polarisation curves obtained at a potentiodynamic sweep rate of 150mV/minutes using a potentiostat and a pulse unit (figure 49a) with no agitation; the polarisation curves were obtained at:

b) frequency and duty cycle of 50Hz and 99%; direct current frequency and duty cycle of 50Hz and 50%; unipolar pulse:

c) potentiostat was switched on a second latter

d) potentiostat and pulse unit were switched together

e) potentiostat and pulse unit were switched together

f) pulse unit was switched on a second latter.

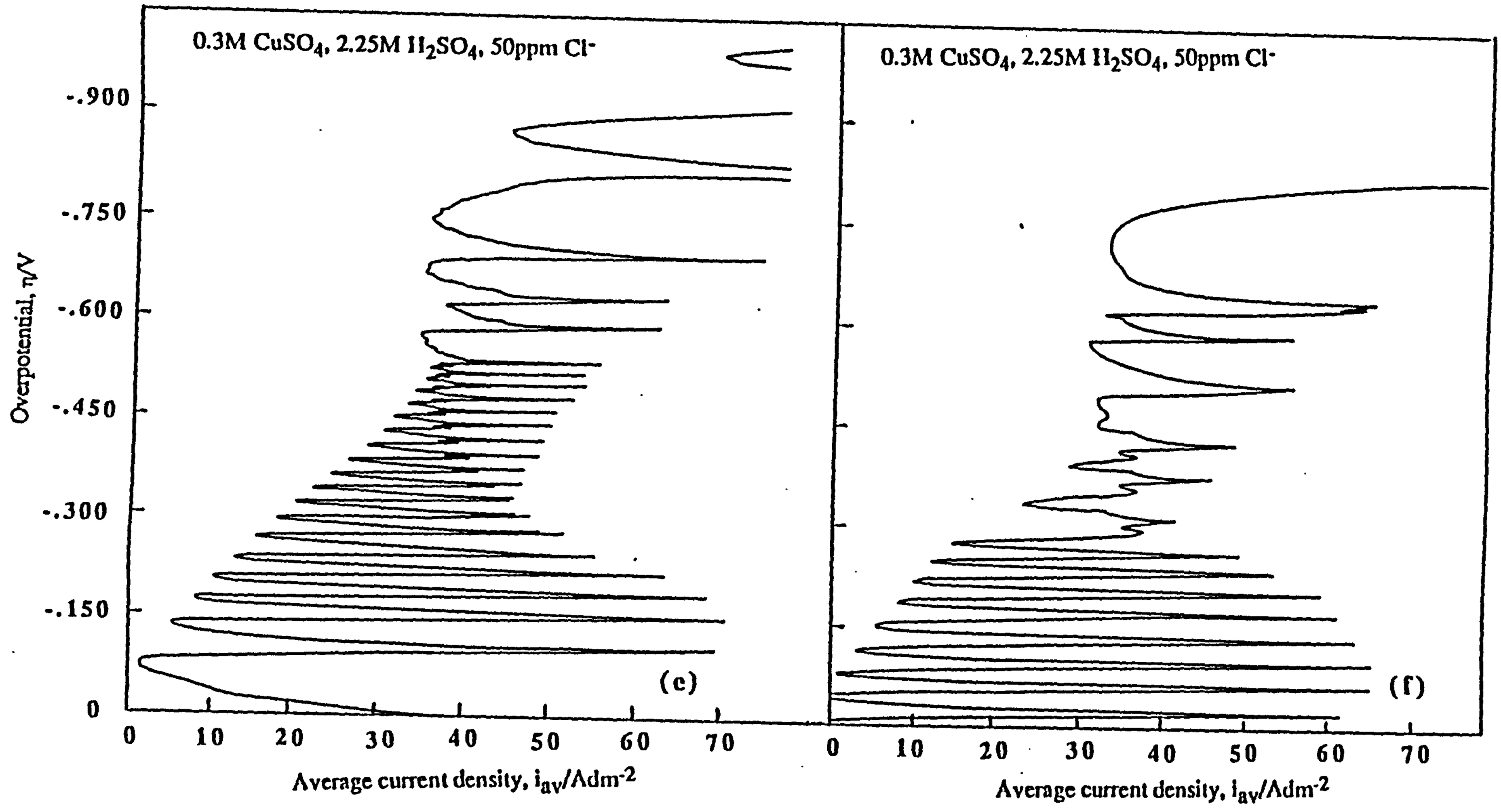

Figure 49 Continued ...

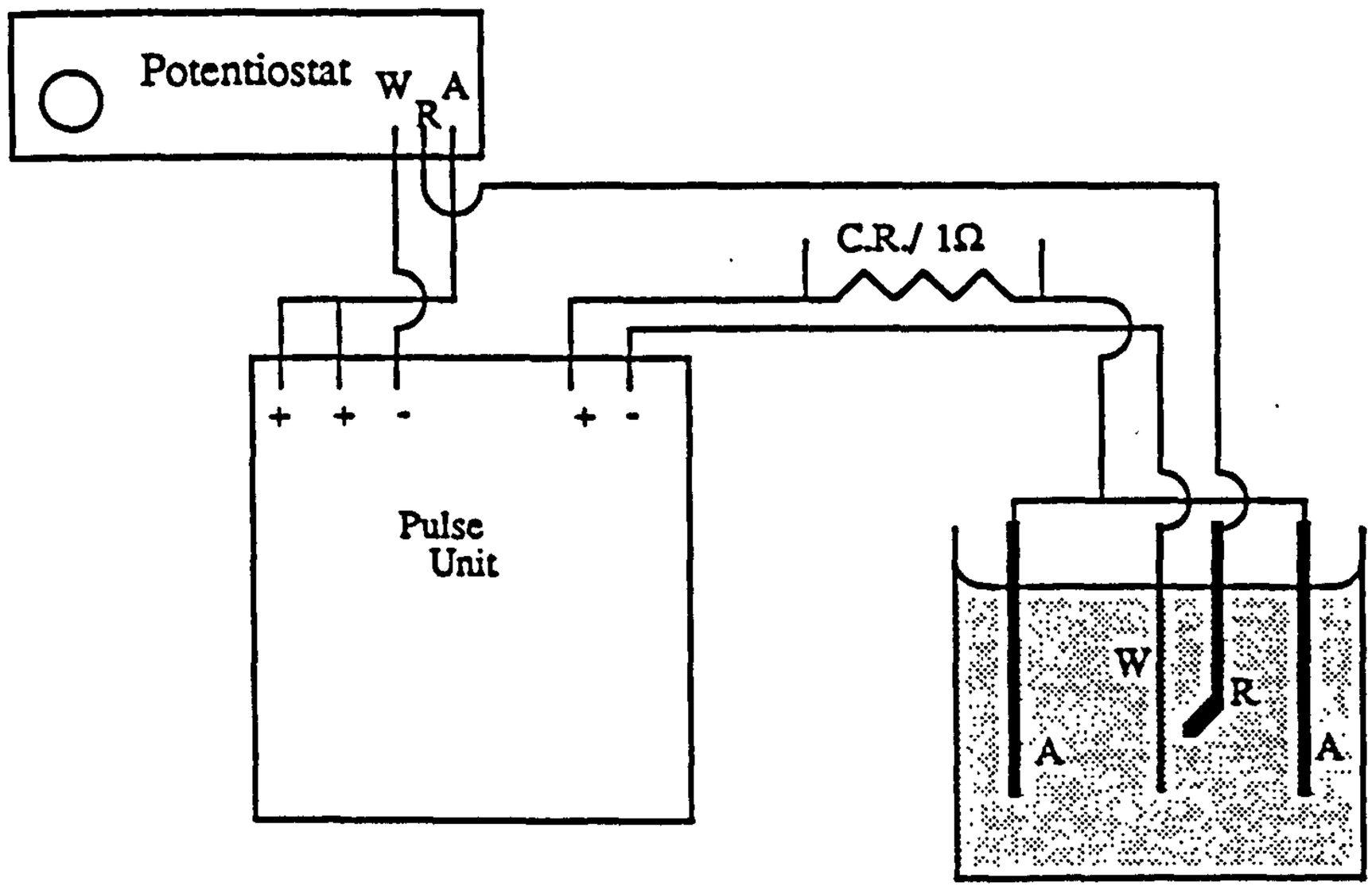

Figure 50 Shows a potentiostat connected to the cell via a pulse unit - step-potential; cell current measurement was carried out via a chart recorder(C.R.) using a 1Ω resistor.

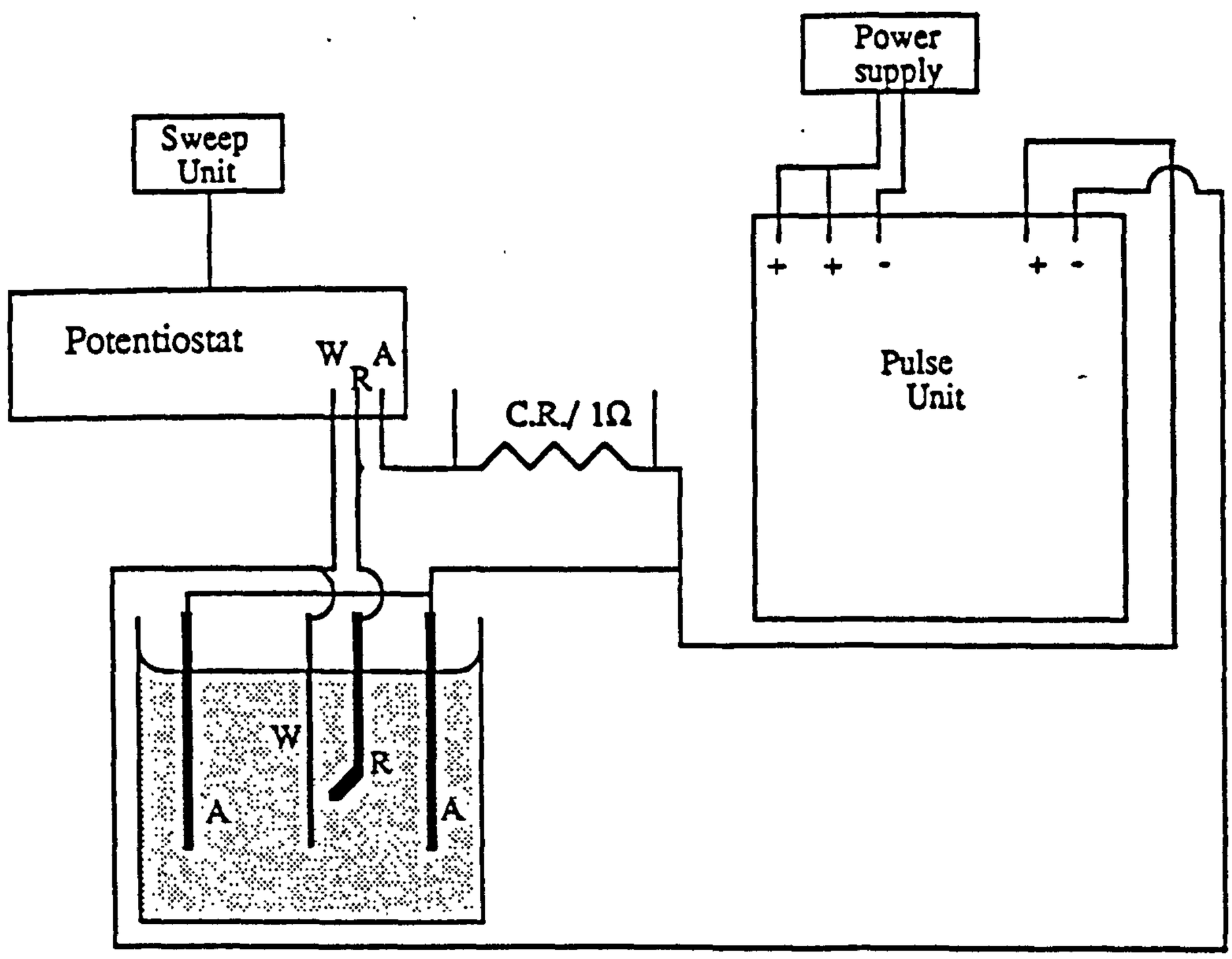

Figure 51 Shows a sweep unit connected to a potentiostat from one end and the power supply via pulse unit to the cell; cell connections are to the same anodes.

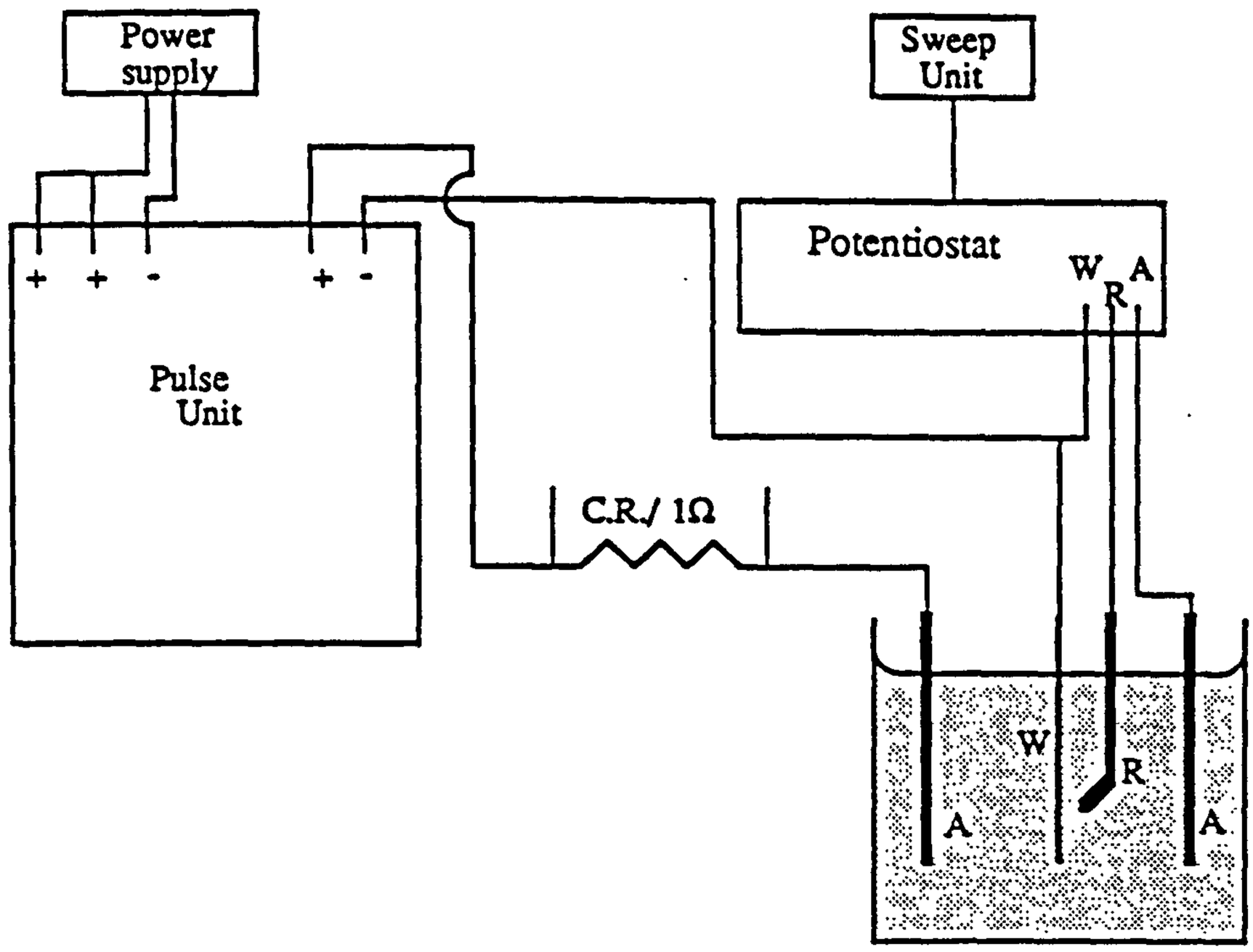

Figure 52 Shows a sweep unit connected to a potentiostat from one end and the power supply via pulse unit to the cell; cell connections are to two different anodes.

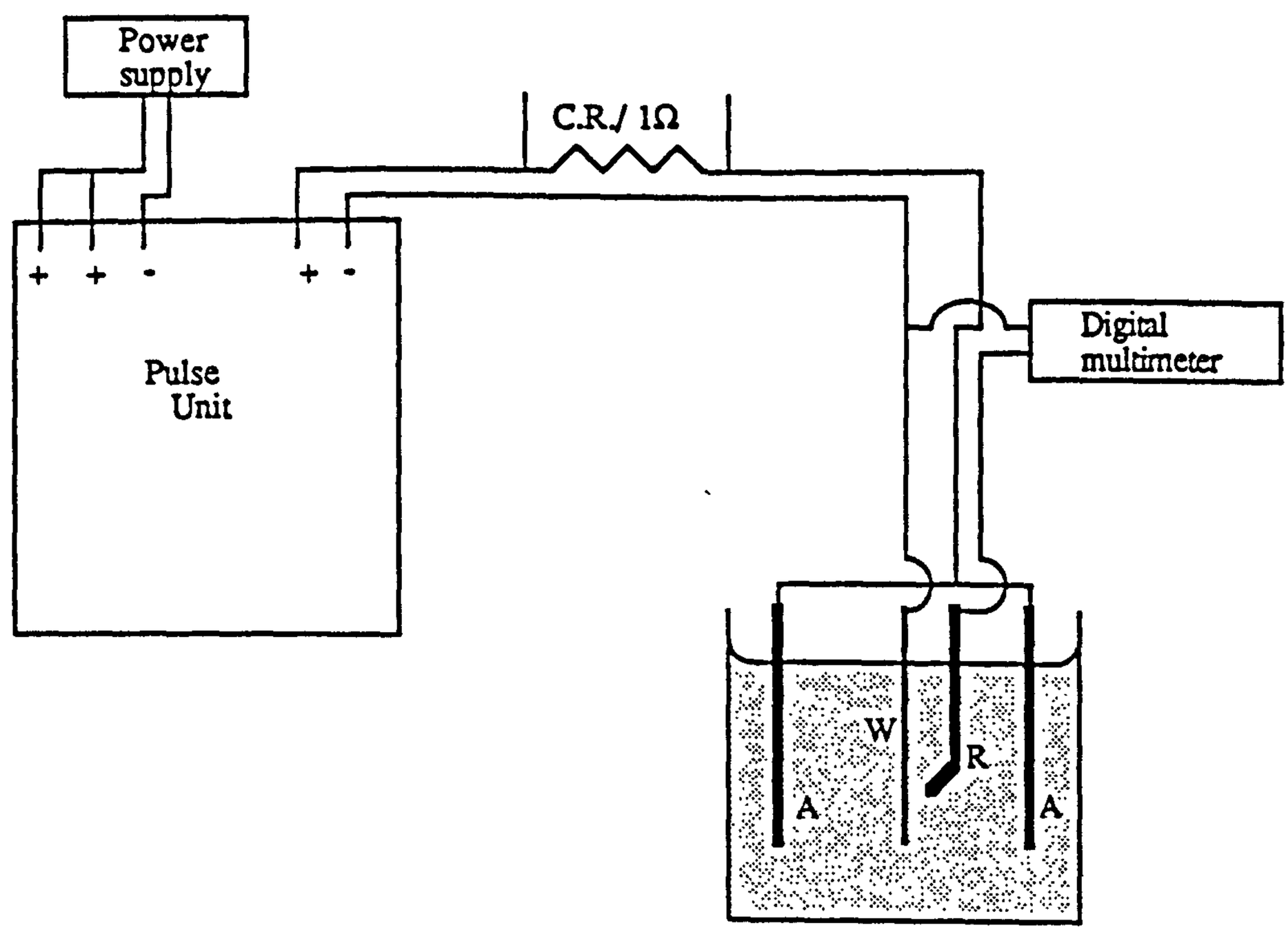

Figure 53 Shows the power supply connected to the pulse unit to the cell (step-potential); cell voltage measured via a voltmeter and the cell current measured via multimeter across a resistor.

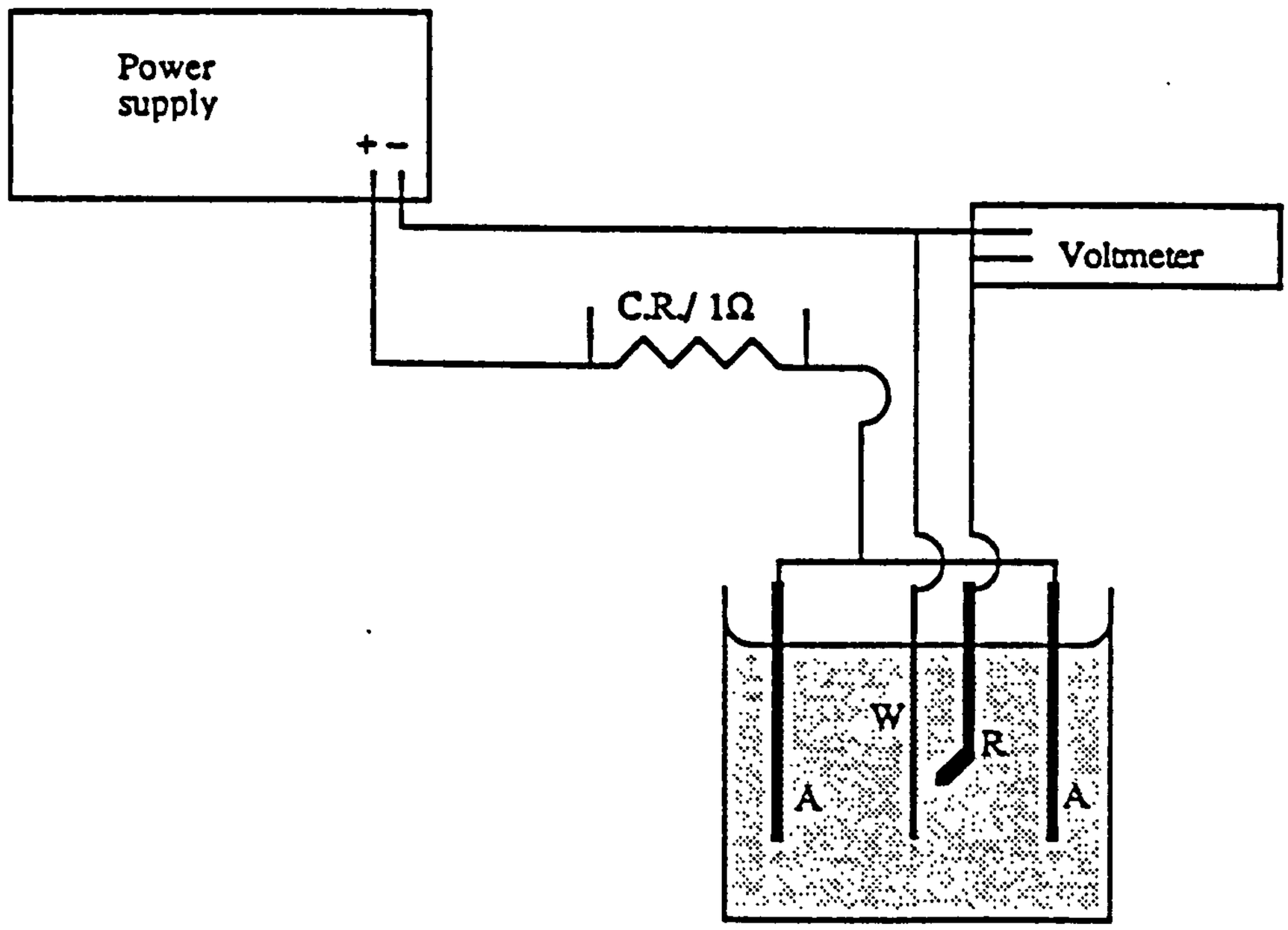

Figure 54a Shows the experimental arrangement used for direct current(DC) studies.

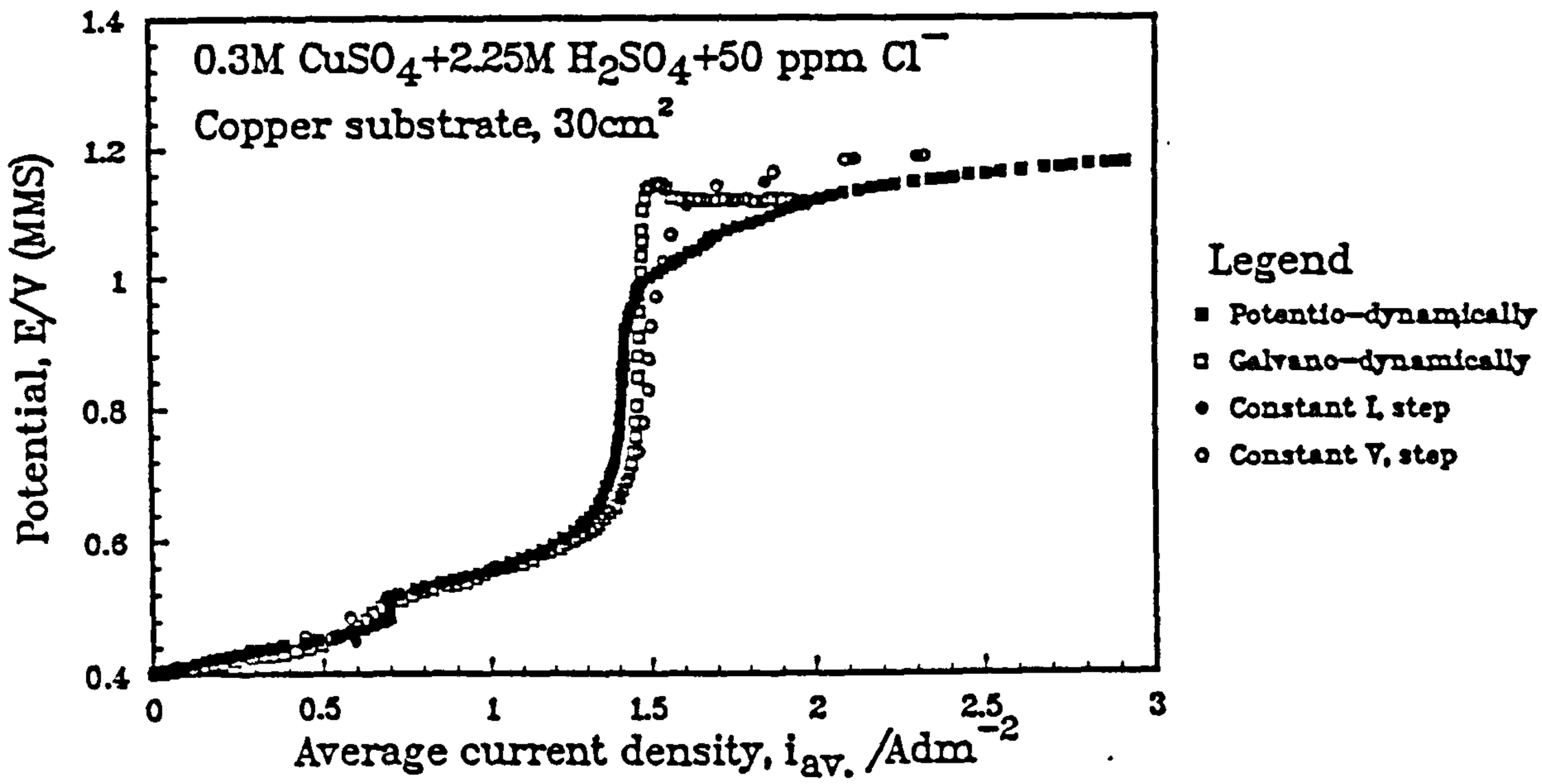

Figure 54b Polarisation curves obtained by potentio-, galvano-dynamically and step-potential method under DC; no agitation.

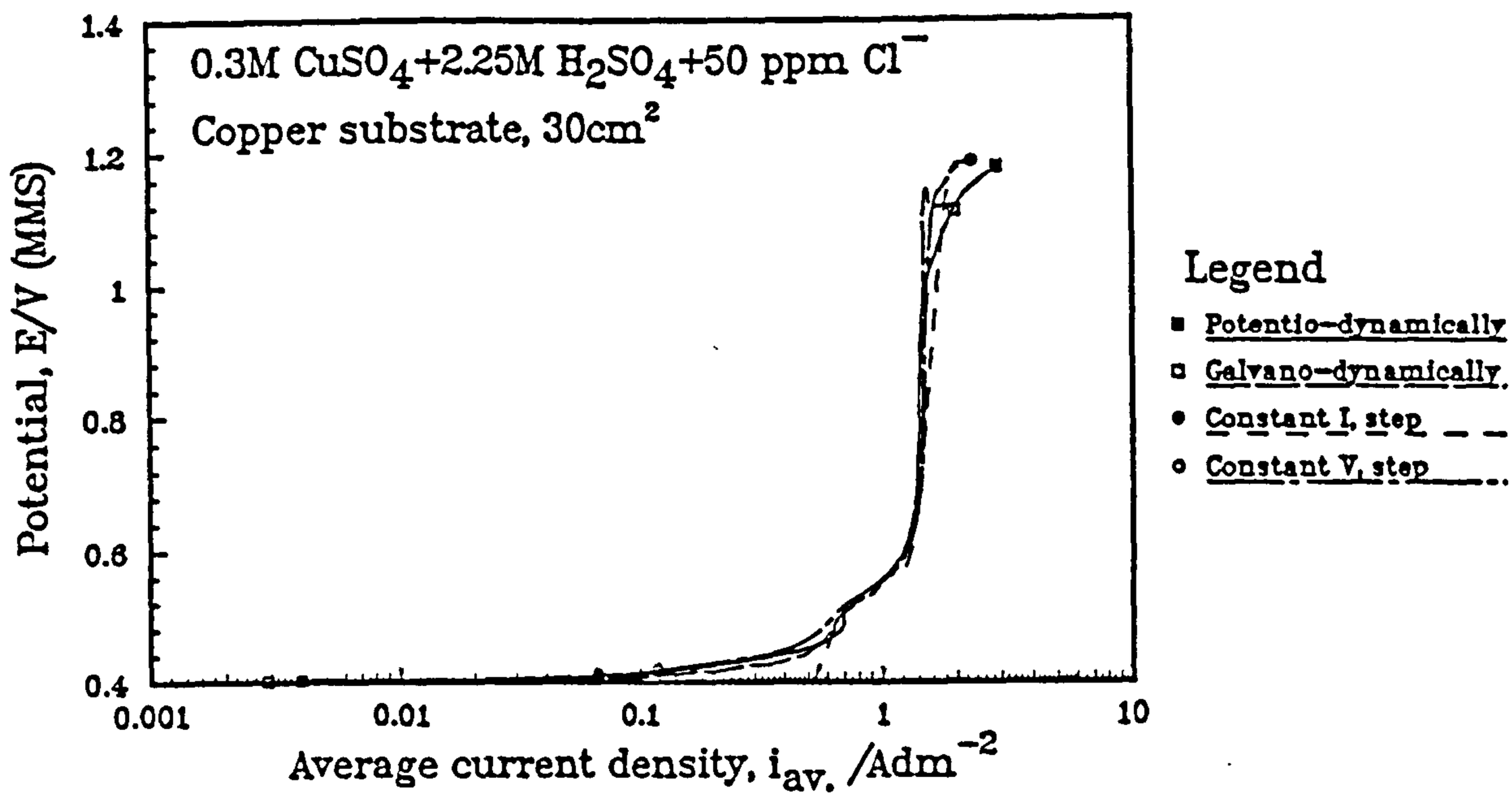

Figure 54c Polarisation curves obtained by potentio-, galvano-dynamically and step-potential method under DC; no agitation.

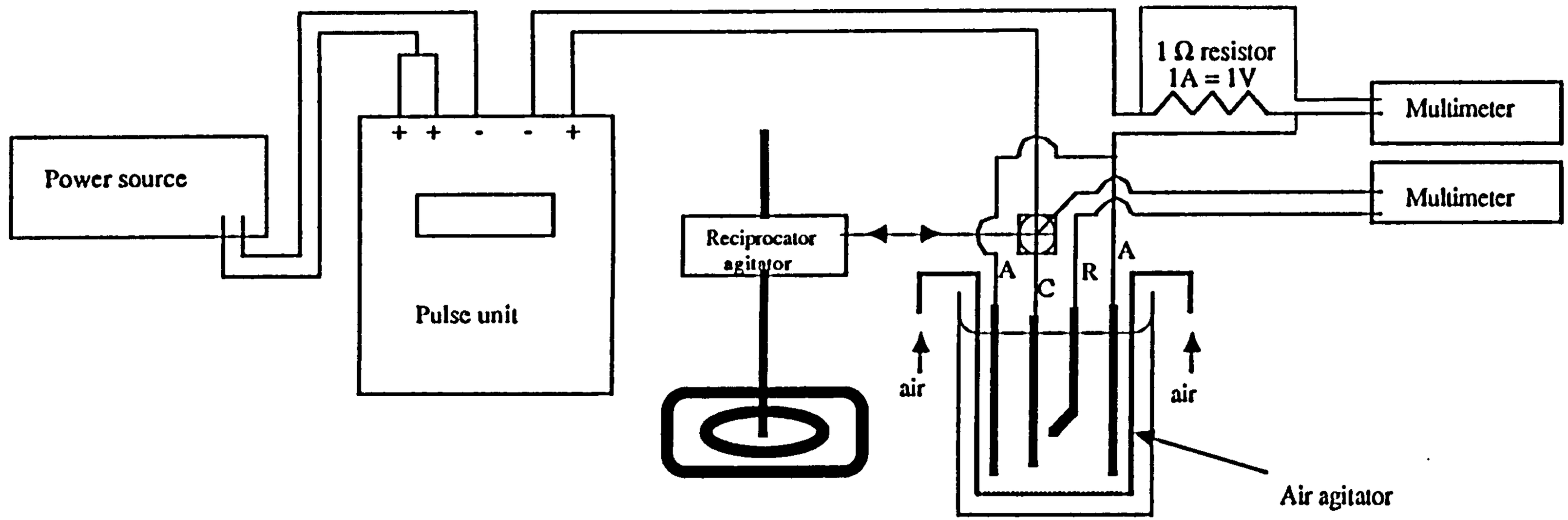

Figure 55 Experimental arrangement used for unipolar pulse polarisation studies using one power supply and also for bipolar pulse reverse using two power supplies.

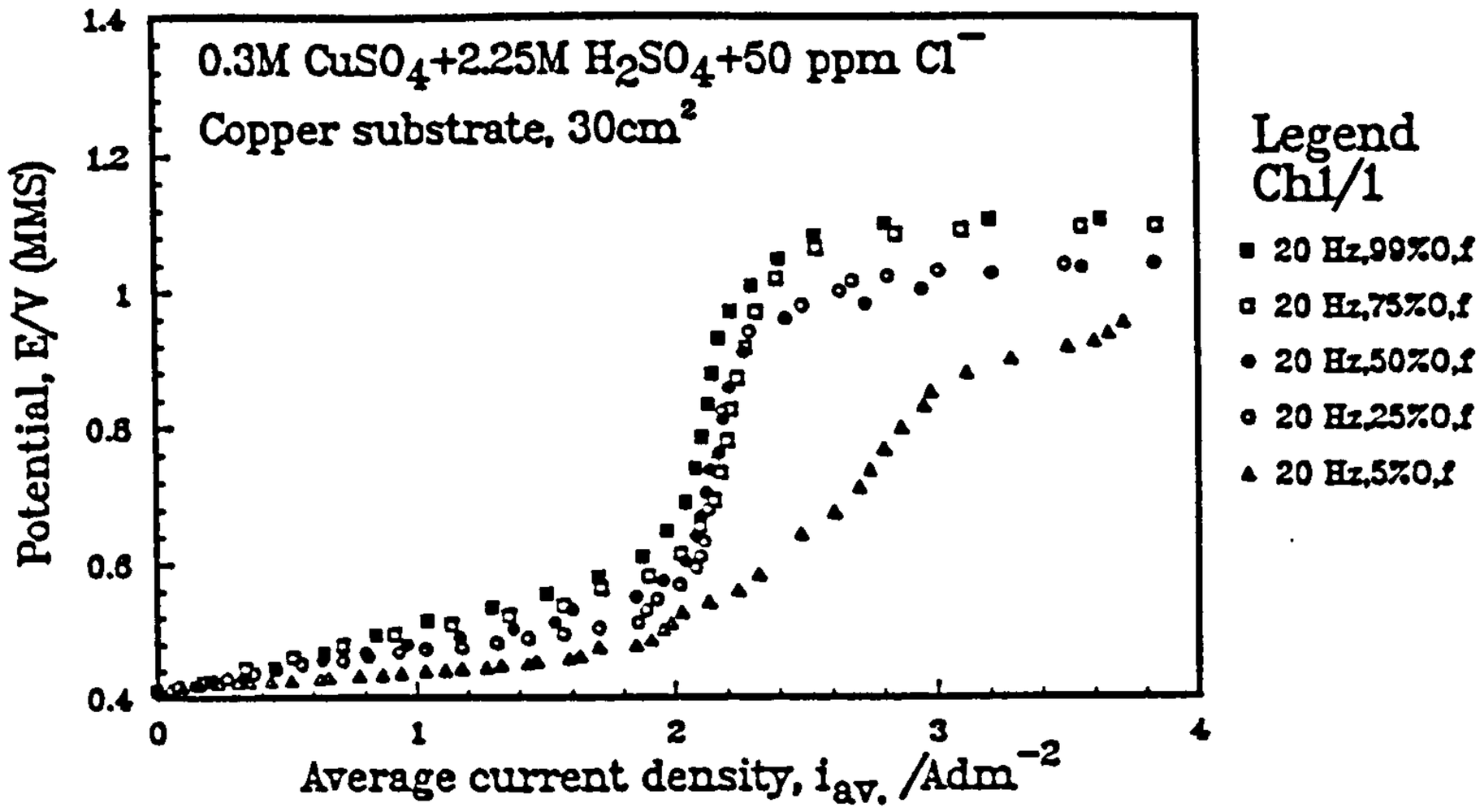

Figure 56a Polarisation curves obtained by step-potential method using a power supply and pulse unit; no agitation.

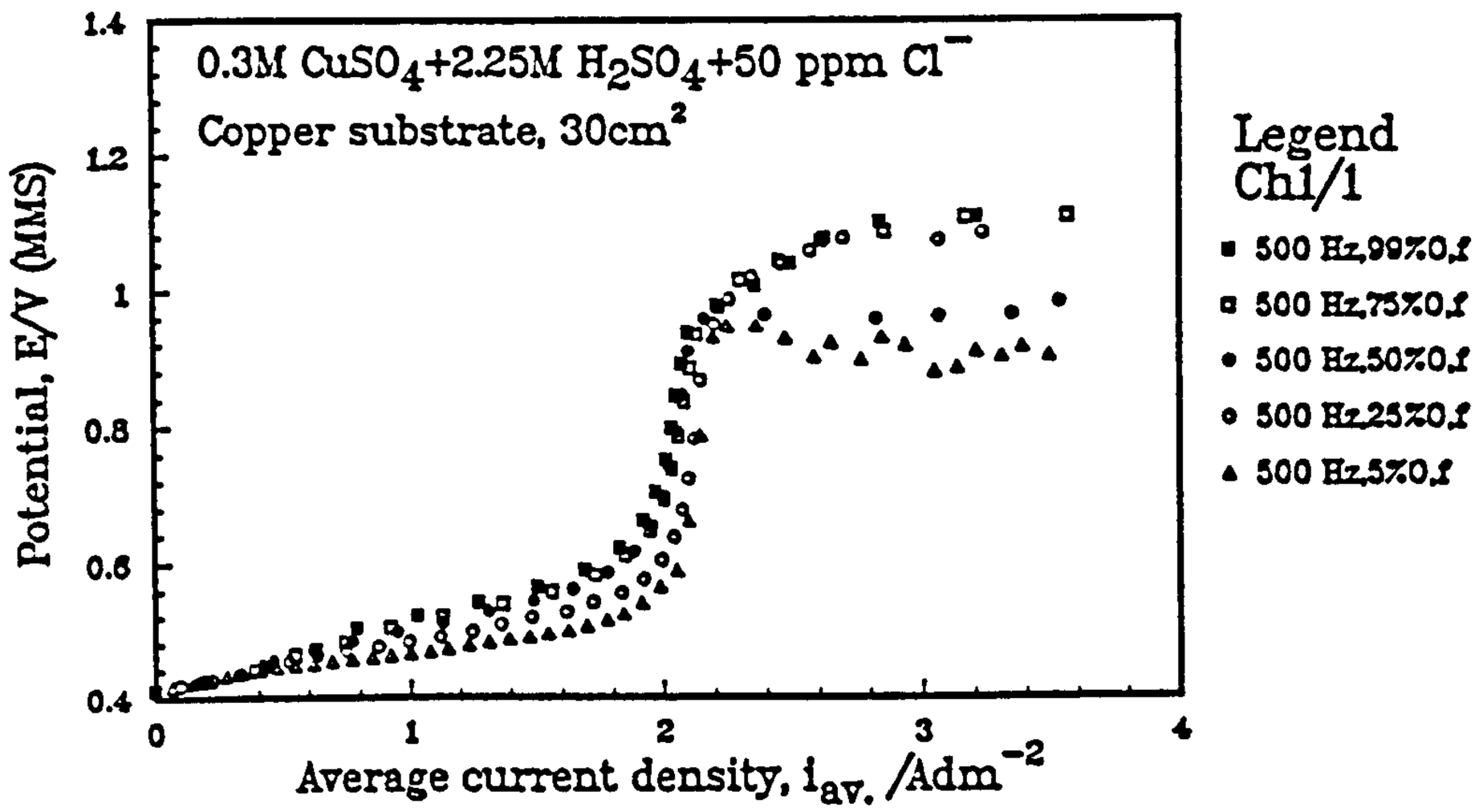

Figure 56b Polarisation curves obtained by step-potential method using a power supply and pulse unit; no agitation.

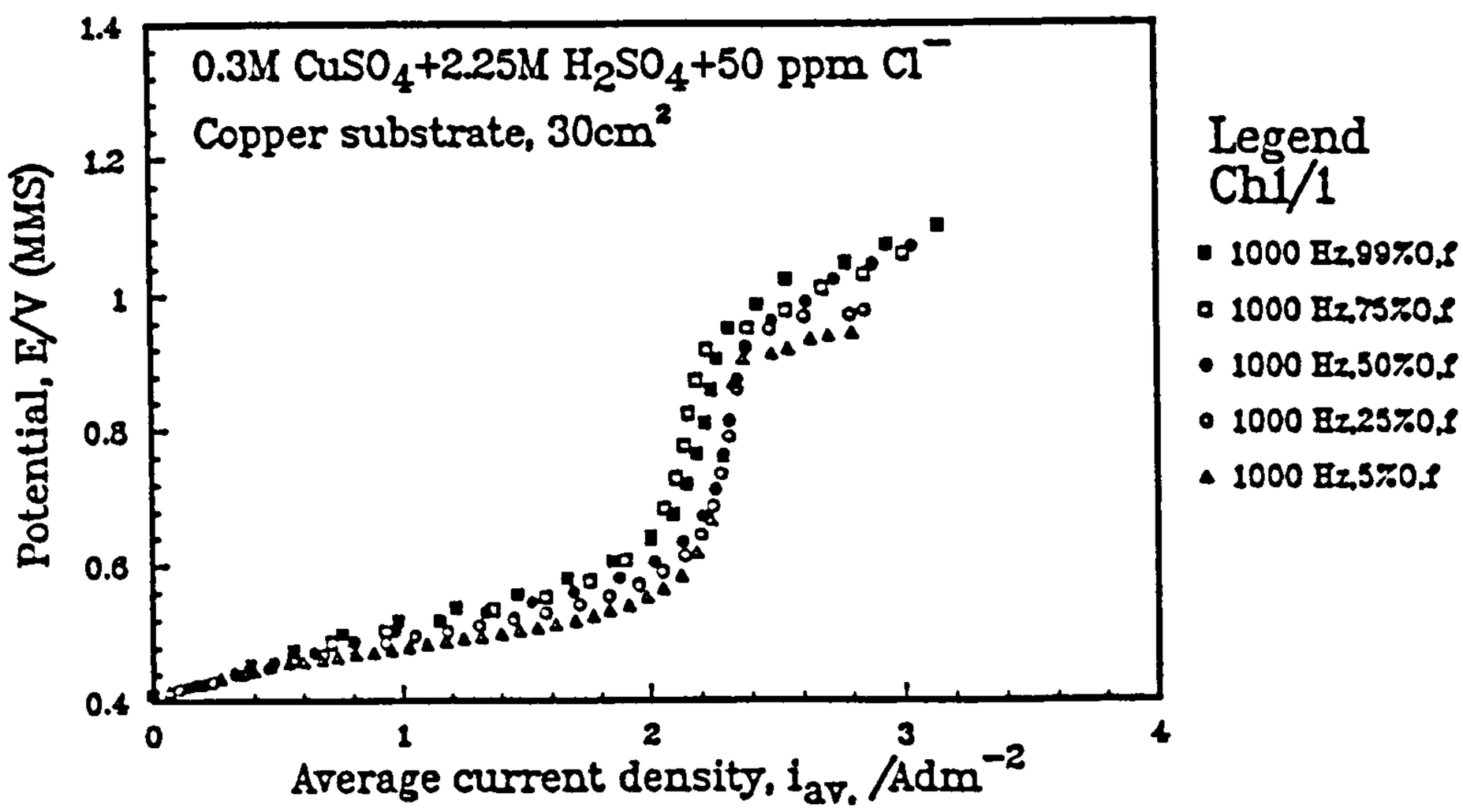

Figure 56c Polarisation curves obtained by step-potential method using a power supply and pulse unit; no agitation.

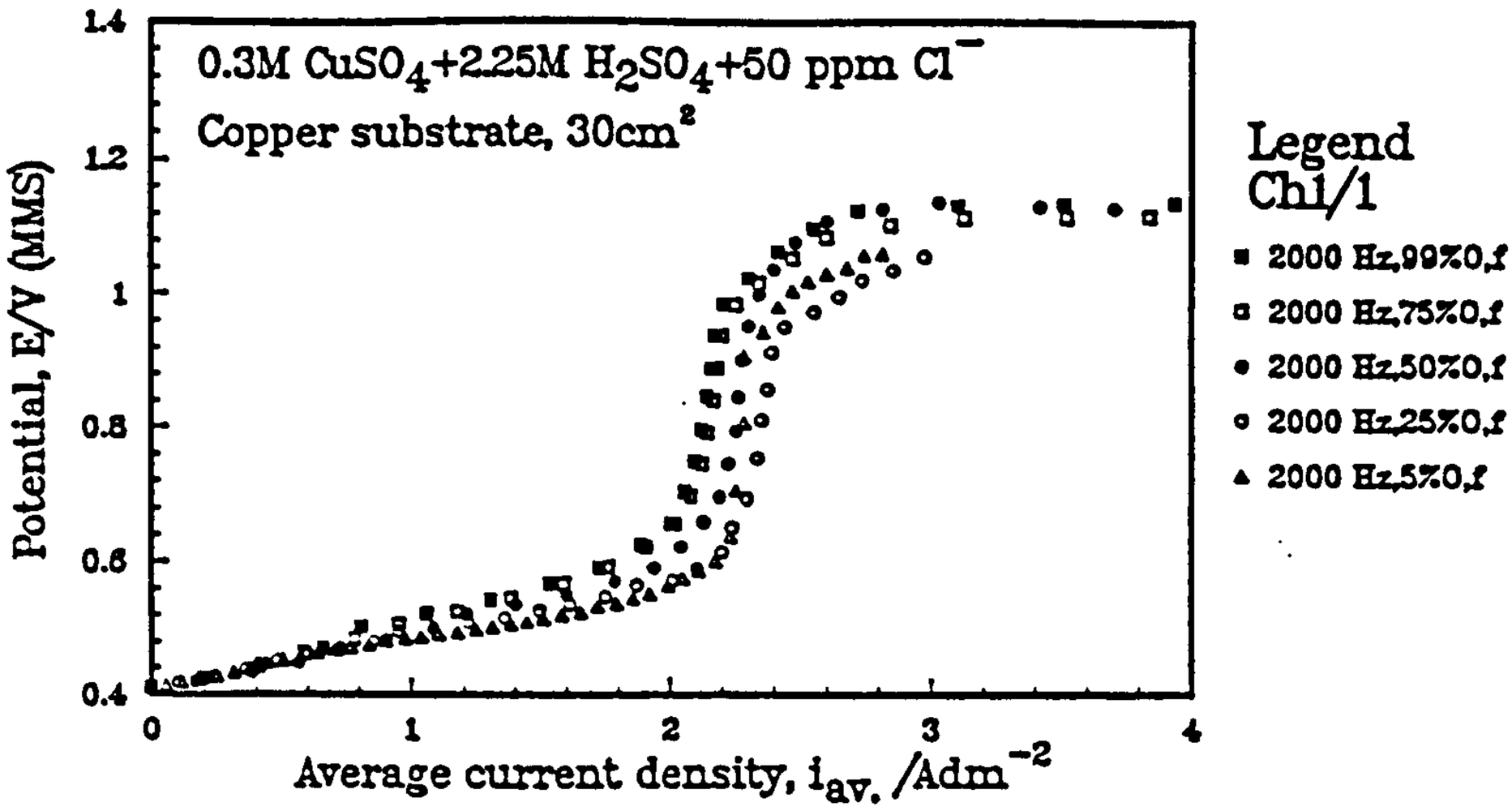

Figure 56d Polarisation curves obtained by step-potential method using a power supply and pulse unit; no agitation.

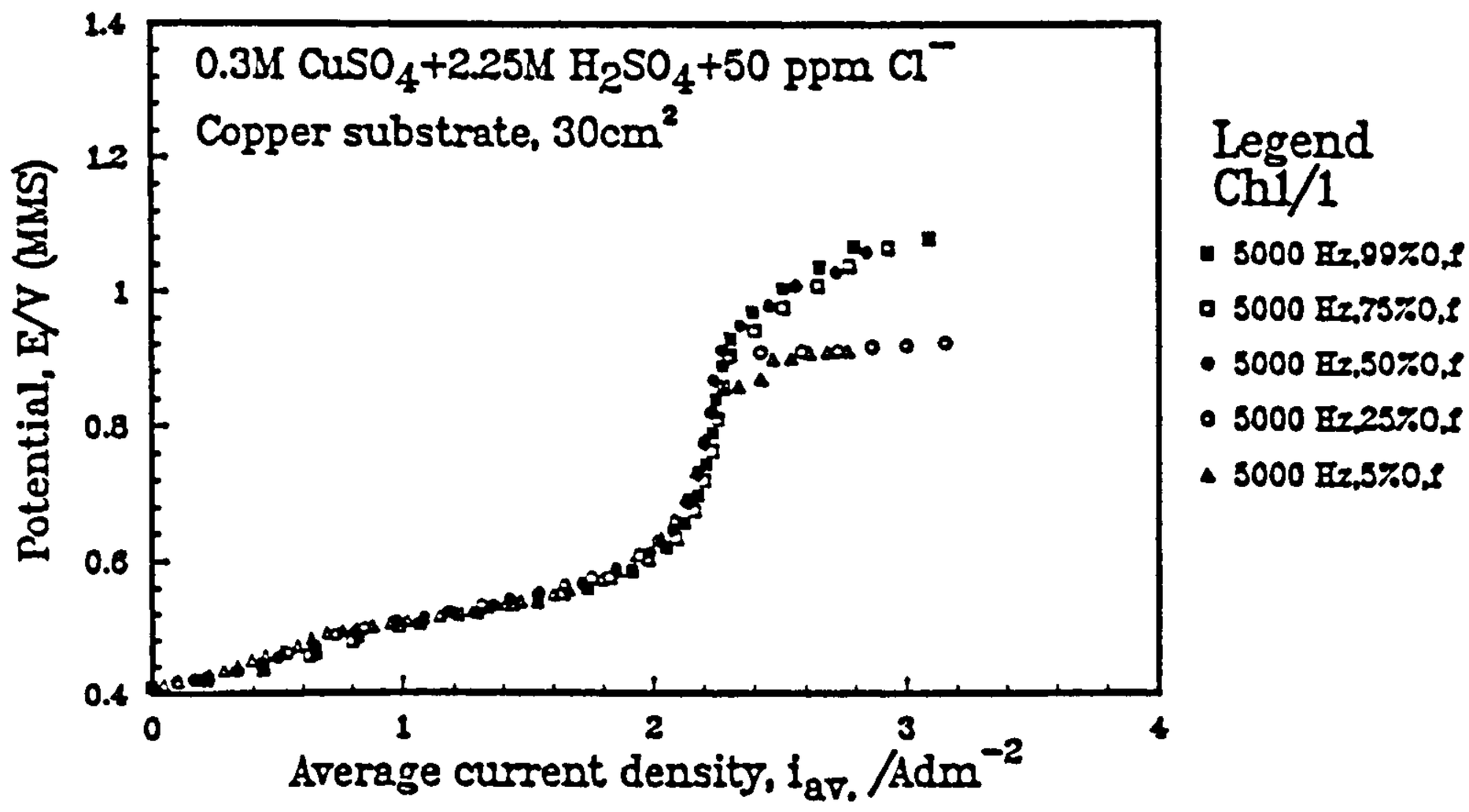

Figure 56e Polarisation curves obtained by step-potential method using a power supply and pulse unit; no agitation.

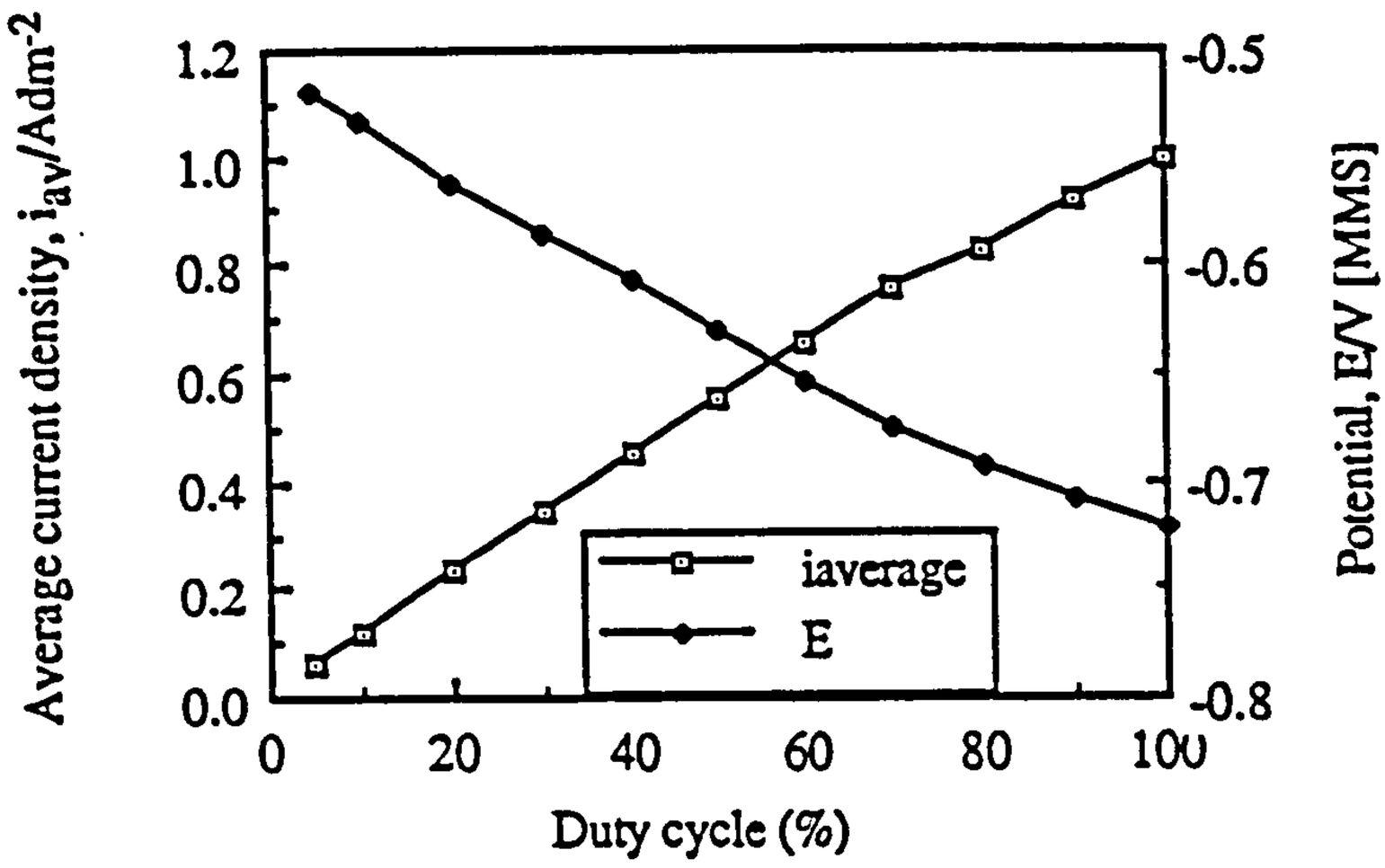

Figure 57a Average current density and potential versus duty cycle at an equivalent DC input current of 1A using electrolyte V and A&R agitations.

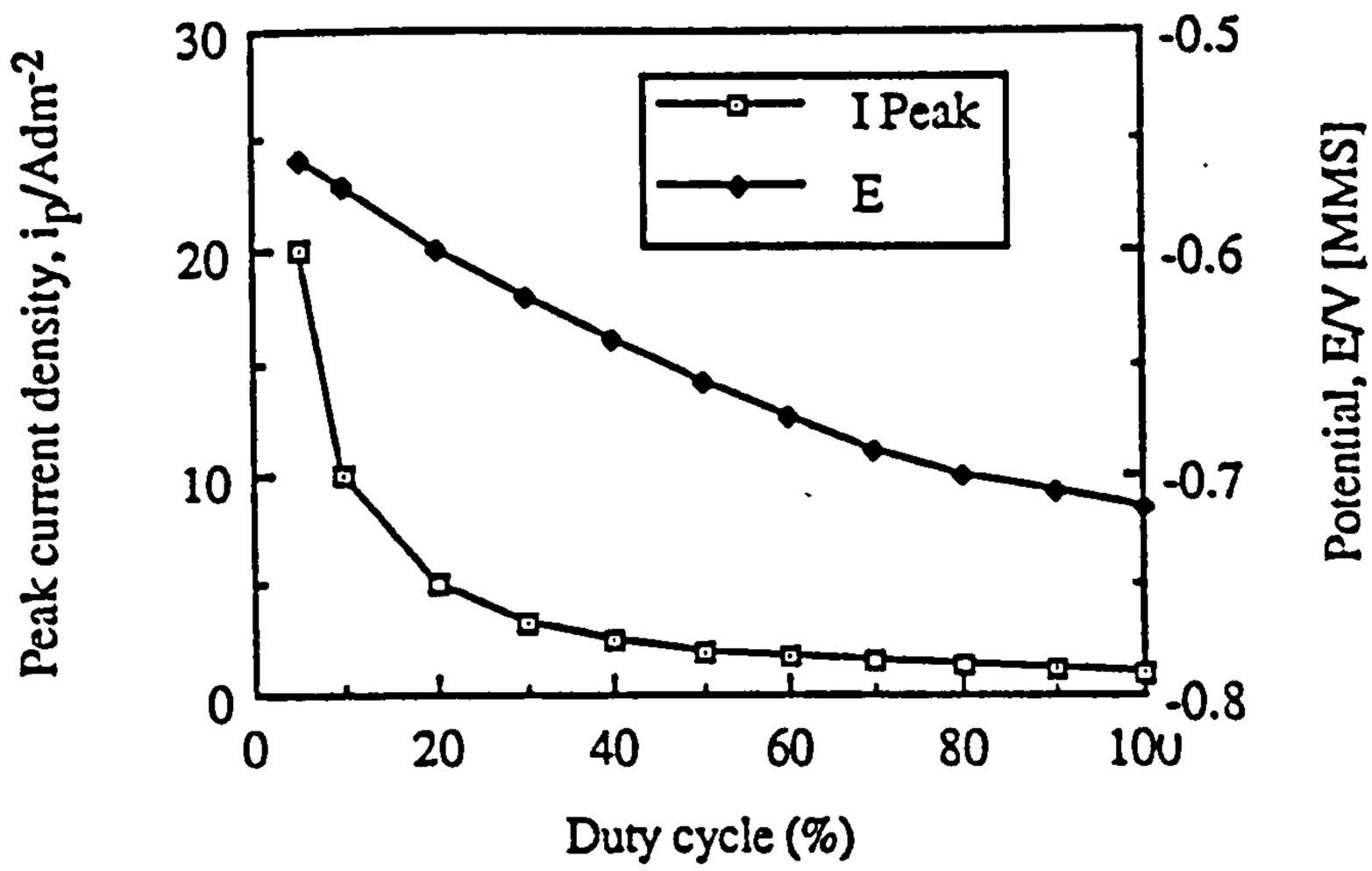

Figure 57b Peak current density and potential versus duty cycle at a constant input current of 1A using electrolyte V and A&R agitations.

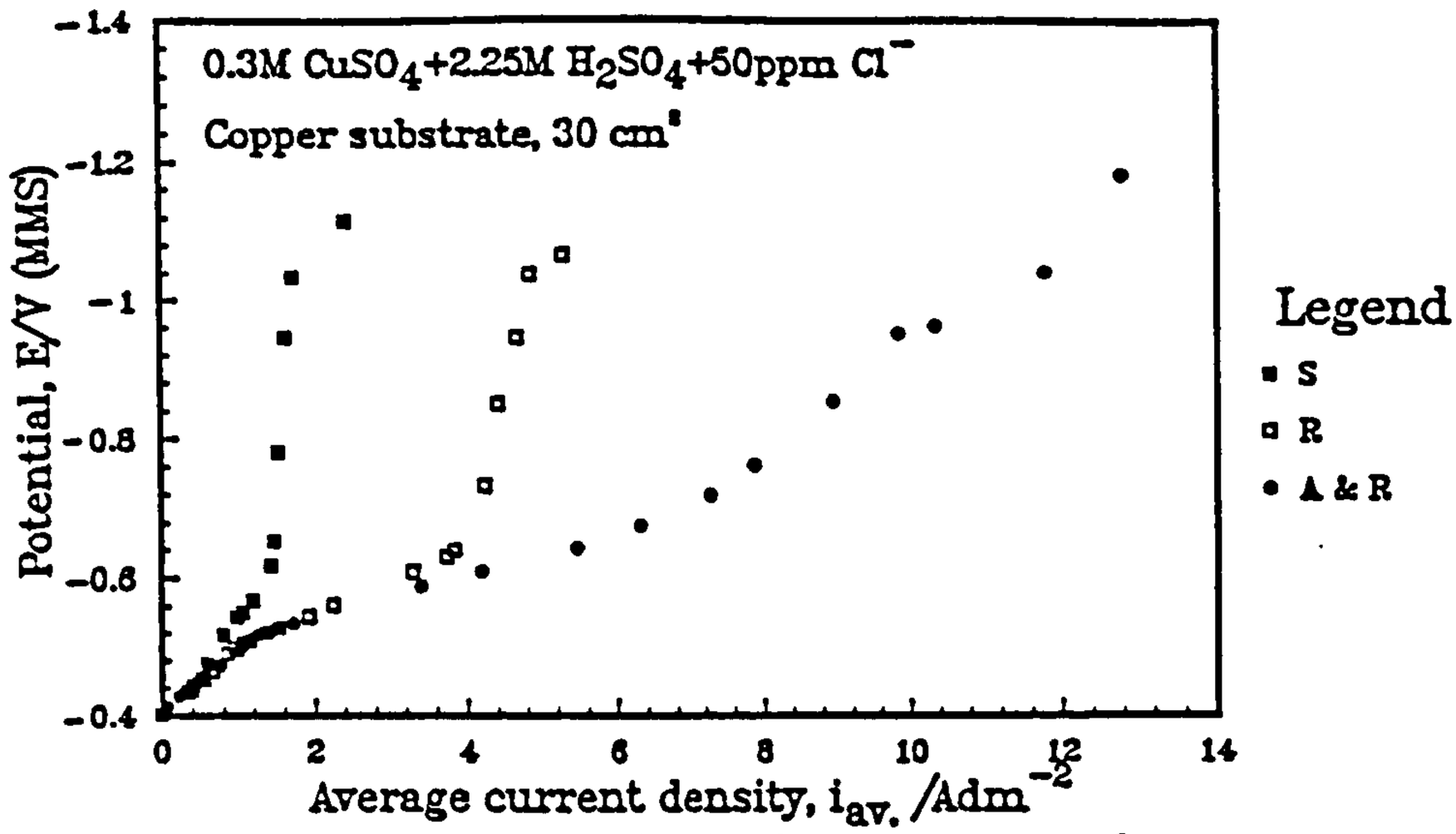

Figure 58a Polarisation curves obtained using a power supply - constant current for different agitation modes; S-Still, R-Reciprocating and A-Air, DVM data.

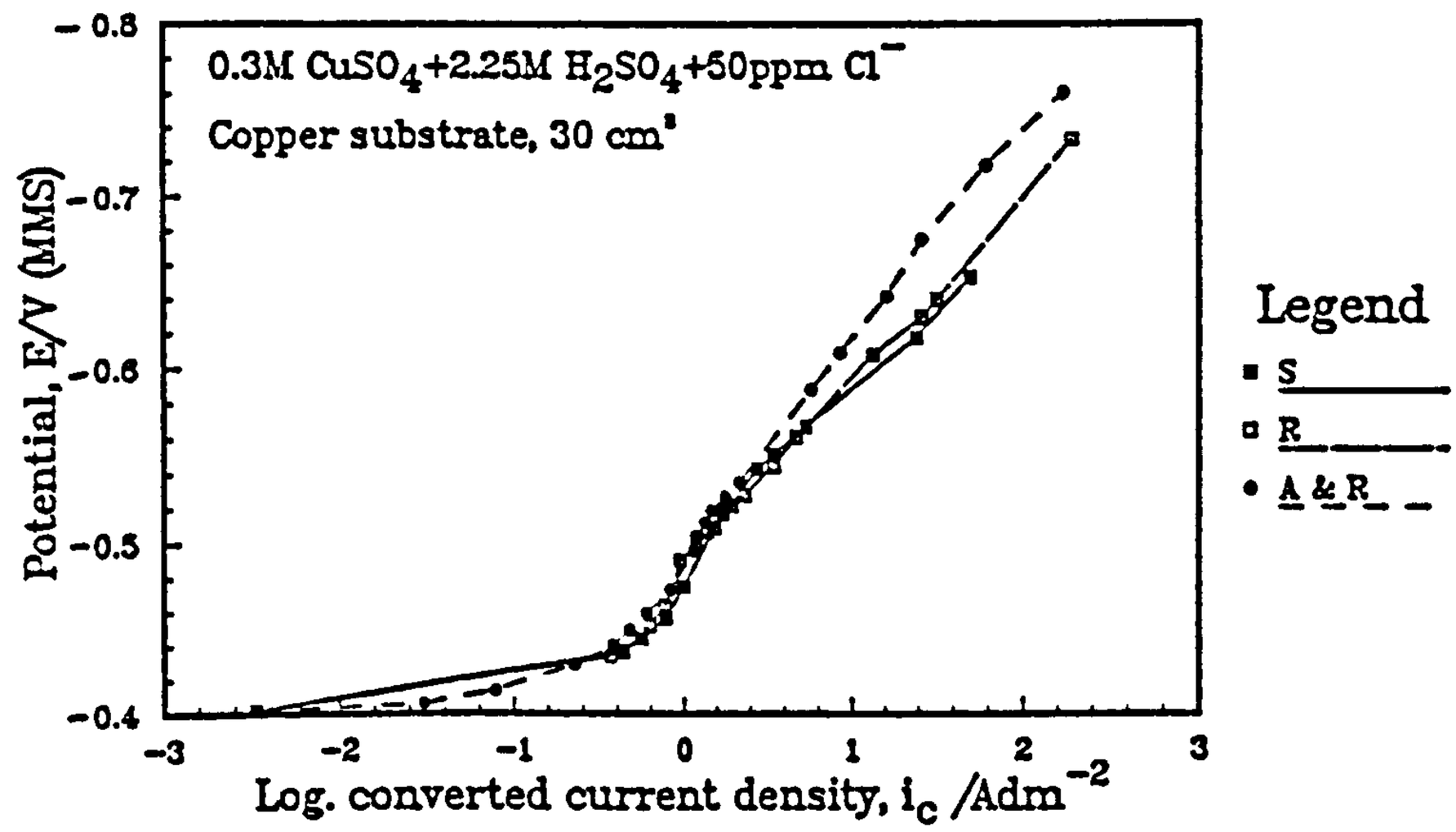

Figure 58b Relationship between potential and logarithmic converted current density, showing the Tafel region for different agitation modes; S-Still, R- Reciprocating and A-Air.

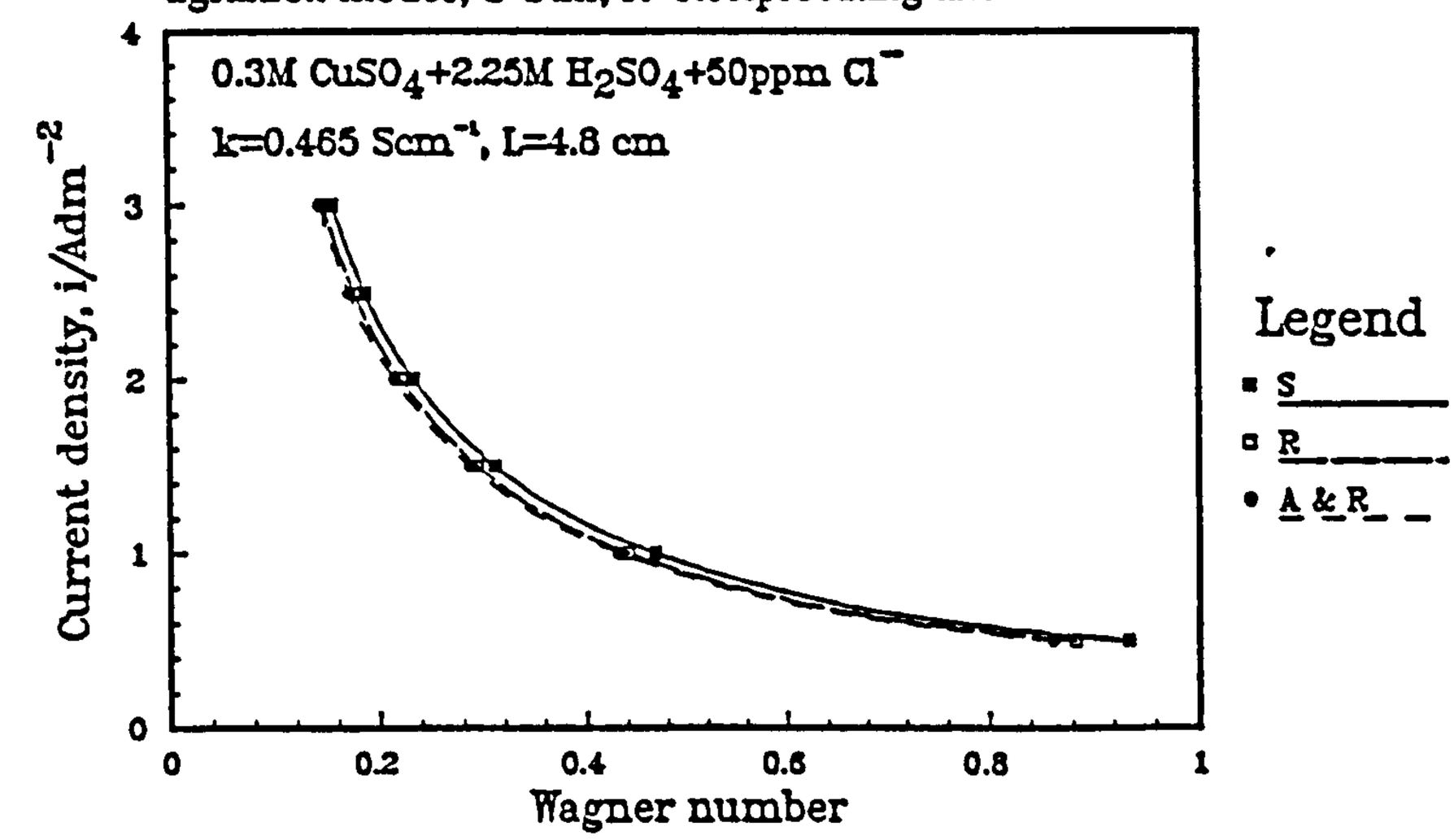

Figure 58c Relationship between current density and Wagner number for different agitation .modes; S-Still, R-Reciprocating and A-Air.

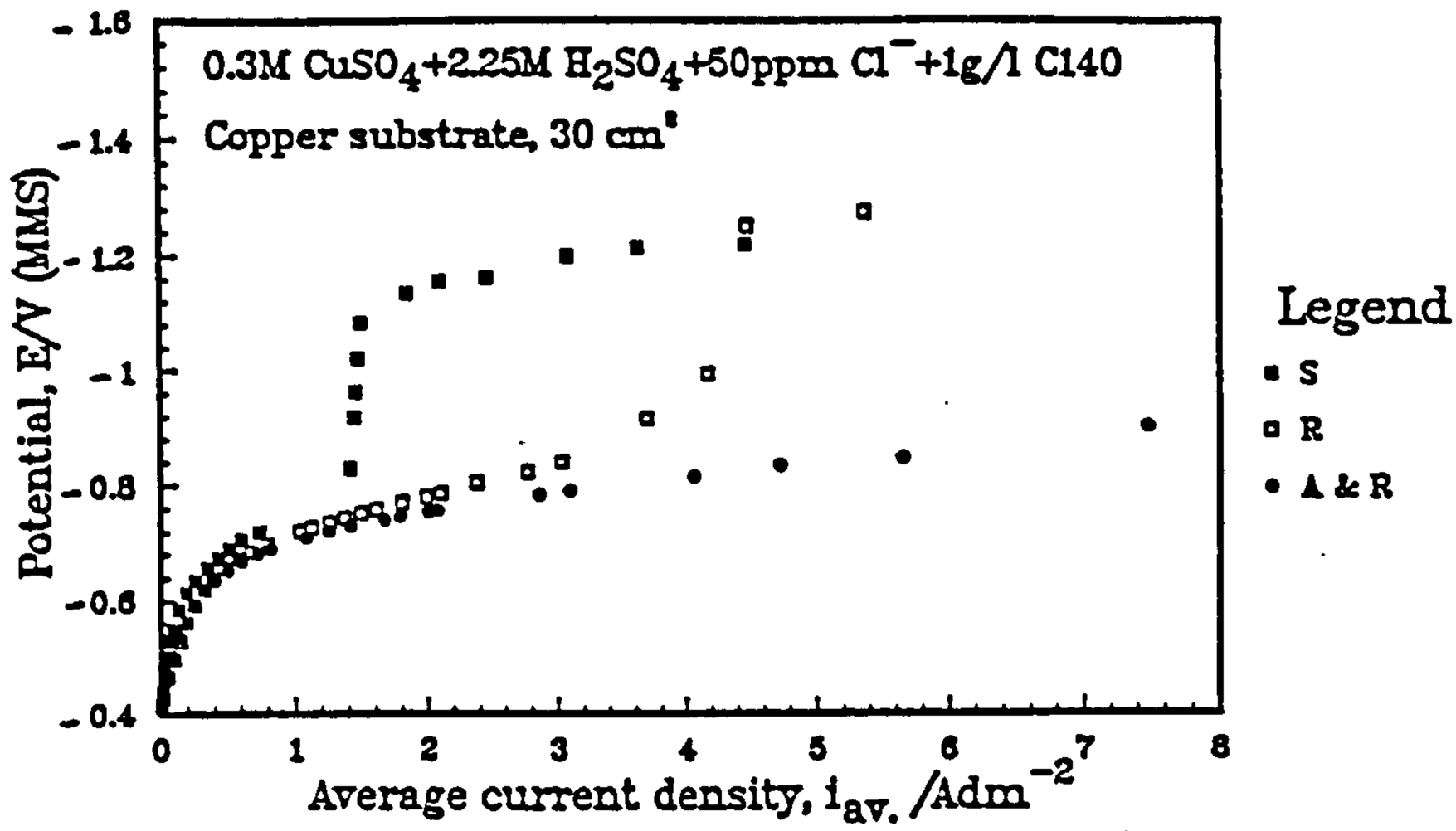

Figure 59a Polarisation curves obtained using a power supply - constant current for different agitation modes; S-Still, R-Reciprocating and A-Air, DVM data.

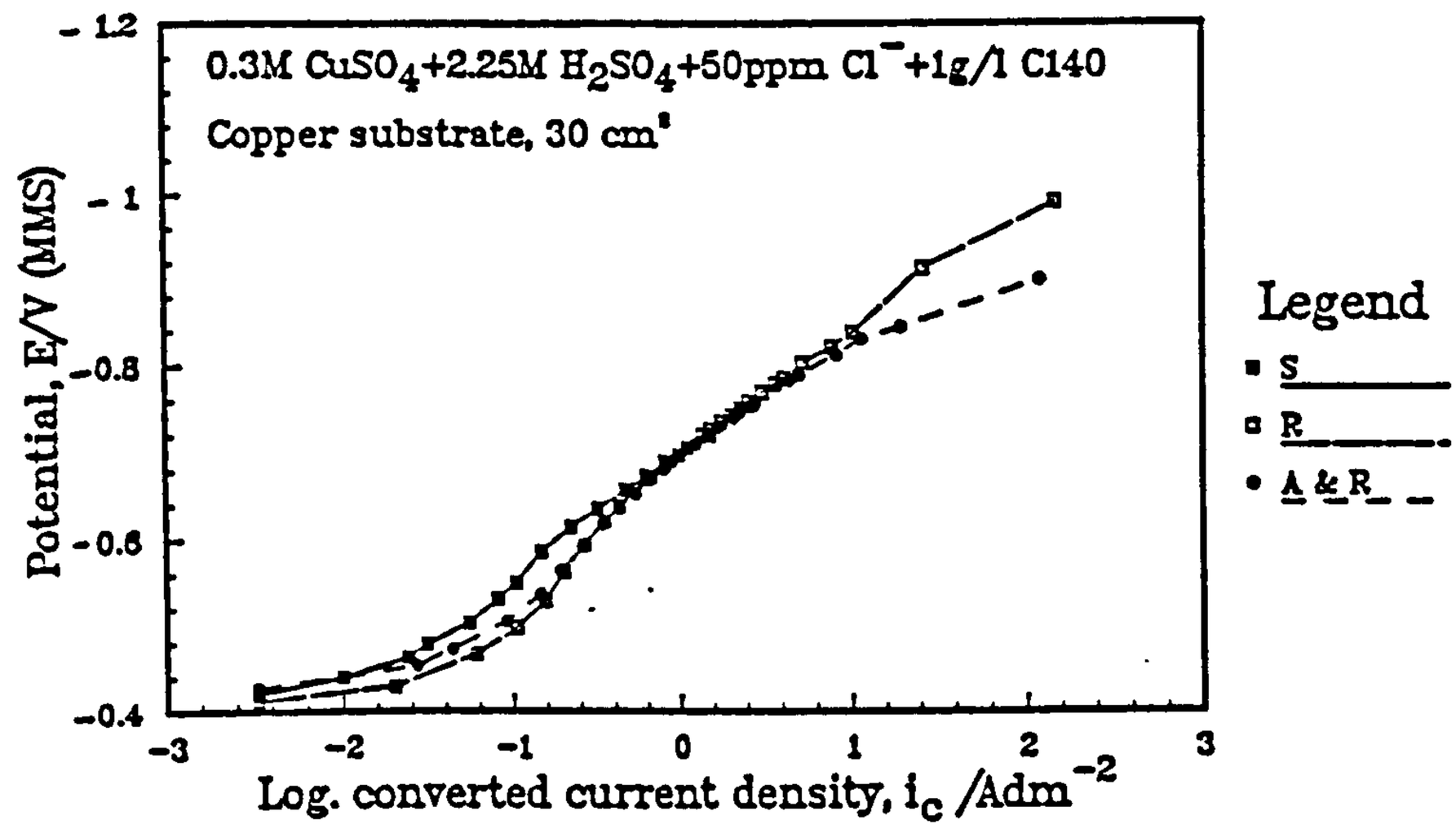

Figure 59b Relationship between potential and logarithmic converted current density, showing the Tafel region for different agitation modes; S-Still, R- Reciprocating and A-Air.

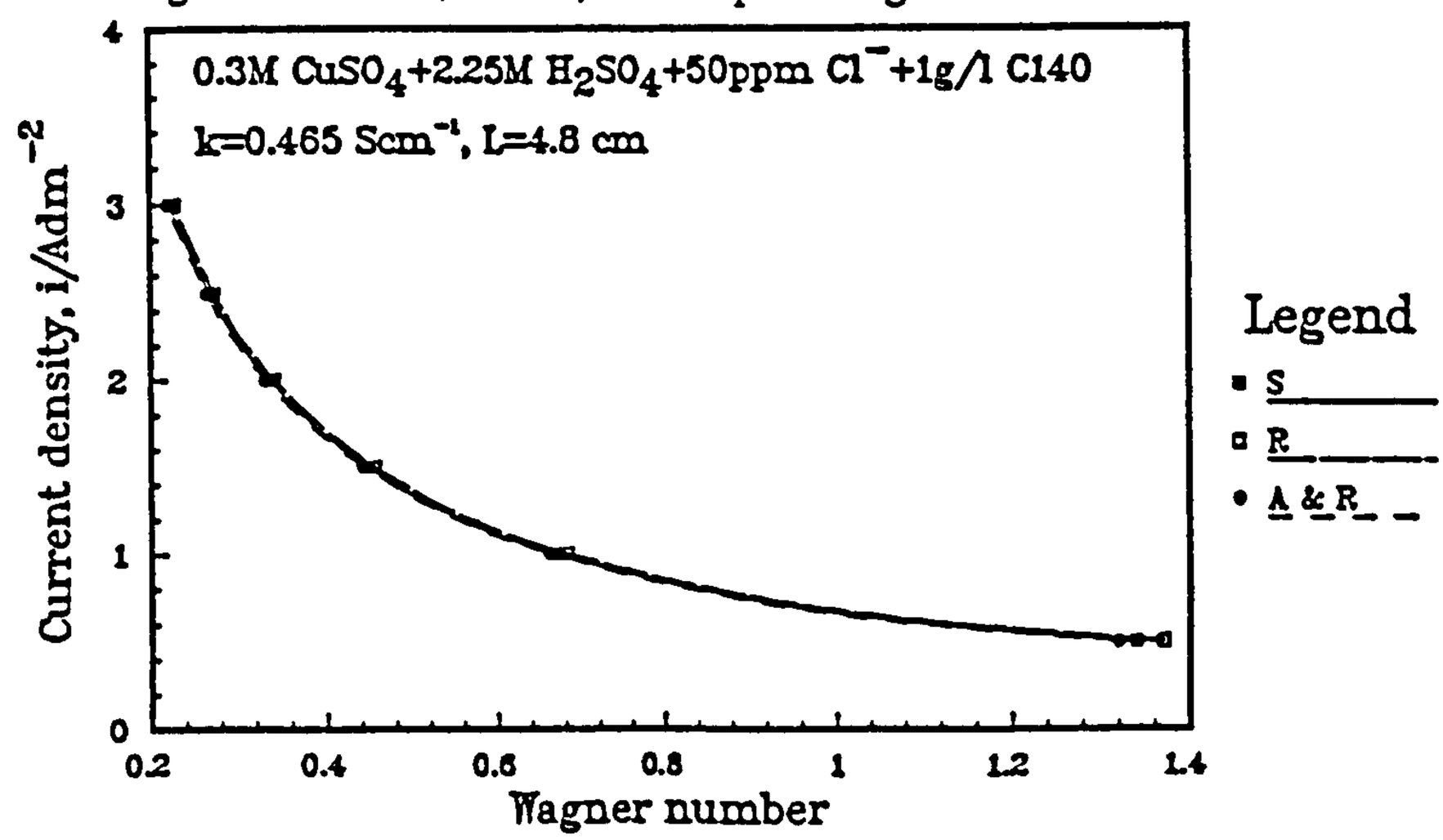

Figure 59c Relationship between current density and Wagner number for different agitation modes; S-Still, R-Reciprocating and A-Air.

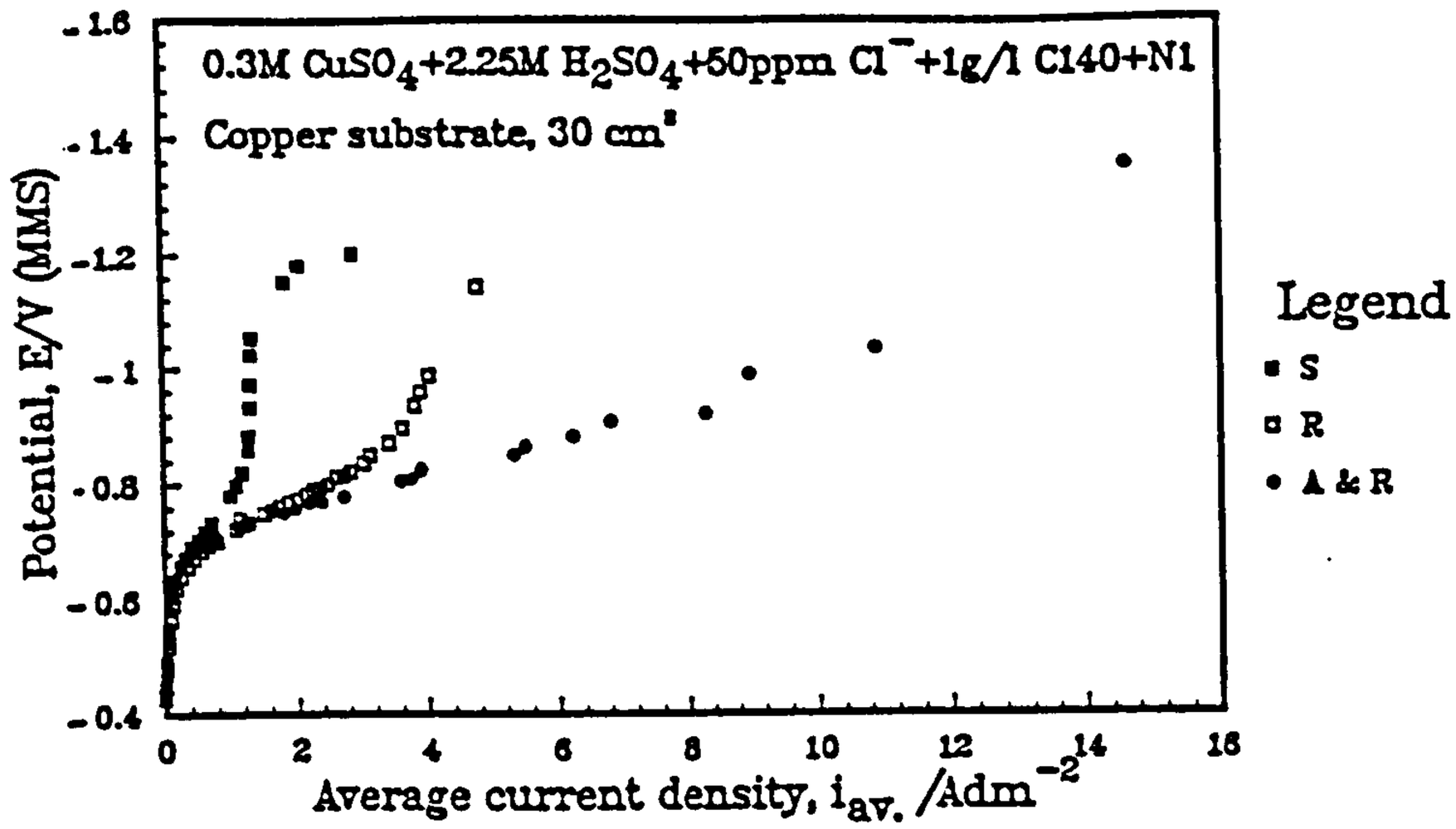

Figure 60a Polarisation curves obtained using a power supply - constant current for different agitation modes; S-Still, R-Reciprocating and A-Air, DVM data.

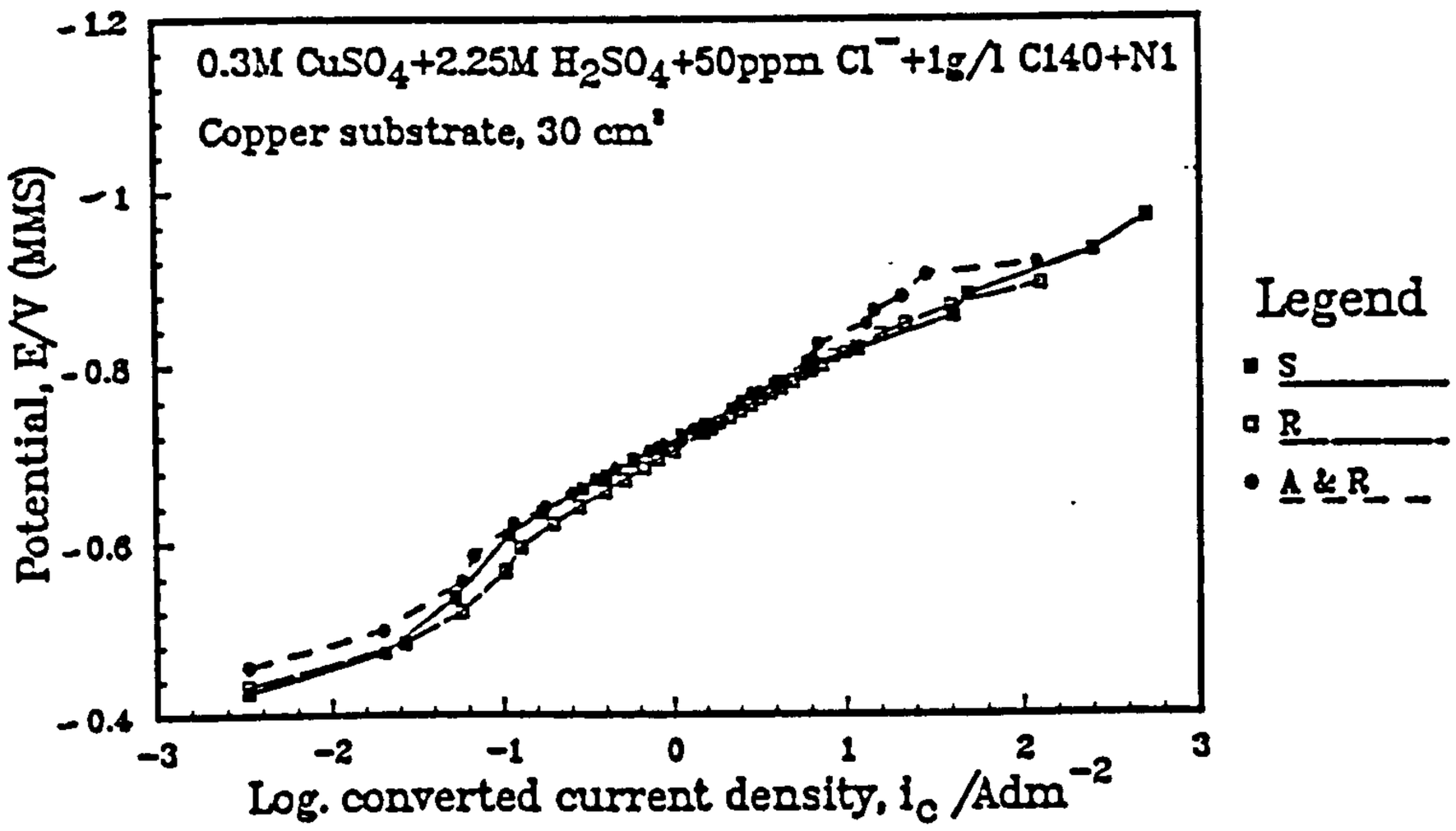

Figure 60b Relationship between potential and logarithmic converted current density, showing the Tafel region for different agitation modes; S-Still, R- Reciprocating and A-Air.

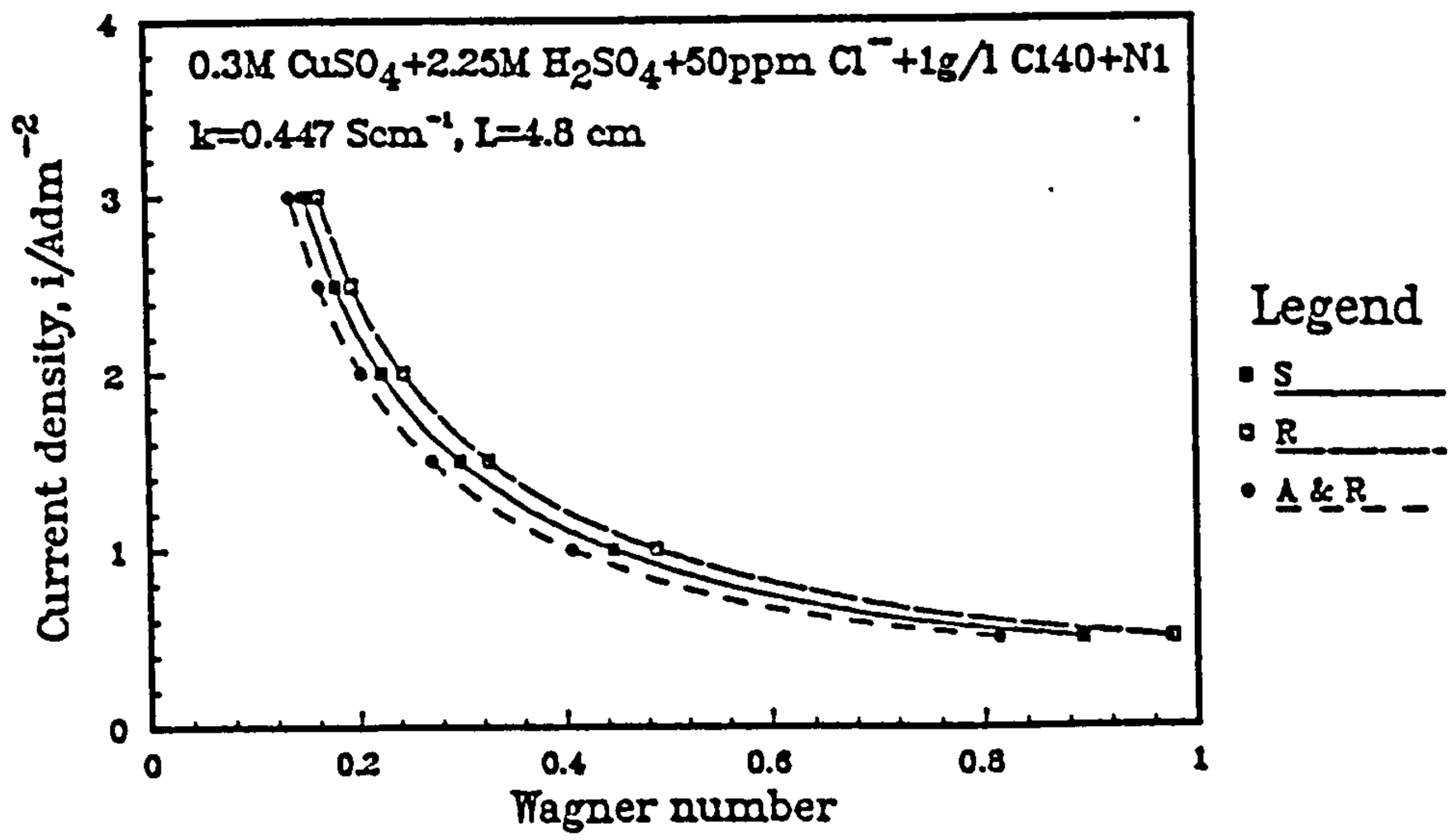

Figure 60c Relationship between current density and Wagner number for different agitation modes; S-Still, R-Reciprocating and A-Air.

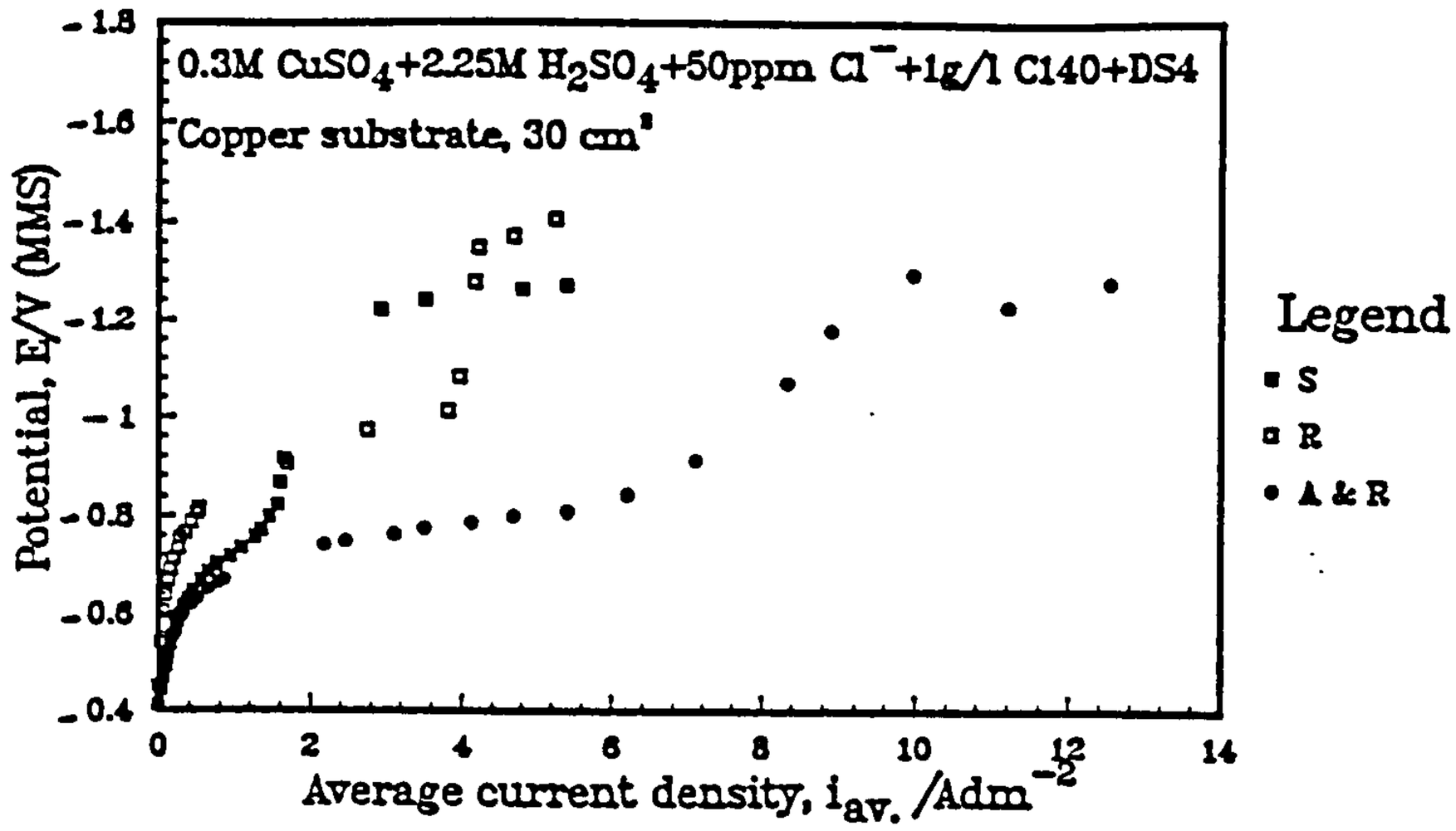

Figure 61a Polarisation curves obtained using a power supply - constant current for different agitation modes; S-Still, R-Reciprocating and A-Air, DVM data.

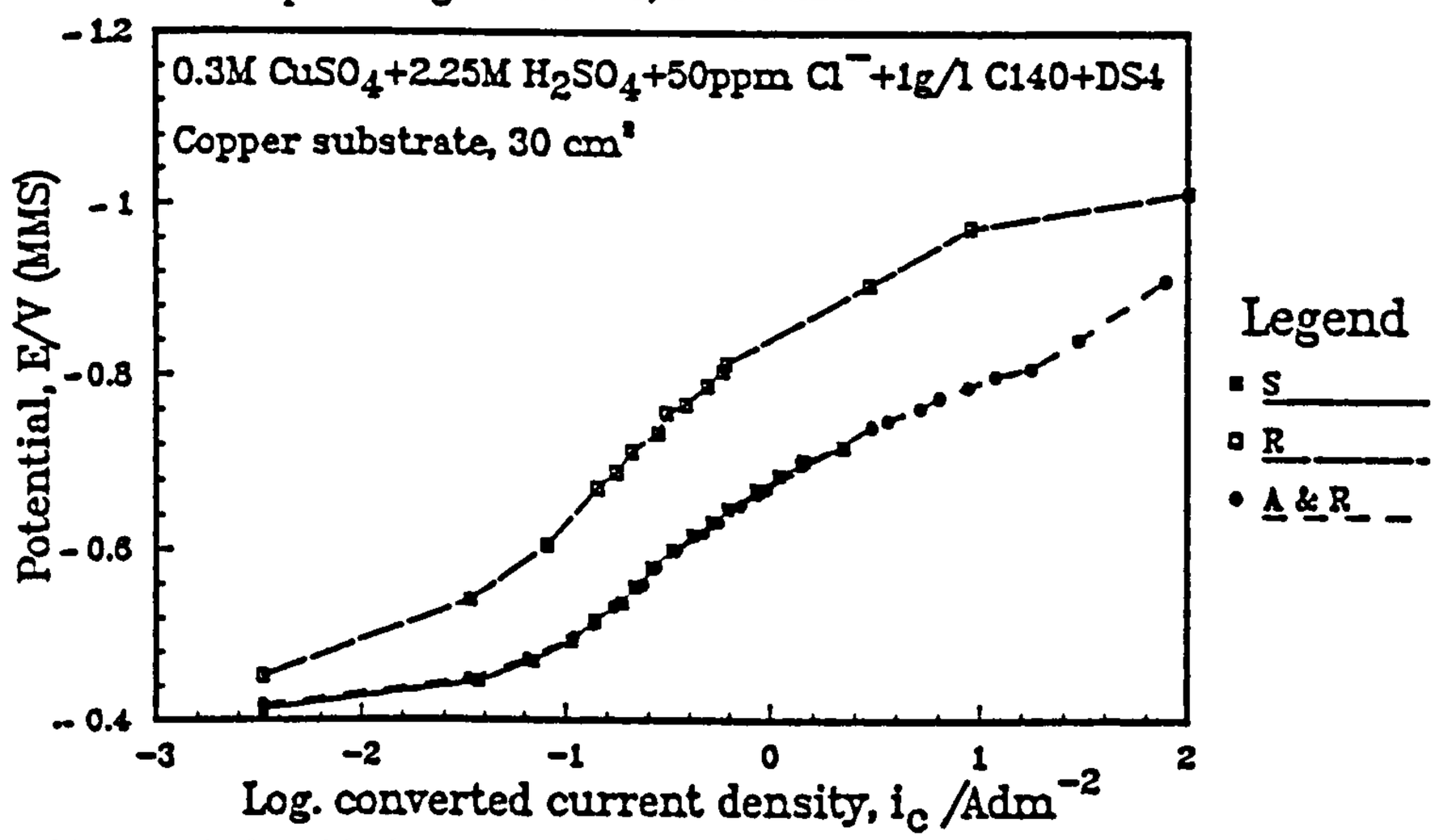

Figure 61b Relationship between potential and logarithmic converted current density, showing the Tafel region for different agitation modes; S-Still, R- Reciprocating and A-Air.

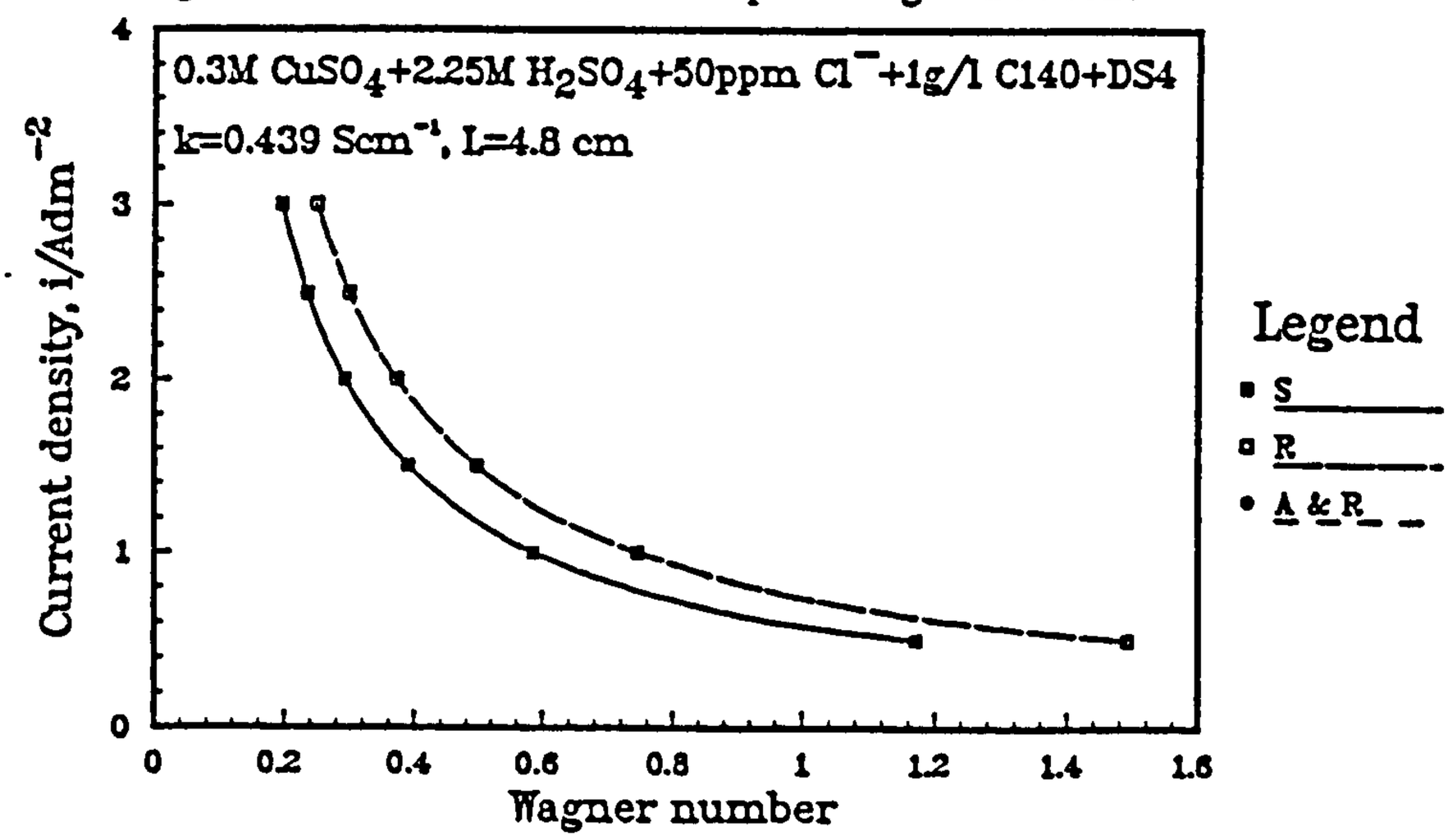

Figure 61c Relationship between current density and Wagner number for different agitation modes; S-Still, R-Reciprocating and A-Air.

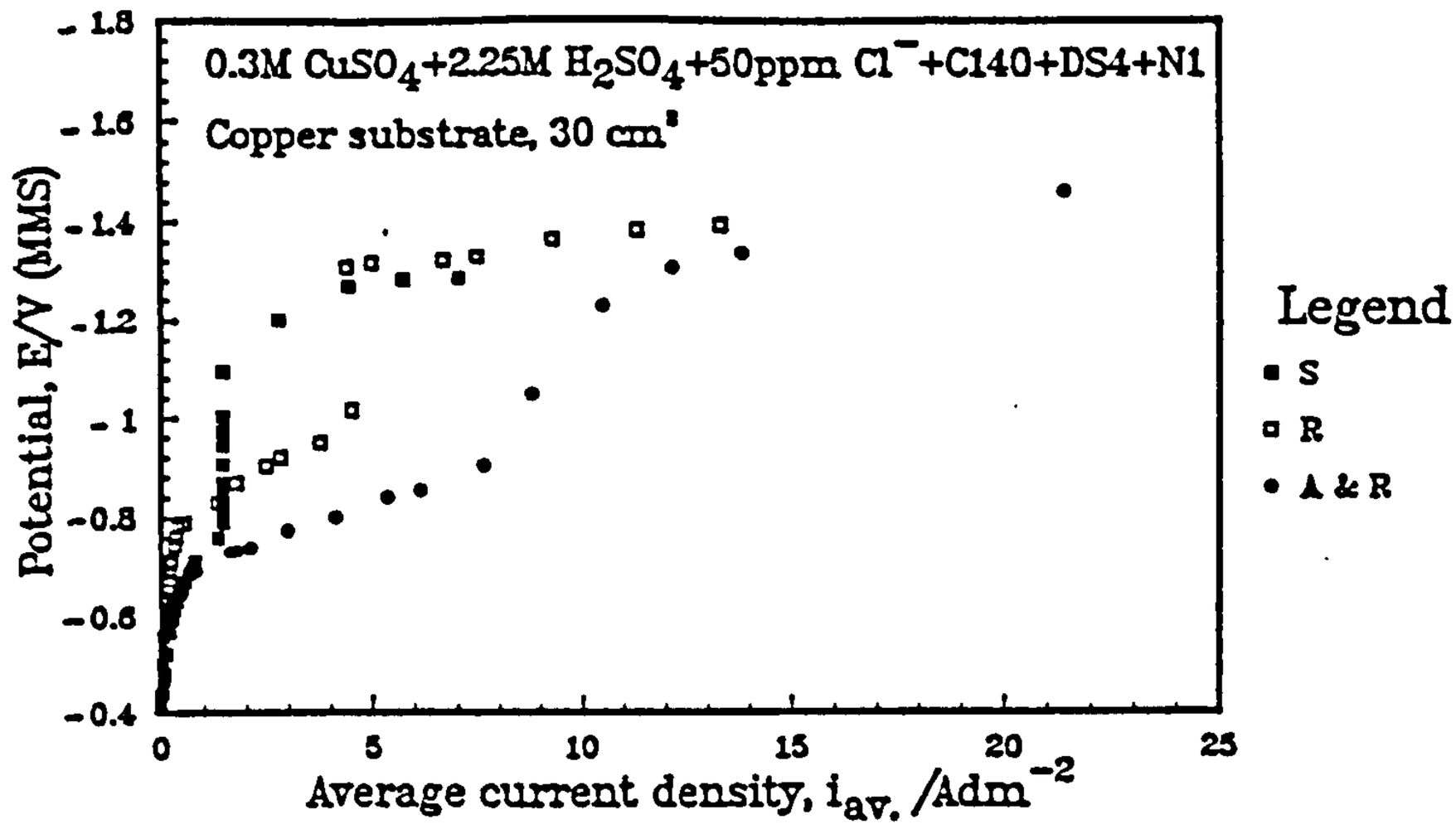

Figure 62a Polarisation curves obtained using a power supply - constant current for different agitation modes; S-Still, R-Reciprocating and A-Air, DVM data.

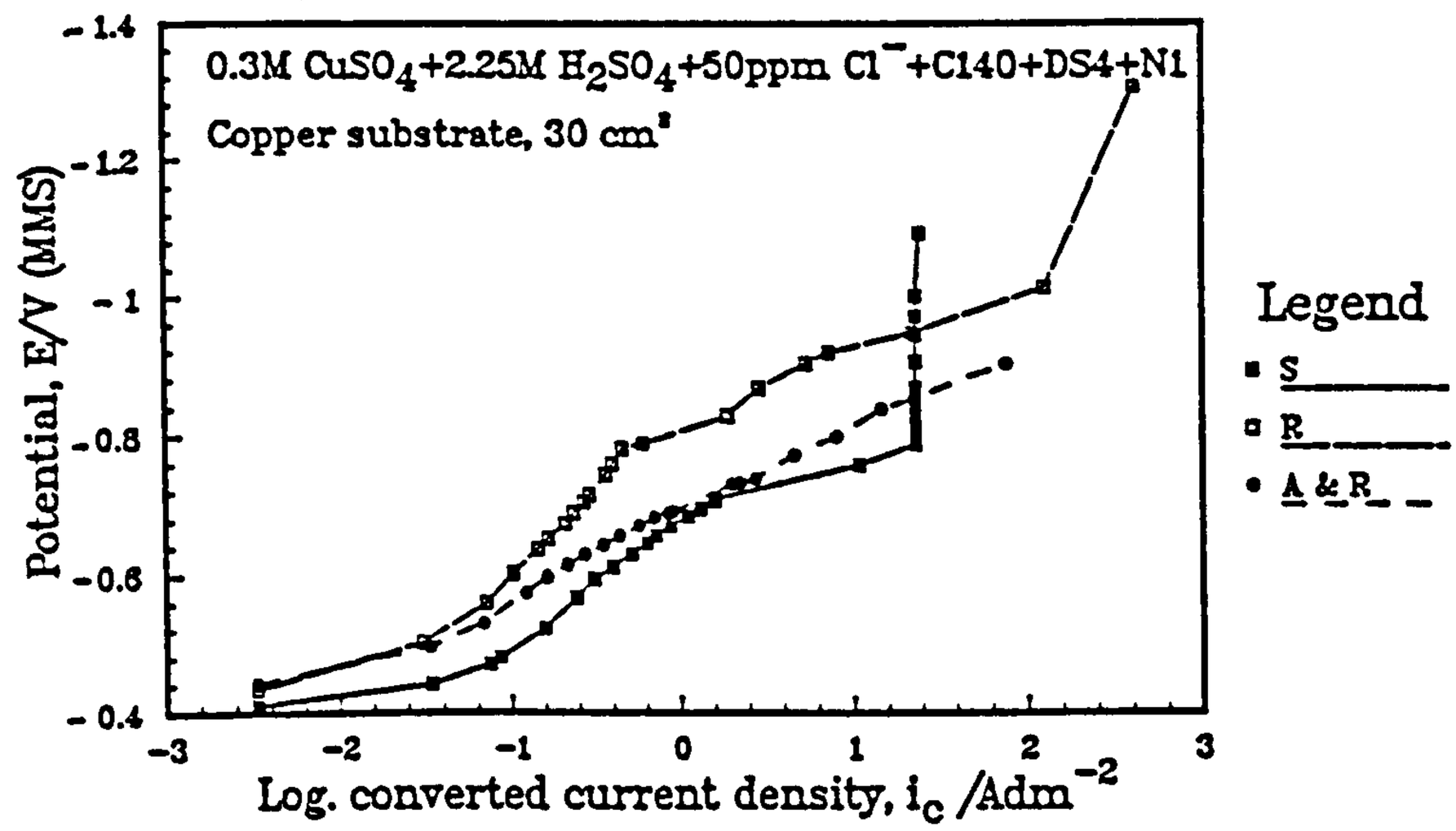

Figure 62b Relationship between potential and logarithmic converted current density, showing the Tafel region for different agitation modes; S-Still, R- Reciprocating and A-Air.

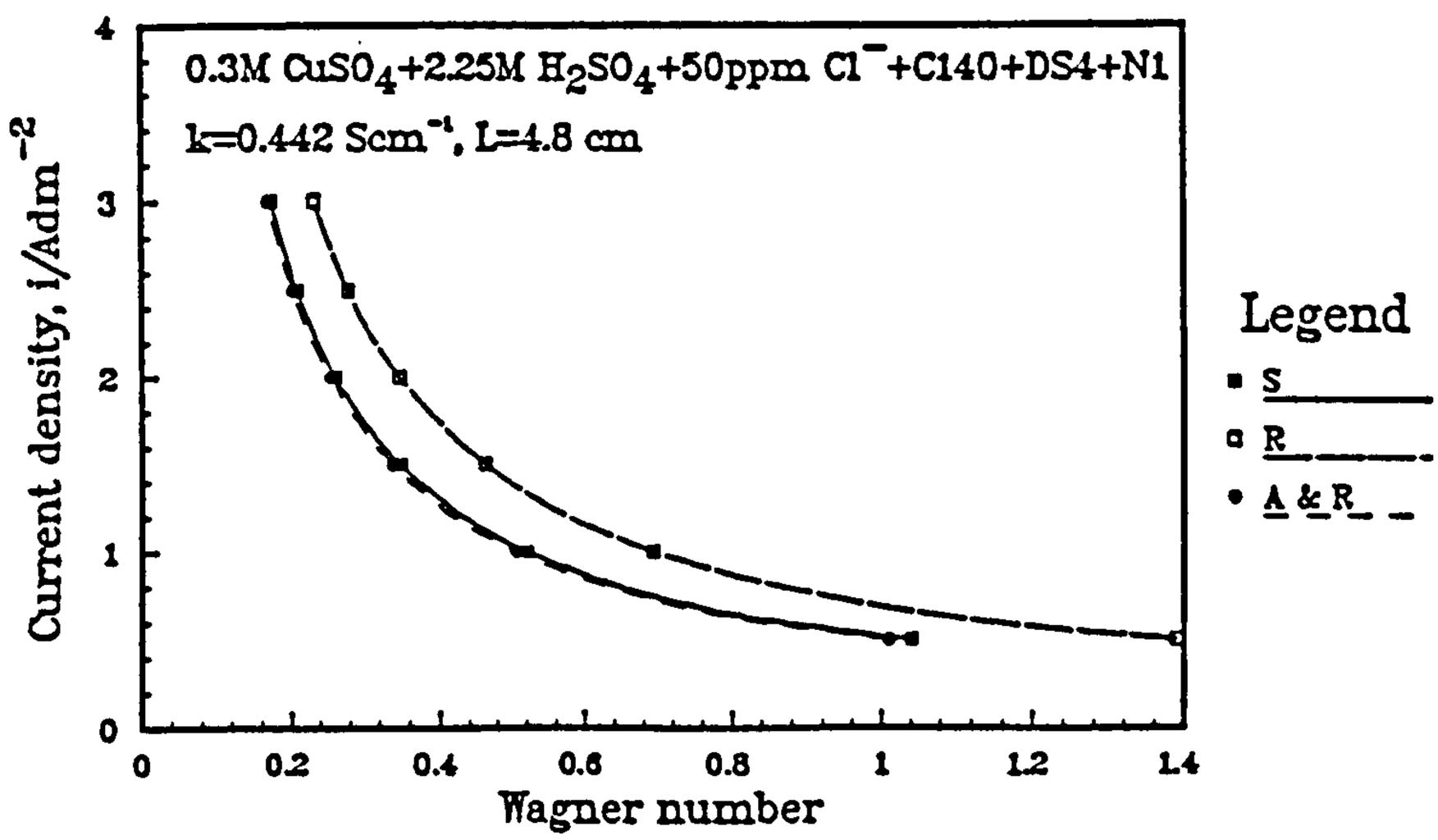

Figure 62c Relationship between current density and Wagner number for different agitation modes; S-Still, R-Reciprocating and A-Air.

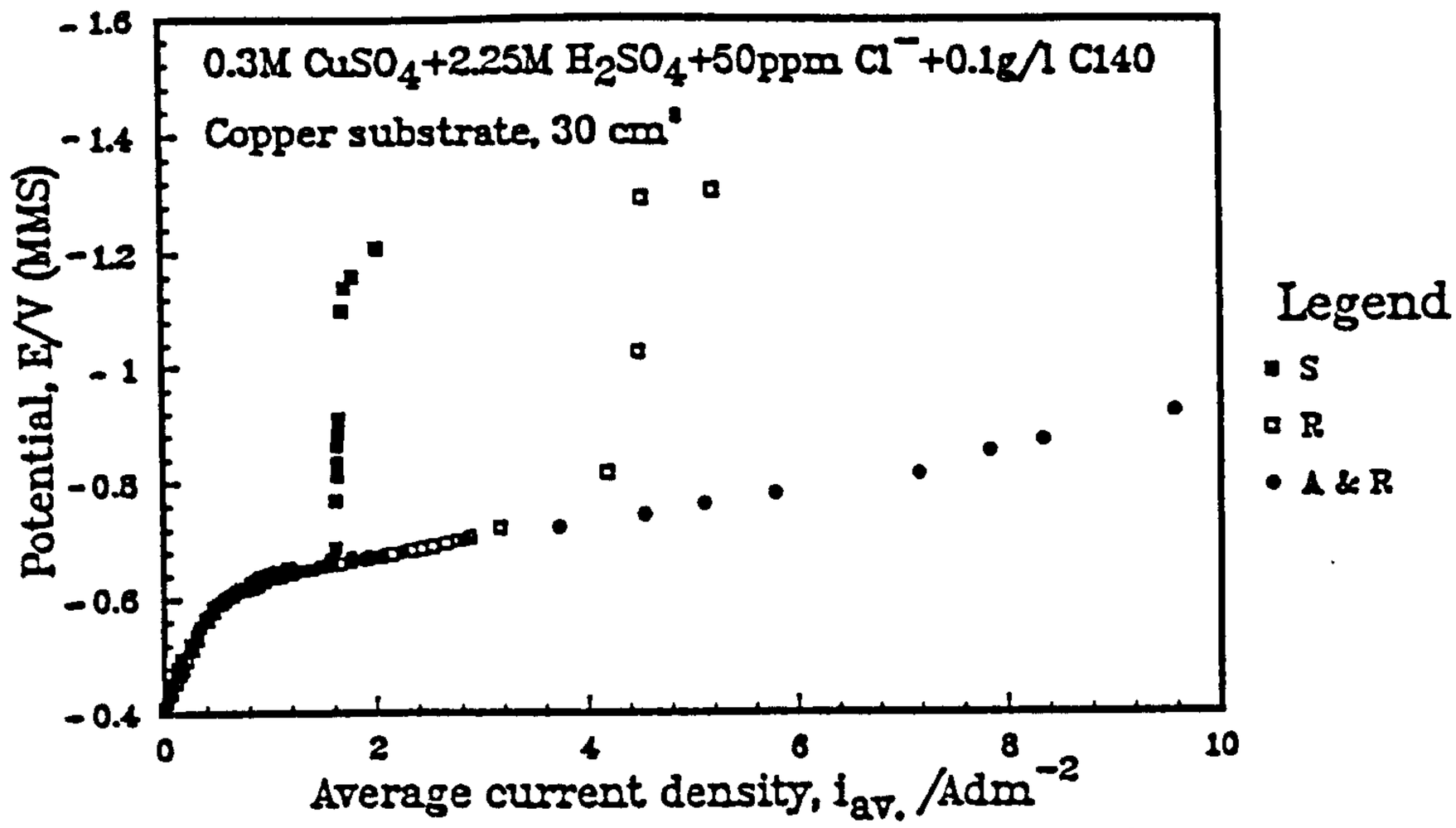

Figure 63a Polarisation curves obtained using a power supply - constant current for different agitation modes; S-Still, R-Reciprocating and A-Air, DVM data.

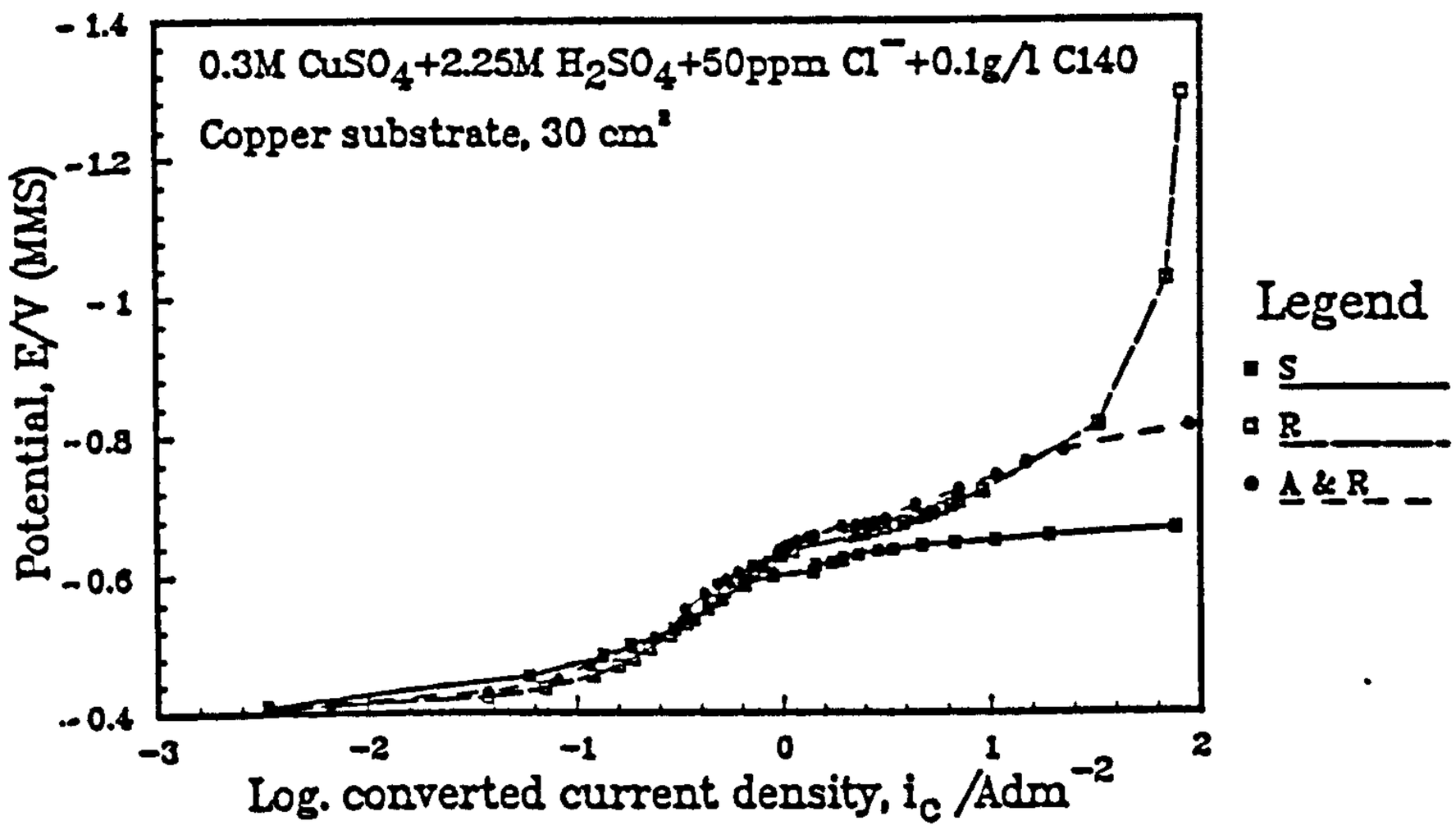

Figure 63b Relationship between potential and logarithmic converted current density, showing the Tafel region for different agitation modes; S-Still, R- Reciprocating and A-Air.

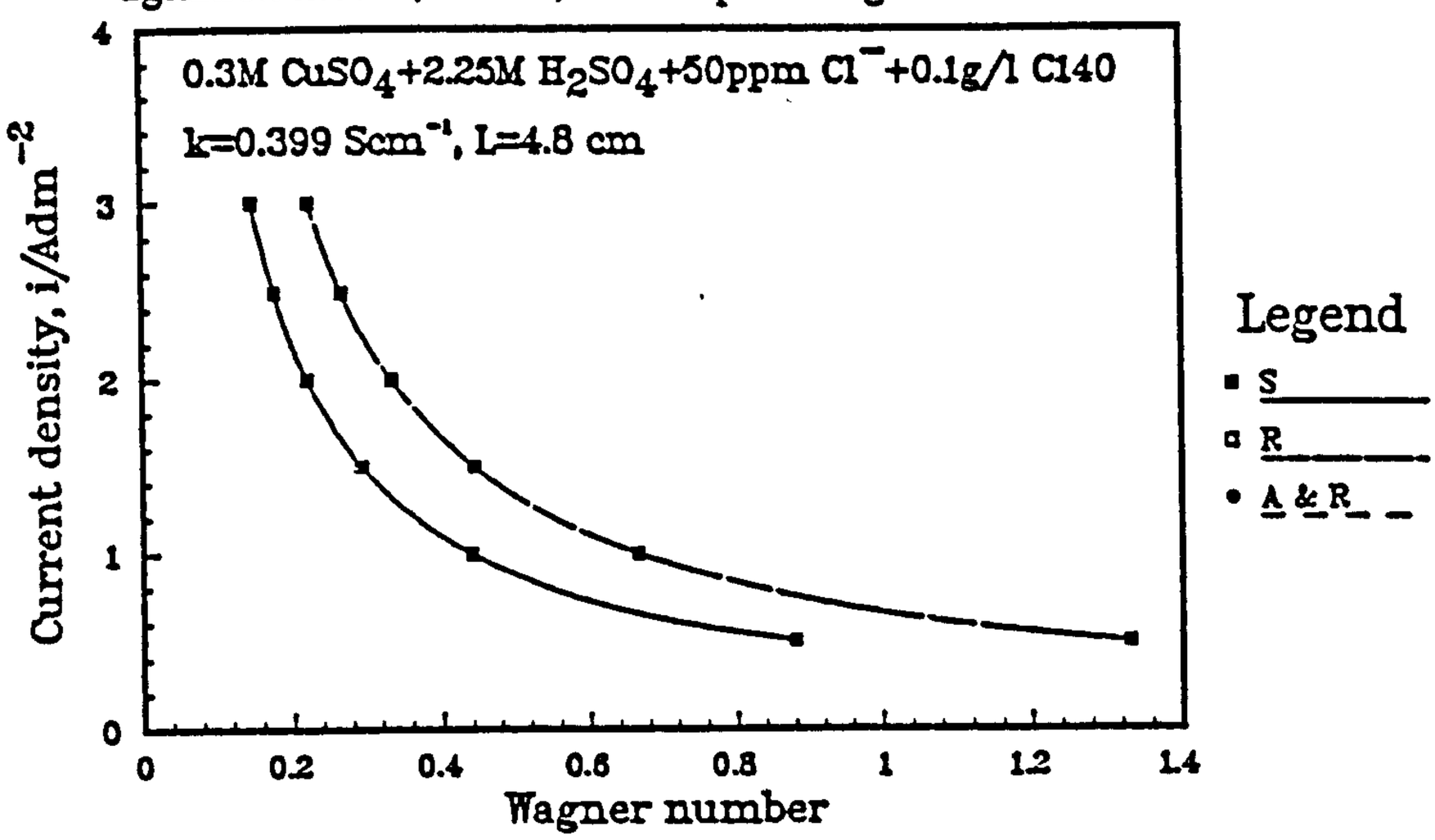

Figure 63c Relationship between current density and Wagner number for different agitation modes; S-Still, R-Reciprocating and A-Air.

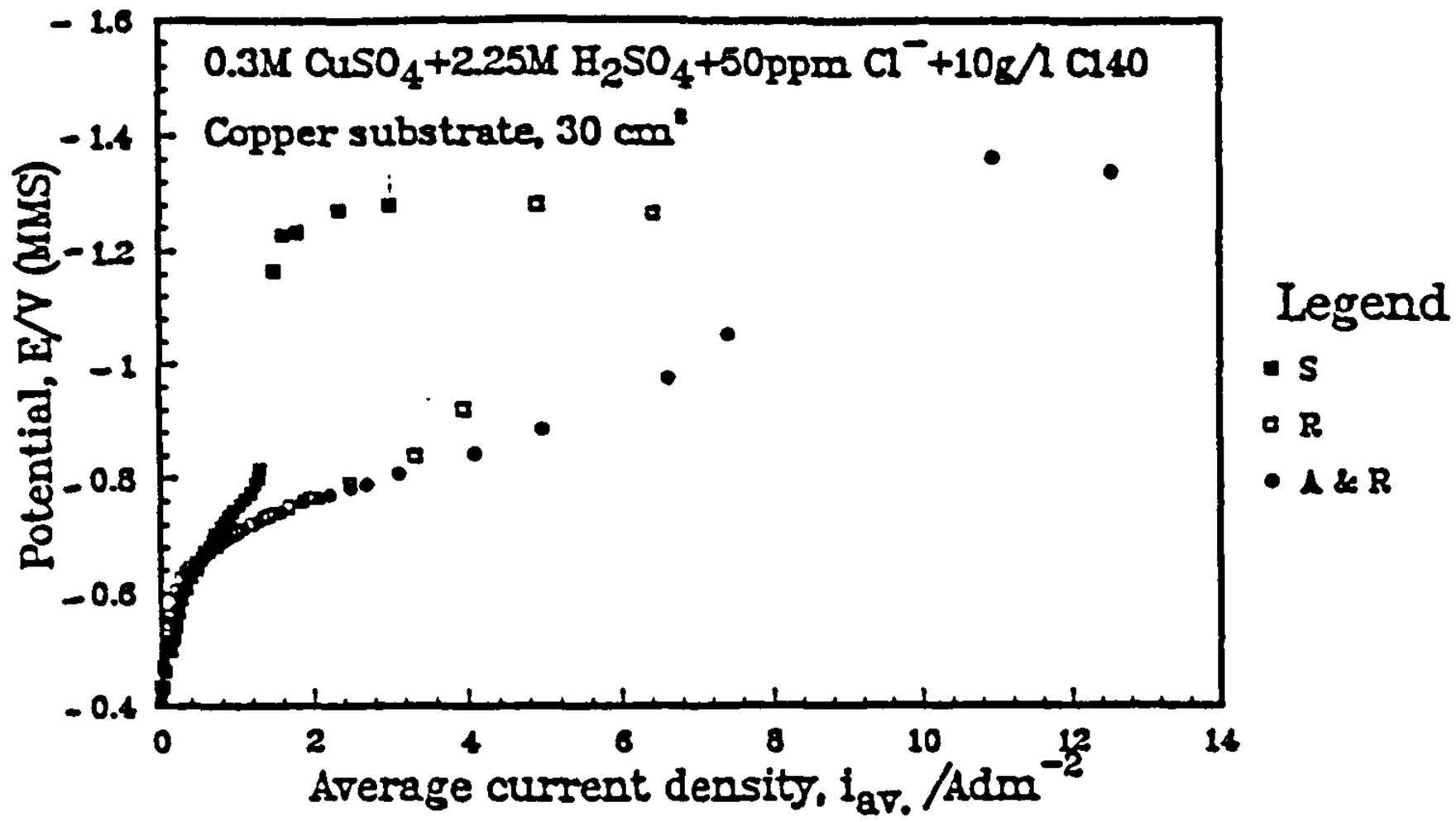

Figure 64a Polarisation curves obtained using a power supply - constant current for different agitation modes; S-Still, R-Reciprocating and A-Air, DVM data.

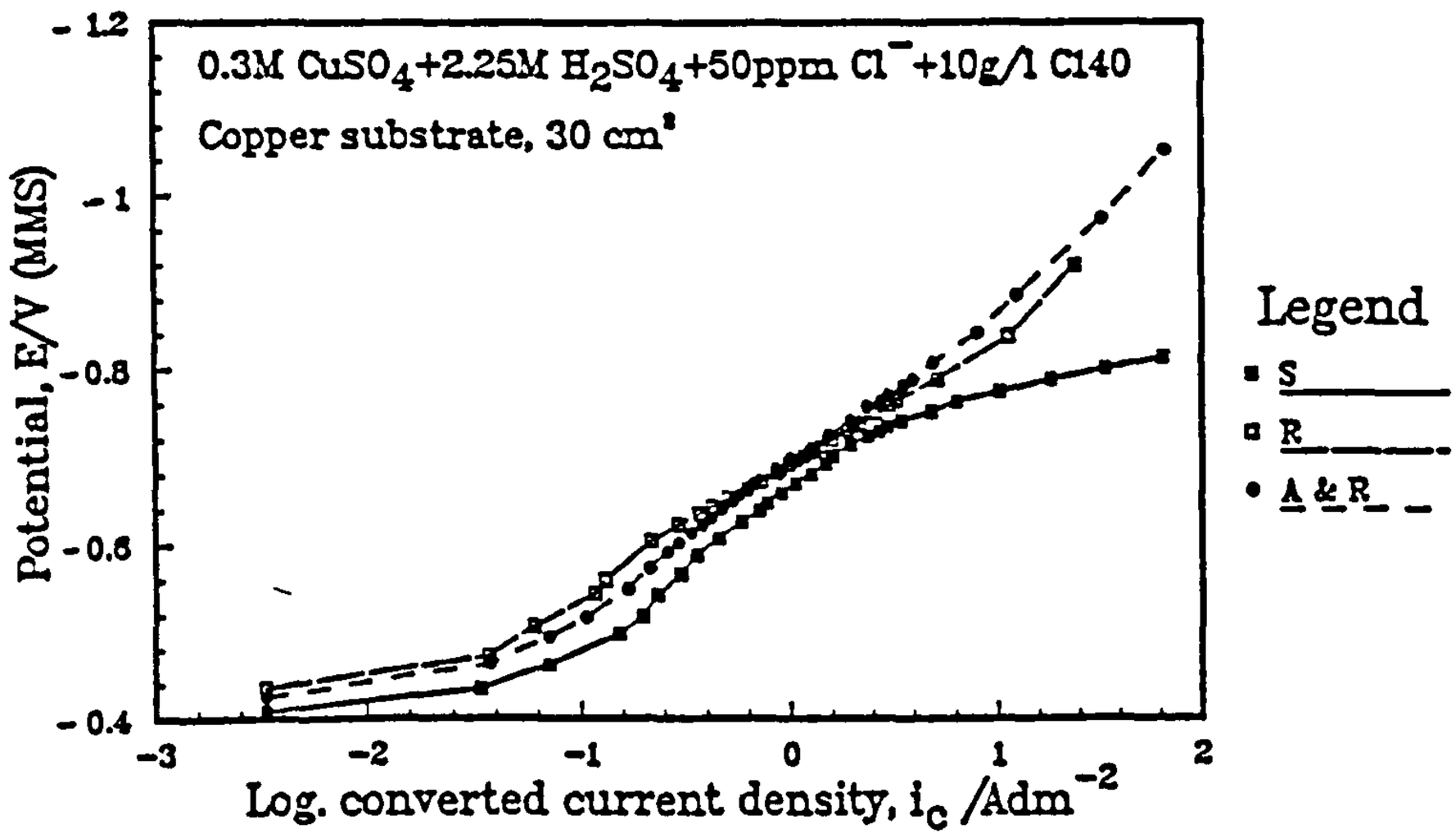

Figure 64b Relationship between potential and logarithmic converted current density, showing the Tafel region for different agitation modes; S-Still, R- Reciprocating and A-Air.

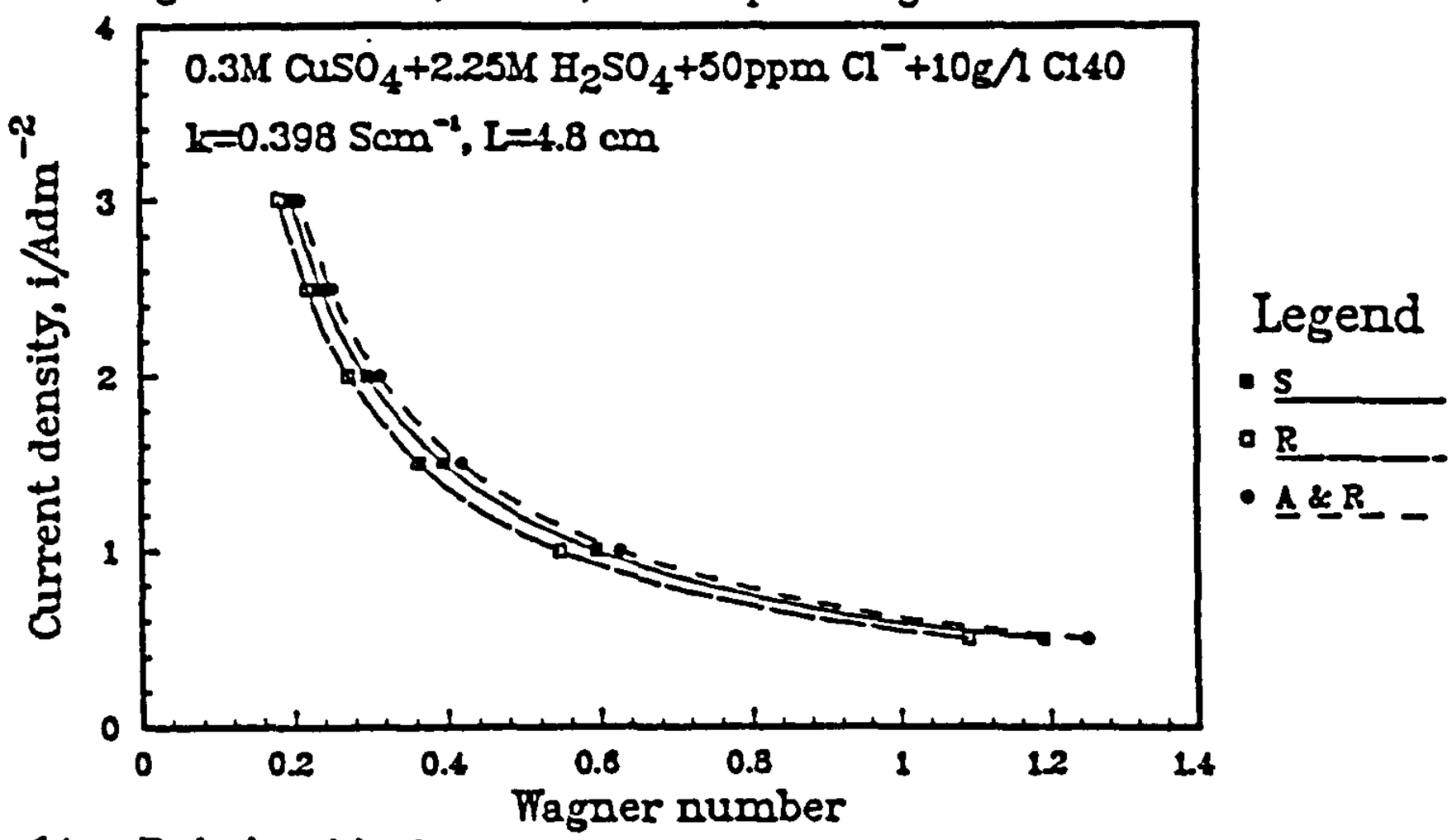

Figure 64c Relationship between current density and Wagner number for different agitation modes; S-Still, R-Reciprocating and A-Air.

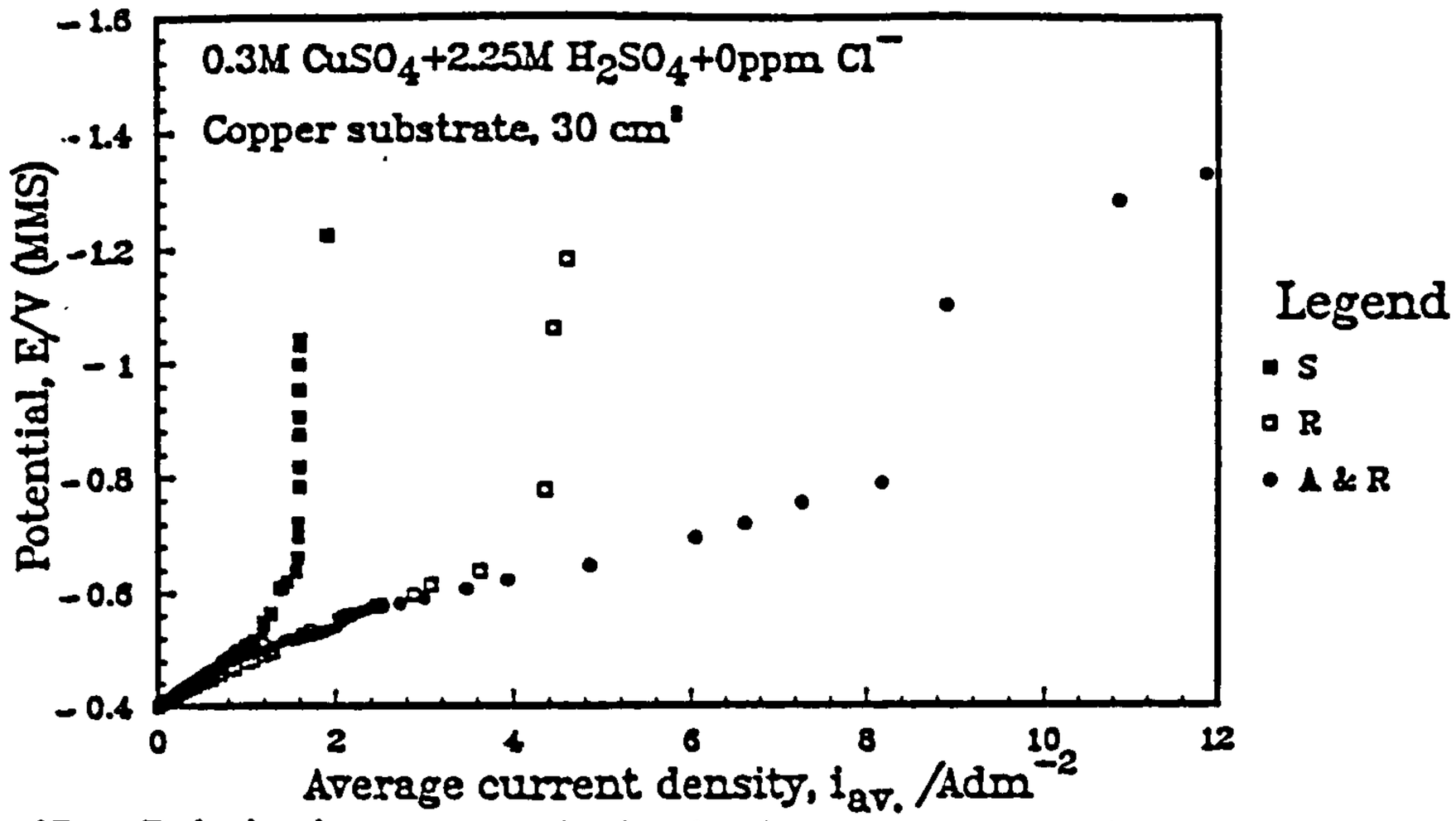

Figure 65a Polarisation curves obtained using a power supply - constant current for different agitation modes; S-Still, R-Reciprocating and A-Air, DVM data.

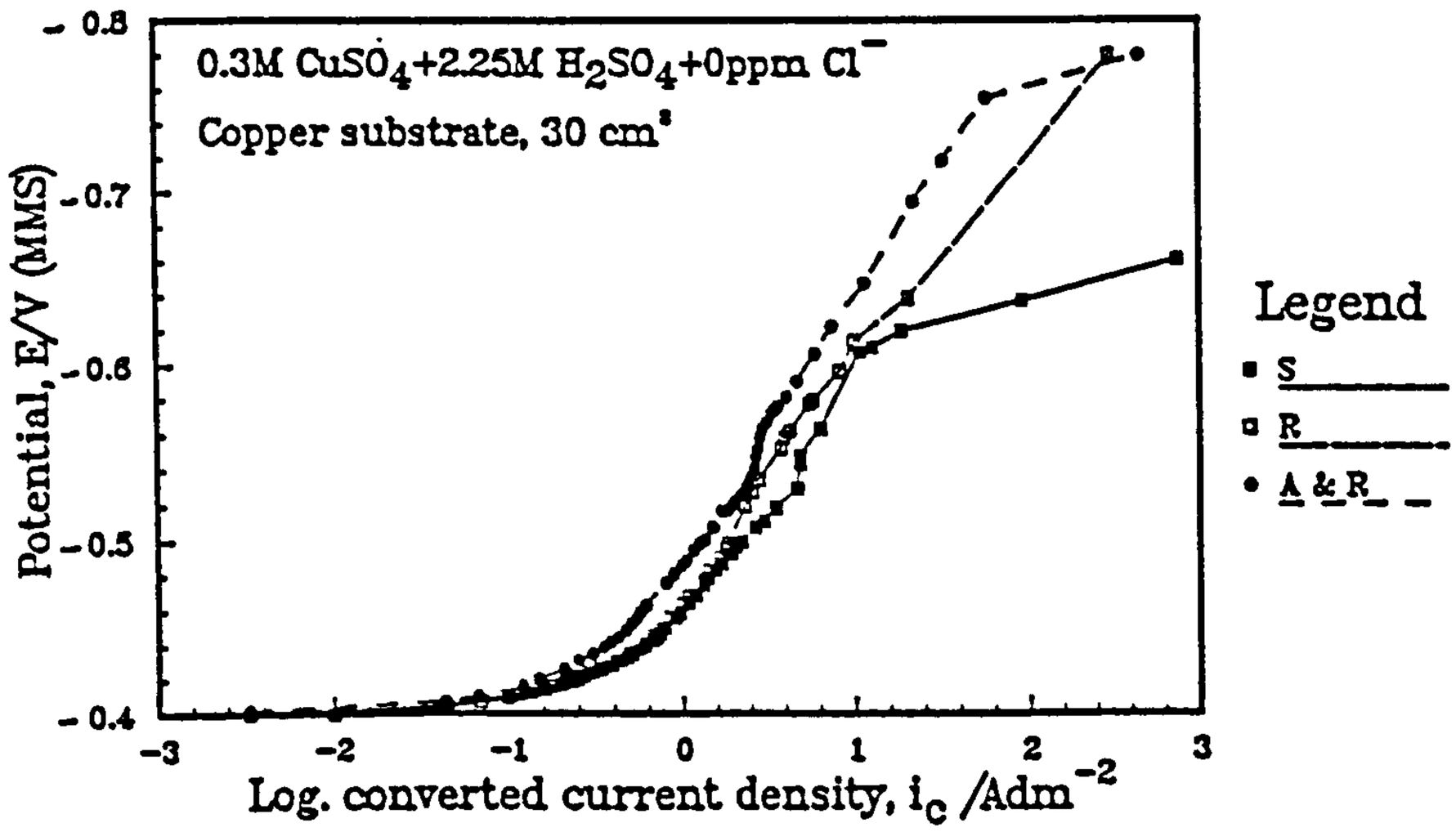

Figure 65b Relationship between potential and logarithmic converted current density, showing the Tafel region for different agitation modes; S-Still, R- Reciprocating and A-Air.

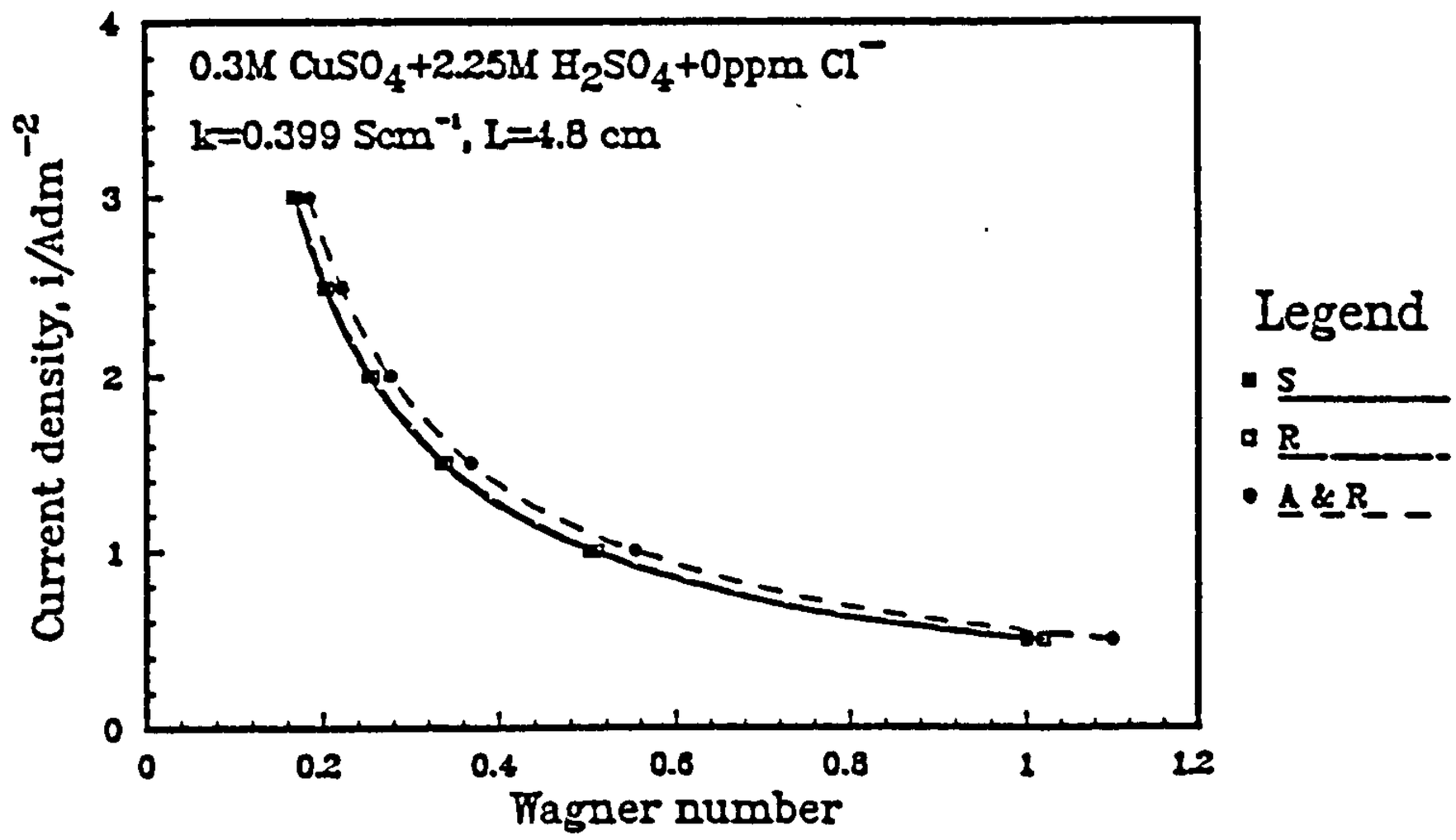

Figure 65c Relationship between current density and Wagner number for different agitation modes; S-Still, R-Reciprocating and A-Air.

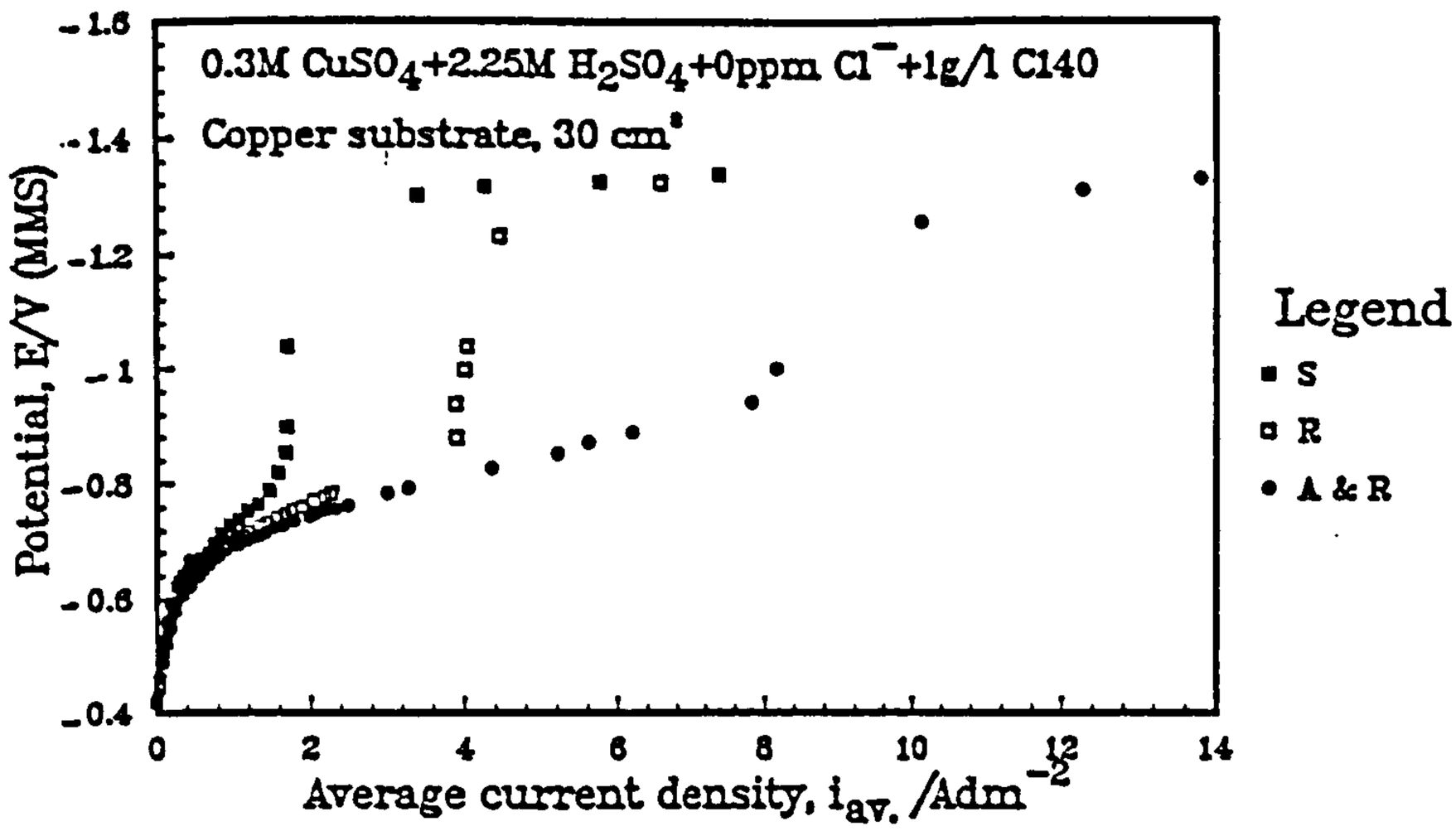

Figure 66a Polarisation curves obtained using a power supply - constant current for different agitation modes; S-Still, R-Reciprocating and A-Air, DVM data.

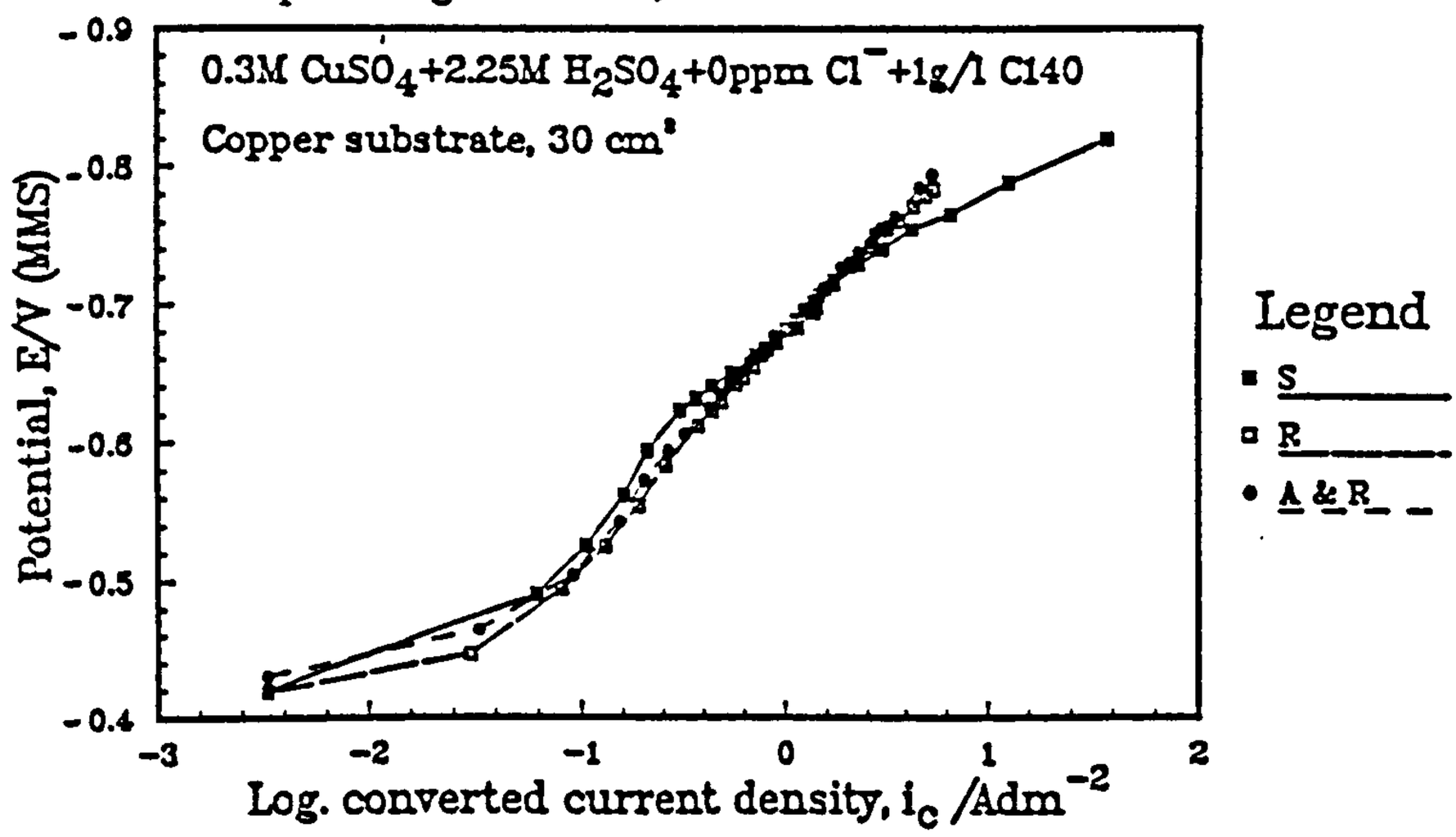

Figure 66b Relationship between potential and logarithmic converted current density, showing the Tafel region for different agitation modes; S-Still, R- Reciprocating and A-Air.

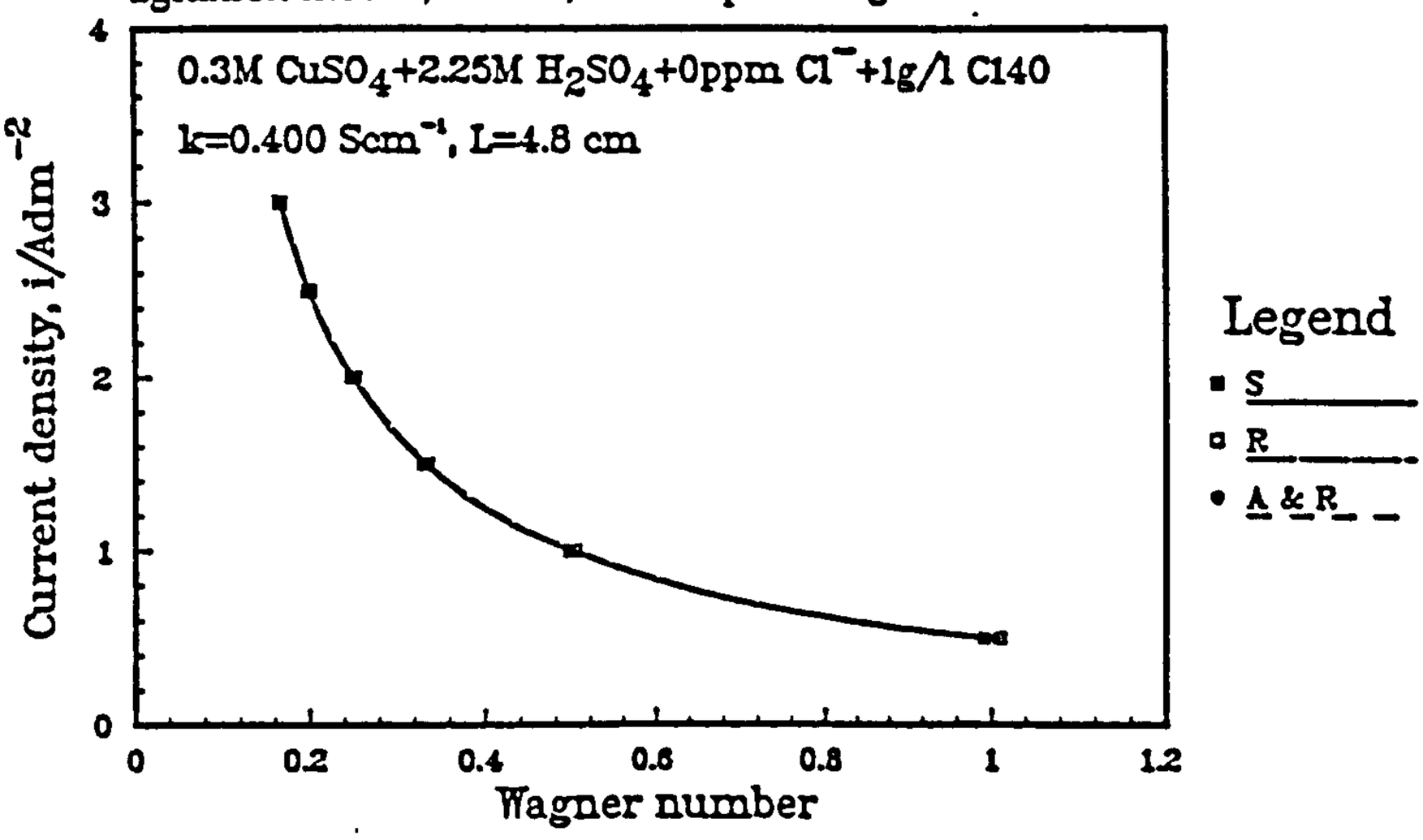

Figure 66c Relationship between current density and Wagner number for different agitation modes; S-Still, R-Reciprocating and A-Air.

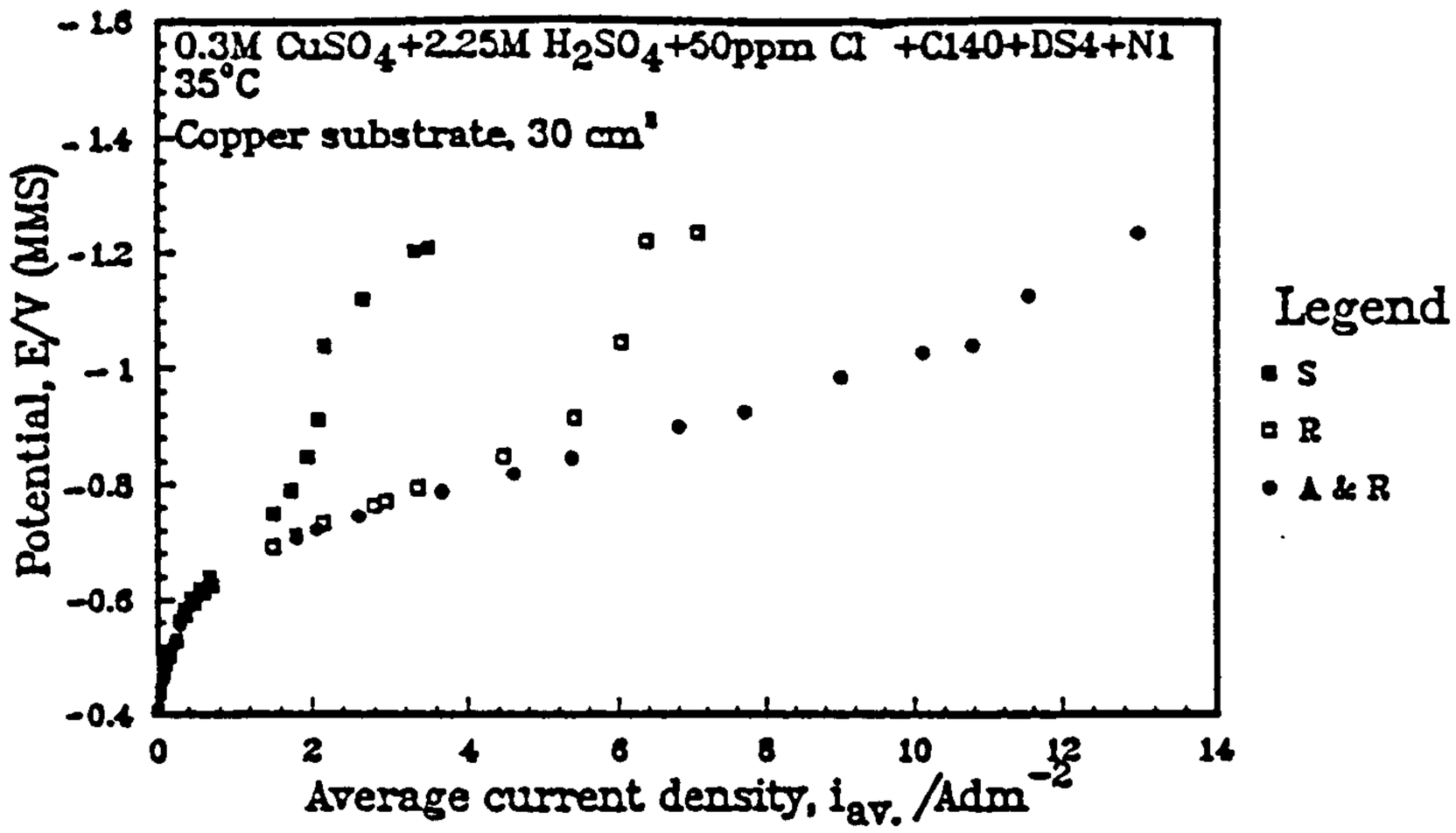

Figure 67a Polarisation curves obtained using a power supply - constant current for different agitation modes; S-Still, R-Reciprocating and A-Air, DVM data.

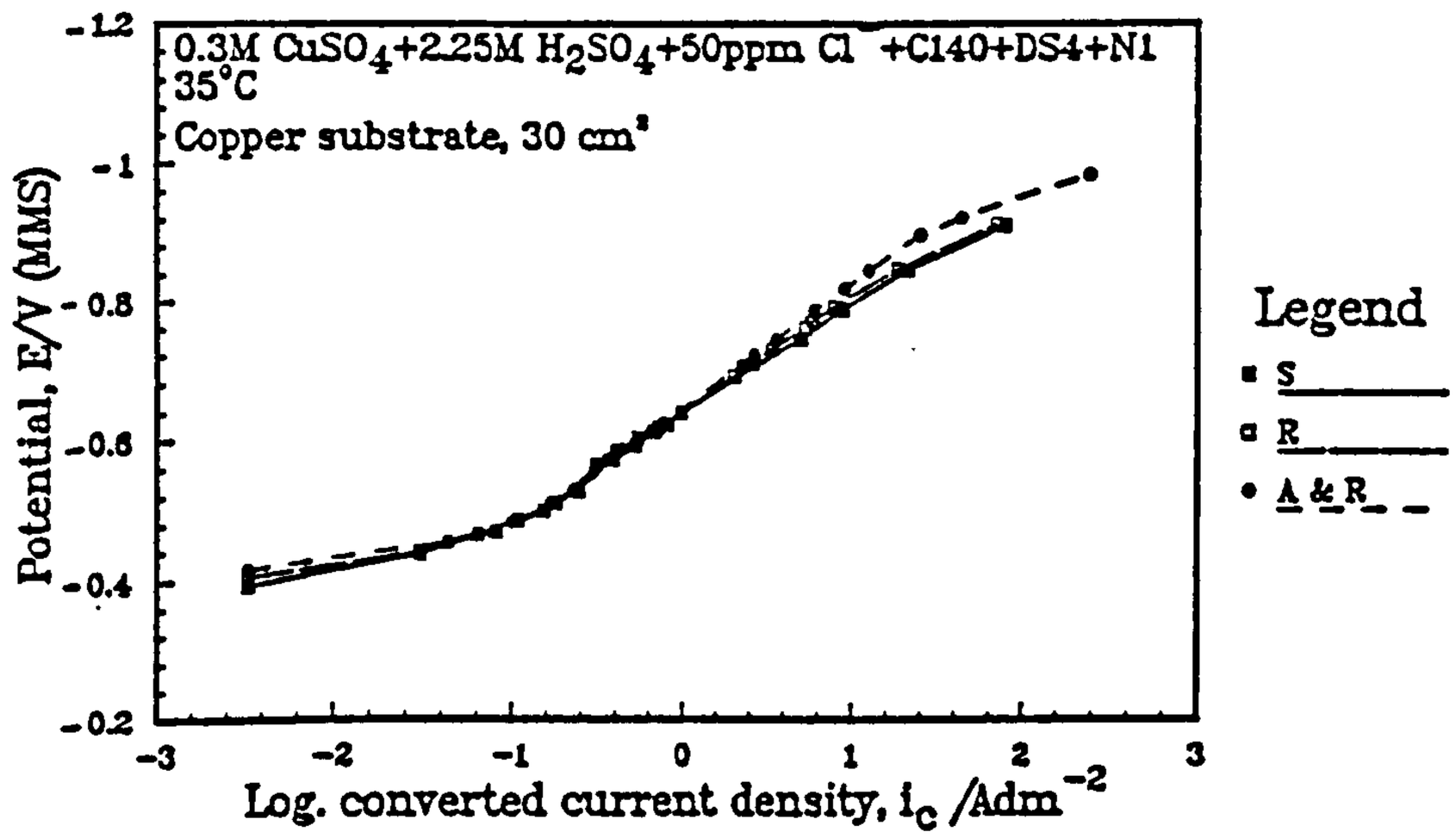

Figure 67b Relationship between potential and logarithmic converted current density, showing the Tafel region for different agitation modes; S-Still, R- Reciprocating and A-Air.

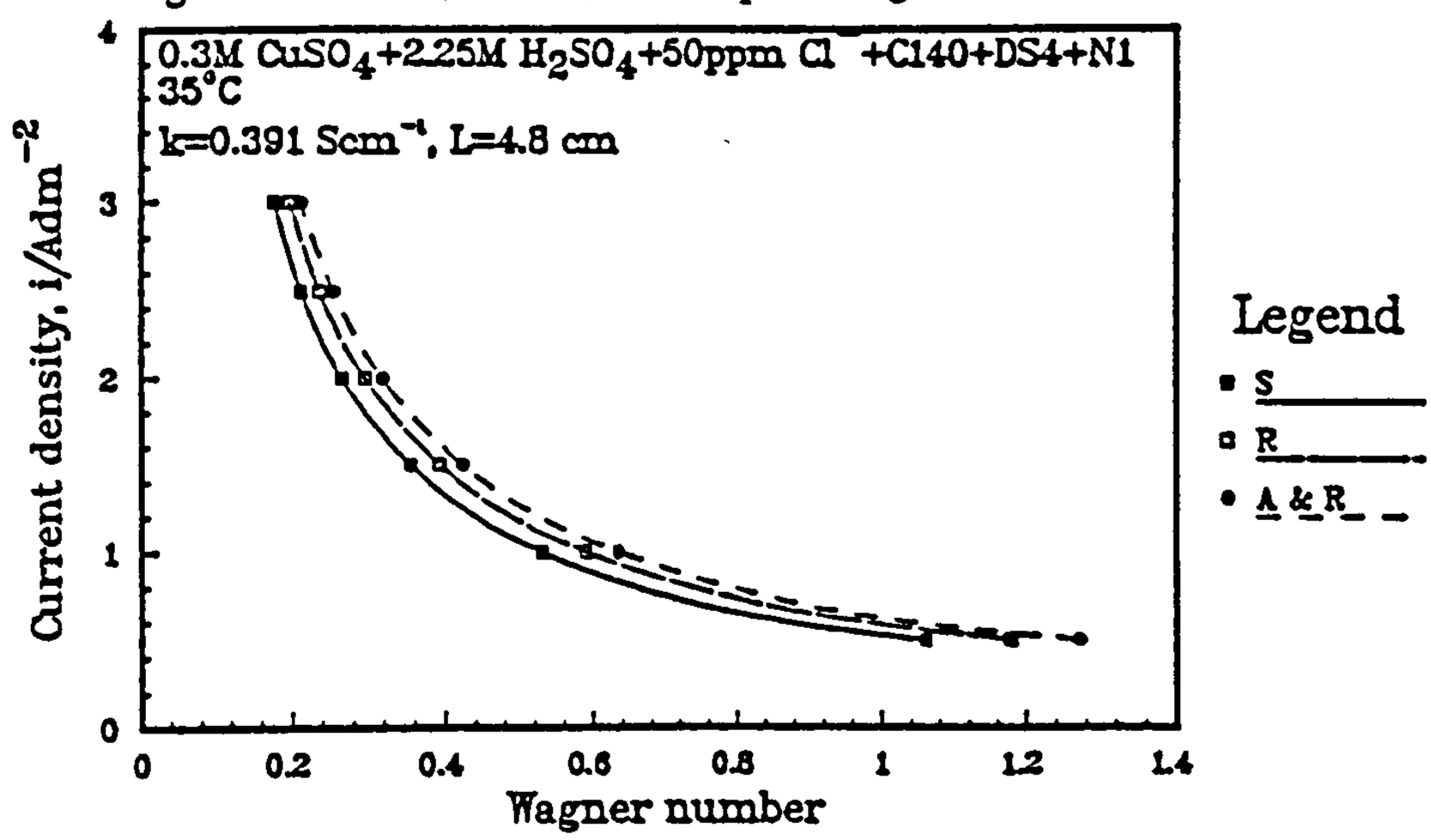

Figure 67c Relationship between current density and Wagner number for different agitation modes; S-Still, R-Reciprocating and A-Air.

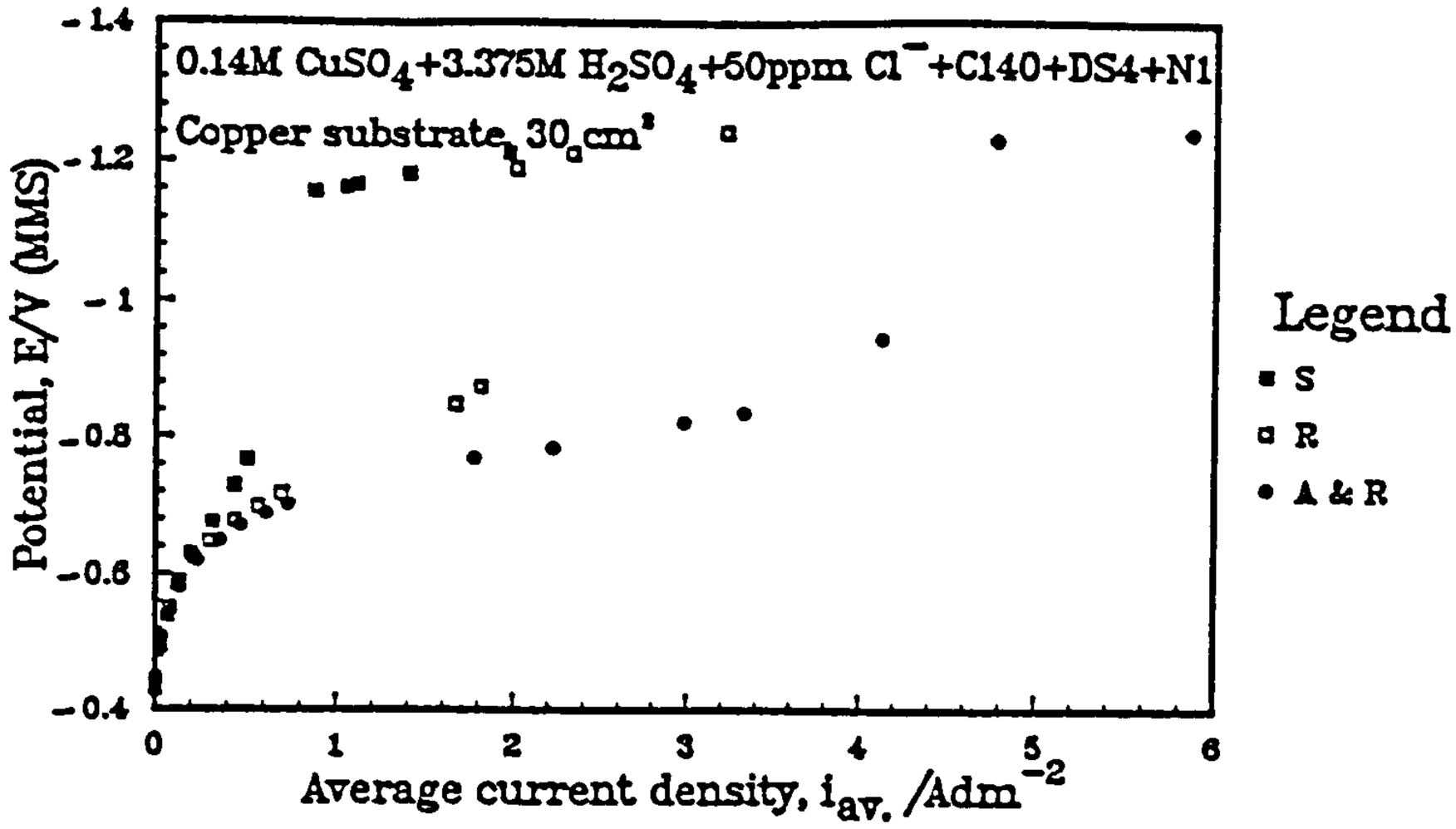

Figure 68a Polarisation curves obtained using a power supply - constant current for different agitation modes; S-Still, R-Reciprocating and A-Air, DVM data.

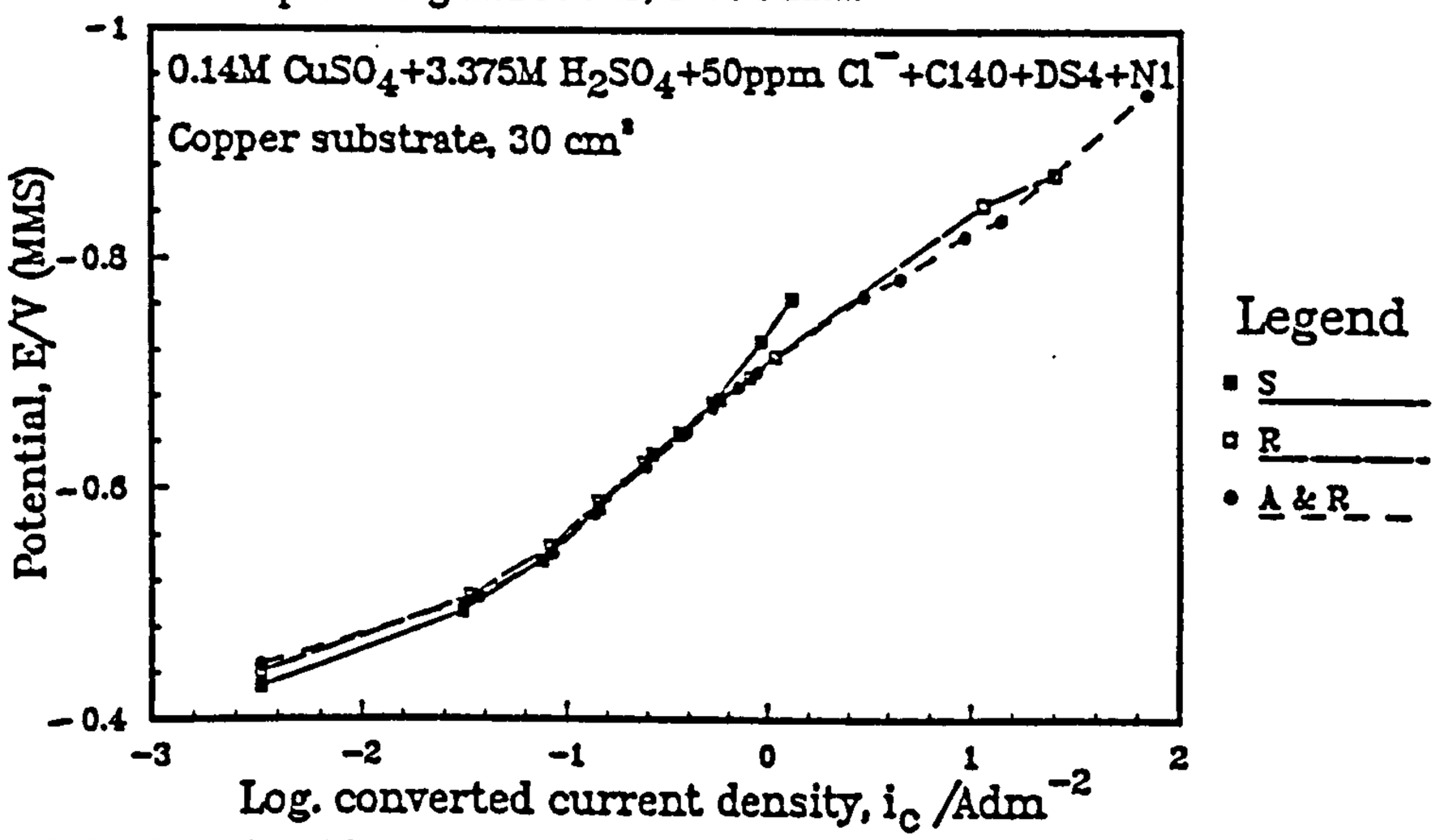

Figure 68b Relationship between potential and logarithmic converted current density, showing the Tafel region for different agitation modes; S-Still, R- Reciprocating and A-Air.

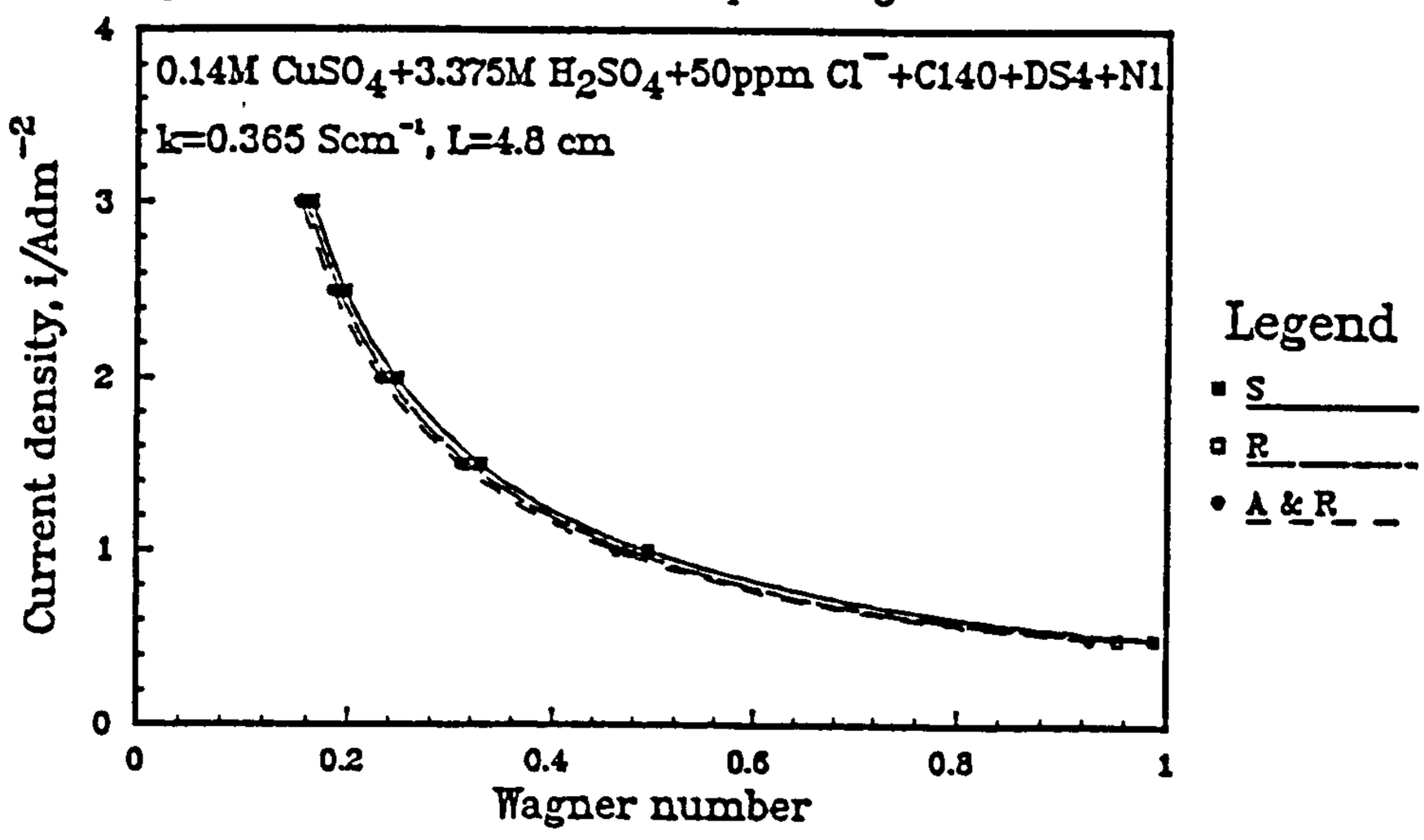

Figure 68c Relationship between current density and Wagner number for different agitation modes; S-Still, R-Reciprocating and A-Air.

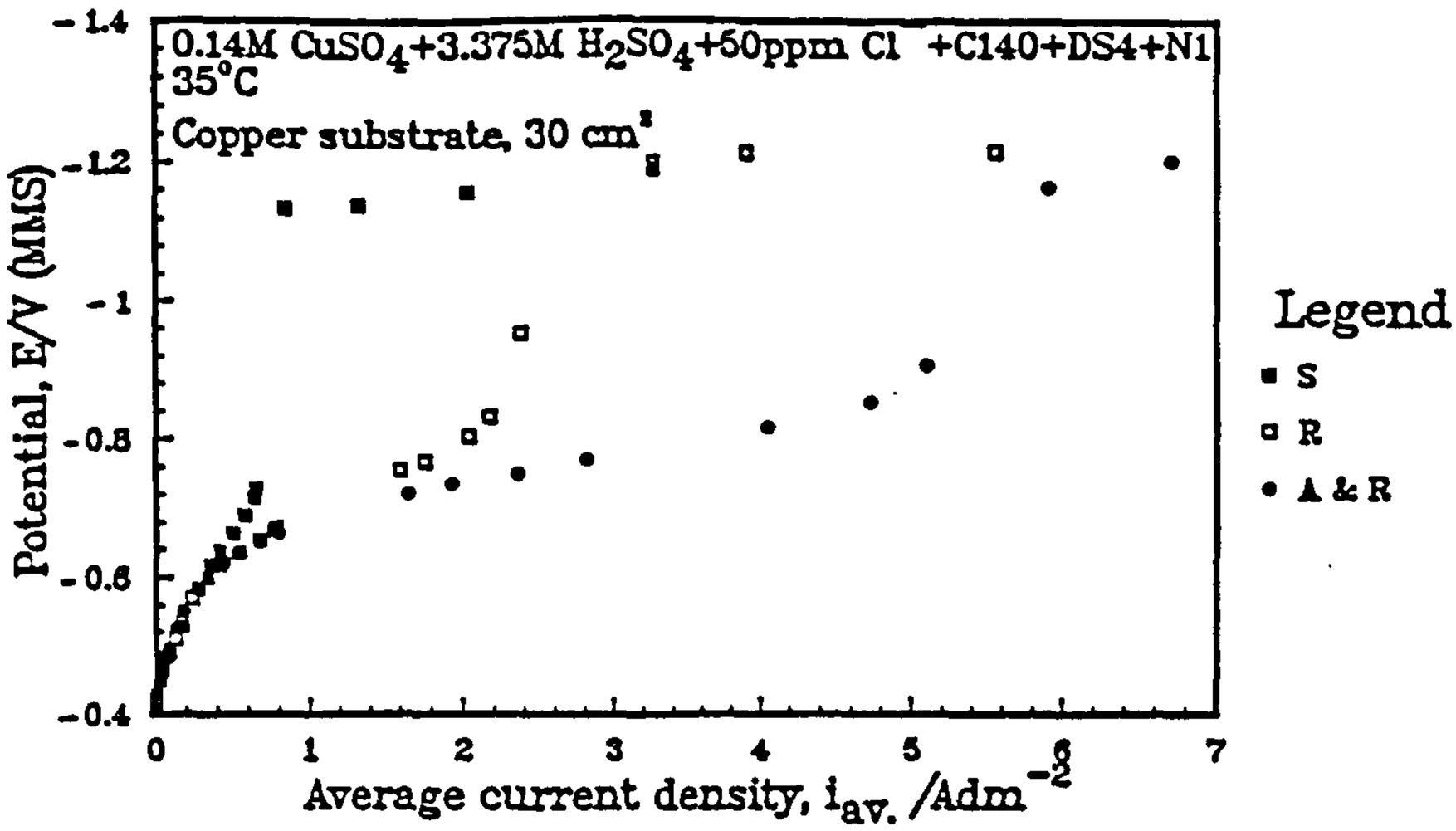

Figure 69a Polarisation curves obtained using a power supply - constant current for different agitation modes; S-Still, R-Reciprocating and A-Air, DVM data.

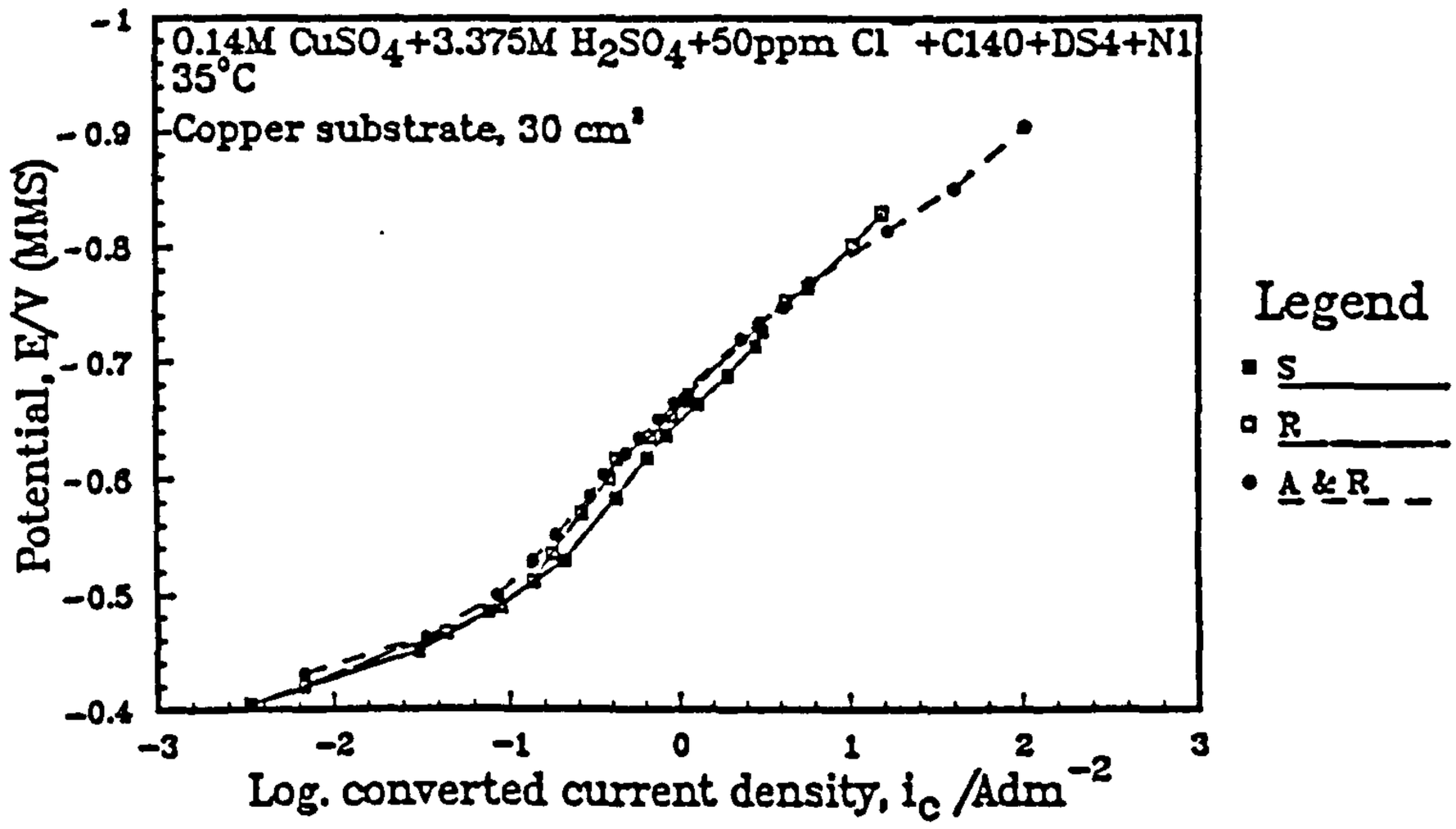

Figure 69b Relationship between potential and logarithmic converted current density, showing the Tafel region for different agitation modes; S-Still, R- Reciprocating and A-Air.

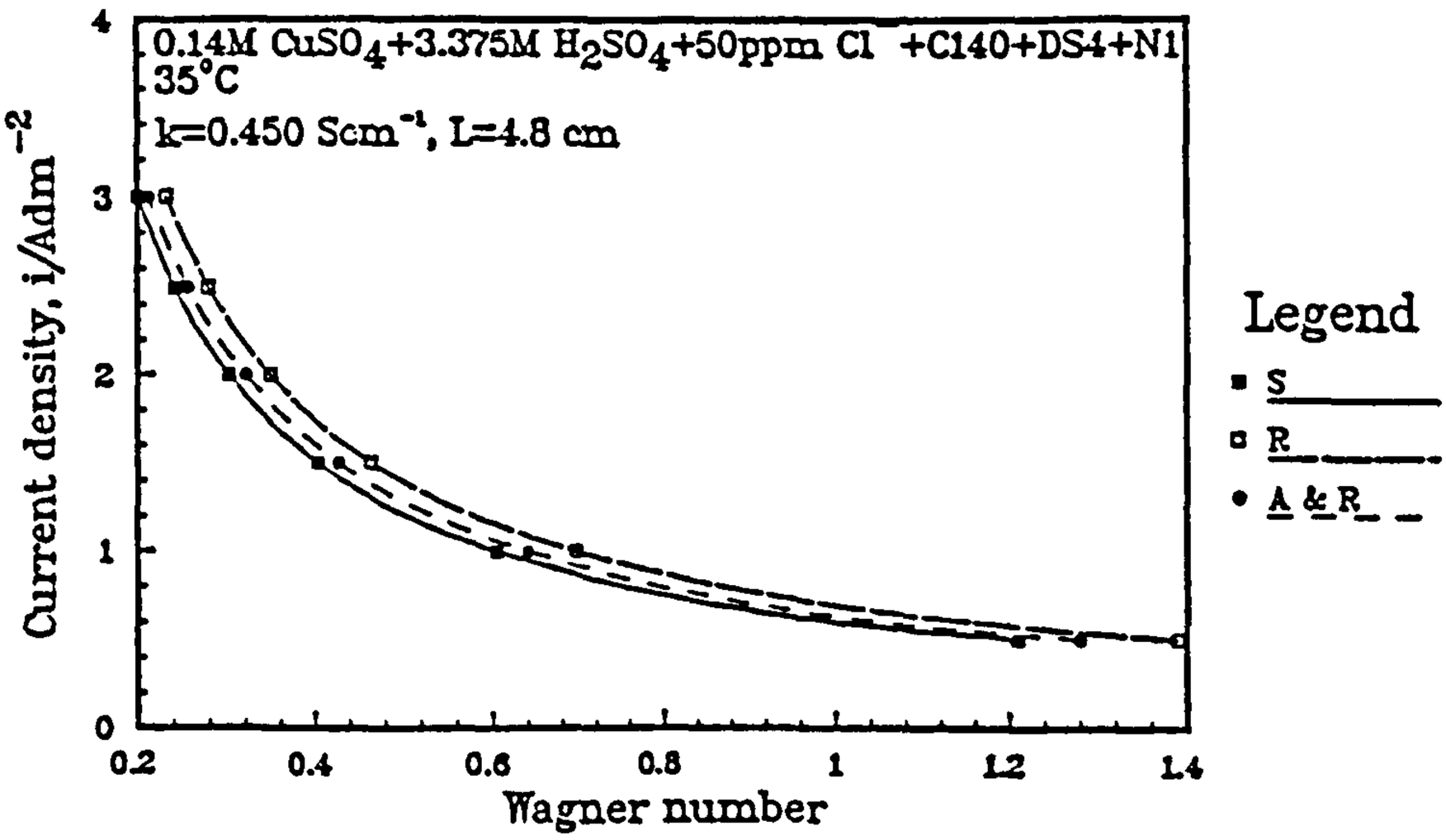

Figure 69c Relationship between current density and Wagner number for different agitation modes; S-Still, R-Reciprocating and A-Air.

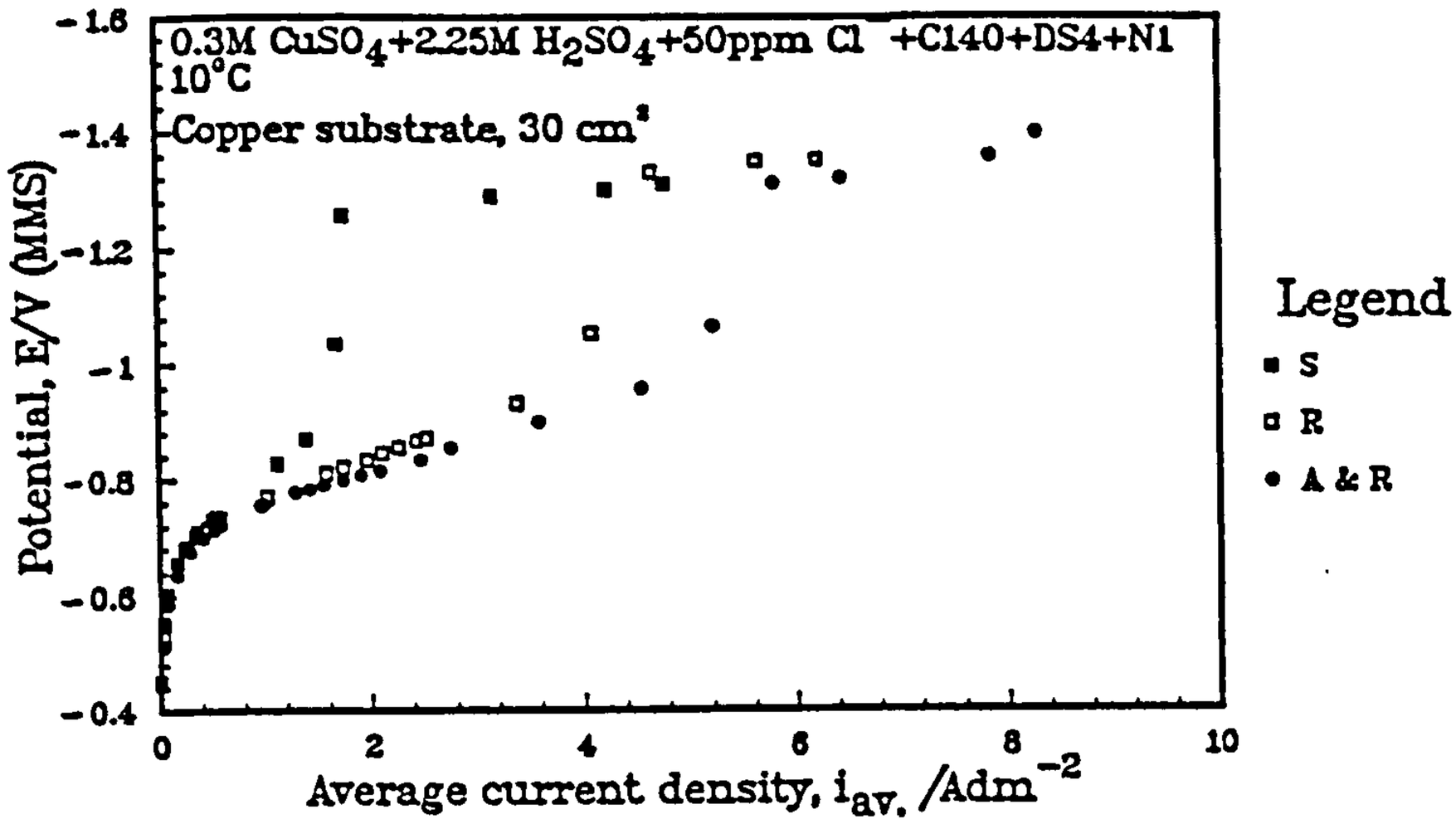

Figure 70a Polarisation curves obtained using a power supply - constant current for different agitation modes; S-Still, R-Reciprocating and A-Air, DVM data.

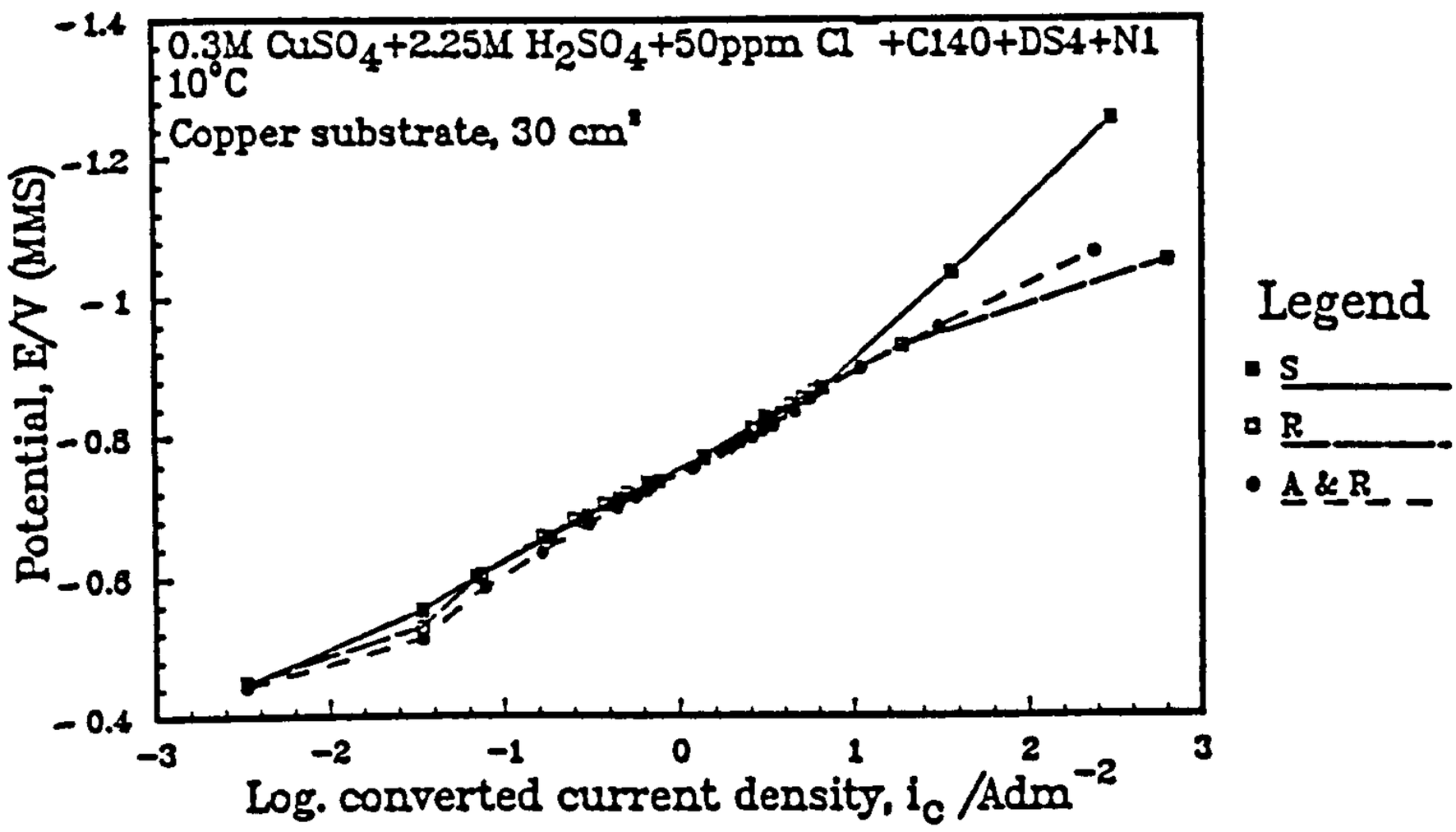

Figure 70b Relationship between potential and logarithmic converted current density, showing the Tafel region for different agitation modes; S-Still, R- Reciprocating and A-Air.

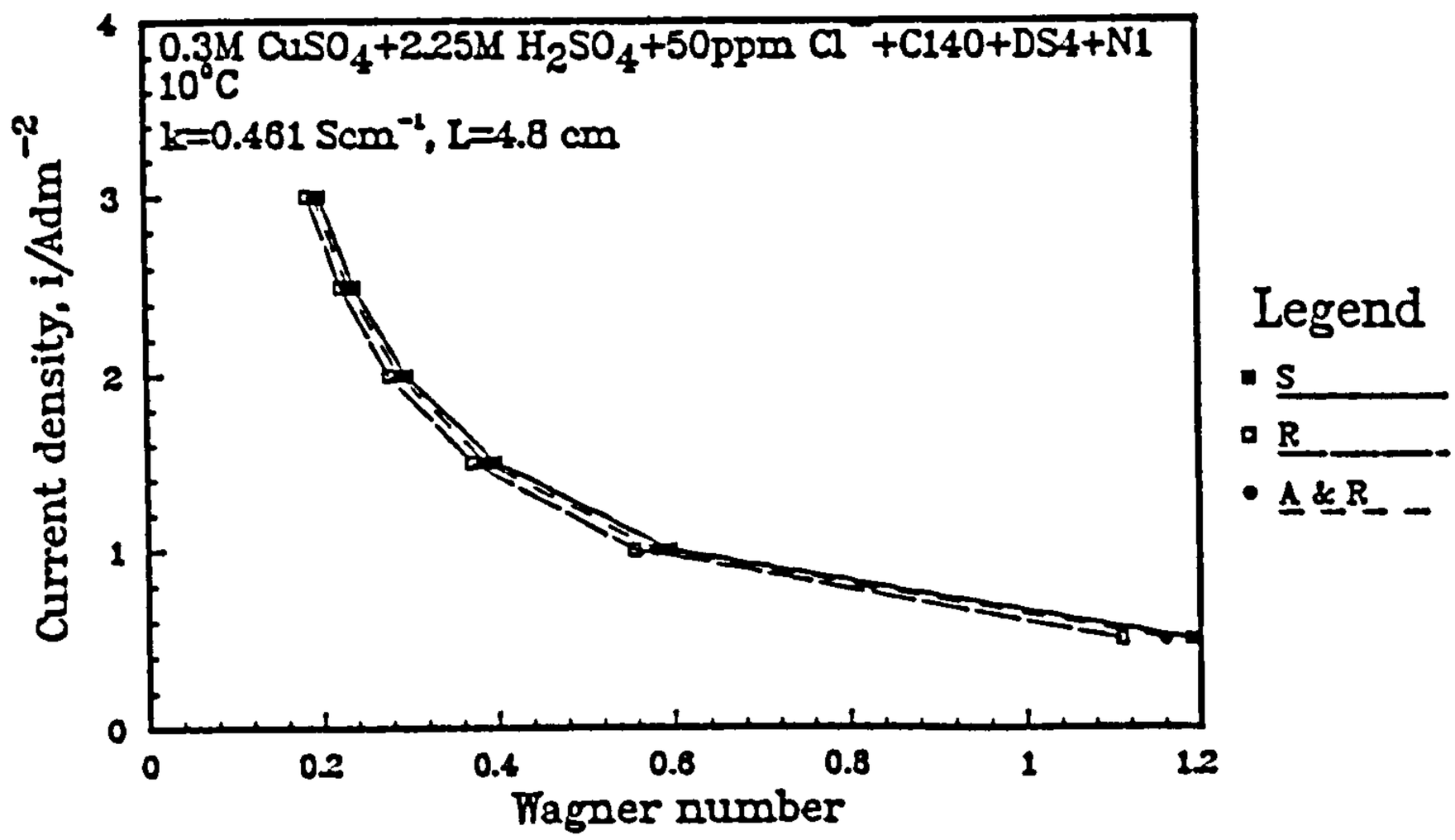

Figure 70c Relationship between current density and Wagner number for different agitation modes; S-Still, R-Reciprocating and A-Air.

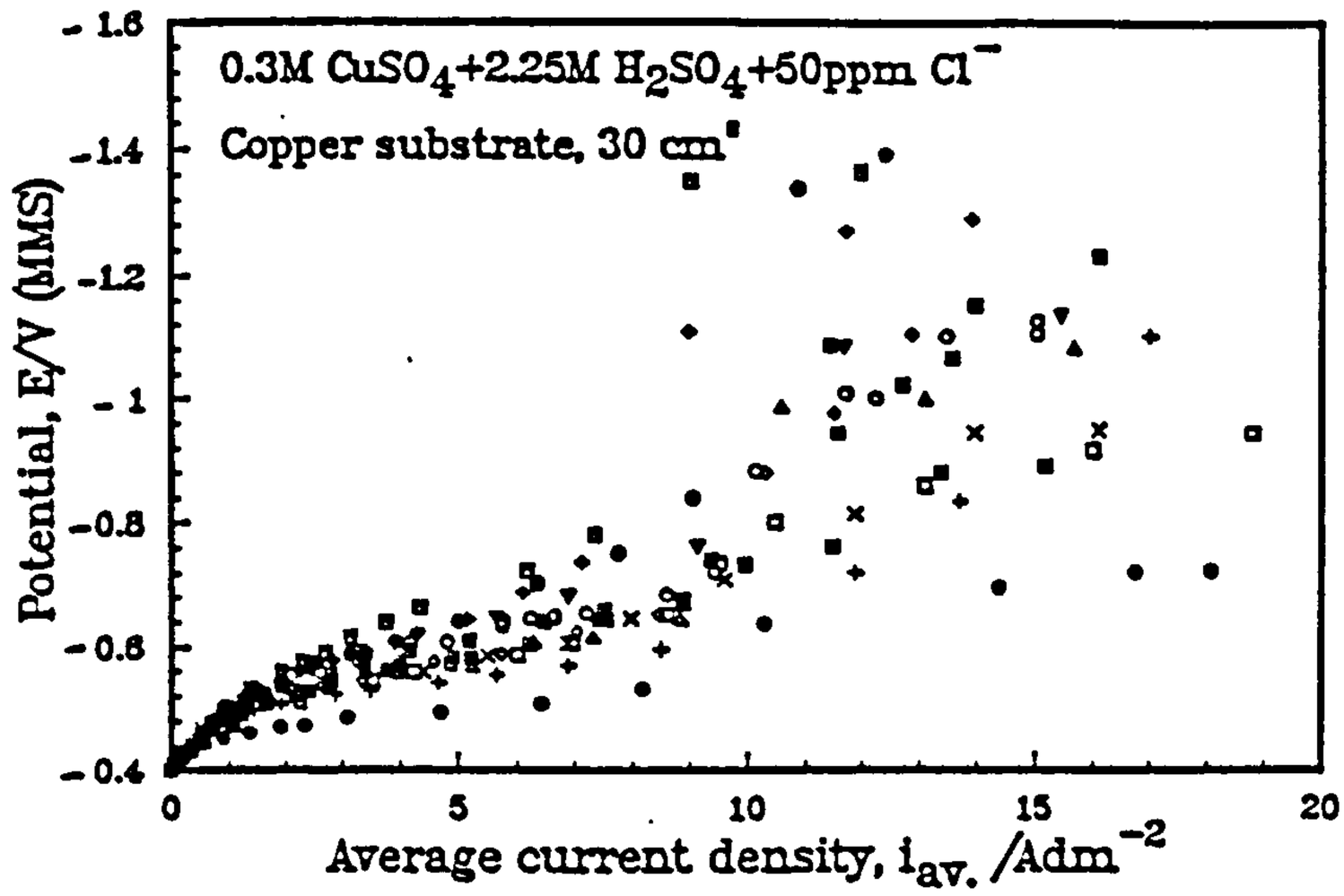

Figure 71a Polarisation curves obtained using the pulse unit and power supply - constant current; air and reciprocating agitations combined, DVM data.

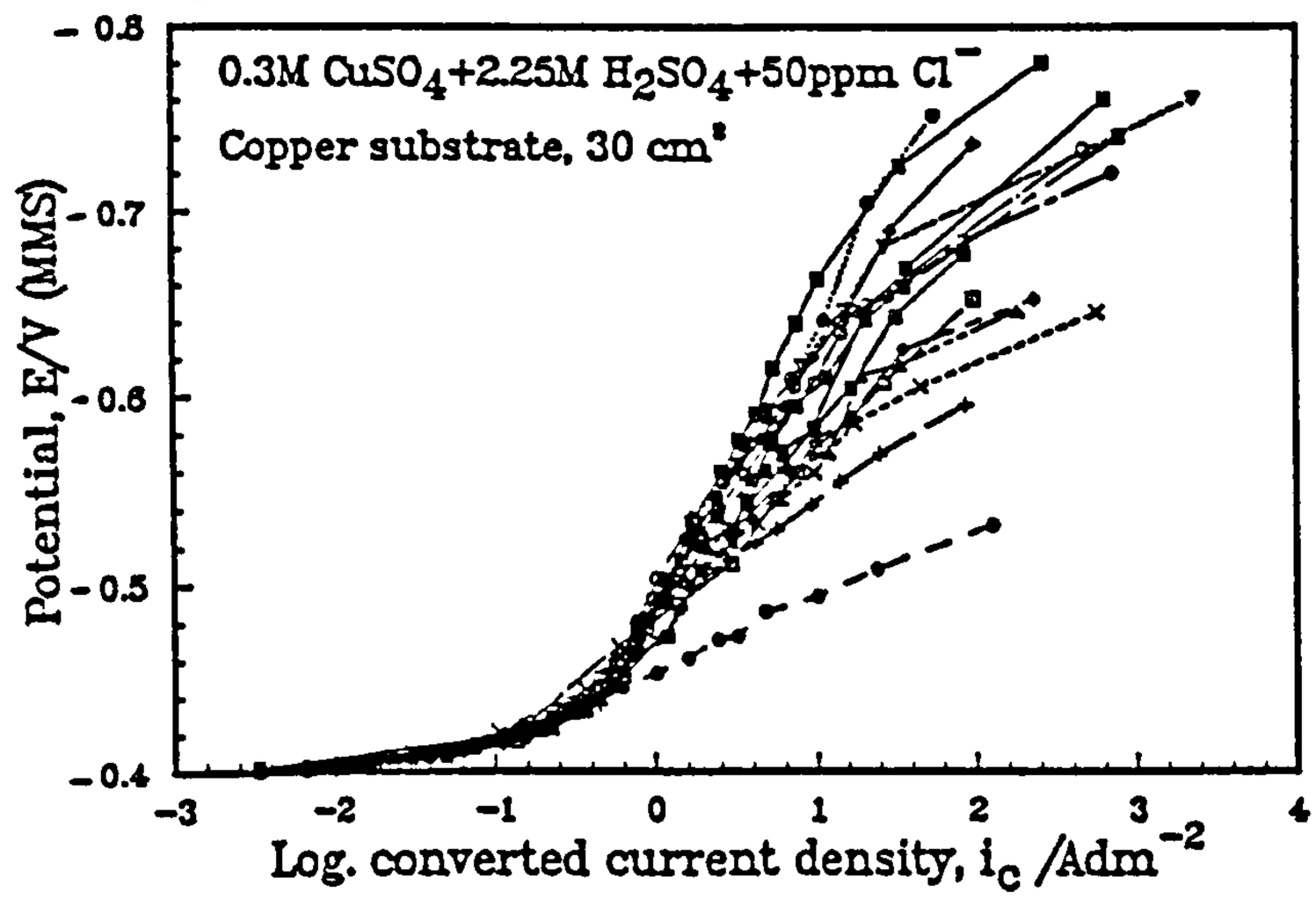

Figure 71b Relationship between potential and logarithmic converted current density, showing the Tafel region under different pulse conditions.

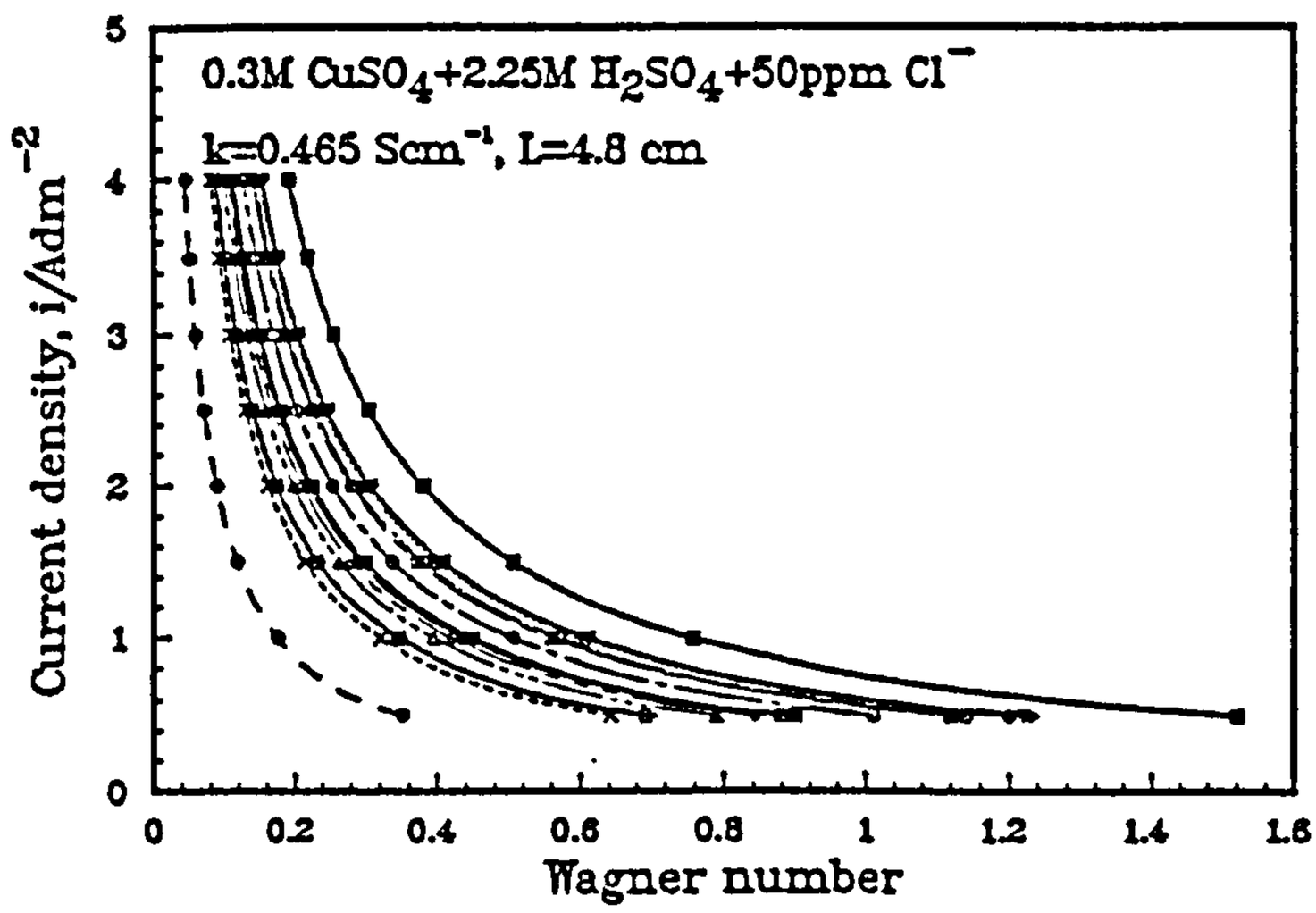

Figure 71c Relationship between current density and Wagner number under different pulse conditions.

Legend

- 20Hz,75%0,f
- 20Hz,50%0,f
- 20Hz,25%0,f
- 500Hz,75%0,f
- 500Hz,50%0,f
- 500Hz,25%0,f
- 1000Hz,75%0,f
- 1000Hz,50%0,f
- 1000Hz,25%0,f
- 2000Hz,75%0,f
- 2000Hz,50%0,f
- 2000Hz,25%0,f
- 5000Hz,75%0,f
- 5000Hz,50%0,f
- 5000Hz,25%0,f

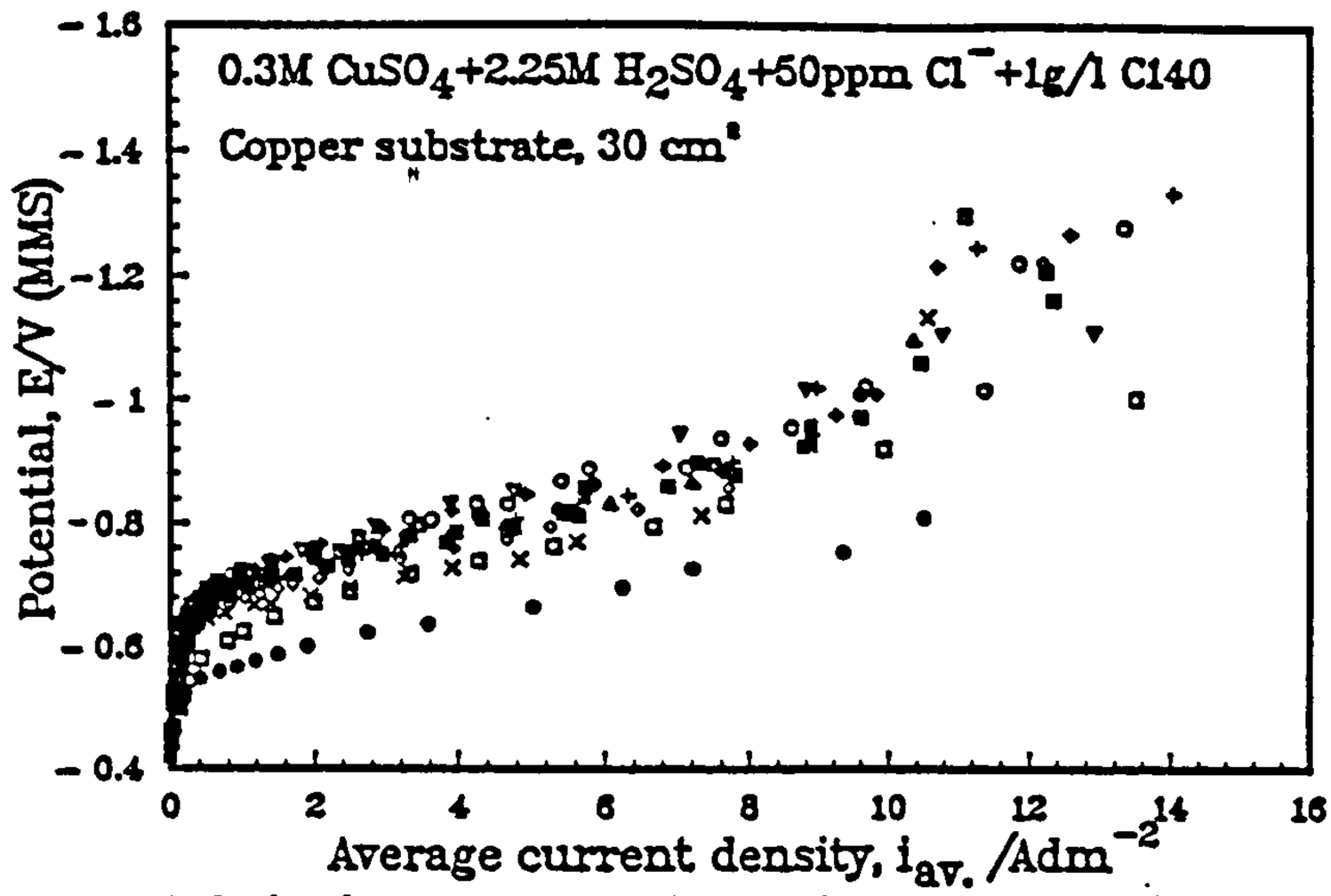

Figure 72a Polarisation curves obtained using the pulse unit and power supply - constant current; air and reciprocating agitations combined, DVM data.

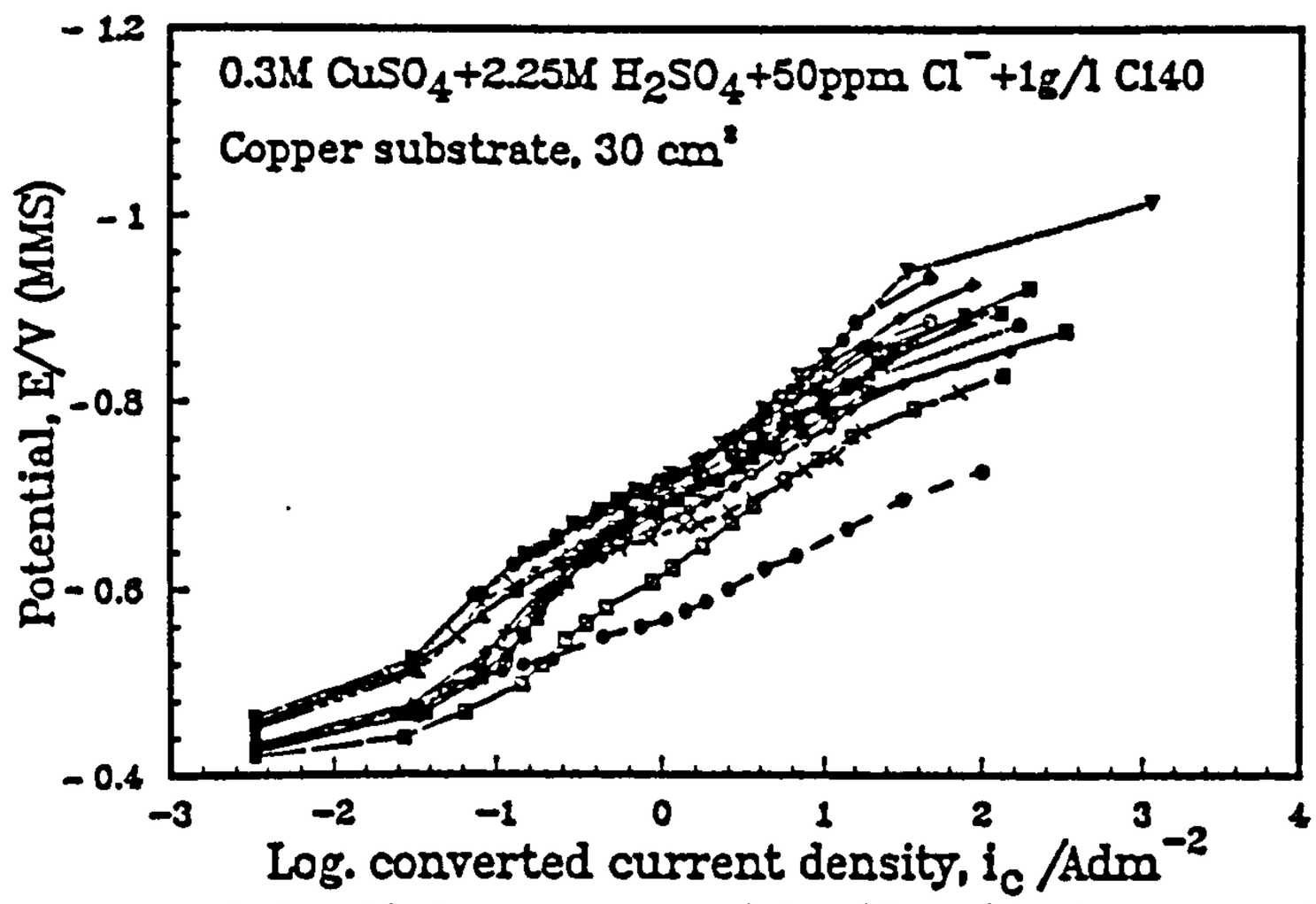

Legend

- 20Hz,75%0,f
- 20Hz,50%0,f
- 20Hz,25%0,f
- 500Hz,75%0,f
- 500Hz,50%0,f
- 500Hz,25%0,f
- 1000Hz,75%0,f
- 1000Hz,50%0,f
- 1000Hz,25%0,f
- 2000Hz,75%0,f
- 2000Hz,50%0,f
- 2000Hz,25%0,f
- 5000Hz,75%0,f
- 5000Hz,50%0,f
- 5000Hz,25%0,f

Figure 72b Relationship between potential and logarithmic converted current density, showing the Tafel region under different pulse conditions.

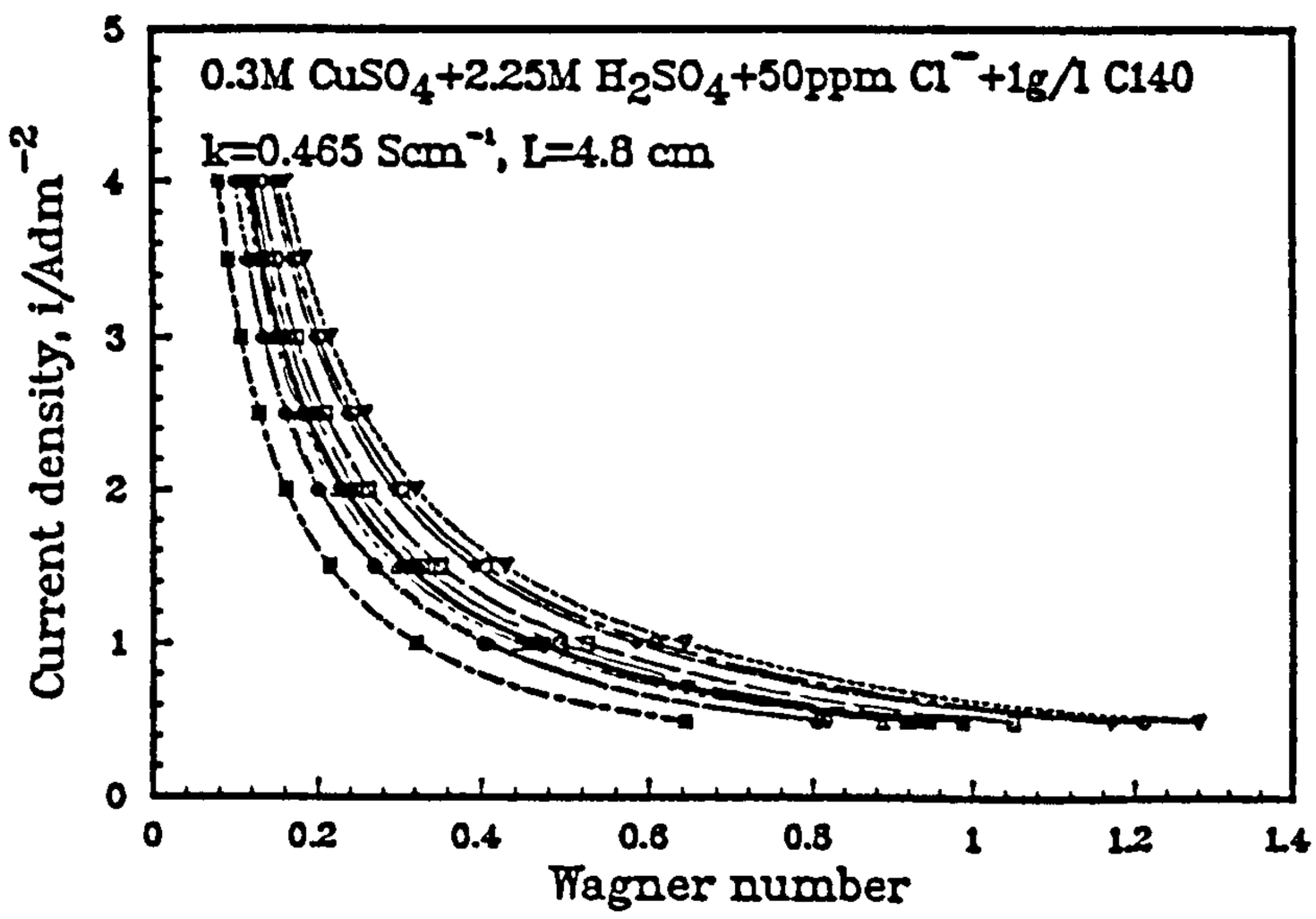

Figure 72c Relationship between current density and Wagner number under different pulse conditions.

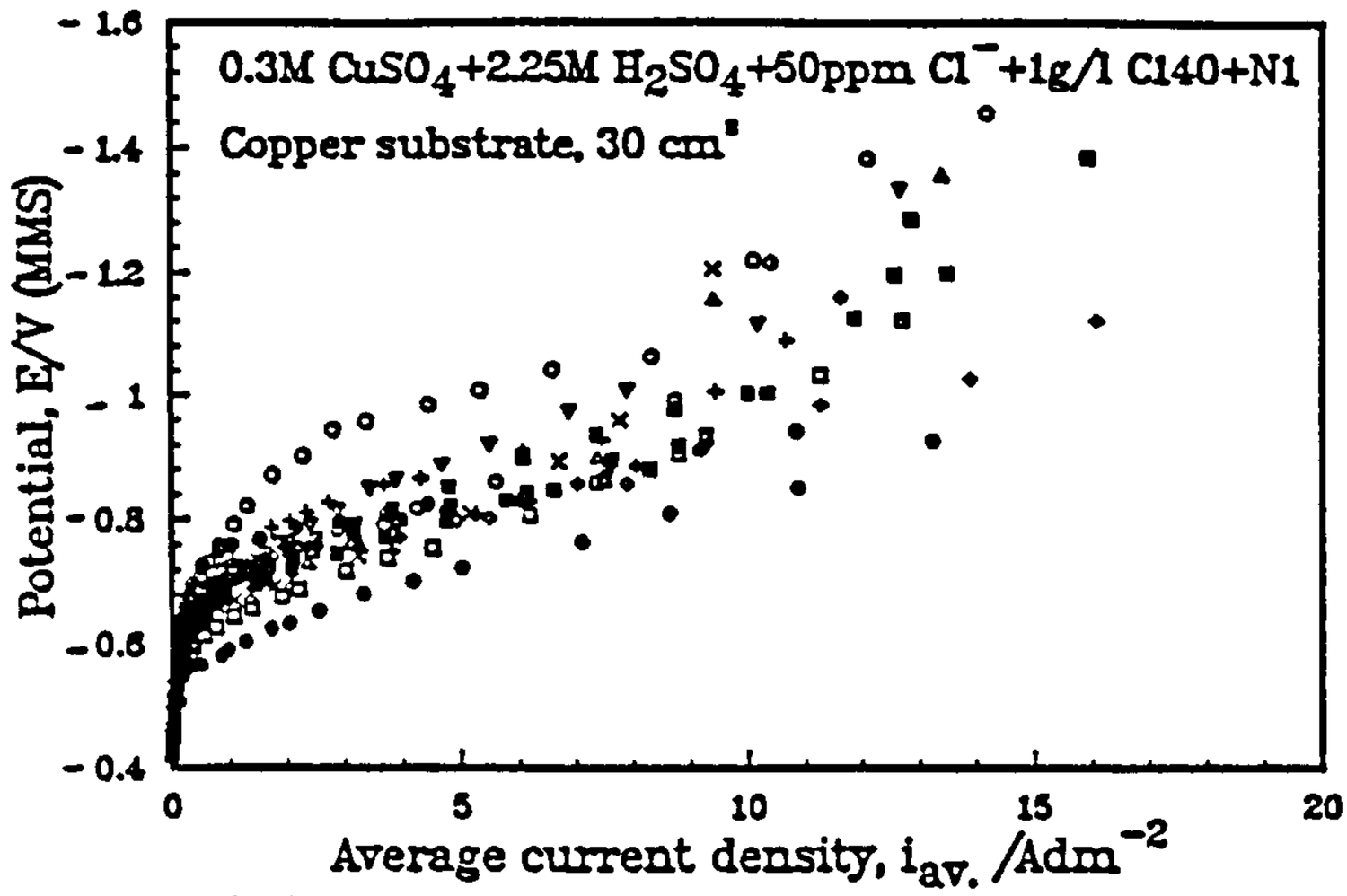

Figure 73a Polarisation curves obtained using the pulse unit and power supply - constant current; air and reciprocating agitations combined, DVM data.

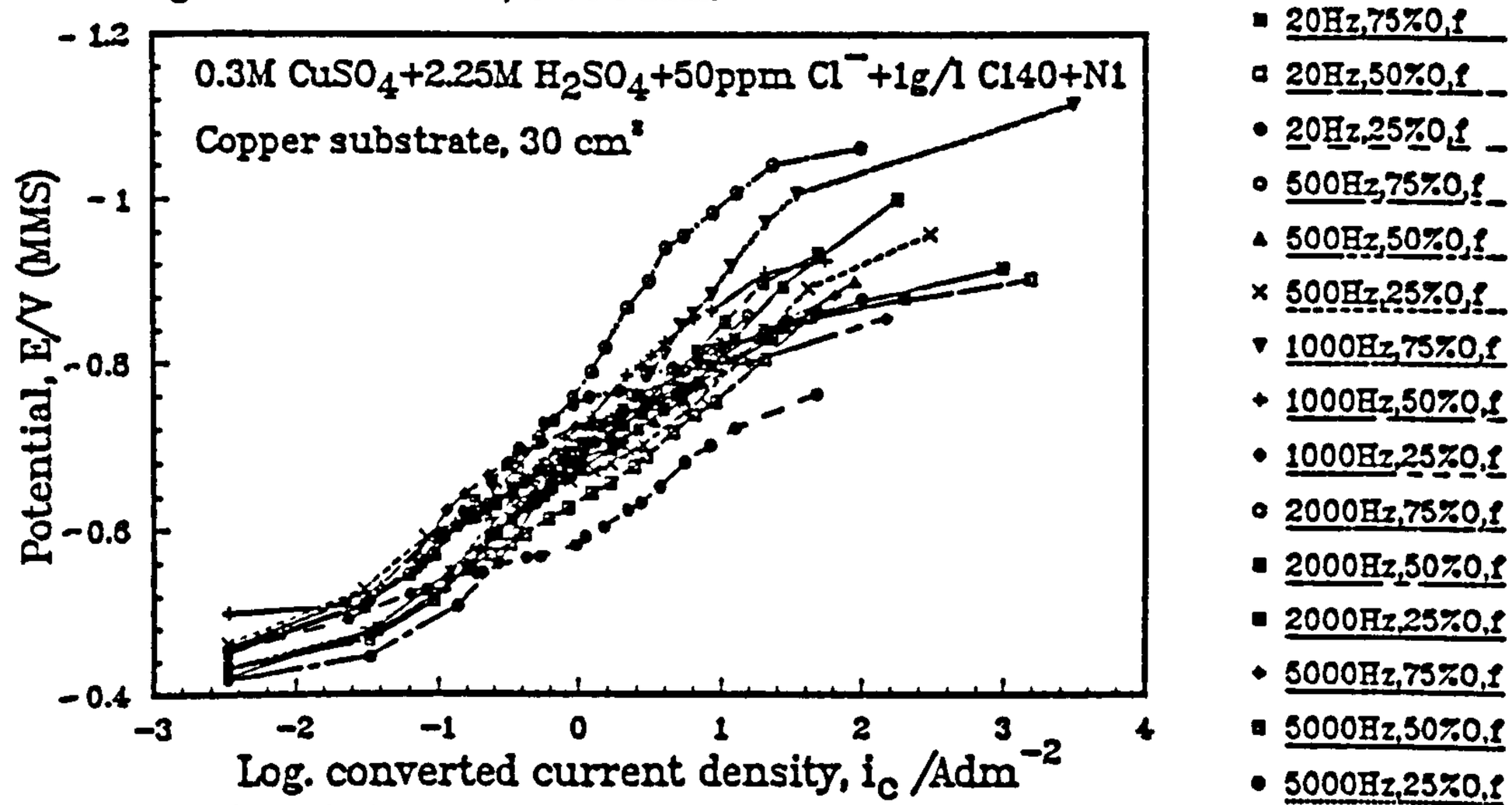

Figure 73b Relationship between potential and logarithmic converted current density, showing the Tafel region under different pulse conditions.

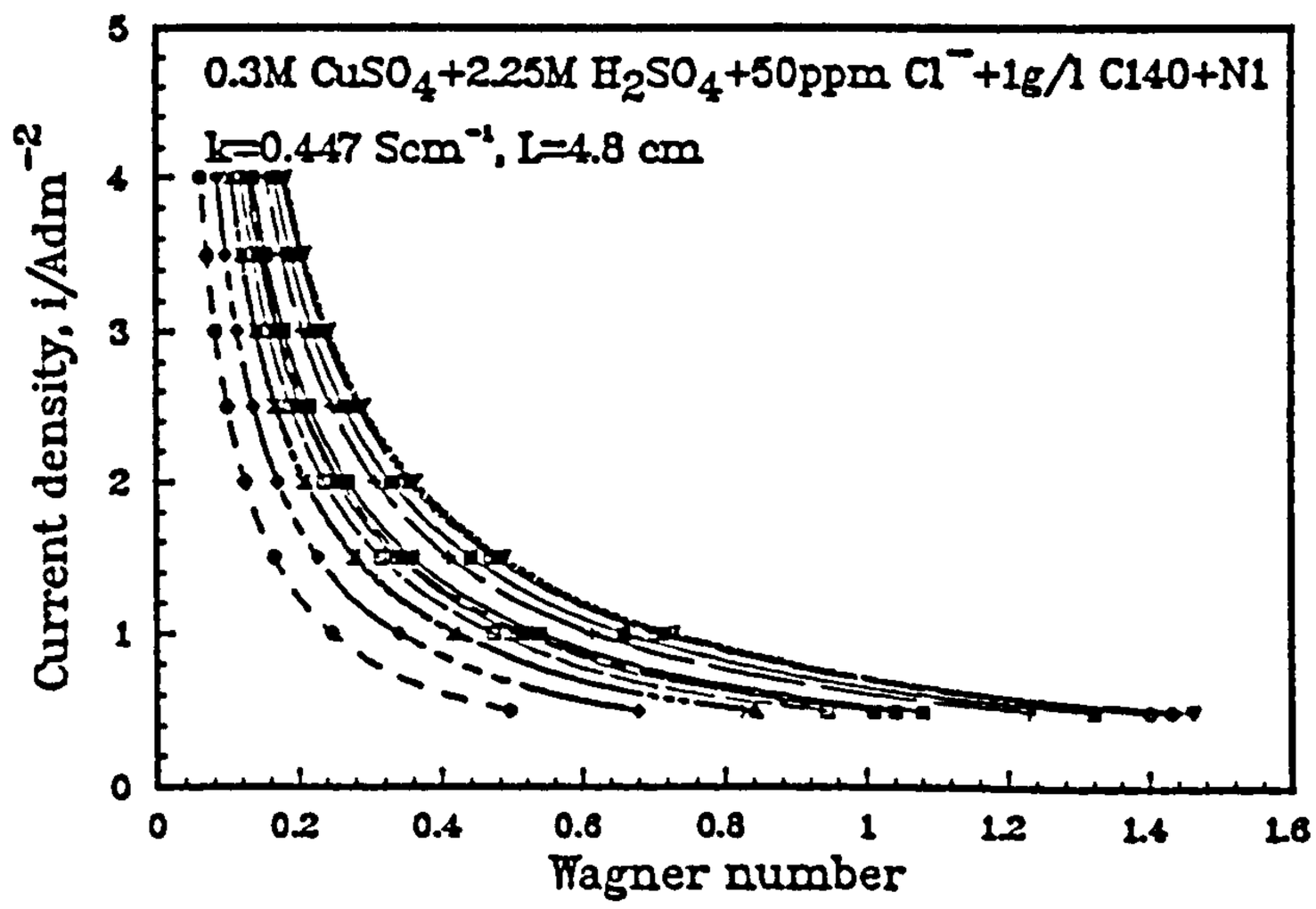

Figure 73c Relationship between current density and Wagner number under different pulse conditions.

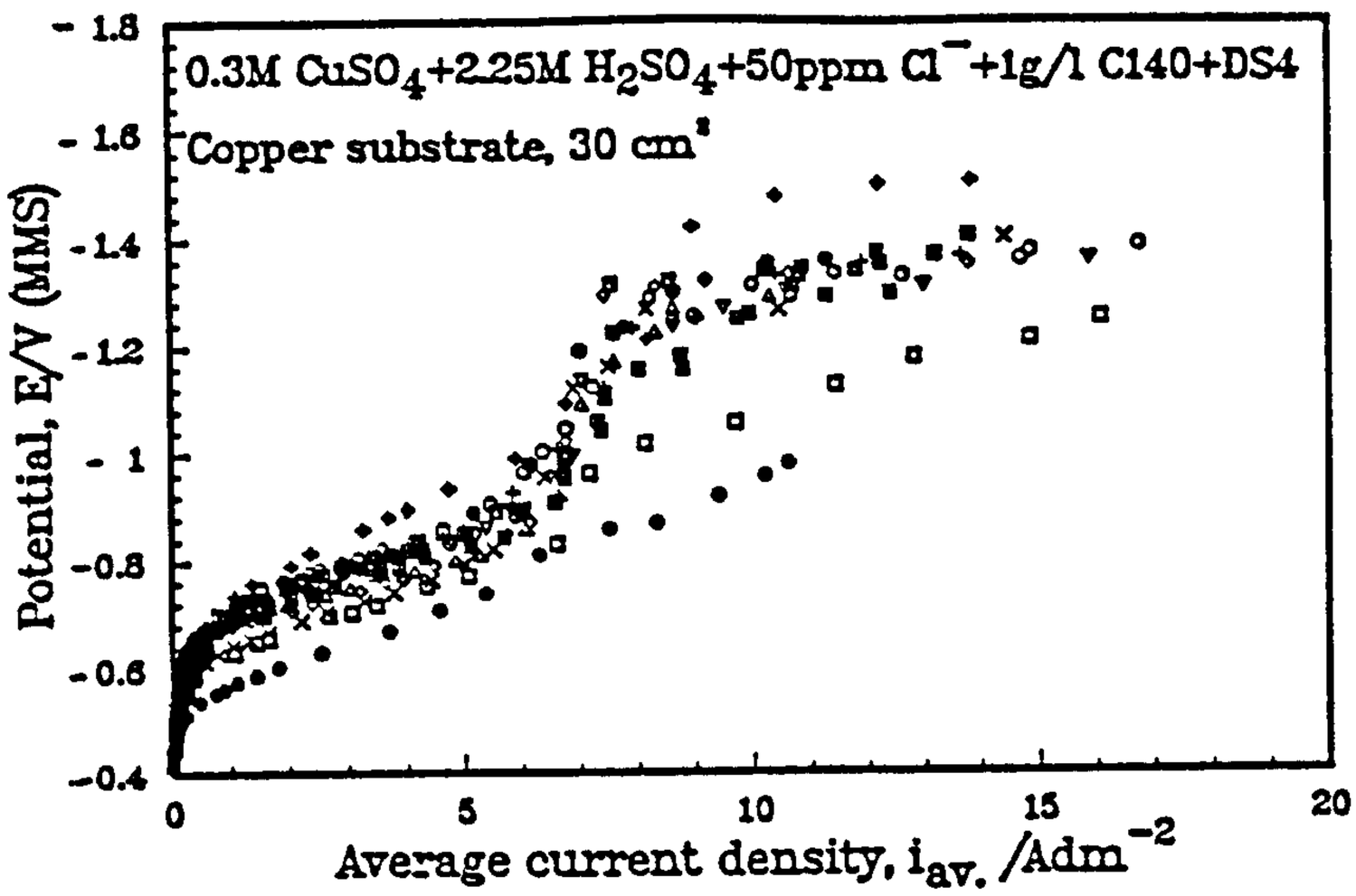

Figure 74a Polarisation curves obtained using the pulse unit and power supply - constant current; air and reciprocating agitations combined, DVM data.

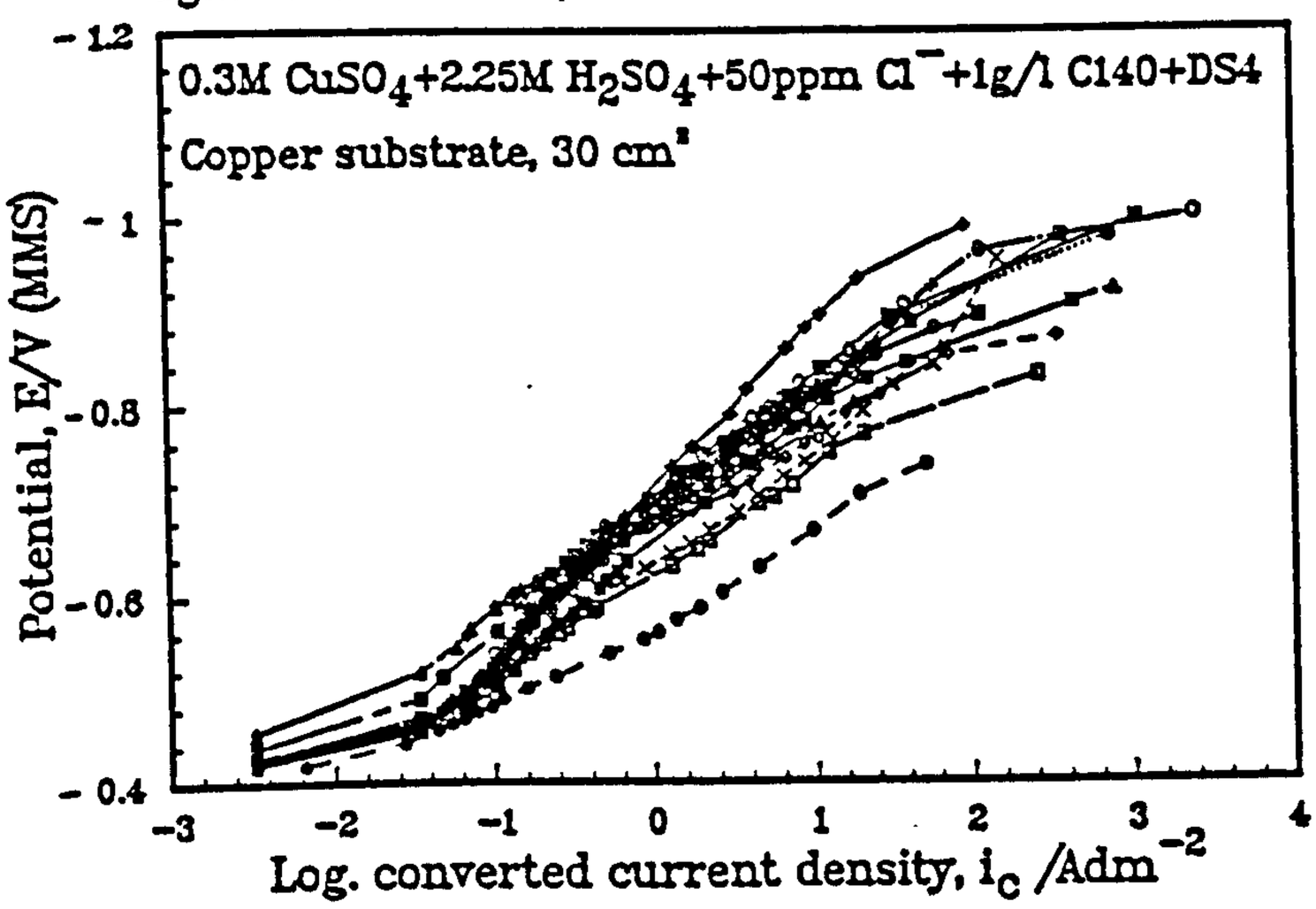

Figure 74b Relationship between potential and logarithmic converted current density, showing the Tafel region under different pulse conditions.

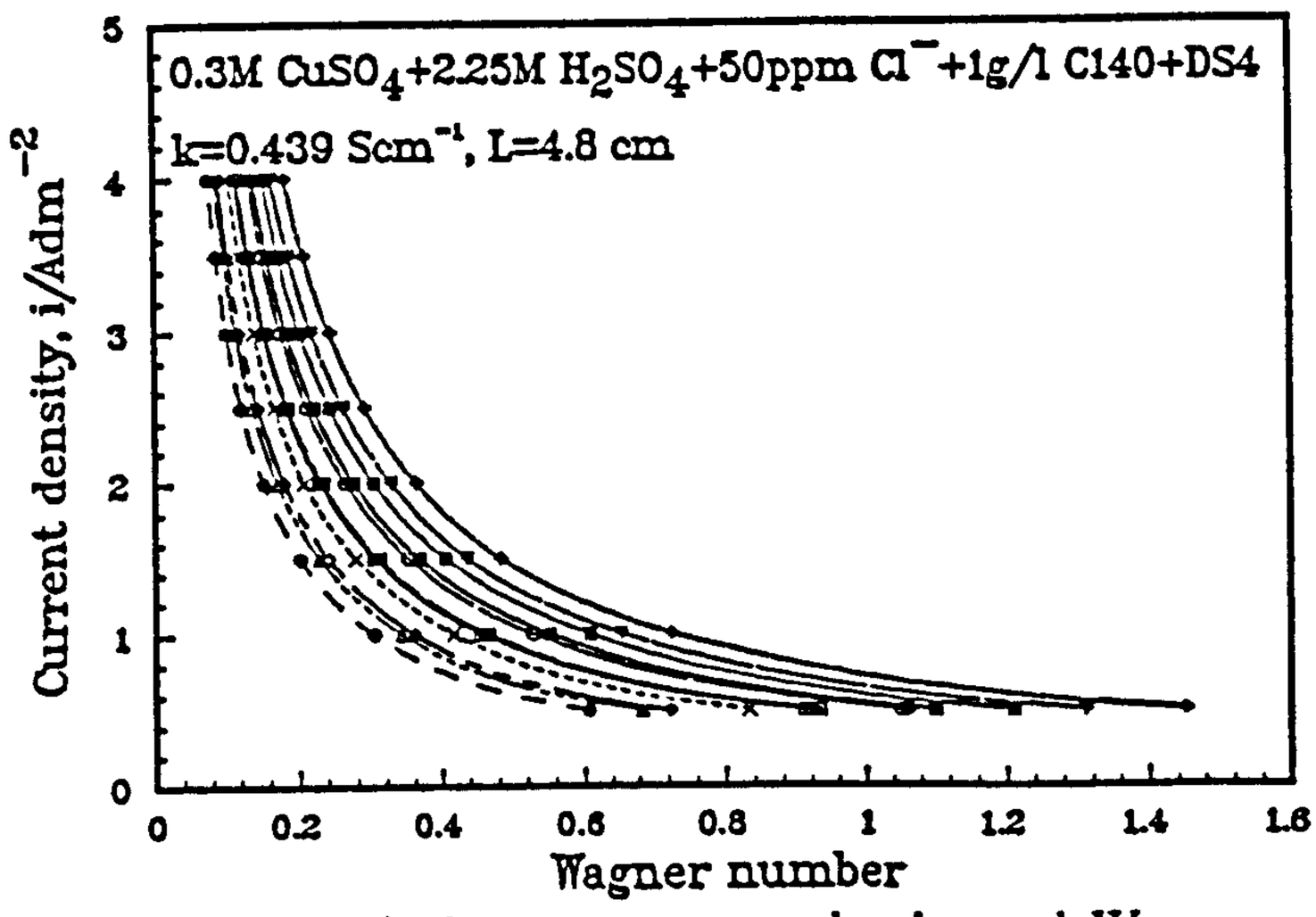

Figure 74c Relationship between current density and Wagner number under different pulse conditions.

Legend

- 20Hz,75%0,f
- 20Hz,50%0,f
- 20Hz,25%0,f
- 500Hz,75%0,f
- 500Hz,50%0,f
- 500Hz,25%0,f
- 1000Hz,75%0,f
- 1000Hz,50%0,f
- 1000Hz,25%0,f
- 2000Hz,75%0,f
- 2000Hz,50%0,f
- 2000Hz,25%0,f
- 5000Hz,75%0,f
- 5000Hz,50%0,f
- 5000Hz,25%0,f

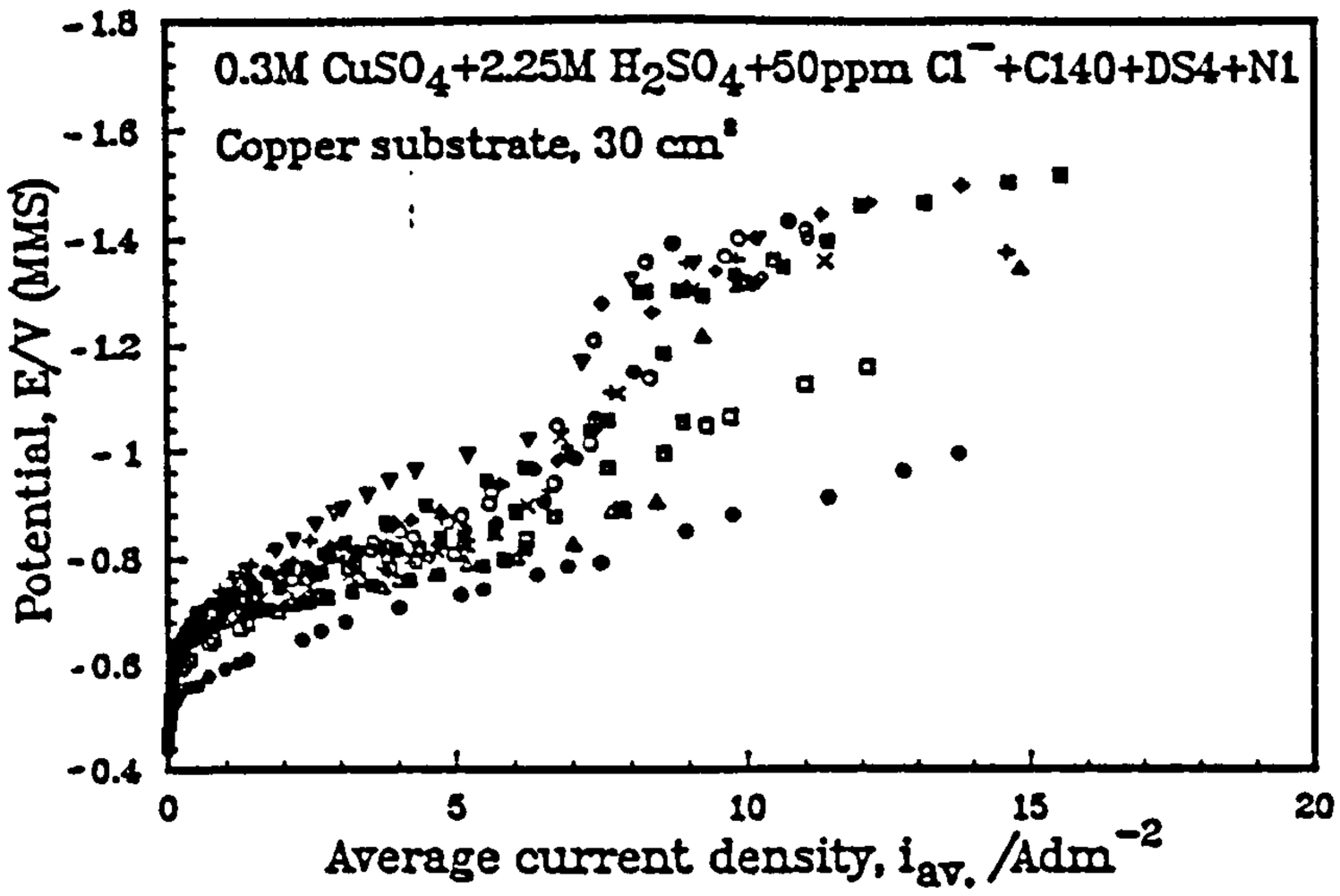

Figure 75a Polarisation curves obtained using the pulse unit and power supply - constant current; air and reciprocating agitations combined, DVM data.

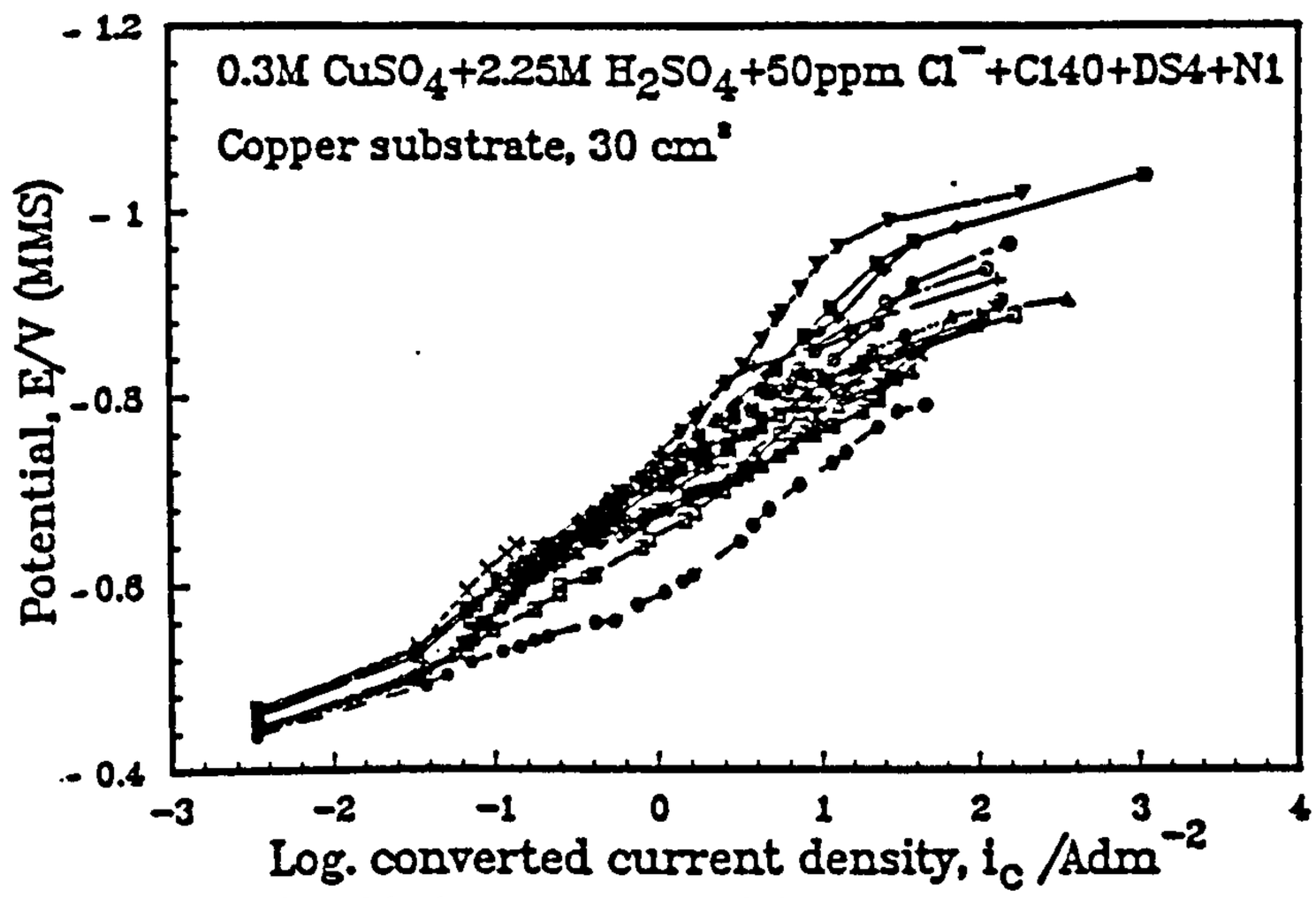

Legend

- 20Hz,75%0,f
- 20Hz,50%0,f
- 20Hz,25%0,f
- 500Hz,75%0,f
- 500Hz,50%0,f
- 500Hz,25%0,f
- 1000Hz,75%0,f
- 1000Hz,50%0,f
- 1000Hz,25%0,f
- 2000Hz,75%0,f
- 2000Hz,50%0,f
- 2000Hz,25%0,f
- 5000Hz,75%0,f
- 5000Hz,50%0,f
- 5000Hz,25%0,f

Figure 75b Relationship between potential and logarithmic converted current density, showing the Tafel region under different pulse conditions.

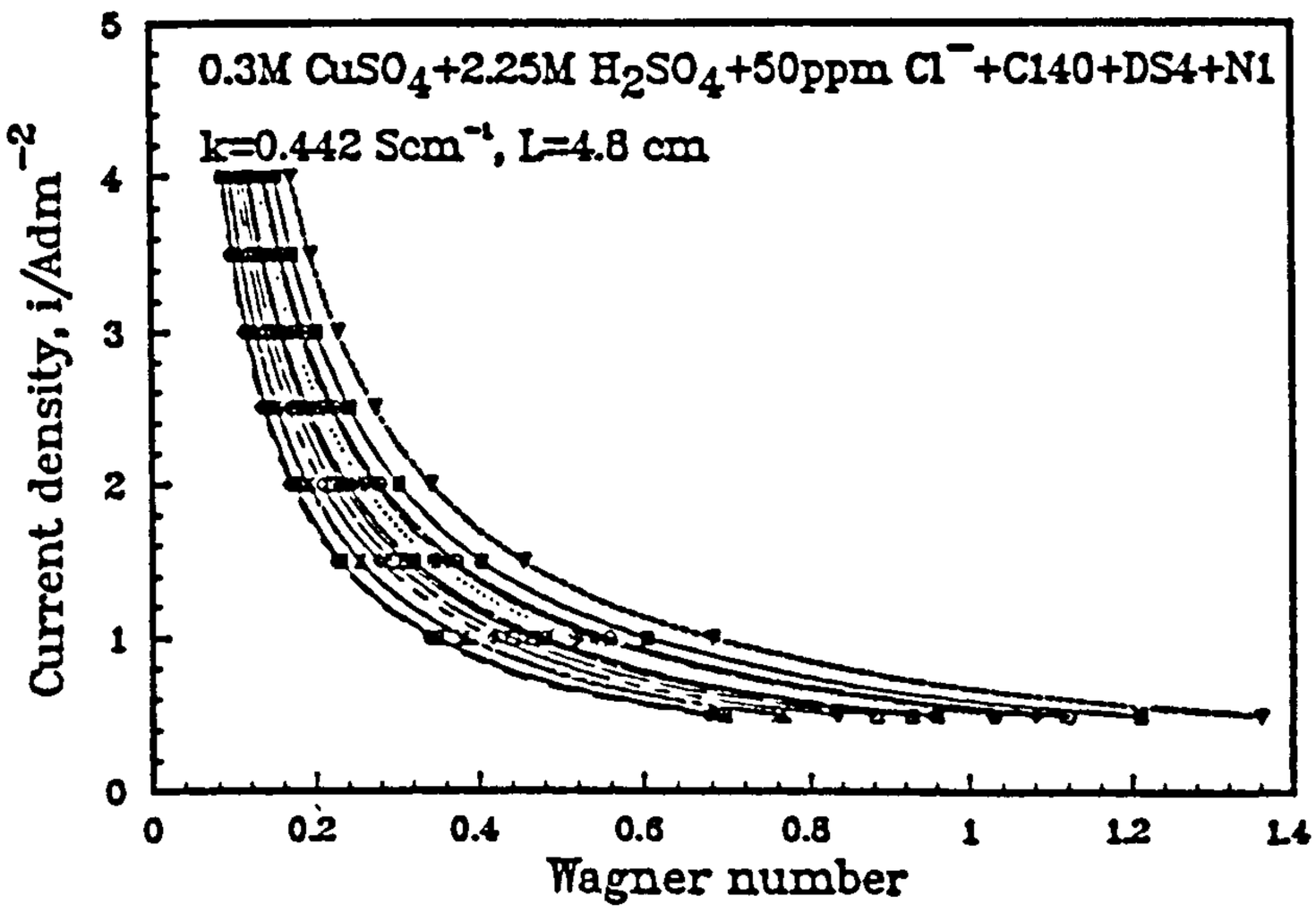

Figure 75c Relationship between current density and Wagner number under different pulse conditions.

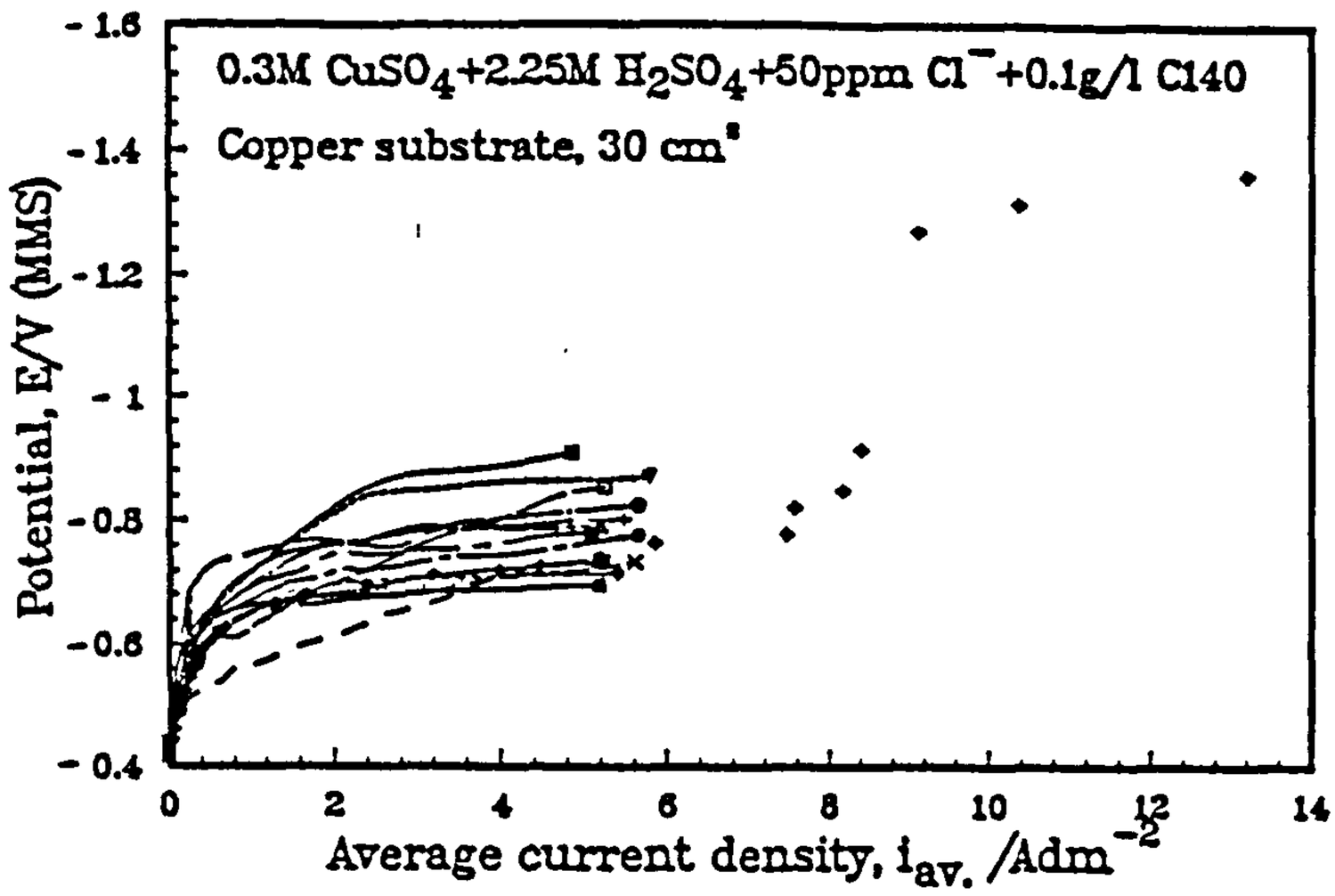

Figure 76a Polarisation curves obtained using the pulse unit and power supply - constant current; air and reciprocating agitations combined, DVM data.

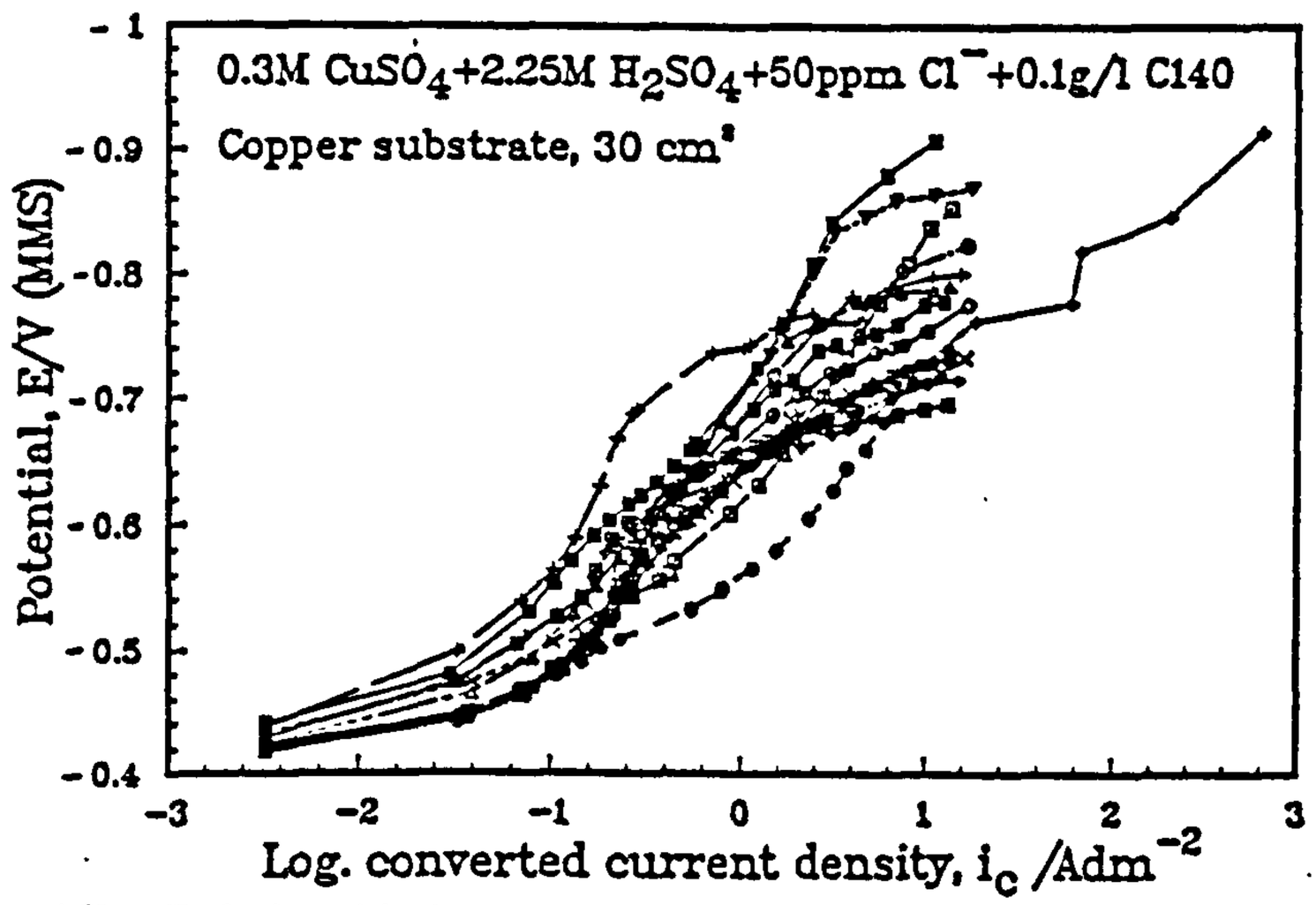

Legend

- 20Hz,75%0,f
- 20Hz,50%0,f
- 20Hz,25%0,f
- 500Hz,75%0,f
- 500Hz,50%0,f
- 500Hz,25%0,f
- 1000Hz,75%0,f
- 1000Hz,50%0,f
- 1000Hz,25%0,f
- 2000Hz,75%0,f
- 2000Hz,50%0,f
- 2000Hz,25%0,f
- 5000Hz,75%0,f
- 5000Hz,50%0,f
- 5000Hz,25%0,f

Figure 76b Relationship between potential and logarithmic converted current density, showing the Tafel region under different pulse conditions.

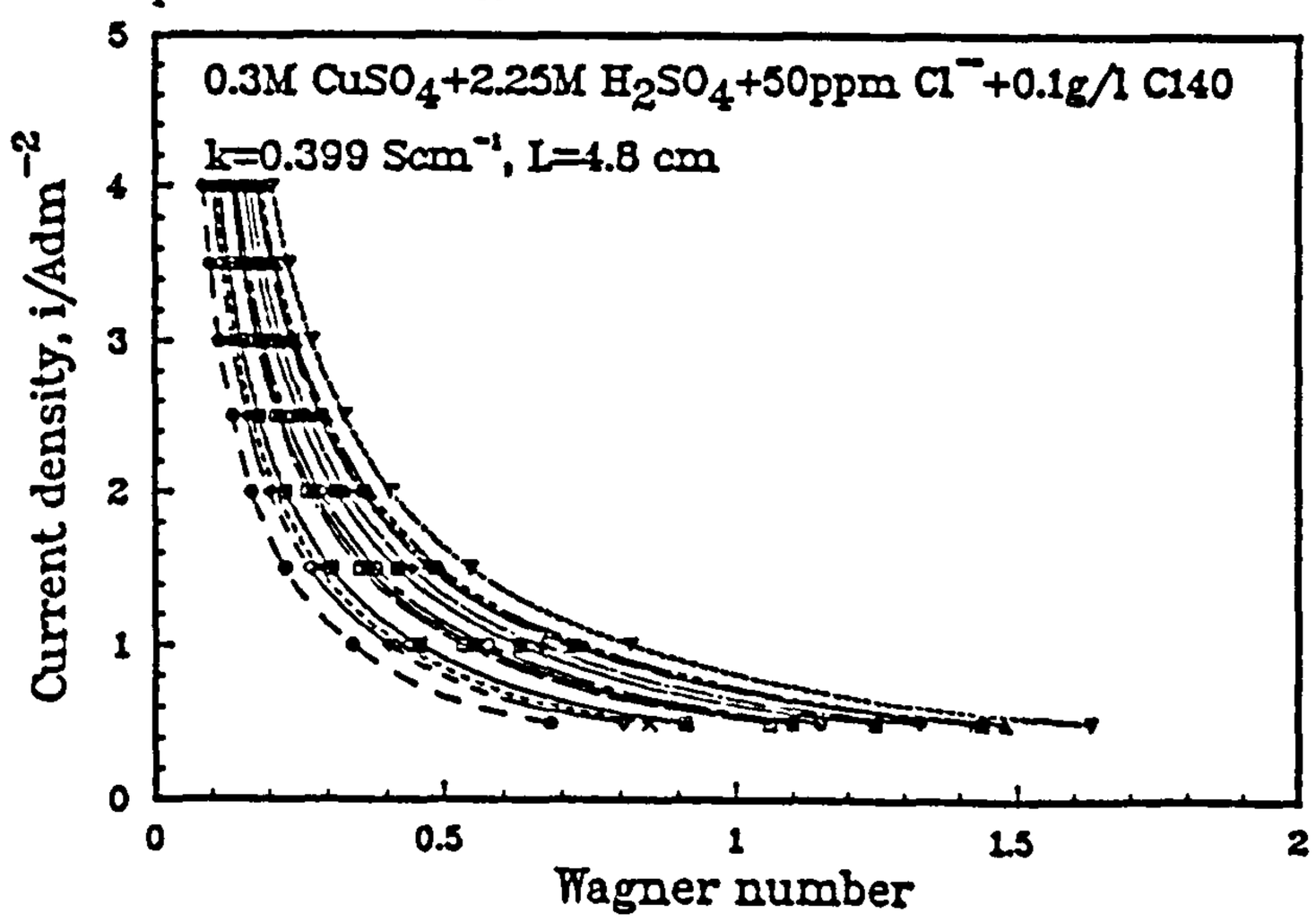

Figure 76c Relationship between current density and Wagner number under different pulse conditions.

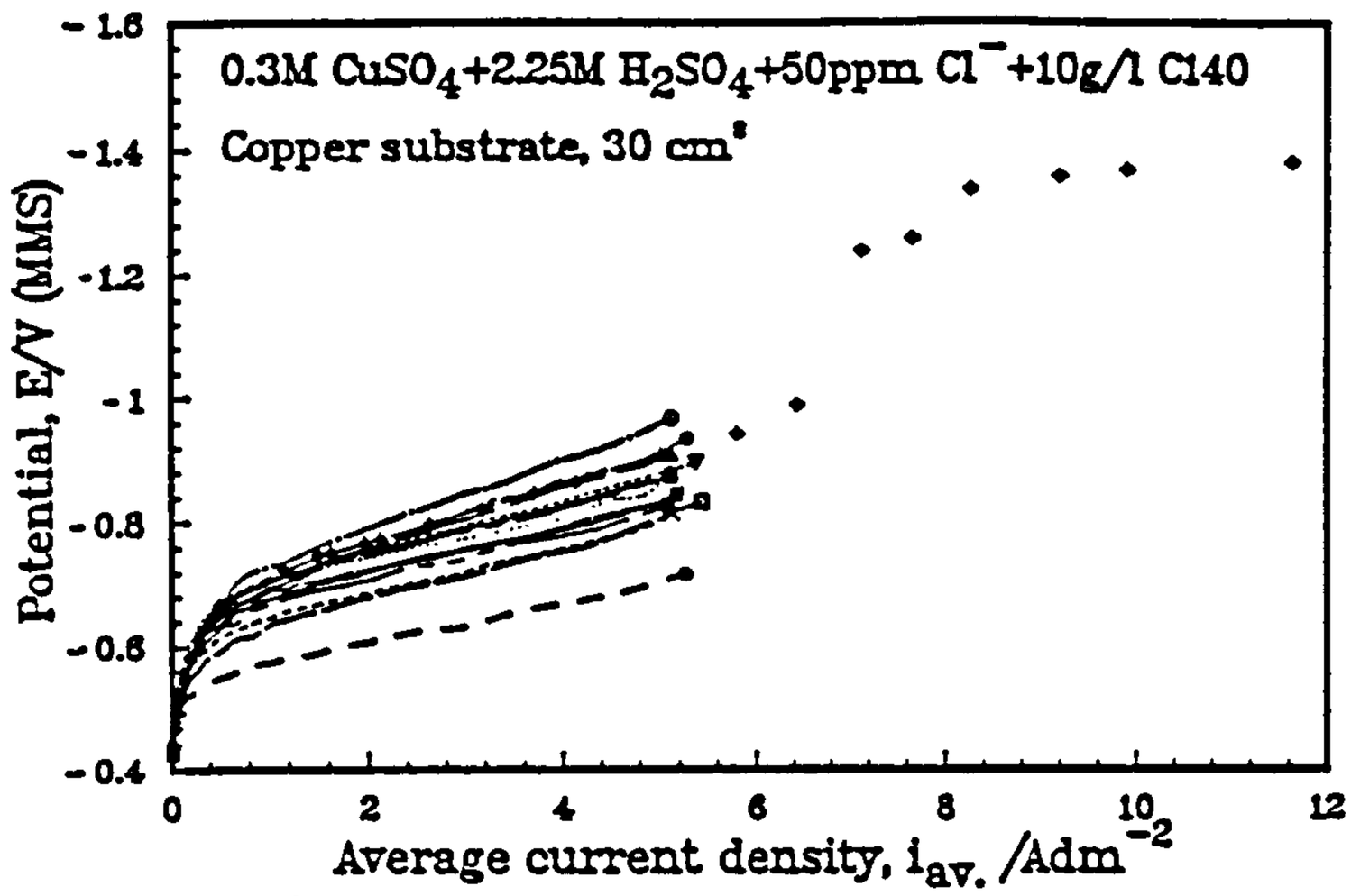

Figure 77a Polarisation curves obtained using the pulse unit and power supply - constant current; air and reciprocating agitations combined, DVM data.

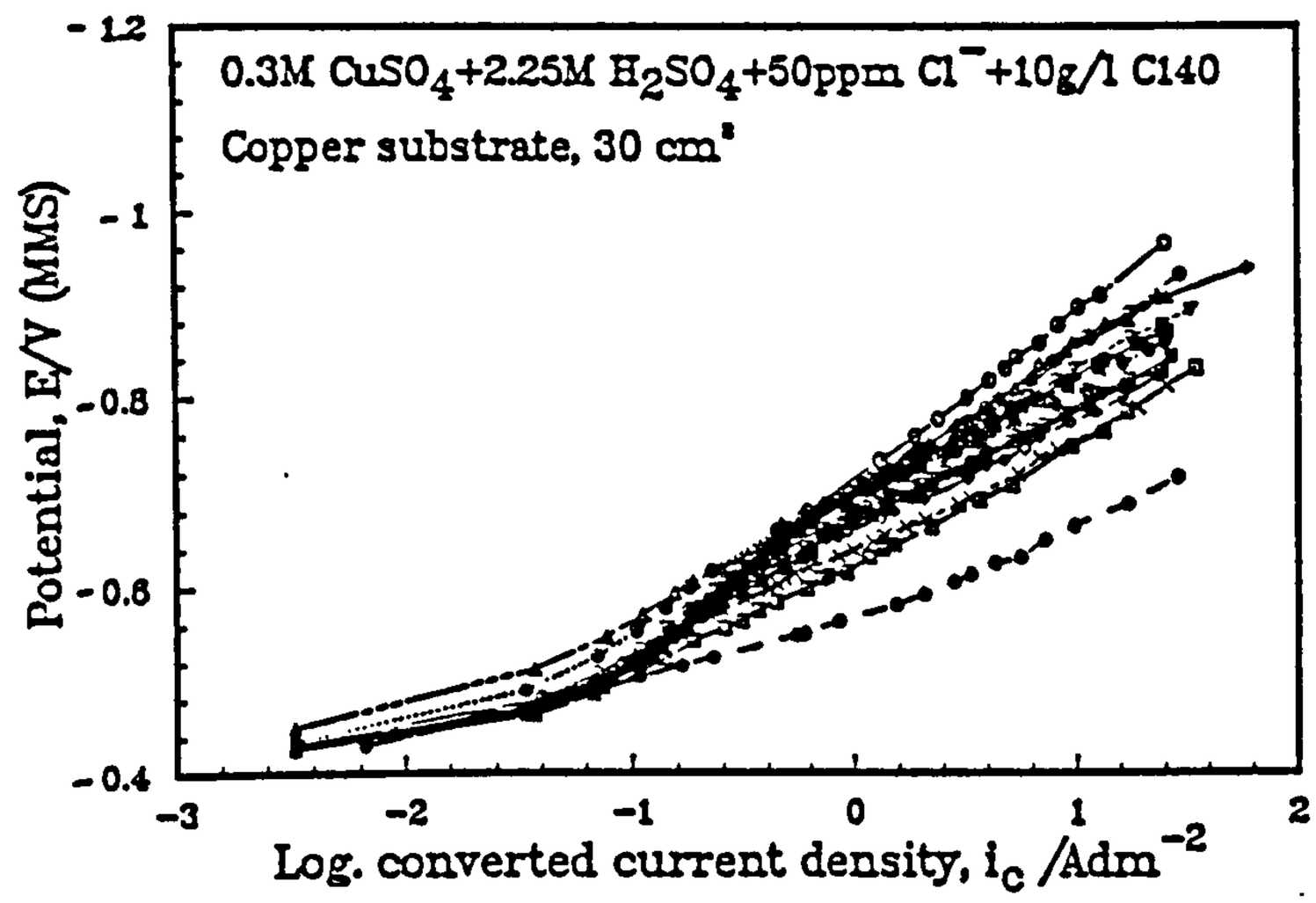

Legend

- 20Hz,75%0,f
- 20Hz,50%0,f
- 20Hz,25%0,f
- 500Hz,75%0,f
- 500Hz,50%0,f
- 500Hz,25%0,f
- 1000Hz,75%0,f
- 1000Hz,50%0,f
- 1000Hz,25%0,f
- 2000Hz,75%0,f
- 2000Hz,50%0,f
- 2000Hz,25%0,f
- 5000Hz,75%0,f
- 5000Hz,50%0,f
- 5000Hz,25%0,f

Figure 77b Relationship between potential and logarithmic converted current density, showing the Tafel region under different pulse conditions.

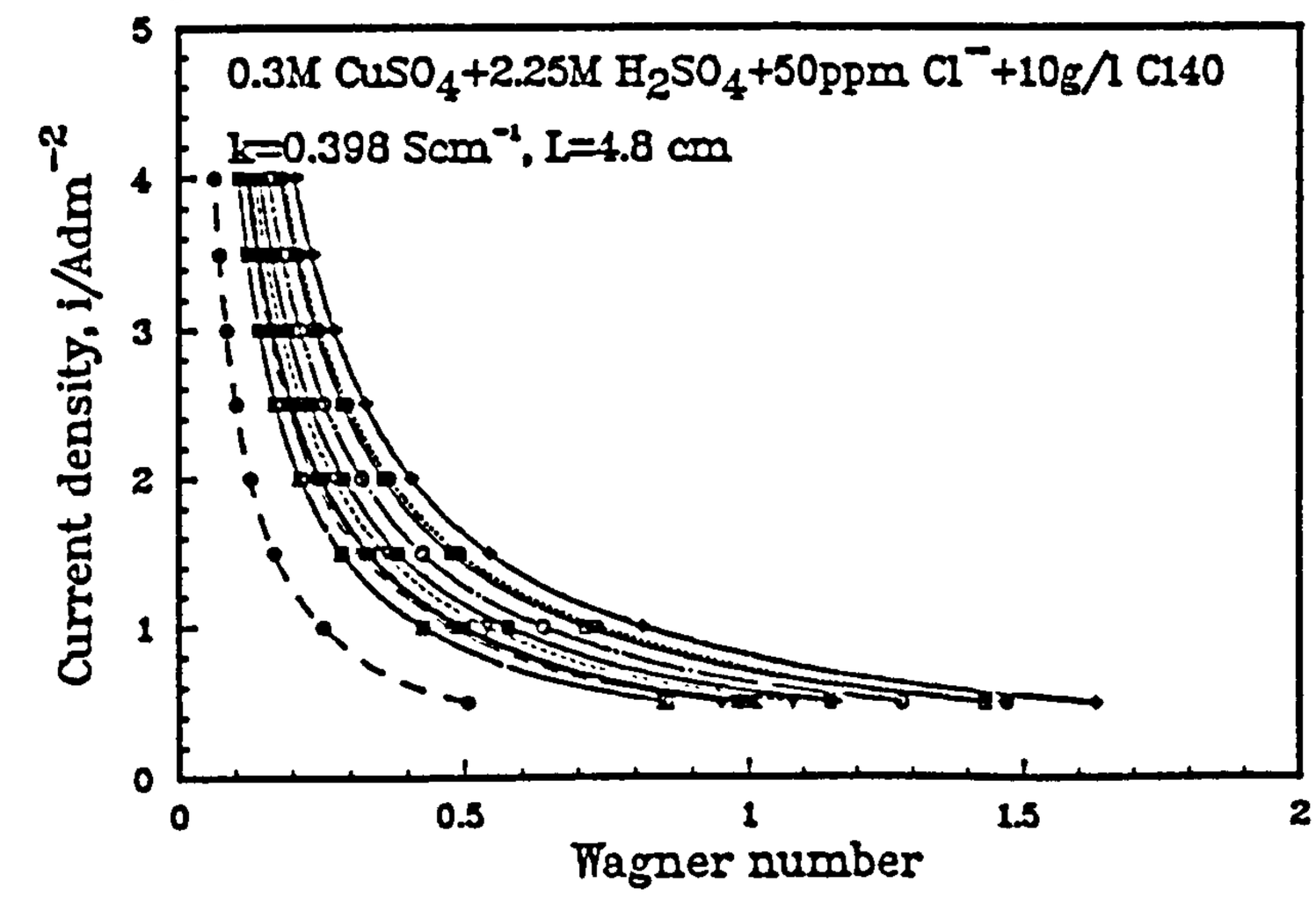

Figure 77c Relationship between current density and Wagner number under different pulse conditions.

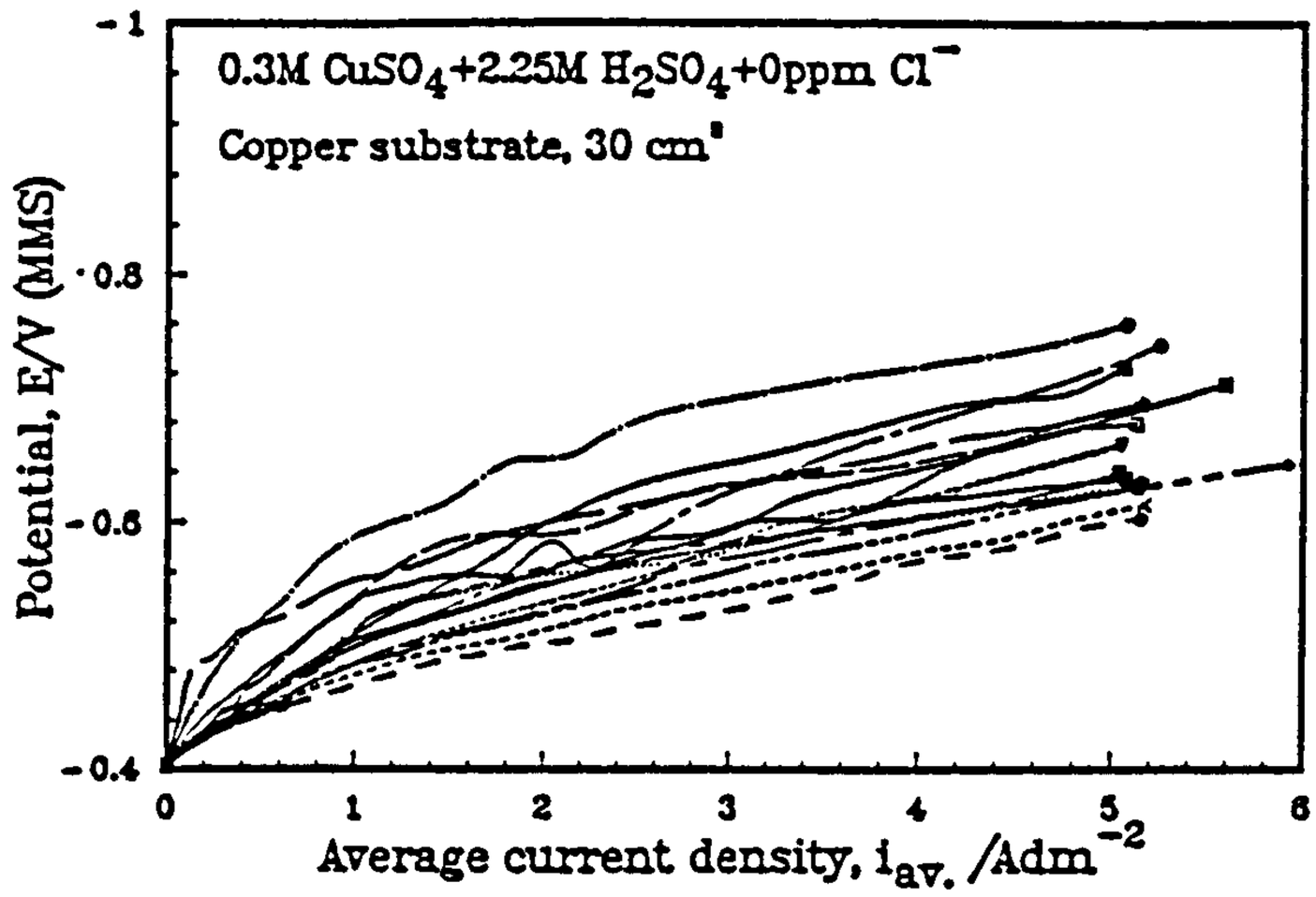

Figure 78a Polarisation curves obtained using the pulse unit and power supply - constant current; air and reciprocating agitations combined, DVM data.

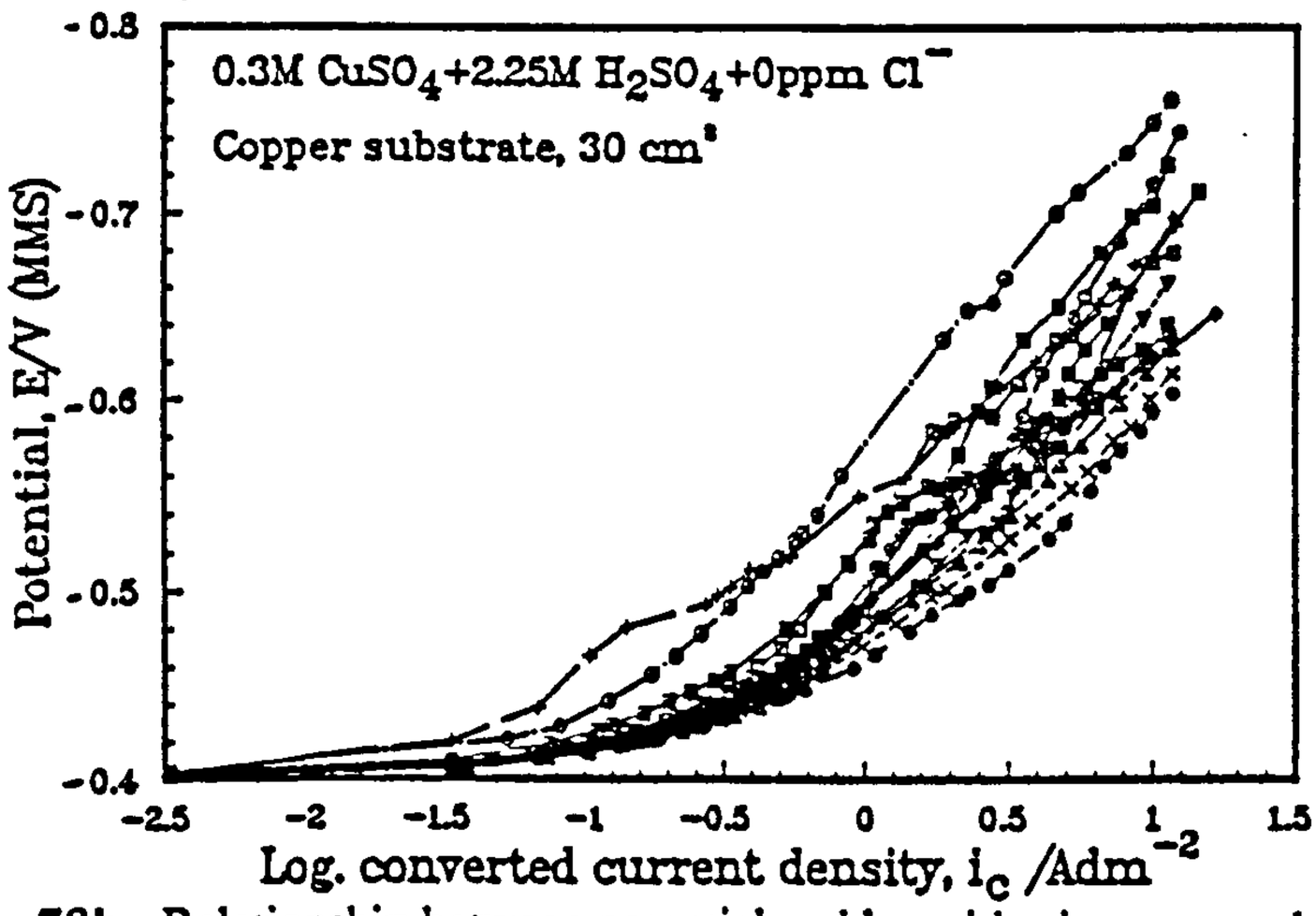

Legend
- 20Hz,75%0,f
- 20Hz,50%0,f
- 20Hz,25%0,f
- 500Hz,75%0,f
- 500Hz,50%0,f
- 500Hz,25%0,f
- 1000Hz,75%0,f
- 1000Hz,50%0,f
- 1000Hz,25%0,f
- 2000Hz,75%0,f
- 2000Hz,50%0,f
- 2000Hz,25%0,f
- 5000Hz,75%0,f
- 5000Hz,50%0,f
- 5000Hz,25%0,f

Figure 78b Relationship between potential and logarithmic converted current density, showing the Tafel region under different pulse conditions.

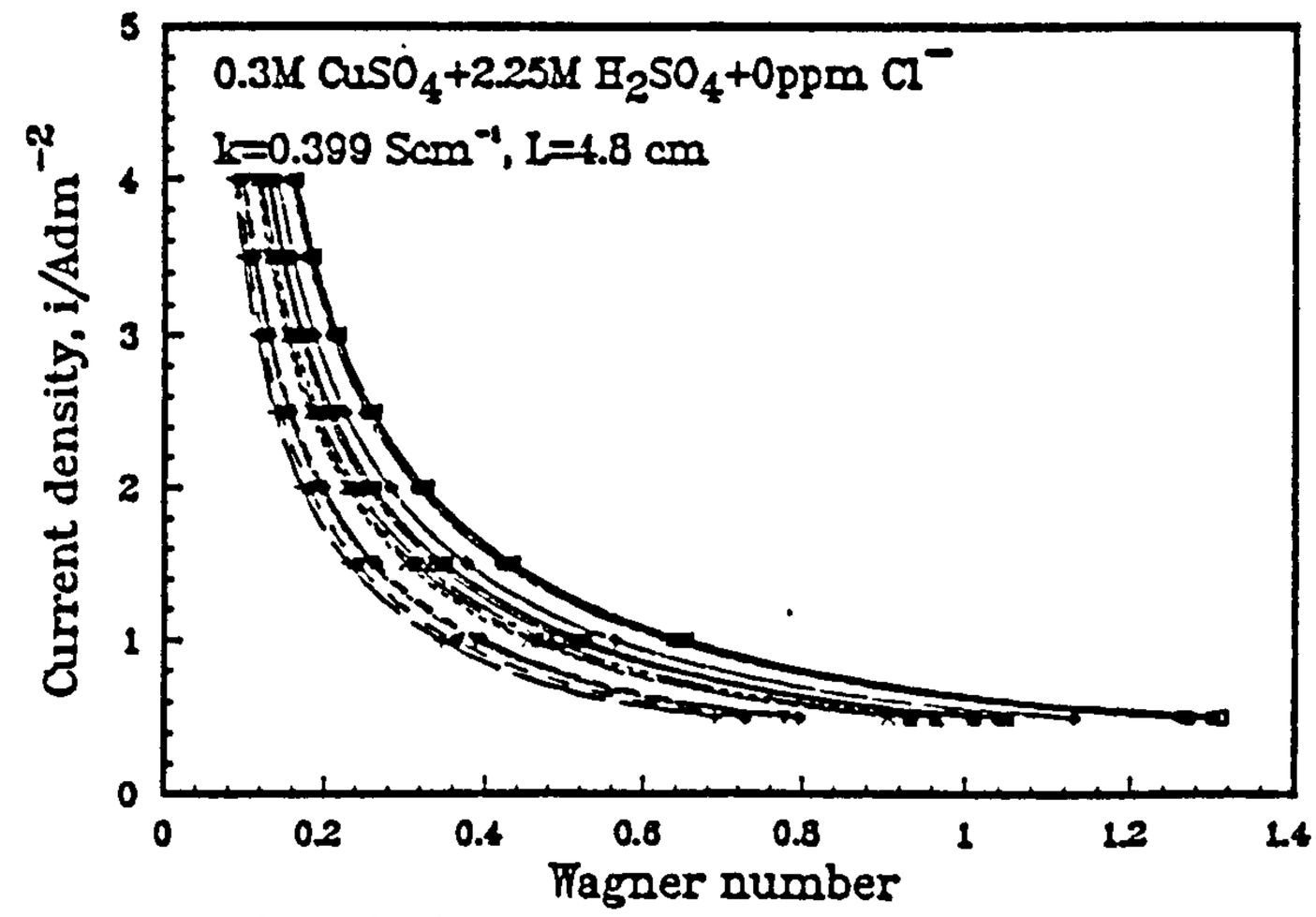

Figure 78c Relationship between current density and Wagner number under different pulse conditions.

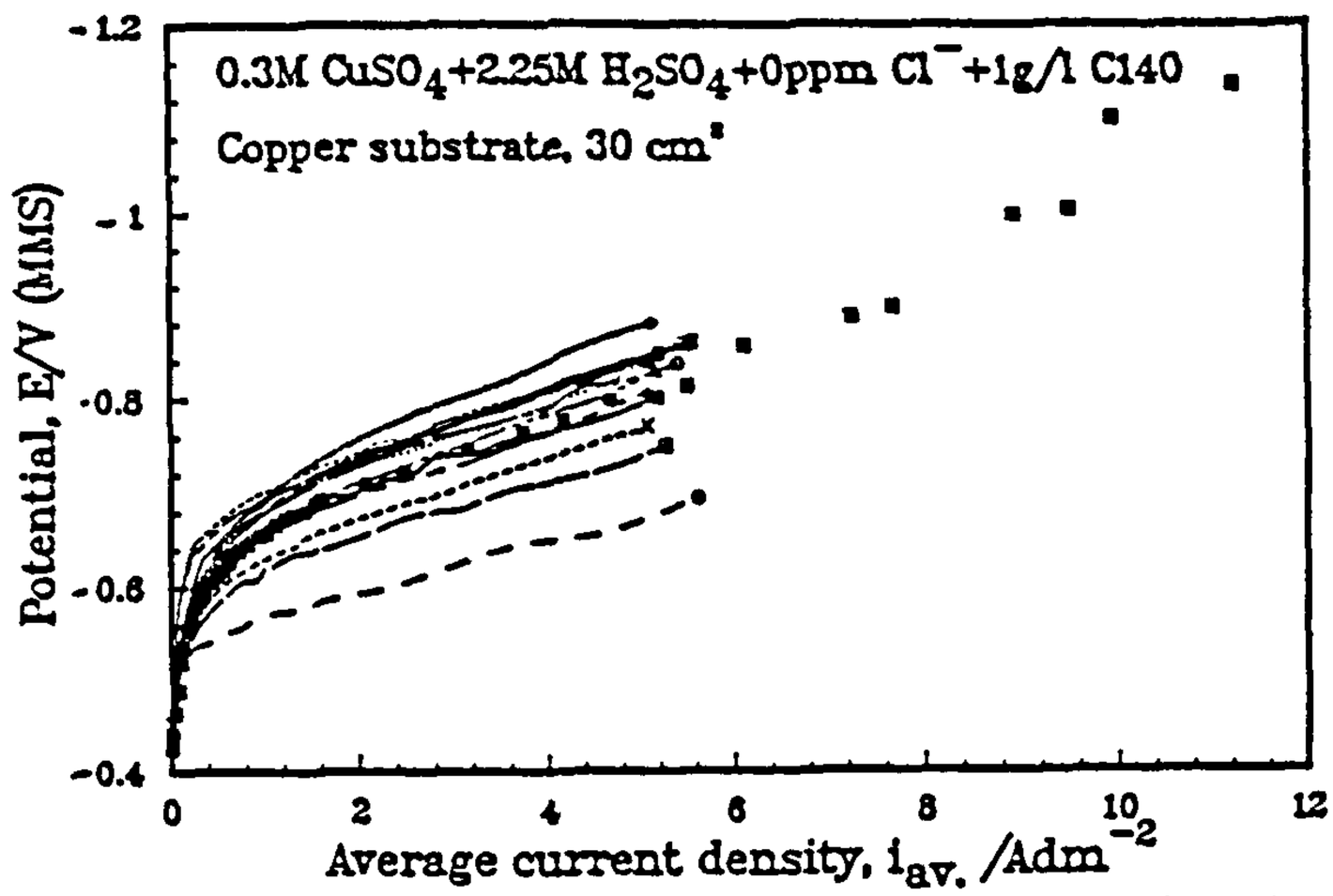

Figure 79a Polarisation curves obtained using the pulse unit and power supply - constant current; air and reciprocating agitations combined, DVM data.

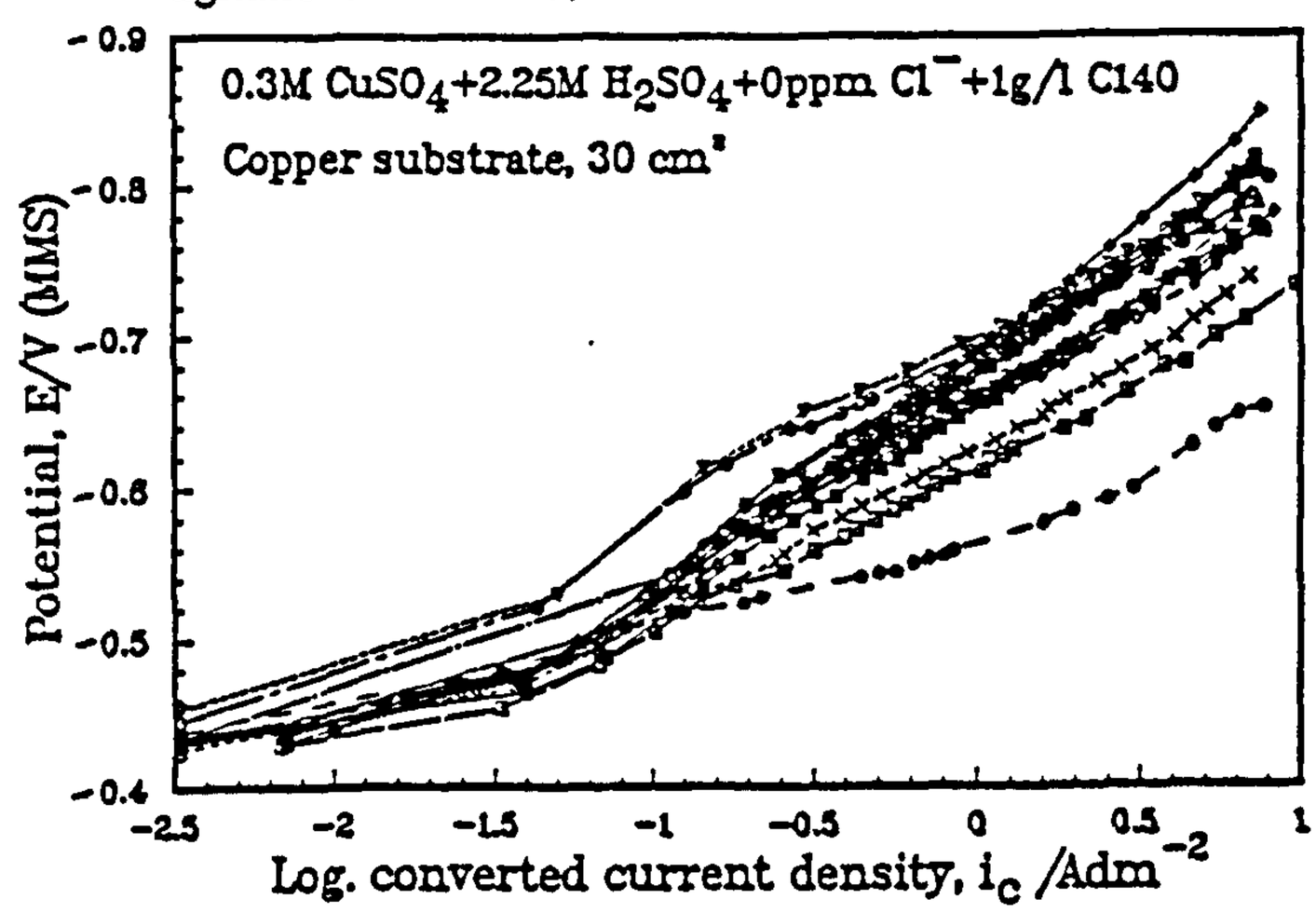

Legend

- 20Hz,75%0,f
- 20Hz,50%0,f
- 20Hz,25%0,f
- 500Hz,75%0,f
- 500Hz,50%0,f
- 500Hz,25%0,f
- 1000Hz,75%0,f
- 1000Hz,50%0,f
- 1000Hz,25%0,f
- 2000Hz,75%0,f
- 2000Hz,50%0,f
- 2000Hz,25%0,f
- 5000Hz,75%0,f
- 5000Hz,50%0,f
- 5000Hz,25%0,f

Figure 79b Relationship between potential and logarithmic converted current density, showing the Tafel region under different pulse conditions.

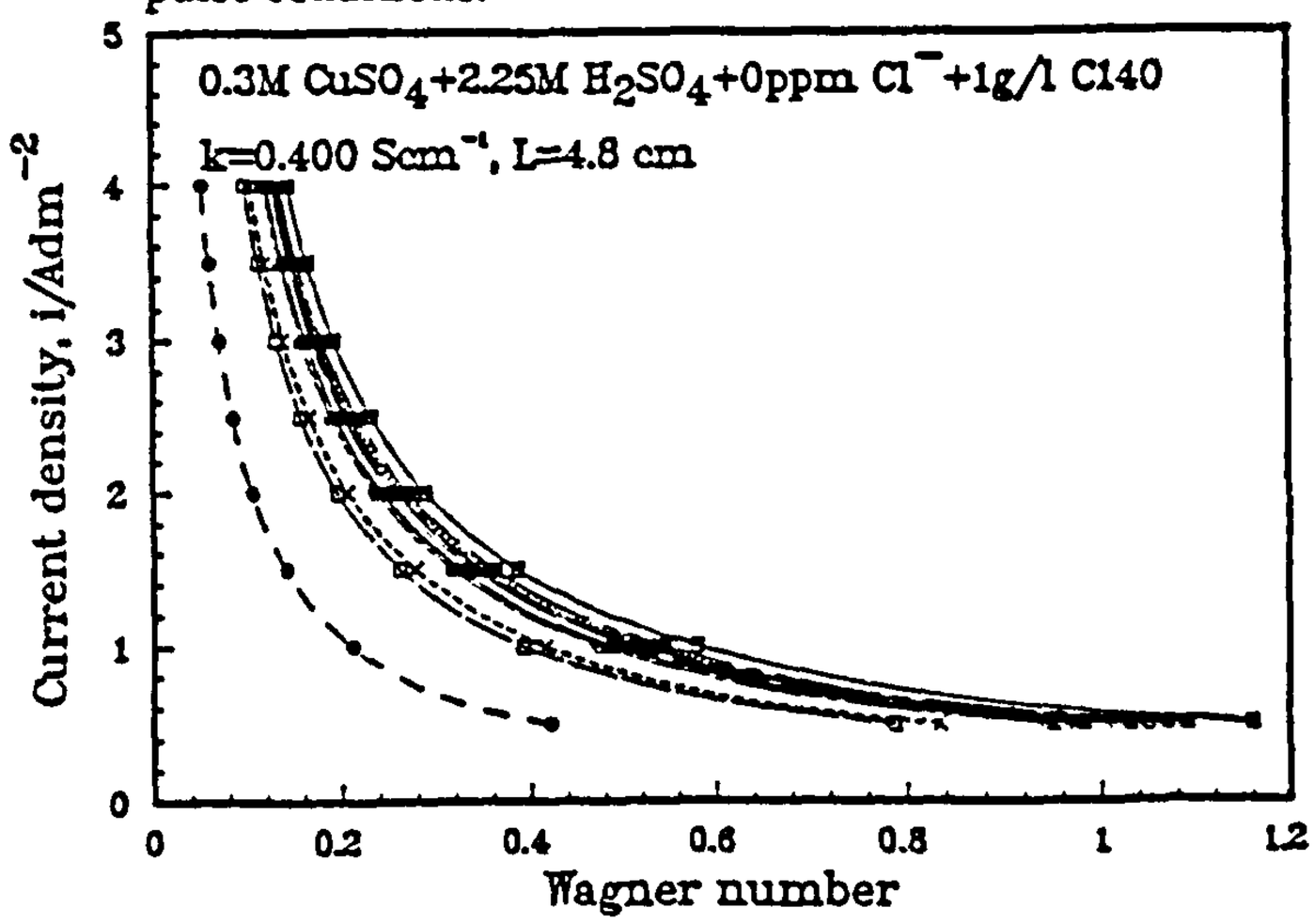

Figure 79c Relationship between current density and Wagner number under different pulse conditions.

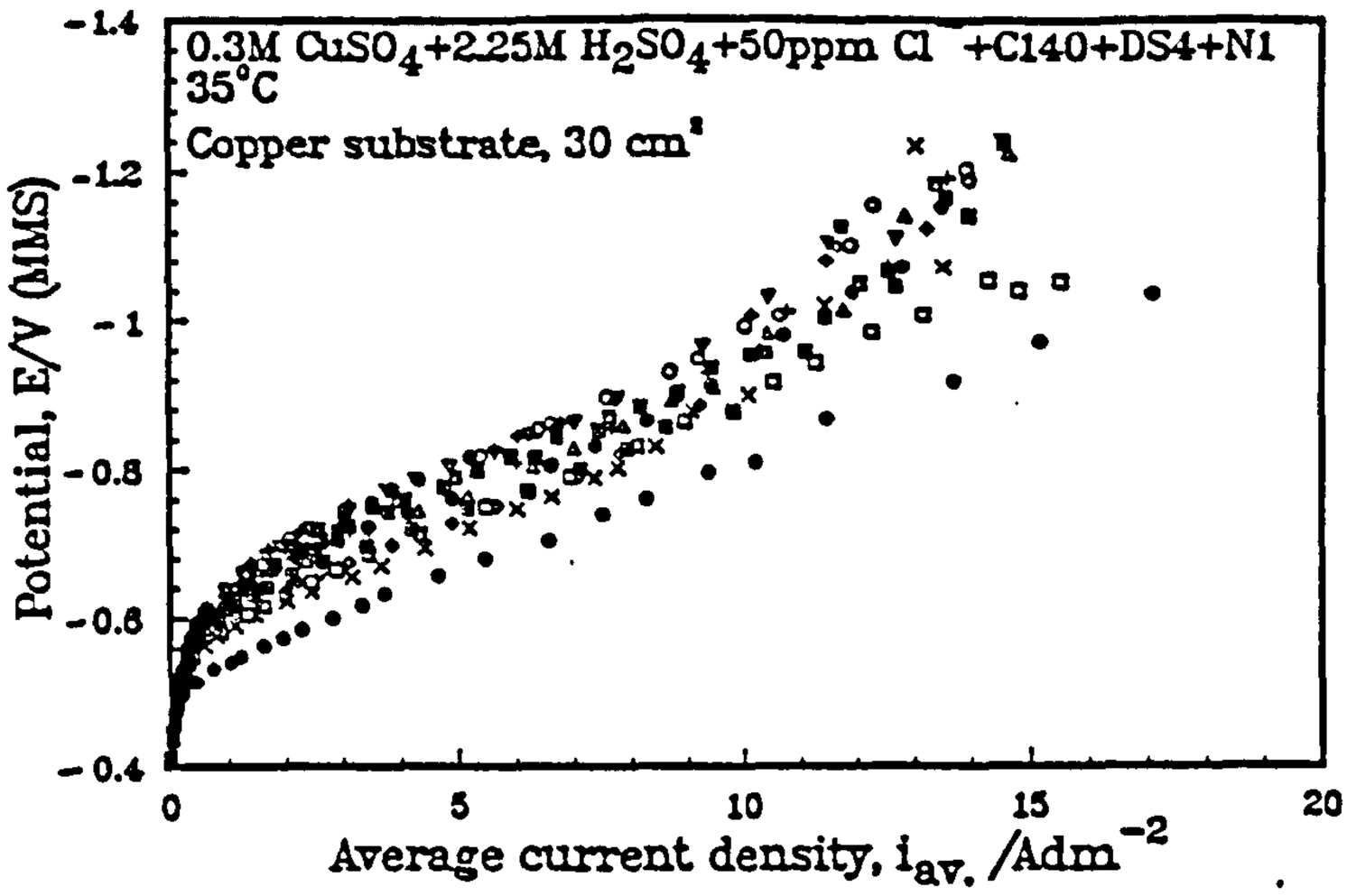

Figure 80a Polarisation curves obtained using the pulse unit and power supply - constant current; air and reciprocating agitations combined, DVM data.

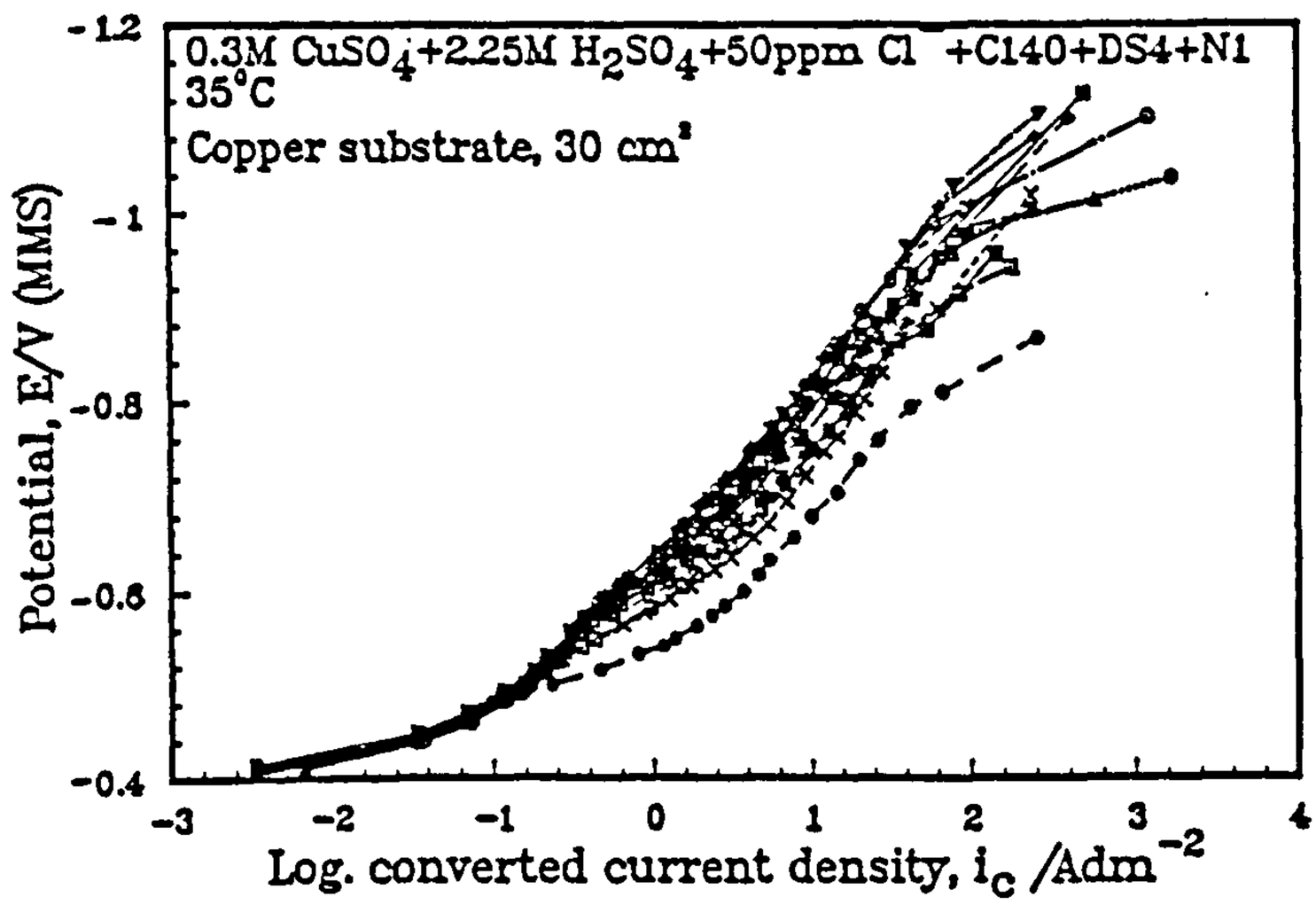

Legend

- 20Hz,75%0,f
- 20Hz,50%0,f
- 20Hz,25%0,f
- 500Hz,75%0,f
- 500Hz,50%0,f
- 500Hz,25%0,f
- 1000Hz,75%0,f
- 1000Hz,50%0,f
- 1000Hz,25%0,f
- 2000Hz,75%0,f
- 2000Hz,50%0,f
- 2000Hz,25%0,f
- 5000Hz,75%0,f
- 5000Hz,50%0,f
- 5000Hz,25%0,f

Figure 80b Relationship between potential and logarithmic converted current density, showing the Tafel region under different pulse conditions.

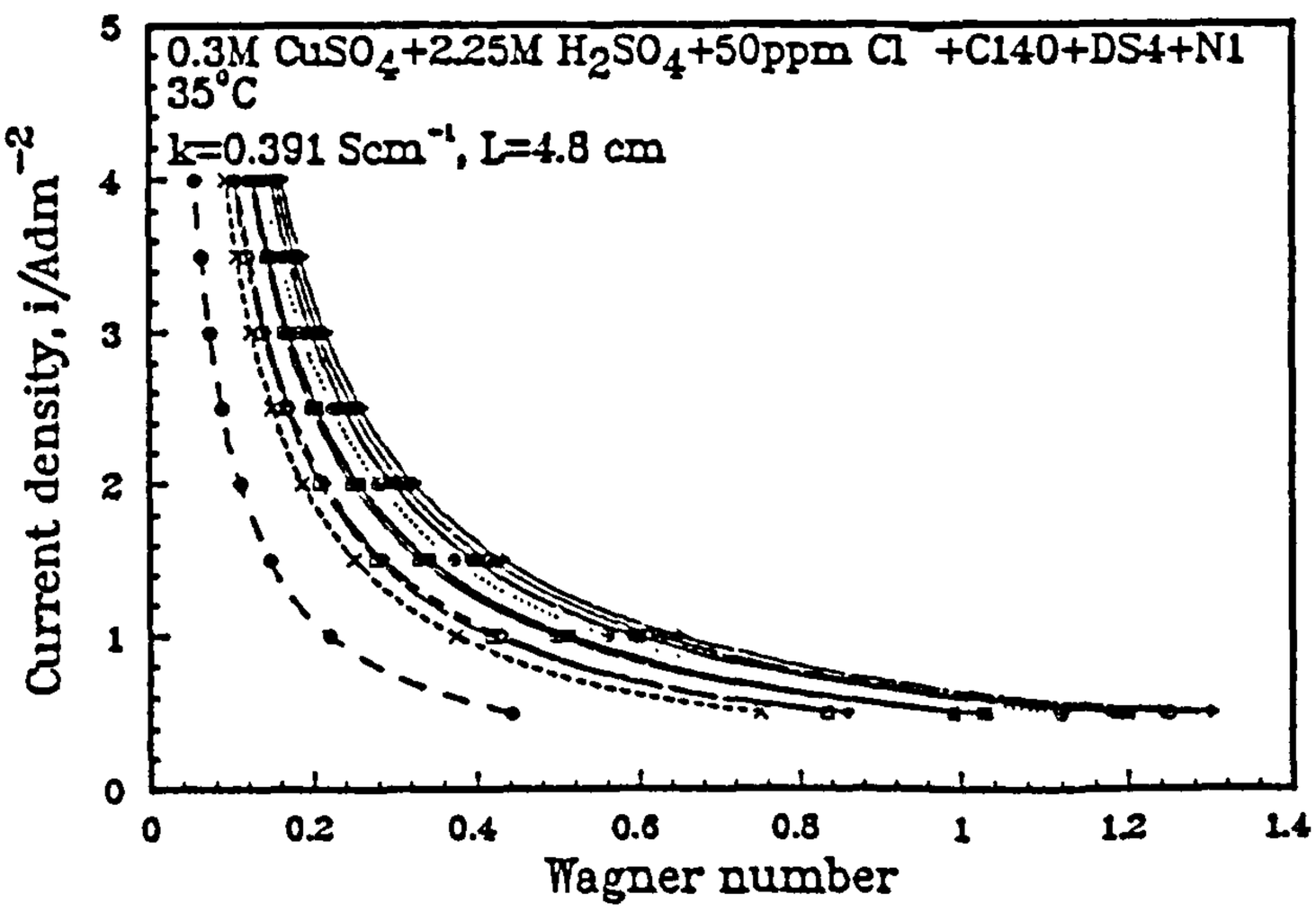

Figure 80c Relationship between current density and Wagner number under different pulse conditions.

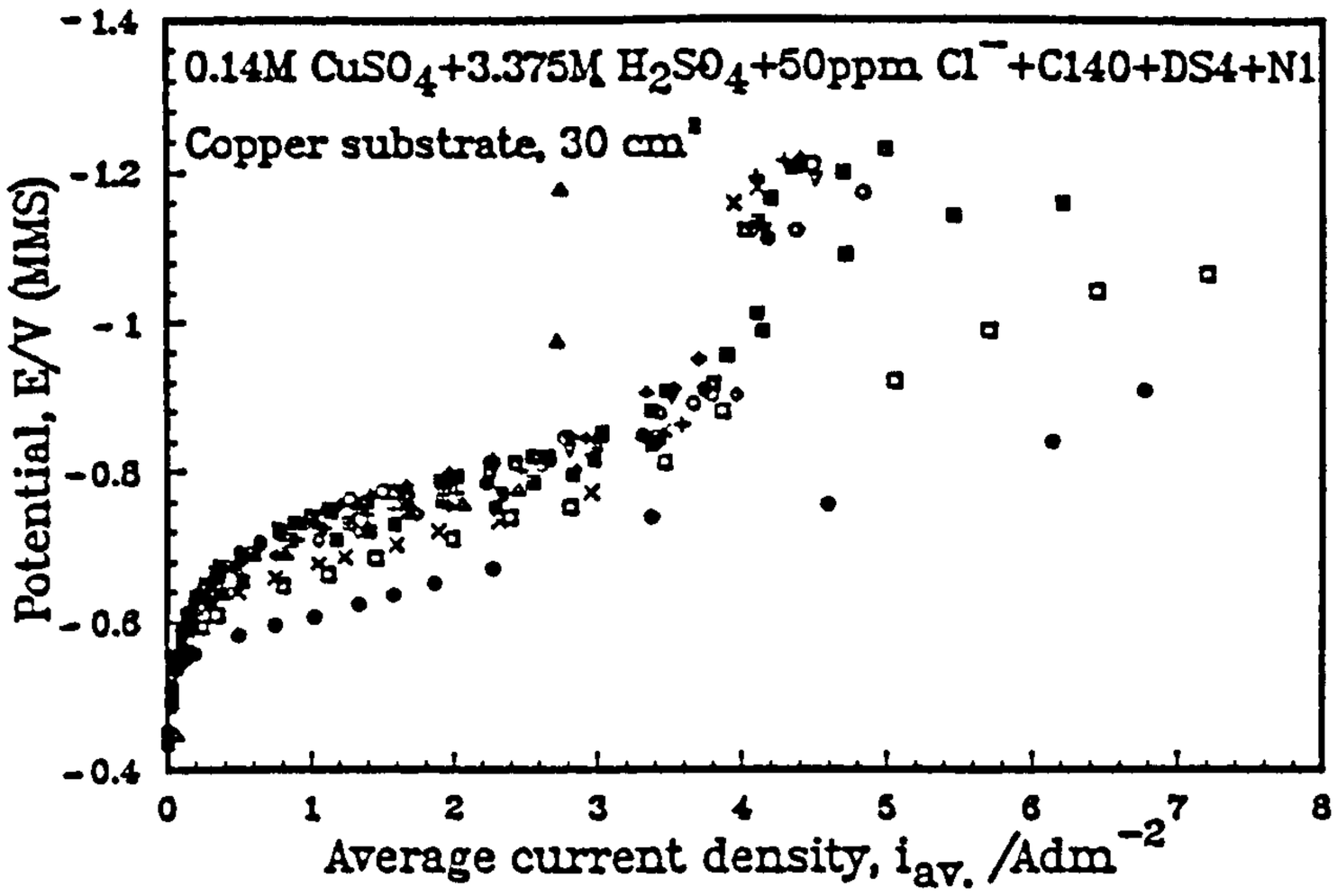

Figure 81a Polarisation curves obtained using the pulse unit and power supply - constant current; air and reciprocating agitations combined, DVM data.

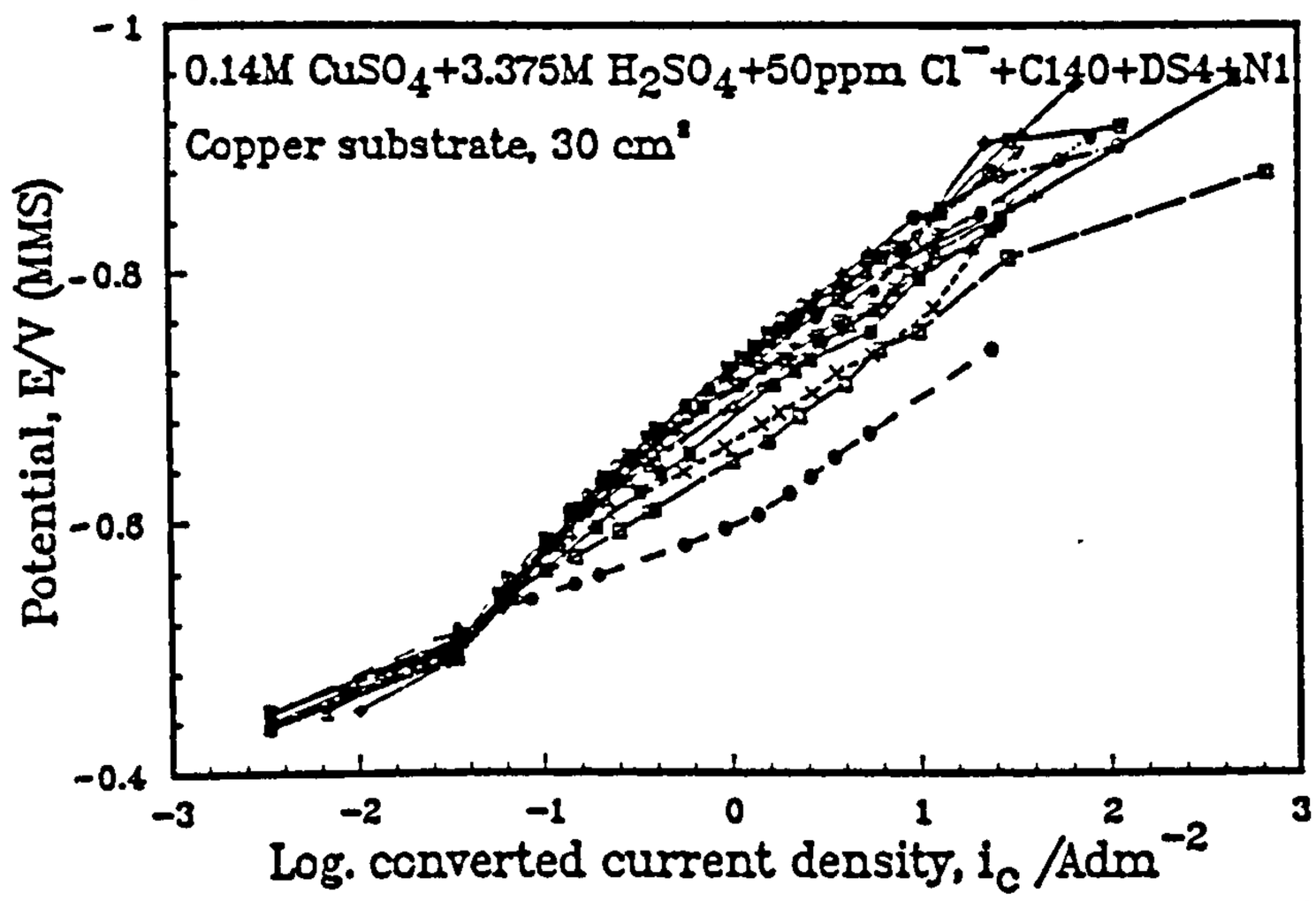

Figure 81b Relationship between potential and logarithmic converted current density, showing the Tafel region under different pulse conditions.

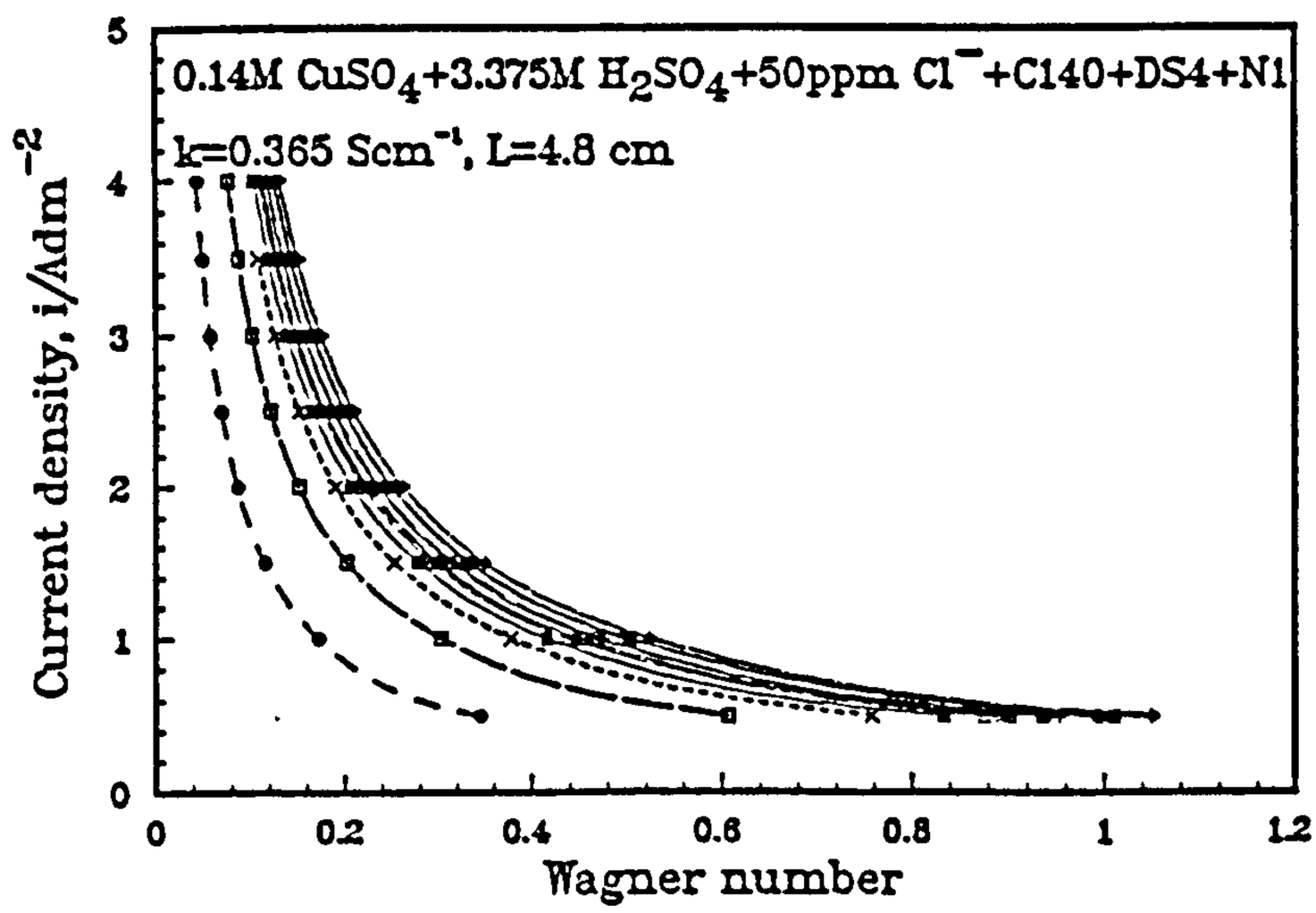

Figure 81c Relationship between current density and Wagner number under different pulse conditions.

Legend

- 20Hz,75%0,f
- 20Hz,50%0,f
- 20Hz,25%0,f
- 500Hz,75%0,f
- 500Hz,50%0,f
- 500Hz,25%0,f
- 1000Hz,75%0,f
- 1000Hz,50%0,f
- 1000Hz,25%0,f
- 2000Hz,75%0,f
- 2000Hz,50%0,f
- 2000Hz,25%0,f
- 5000Hz,75%0,f
- 5000Hz,50%0,f
- 5000Hz,25%0,f

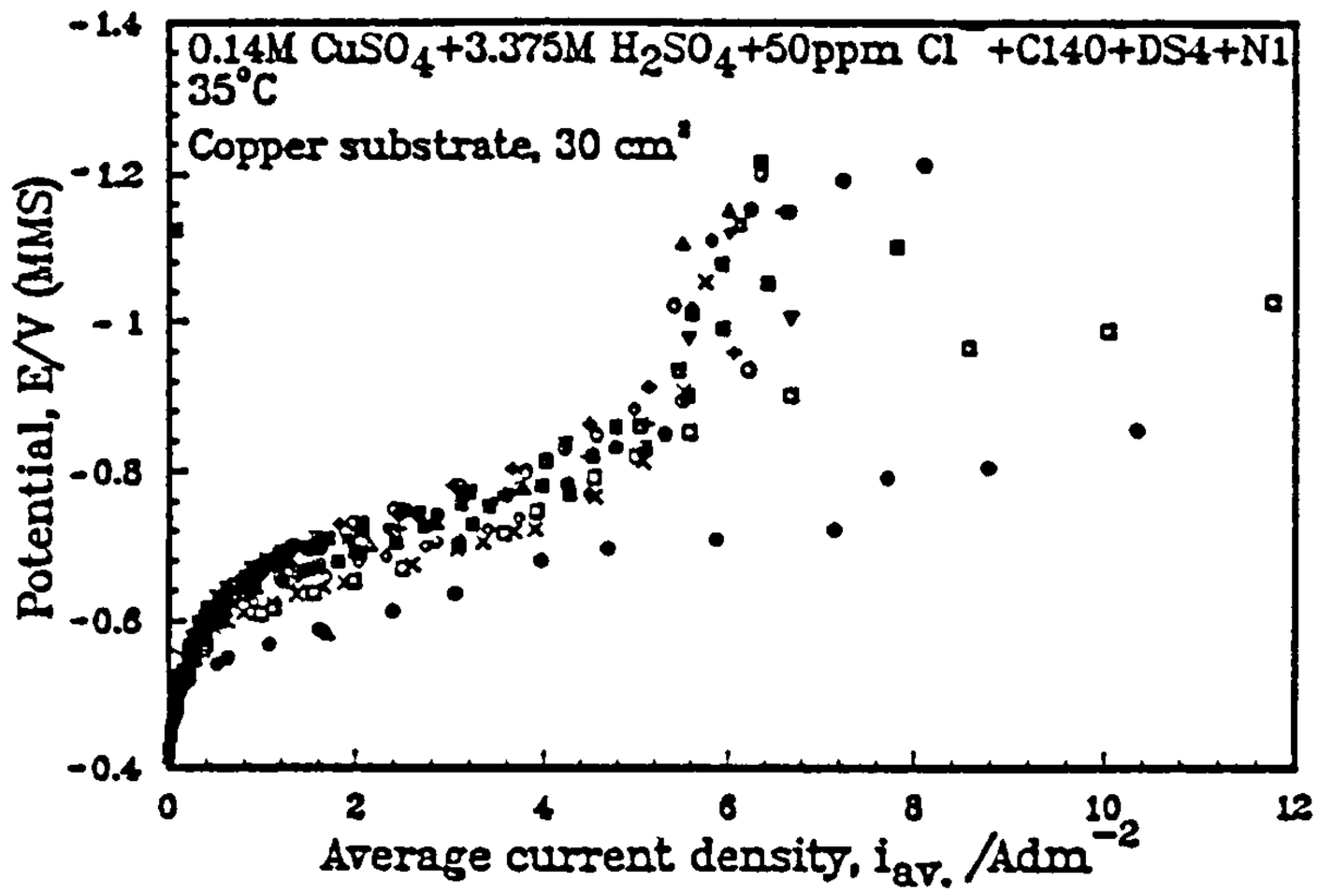

Figure 82a Polarisation curves obtained using the pulse unit and power supply - constant current; air and reciprocating agitations combined, DVM data.

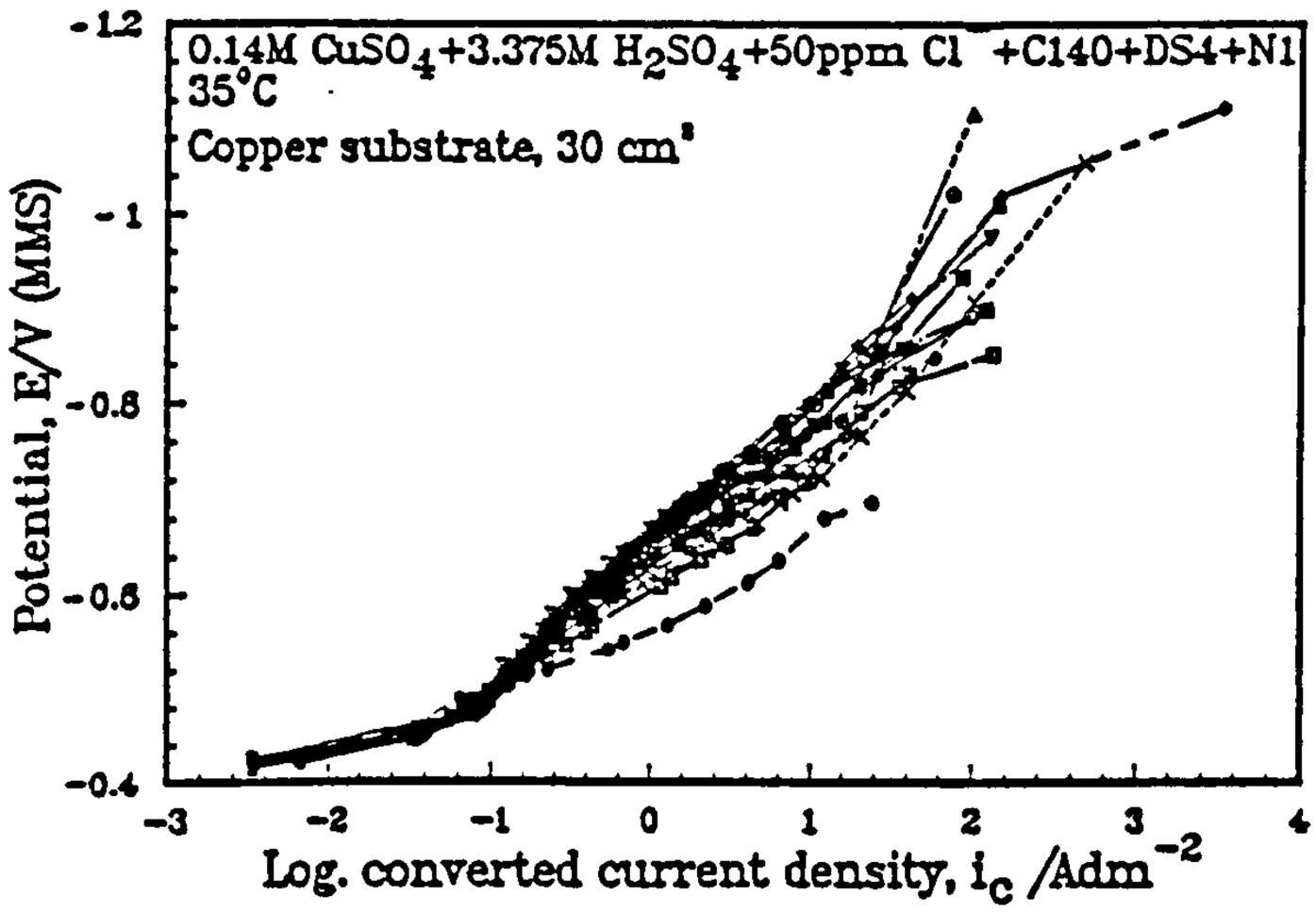

Legend

- 20Hz,75%0,f
- 20Hz,50%0,f
- 20Hz,25%0,f
- 500Hz,75%0,f
- 500Hz,50%0,f
- 500Hz,25%0,f
- 1000Hz,75%0,f
- 1000Hz,50%0,f
- 1000Hz,25%0,f
- 2000Hz,75%0,f
- 2000Hz,50%0,f
- 2000Hz,25%0,f
- 5000Hz,75%0,f
- 5000Hz,50%0,f
- 5000Hz,25%0,f

Figure 82b Relationship between potential and logarithmic converted current density, showing the Tafel region under different pulse conditions.

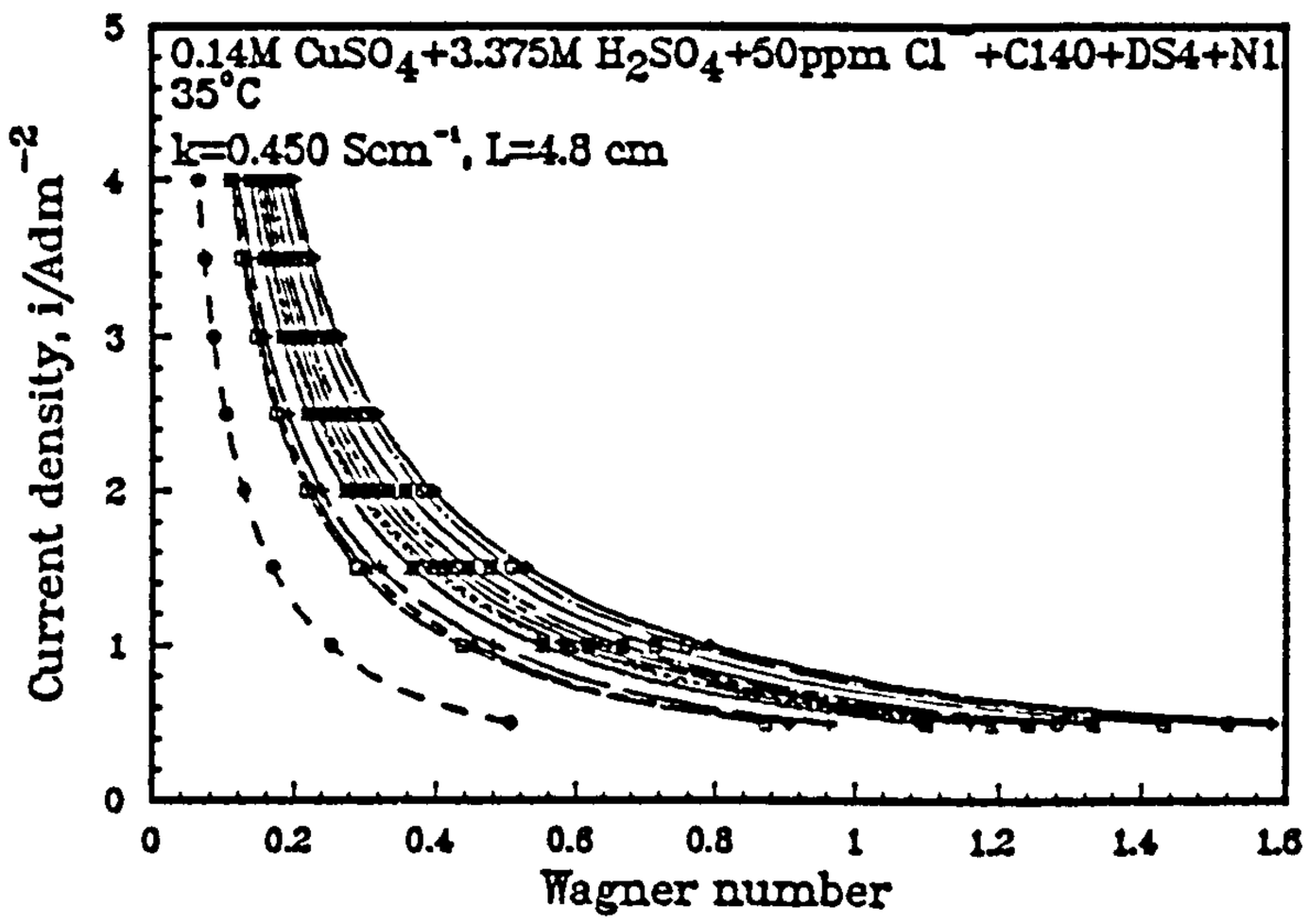

Figure 82c Relationship between current density and Wagner number under different pulse conditions.

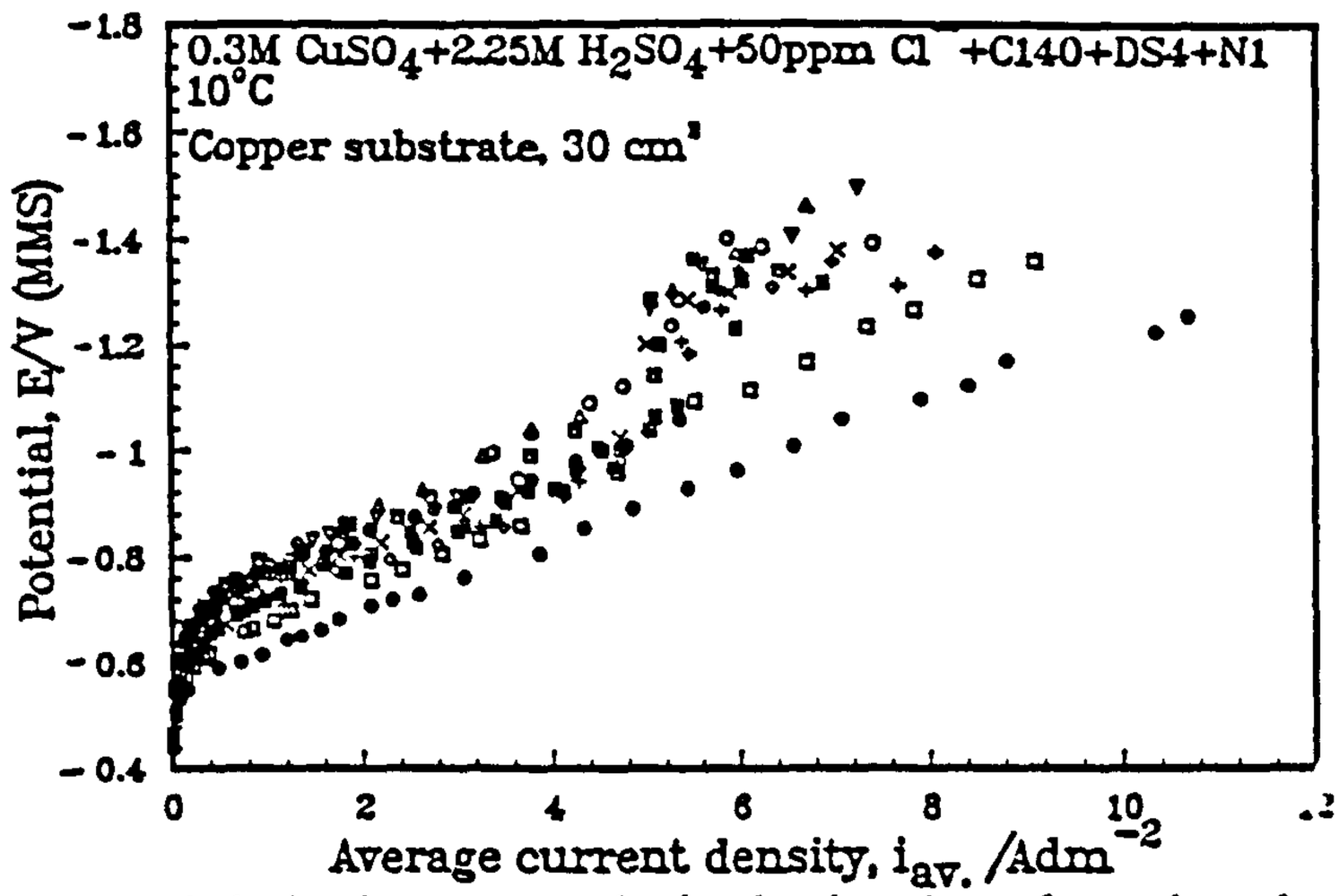

Figure 83a Polarisation curves obtained using the pulse unit and power supply - constant current; air and reciprocating agitations combined, DVM data.

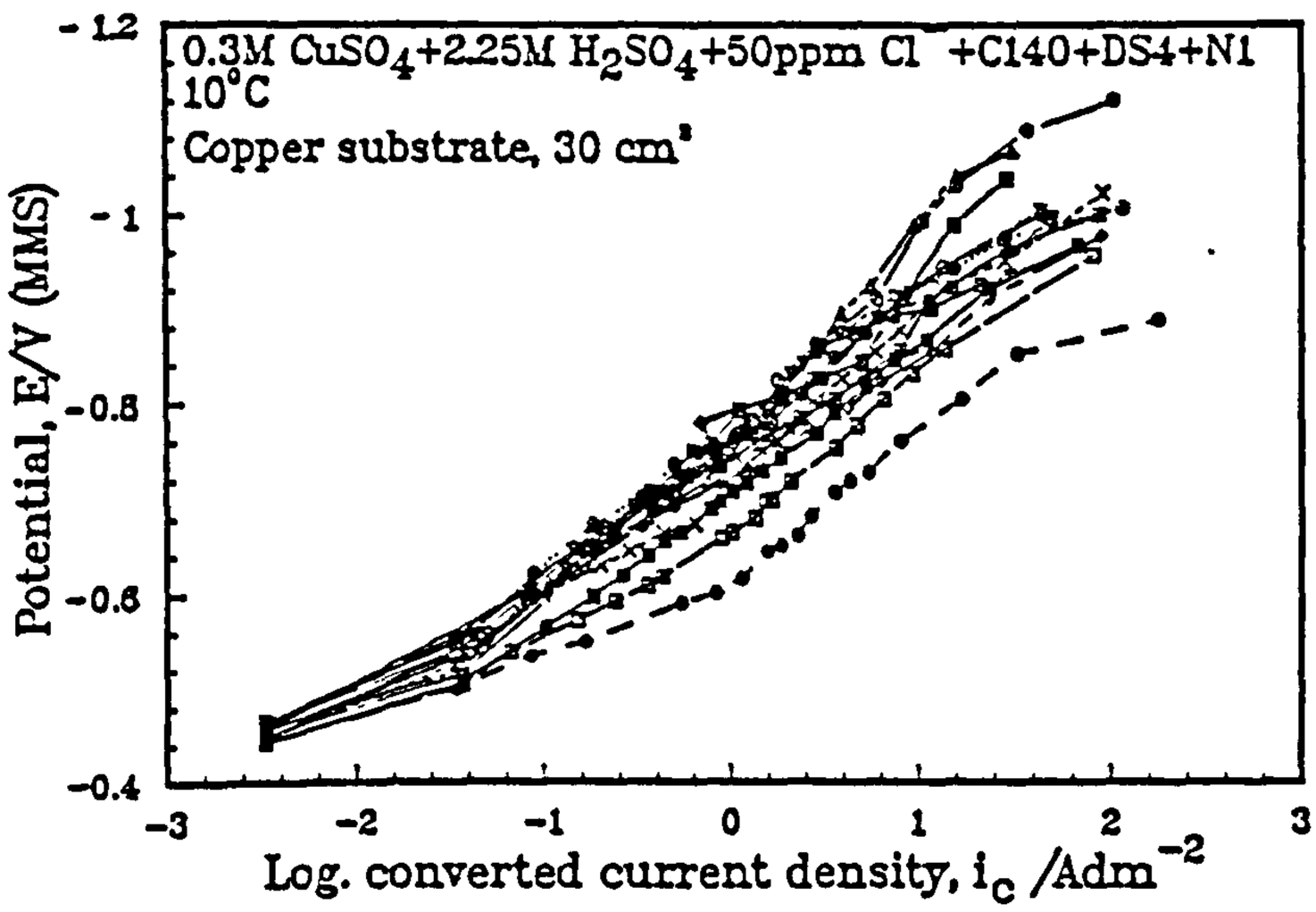

Legend

- 20Hz,75%0,f
- 20Hz,50%0,f
- 20Hz,25%0,f
- 500Hz,75%0,f
- 500Hz,50%0,f
- 500Hz,25%0,f
- 1000Hz,75%0,f
- 1000Hz,50%0,f
- 1000Hz,25%0,f
- 2000Hz,75%0,f
- 2000Hz,50%0,f
- 2000Hz,25%0,f
- 5000Hz,75%0,f
- 5000Hz,50%0,f
- 5000Hz,25%0,f

Figure 83b Relationship between potential and logarithmic converted current density, showing the Tafel region under different pulse conditions.

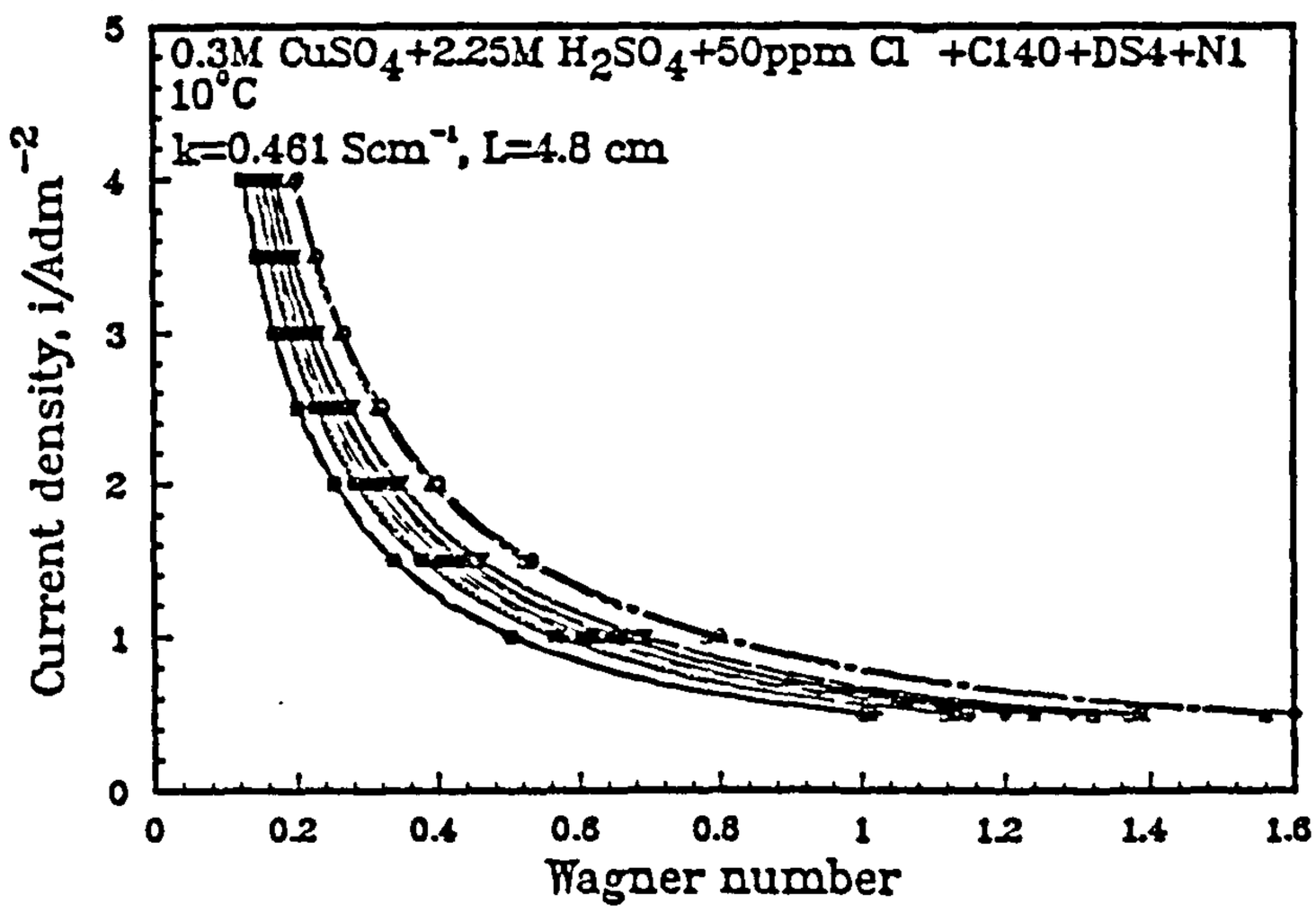

Figure 83c Relationship between current density and Wagner number under different pulse conditions.

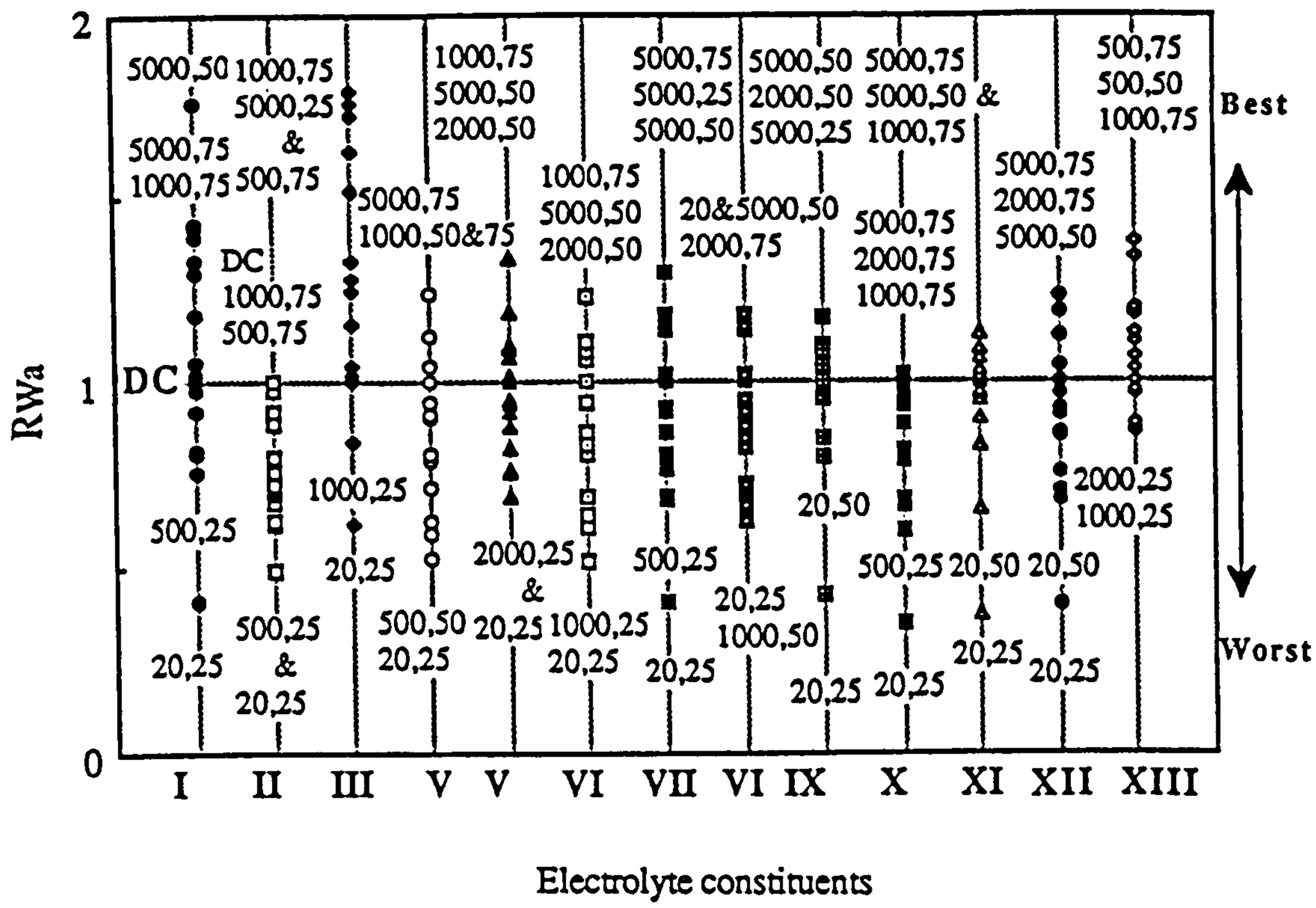

Figure 84 RWa versus electrolyte constituents, at current density of 2.0Adm^{-2}; also shows three best and two worst pulse conditions(Hz,%ϕ).

I- 0.3M $CuSO_4$, 2.25M 98%H_2SO_4, 50ppm Cl^-
II- 0.3M$CuSO_4$, 2.25M 98%H_2SO_4, 50ppm Cl^-, 1g/l C140
III- 0.3M $CuSO_4$, 2.25M 98%H_2SO_4, 50ppm Cl^-, 1g/l C140, 6.25mg/l N1
IV- 0.3M CuSO4, 2.25M 98%H_2SO_4, 50ppm Cl^-, 1g/l C140, 0.625mg/l DS4
V- 0.3M $CuSO_4$, 2.25M 98%H_2SO_4, 50ppm Cl^-, 1g/l C140, 0.625mg/l DS4, 6.25mg/l N1
VI- 0.3M$CuSO_4$, 2.25M 98%H_2SO_4, 50ppm Cl^-, 0.1g/l C140
VII- 0.3M$CuSO_4$, 2.25M 98%H_2SO_4, 50ppm Cl^-, 10g/l C140
VIII- 0.3M $CuSO_4$, 2.25M 98%H_2SO_4, 0ppm Cl^-
IX- 0.3M $CuSO_4$, 2.25M 98%H_2SO_4, 0ppm Cl^-, 1g/l C140
X- 0.3M $CuSO_4$, 2.25M 98%H_2SO_4, 50ppm Cl^-, 1g/l C140, 0.625mg/l DS4, 6.25mg/l N1; 35°C
XI- 0.14M $CuSO_4$, 3.375M 98%H_2SO_4, 50ppm Cl^-, 1g/l C140, 0.625mg/l DS4, 6.25mg/l N1
XII- 0.14M $CuSO_4$, 3.375M 98%H_2SO_4, 50ppm Cl^-, 1g/l C140, 0.625mg/l DS4, 6.25mg/l N1; 35°C
XIII- 0.3M $CuSO_4$, 2.25M 98%H_2SO_4, 50ppm Cl^-, 1g/l C140, 0.625mg/l DS4, 6.25mg/l N1; 10°C

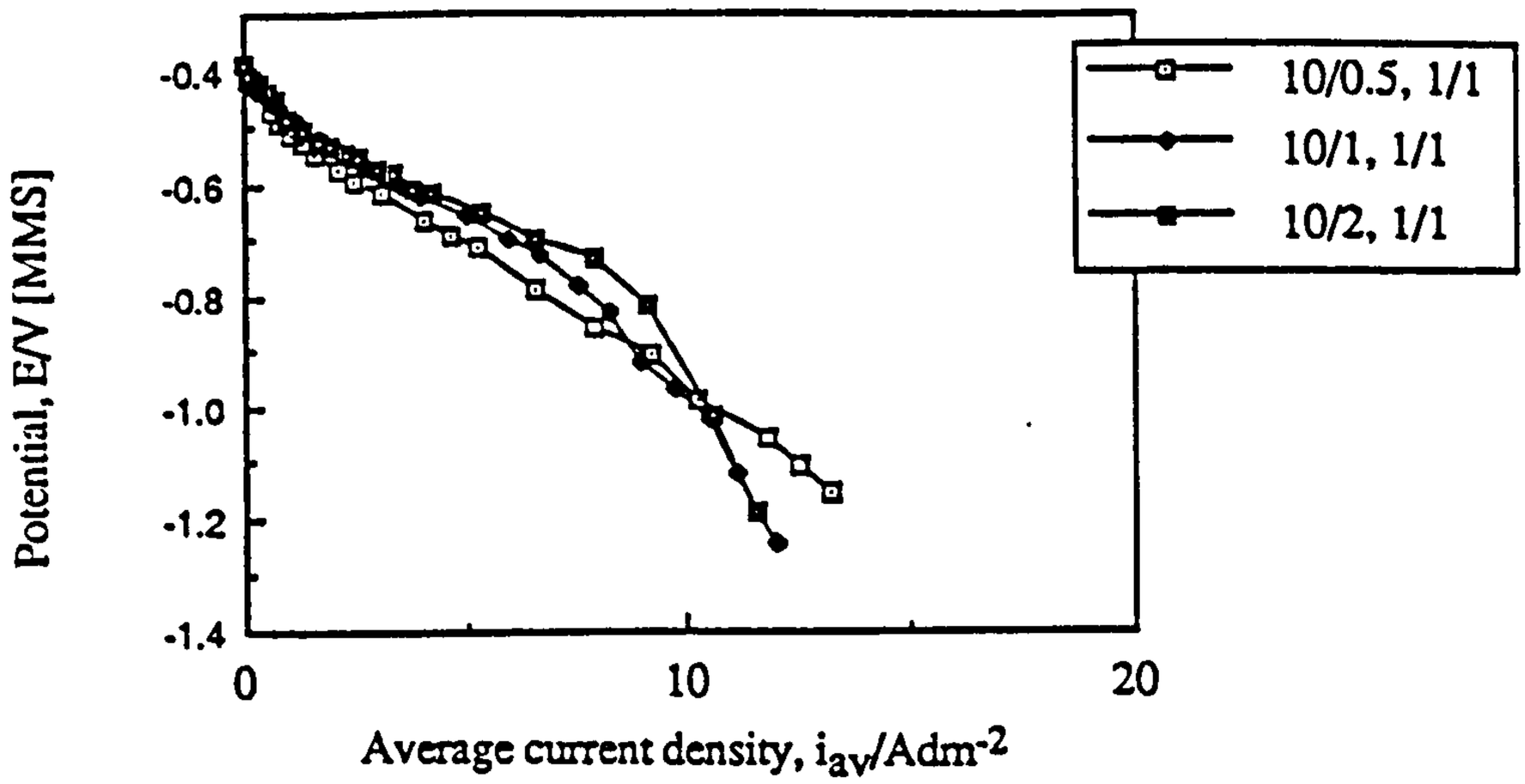

Figure 85a Pulse reverse polarisation curves for different $t_{on(c)}/t_{on(a)}$ ratios but at a $i_{p(c)}/i_{p(a)}$ ratio of 1/1 using electrolyte I.

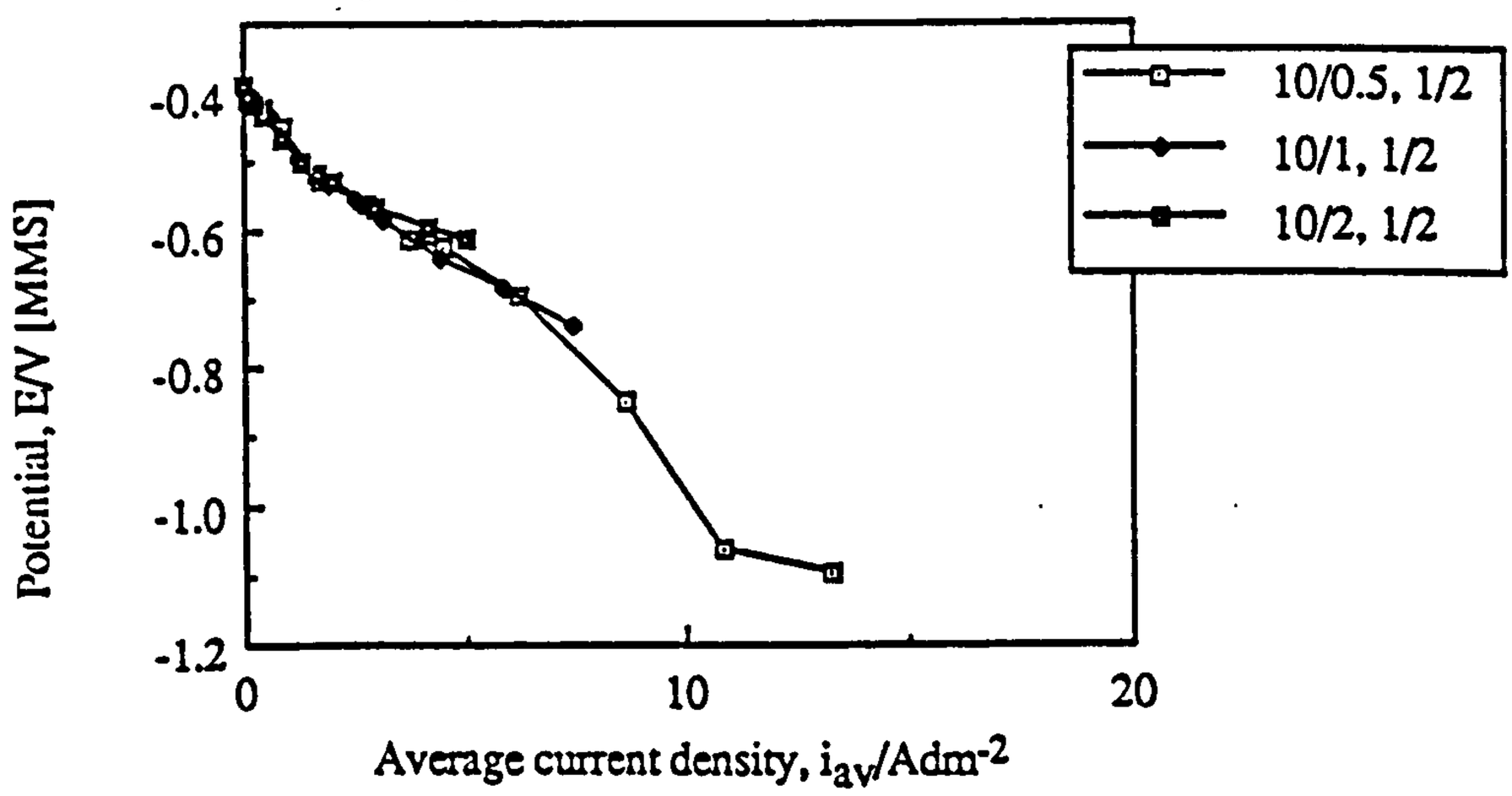

Figure 86a Pulse reverse polarisation curves for different $t_{on(c)}/t_{on(a)}$ ratios but at a $i_{p(c)}/i_{p(a)}$ ratio of 1/2 using electrolyte I.

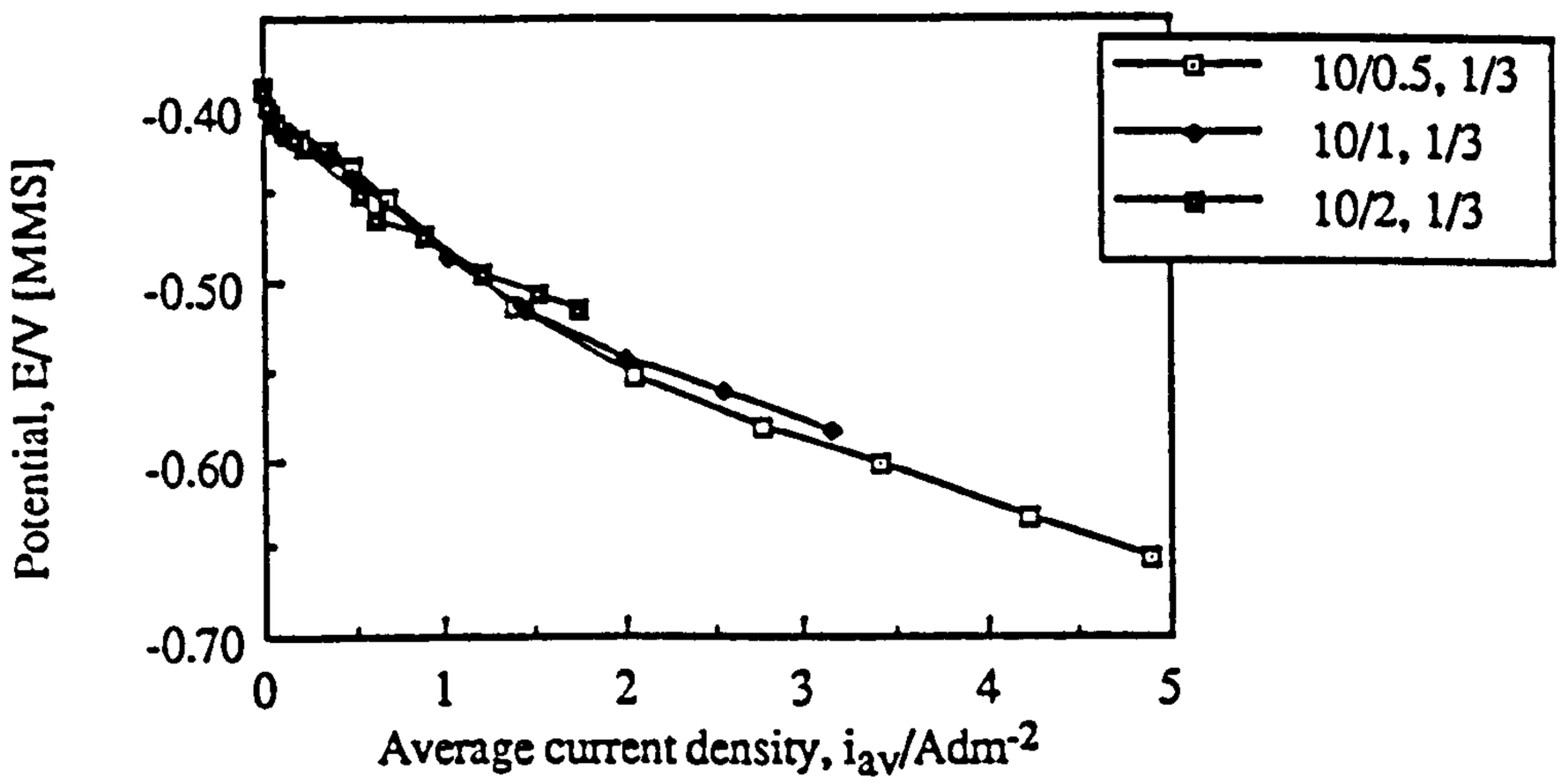

Figure 87a Pulse reverse polarisation curves for different $t_{on(c)}/t_{on(a)}$ ratios but at a $i_{p(c)}/i_{p(a)}$ ratio of 1/3 using electrolyte I.

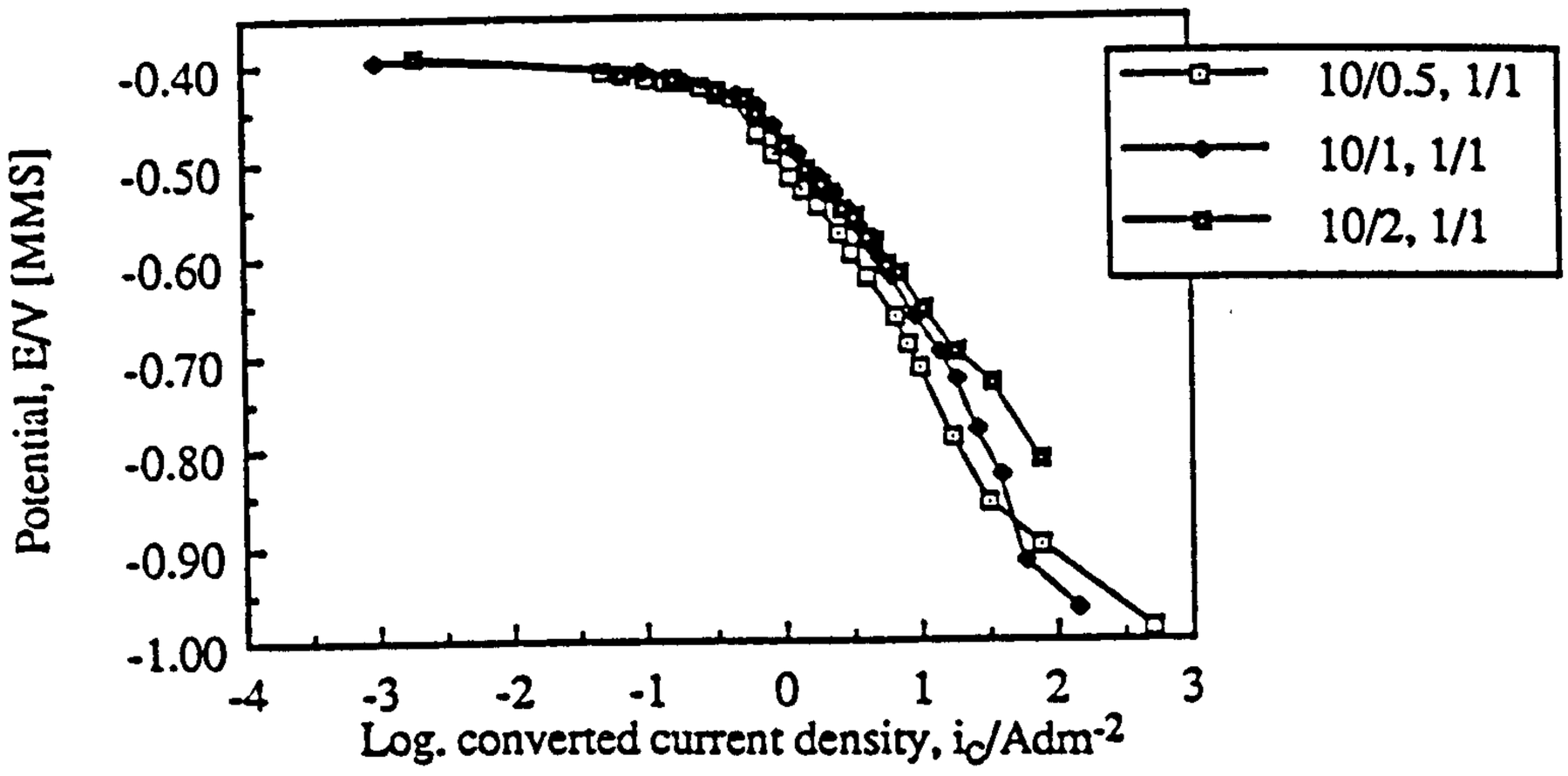

Figure 85b Potential versus logarithmic converted current density pulse reverse curves for different $t_{on(c)}/t_{on(a)}$ ratios but at a $i_{p(c)}/i_{p(a)}$ ratio of 1/1 using electrolyte I.

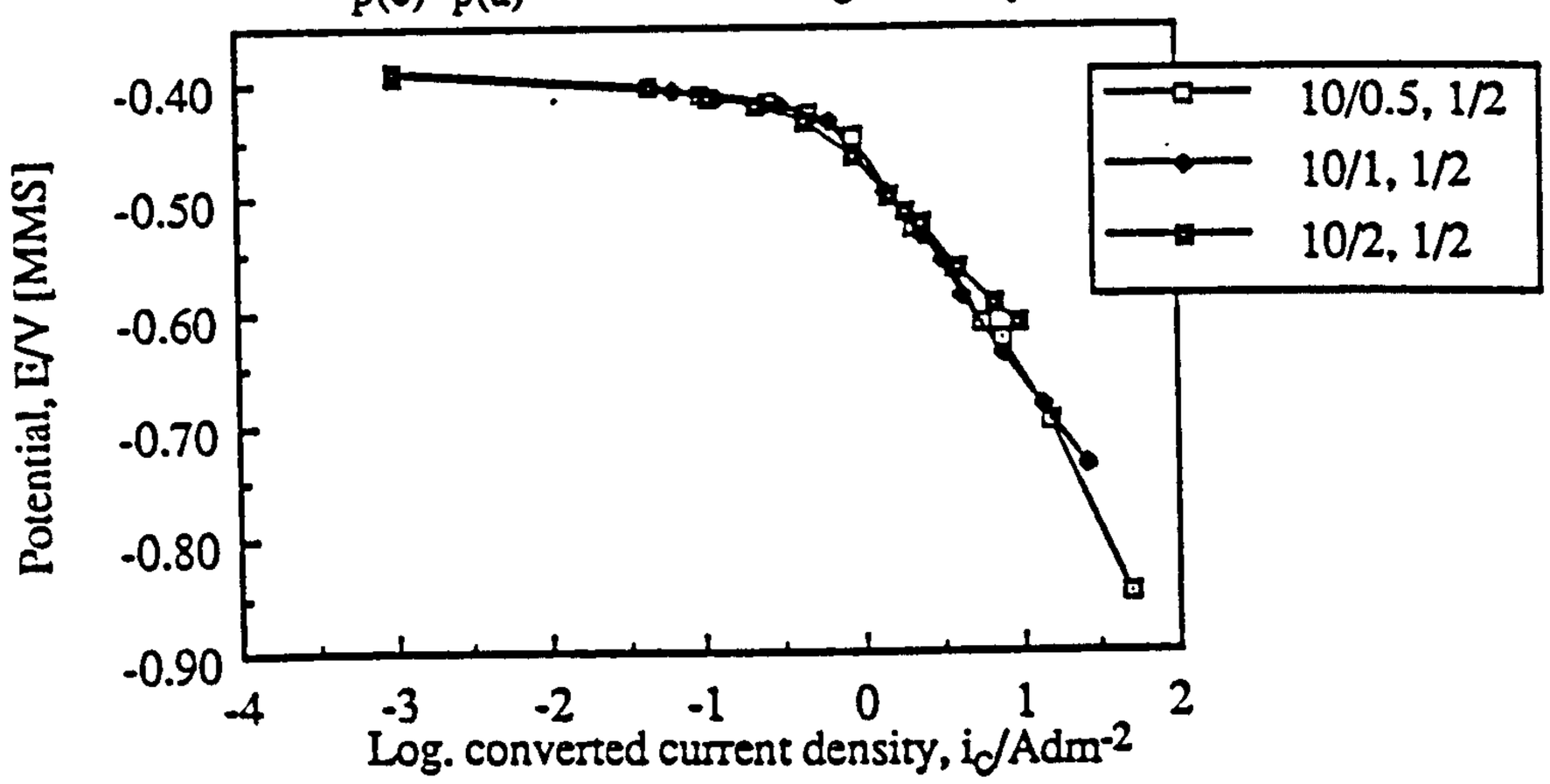

Figure 86b Potential versus logarithmic converted current density pulse reverse curves for different $t_{on(c)}/t_{on(a)}$ ratios but at a $i_{p(c)}/i_{p(a)}$ ratio of 1/2 using electrolyte I.

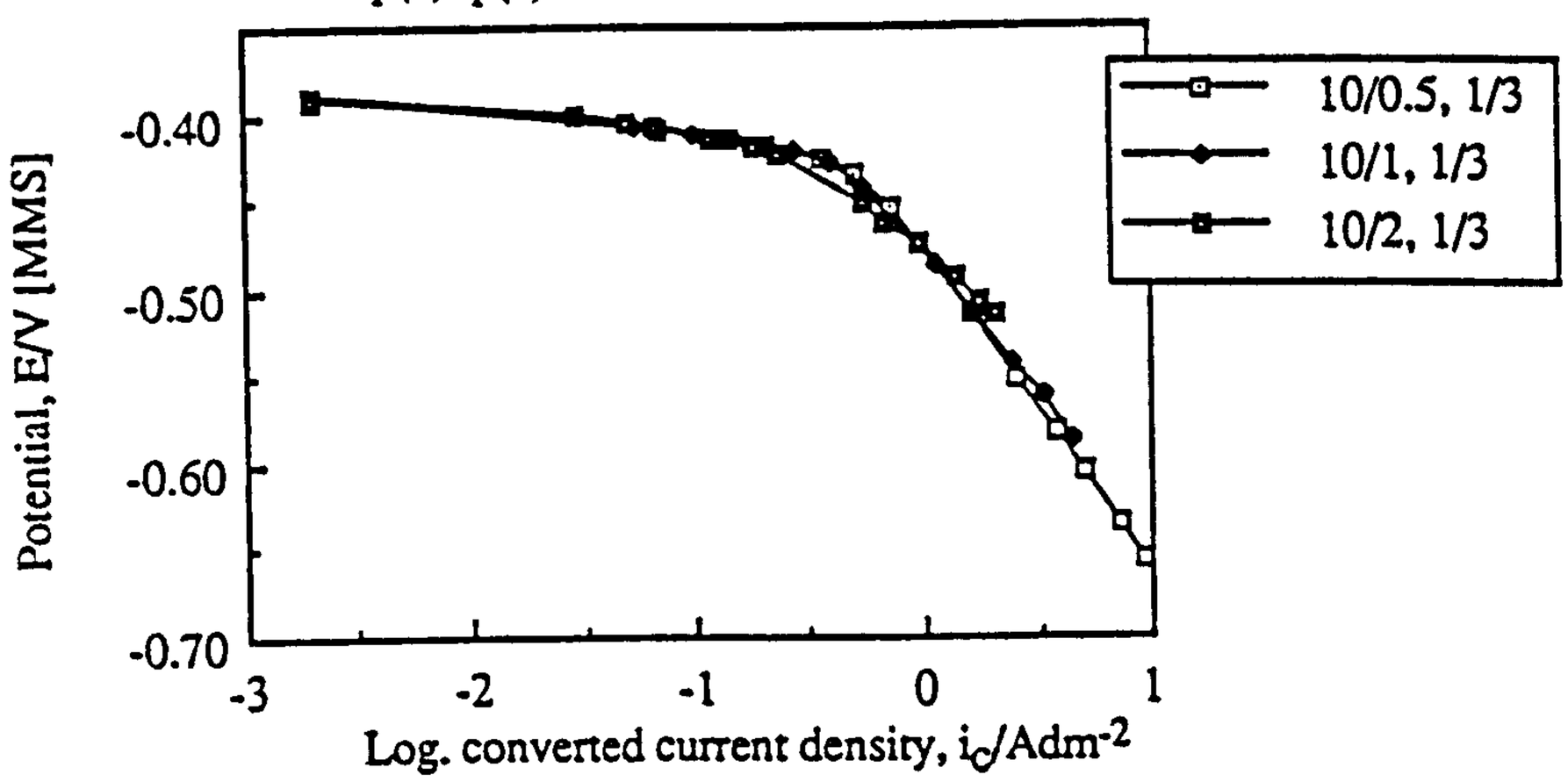

Figure 87b Potential versus logarithmic converted current density pulse reverse curves for different $t_{on(c)}/t_{on(a)}$ ratios but at a $i_{p(c)}/i_{p(a)}$ ratio of 1/3 using electrolyte I.

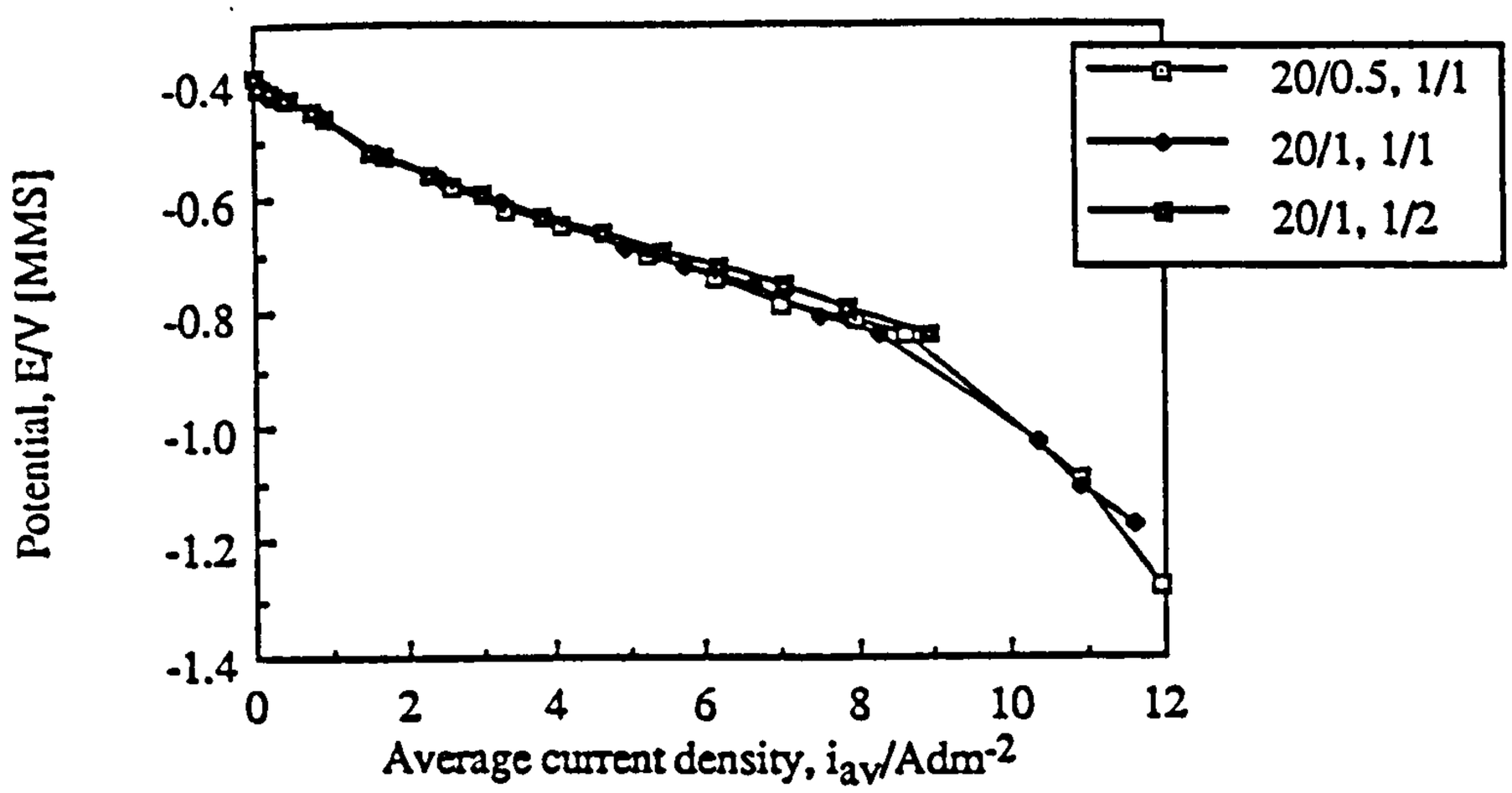

Figure 88a Pulse reverse polarisation curves for different $t_{on(c)}/t_{on(a)}$ and also different $i_{p(c)}/i_{p(a)}$ ratios using electrolyte I.

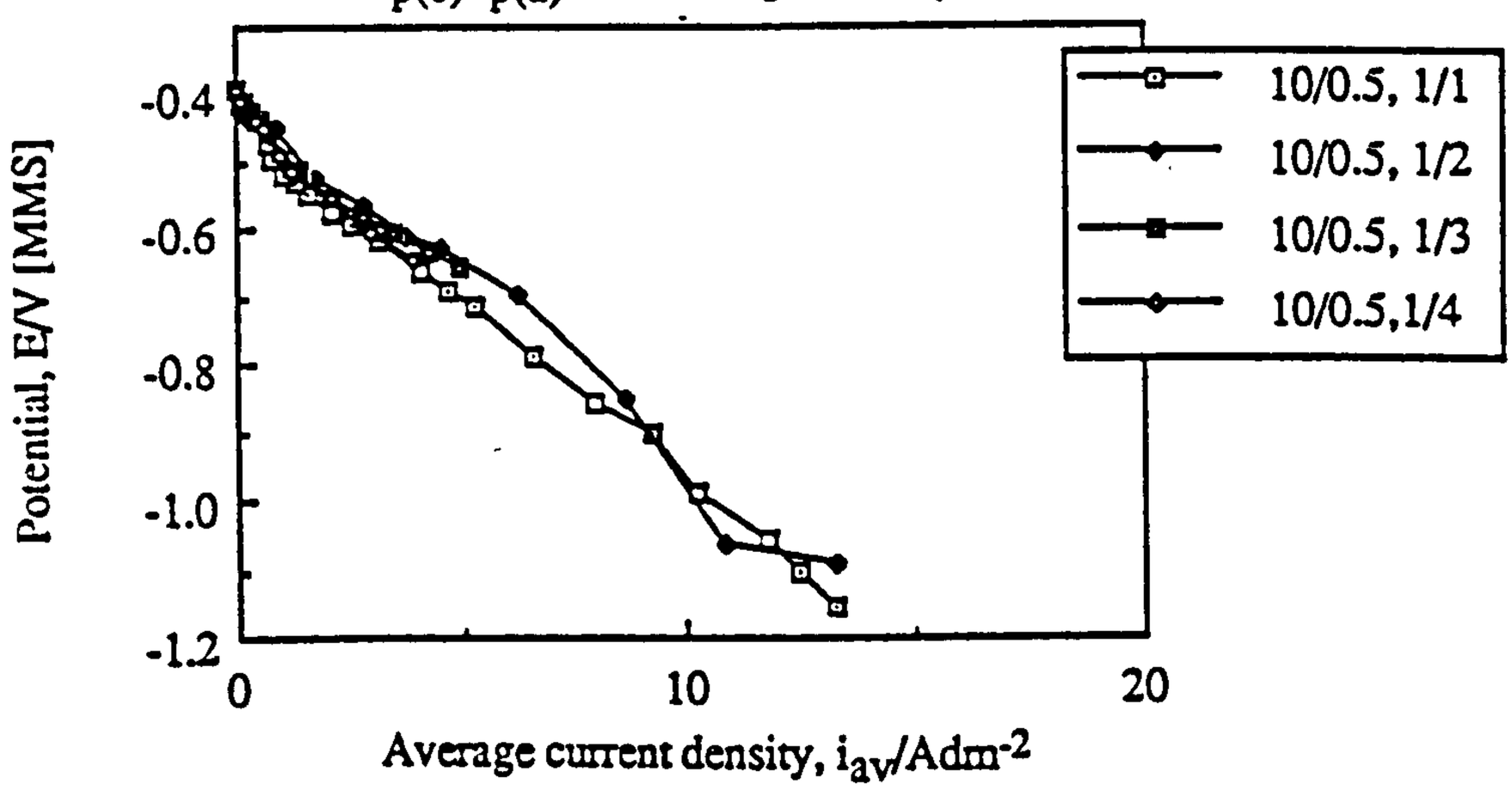

Figure 89a Pulse reverse polarisation curves for $t_{on(c)}/t_{on(a)}$ ratio of 10ms/0.5ms but different $i_{p(c)}/i_{p(a)}$ ratios using electrolyte I.

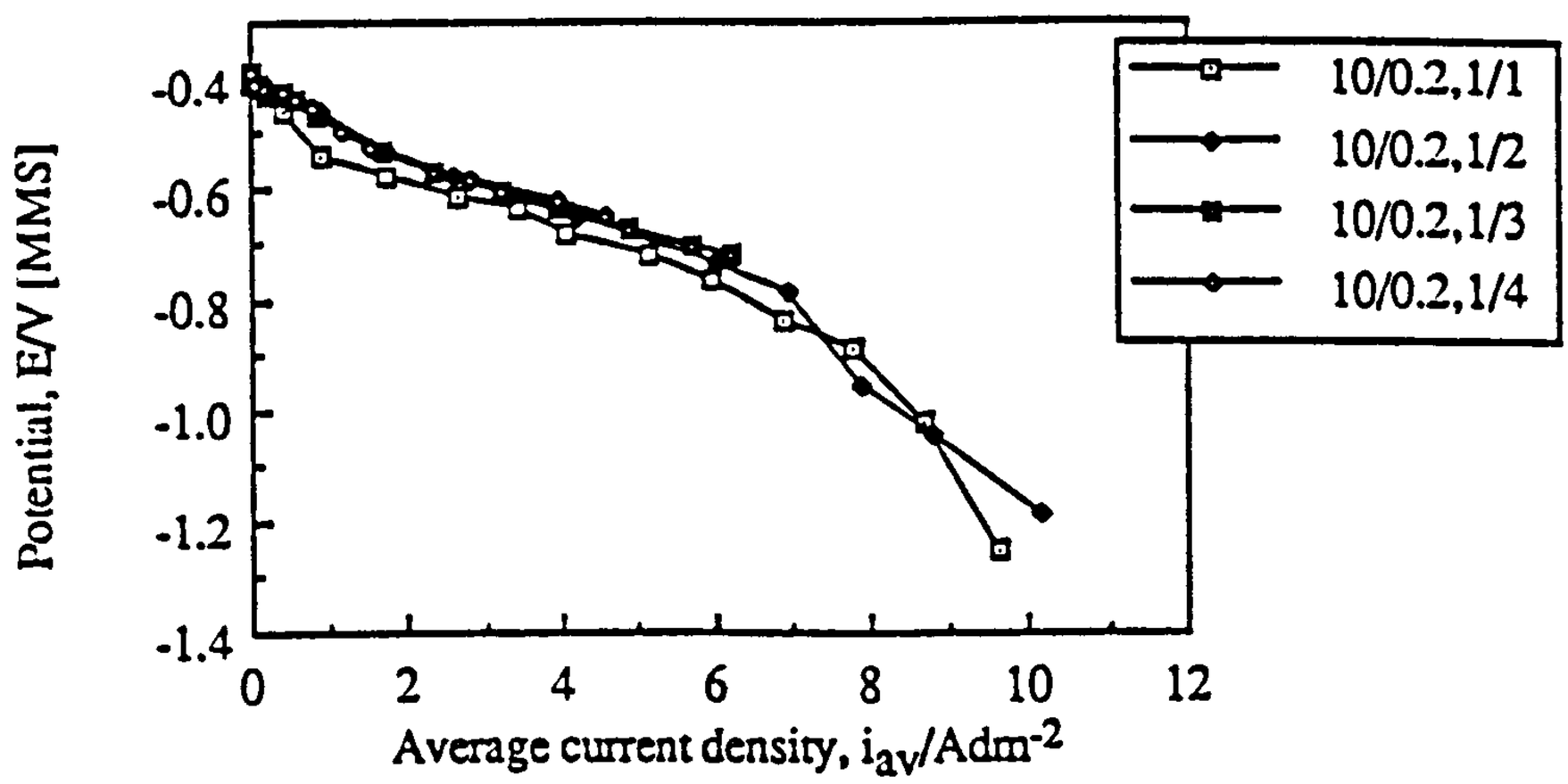

Figure 90a Pulse reverse polarisation curves for $t_{on(c)}/t_{on(a)}$ ratio of 10ms/0.2ms but different $i_{p(c)}/i_{p(a)}$ ratios using electrolyte I.

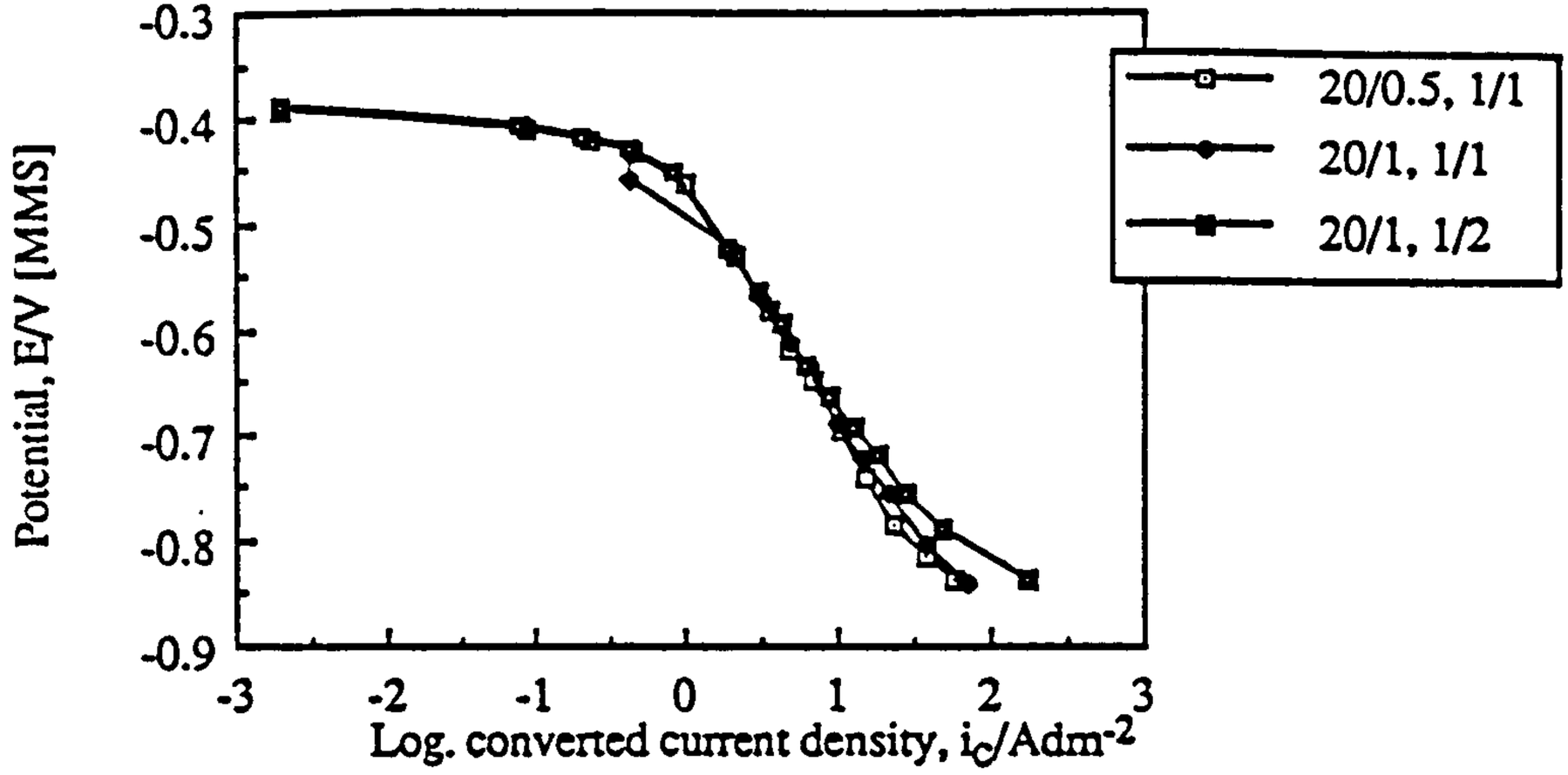

Figure 88b Potential versus logarithmic converted current density pulse reverse curves for different $t_{on(c)}/t_{on(a)}$ and also different $i_{p(c)}/i_{p(a)}$ ratios using electrolyte I.

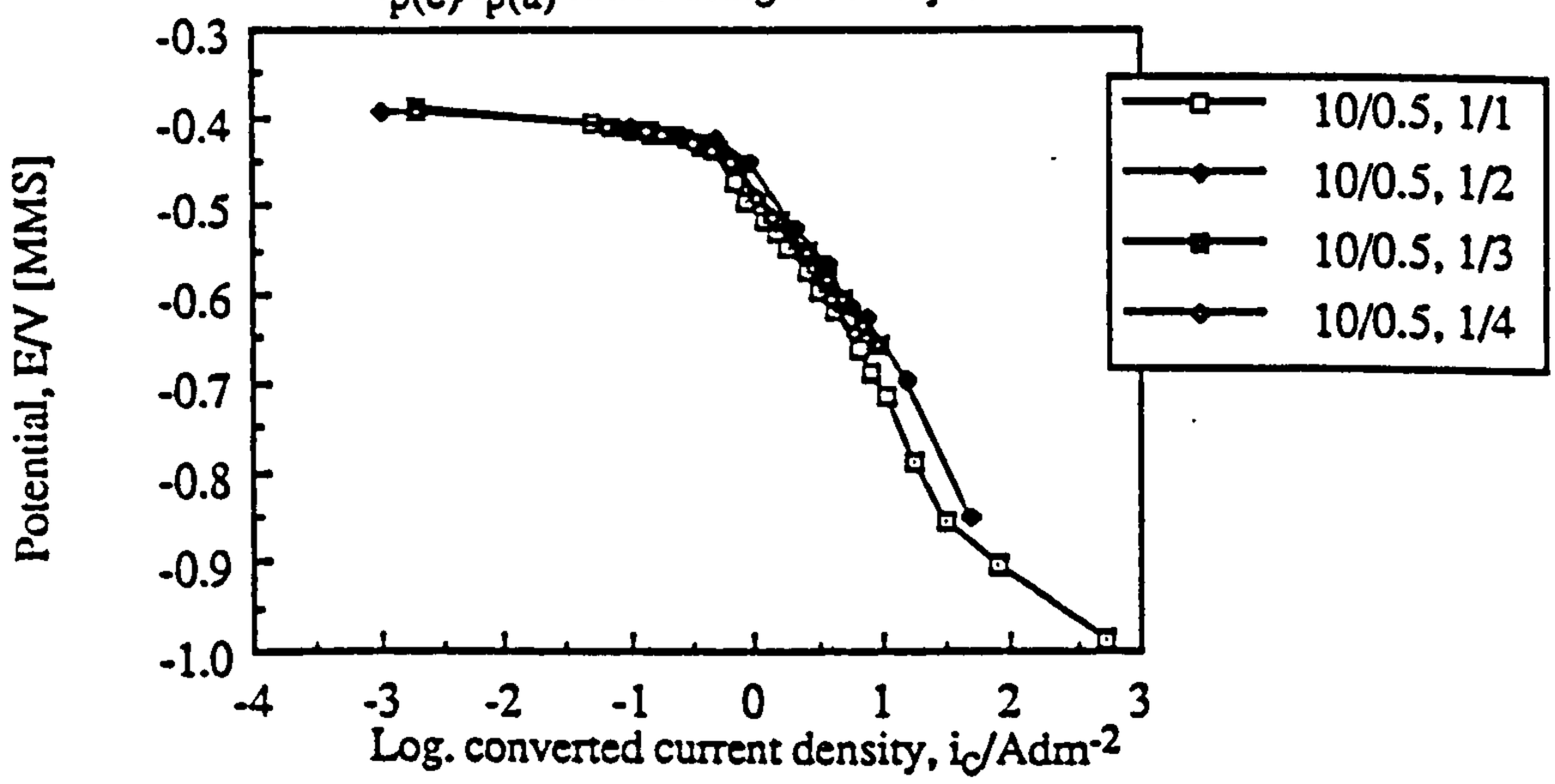

Figure 89b Potential versus logarithmic converted current density pulse reverse curves for $t_{on(c)}/t_{on(a)}$ ratio of 10ms/0.5ms but different $i_{p(c)}/i_{p(a)}$ ratios using electrolyte I.

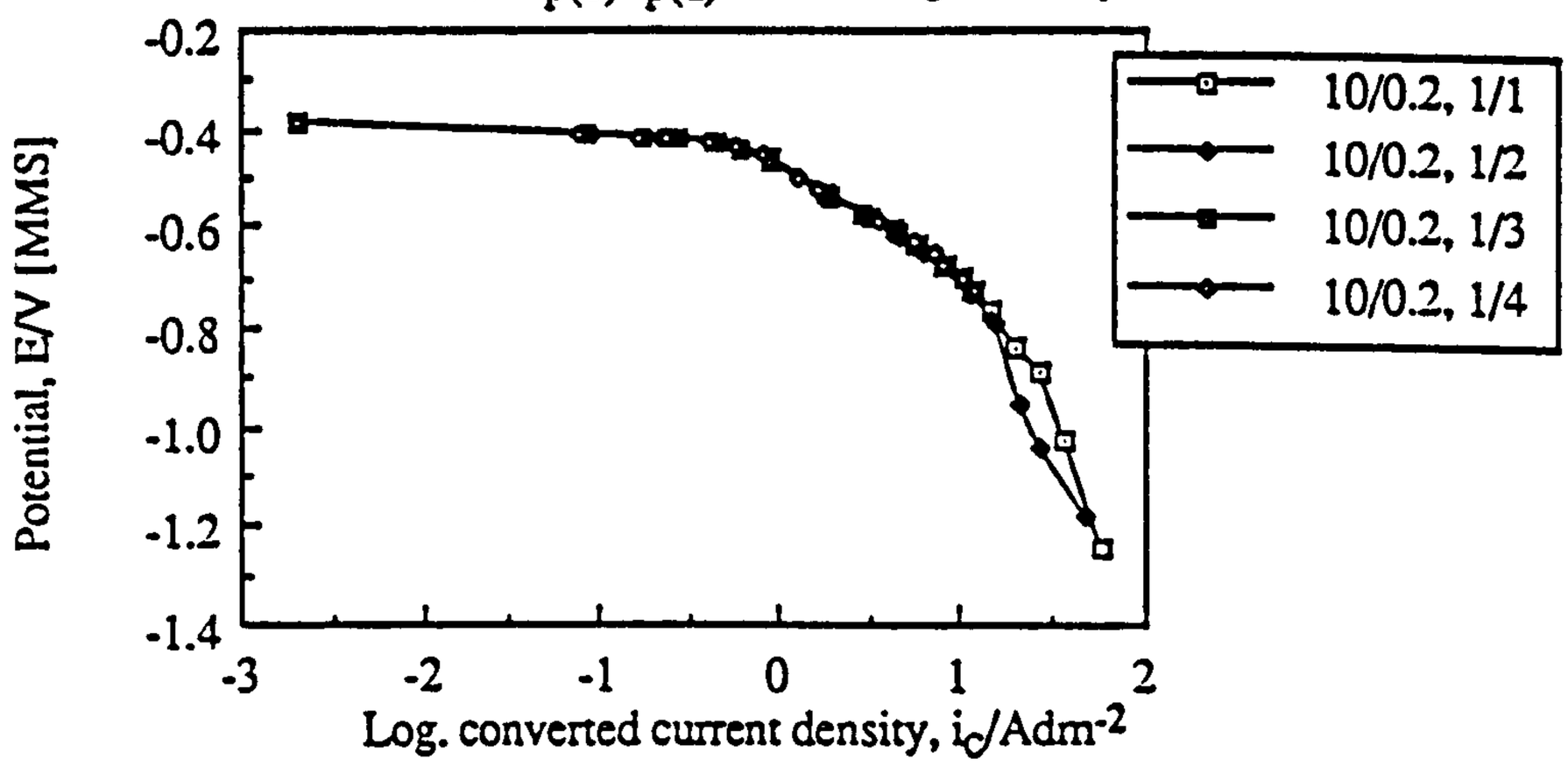

Figure 90b Potential versus logarithmic converted current density pulse reverse curves for $t_{on(c)}/t_{on(a)}$ ratio of 10ms/0.2ms but different $i_{p(c)}/i_{p(a)}$ ratios using electrolyte I.

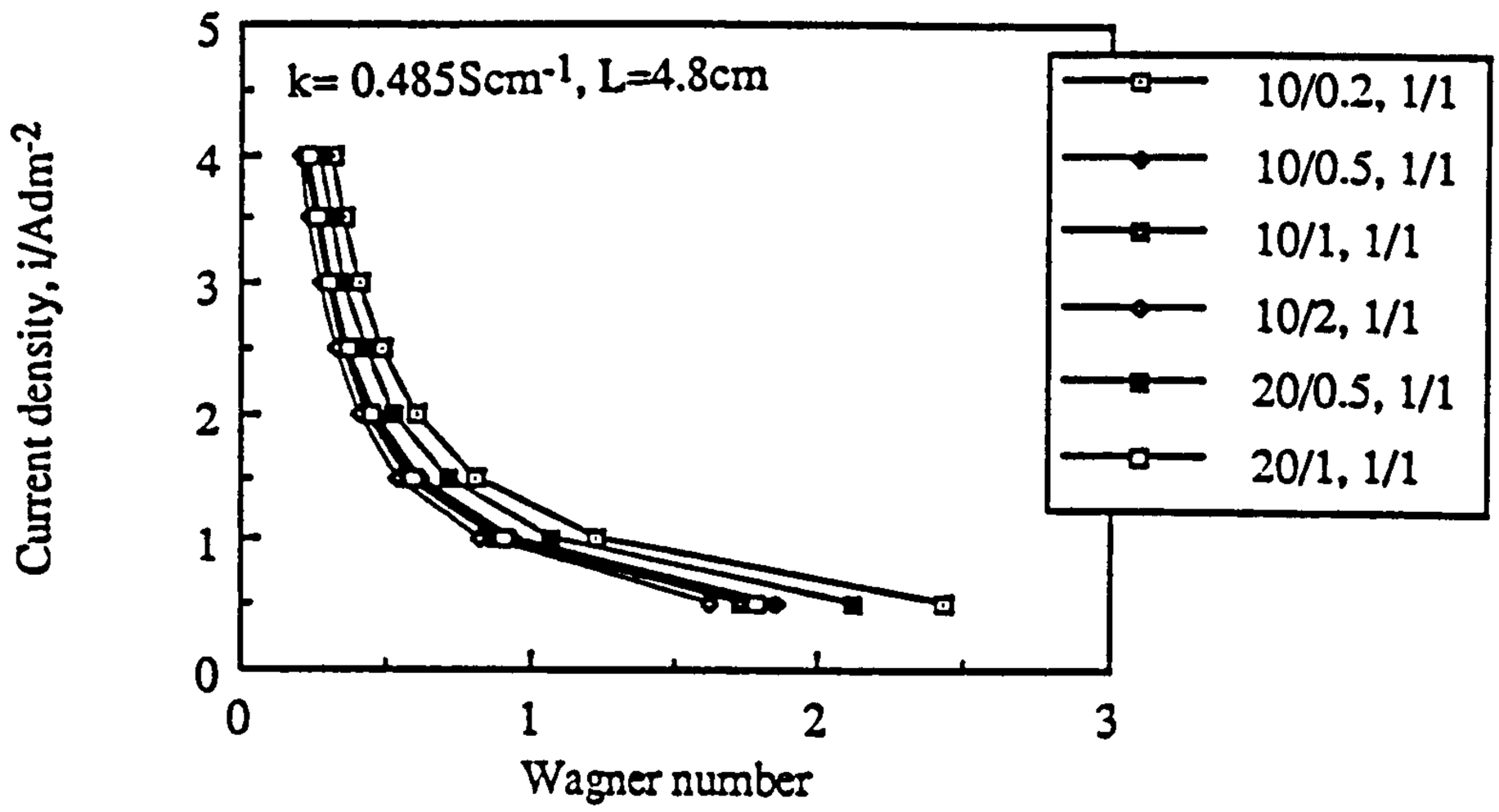

Figure 91 Relationship between current density and Wagner number under PR for different ton(c)/ton(a) ratios but at a $i_{p(c)}/i_{p(a)}$ ratio of 1/1 using electrolyte I.

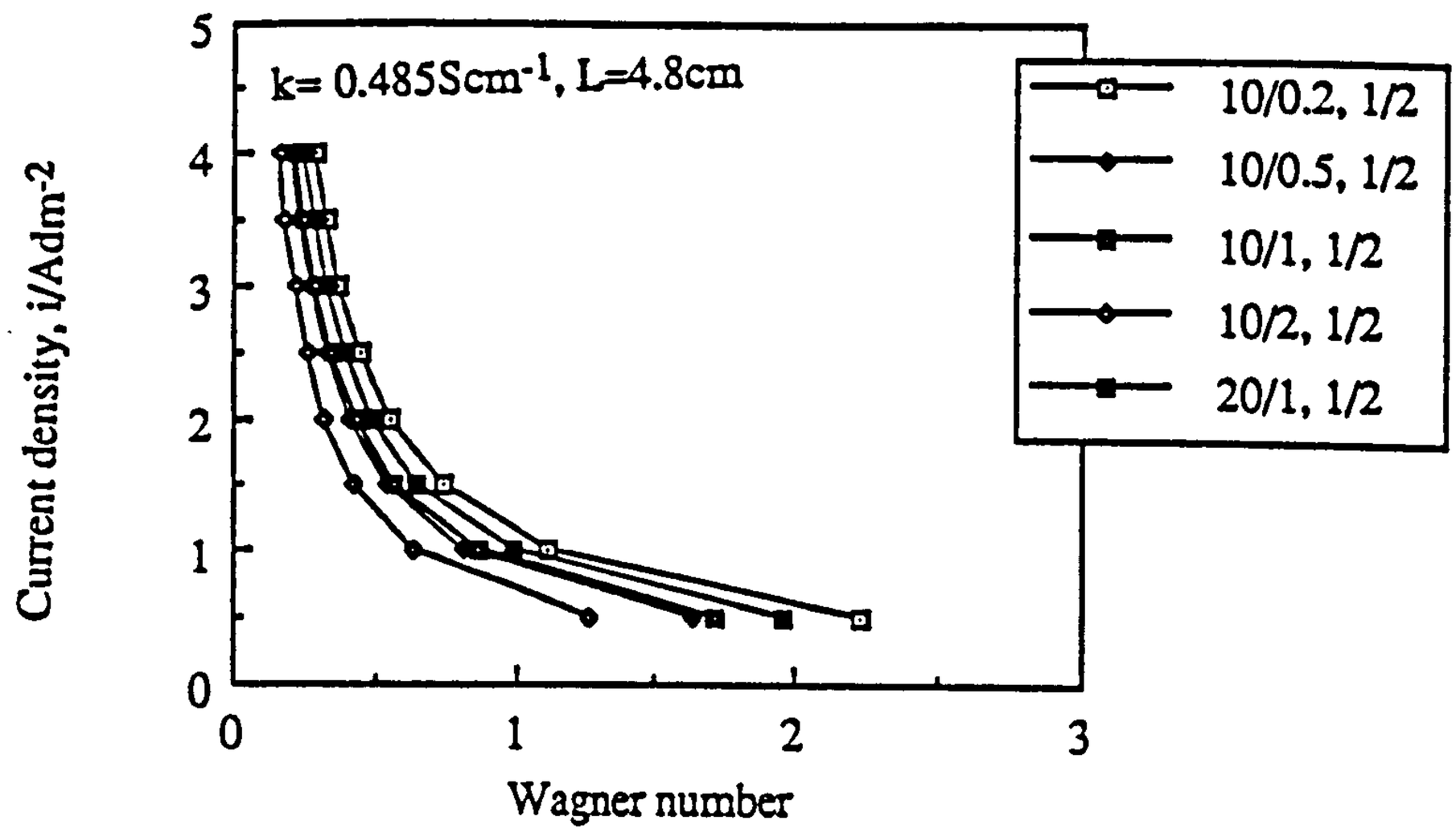

Figure 92 Relationship between current density and Wagner number under PR for different ton(c)/ton(a) ratios but at a $i_{p(c)}/i_{p(a)}$ ratio of 1/2 using electrolyte I.

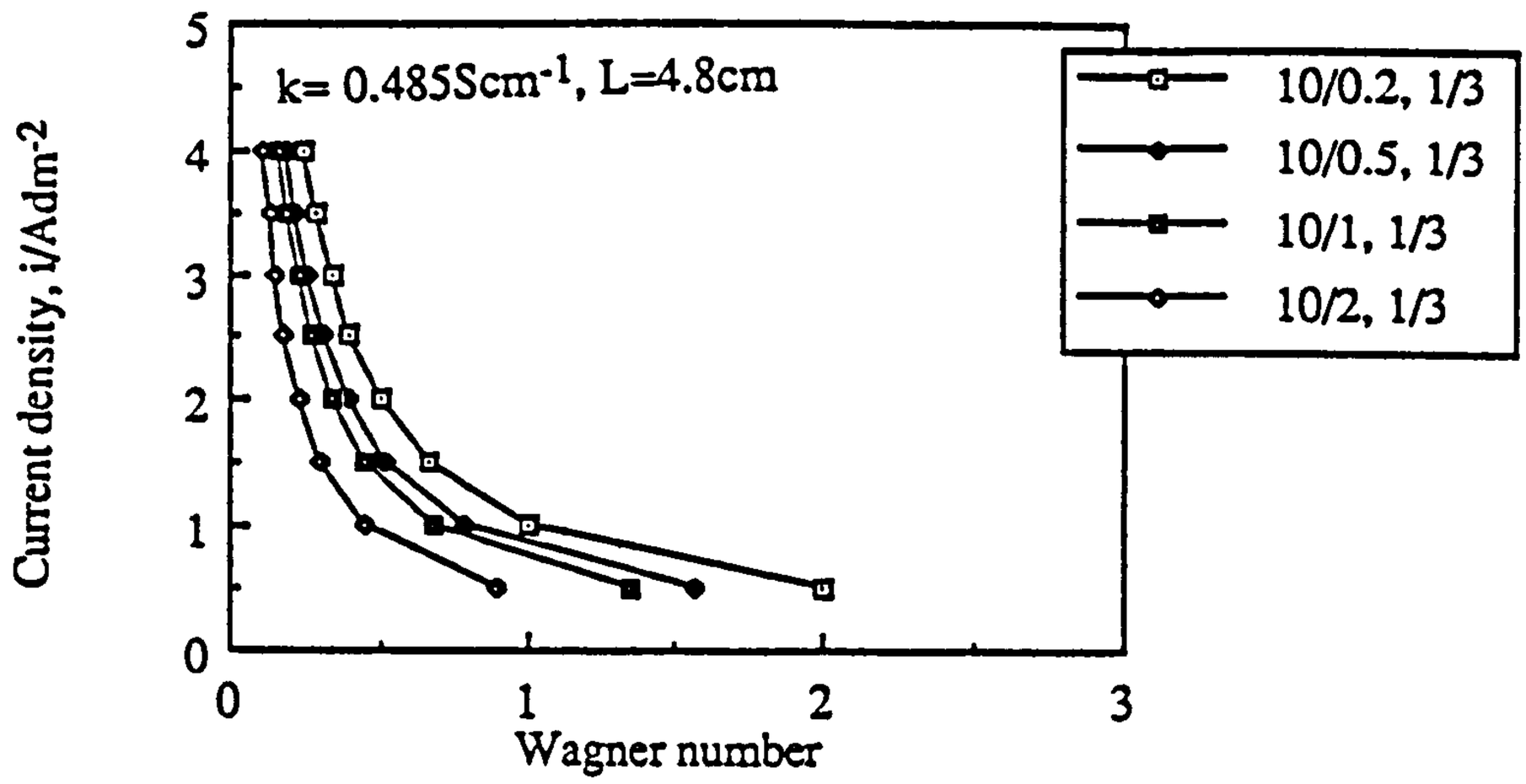

Figure 93 Relationship between current density and Wagner number under PR for different ton(c)/ton(a) ratios but at a $i_{p(c)}/i_{p(a)}$ ratio of 1/3 using electrolyte I.

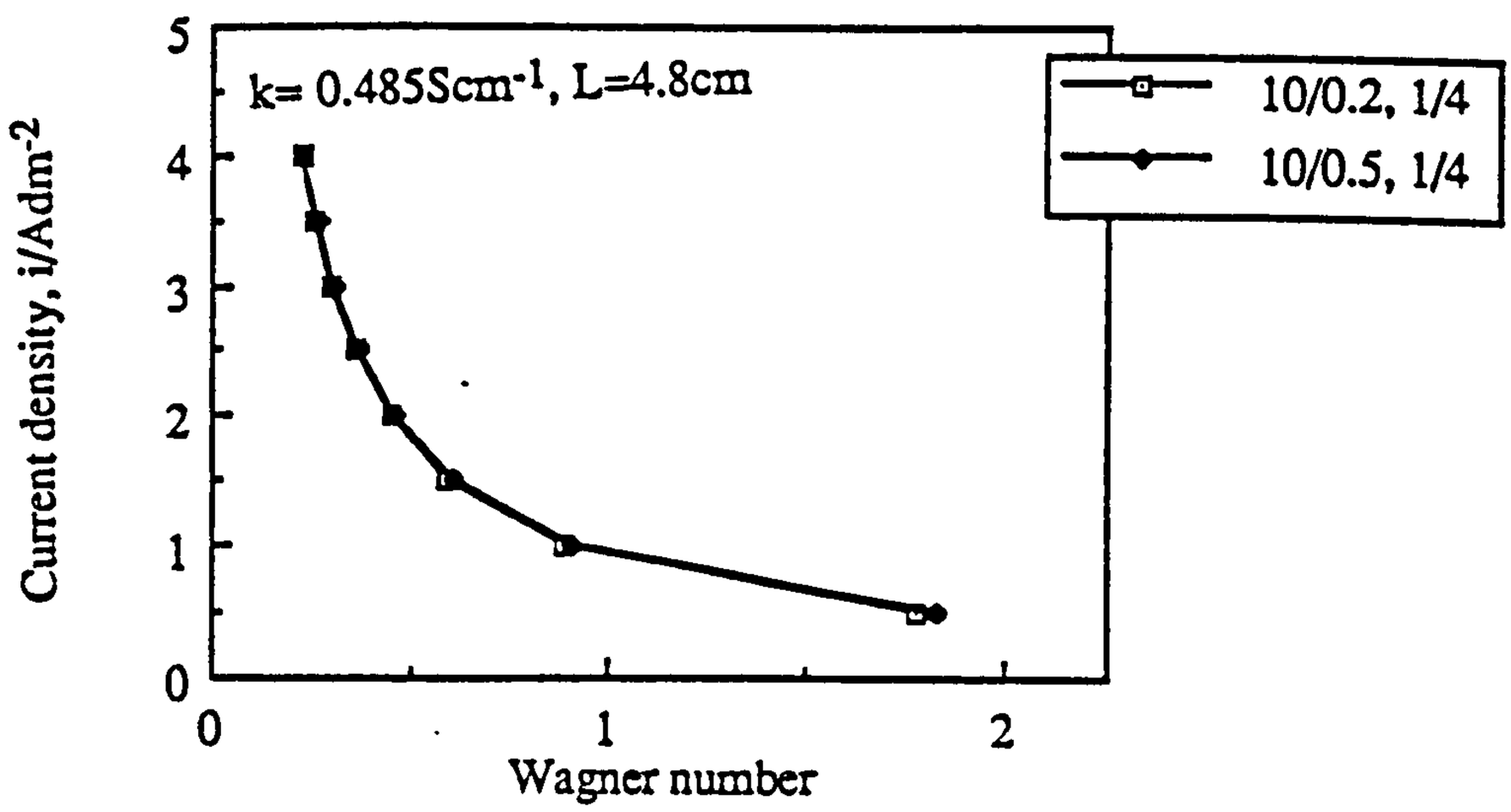

Figure 94 Relationship between current density and Wagner number under PR for different ton(c)/ton(a) ratios but at a $i_{p(c)}/i_{p(a)}$ ratio of 1/4 using electrolyte I.

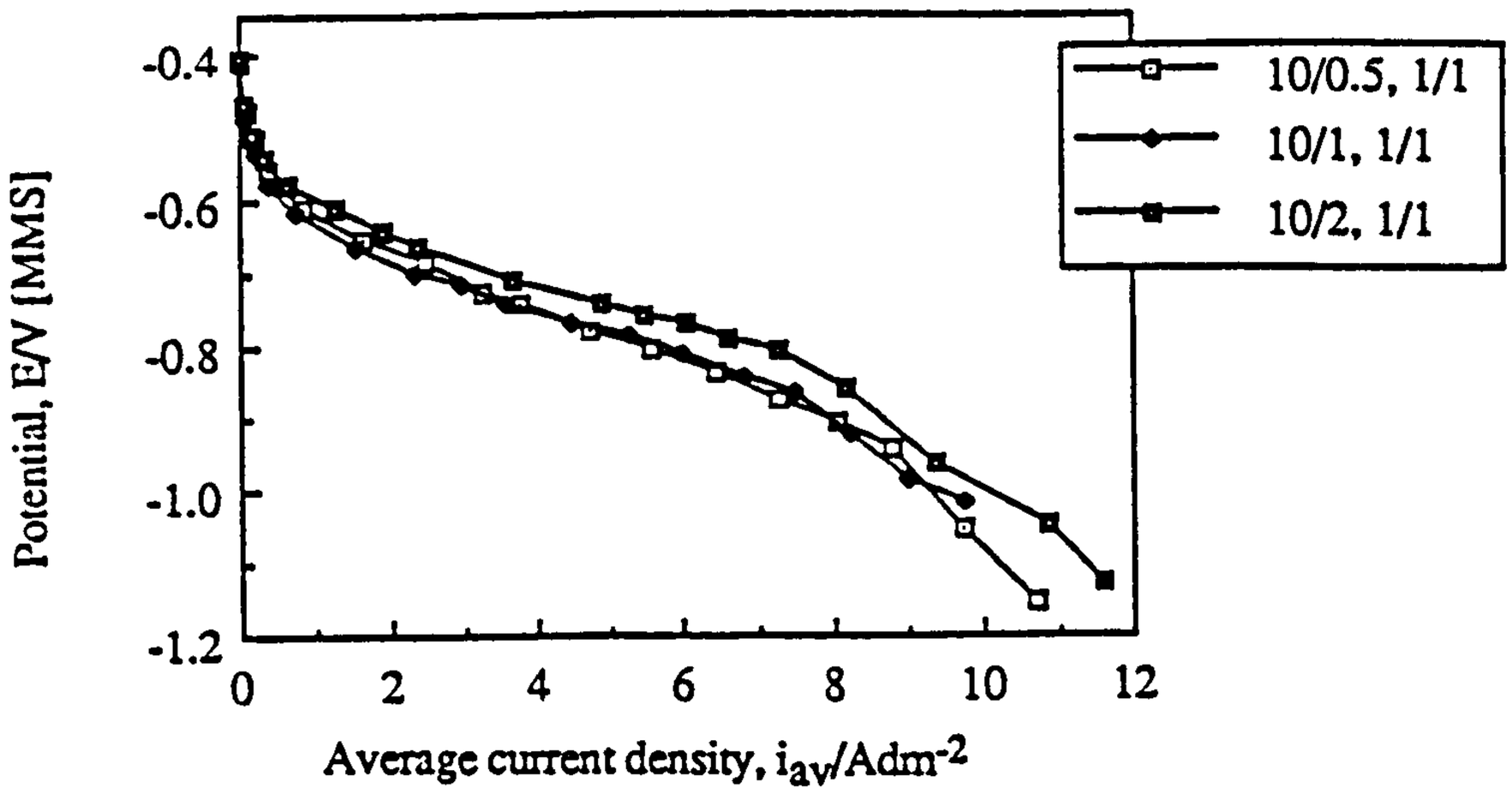

Figure 95a Pulse reverse polarisation curves for different $t_{on(c)}/t_{on(a)}$ ratios but at a $i_{p(c)}/i_{p(a)}$ ratio of 1/1 using electrolyte V.

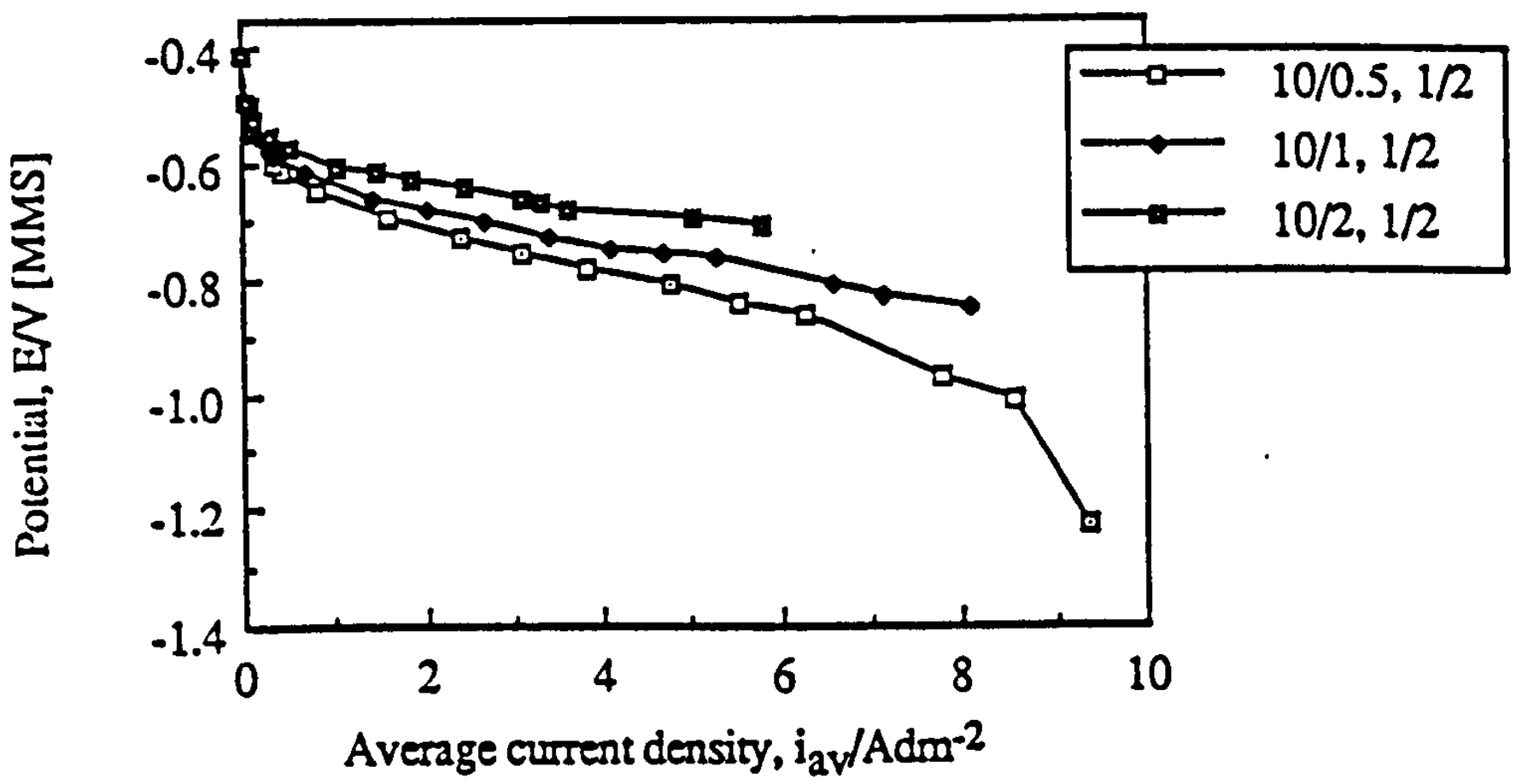

Figure 96a Pulse reverse polarisation curves for different $t_{on(c)}/t_{on(a)}$ ratios but at a $i_{p(c)}/i_{p(a)}$ ratio of 1/2 using electrolyte V.

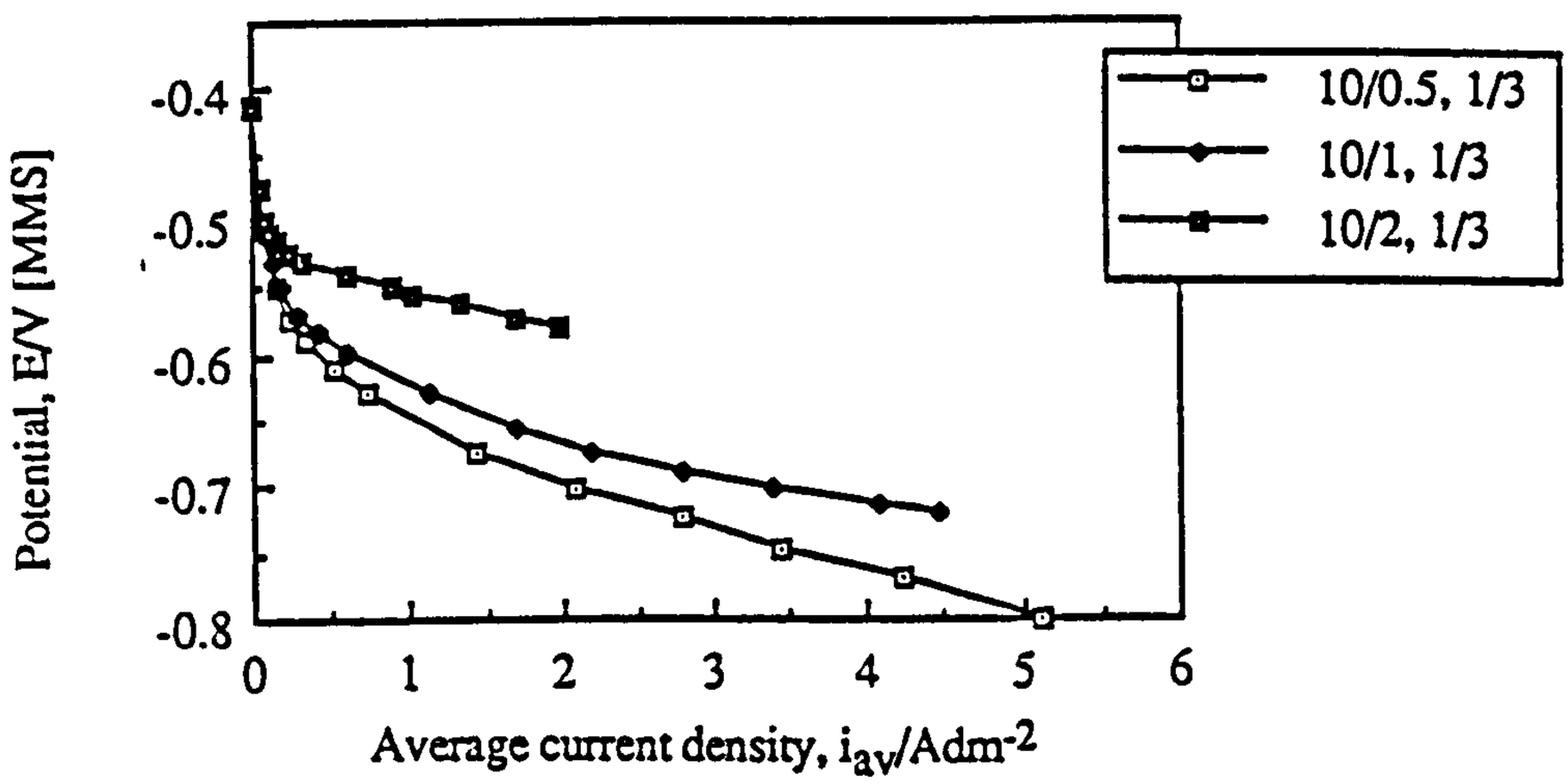

Figure 97a Pulse reverse polarisation curves for different $t_{on(c)}/t_{on(a)}$ ratios but at a $i_{p(c)}/i_{p(a)}$ ratio of 1/3 using electrolyte V.

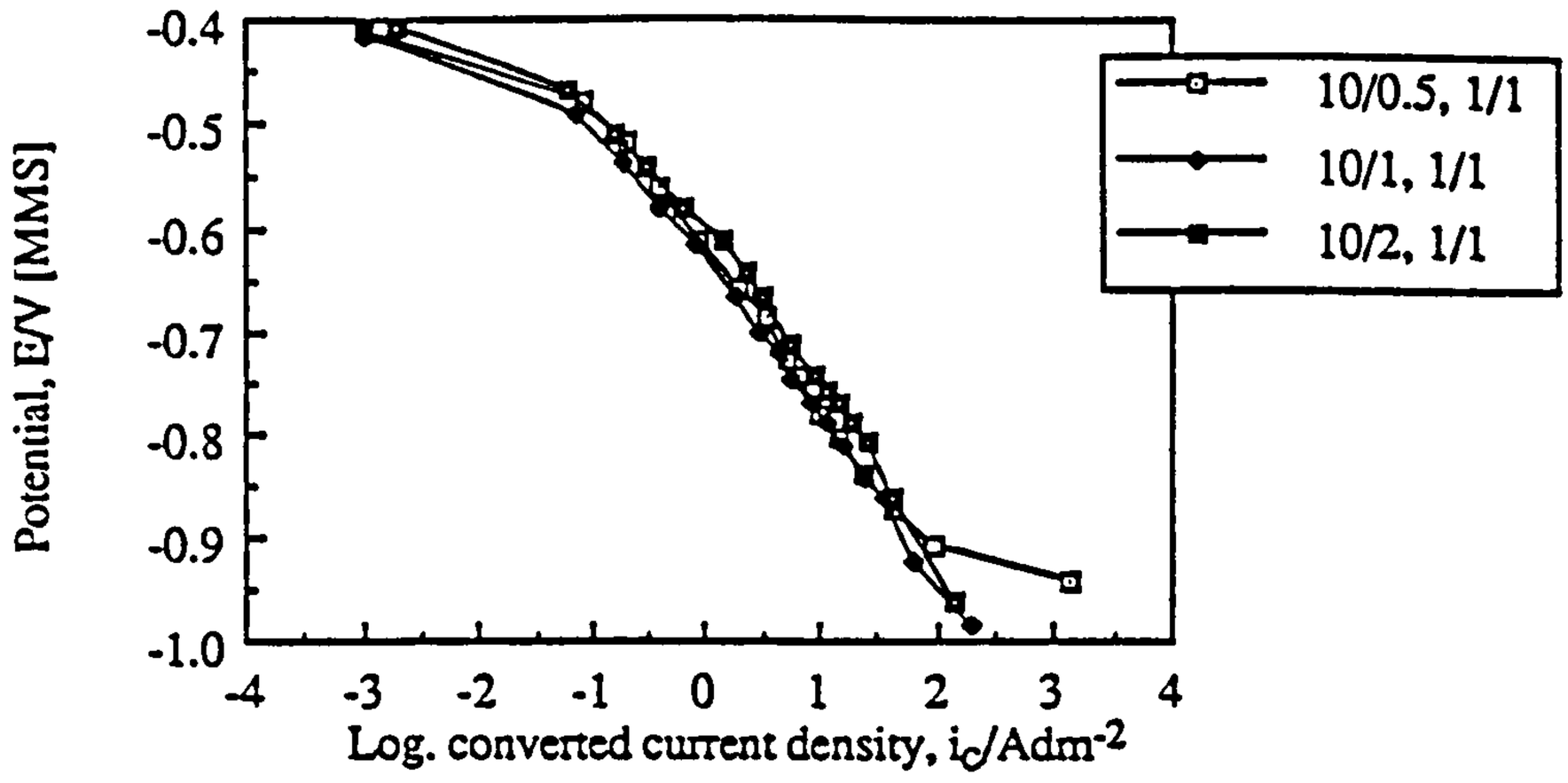

Figure 95b Potential versus logarithmic converted current density pulse reverse curves for different $t_{on(c)}/t_{on(a)}$ ratios but at a $i_{p(c)}/i_{p(a)}$ ratio of 1/1 using electrolyte V.

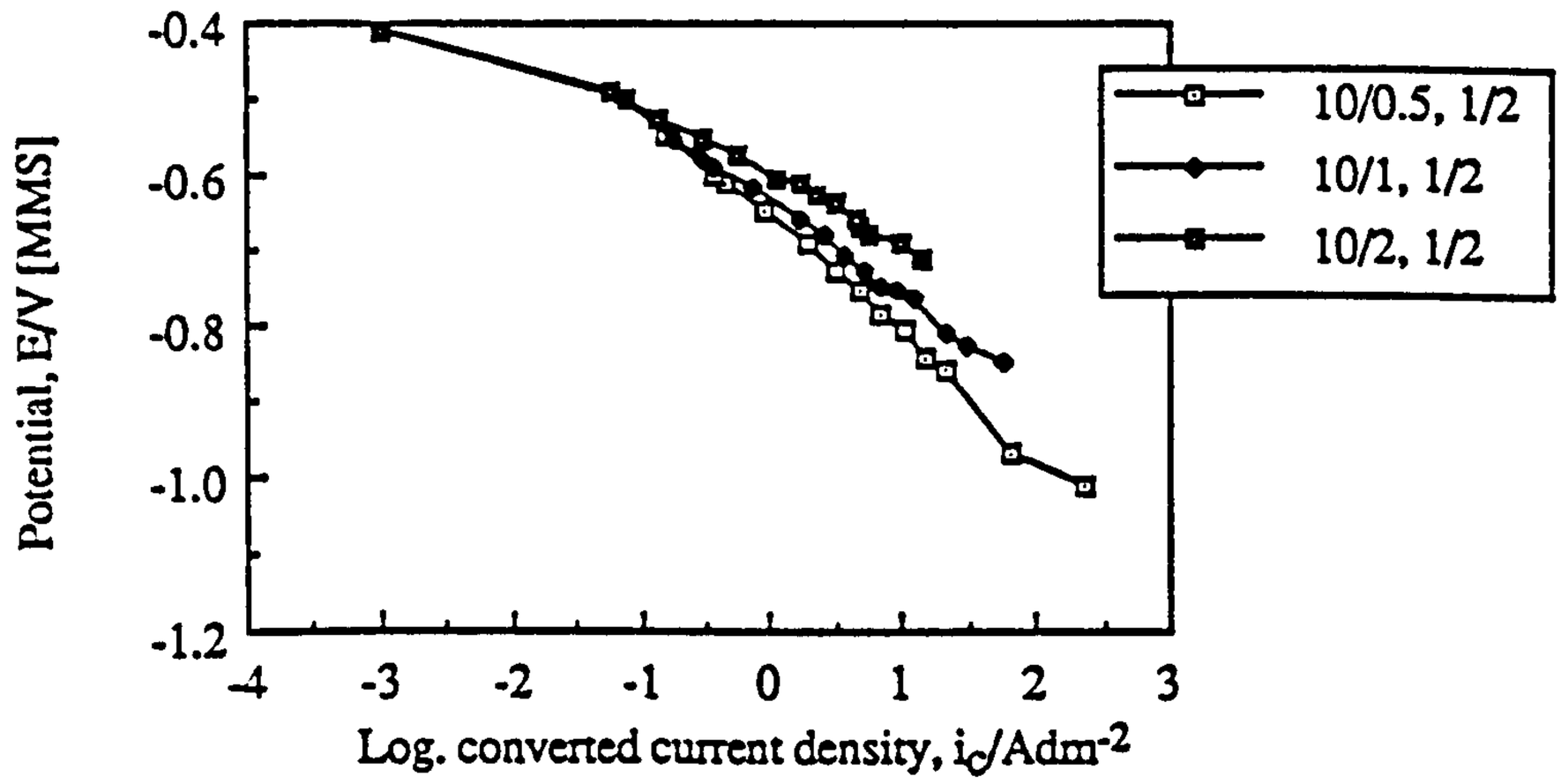

Figure 96b Potential versus logarithmic converted current density pulse reverse curves for different $t_{on(c)}/t_{on(a)}$ ratios but at a $i_{p(c)}/i_{p(a)}$ ratio of 1/2 using electrolyte V.

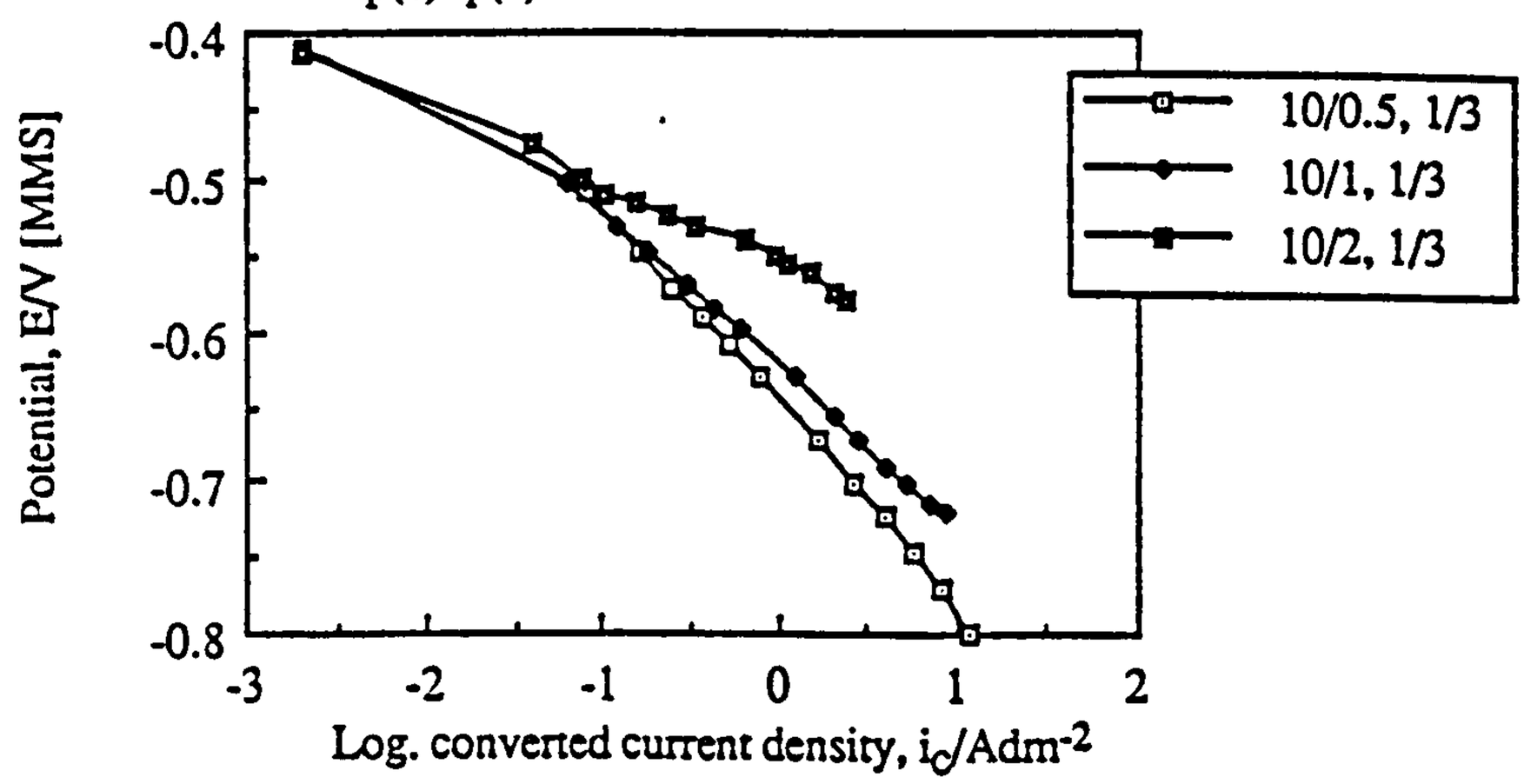

Figure 97b Potential versus logarithmic converted current density pulse reverse curves for different $t_{on(c)}/t_{on(a)}$ ratios but at a $i_{p(c)}/i_{p(a)}$ ratio of 1/3 using electrolyte V.

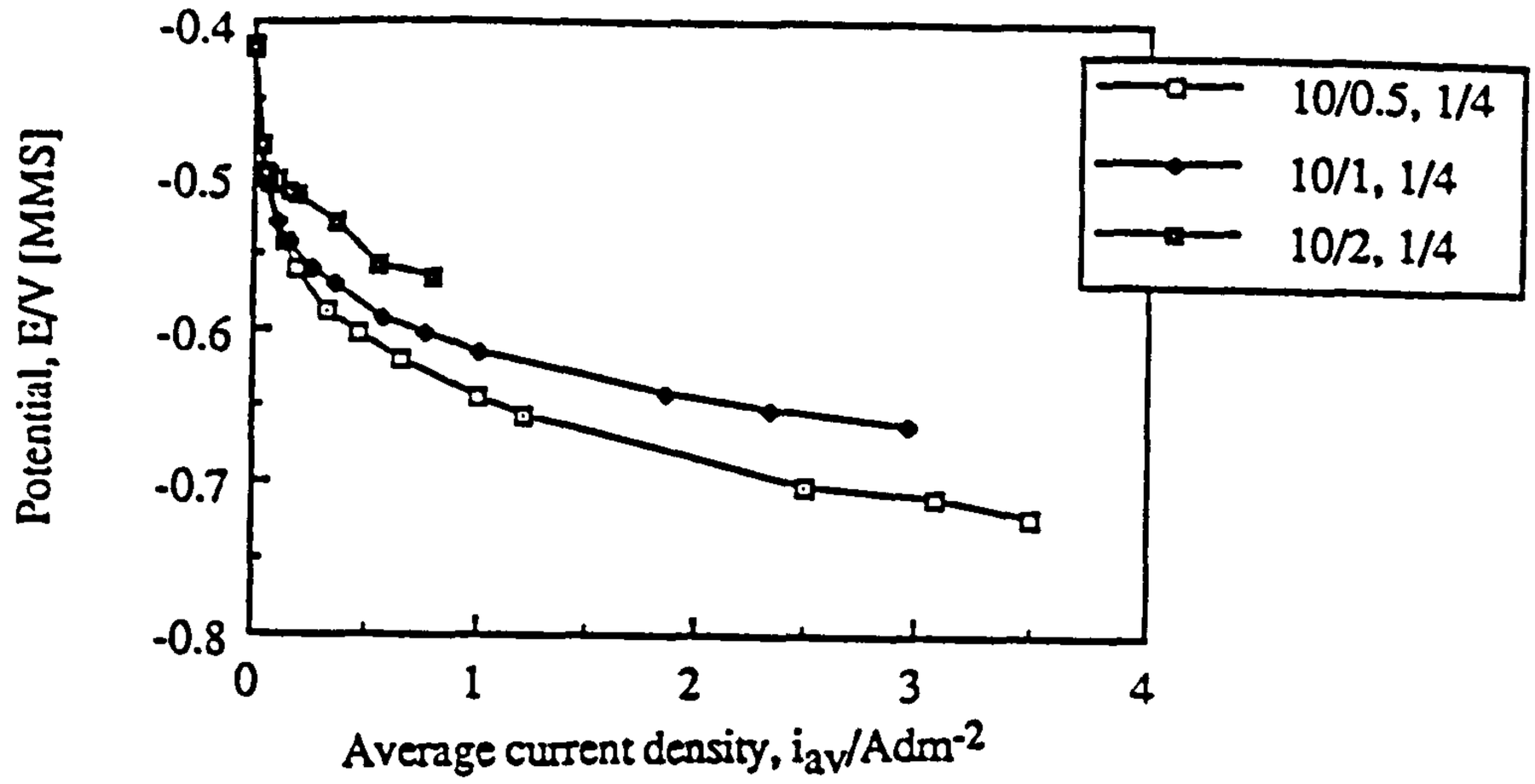

Figure 98a Pulse reverse polarisation curves for different $t_{on(c)}/t_{on(a)}$ ratios but at a $i_{p(c)}/i_{p(a)}$ ratio of 1/4 using electrolyte V.

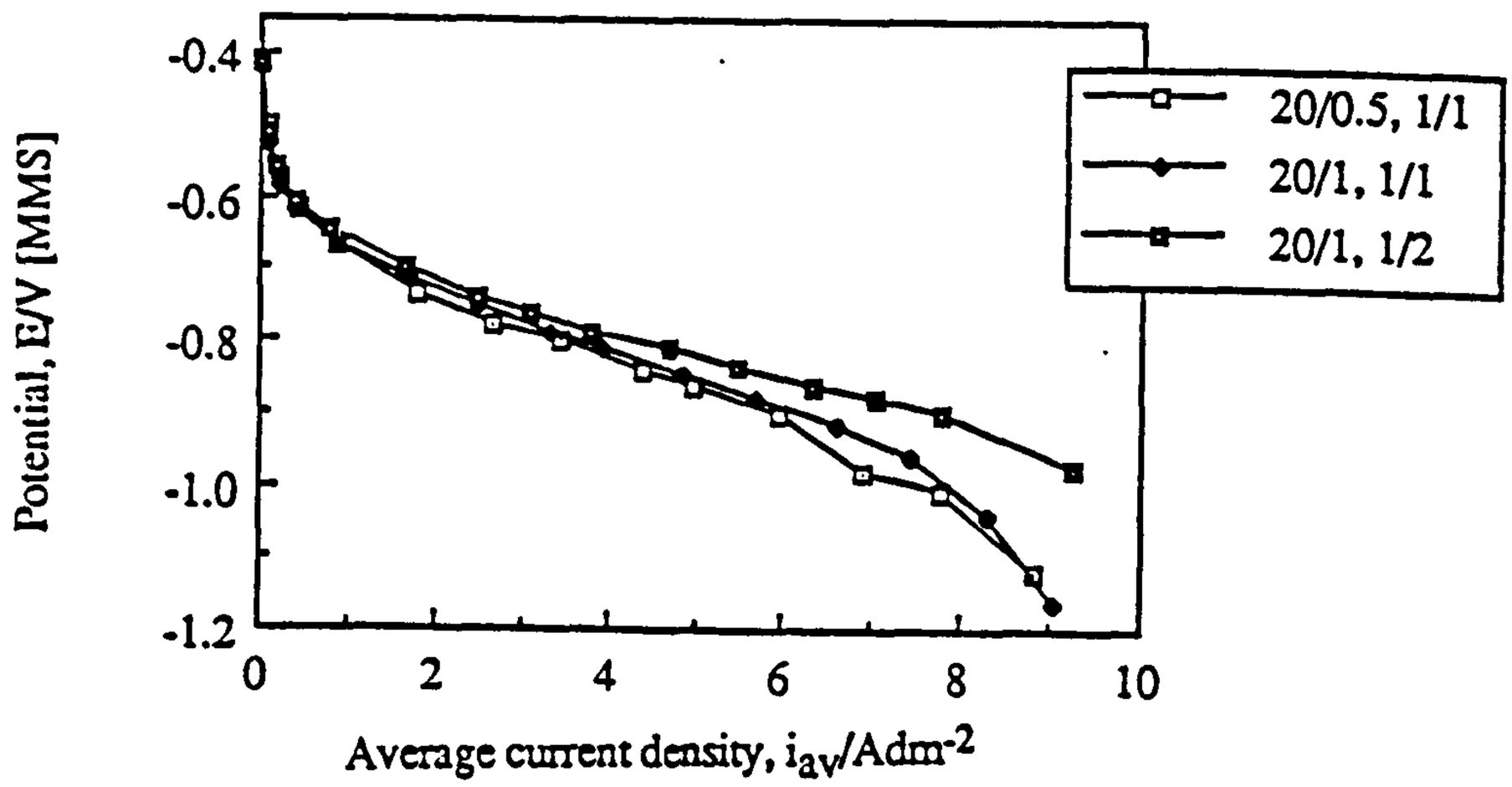

Figure 99a Pulse reverse polarisation curves for different $t_{on(c)}/t_{on(a)}$ and also different $i_{p(c)}/i_{p(a)}$ ratios using electrolyte V.

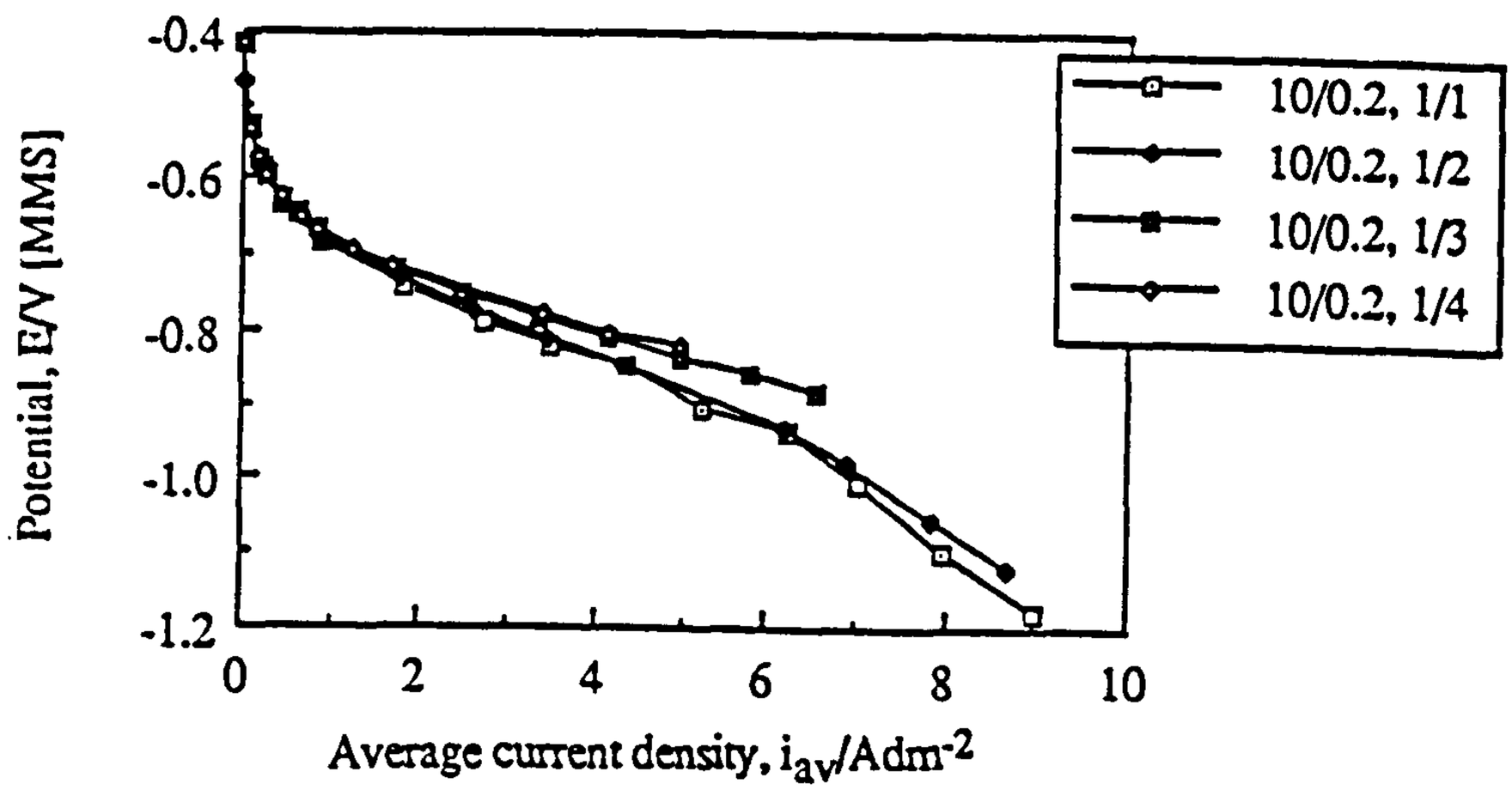

Figure 100a Pulse reverse polarisation curves for $t_{on(c)}/t_{on(a)}$ ratio of 10ms/0.2ms but different $i_{p(c)}/i_{p(a)}$ ratios using electrolyte V.

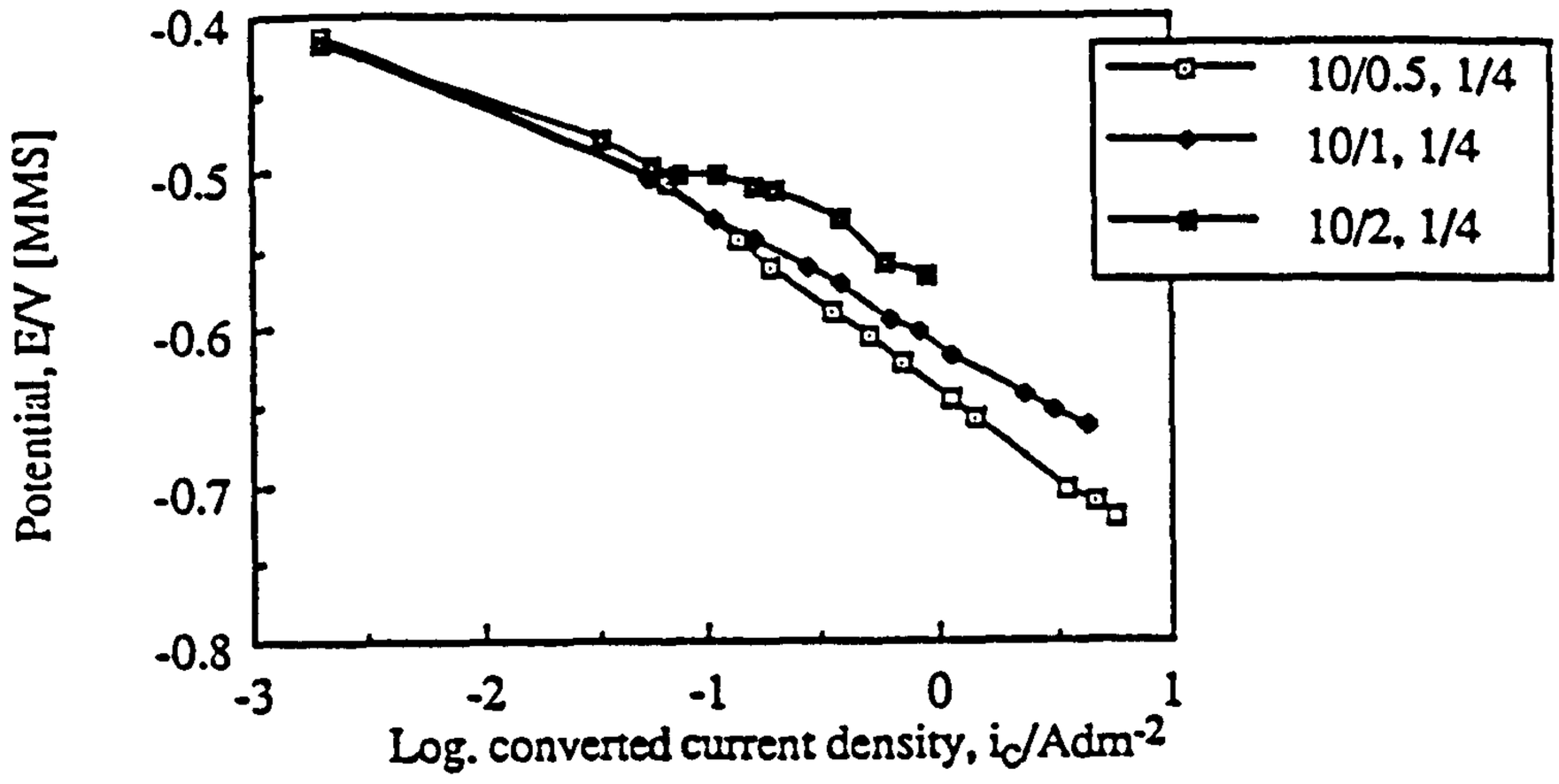

Figure 98b Potential versus logarithmic converted current density pulse reverse curves for different $t_{on(c)}/t_{on(a)}$ ratios but at a $i_{p(c)}/i_{p(a)}$ ratio of 1/4 using electrolyte V.

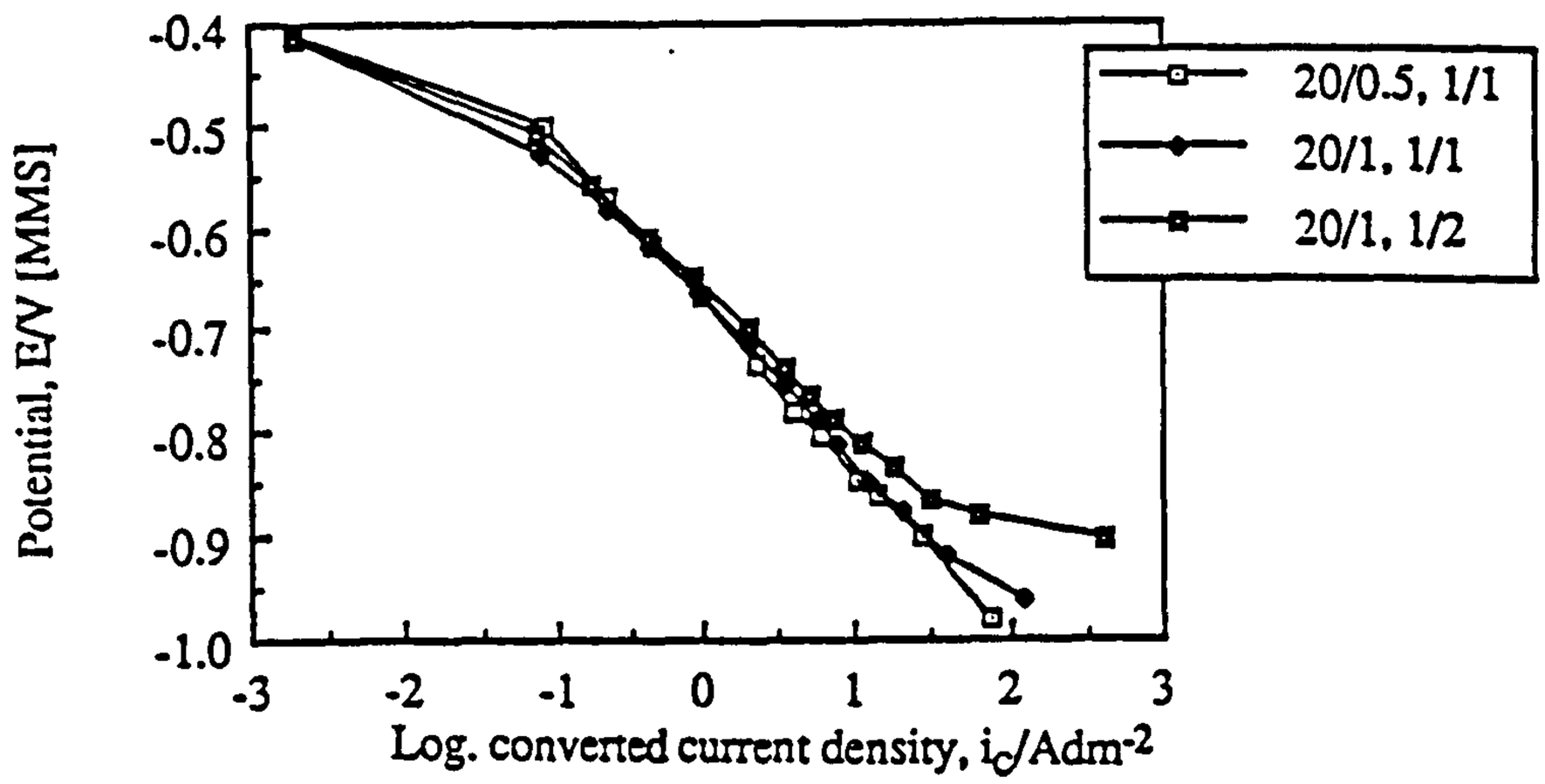

Figure 99b Potential versus logarithmic converted current density pulse reverse curves for different $t_{on(c)}/t_{on(a)}$ and also different $i_{p(c)}/i_{p(a)}$ ratios using electrolyte V.

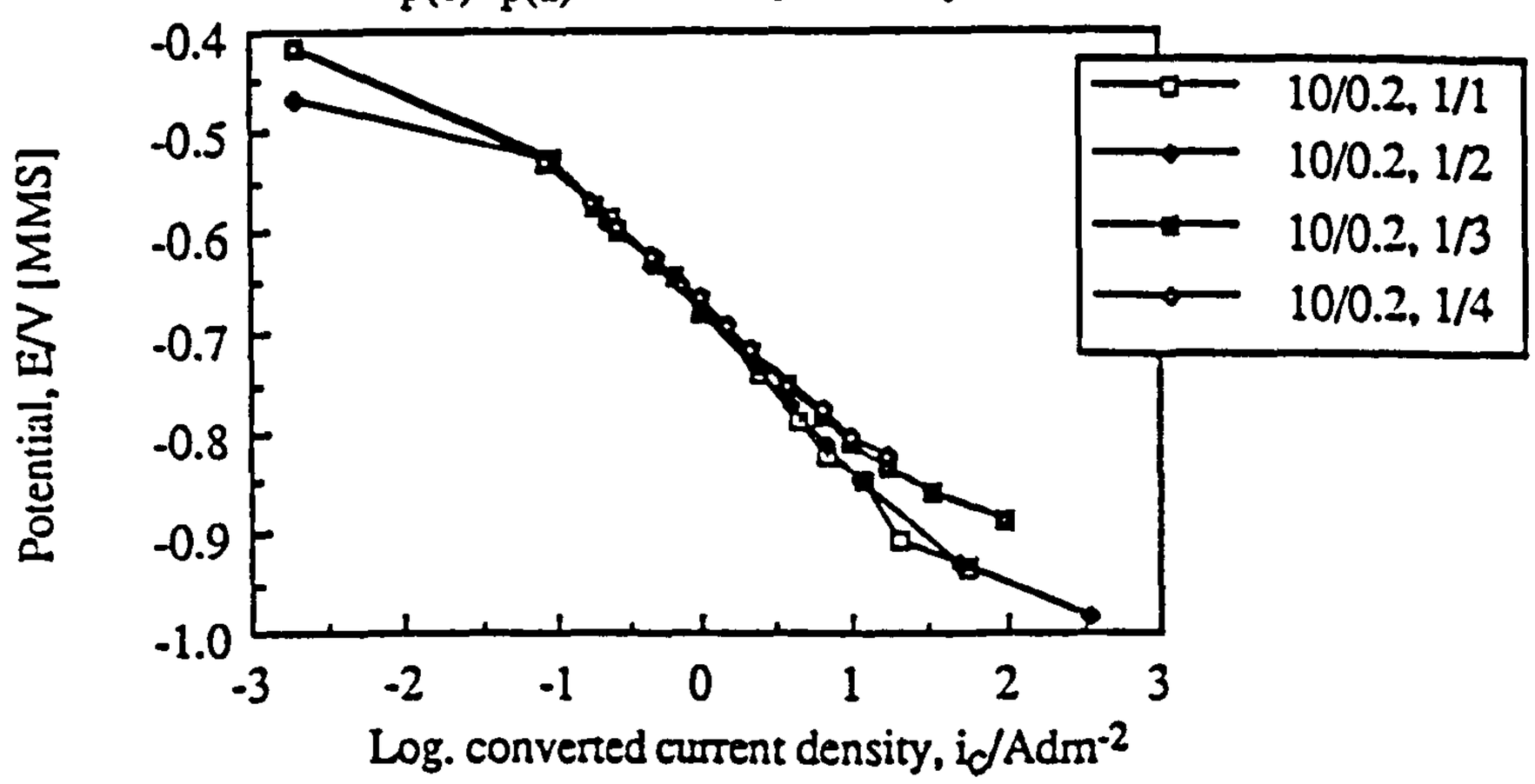

Figure 100b Potential versus logarithmic converted current density pulse reverse curves for $t_{on(c)}/t_{on(a)}$ ratio of 10ms/0.2ms but different $i_{p(c)}/i_{p(a)}$ ratios using electrolyte I.

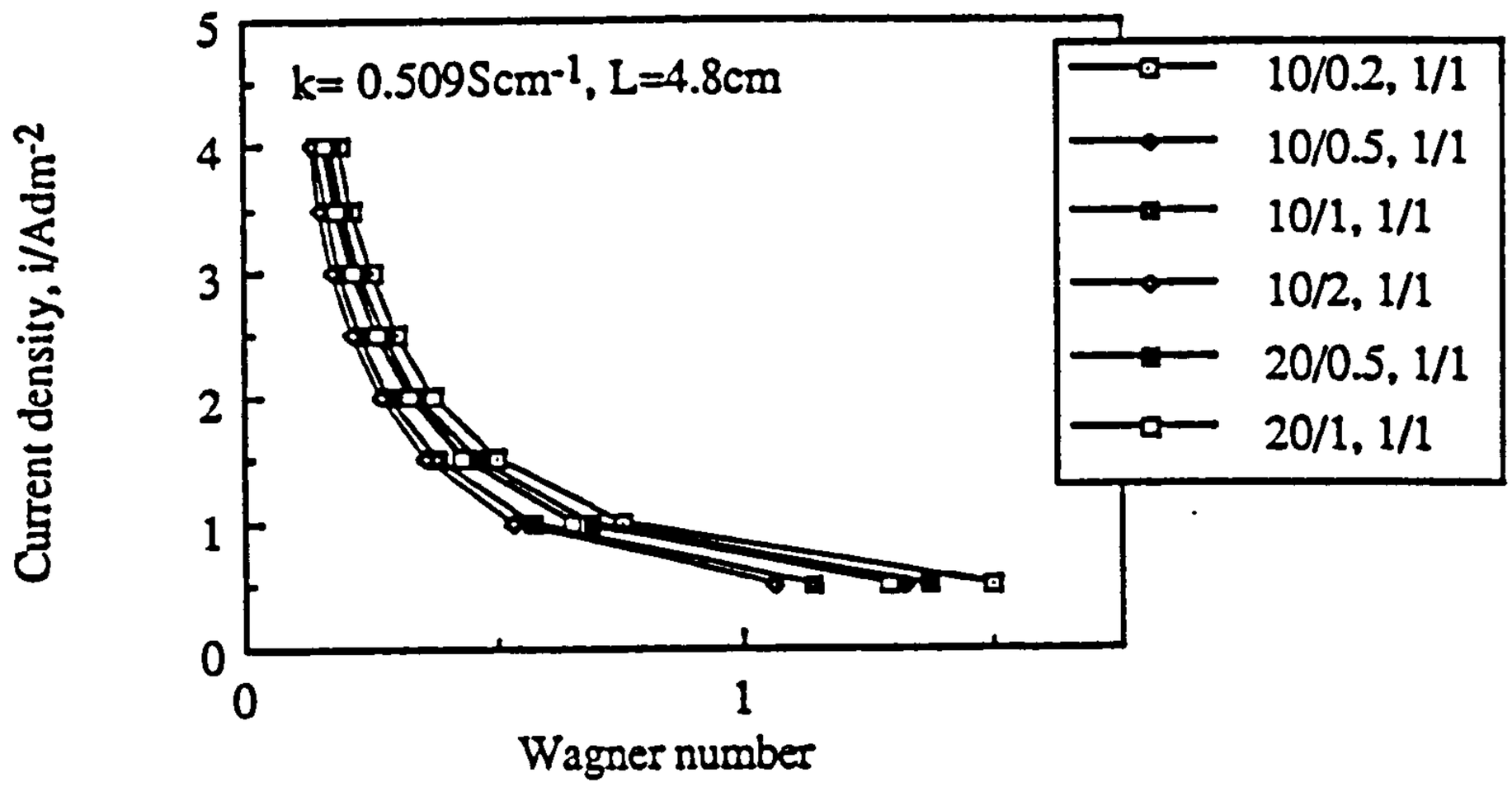

Figure 101 Relationship between current density and Wagner number under PR for different ton(c)/ton(a) ratios but at a $i_{p(c)}/i_{p(a)}$ ratio of 1/1 using electrolyte I.

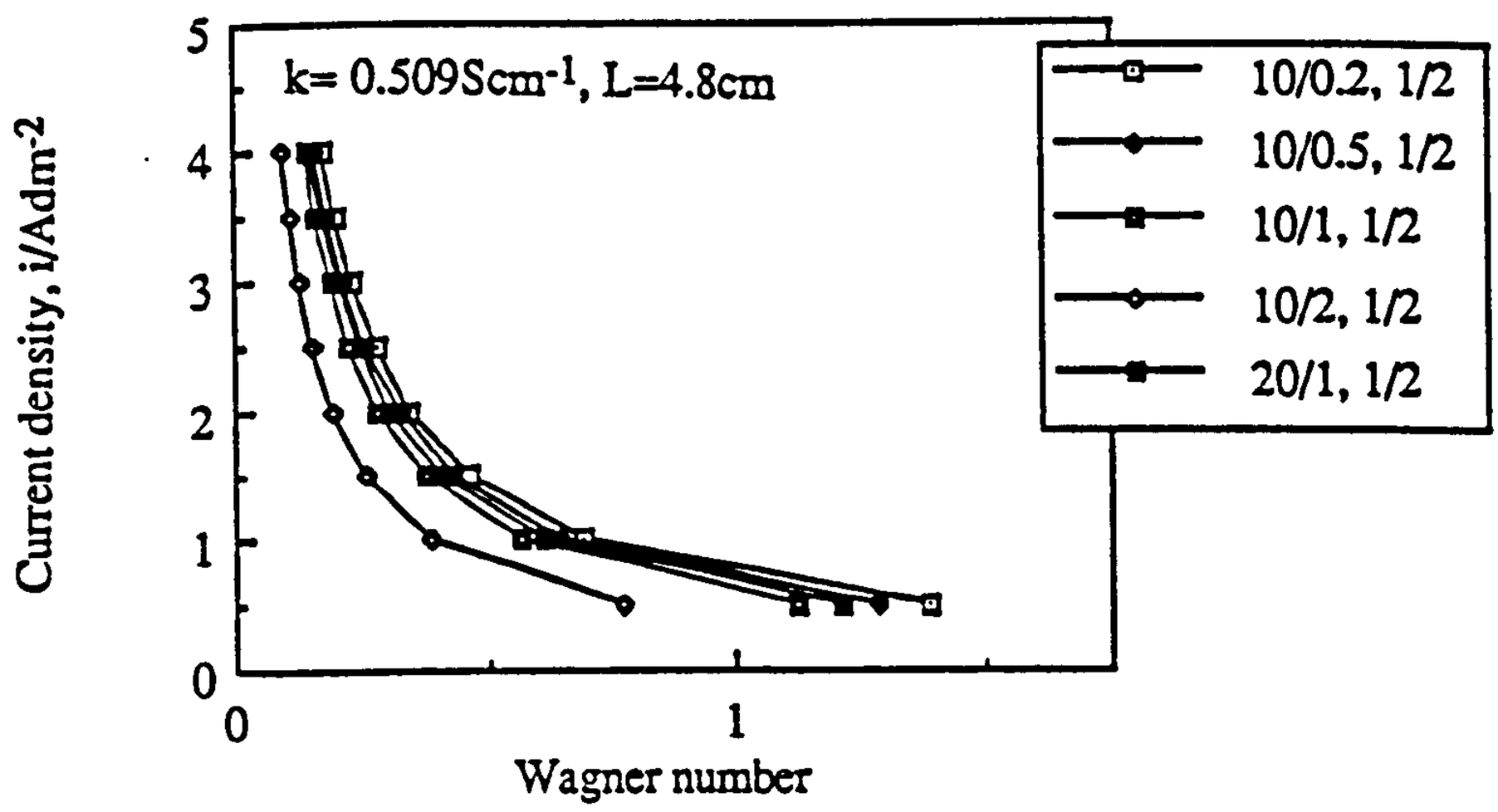

Figure 102 Relationship between current density and Wagner number under PR for different ton(c)/ton(a) ratios but at a $i_{p(c)}/i_{p(a)}$ ratio of 1/2 using electrolyte I.

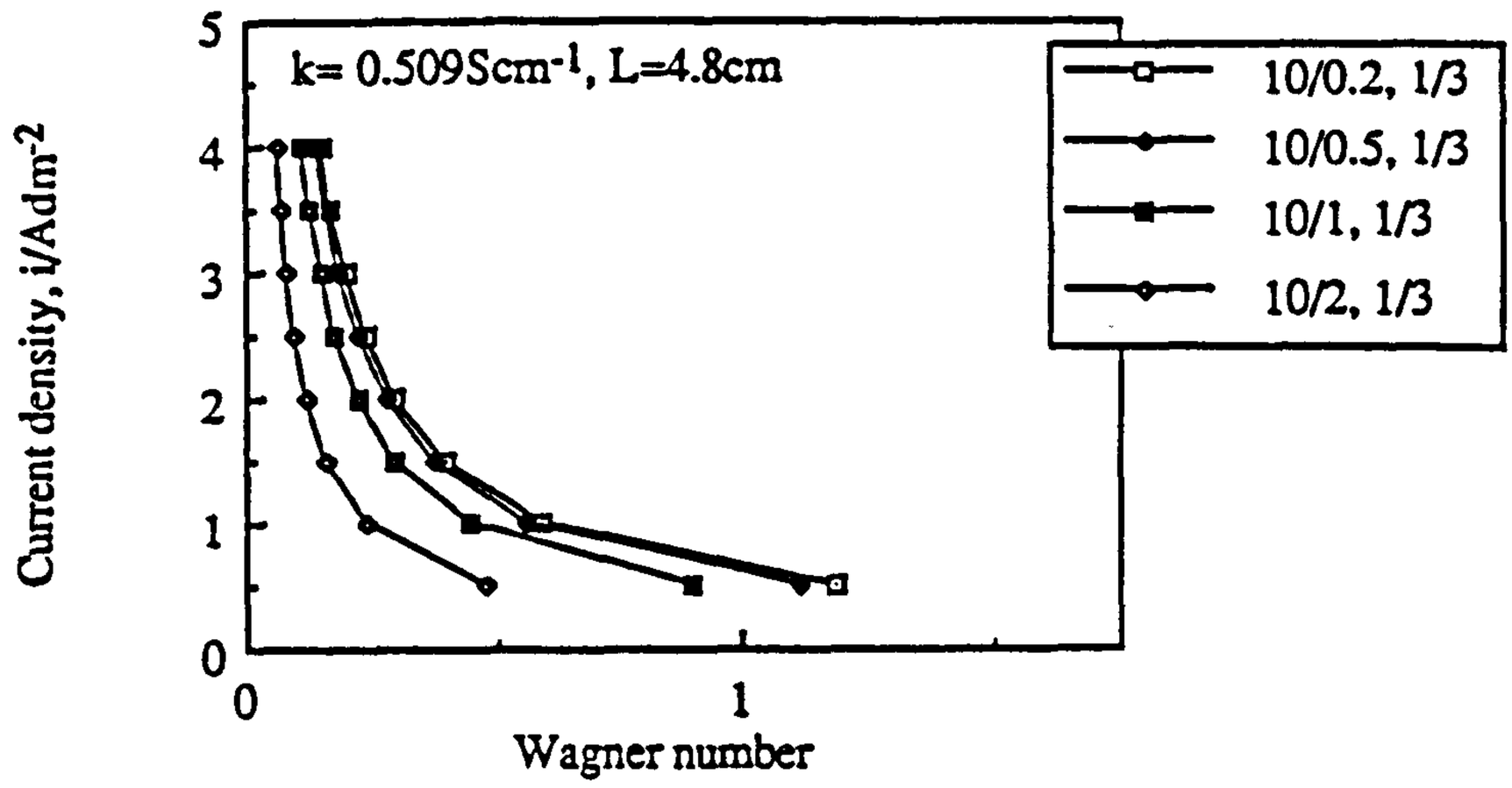

Figure 103 Relationship between current density and Wagner number under PR for different ton(c)/ton(a) ratios but at a $i_{p(c)}/i_{p(a)}$ ratio of 1/3 using electrolyte I.

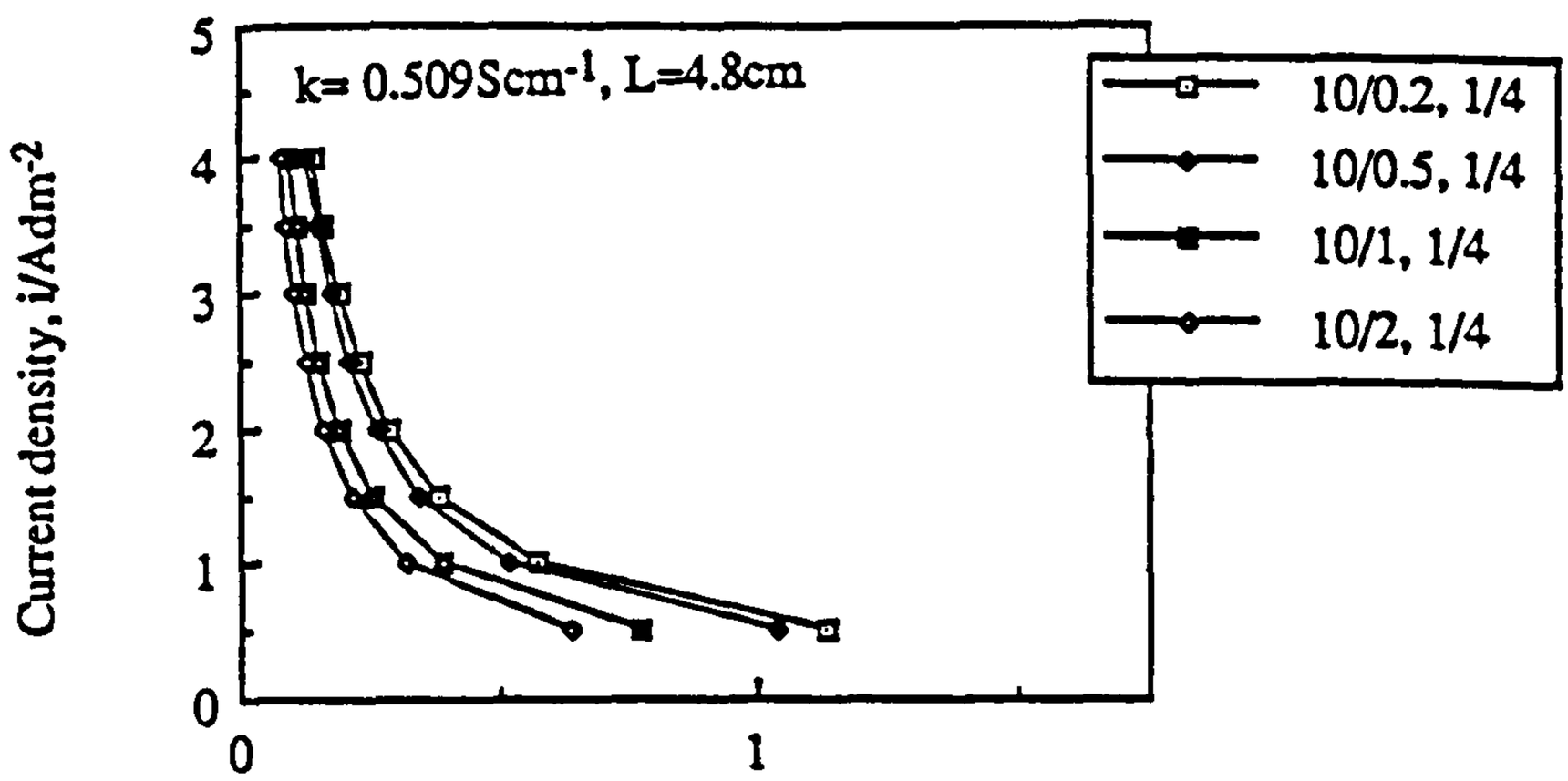

Figure 104 Relationship between current density and Wagner number under PR for different ton(c)/ton(a) ratios but at a $i_{p(c)}/i_{p(a)}$ ratio of 1/4 using electrolyte I.

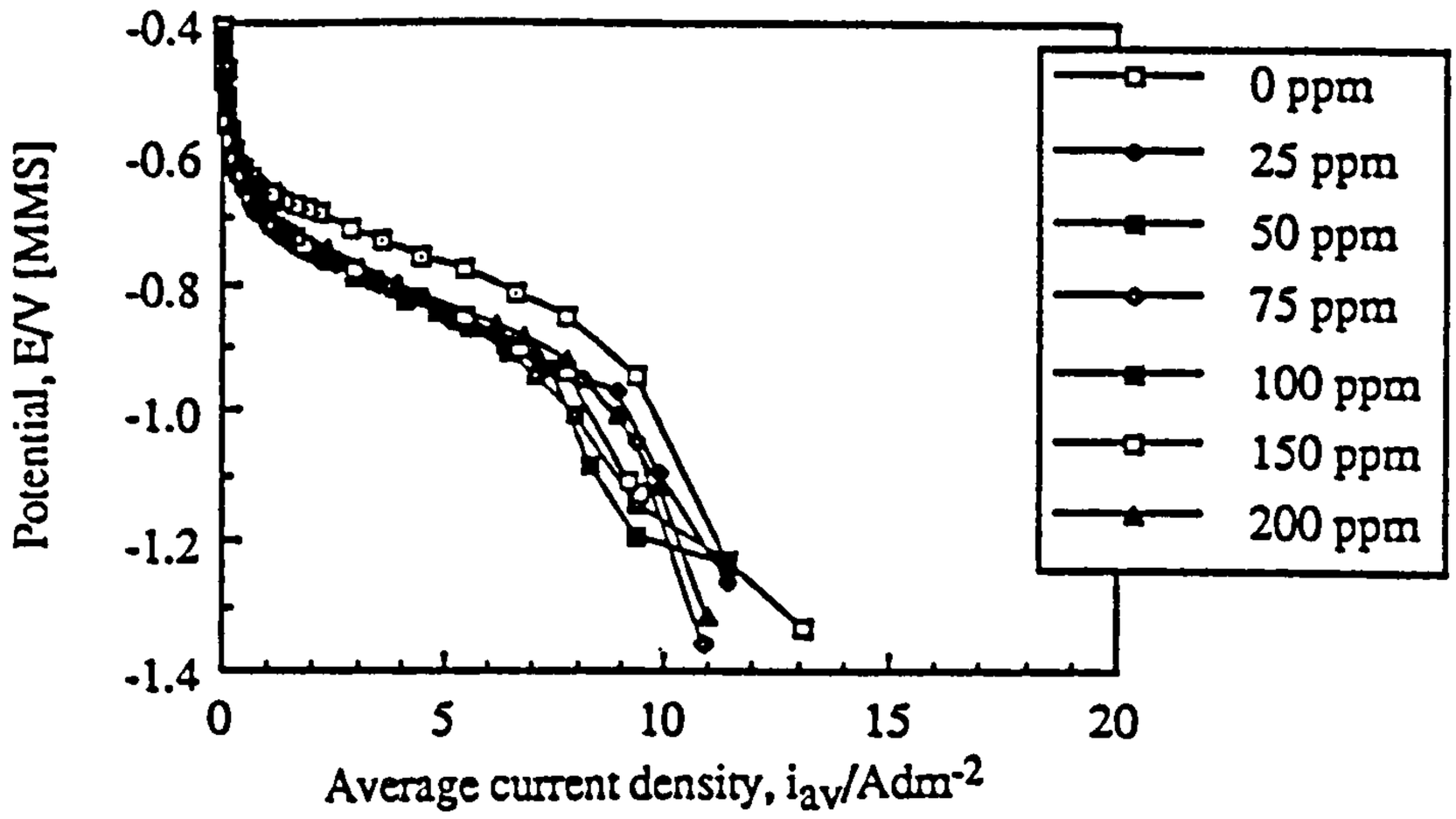

Figure 105a Polarisation curves obtained under DC condition with respect to Cl^- concentrations using electrolyte VIII and A&R agitation.

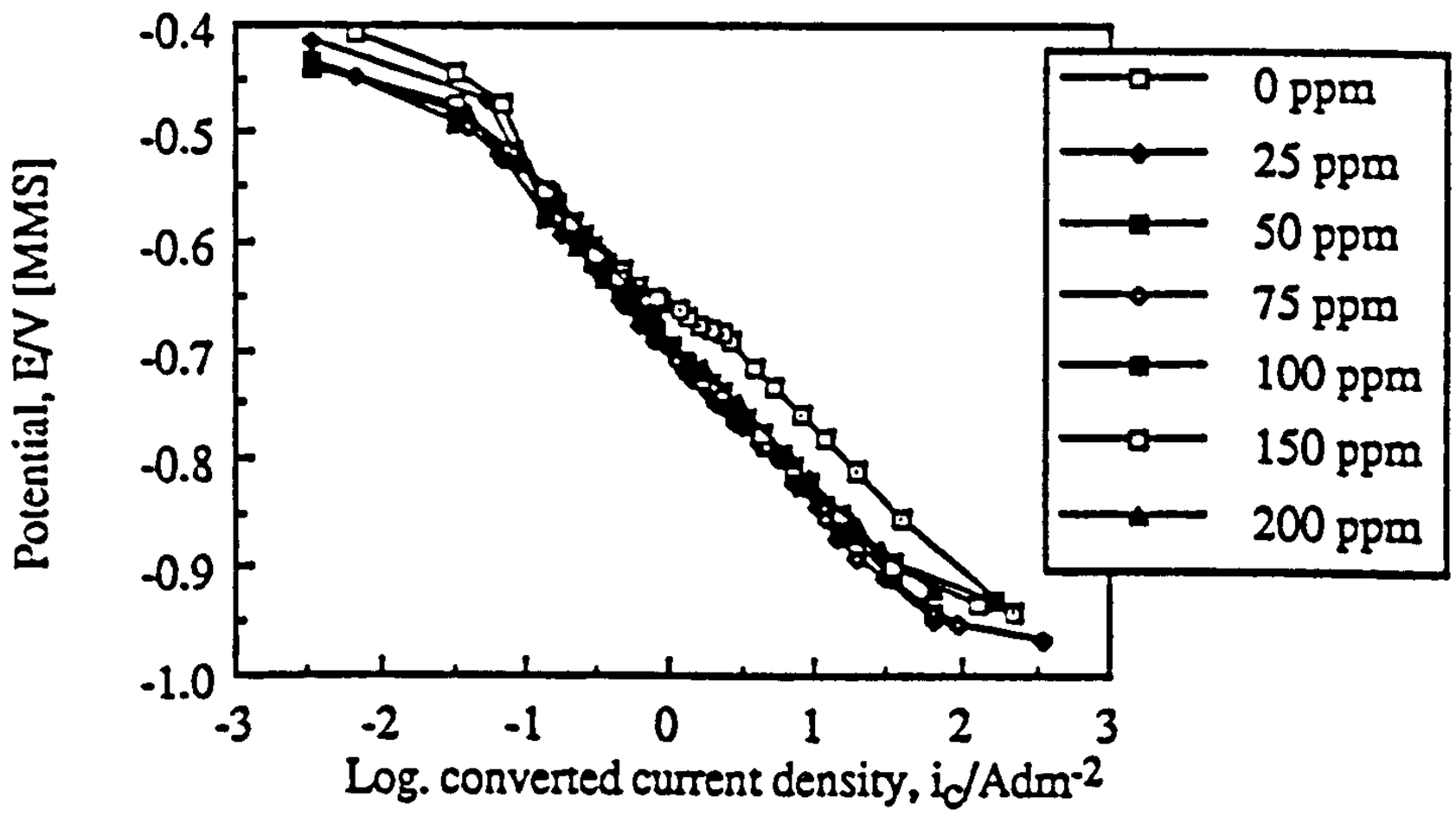

Figure 105b Potential versus logarithmic converted current density curves for different concentrations of Cl^- using electrolyte VIII under DC condition.

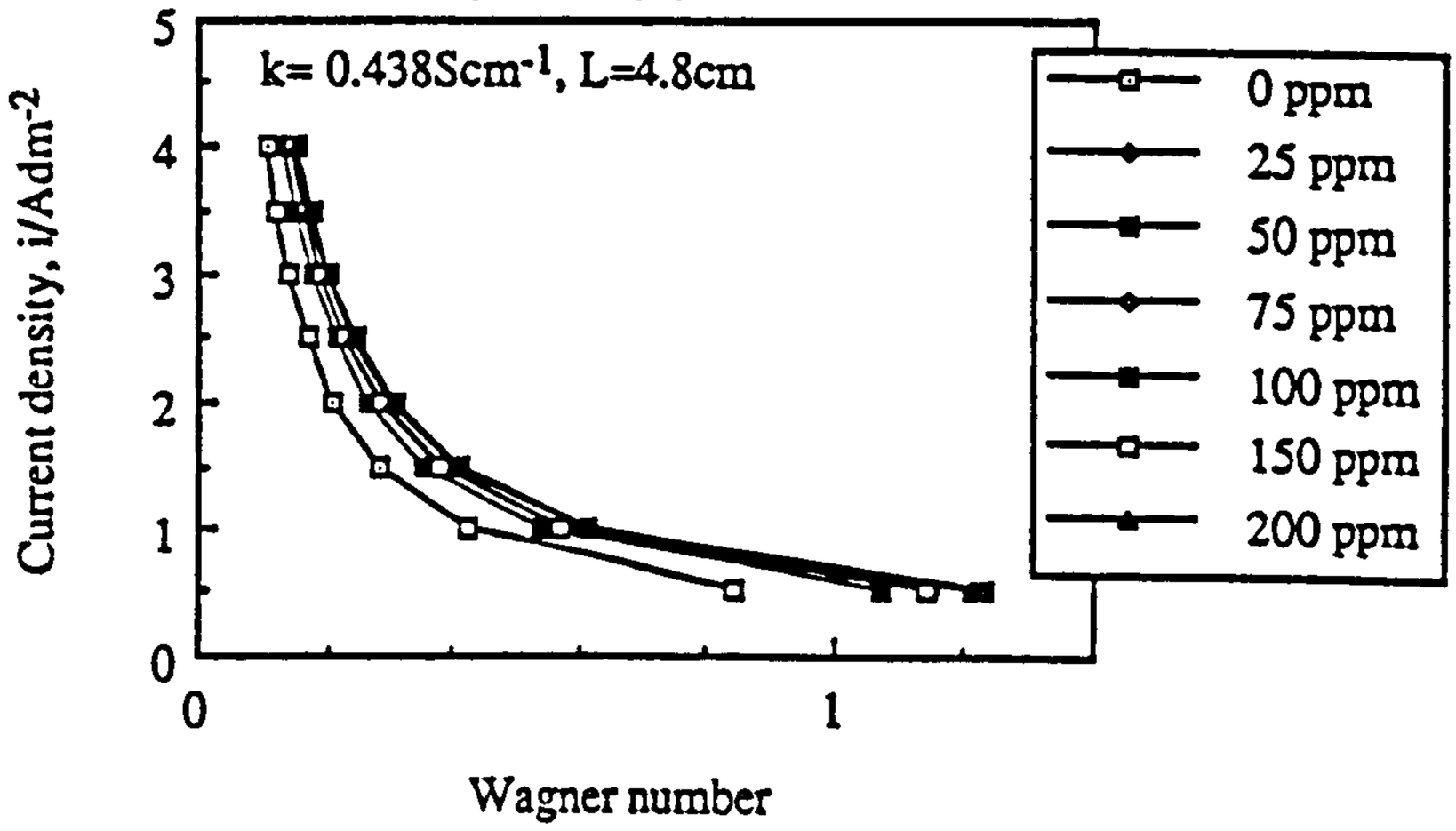

Figure 105c Current density versus Wagner number for different concentrations of Cl^- using electrolyte VIII under DC condition.

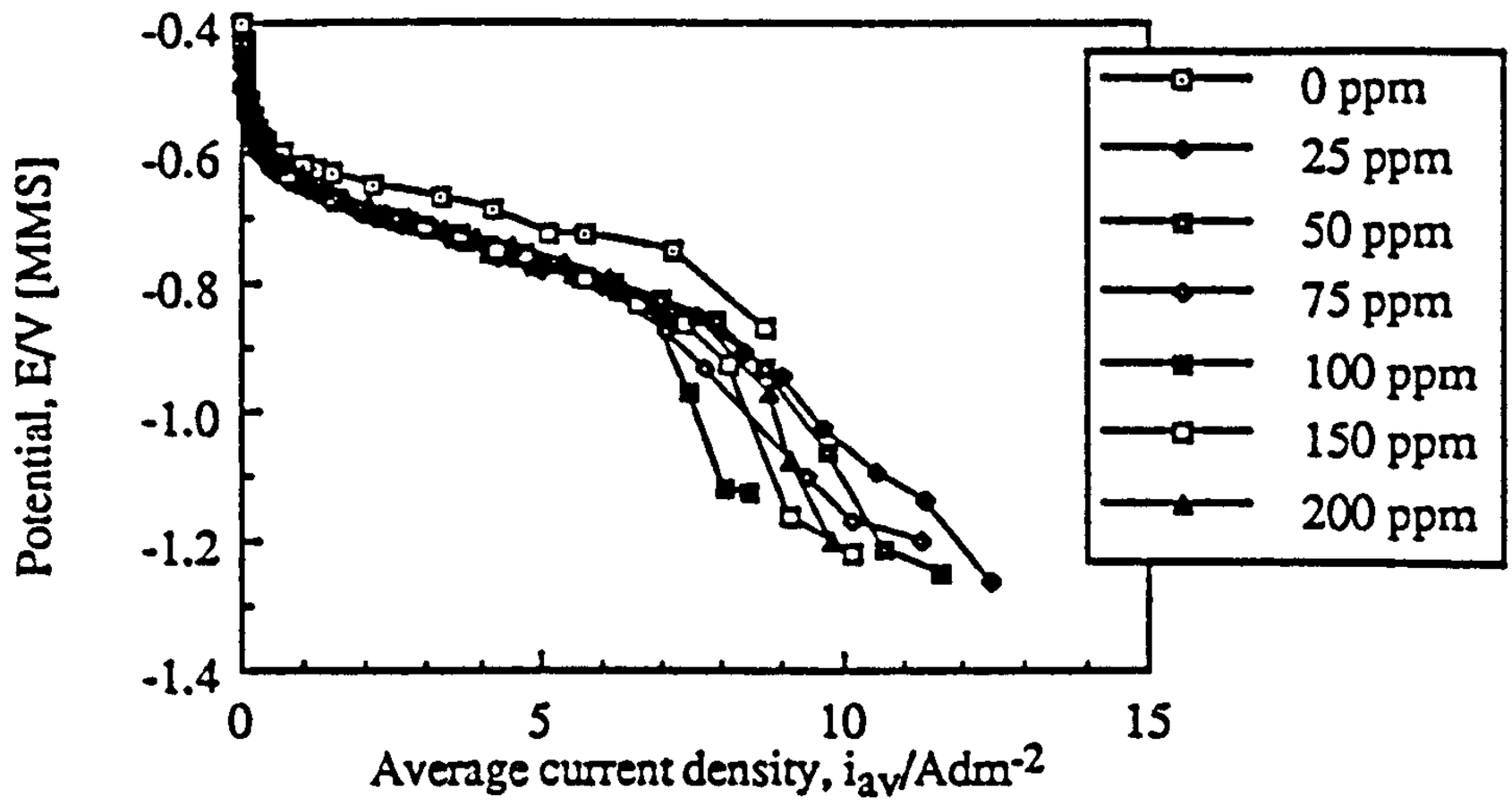

Figure 106a Polarisation curves obtained under P (100Hz,50%ϕ) condition with respect to Cl^- concentrations using electrolyte I and A&R agitation.

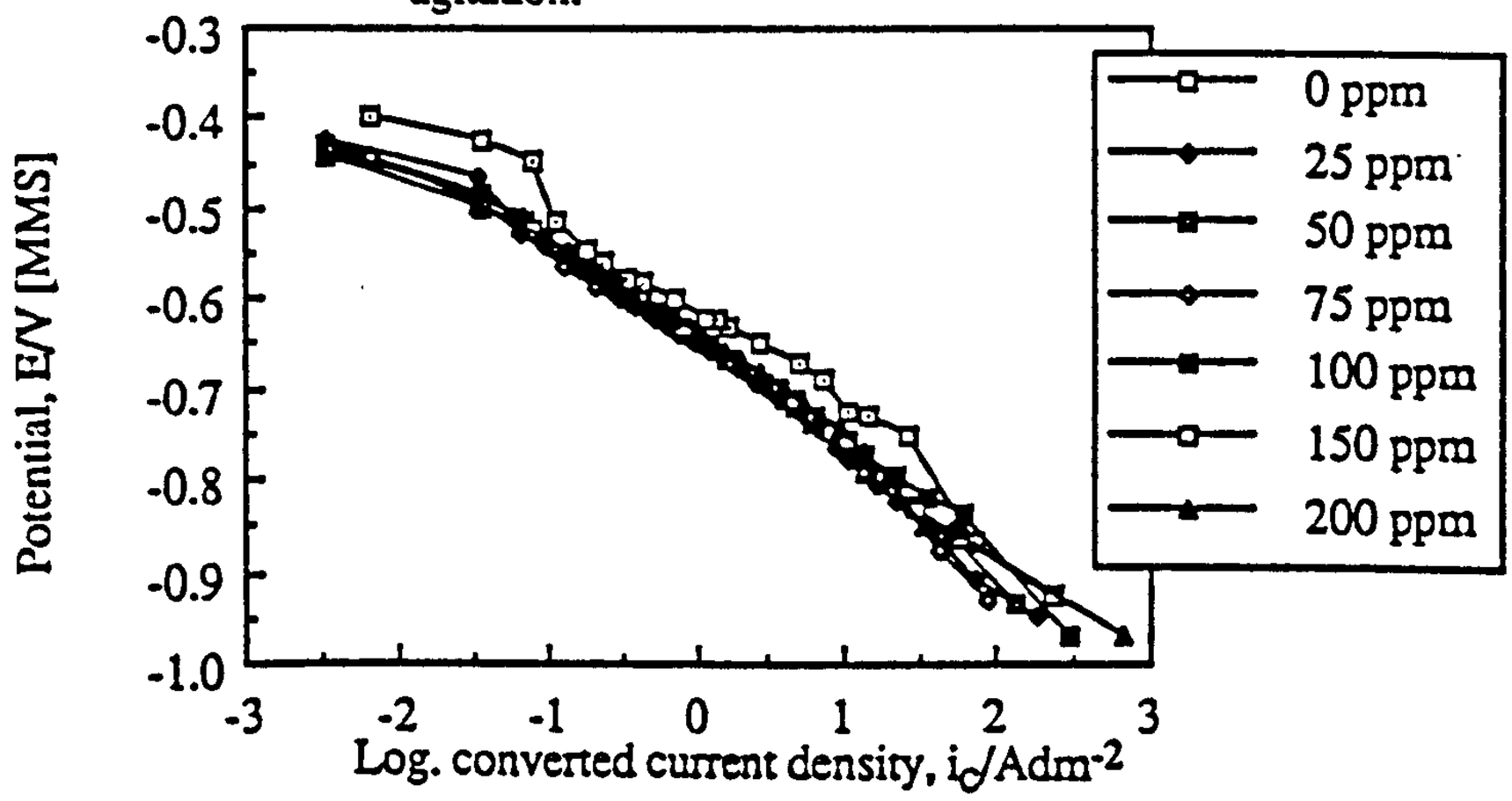

Figure 106b Potential versus logarithmic converted current density curves for different concentrations of Cl^- using electrolyte VIII under P (100Hz,50%ϕ) condition.

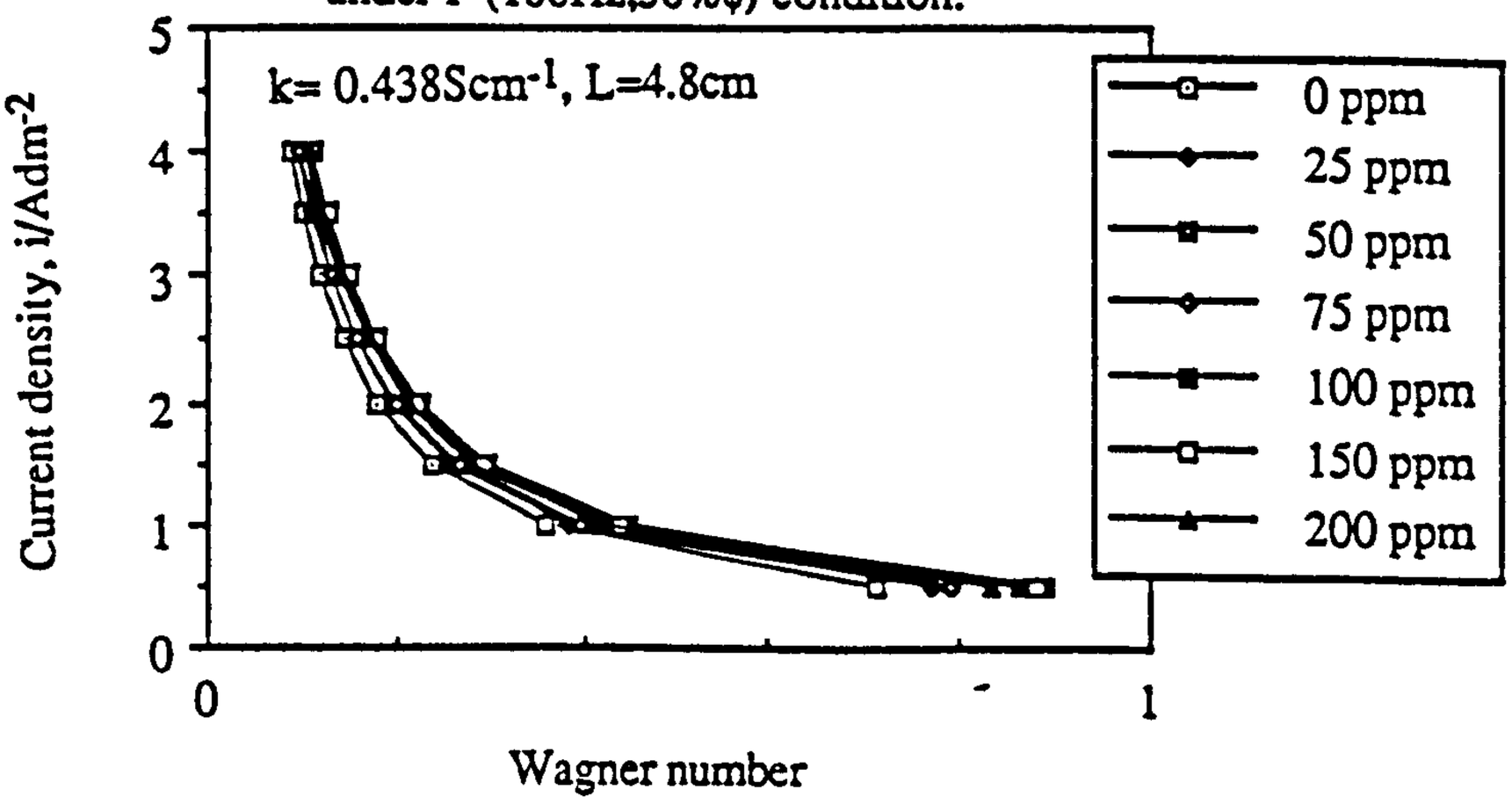

Figure 106c Current density versus Wagner number for different concentrations of Cl^- using electrolyte VIII under P (100Hz,50%ϕ) condition.

Figure 107

Representation of PCB's in cross-section for various hole diameters, current densities and electrolytes and also comparing DC to different Pulse conditions for different aspect ratios; suface:hole thickness ratios are also shown.

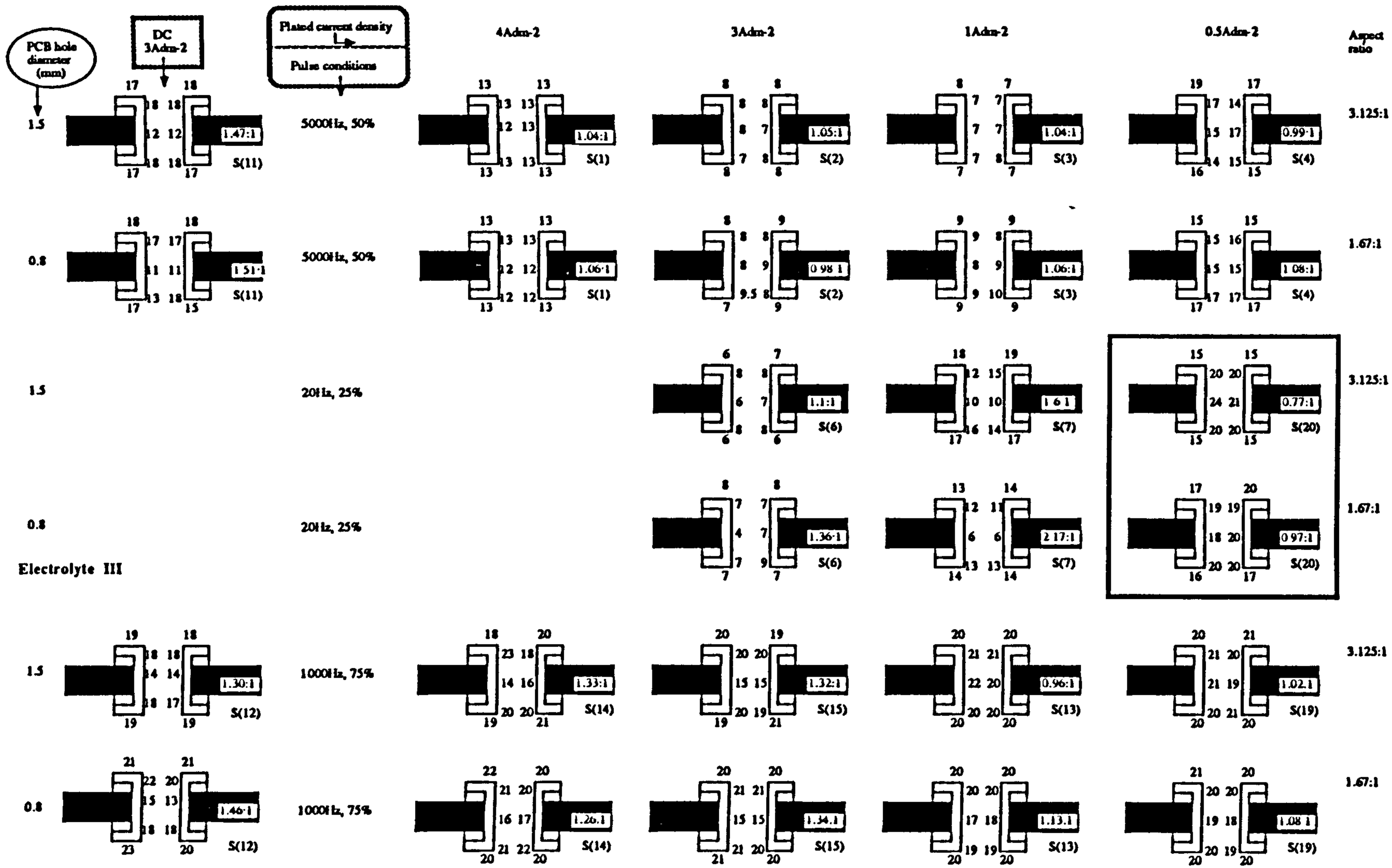

Figure 107 Continued ...

1.5	1000Hz, 75%	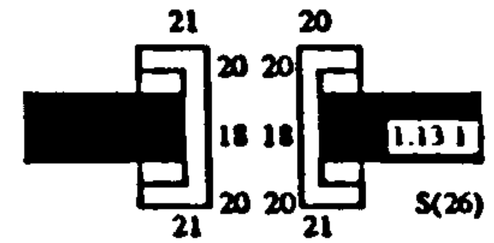			2:1
0.8	1000Hz, 75%	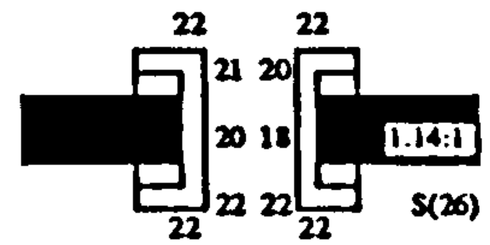			1.06:1
1.5	20Hz, 25%	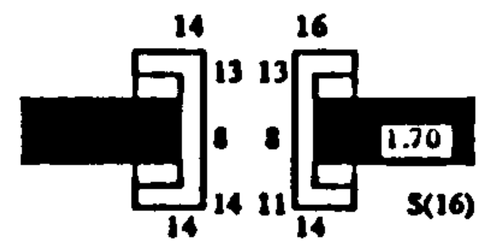	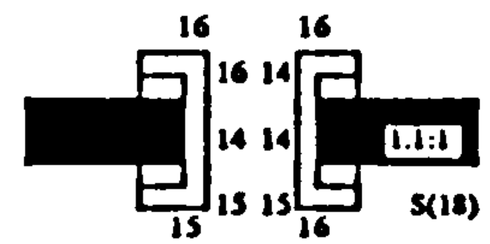	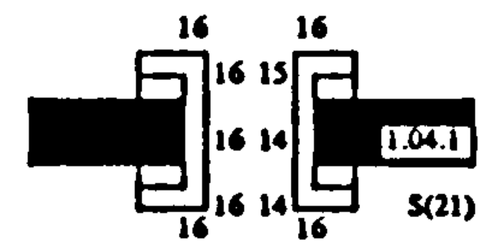	3.125:1
0.8	20Hz, 25%	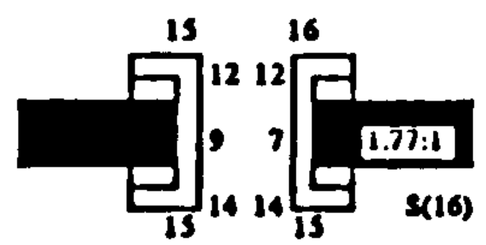	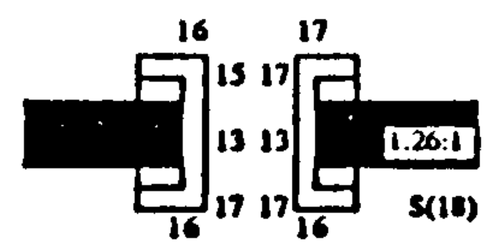	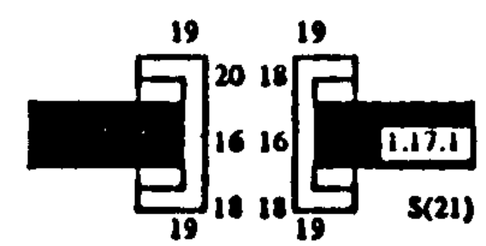	1.67:1
1.5	20Hz, 25%	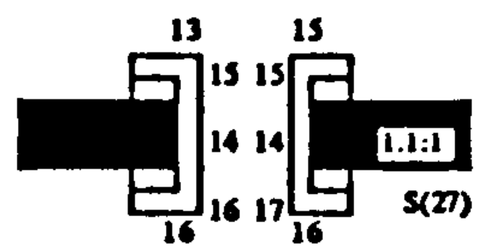			2:1
0.8	20Hz, 25%	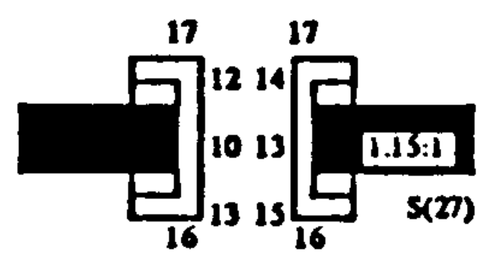			1.06:1

Figure 107 Continued ...

Electrolyte V

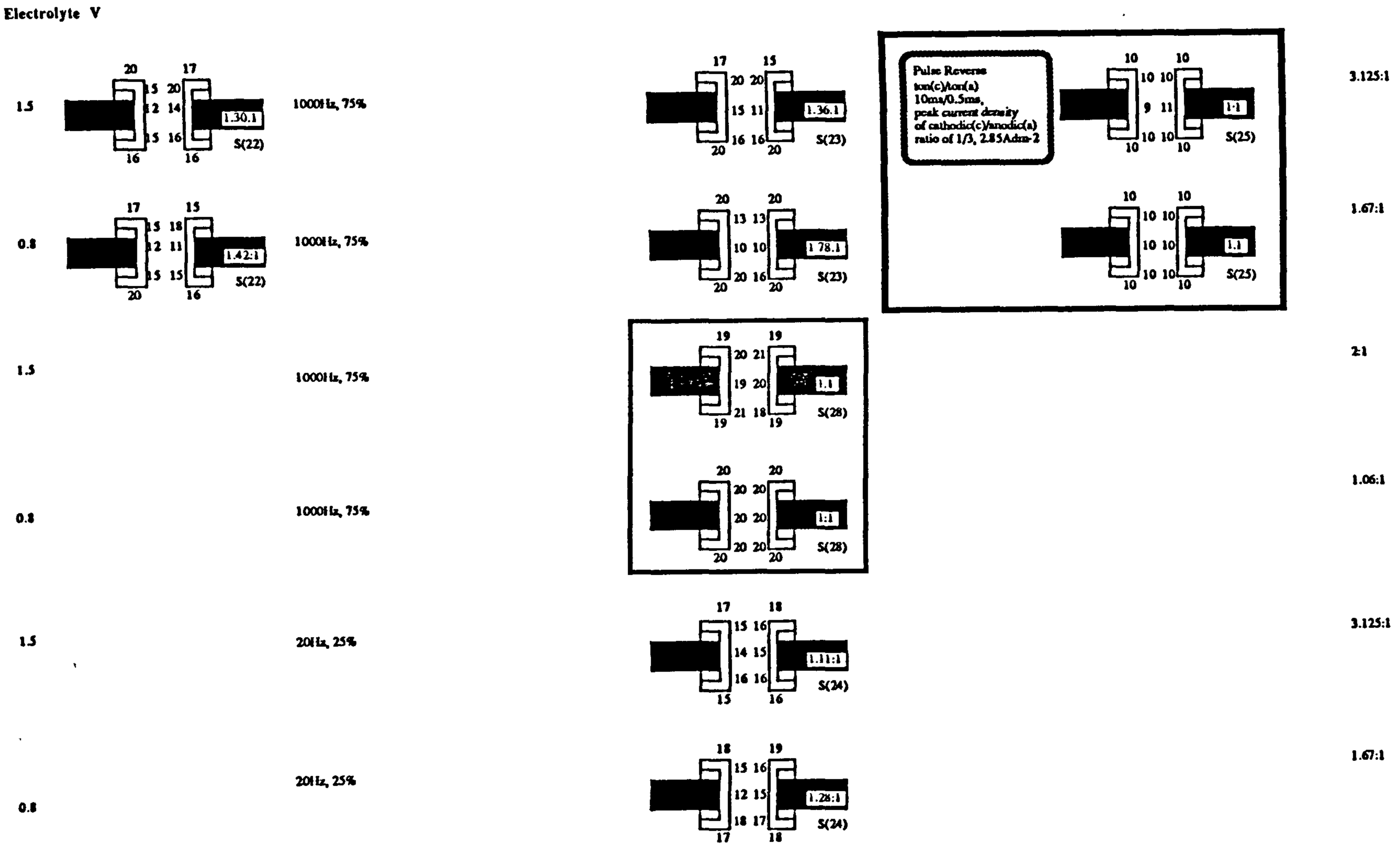

S indicates sample and ( ) indicates the sample number

Figure 108

Representation of PCB's in cross-section for various hole diameters and electrolytes at 3.0Adm-2 and also comparing DC to different Pulse conditions for different aspect ratios; suface:hole thickness ratios are also shown.

Electrolyte I

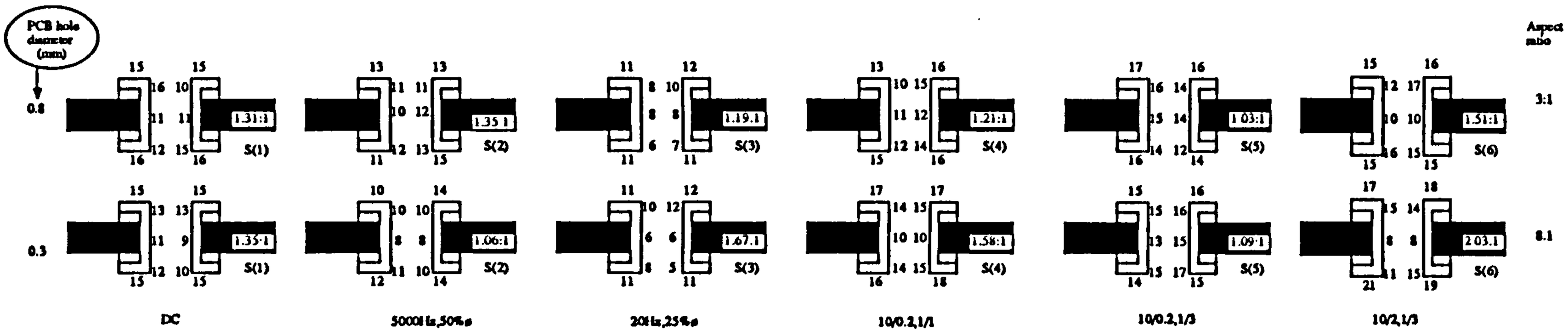

Electrolyte III

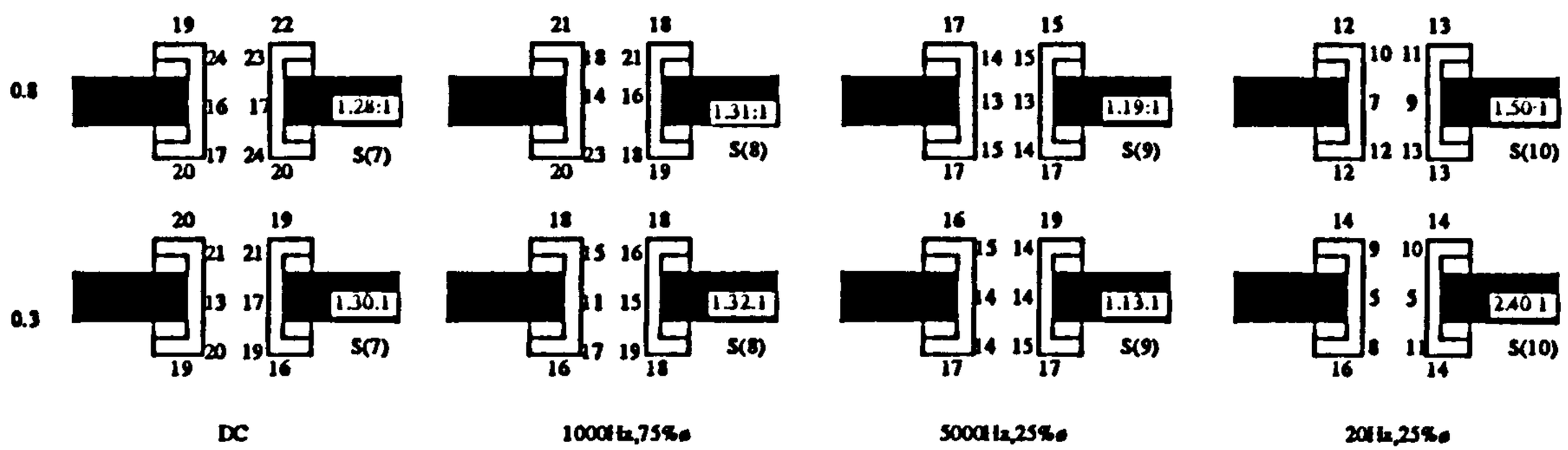

Figure 108 Continued ...

Electrolyte V

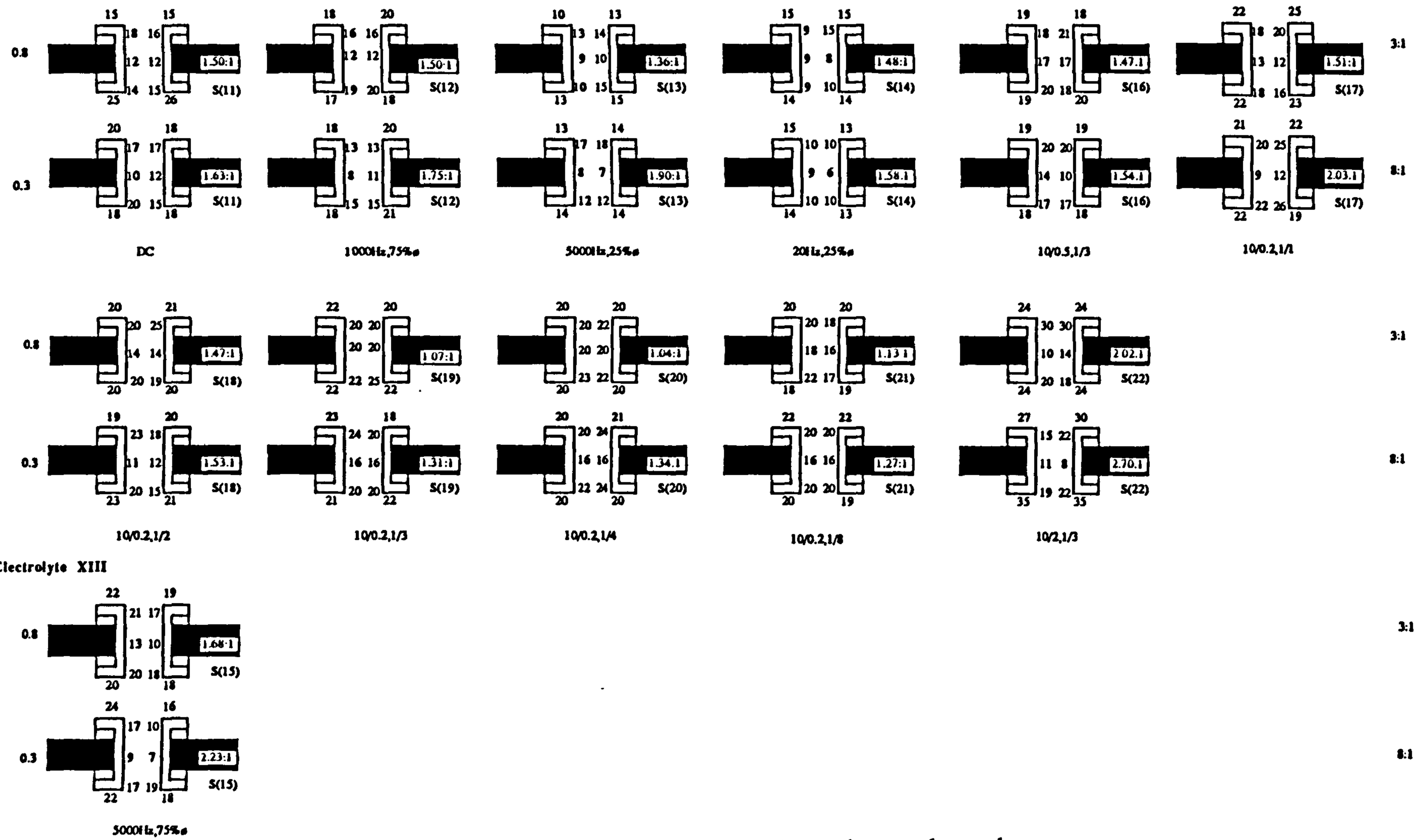

Electrolyte XIII

S indicates sample and ( ) indicates the sample number

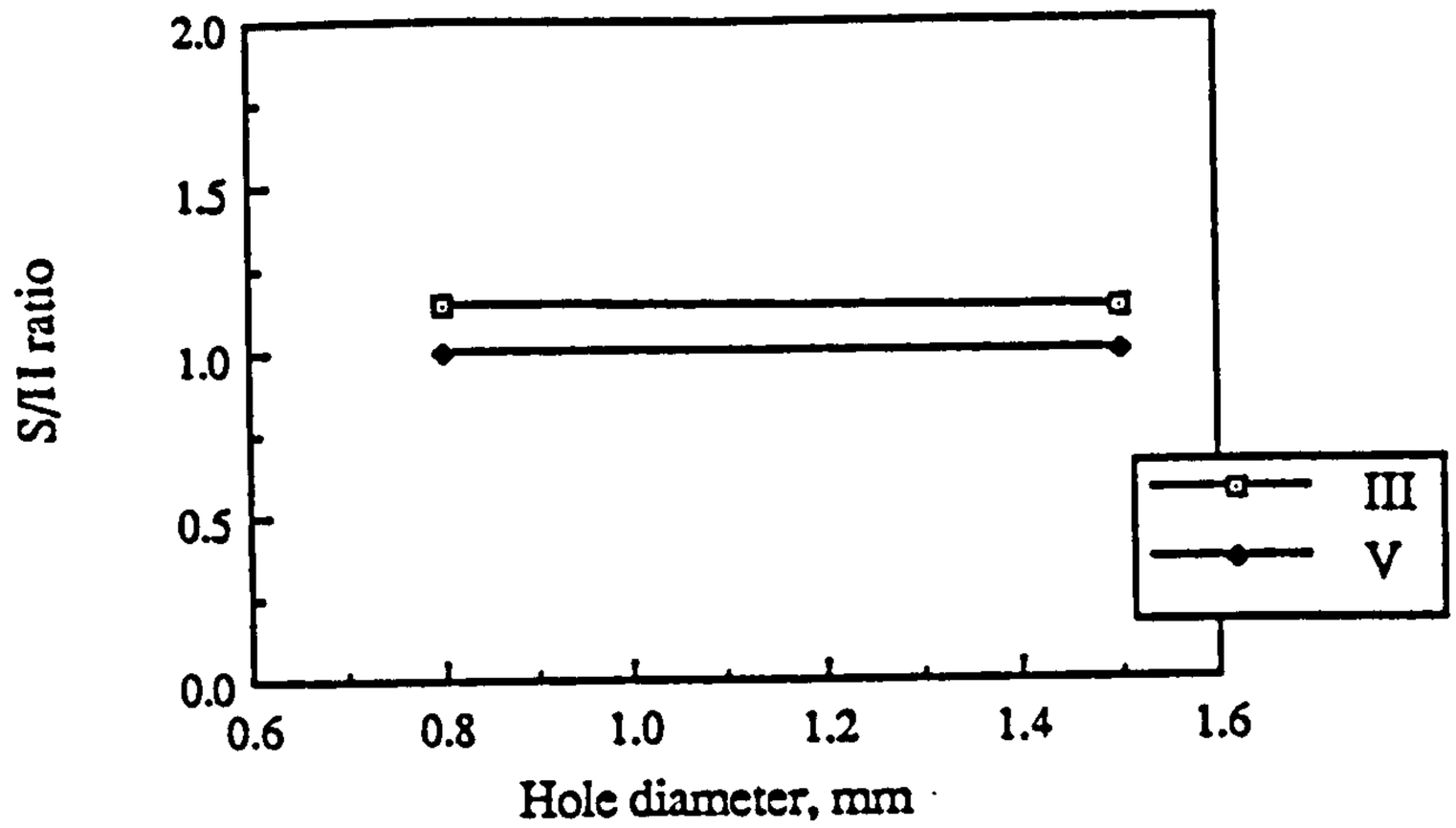

Figure 109a Shows the surface to hole thickness ratio against hole diameter having board thickness of 1.6mm for electrolytes III and V.

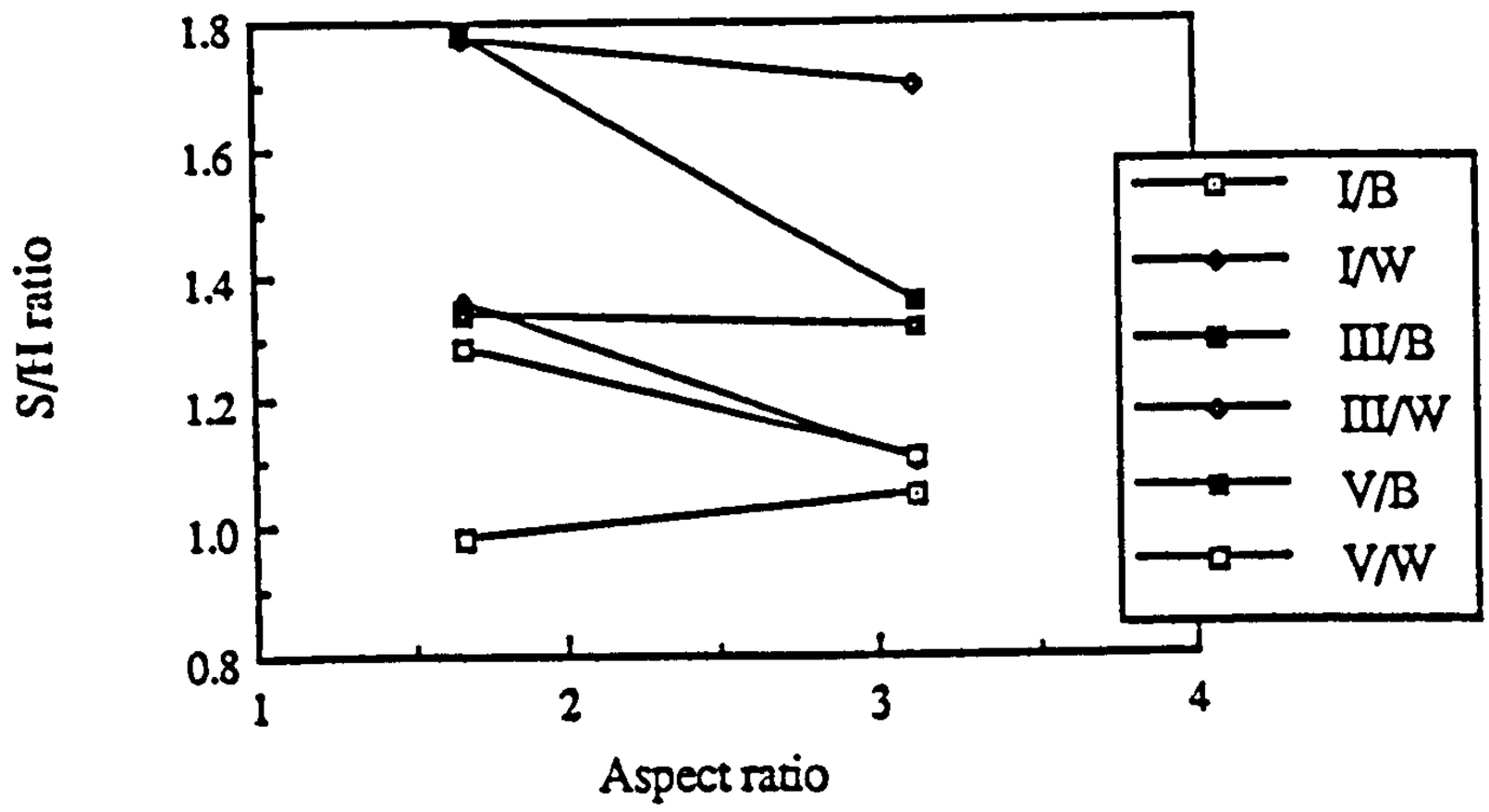

Figure 109b Shows the surface to hole thickness ratio versus aspect ratio; board thickness of 2.5mm using electrolytes I, III and V under best(B) and worst(W) conditions.

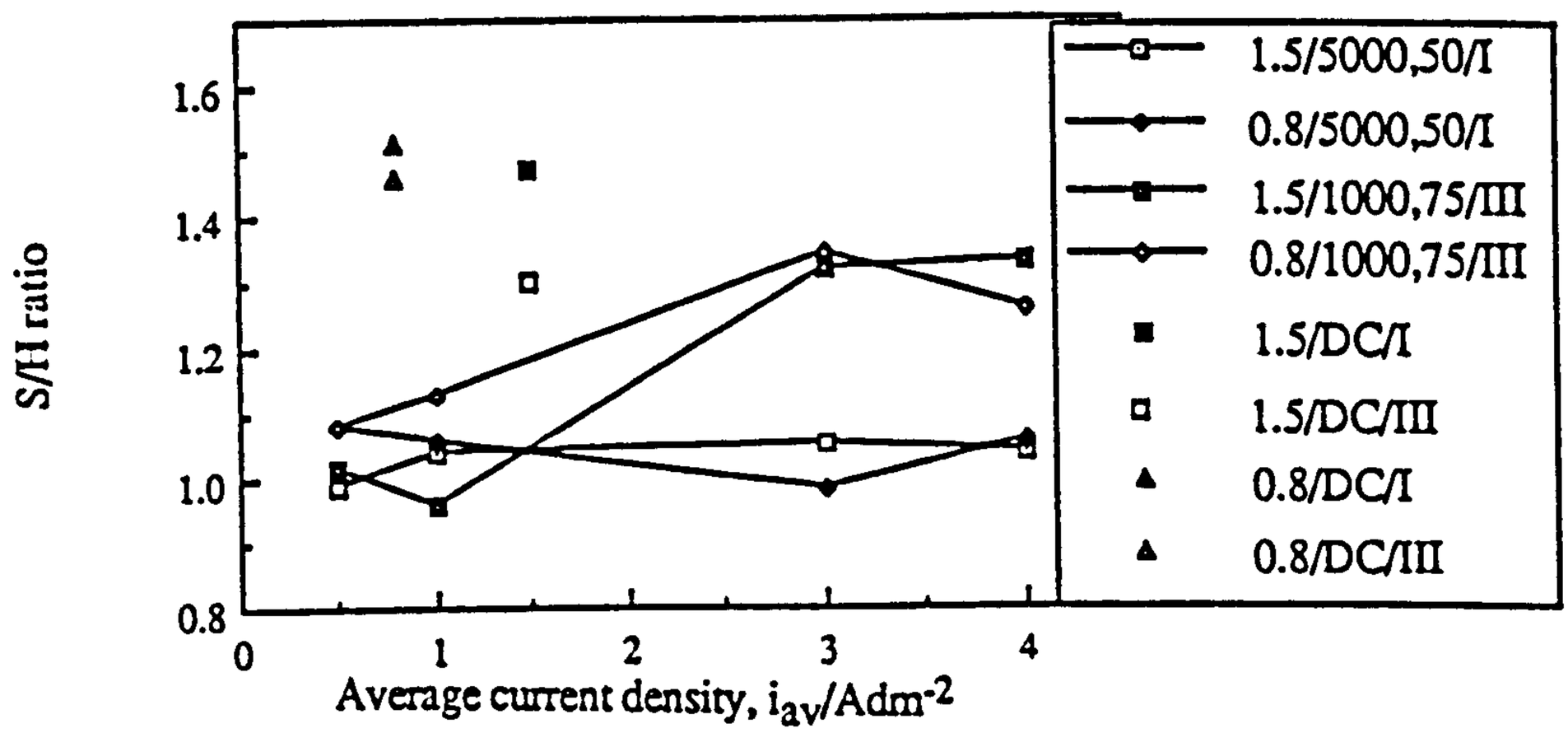

Figure 109c Shows the surface to hole thickness ratio against average current density for different hole diameters under DC and best pulse conditions using electrolytes I and III for board thickness of 2.5mm.

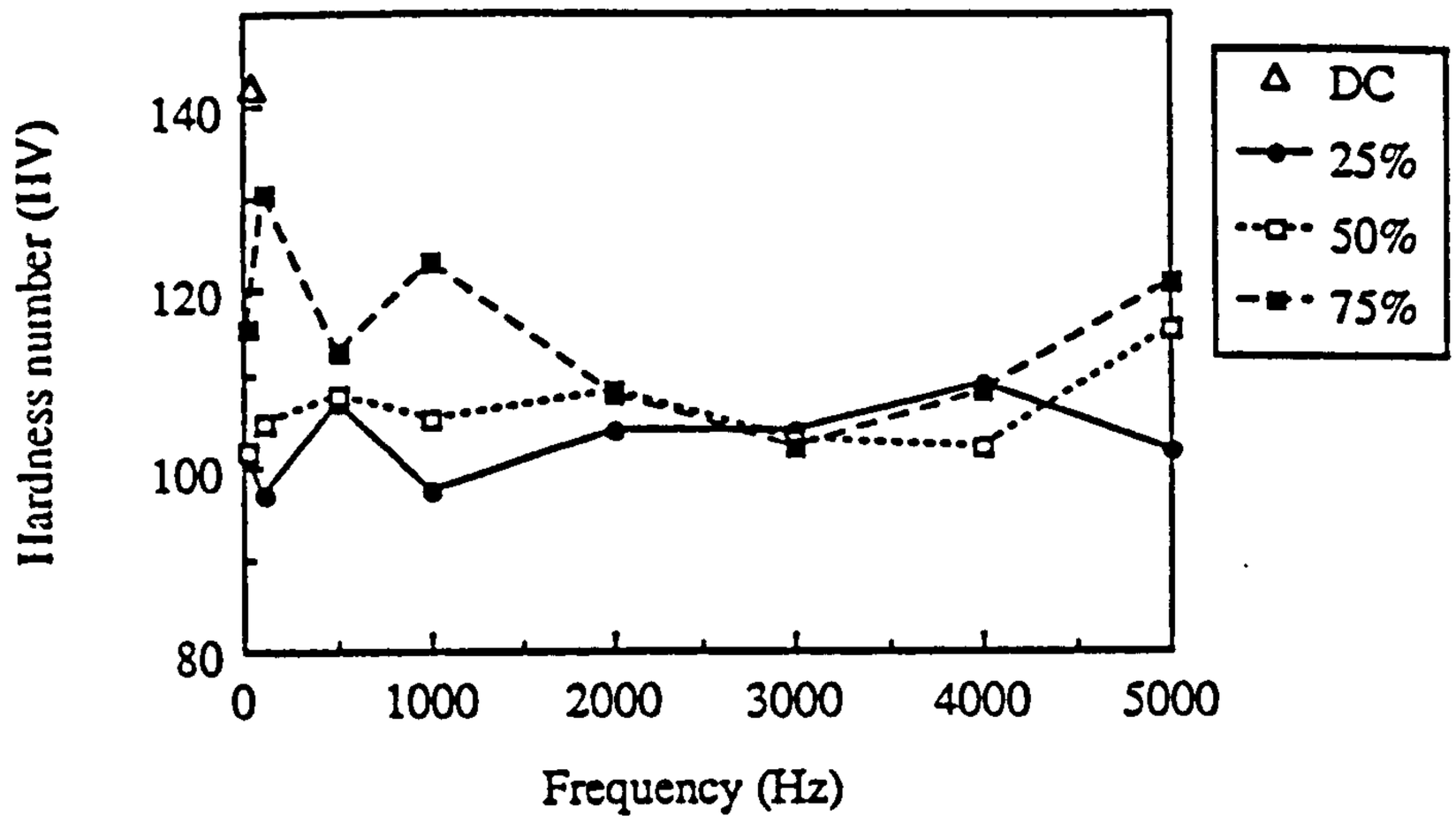

Figure 110a Hardness number against frequency using electrolyte I.

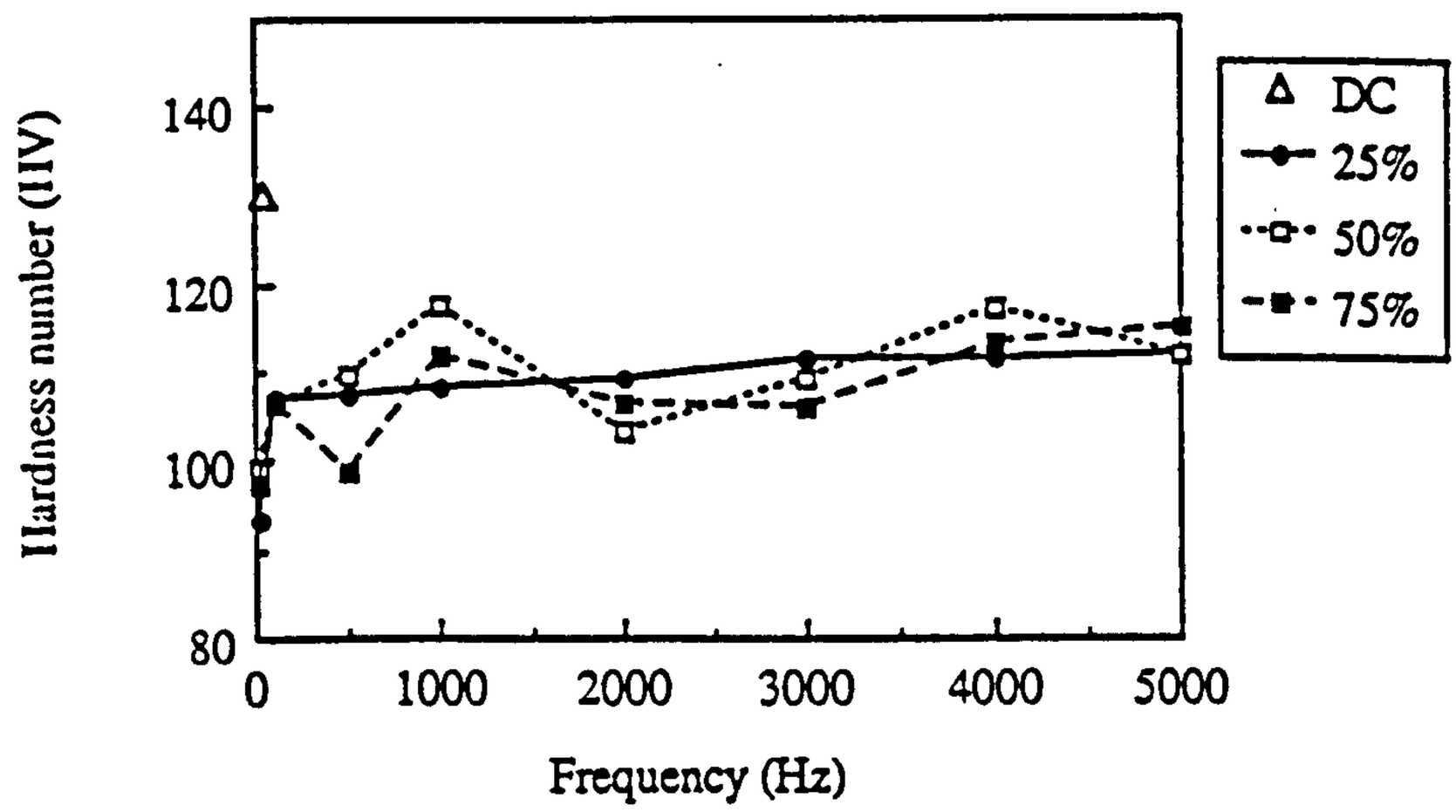

Figure 110b Hardness values against frequency using electrolyte V.

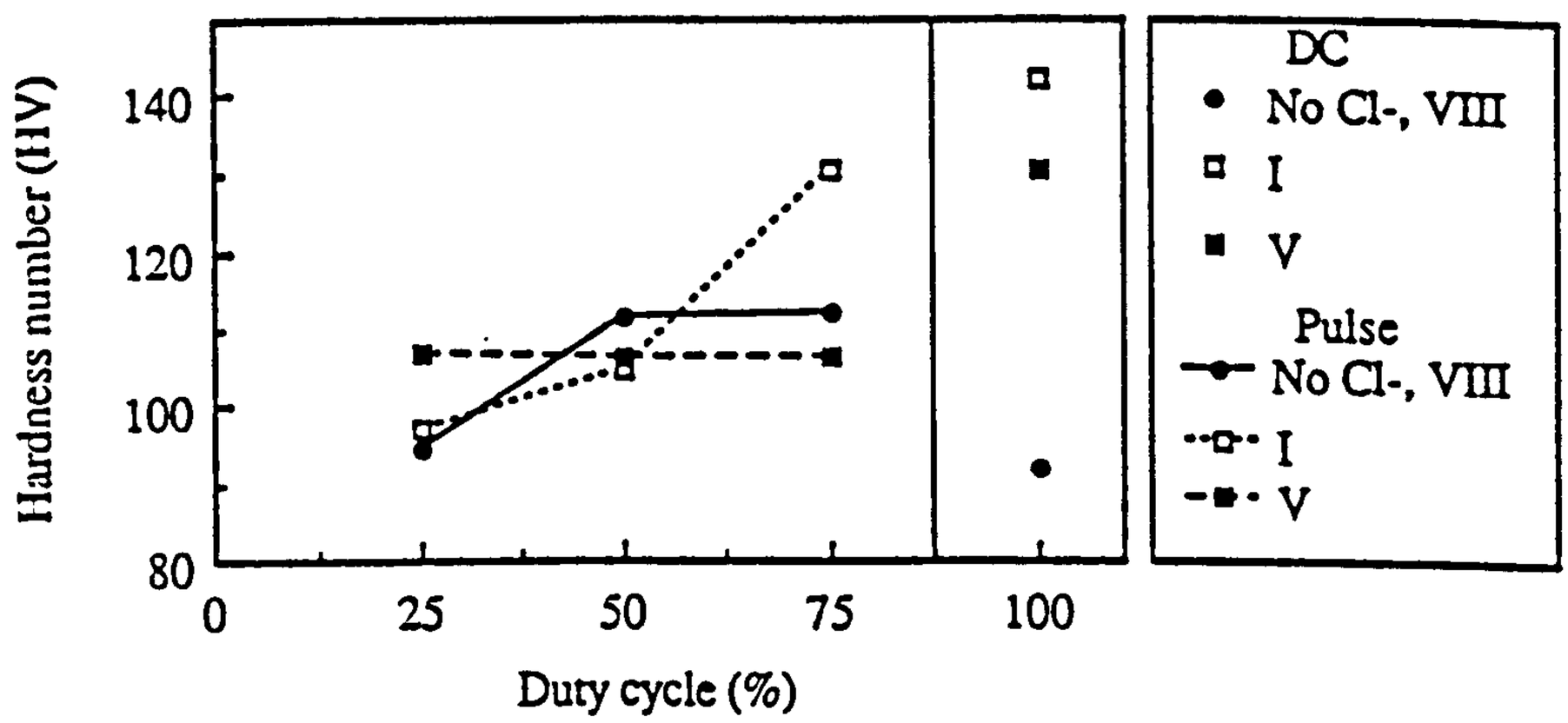

Figure 110c Hardness values against duty cycle using electrolytes VIII, I and V at a frequency of 100Hz and also DC values for the three electrolytes.

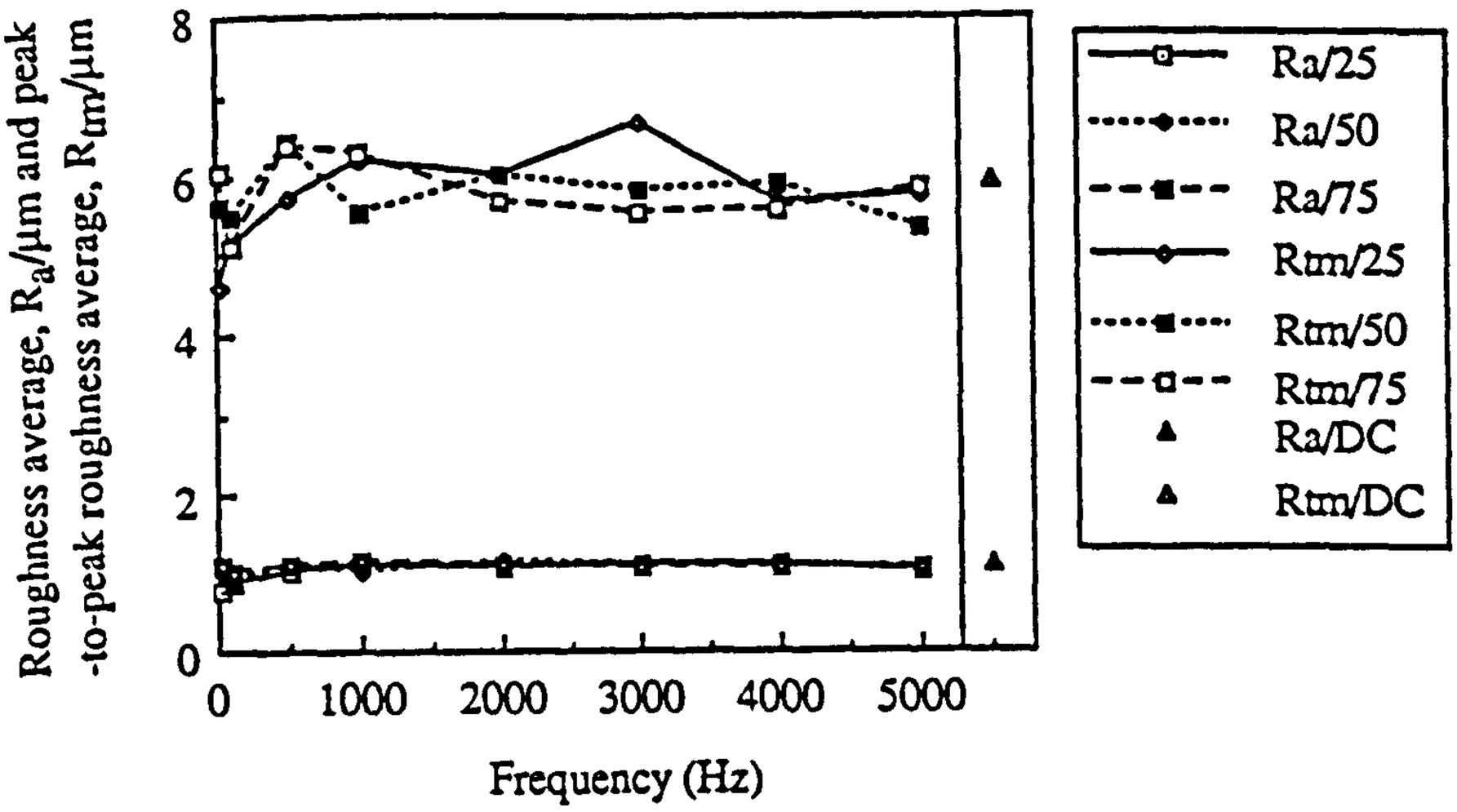

Figure 111a Roughness average and peak-to-peak average roughness against frequency using electrolyte I.

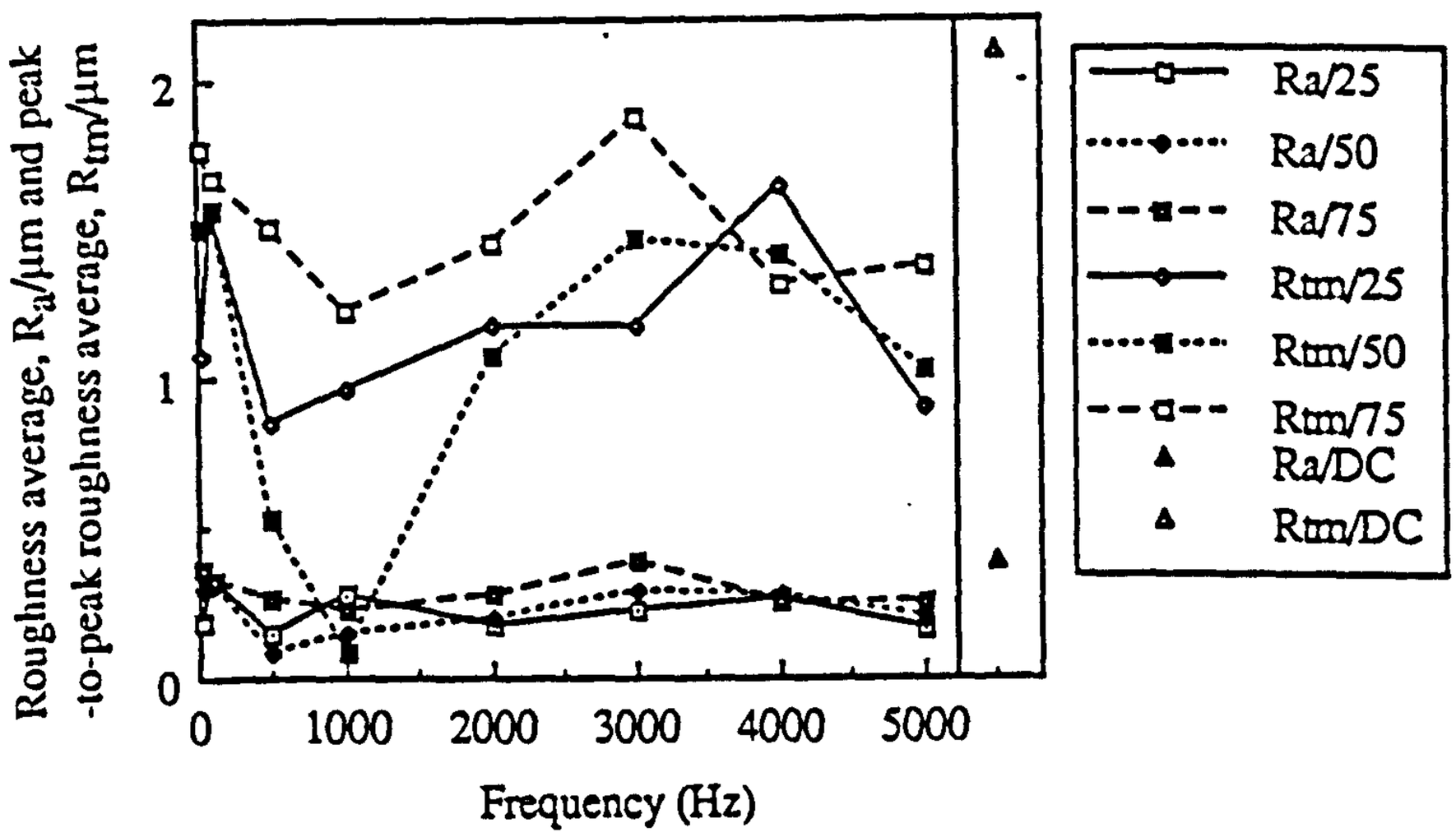

Figure 111b Roughness average and peak-to-peak average roughness against frequency using electrolyte V.

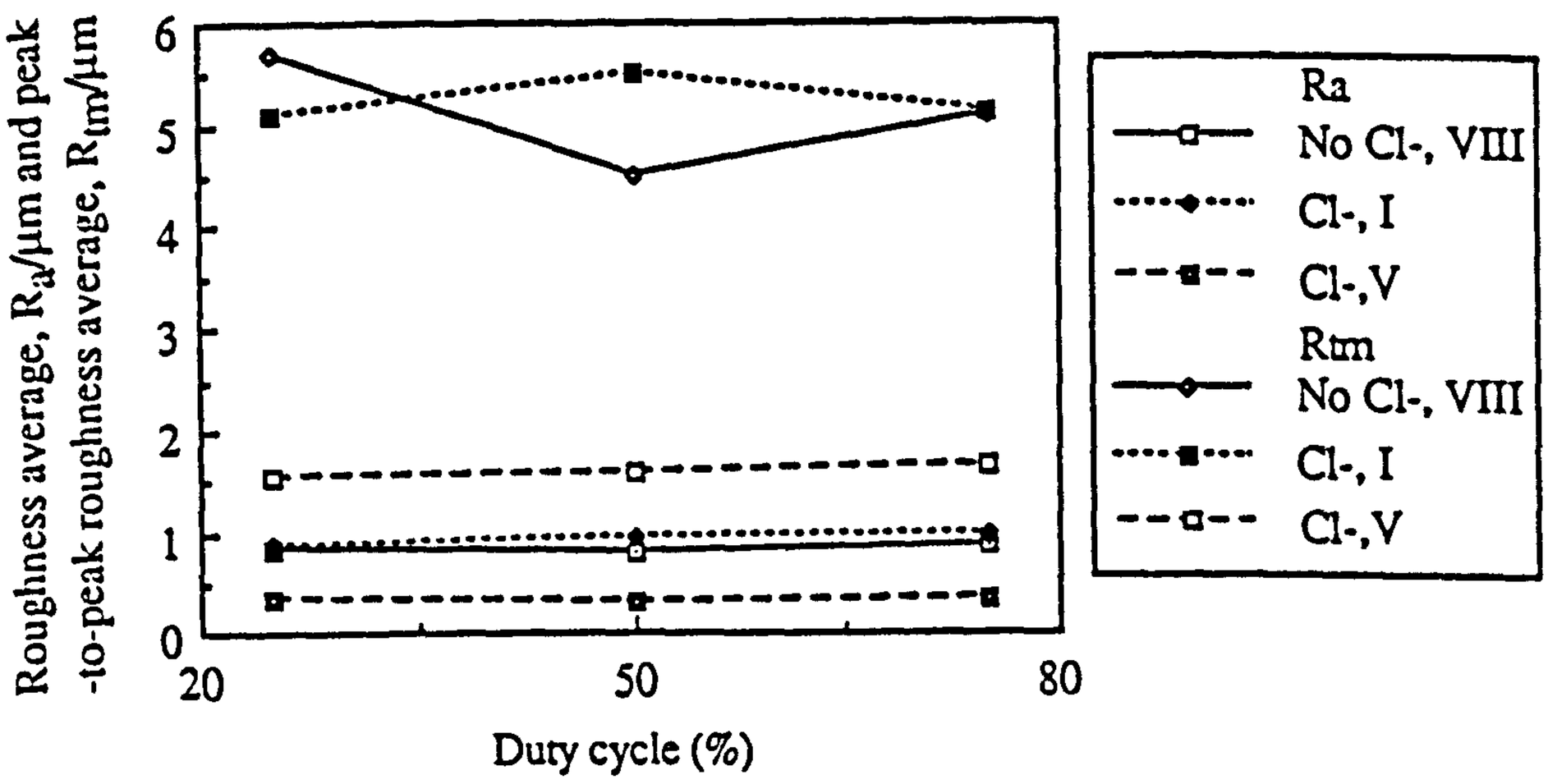

Figure 111c Roughness average and peak-to-peak average roughness against duty cycle using electrolytes VIII, I and V at a frequency of 100Hz.

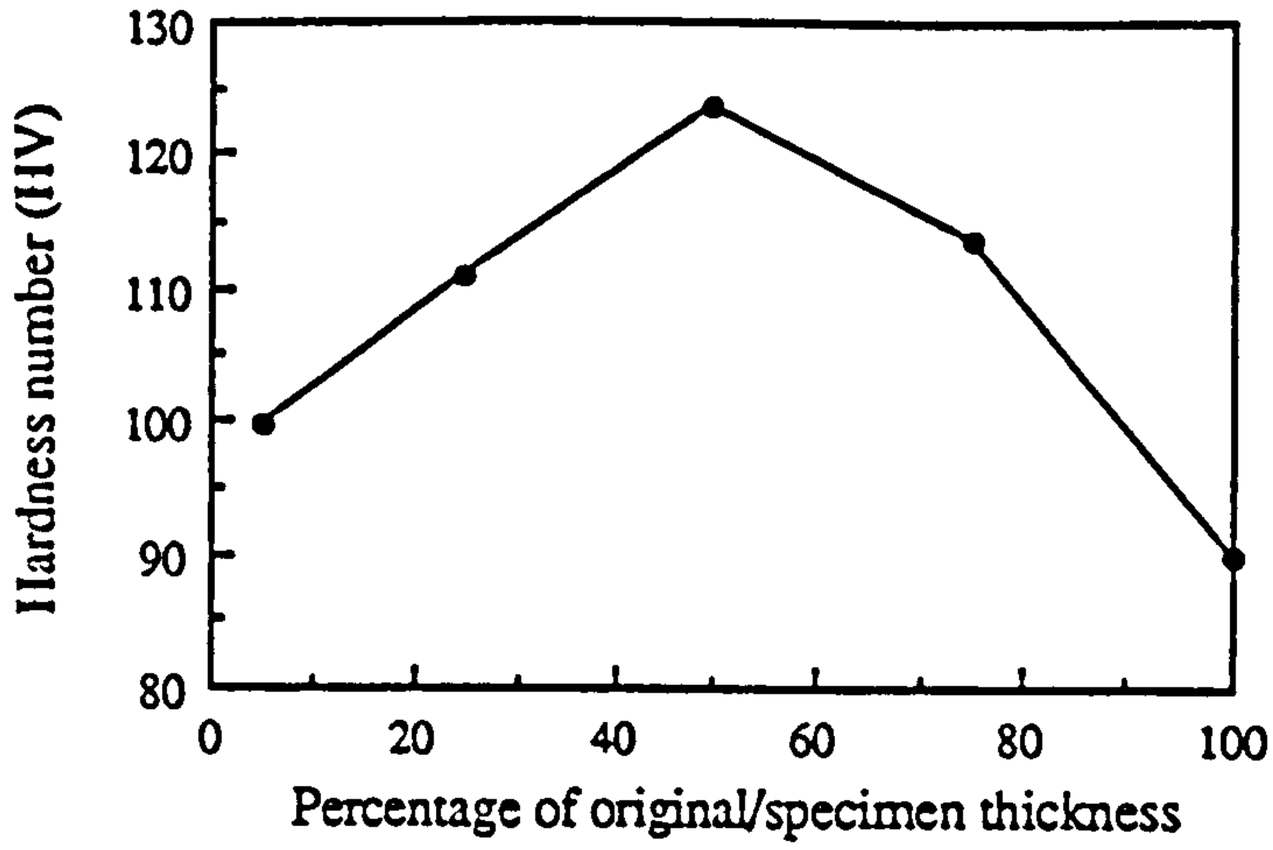

Figure 112a Hardness versus percentage of original thickness to specimen (cold rolled) thickness.

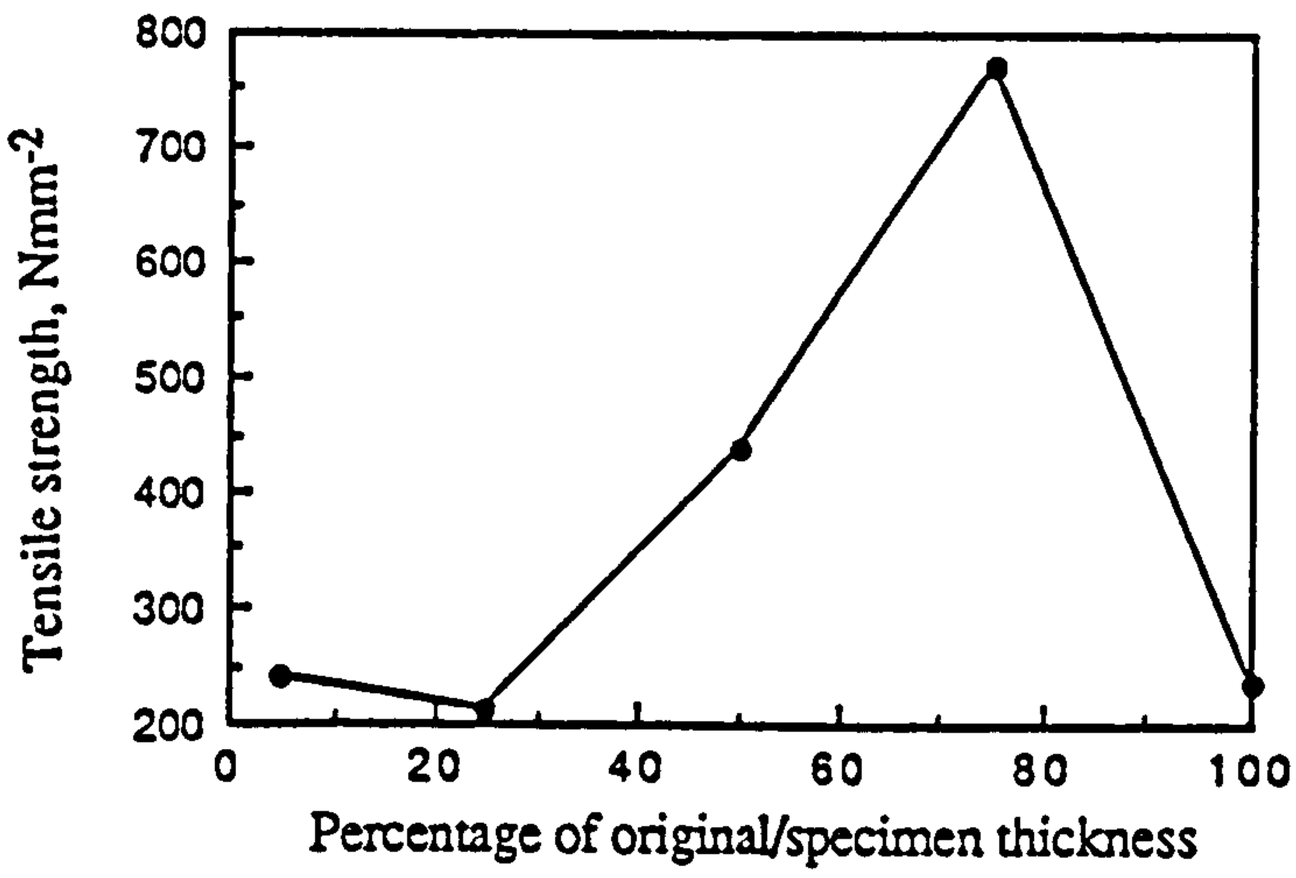

Figure 112b Tensile strength versus percentage of original thickness to specimen (cold rolled) thickness.

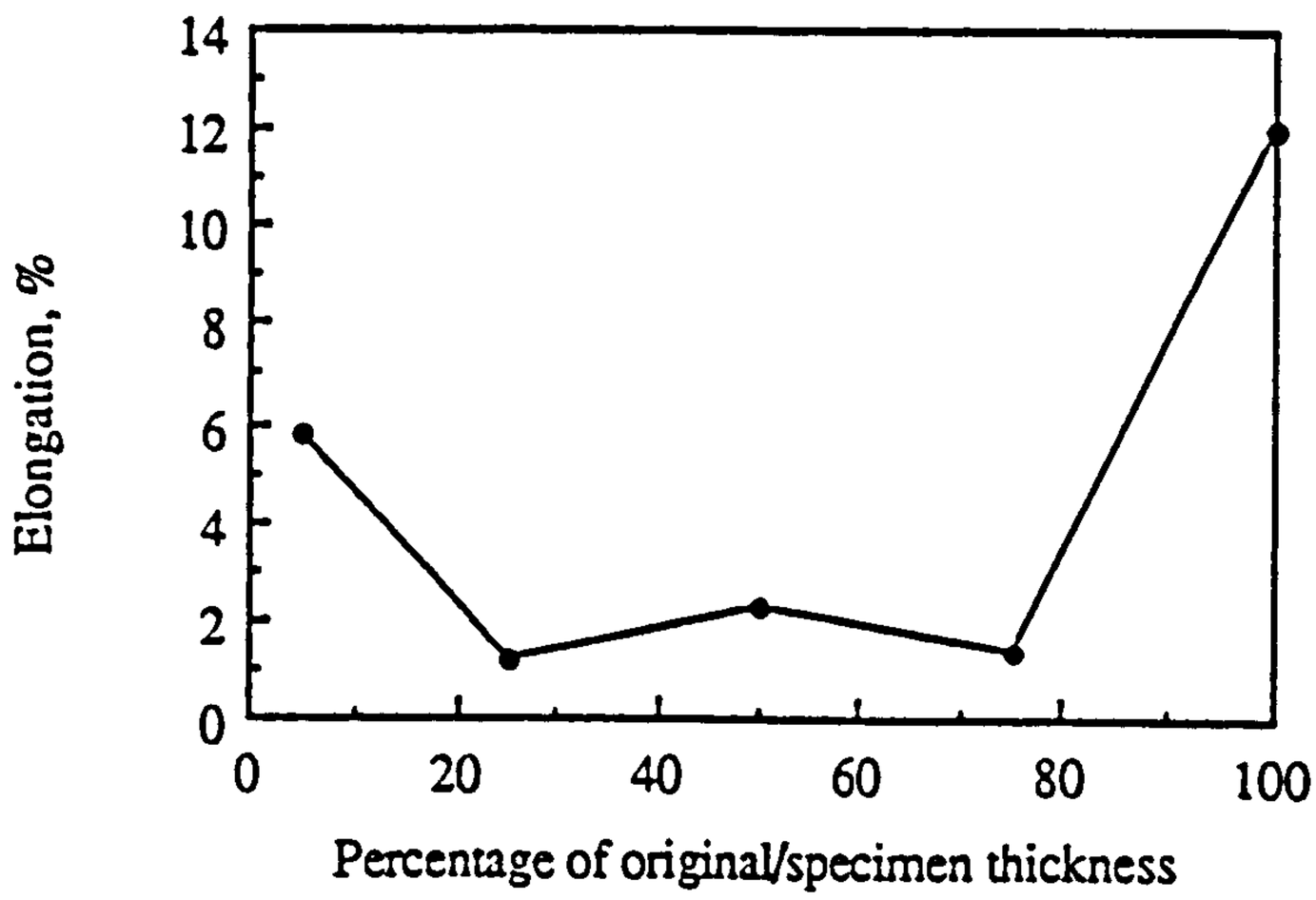

Figure 112c Elongation versus percentage of original thickness to specimen (cold rolled) thickness.

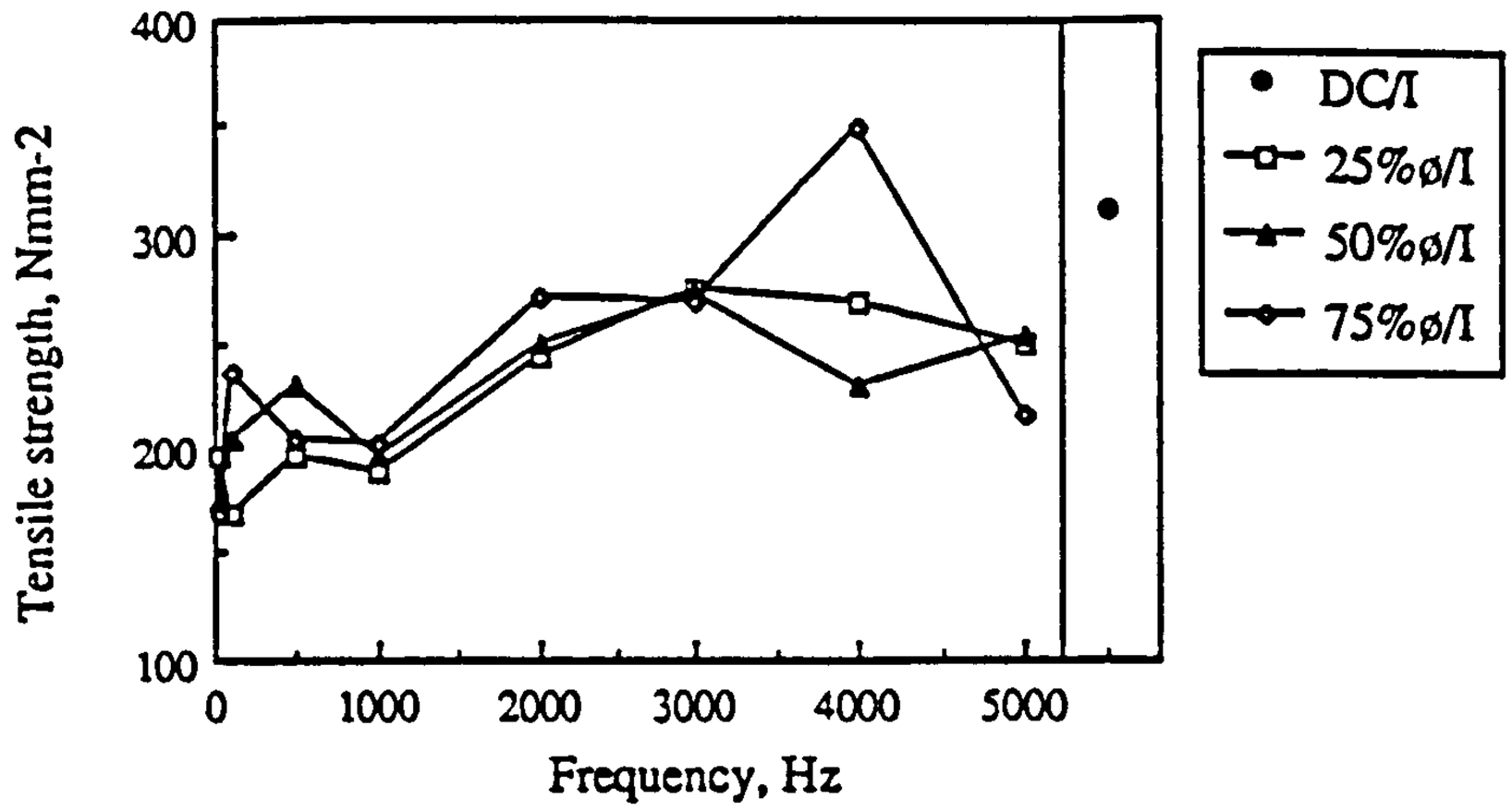

Figure 113a Tensile strength verses frequency for different duty cycles and also DC for electrolyte I.

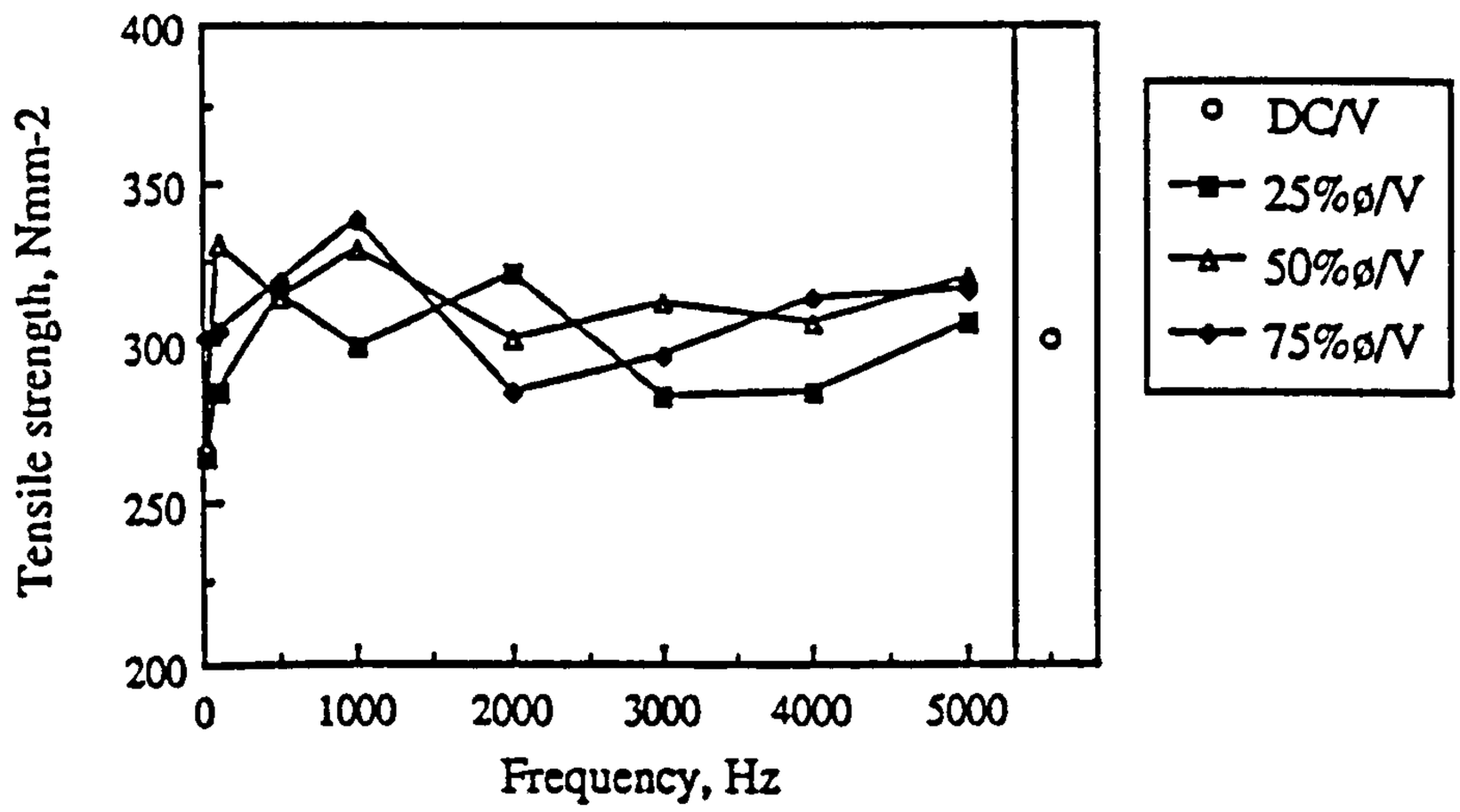

Figure 113b Tensile strength verses frequency for different duty cycles and also DC for electrolyte V.

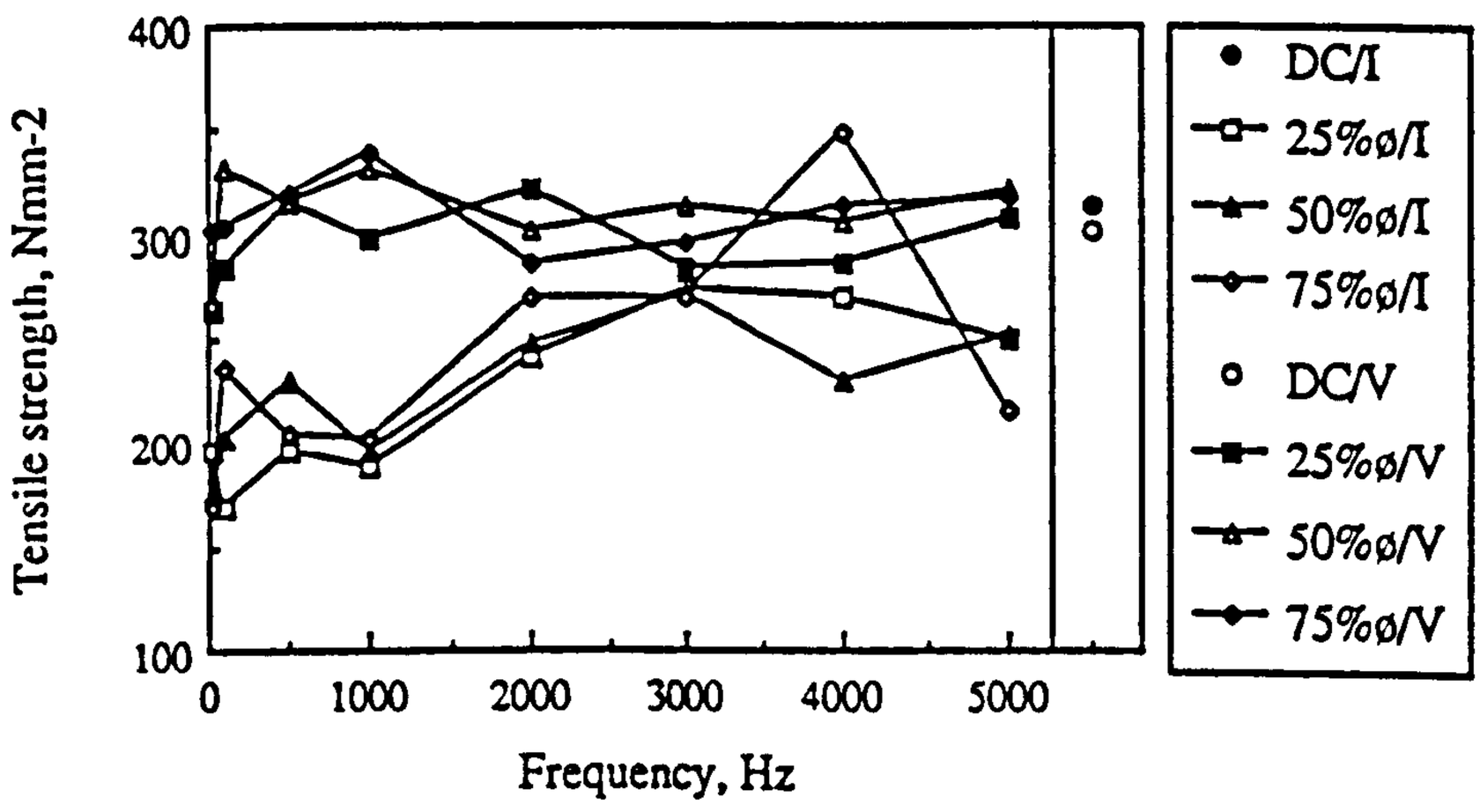

Figure 113c Tensile strength verses frequency for different duty cycles and also DC using electrolyte I and V.

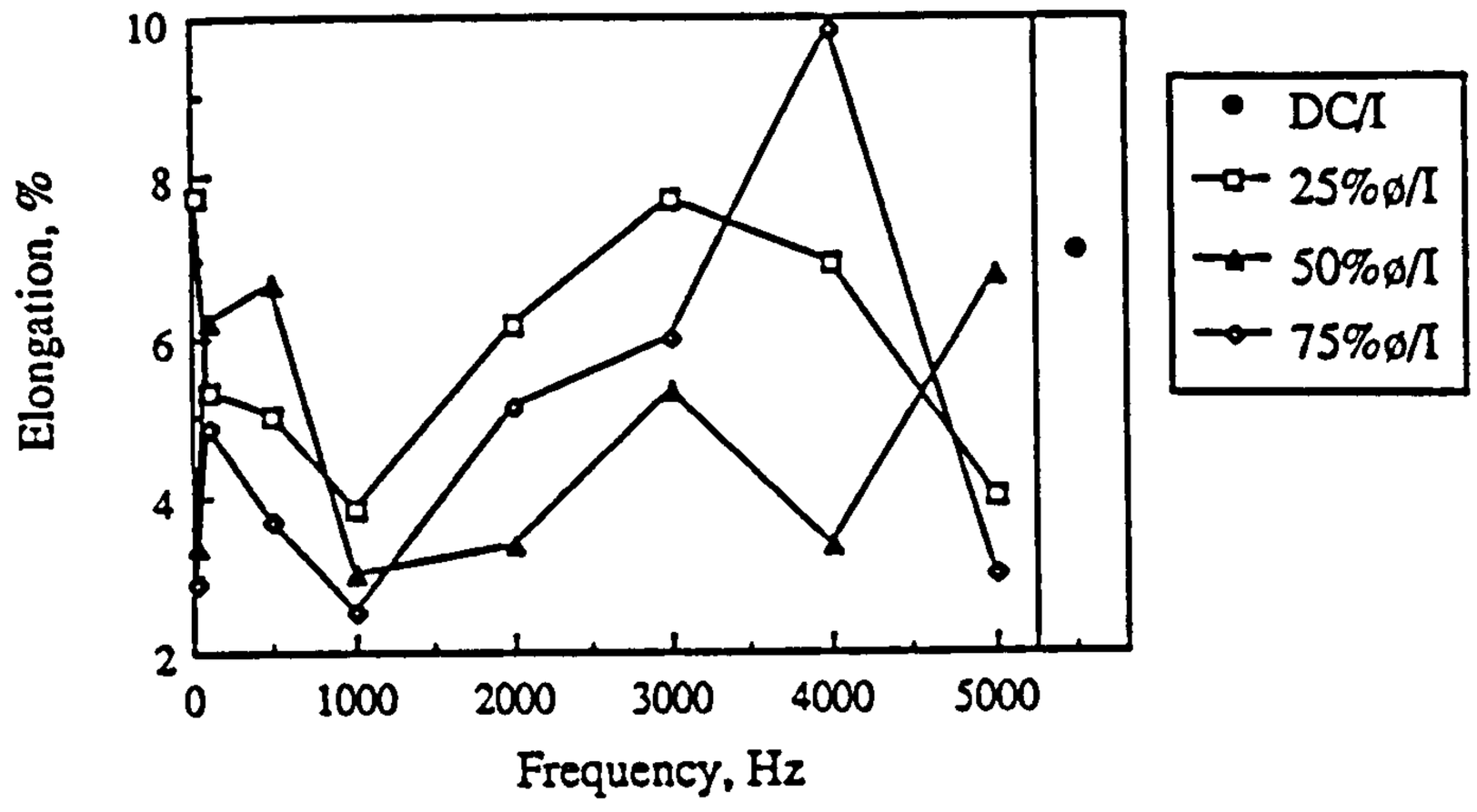

Figure 114a Elongation verses frequency for different duty cycles and also DC using electrolyte V.

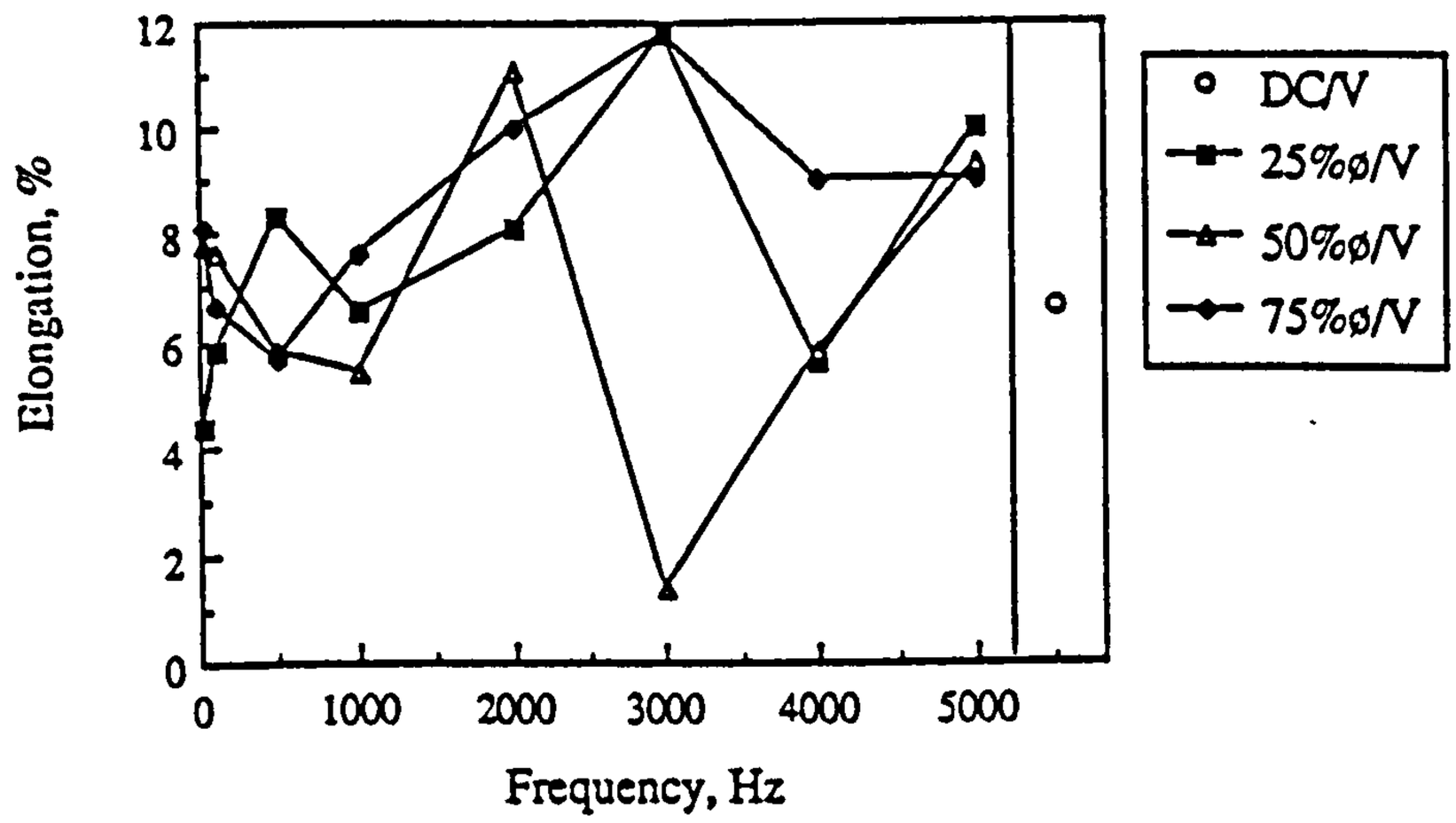

Figure 114b Elongation verses frequency for different duty cycle and also DC for electrolyte V.

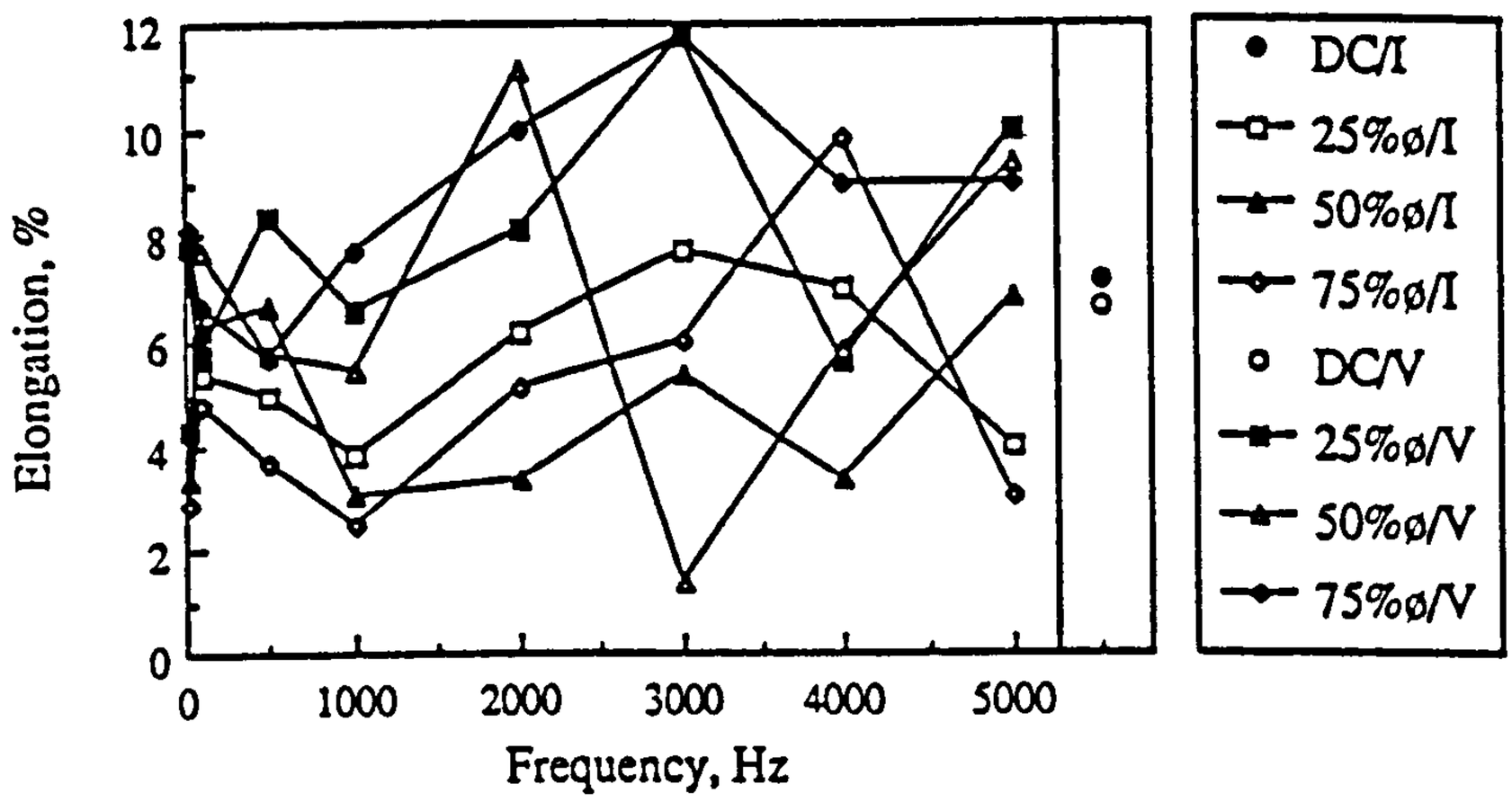

Figure 114c Elongation verses frequency for different duty cycles and also DC using electrolyte I and V.

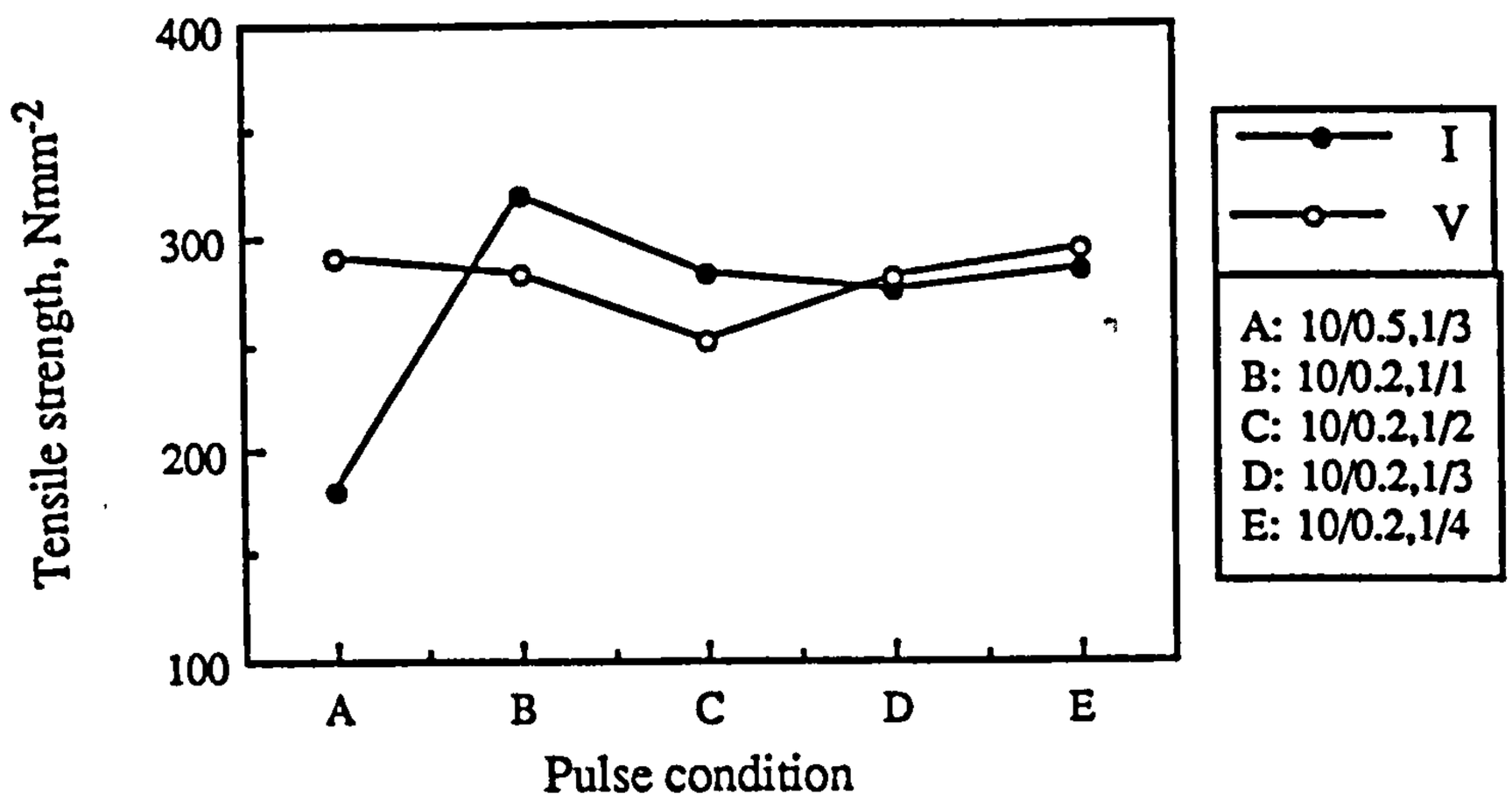

Figure 115 Tensile strength versus different pulse conditions, $t_{on(c)}/t_{on(a)}$, $i_{p(c)}/i_{p(a)}$, using electrolyte I and V.

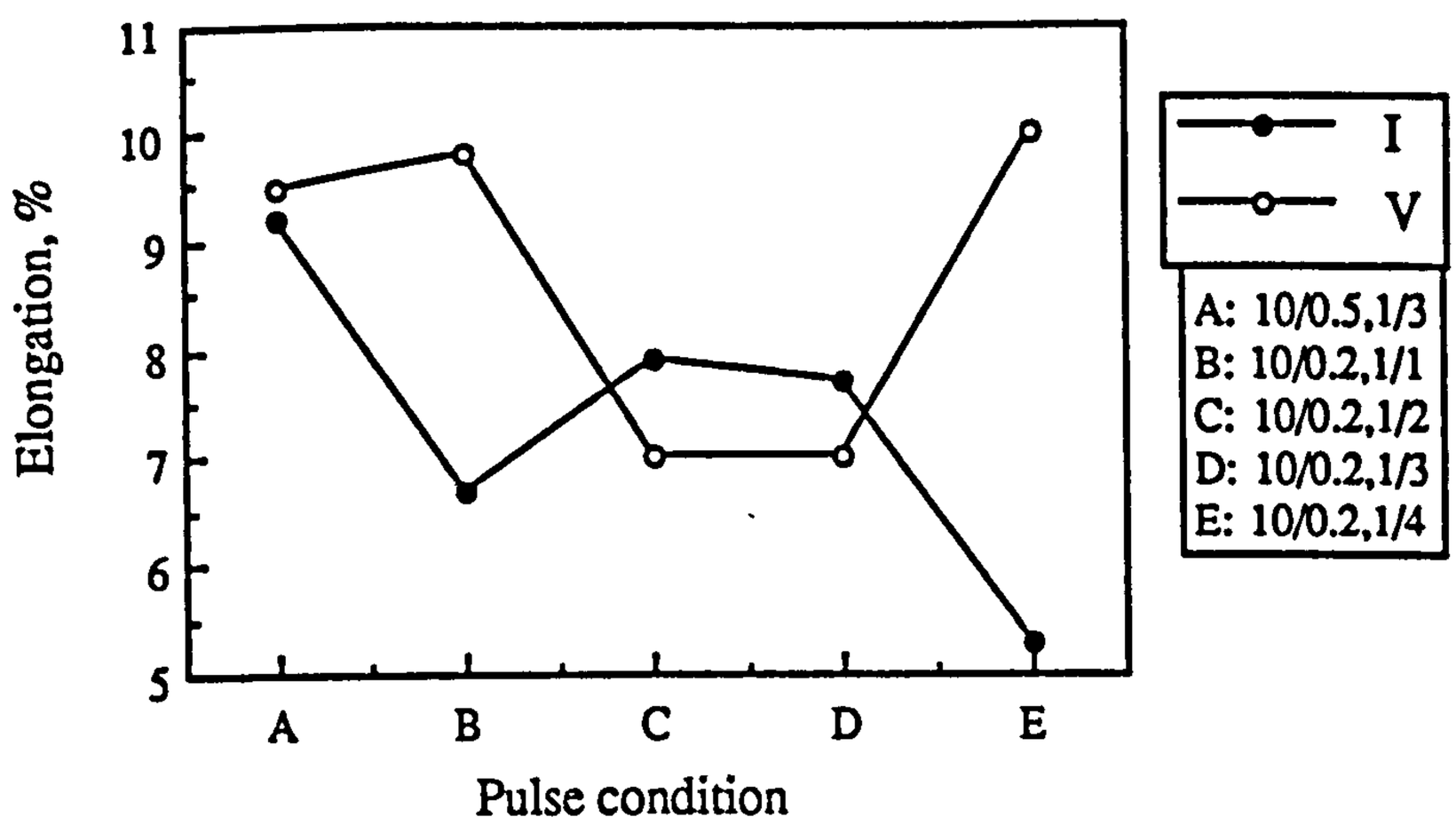

Figure 116 Elongation versus different pulse conditions, $t_{on(c)}/t_{on(a)}$, $i_{p(c)}/i_{p(a)}$, using electrolyte I and V.

Figure 117 Results showing the surface coverage of plated samples at $3.0Adm^{-2}$ for 37 minutes using electrolyte I under DC, P and PR; expected coating thickness of 50μm.

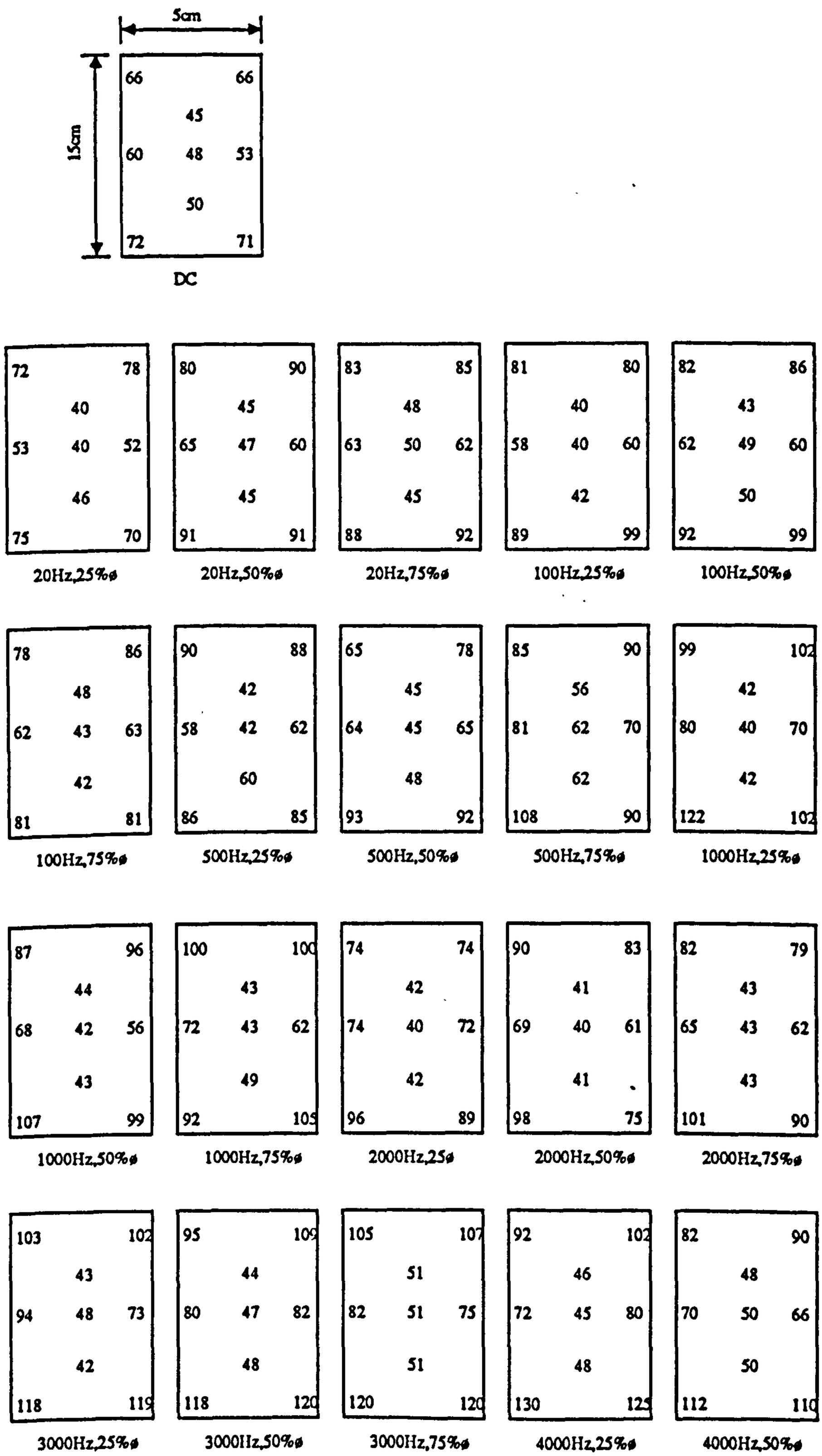

Figure 117 Continued ...

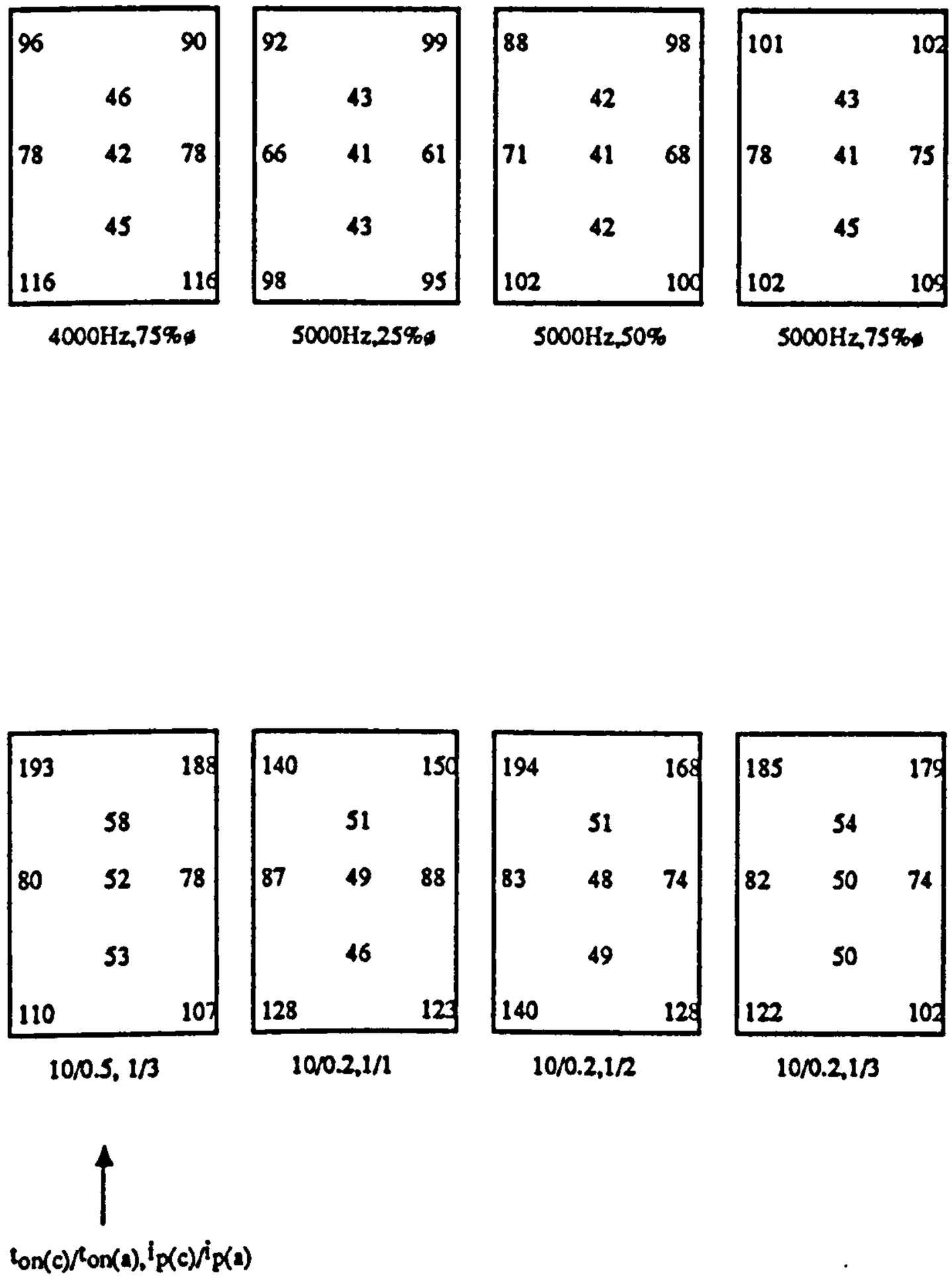

Figure 118 Results showing the surface coverage of plated samples at $3.0Adm^{-2}$ for 37 minutes using electrolyte V under DC, P and PR; expected coating thickness of 50μm.

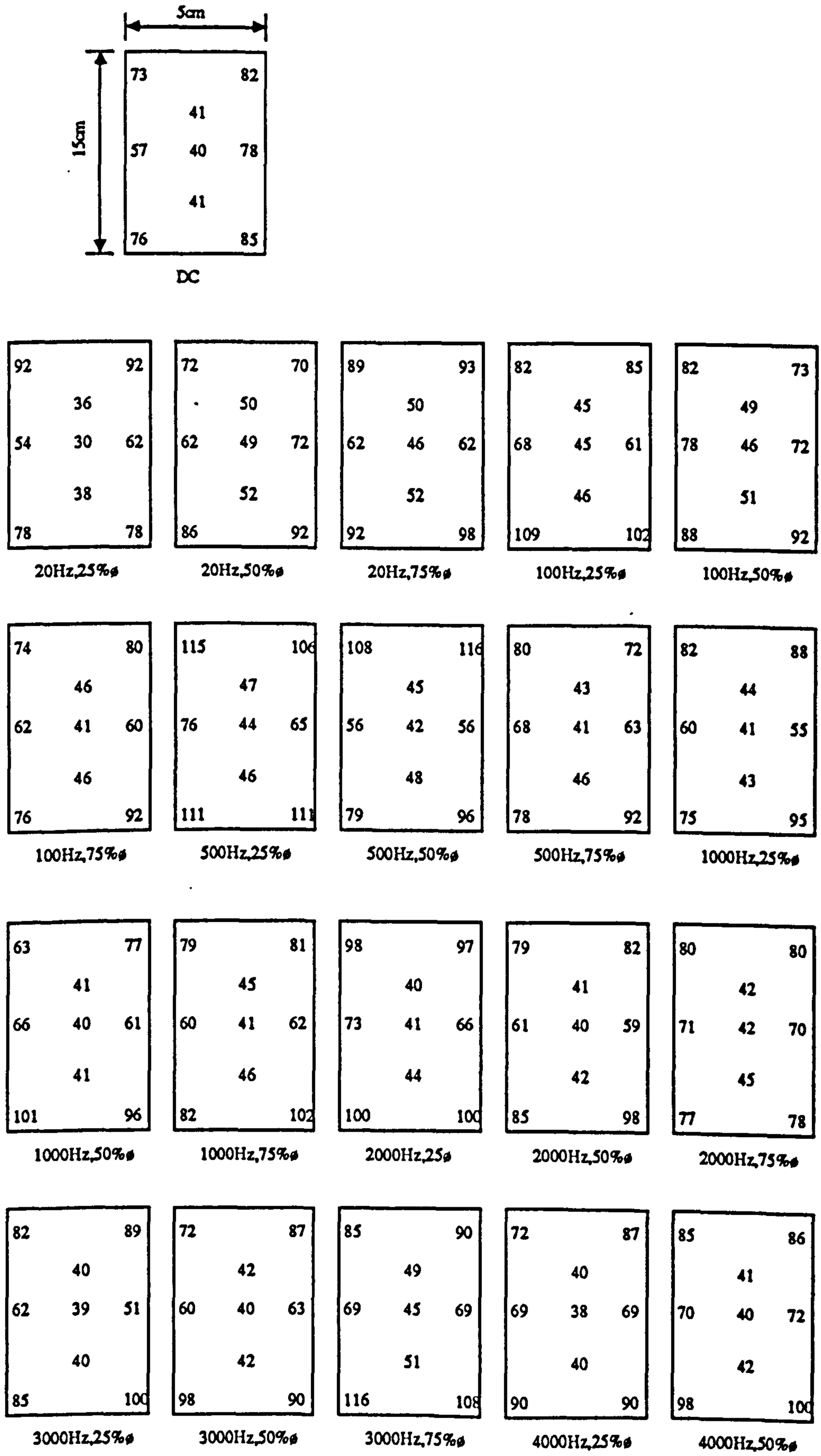

Figure 118 Continued ...

81		85
	40	
56	36	55
	40	
81		99

4000Hz,75%ø

92		86
	38	
61	36	70
	40	
85		88

5000Hz,25%ø

68		70
	36	
55	35	53
	37	
78		82

5000Hz,50%

60		67
	40	
52	37	57
	39	
83		90

5000Hz,75%ø

70		70
	42	
56	42	62
	42	
84		86

10/0.5, 1/3

92		90
	43	
60	40	72
	42	
98		86

10/0.2,1/1

72		72
	42	
60	40	64
	41	
78		80

10/0.2,1/2

95		88
	38	
53	38	57
	38	
80		77

10/0.2,1/3

75		76
	45	
51	38	55
	40	
76		90

10/0.2,1/4

$t_{on(c)}/t_{on(a)}, i_{p(c)}/i_{p(a)}$

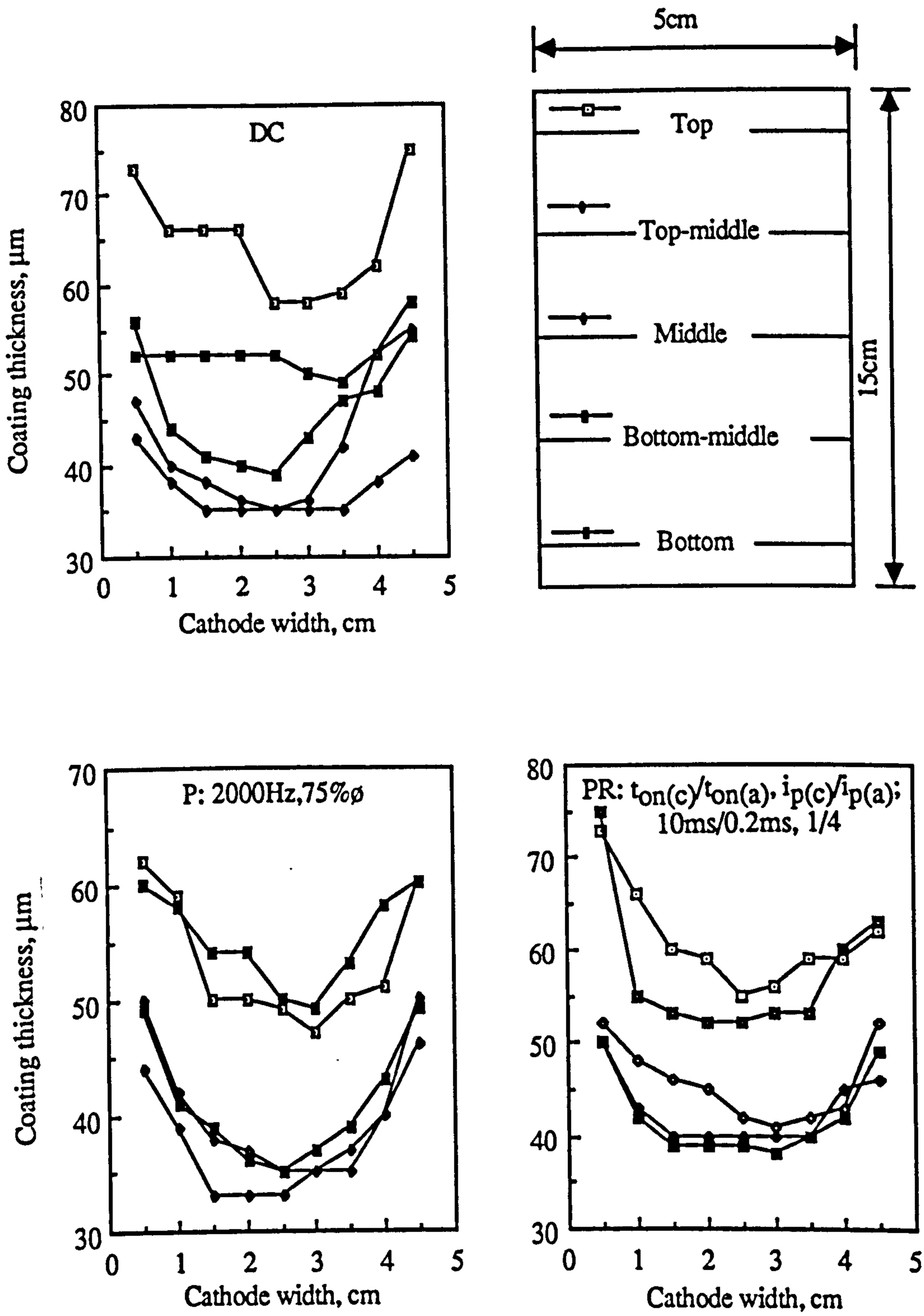

Figure 119 Shows the coating distribution of of electrodeposited foils under DC, unipolar pulse(P) and bipolar pulse reverse(PR) using electrolyte I and also showing the positions which the thicknesses were measured.

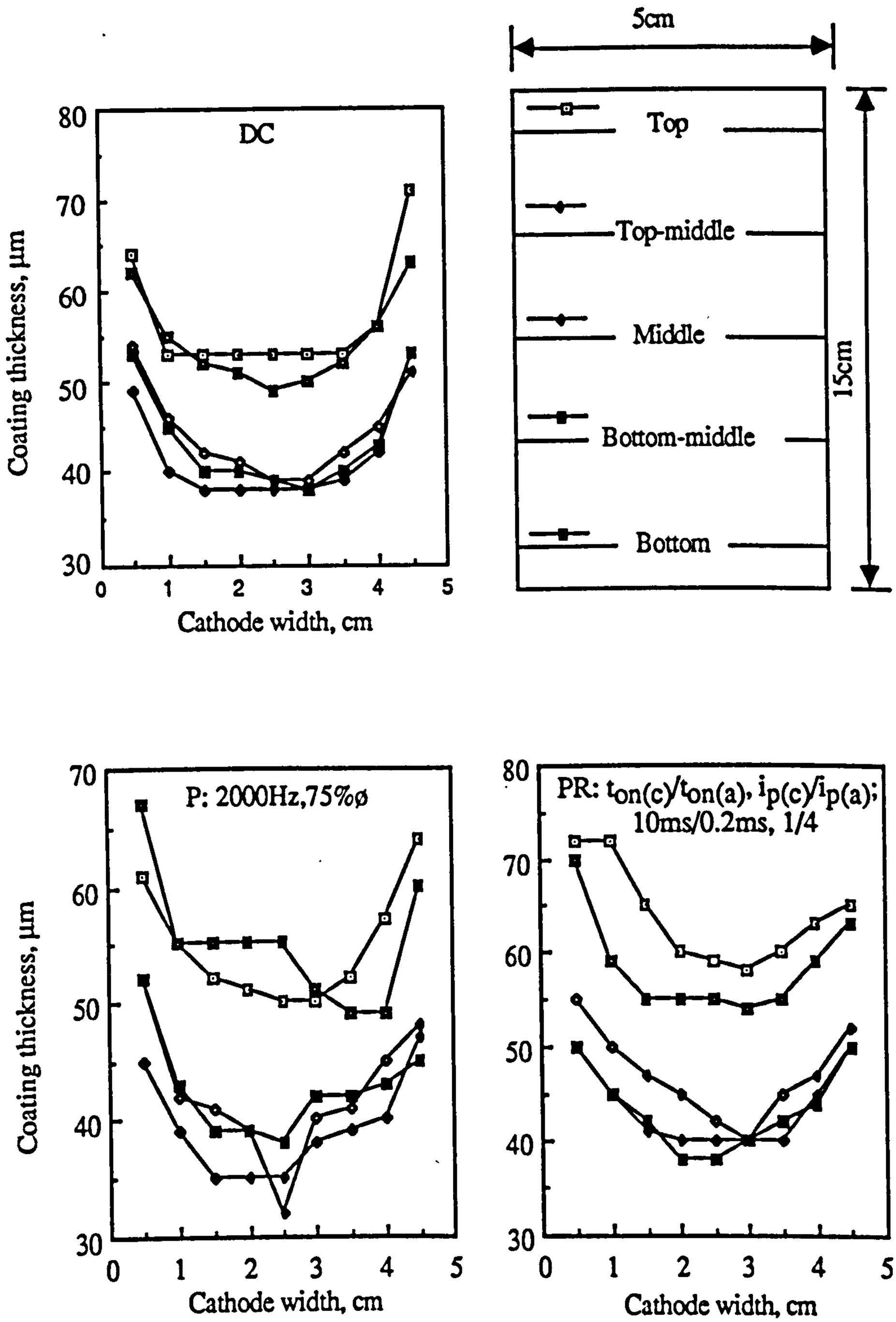

Figure 120 Shows the coating distribution of of electrodeposited foils under DC, unipolar pulse(P) and bipolar pulse reverse(PR) using electrolyte V and also showing the positions which the thicknesses were measured.

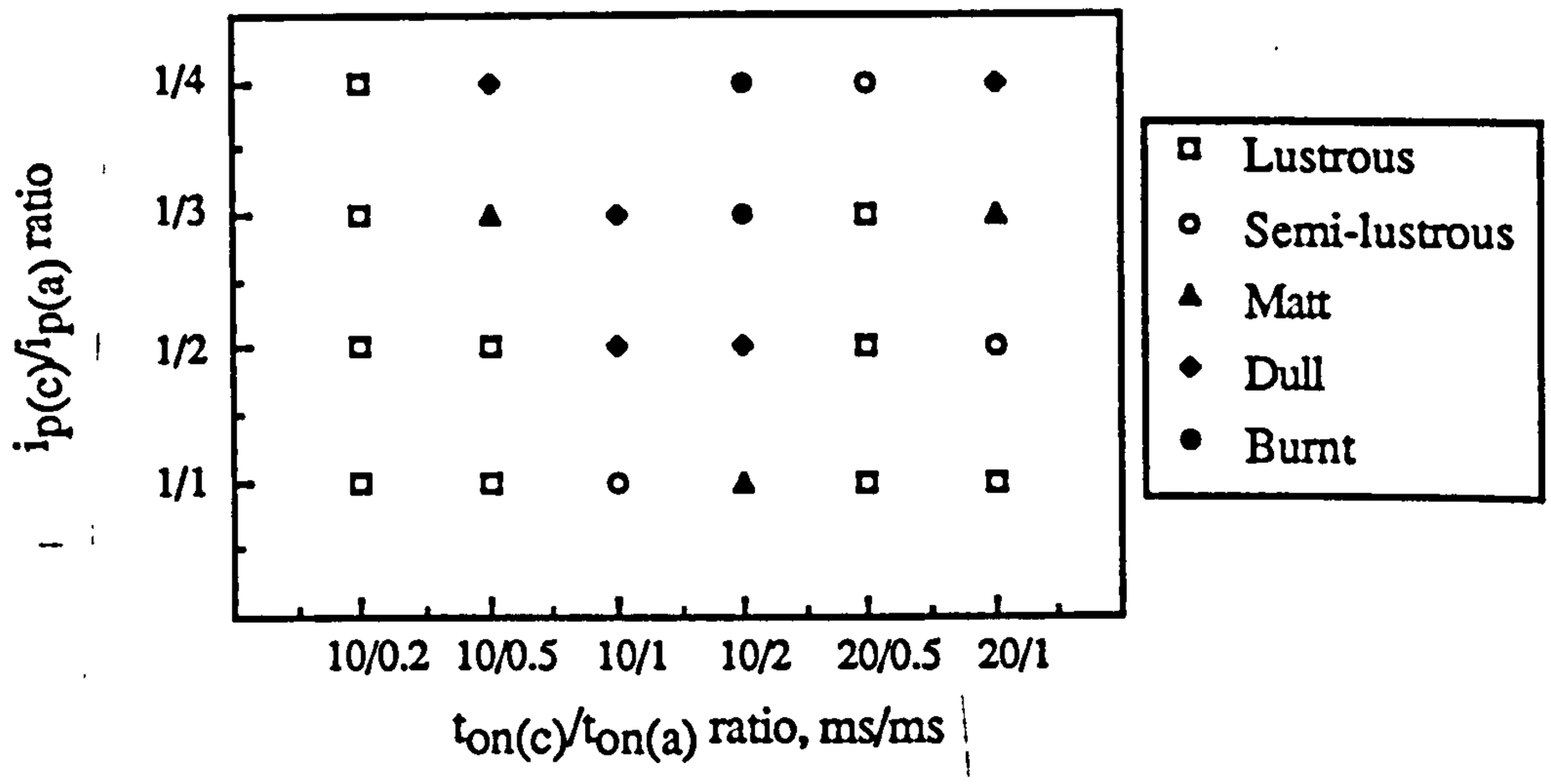

Figure 121 Shows the surface finish of the coatings under PR conditions for different $t_{on(c)}/t_{on(a)}$ ratios and also different $i_{p(c)}/i_{p(a)}$ ratios using electrolyte V.

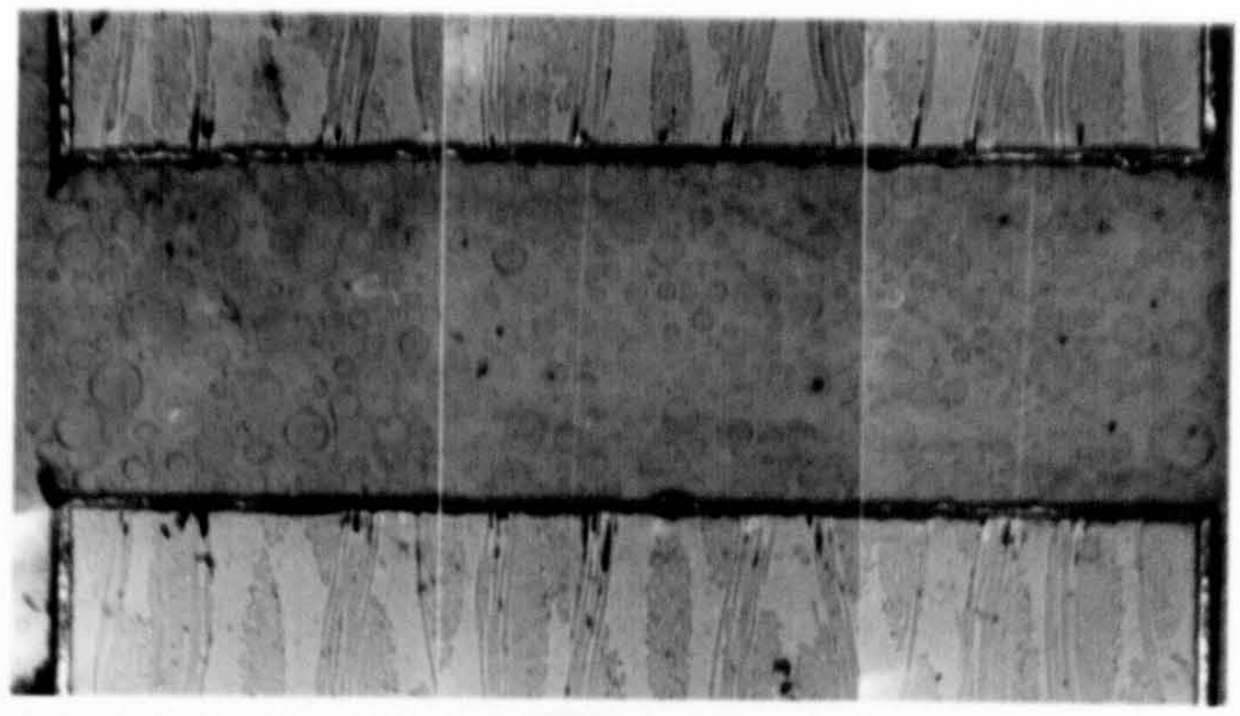

a

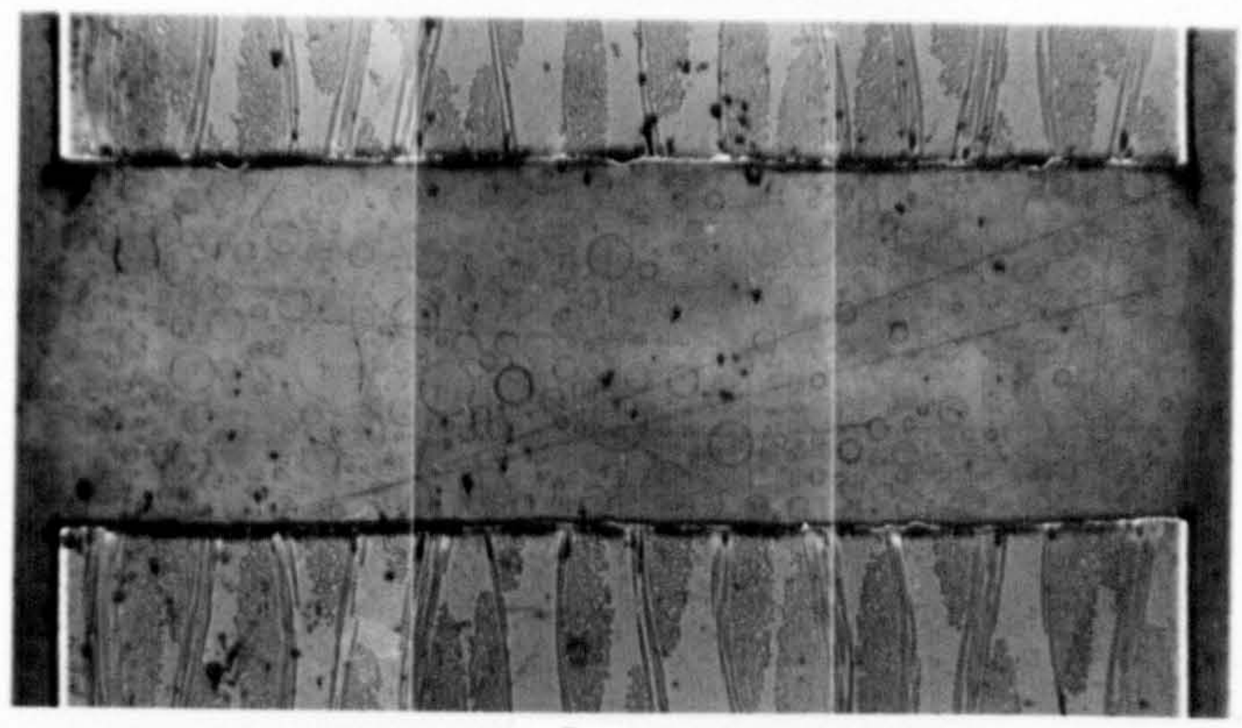

b

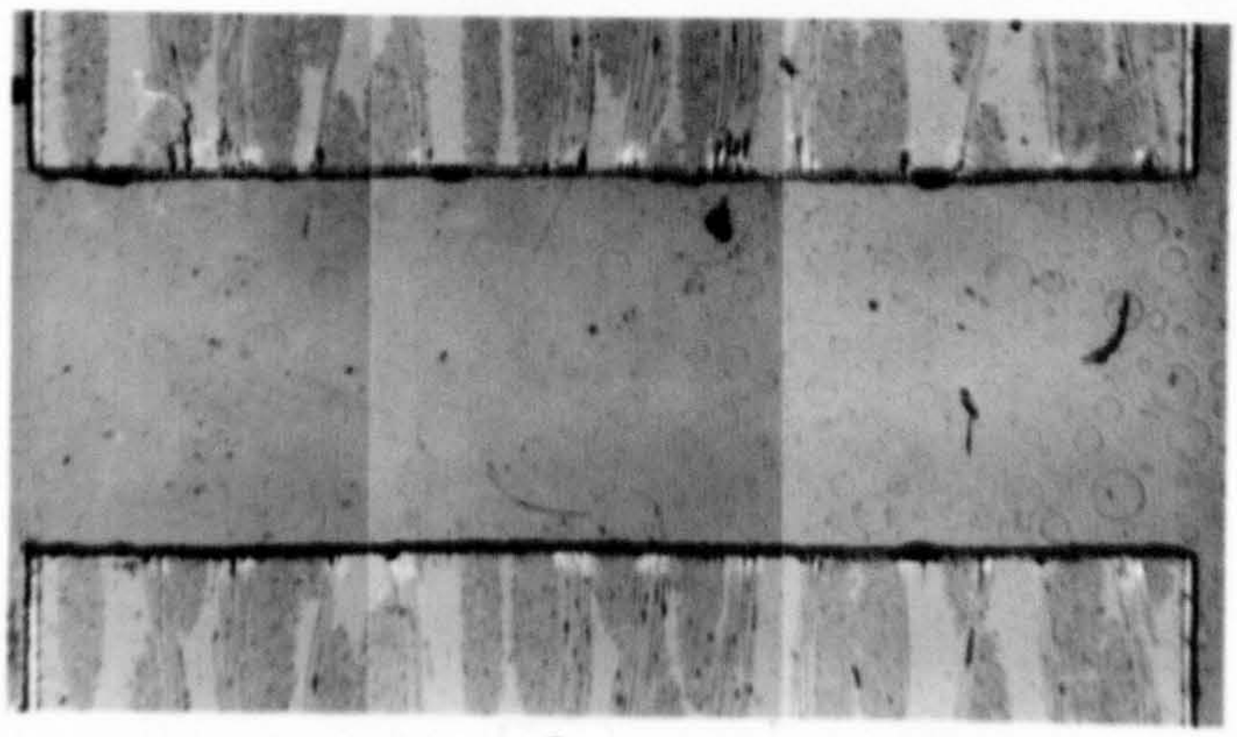

c

Figure 122 Optical micrographs showing the coating thickness distributions using electrolyte I at a plating rate of $3.0Adm^{-2}$ for board thickness of 2.5mm and hole diameter of 0.8mm under:
a) direct current
b) best unipolar pulse condition: 5000Hz, 50%ϕ
c) worst unipolar pulse condition: 20Hz, 25%ϕ.

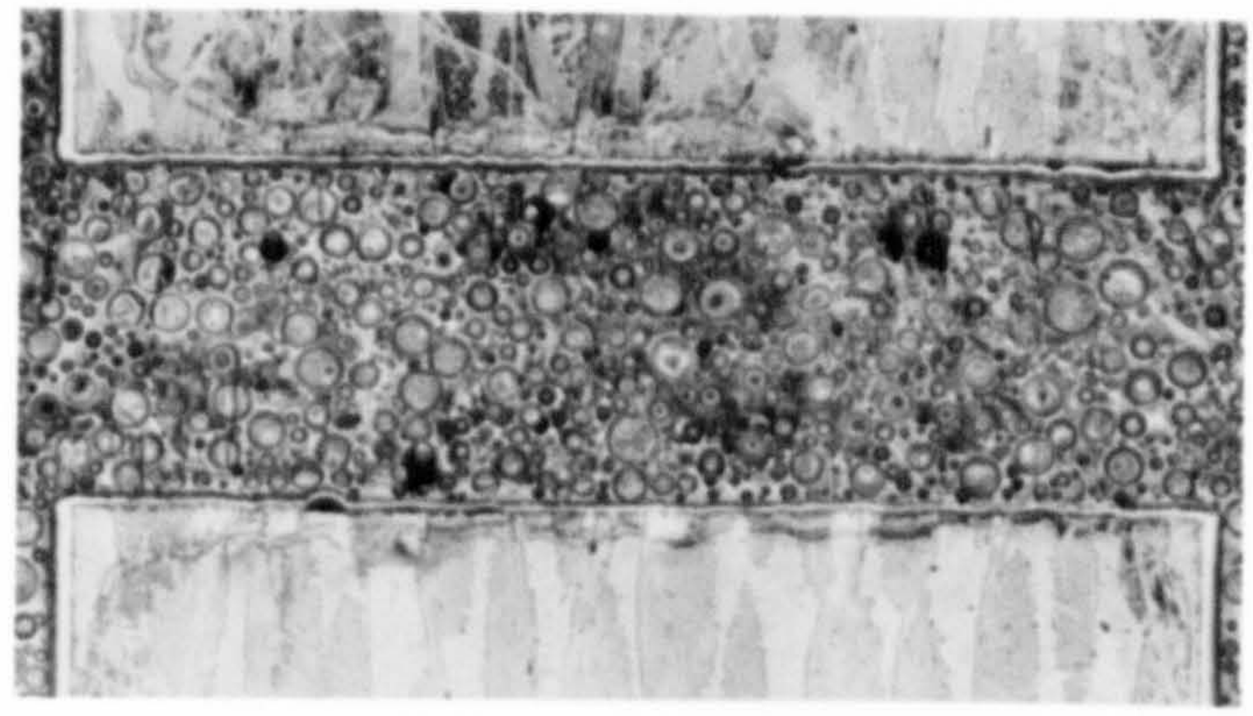

a

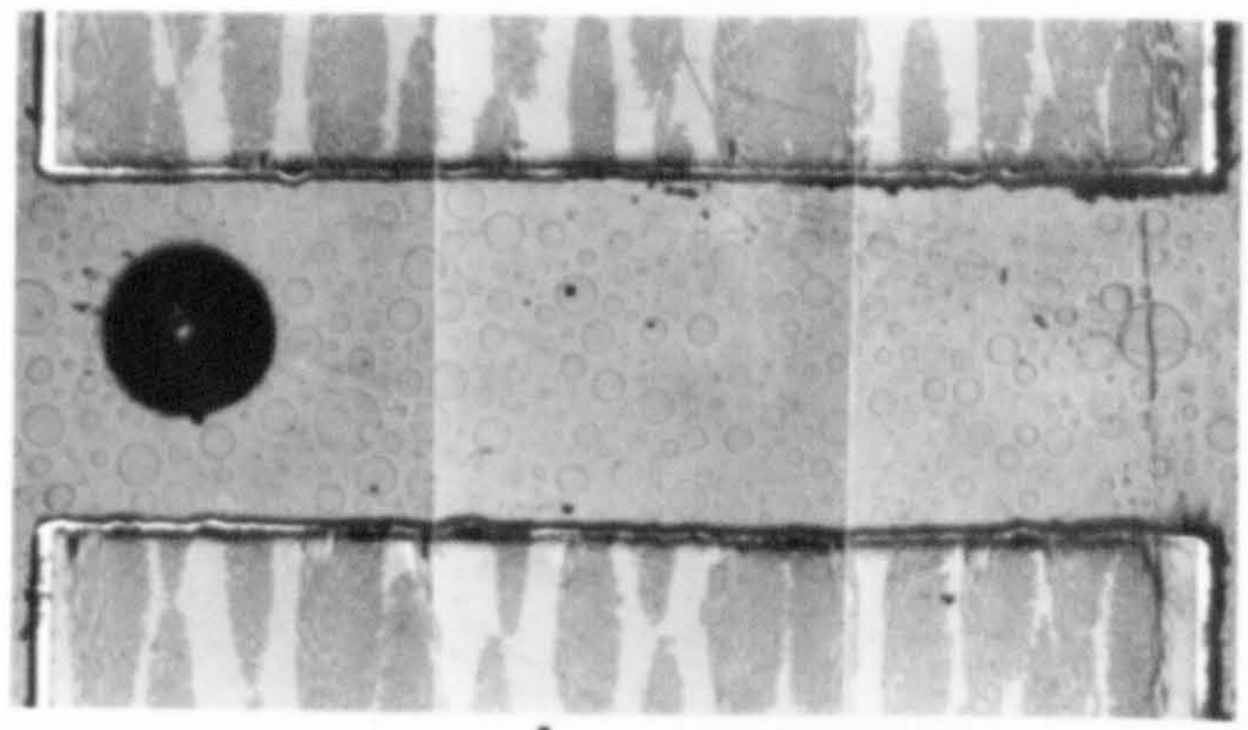

b

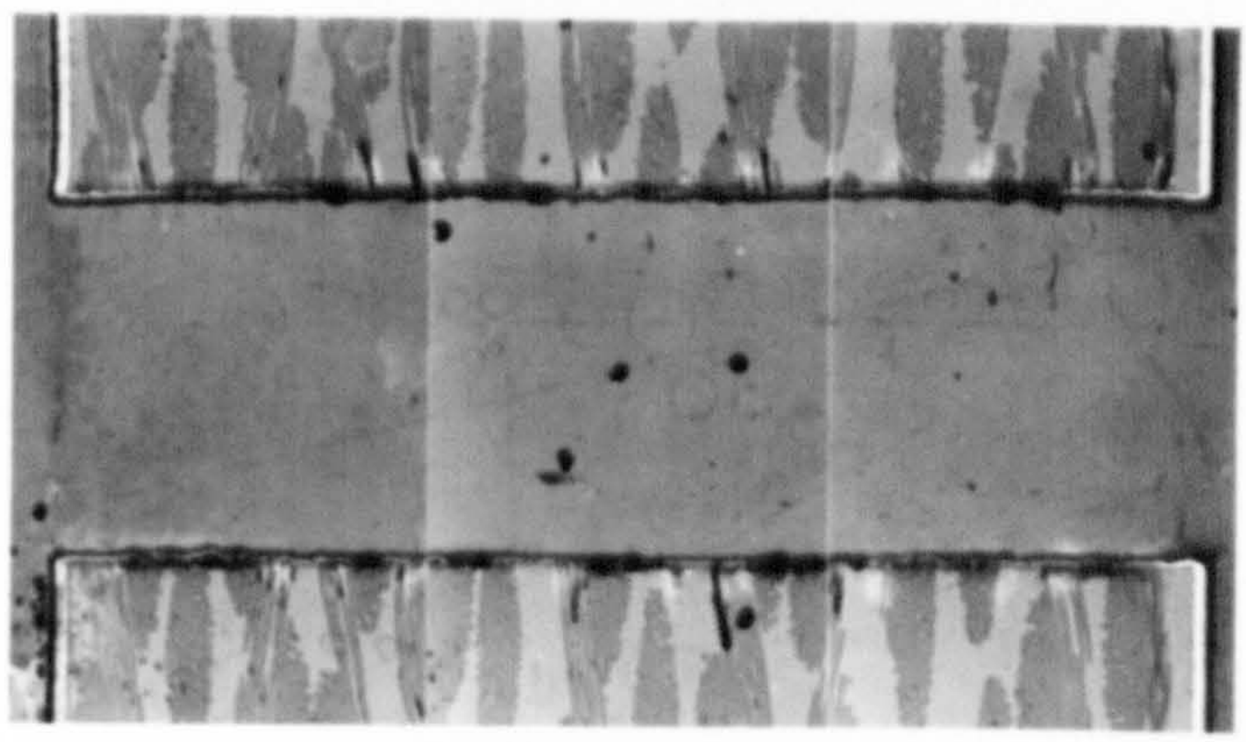

c

Figure 123 Optical micrographs showing the coating thickness distributions using electrolyte III at a plating rate of $3.0Adm^{-2}$ for board thickness of 2.5mm and hole diameter of 0.8mm under:
a) direct current
b) best unipolar pulse condition: 1000Hz, 75%ϕ
c) worst unipolar pulse condition: 20Hz, 25%ϕ.

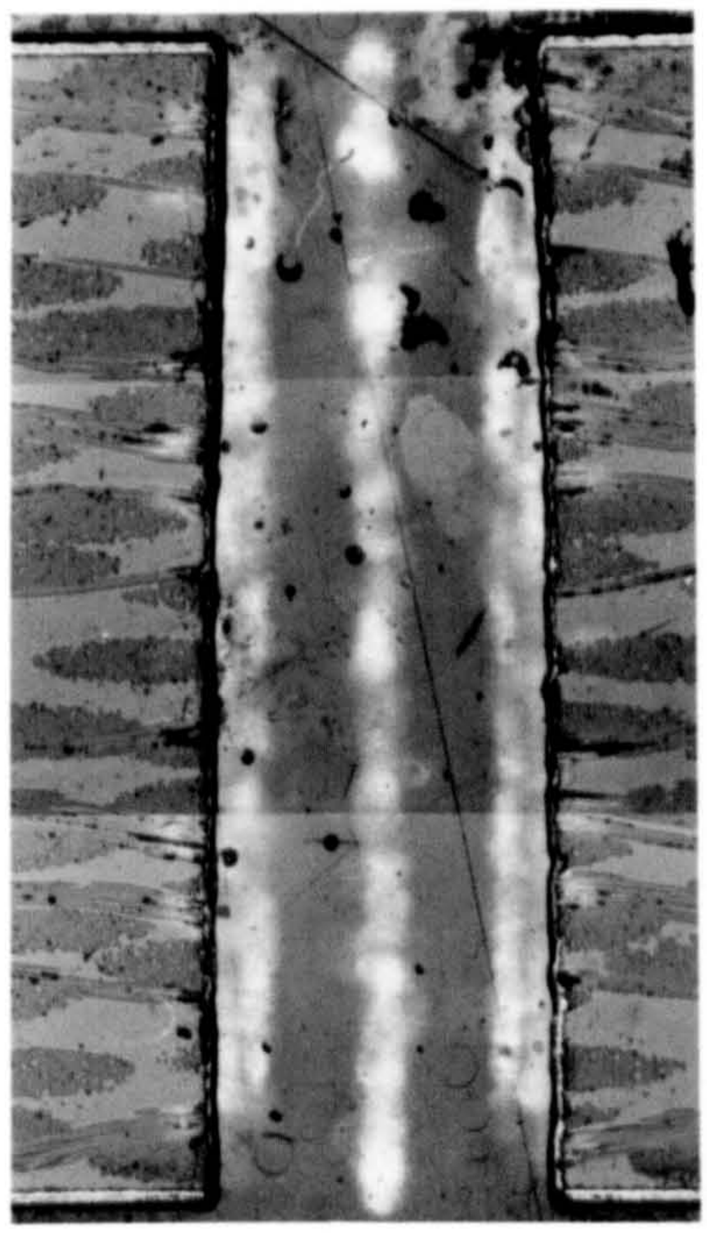

a

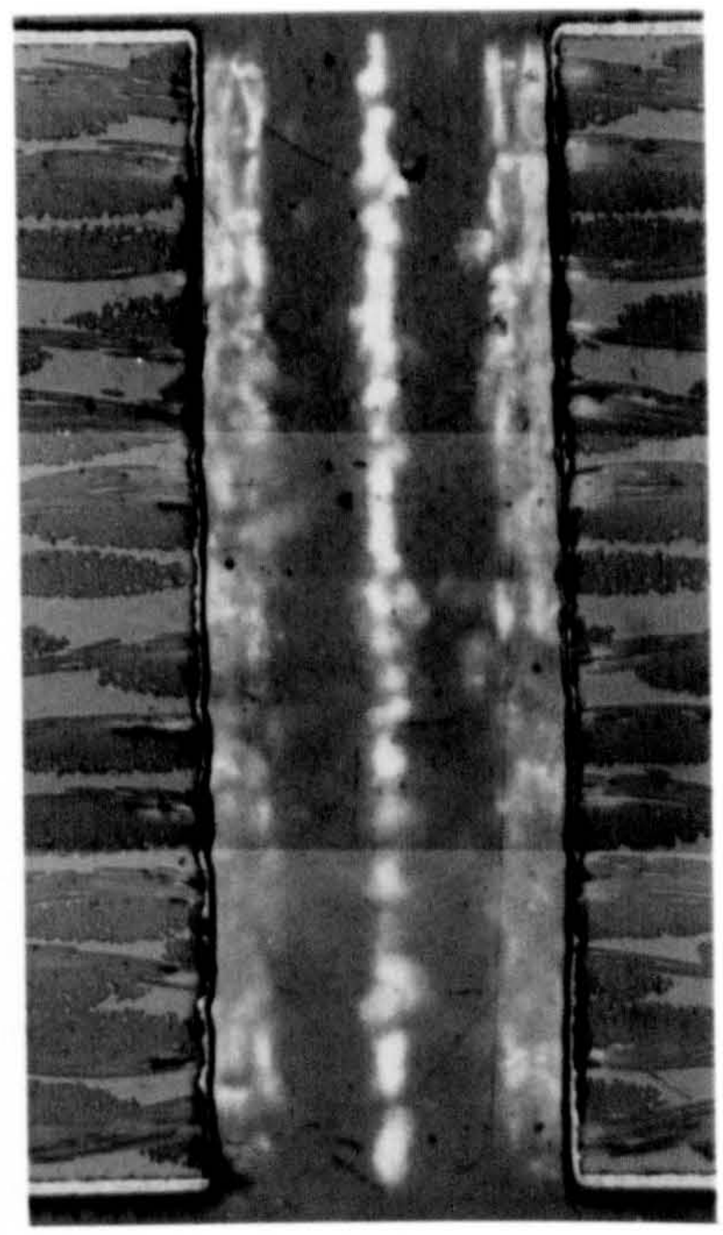

b

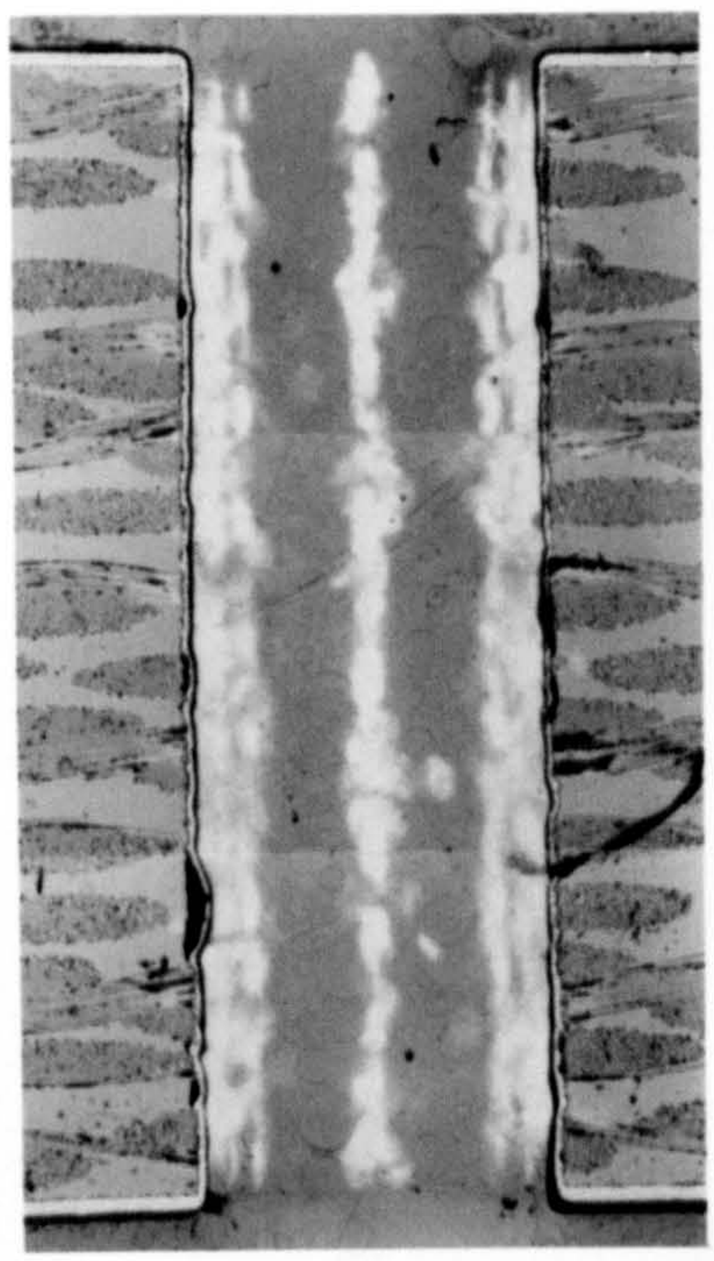

c

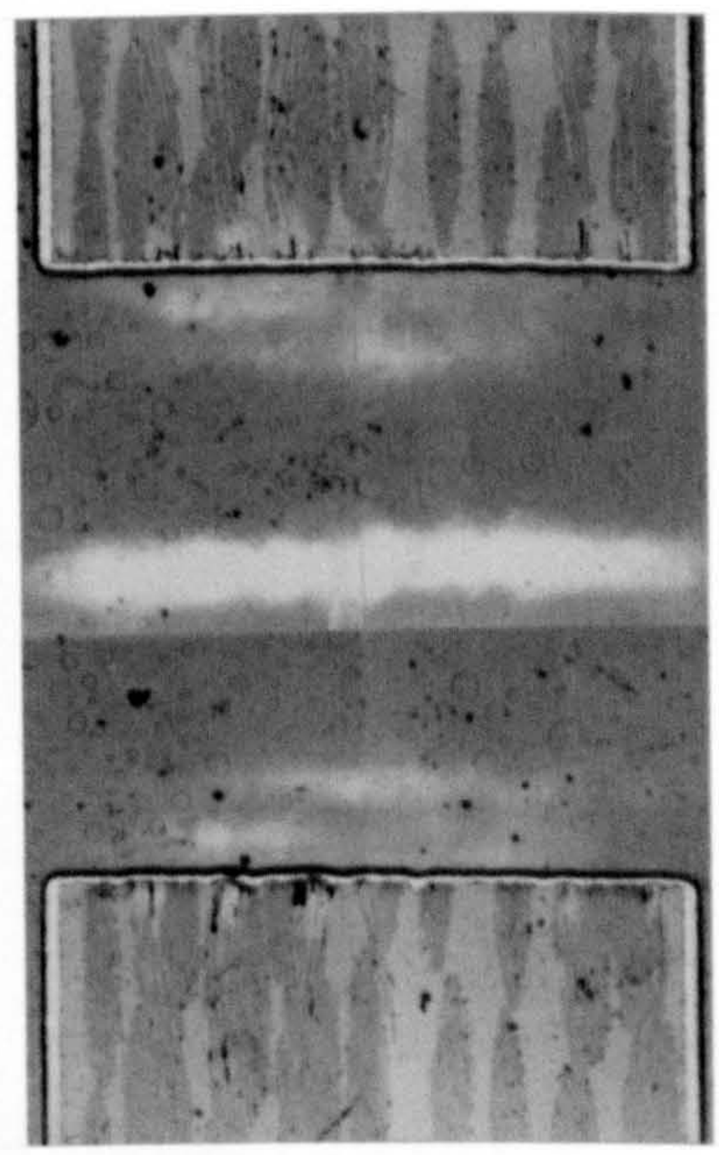

d

Figure 124 Optical micrographs showing the coating thickness distributions using electrolyte V at a plating rate of $3.0 Adm^{-2}$ for board thickness of 2.5mm and hole diameter of 0.8mm under:

a) direct current
b) best unipolar pulse condition: 1000Hz, 75%ϕ
c) worst unipolar pulse condition: 20Hz, 25%ϕ
d) best unipolar pulse condition: 1000Hz, 75%ϕ, board thickness 1.6mm.

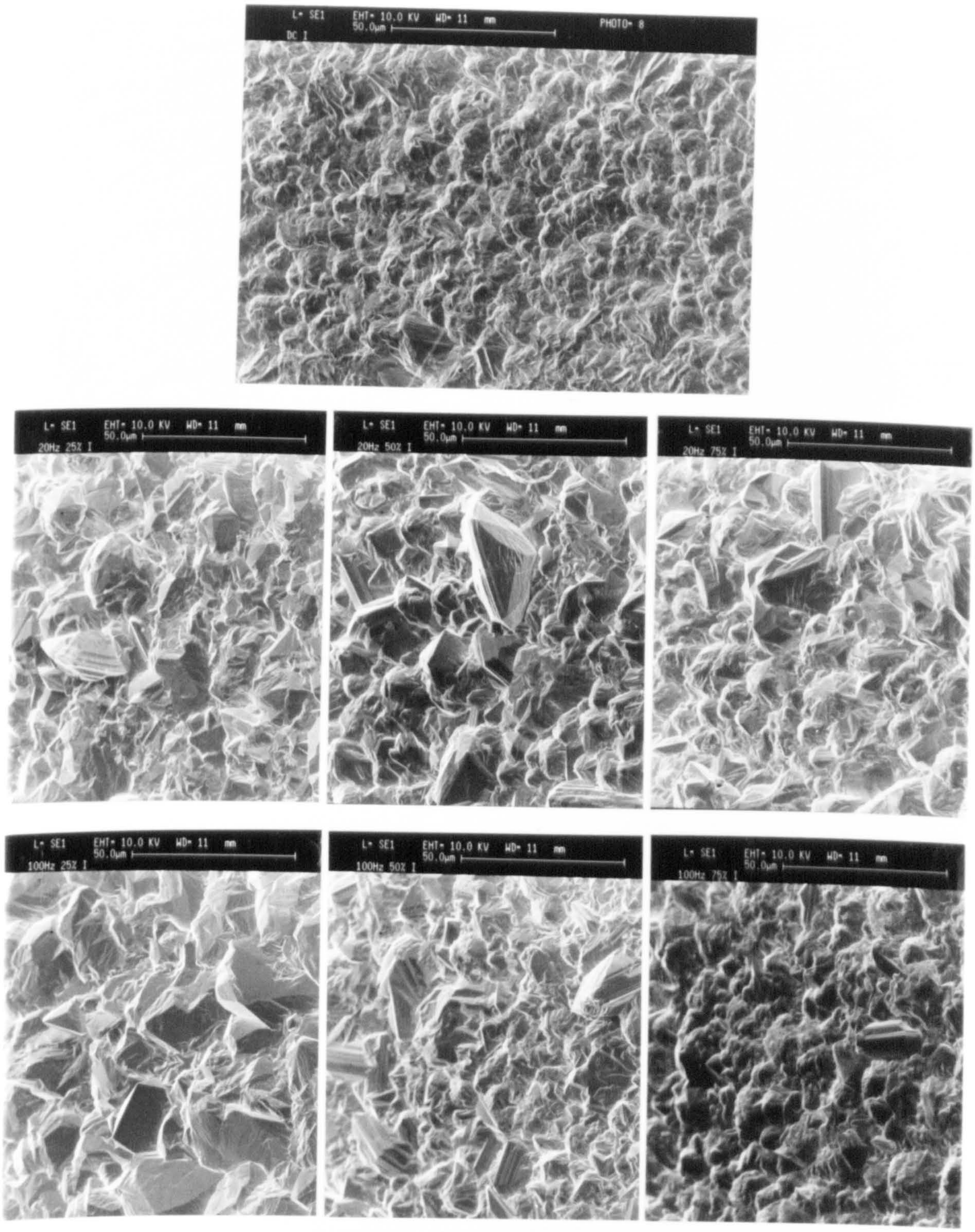

Figure 125 Scanning electron micrographs showing the crystal structures obtained under DC and unipolar pulse using electrolyte I; the conditions are specified on each micrographs.

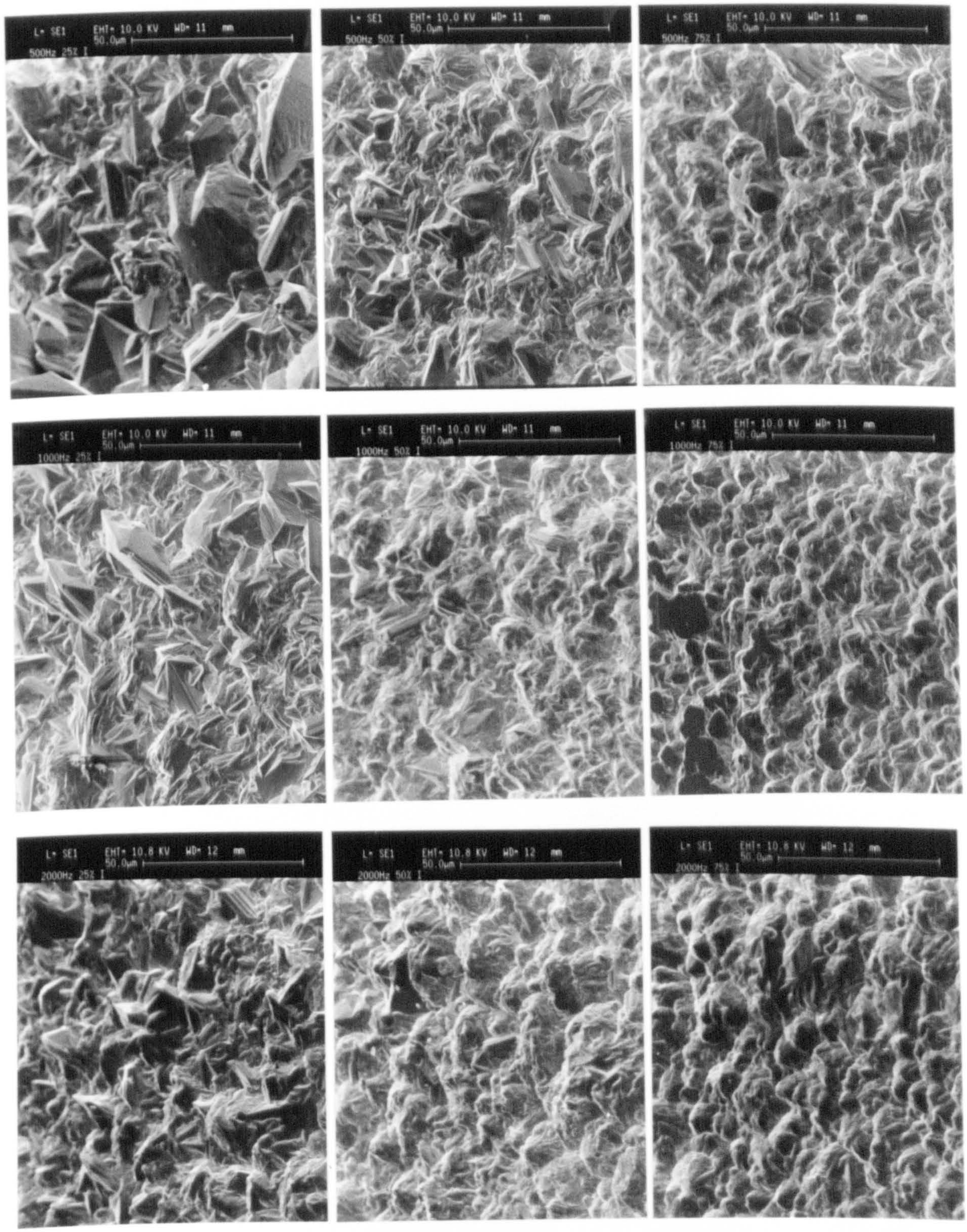

Figure 125 Continued ...

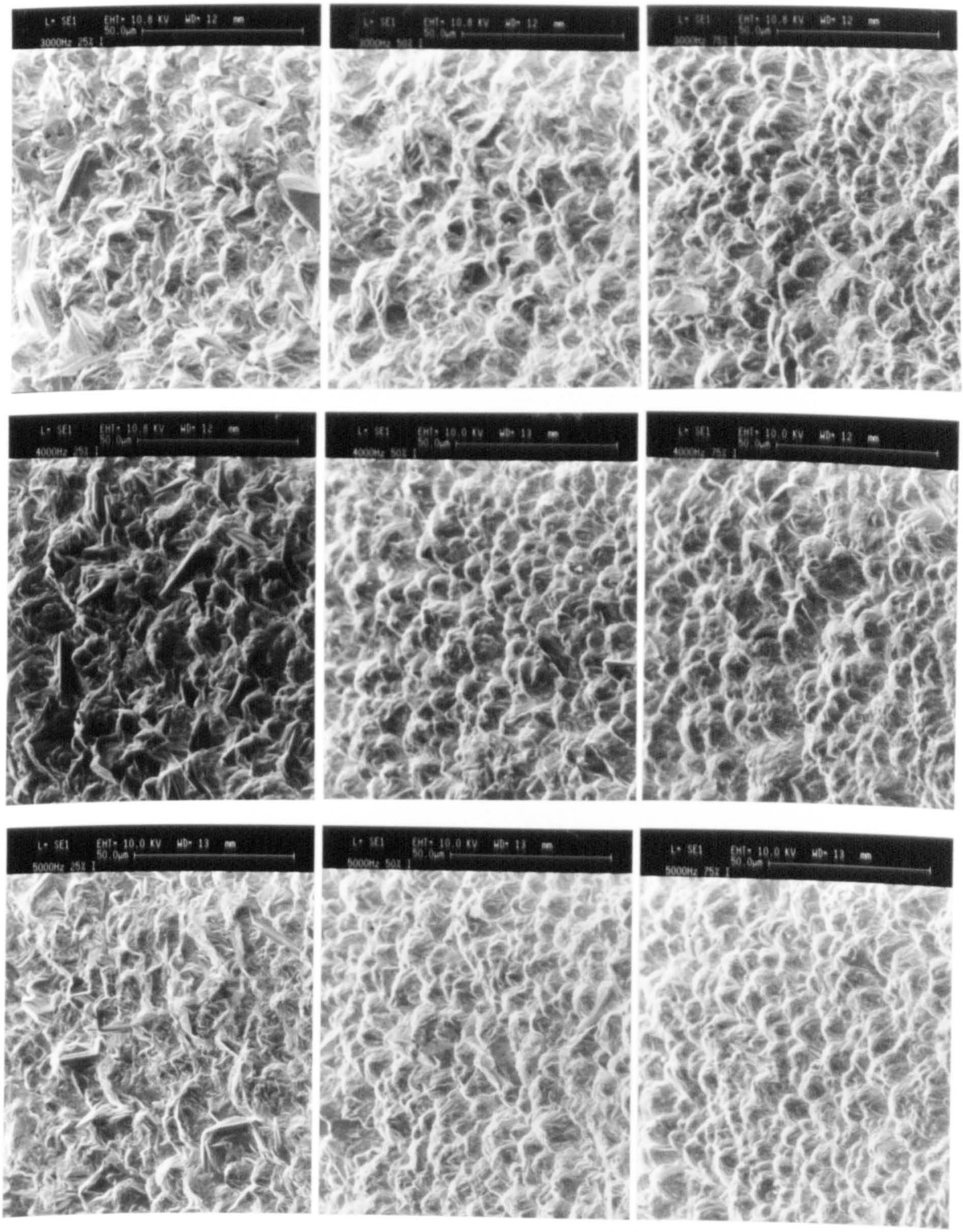

Figure 125 Continued ...

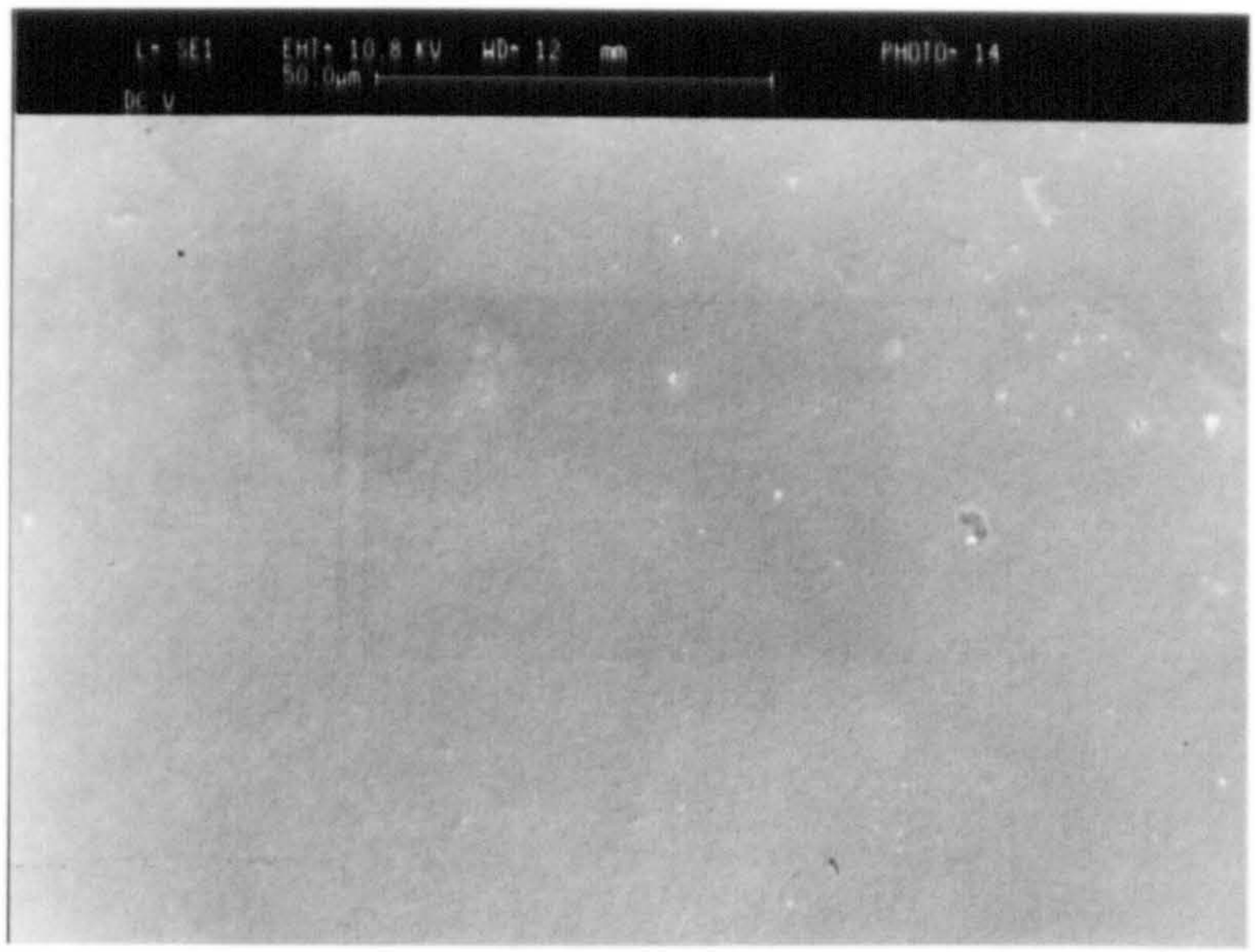

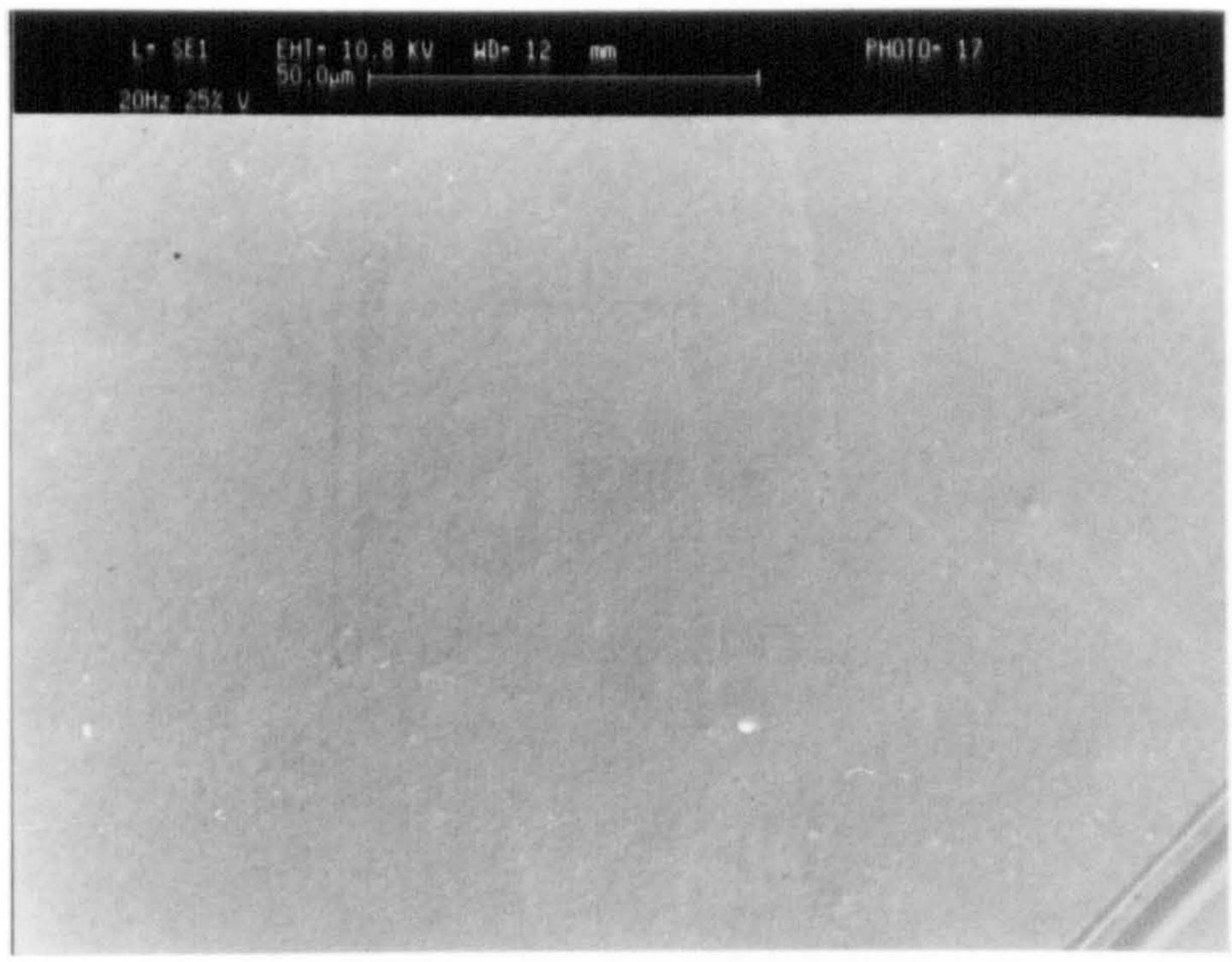

Figure 126 Scanning electron micrographs showing the crystal structures obtained under DC and unipolar pulse using electrolyte V; the conditions are specified on each micrographs.

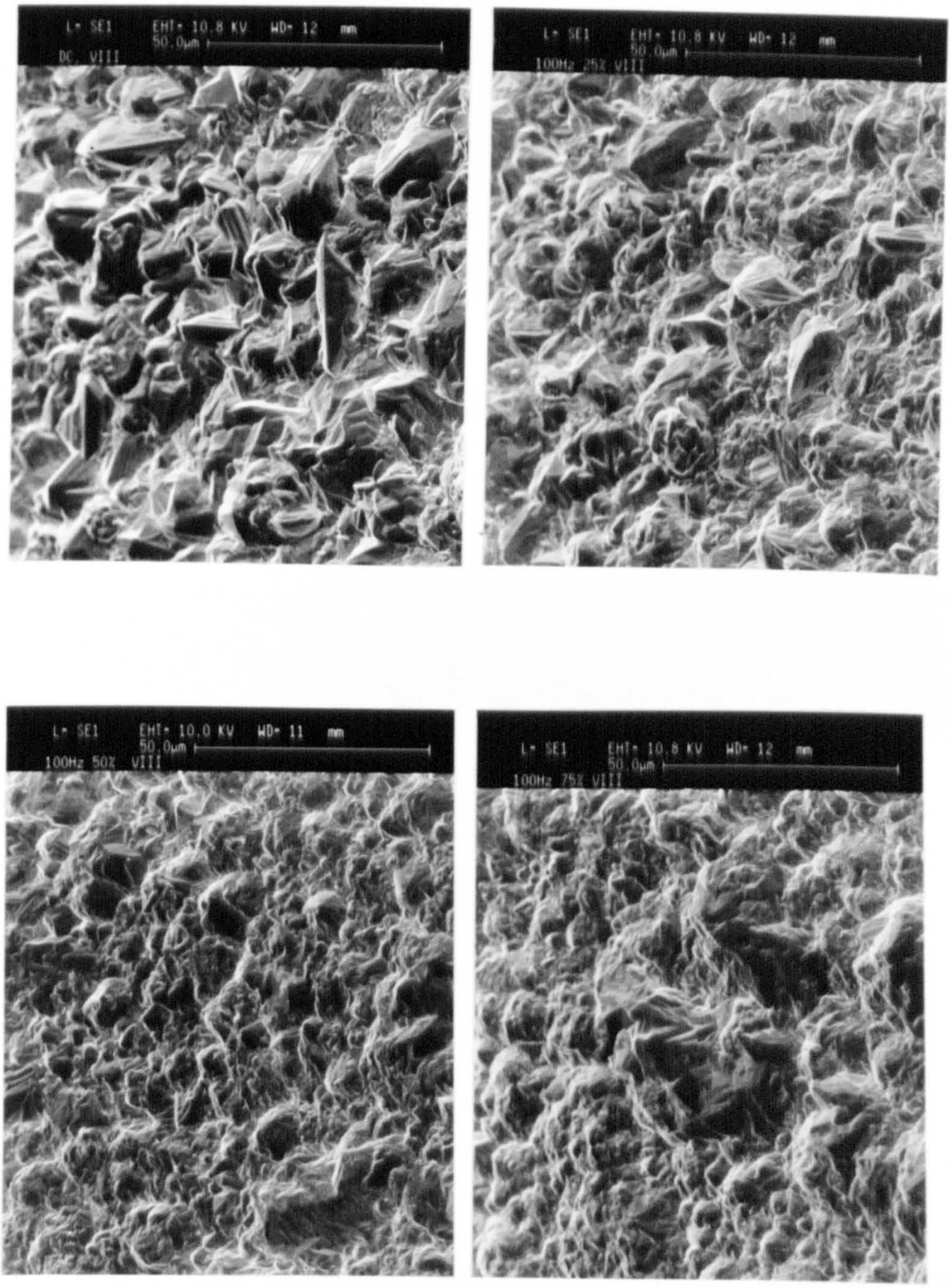

Figure 127 Scanning electron micrographs showing the crystal structures obtained under DC and unipolar pulse using electrolyte VIII; the conditions are specified on each micrographs.

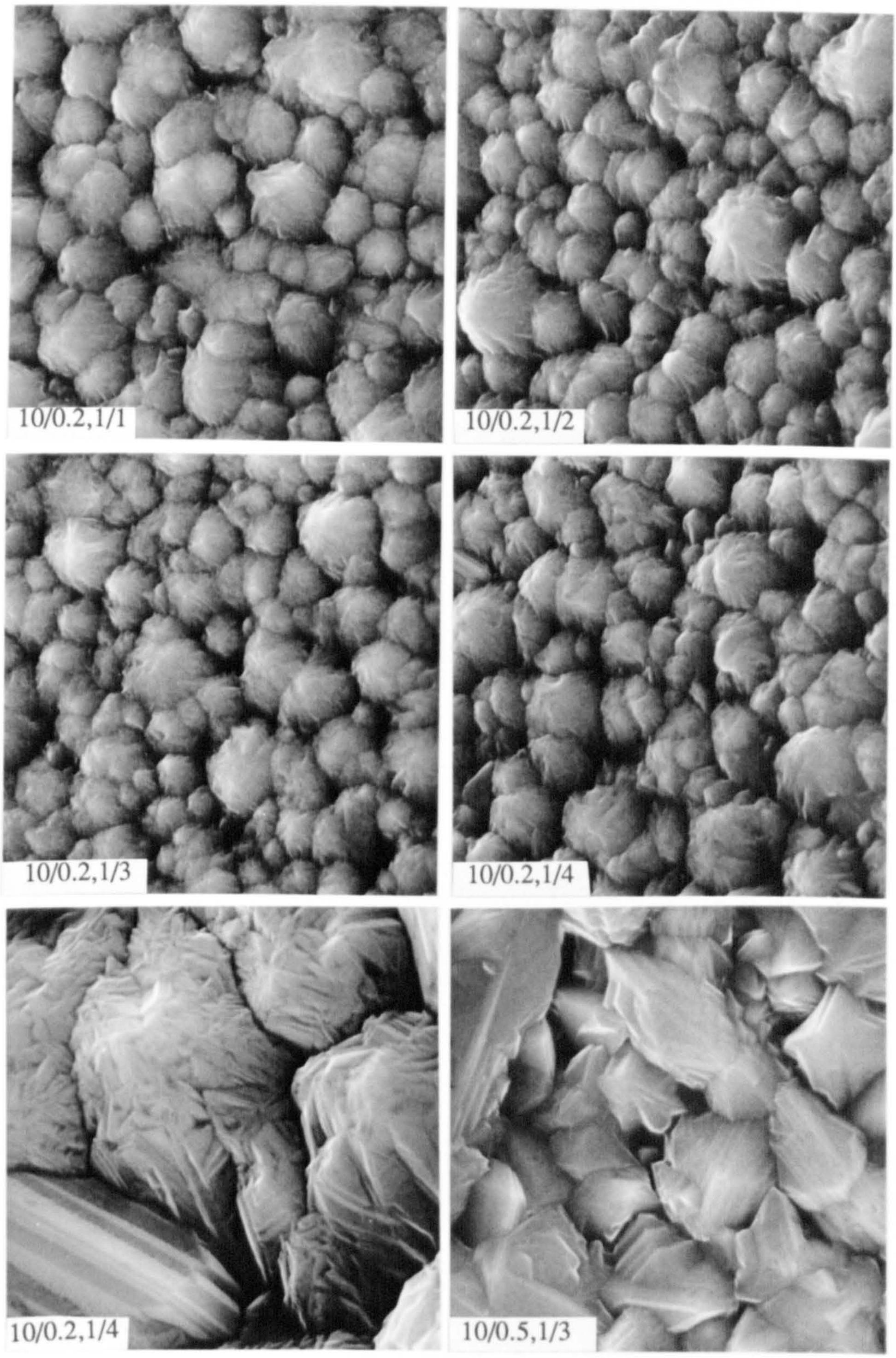

Figure 128 Scanning transmission electron micrographs showing the crystal structures obtained under bipolar pulse reverse at various $t_{on(c)}/t_{on(a)}$ and $i_{p(c)}/i_{p(a)}$ ratios using electrolyte I; the conditions are specified on each micrographs. Magnification: x1000 or x5000.

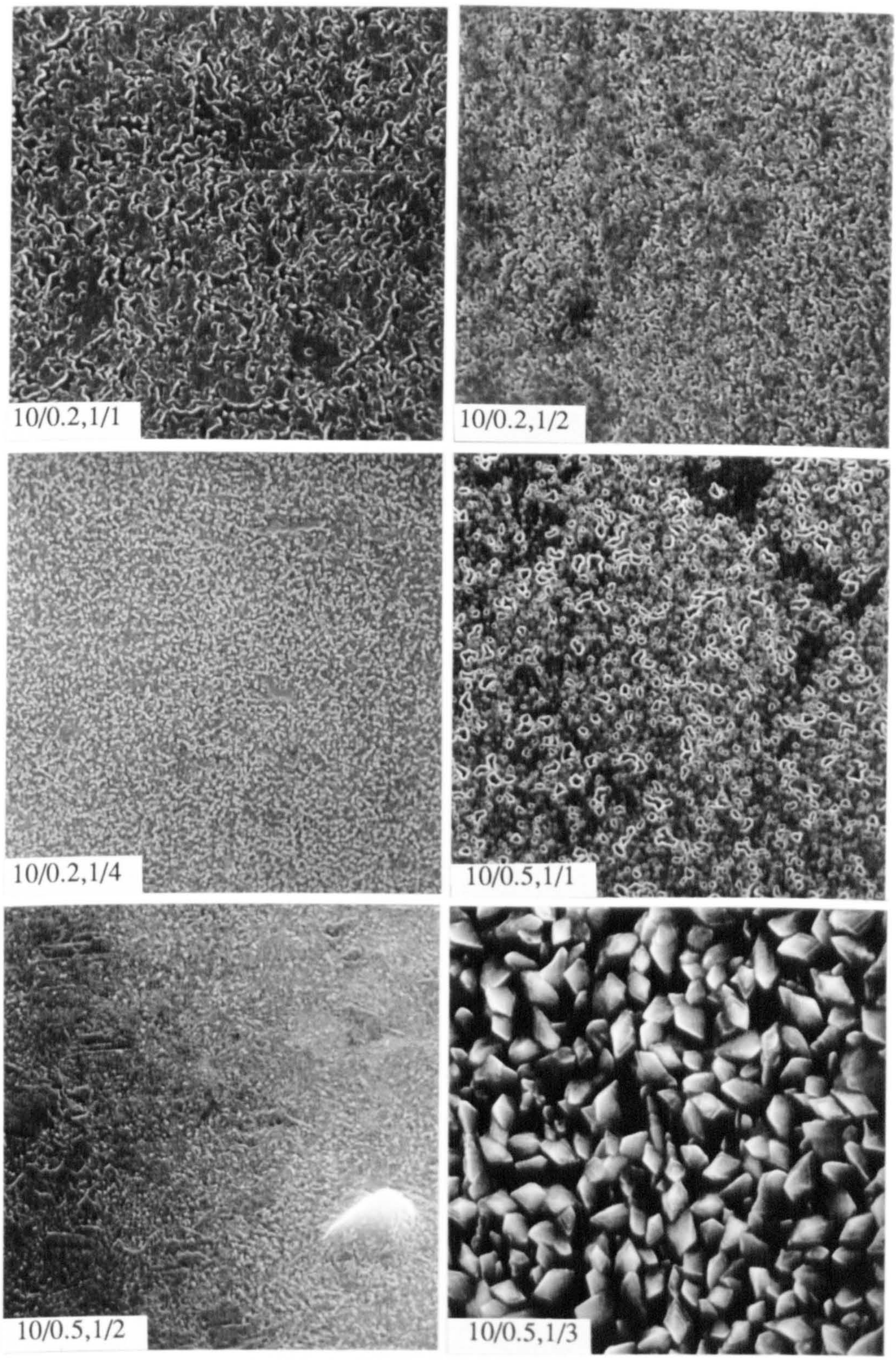

Figure 129 Scanning transmission electron micrographs showing the crystal structures obtained under bipolar pulse reverse at various $t_{on(c)}/t_{on(a)}$ and $i_{p(c)}/i_{p(a)}$ ratios using electrolyte V; the conditions are specified on each micrographs. Magnification: x1000 and x5000 for very small grains (or samples with lustrous appearance) and very large grains.

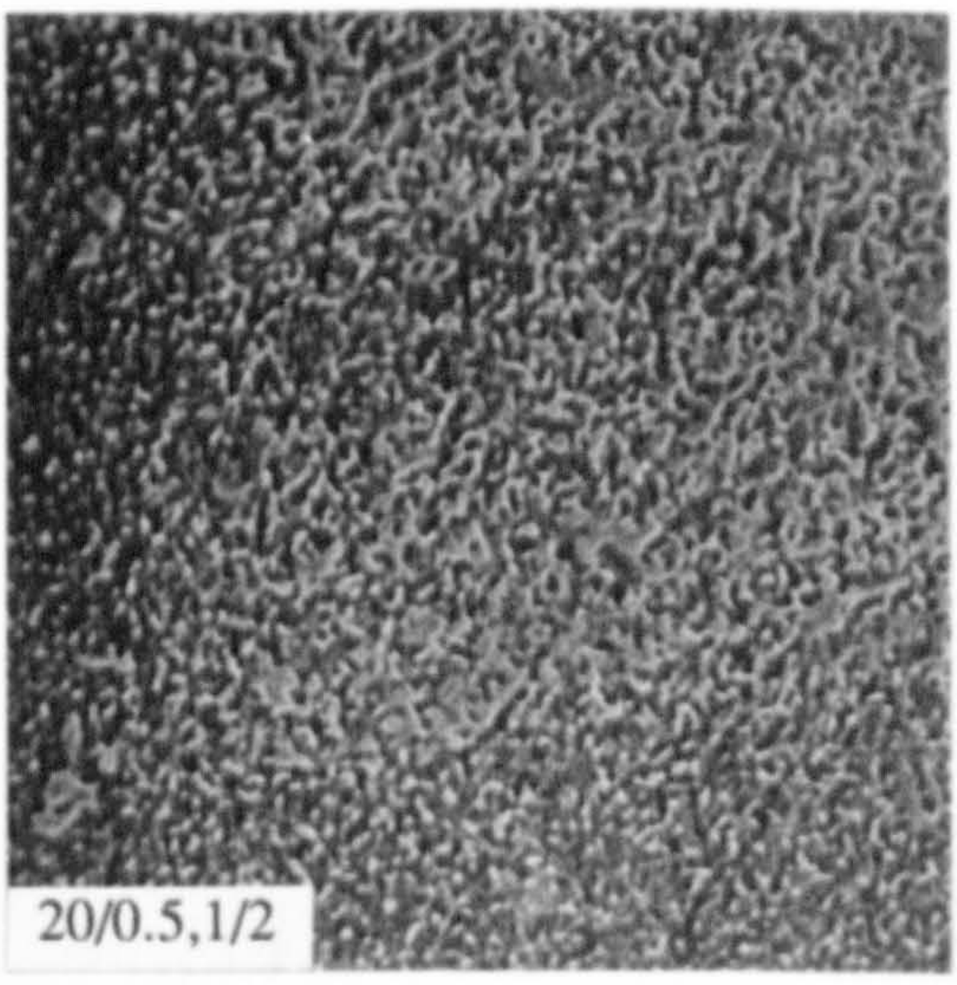

Figure 129 Continued ...

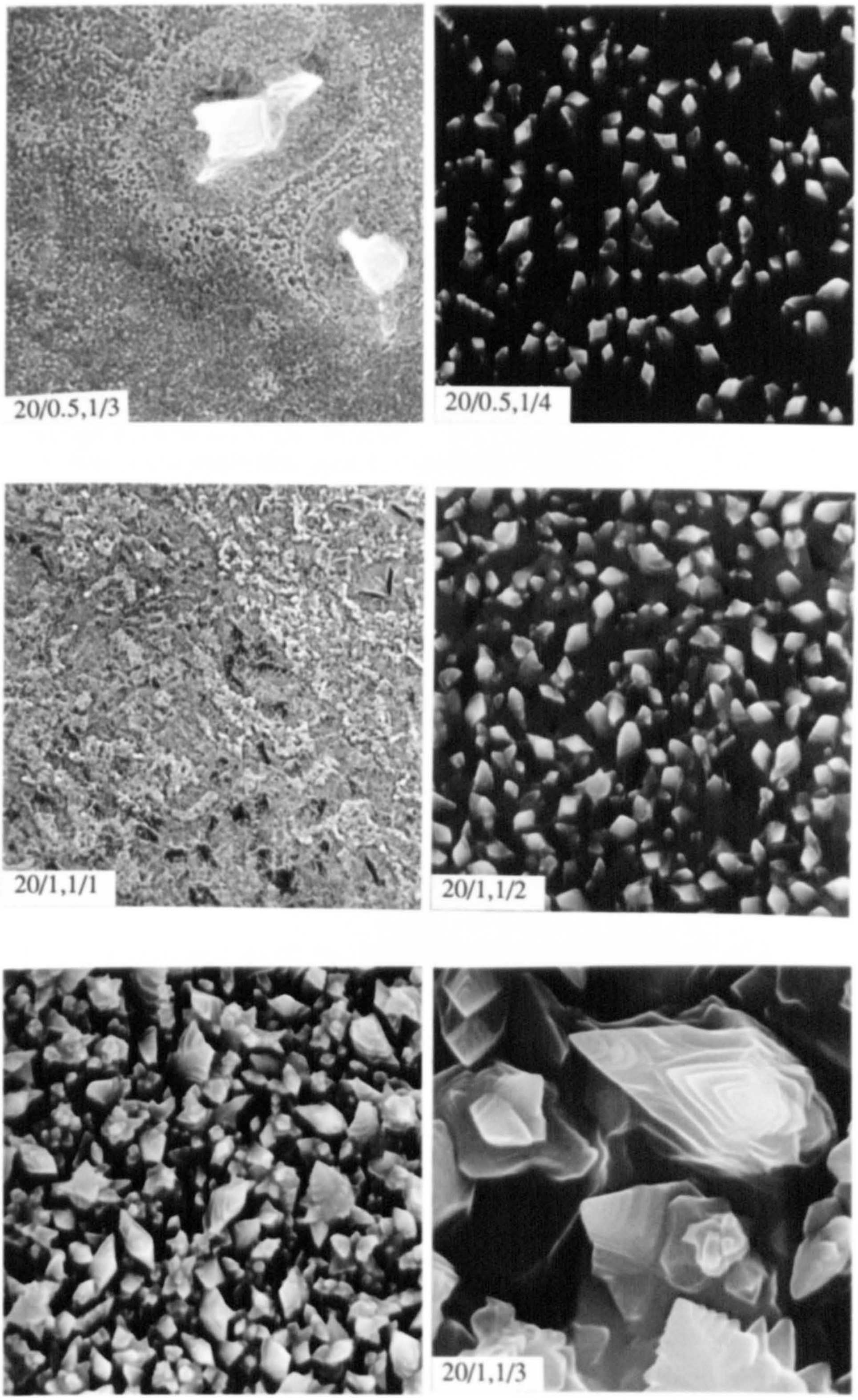

Figure 129 Continued ...

Appendix 1

Electrolyte composition used for DC, forward pulse and PR, conductivity values and Wagner number and Enhancement Wagner number ratio definitions

Electrolyte composition used for DC and forward pulse

I- 0.3M $CuSO_4$, 2.25M 98%H_2SO_4, 50ppm Cl^-
II- 0.3M$CuSO_4$, 2.25M 98%H_2SO_4, 50ppm Cl^-, 1g/l C140
III- 0.3M $CuSO_4$, 2.25M 98%H_2SO_4, 50ppm Cl^-, 1g/l C140, 6.25mg/l N1
IV- 0.3M CuSO4, 2.25M 98%H_2SO_4, 50ppm Cl^-, 1g/l C140, 0.625mg/l DS4
V- 0.3M $CuSO_4$, 2.25M 98%H_2SO_4, 50ppm Cl^-, 1g/l C140, 0.625mg/l DS4, 6.25mg/l N1
VI- 0.3M$CuSO_4$, 2.25M 98%H_2SO_4, 50ppm Cl^-, 0.1g/l C140
VII- 0.3M$CuSO_4$, 2.25M 98%H_2SO_4, 50ppm Cl^-, 10g/l C140
VIII- 0.3M $CuSO_4$, 2.25M 98%H_2SO_4, 0ppm Cl^-
IX- 0.3M $CuSO_4$, 2.25M 98%H_2SO_4, 0ppm Cl^-, 1g/l C140
X- 0.3M $CuSO_4$, 2.25M 98%H_2SO_4, 50ppm Cl^-, 1g/l C140, 0.625mg/l DS4, 6.25mg/l N1; 35^oC
XI- 0.14M $CuSO_4$, 3.375M 98%H_2SO_4, 50ppm Cl^-, 1g/l C140, 0.625mg/l DS4, 6.25mg/l N1
XII- 0.14M $CuSO_4$, 3.375M 98%H_2SO_4, 50ppm Cl^-, 1g/l C140, 0.625mg/l DS4, 6.25mg/l N1; 35^oC
XIII- 0.3M $CuSO_4$, 2.25M 98%H_2SO_4, 50ppm Cl^-, 1g/l C140, 0.625mg/l DS4, 6.25mg/l N1; 10^oC

Electrolyte conductivity used for DC and forward pulse

$\kappa_I = 0.465 Scm^{-1}$
$\kappa_{II} = 0.465 Scm^{-1}$
$\kappa_{III} = 0.447 Scm^{-1}$
$\kappa_{IV} = 0.439 Scm^{-1}$
$\kappa_V = 0.442 Scm^{-1}$
$\kappa_{VI} = 0.399 Scm^{-1}$
$\kappa_{VII} = 0.398 Scm^{-1}$
$\kappa_{VIII} = 0.399 Scm^{-1}$
$\kappa_{IX} = 0.400 Scm^{-1}$
$\kappa_X = 0.391 Scm^{-1}$
$\kappa_{XI} = 0.365 Scm^{-1}$
$\kappa_{XII} = 0.450 Scm^{-1}$
$\kappa_{XIII} = 0.461 Scm^{-1}$

Electrolyte composition used for PR

I- 0.3M $CuSO_4$, 2.25M 98%H_2SO_4, 50ppm Cl^-
V- 0.3M $CuSO_4$, 2.25M 98%H_2SO_4, 50ppm Cl^-, 1g/l C140, 0.625mg/l DS4, 6.25mg/l N1

Electrolyte conductivity used for PR

$\kappa_I = 0.485 Scm^{-1}$
$\kappa_V = 0.509 Scm^{-1}$

Wagner number

$$Wa = \frac{\text{Tafel Slope}}{2.303\ i} \times \frac{\kappa}{L}$$ where L=shortest distance between cathode to reference electrodes= 4.8cm

Wagner number enhancement ratio

$$R_{Wa} = \frac{\text{Pulse Wagner number } (Wa_P)}{\text{DC Wagner number } (Wa_{DC})}$$

Appendix 2

Table of plating additives

Code	Chemical Name/Formula	Comment/Effectiveness
C140	Polyethylene glycol $HOCH_2(CHOCH_2)_n CH_2O$ or $H(OCH_2CH_2)_n OH$	Average M.W. 14000 Usually M.W. is from 200 to 6000 Intermediate from non-ionic surfactants and alkyd resins. - Suppresses the deposition process - Surface prohibitor.
N1	1, 3, 6 - naphthalenetrisulphonic acid trisodium salt $C_{10}H_5(SO_3Na)_3$ 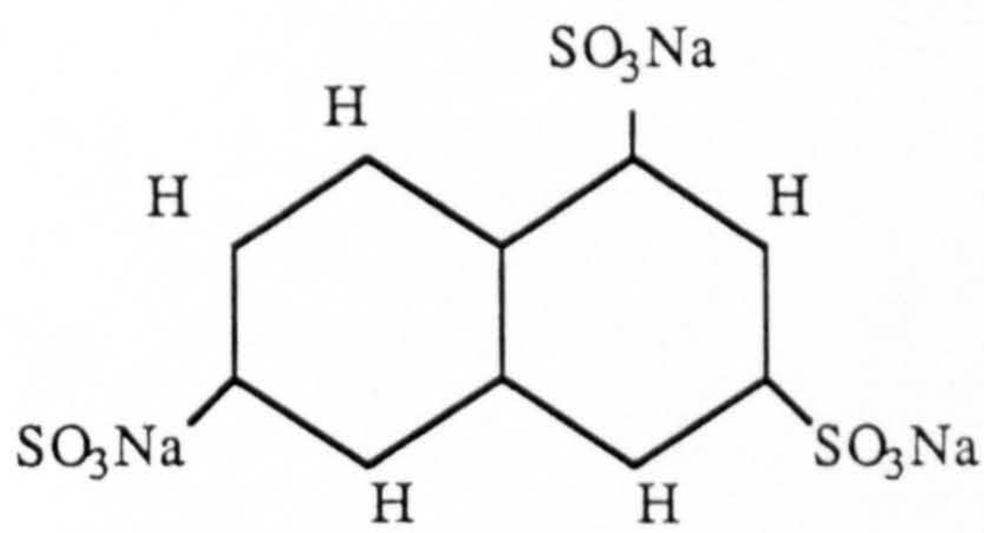	For low current density brightness.
DS4	33, Dithiobispropane sulphonic acid $-(S-(CH_2)_3SO_3H)_2$	Fine buff crystals usually used as a diazo type stabilizer - Activator; re-activates the surface - Little effect on its own - Effects crystal structure - Its a sulphur compound similar to thiourea - Brighter agent.
Cl^-	Cl^- as NaCl	Essential for C140 to work or may activate the surface. It is believed that it acts as a bridge on the surface of the electrode.

APPENDIX 3

2-D and 3-D maps of the results obtained under unipolar pulse conditions for electrolytes I-IX.

2-D profiles showing the duty cycle and the frequency in relation to the Wagner number values as a contour map for different acid copper sulphate electrolyte constituents.

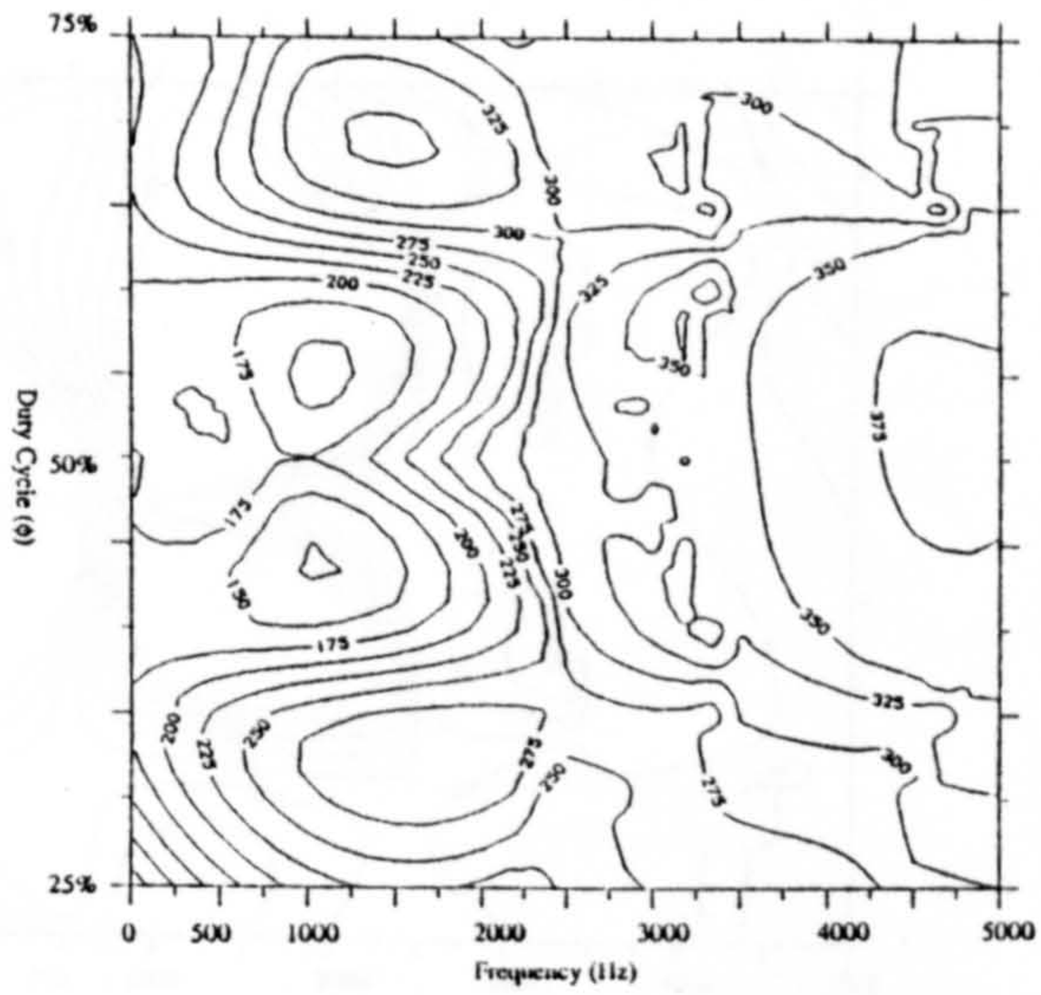

Electrolyte I- 0.3M $CuSO_4$, 2.25M 98%H_2SO_4, 50ppm Cl^-

Wagner Number Contour Height • 10^{-3}

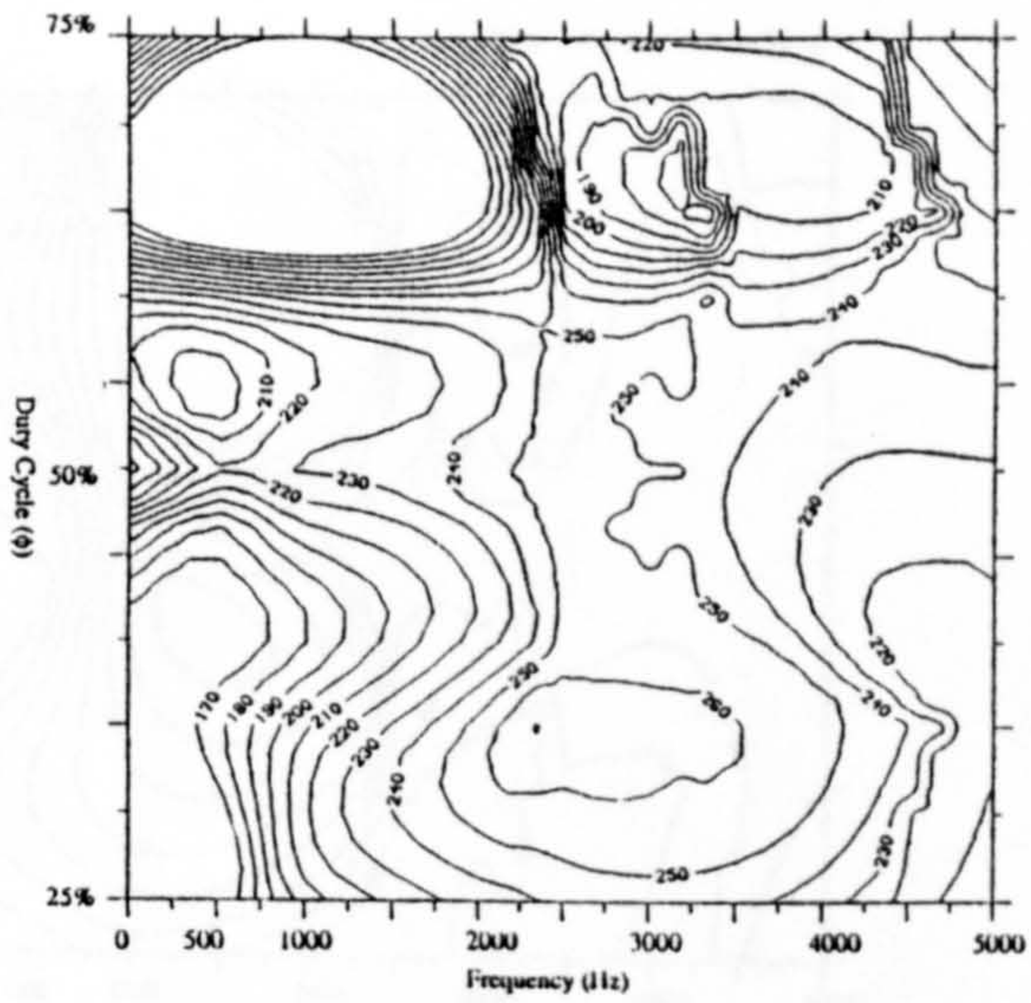

Electrolyte II - 0.3M $CuSO_4$, 2.25M 98%H_2SO_4, 50ppm Cl^-, 1g/l C140

Wagner Number Contour Height • 10^{-3}

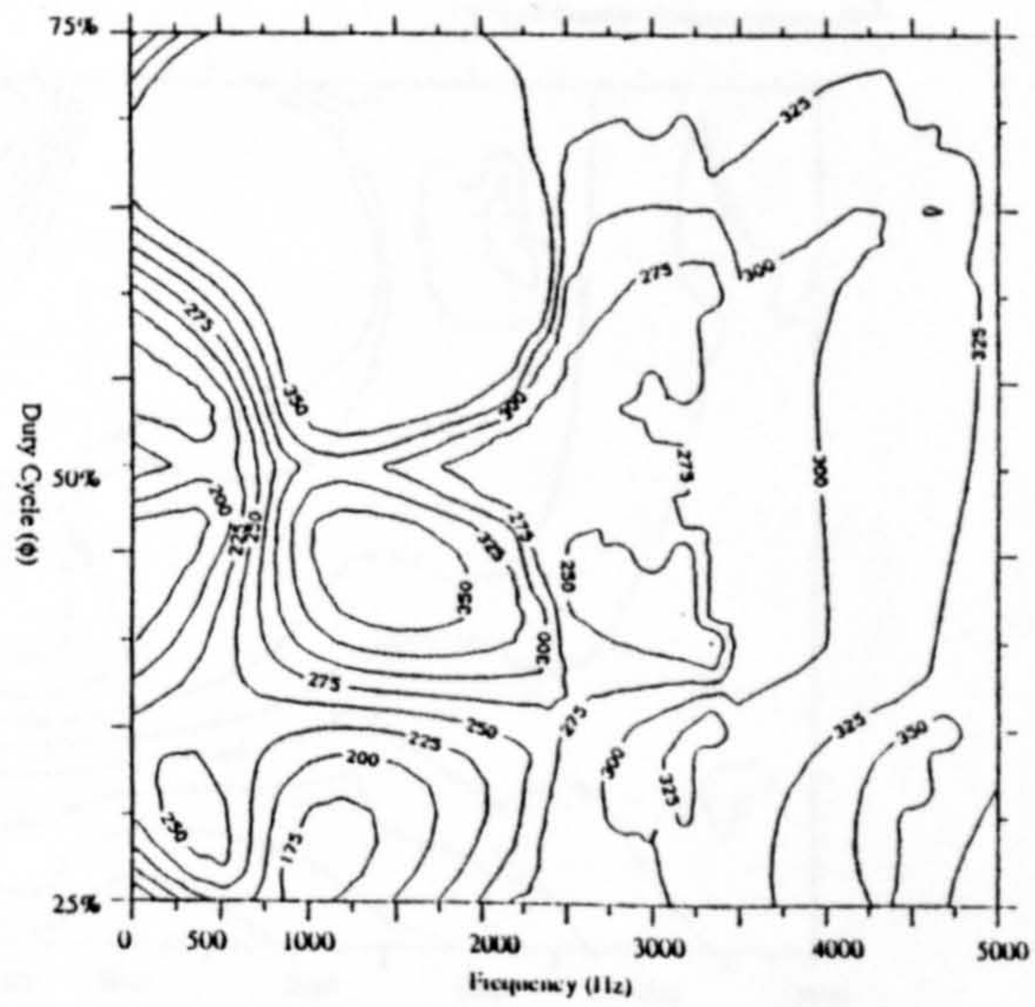

Electrolyte III - 0.3M $CuSO_4$, 2.25M 98%H_2SO_4, 50ppm Cl^-, 1g/l C140, 0.25mg/l Ni

Wagner Number Contour Height • 10^{-3}

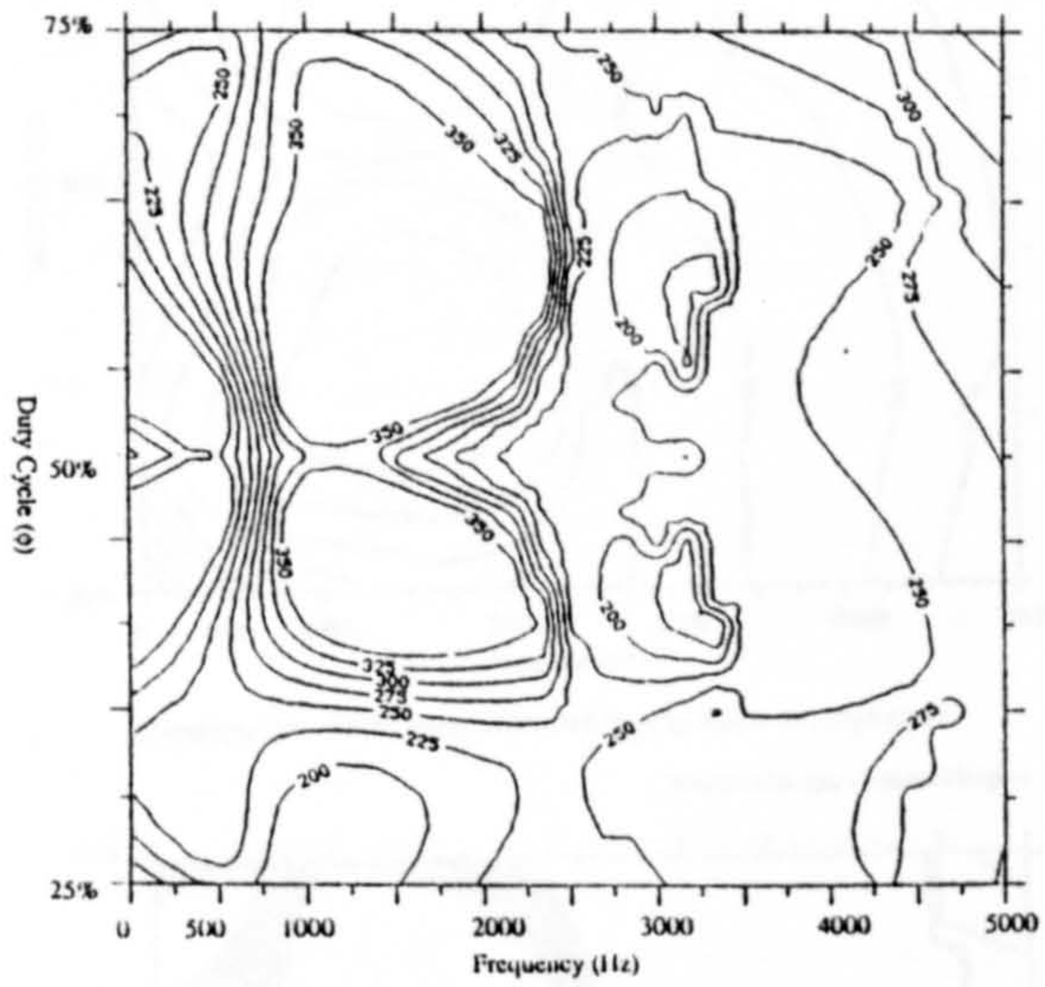

Electrolyte IV - 0.3M $CuSO_4$, 2.25M 98% H_2SO_4, 50ppm Cl^-, 1g/l C140, 0.625mg/l DS4

Wagner Number Contour Height • 10^{-3}

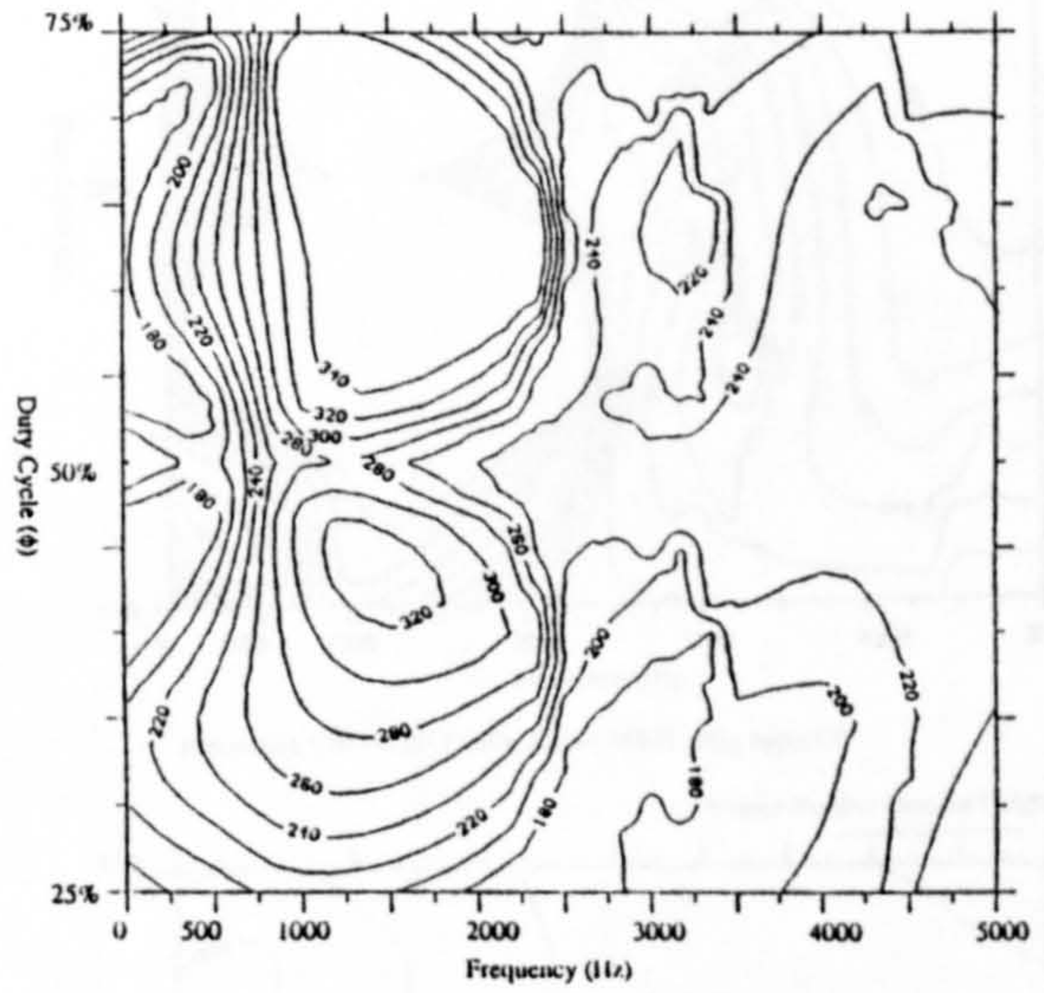

Electrolyte V - 0.3M $CuSO_4$, 2.25M 98% H_2SO_4, 50ppm Cl^-, 1g/l C140, 0.625mg/l DS4, 6.25mg/l Ni

Wagner Number Contour Height • 10^{-3}

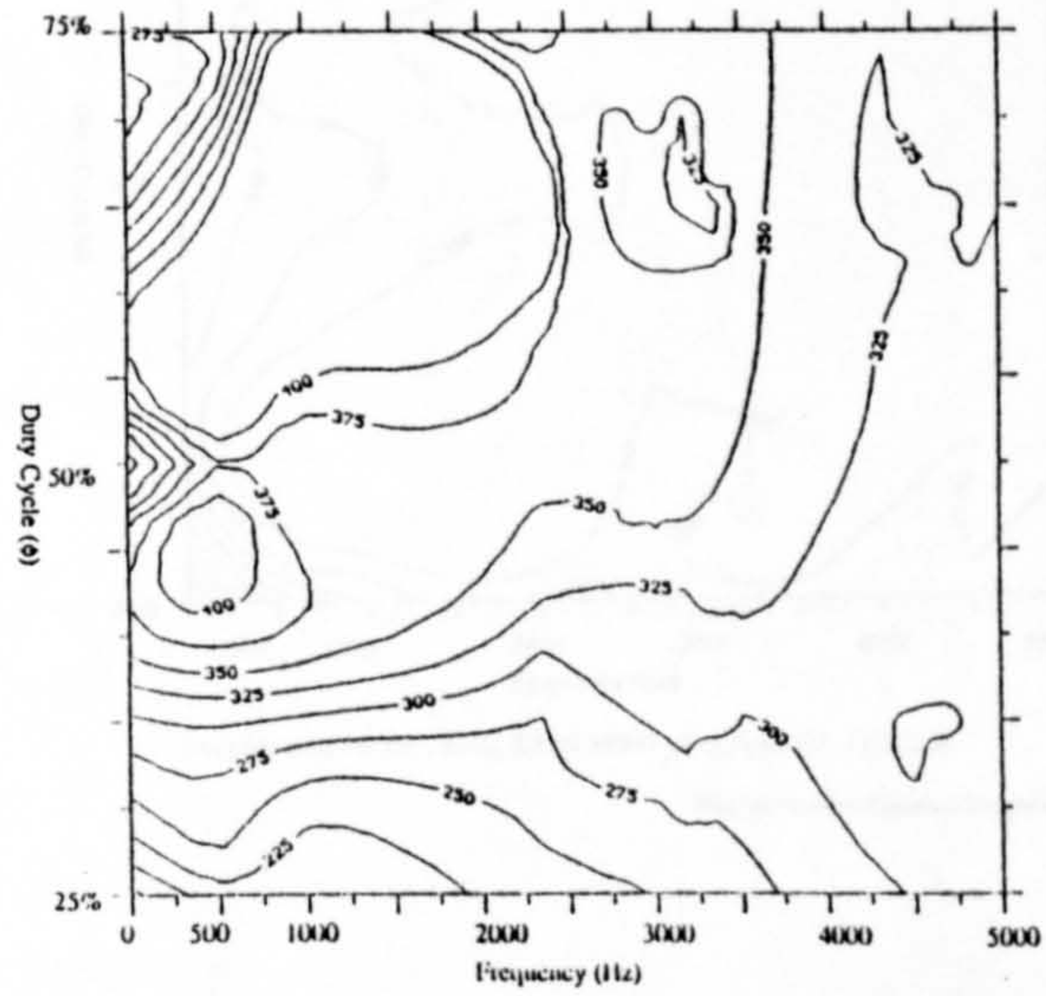

Electrolyte VI - 0.3M $CuSO_4$, 2.25M 98% H_2SO_4, 50ppm Cl^-, 0.1g/l C140

Wagner Number Contour Height • 10^{-3}

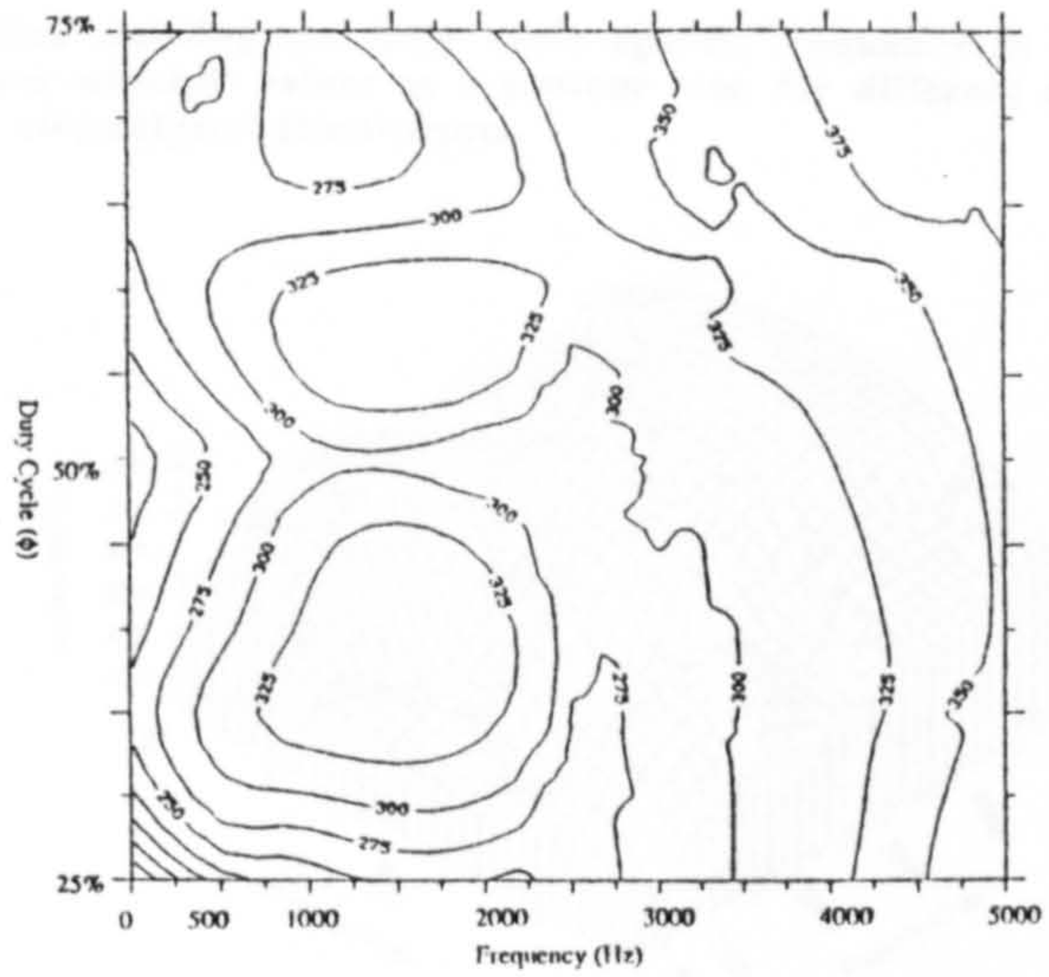

Electrolyte VII - 0.3M $CuSO_4$, 2.25M 98%H_2SO_4, 50ppm Cl^-, 10g/l C140

Wagner Number Contour Height• 10^{-3}

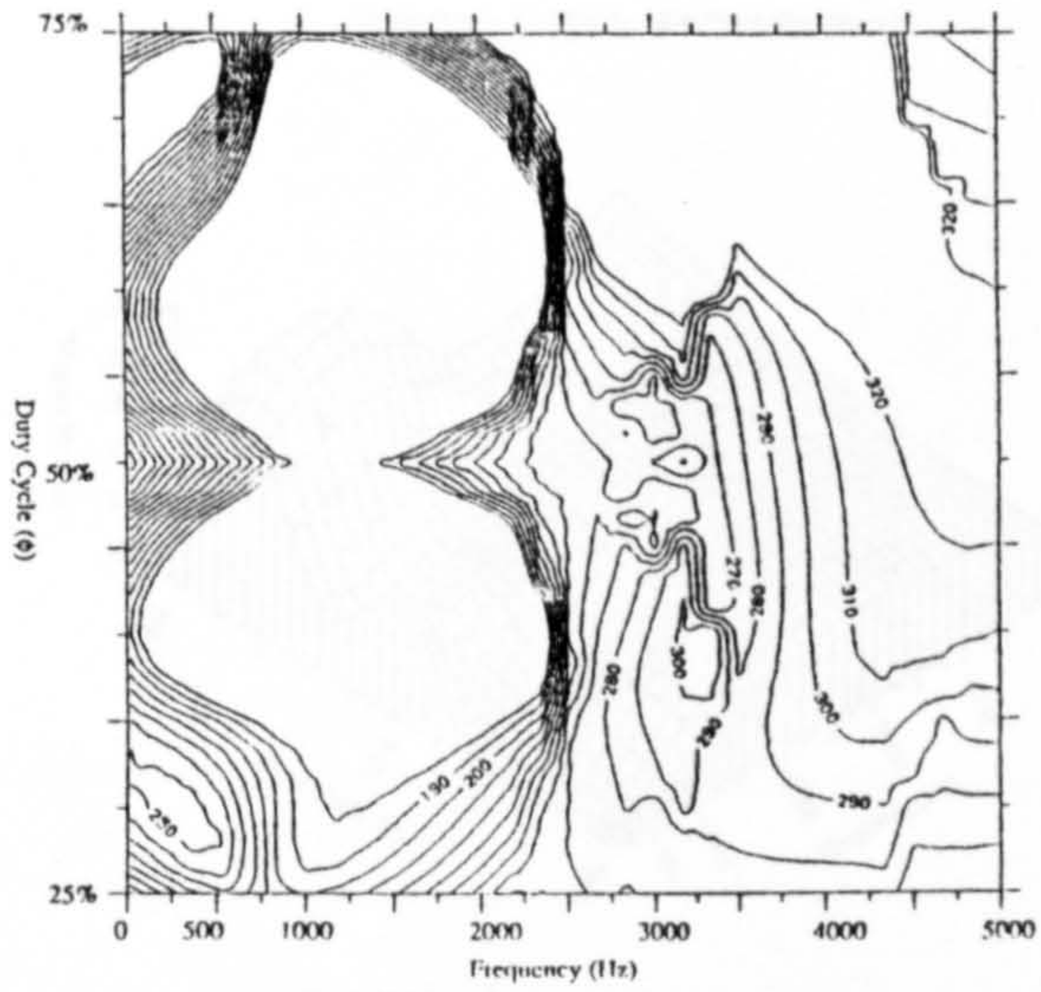

Electrolyte VIII - 0.3M $CuSO_4$, 2.25M 98%H_2SO_4, 0ppm Cl^-

Wagner Number Contour Height• 10^{-3}

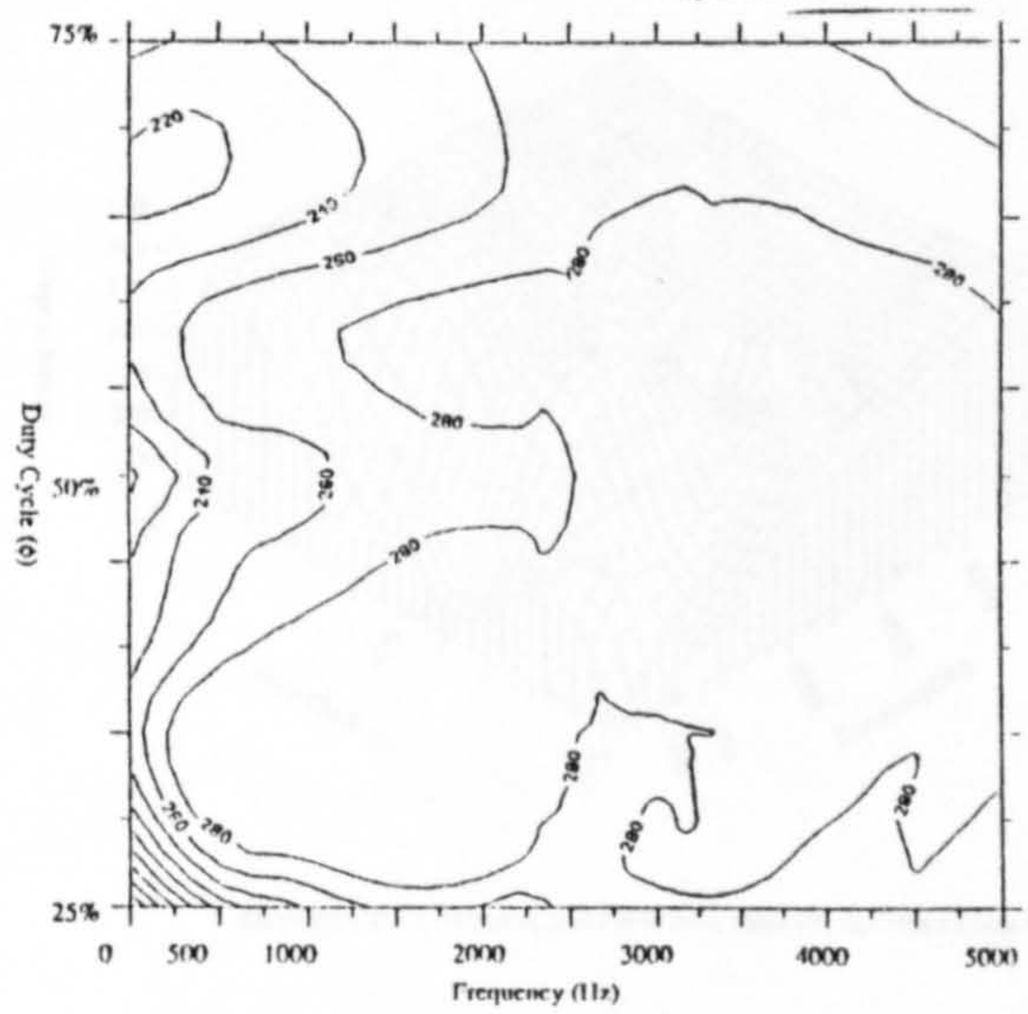

Electrolyte IX - 0.3M $CuSO_4$, 2.25M 98%H_2SO_4, 0ppm Cl^-, 1g/l C140

Wagner Number Contour Height• 10^{-3}

3-D profiles showing the duty cycle against frequency in relation to the Wagner number values as a contour map for different acid copper sulphate electrolytes constituents.

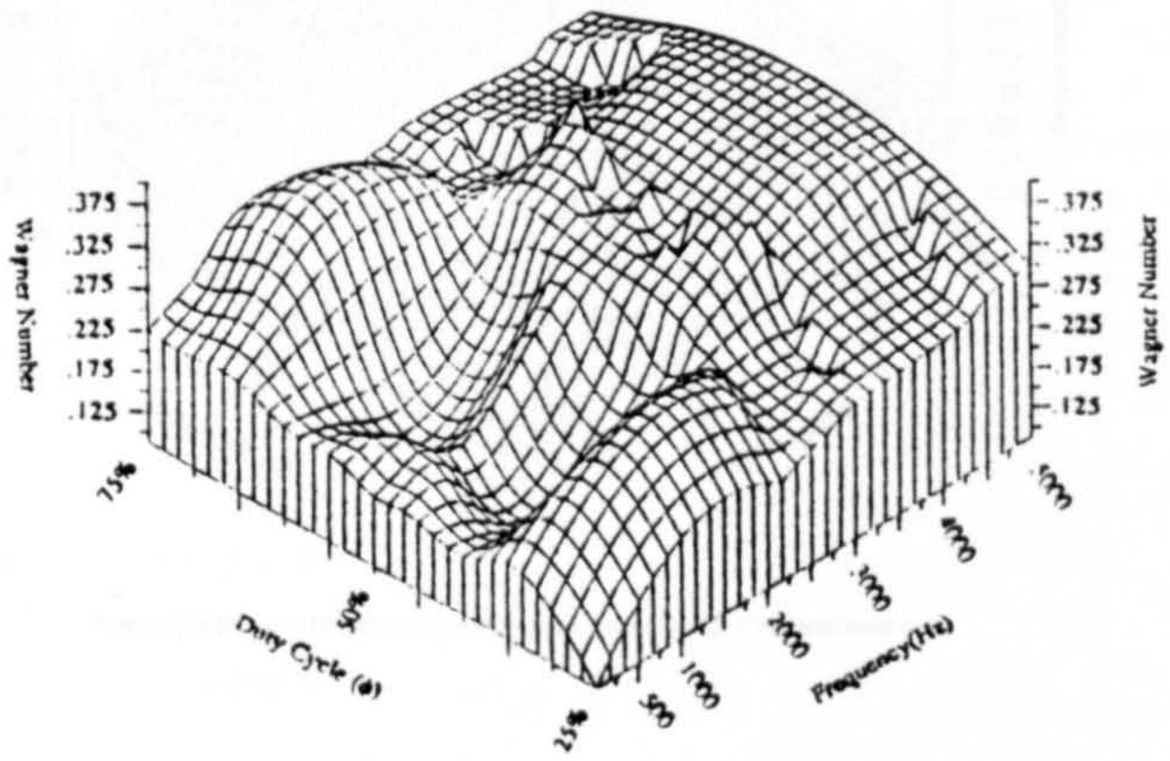

Electrolyte I- 0.3M $CuSO_4$, 2.25M 98%H_2SO_4, 50ppm Cl^-

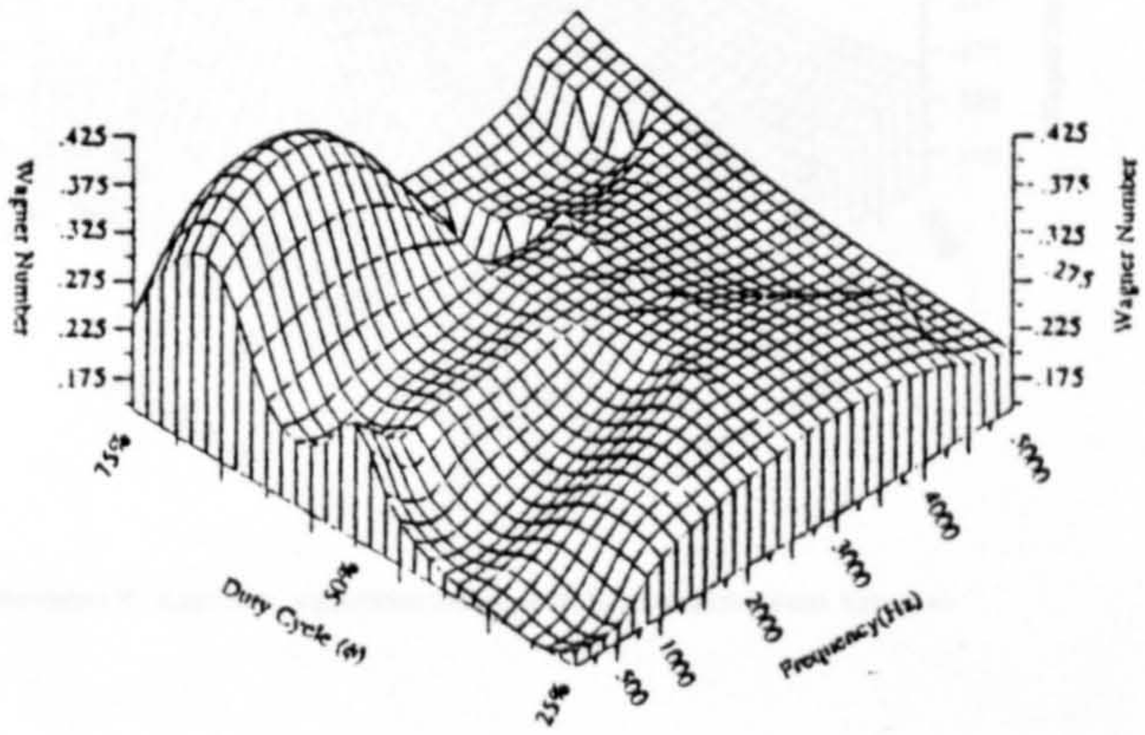

Electrolyte II- 0.3M$CuSO_4$, 2.25M 98%H_2SO_4, 50ppm Cl^-, 1g/l C140

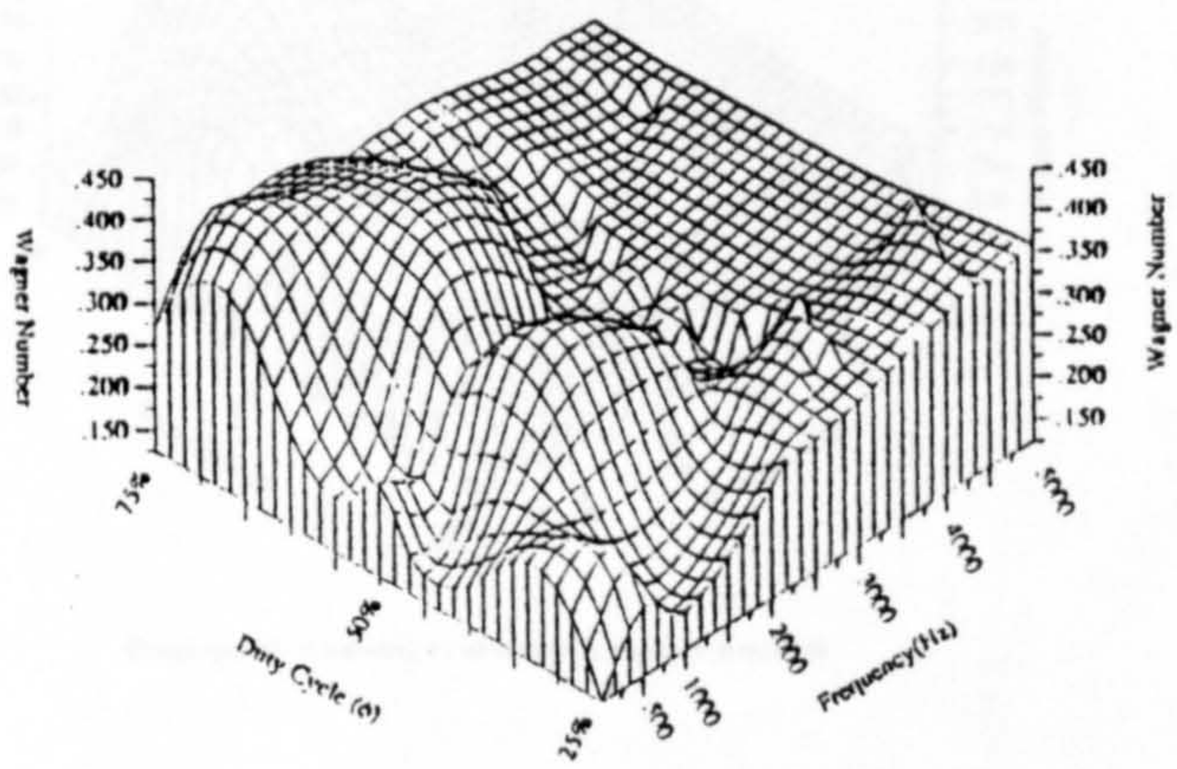

Electrolyte III- 0.3M $CuSO_4$, 2.25M 98%H_2SO_4, 50ppm Cl^-, 1g/l C140, 6.25mg/l Ni

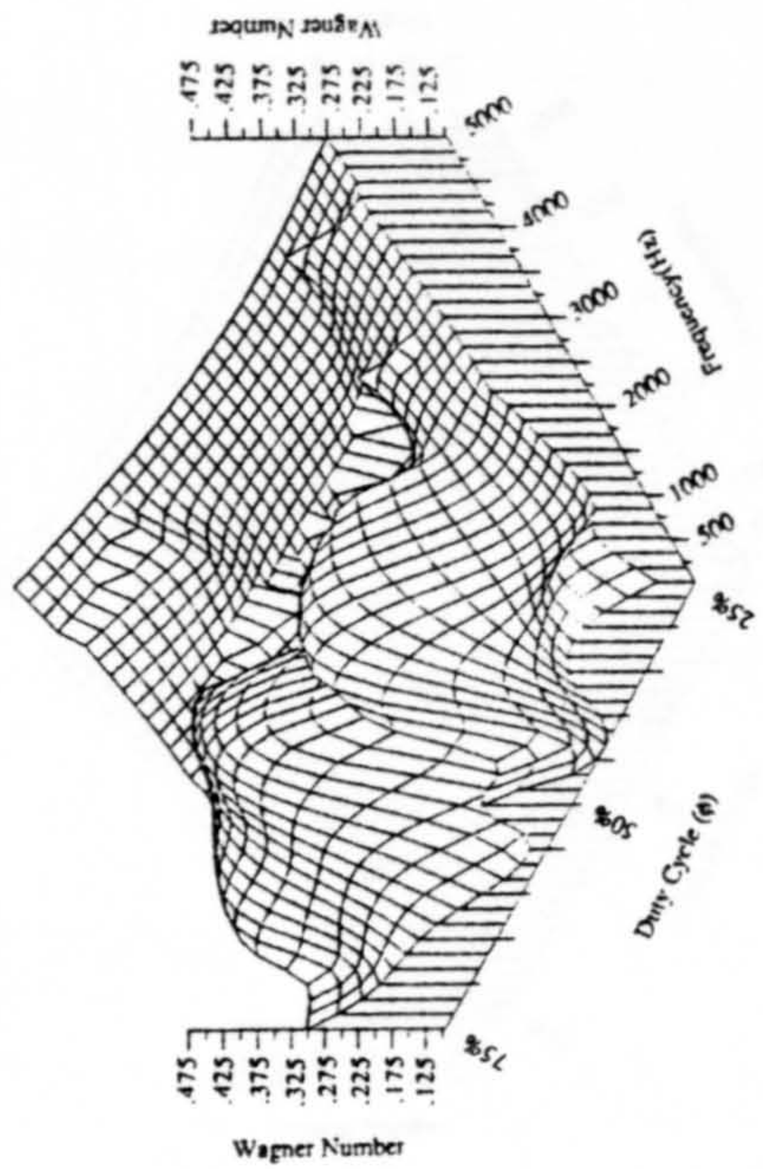

Electrolyte IV- 0.3M $CuSO_4$, 2.25M 98% H_2SO_4, 50ppm Cl^-, 1µl C140, 0.625mg/l DS4

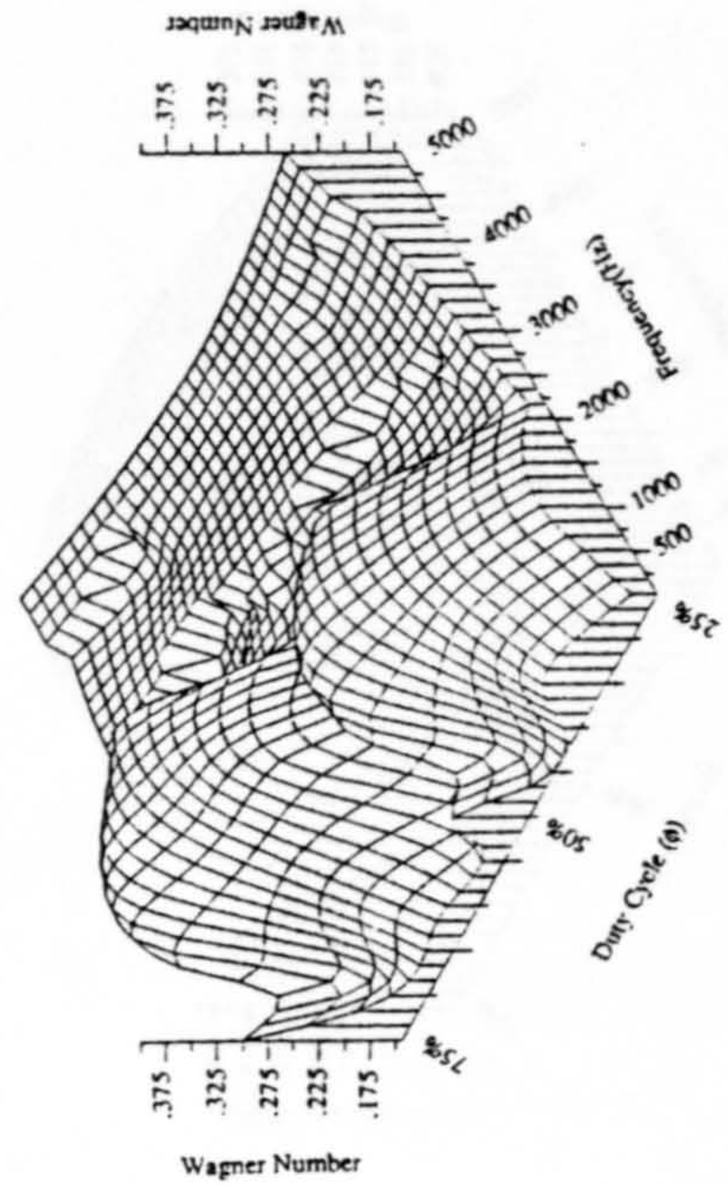

Electrolyte V- 0.3M $CuSO_4$, 2.25M 98% H_2SO_4, 50ppm Cl^-, 1µl C140, 0.625mg/l DS4, 6.25mg/l N1

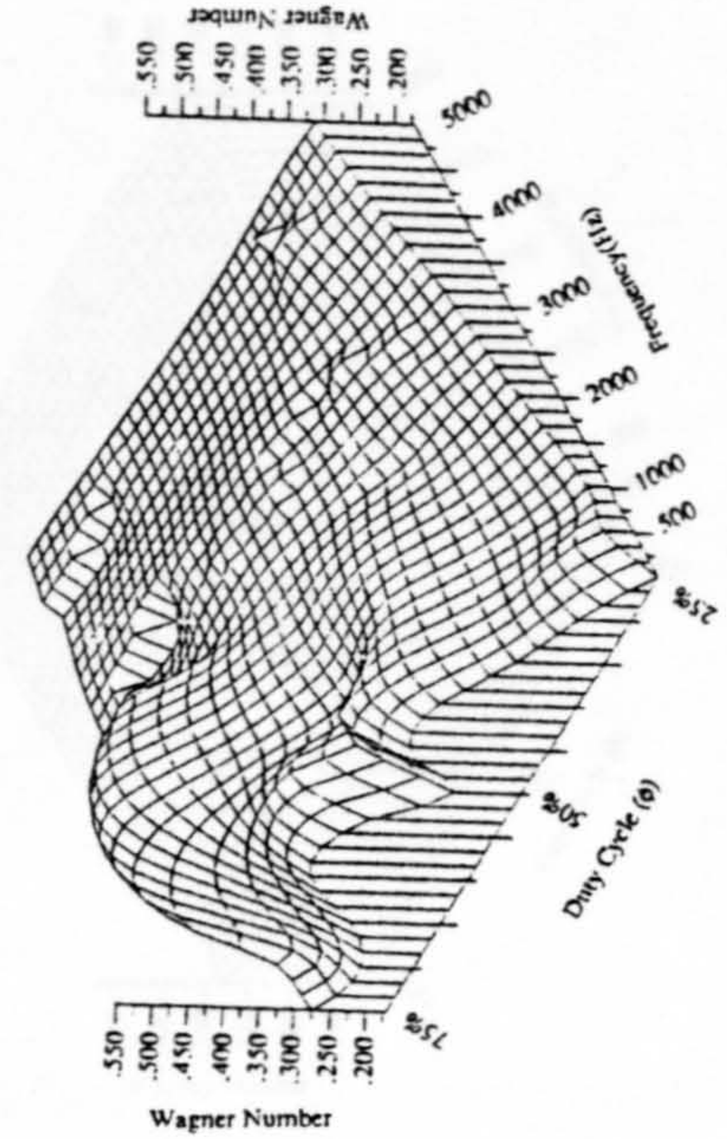

Electrolyte VI- 0.3M $CuSO_4$, 2.25M 98% H_2SO_4, 50ppm Cl^-, 0.1µl C140

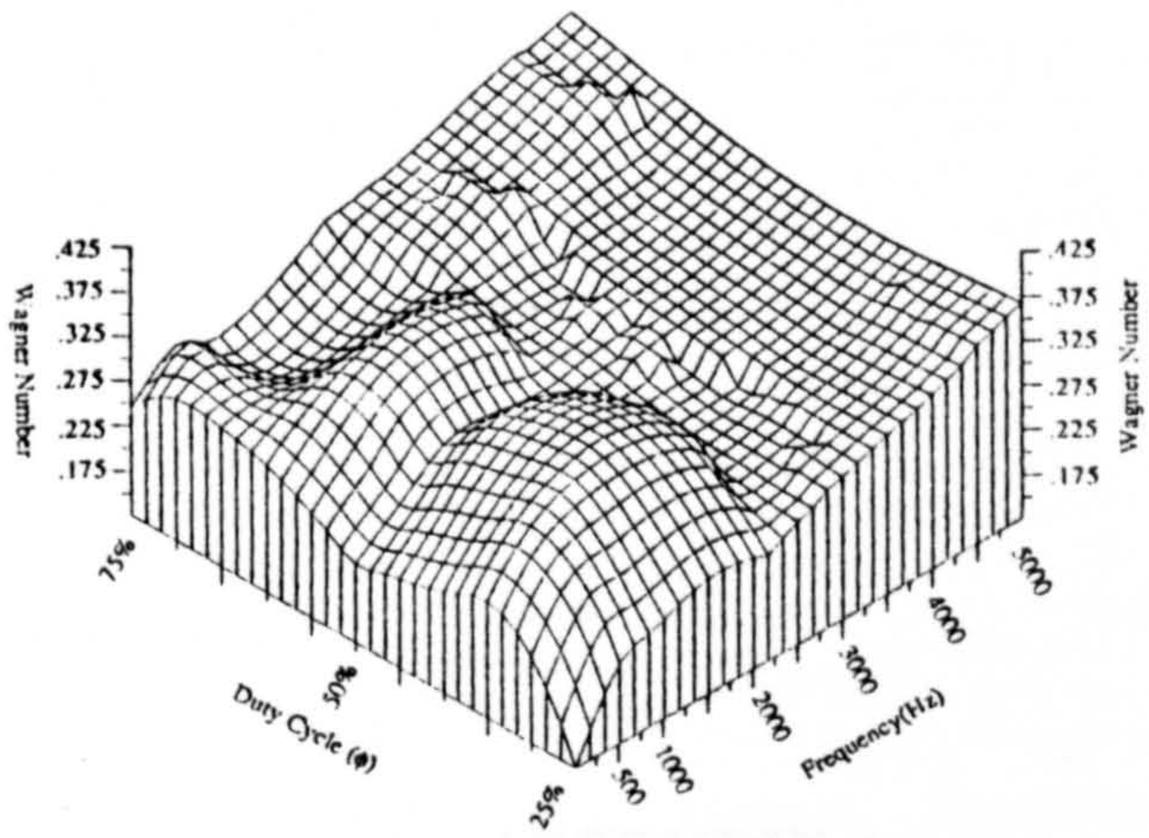

Electrolyte VII- 0.3M $CuSO_4$, 2.25M 98% H_2SO_4, 50ppm Cl^-, 10g/l C140

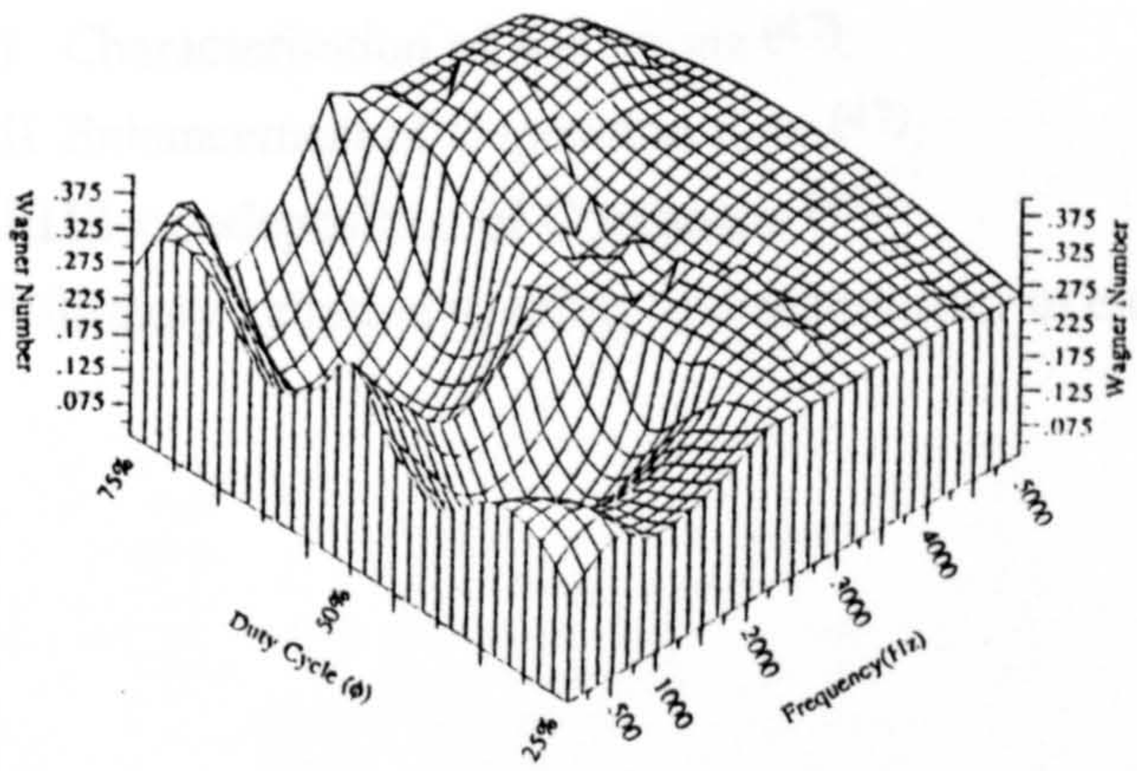

Electrolyte VIII- 0.3M $CuSO_4$, 2.25M 98% H_2SO_4, 0ppm Cl^-

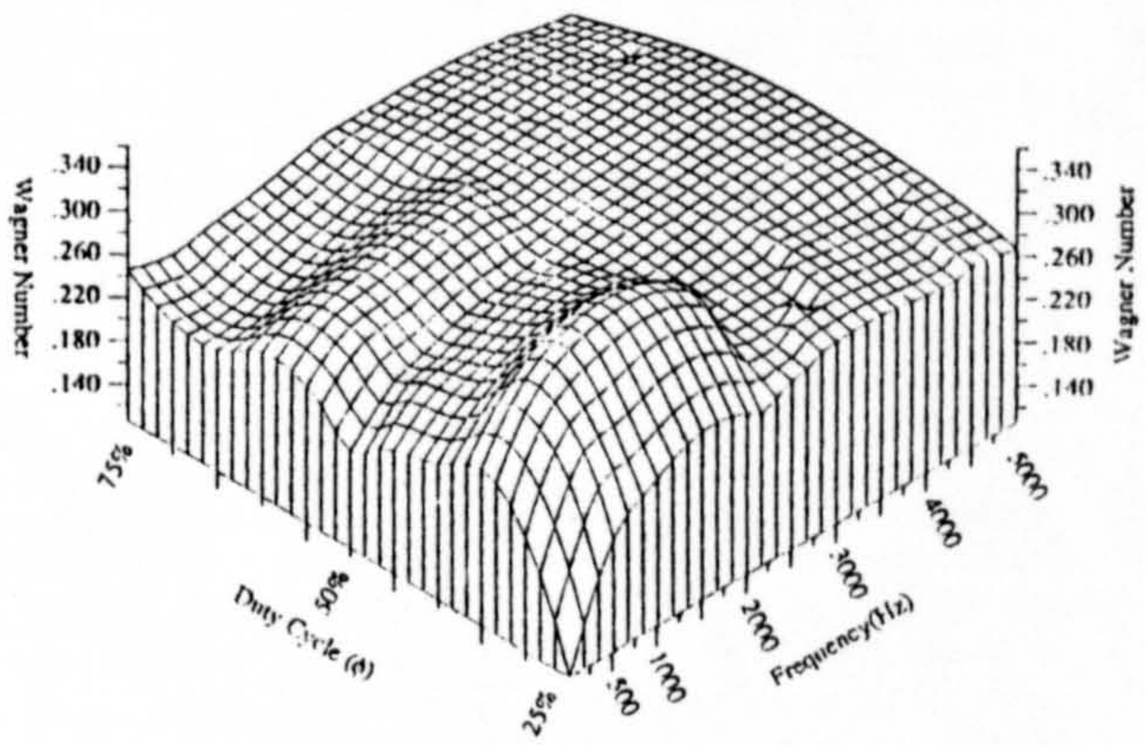

Electrolyte IX- 0.3M $CuSO_4$, 2.25M 98% H_2SO_4, 0ppm Cl^-, 1g/l C140

APPENDIX 4

Papers published prior to submission of thesis.

Vibratory Agitation for Electrodeposition:

I Characterisation of Agitations [47].

II Enhancement of Deposition Rate [47].

III Electrodeposition of Composite [48].

Vibratory agitation to enhance mass transfer in electrodeposition [49].

Vibratory agitation for electrodeposition: I Characterization of agitation

Mehrdad R. Kalantary and D. R. Gabe

Institute of Polymer Technology and Materials Engineering, Loughborough University of Technology, LE11 3TU.

SUMMARY – *A technique of vibratory agitation for electroplating solutions is described and methods of measuring the amplitude of vibration investigated. The pattern of agitation induced has been examined for flat and perforated disc vibrators. The use of Reynolds number to characterize the agitation is proposed, where* $Re = \frac{2fad}{v}$: *a is the amplitude, f is the frequency (in this case 50Hz), d the diameter of the disc and v the solution viscosity. Turbulent eddy patterns commence at Re ≈ 2500.*

Mehrdad R. Kalantary is a research student at Loughborough University where he completed his MSc degree in Materials Protection in 1986. He was formerly at Buckinghamshire College of Higher Education and Brunel University and his research interests are in electroplating with novel pulsing and agitation.

Dr David R. Gabe leads a research group at Loughborough University of Technology with a special interest in high speed electrodeposition. This paper forms part of the programme concerned with novel methods of agitation.

Mehrdad R. Kalantary and D. R. Gabe
Trans IMF 1989, **67**, 24

INTRODUCTION

The use of vibration in electrodeposition processes as a means of agitation has received limited attention and is rarely used at present in industrial processing largely because air agitation (or gas sparging) is cheap, easy to use and its general effects well-known. However, unlike air agitation, it can readily be described directly in a quantitative manner and its effects are not entirely dependent upon analysing the resultant process performance. Vibrational energy can be transmitted or generated either electromagnetically or mechanically and may be applied to either the electrode itself or to the solution. Most systematic studies have been concerned with vibrated electrodes either for rapid electro-analysis [1-3] or for enhanced mass transfer.[4-9] Alternatively, studies of vibrated solutions have been concerned with ultrasonic agitation[10-11] which is a special case having some specific advantages, and which also has other uses such as cleaning processes. When applied to the solution conventional vibrational energy has been used for processes other than electrodeposition, e.g. liquid-liquid solvent extraction.[12-13]

Vibrational agitation has a particular advantage for the electrodeposition of composite coatings where there is a requirement to maintain particles in suspension so that they may be entrapped in the growing electrodeposit – other methods of agitation have been employed but cannot offer such a wide range of incorporation behaviour.[14-15] It is in such a context that this detailed study of solution vibrational agitation has been made using a standard commercial vibro-mixer as agitator. The flow patterns induced by the agitator plates have been studied by a dye-tracer technique and methods of calibrating the vibrator explored as a means of measuring the degree of agitation quantitatively. In part 11 the effects of vibratory agitation on electroplating pure metal and composite deposits are explored and an analysis using mass transport methods is provided.

EXPERIMENTAL

Vibratory stirrer

Vibratory agitation was by means of a commercial vibromixer-motor E1 model Chemap A.G.* – operating at 220V, 0.5-1.0A and 50Hz. It was designed to operate at a constant rate or amplitude for a given power supply and at constant frequency. An armature coil assembly was suspended from a balanced set of heavy coils; application of alternating current caused the coil assembly to be pulled downwards and on reversal the coil sprang back, the shaft describing a sine curve amplitude waveform. A series of discs can be attached to the bottom end of the shaft to act as agitators, various sizes and designs of discs being possible and the use of 316-type stainless steel ensured inertness in typical electroplating solutions. The discs were attached to the shaft with a swivel-screw threaded into the shaft. Both flat and perforated discs were employed to investigate the effect of size and design; the standard supplier's perforated discs had 14 equi-size (3mm) truncated cones which induced a jetflow pumping action especially valuable for fluidizing fine particles.

Amplitude measurement

Vibratory amplitude was measured by several methods. A 'xenon' stroboscope enabled the image of the vibrating shaft to be slowed down or frozen and was calibrated against a rotating shaft motor and provided a check on the frequency of vibration.

By providing a travelling microscope and a graduated graticule lens a marker line on the shaft could be observed and a direct measurement of amplitude made from the maximum and minimum positions.

A further although less accurate check was provided by a 'Chemap Indicator' (Alfa-Laval Ltd) – a self-adhesive strip attached to the shaft coupling – which exhibits two arrows during operation and by observing intersection points the amplitude could be measured to ±0.1mm.

Experimental arrangement

The vibromixer was used to provide agitation in a potentiostatically controlled electroplating cell. Power was provided to the vibromixer by a Zenith Variac and both voltage and current were measured with digital multimeters. The permanent ex-

* Swiss manufacturers tradename, marketed in the UK by Alfa-Laval Co.

perimental arrangement enabled the amplitude and frequency to be measured at any stage of operation (Fig. 1), X-X being the horizontal optical axis.

For electroplating, power was supplied by a Thompson Ministat series E capable of providing ±12A at ±18V, and driven by a conventional potential/time sweep rate. Current was measured by a digital meter and potentiometric chart recorder which provided potential-current polarization curves. A mercury/mercury sulphate (MMS) reference electrode was used throughout.

Solutions used

To study fully the effect of vibration two sets of three variables were used. First,

a. tap water
b. tap water containing iron powder
c. Dow Corning oil

which enabled the solution fluid characteristics to be assessed.

Secondly,

d. perforated disc plates
e. flat disc plates

to enable the vibration characteristics to be assessed. Discs of 45mm diameter were used in a 1 litre beaker for most of the tests, but both 400 ml and 4 litre beakers were used to investigate possible container construction effects. Flow patterns were studied using red-brown dye tracers. The scheme of perforations is shown in Fig. 2.

Electroplating was carried out using a dilute acid copper sulphate solution whose electrochemical characteristics were well-known. For polarization and mass transport studies a dilute copper solution of high acidity was used to ensure that the transport number of Cu^{2+} was almost zero.

$CuSO_4 . 5H_2O$	3.75g
H_2SO_4 (98%)	26.65ml

Deionised water to 1 litre, pH = 0.6

The active areas of anode and cathode were 15cm² and 3cm² respectively and a remote junction MMS reference electrode employed a 1M sodium sulphate salt bridge.

For composite plating a less acid copper solution was preferred to ensure minimal attack on the second phase particles in suspension. It was less acid to avoid oxide particle dissolution and based on:

$CuSO_4 . 5H_2O$	200g
Deionized water to 1 litre	
H_2SO_4	100ml/l to pH = 2
Current density	3-10A/dm²
Deposit thickness	25µm

Soluble copper anodes were used (flat sheet, total area 32cm²) and the cathode flat sheet area was 24cm² for a total electrolyte volume of 500ml in a 1 litre beaker. For composite plating a known quantity of particles was added to the standard copper sulphate solution, typically 10-70g/l. Two materials were used:

a. Silicon carbide, SiC: grit 700 carborundum.
b. Alumina, $\alpha - Al_2O_3$: 3µm Buehler polishing grade.

The SiC particles were particularly useful in this work as they could be seen easily in the scanning electron microscope and the degree of incorporation could be measured visually.

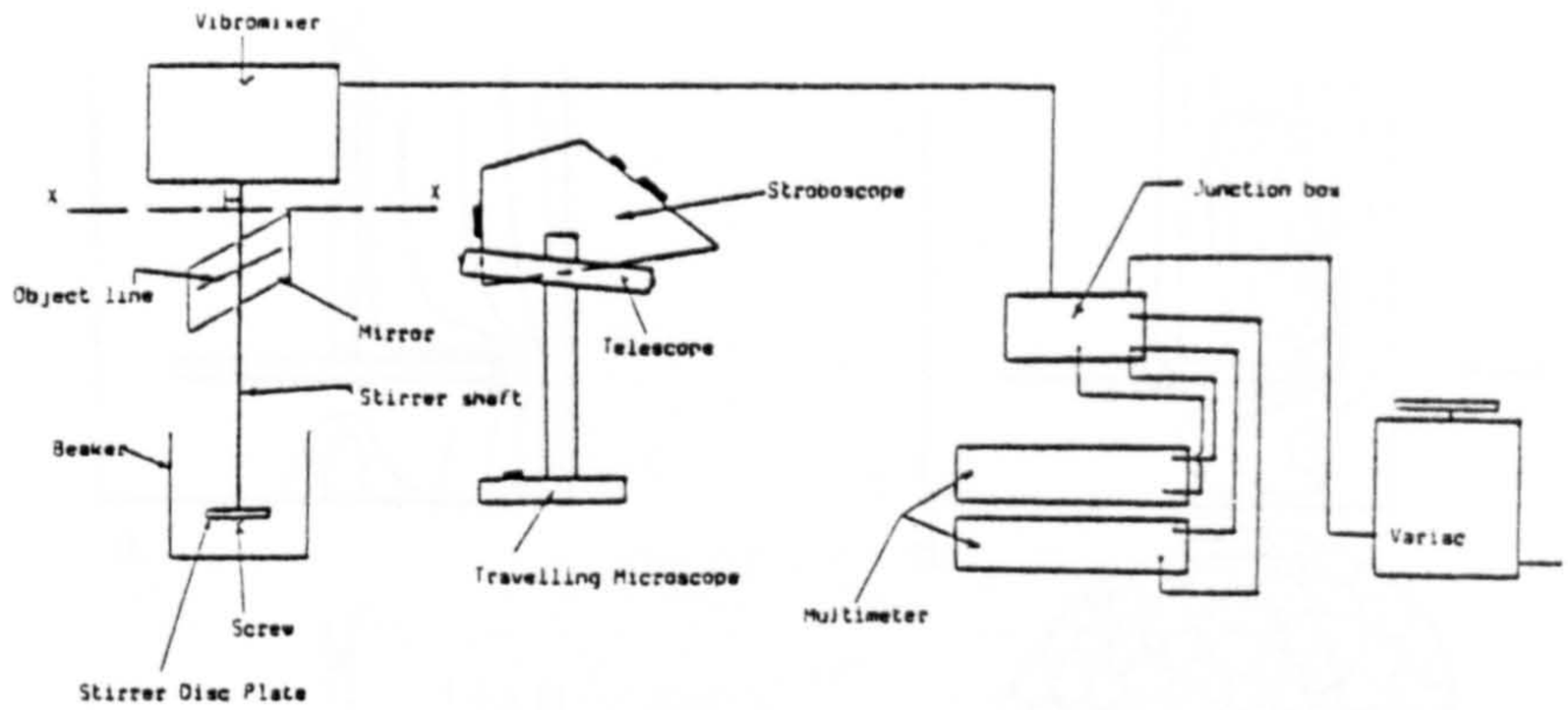

Fig. 1. Schematic arrangement used for measuring amplitude of vibration.

Analysis of electrodeposits

The estimation of the Al_2O_3 content was by means of selective dissolution of the deposit in:

H_2SO_4 (98%)	100ml
H_2O_2 (30%)	100ml
H_2O	to 1 litre
temperature	45-55°C

After dissolution and dilution, copper was removed by electrolysis either on to platinum or into mercury cathodes whereupon the residue was evaporated to dryness in a nickel crucible. The residue was fused with 2g Na_2CO_3 at 850°C for 20 min., dissolved in HCl with KNO_3 added and analysed by atomic absorption spectroscopy.

PATTERNS OF AGITATION

The types of agitation induced by vibratory agitation were studied primarily by injection of red-brown dye and sketches of the flow patterns observed are shown in Figs. 3-5 at two ranges of amplitude or input

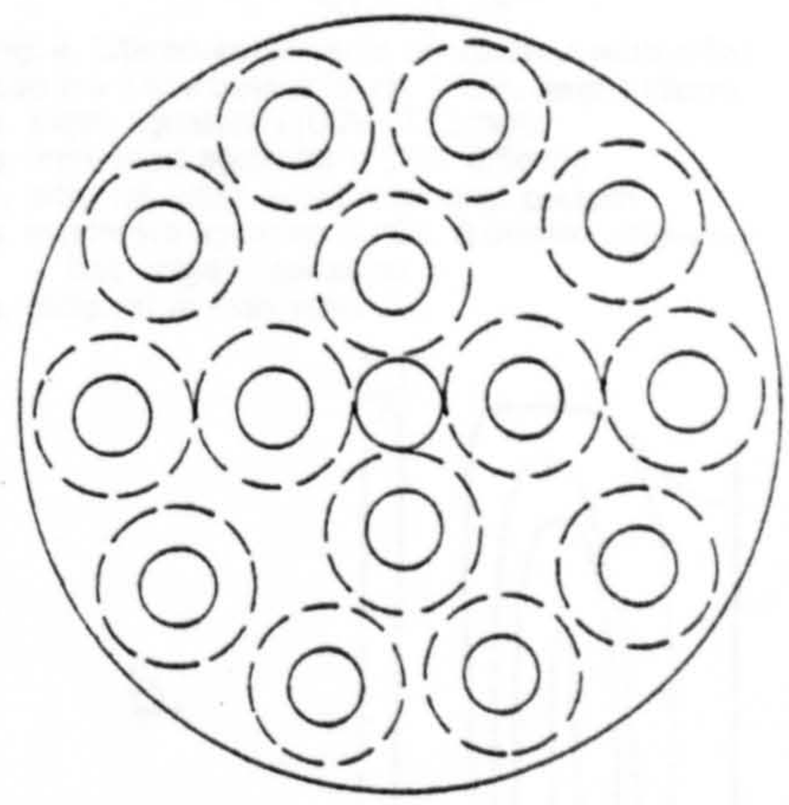

Fig. 2. Plan view of perforated disc.

Disc diameter	45mm
Plate thickness	1mm
Perforation hole diameter	3mm
Hole truncation diameter	9mm
Number of holes	14

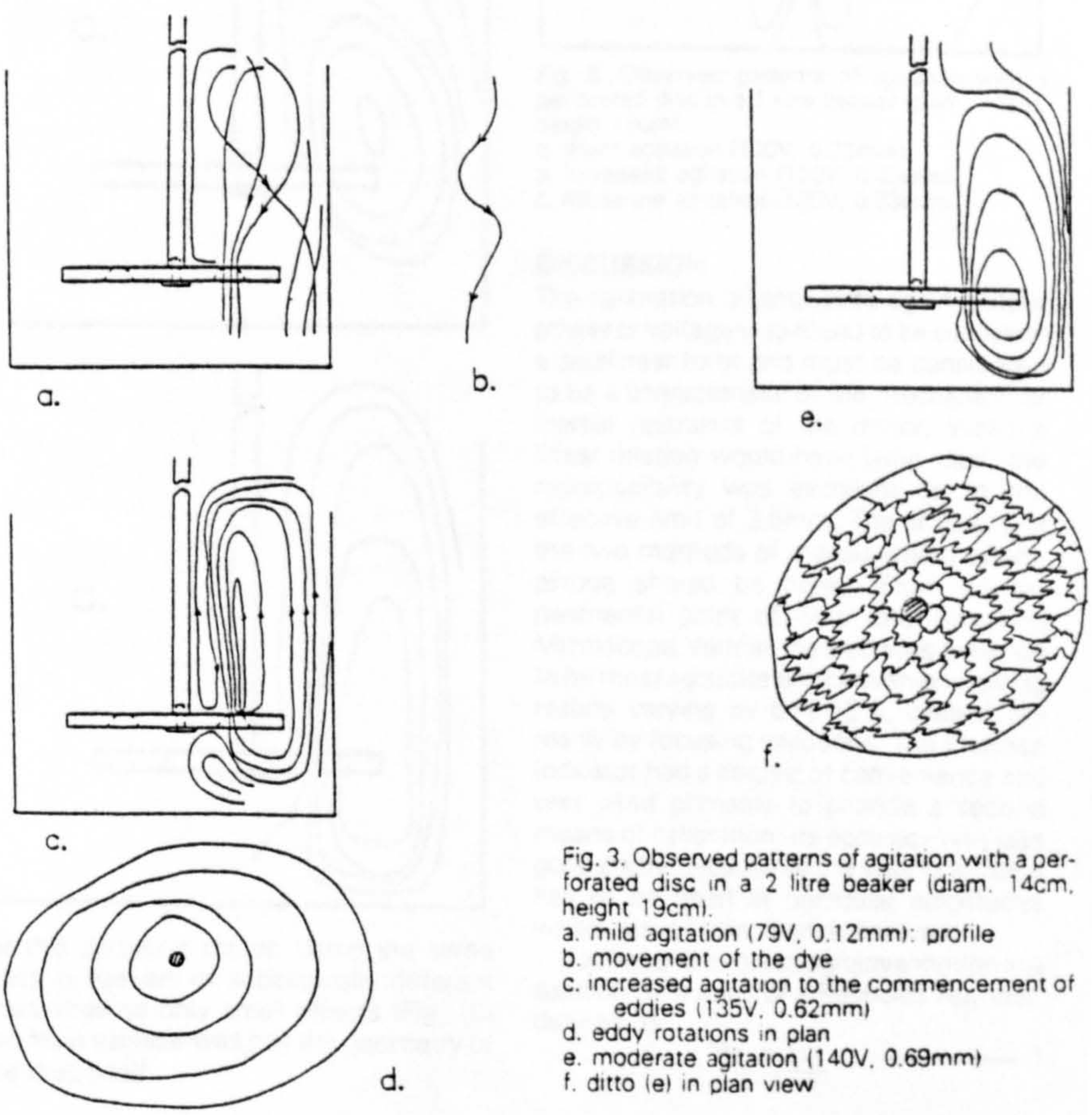

Fig. 3. Observed patterns of agitation with a perforated disc in a 2 litre beaker (diam. 14cm, height 19cm).
a. mild agitation (79V, 0.12mm): profile
b. movement of the dye
c. increased agitation to the commencement of eddies (135V, 0.62mm)
d. eddy rotations in plan
e. moderate agitation (140V, 0.69mm)
f. ditto (e) in plan view

ɔwer. In order to standardise the procedure a 2 litre beaker was used throughout with the stationary disc positioned 6.25cm above the bottom.

Using a perforated disc (Fig. 3) the agitation was observed to be essentially laminar up to 135V (a = 0.62mm) when the commencement of an eddy pattern was noted. With increasing input voltages the pattern was clearly defined as an increased flow velocity, becoming one of equi-sized waves creating rapid vibratory agitation effects.

Although the vibratory shaft showed no rotational motion, solution rotation was apparent once eddying commenced.

Using a flat, non-perforated disc quite a different pattern was observed (Fig. 4). The cause of the difference was that the perforations allowed fluid to pass through and jet upwards but in the absence of holes the fluid hit the disc and was diverted laterally around the disc edge. Up to about 125V (a = 0.5mm) the pattern remained similar but above that value there was a fast peeling or breakaway motion at the edge of the disc, shown in Fig. 4d.

When a smaller beaker (1 litre) was employed the pattern changed only in relation to the voltage employed to induce vibration. Thus in Fig. 5 the eddy patterns occurred at lower voltage values but remained similar in general form. Clearly the container size is an important parameter and may be a factor in governing the mass transport analysis of agitation. Other factors are also of some importance – bath volume size, bath shape, disc diameter and thickness etc. – but none are believed to have a vital influence on the mode of agitation.

CALIBRATION OF VIBRATORY AGITATION

The *experimental* variables used to vary the degree of agitation were input voltage and input power, although input current might be used equally well.[14] The amplitude of vibration was considered to be the main quantitative expression of the degree of vibration and measurement was attempted by several techniques described variously as 'Travelling Microscope/Vernier' and 'Chemap Indicator' methods. Initially measurements were made to study the damping of vibration by different media and to assess the accuracy and precision of each technique of amplitude measurement.

For a given disc size and geometry no significant damping was caused by fluids of differing viscous character, the results of Fig. 6 relating to low degrees of vibration for a perforated disc in three media. Thus the calibration for a given disc is virtually absolute and the vibro-motor can be considered to have substantial power reserve to overcome differences in the solution's physical properties. However, differences in disc geometry cause different but similar responses. Figs. 7 and 8 compare the calibration obtained by two methods and illustrates individual calibration as well as small differences between the two techniques. If power were used as the experimental variable the results were essentially the same (Fig. 9) and no preference for power over voltage could be deduced for this particular motor. Using the same discs in beakers of substantially different sizes showed only small effects (Fig. 10) the main variable was still the geometry of the disc itself.

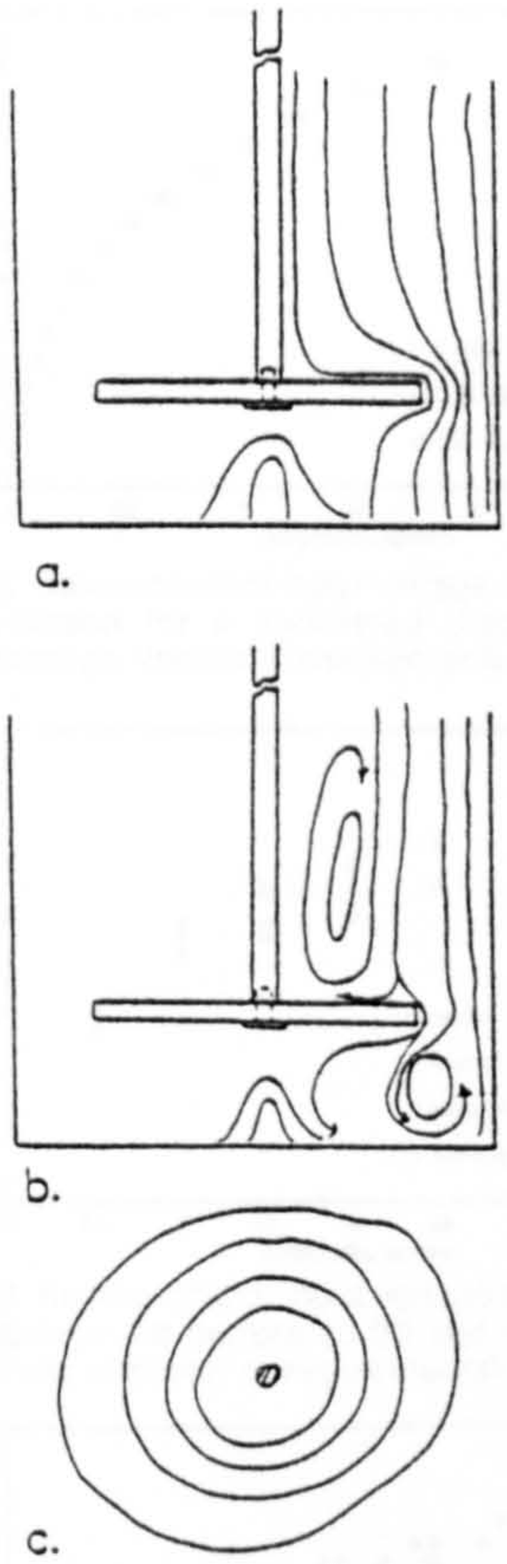

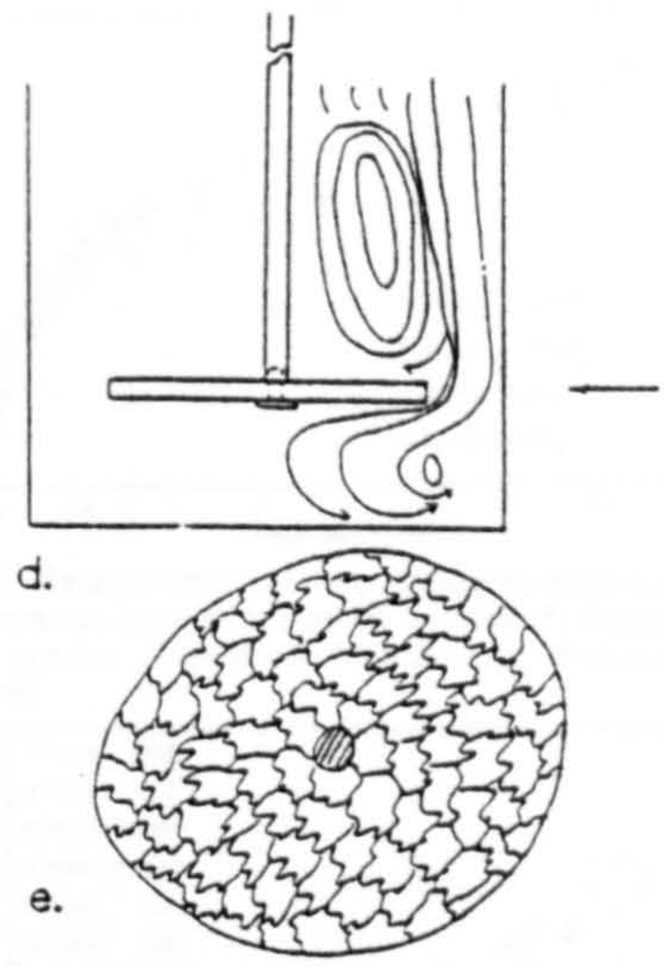

Fig. 4. Observed patterns of agitation with a flat disc in a 2 litre beaker (diam. 14cm, height 19cm).
a. slight agitation (100V, 0.22mm)
b. increased agitation (125V, 0.5mm)
c. ditto (b) eddy wave rotational pattern
d. moderate agitation (140V, 0.86mm) showing fast edge breakaway
e. ditto (d) in plan view

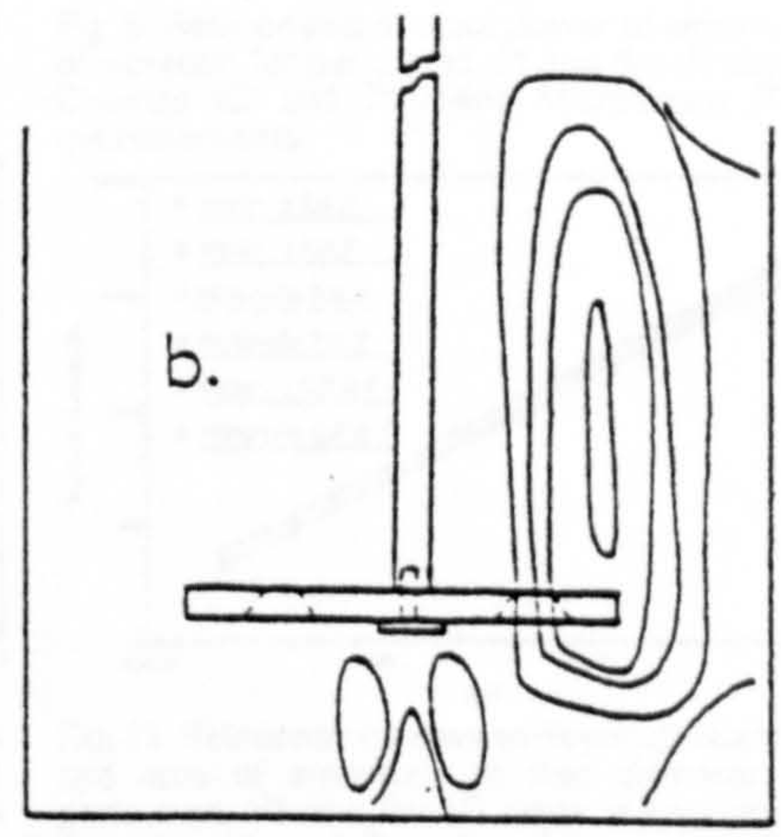

Fig. 5. Observed patterns of agitation with a perforated disc in a 1 litre beaker (diam. 10cm, height 14cm).
a. slight agitation (100V, 0.23mm)
b. increased agitation (120V, 0.43mm)
c. moderate agitation (130V, 0.53mm)

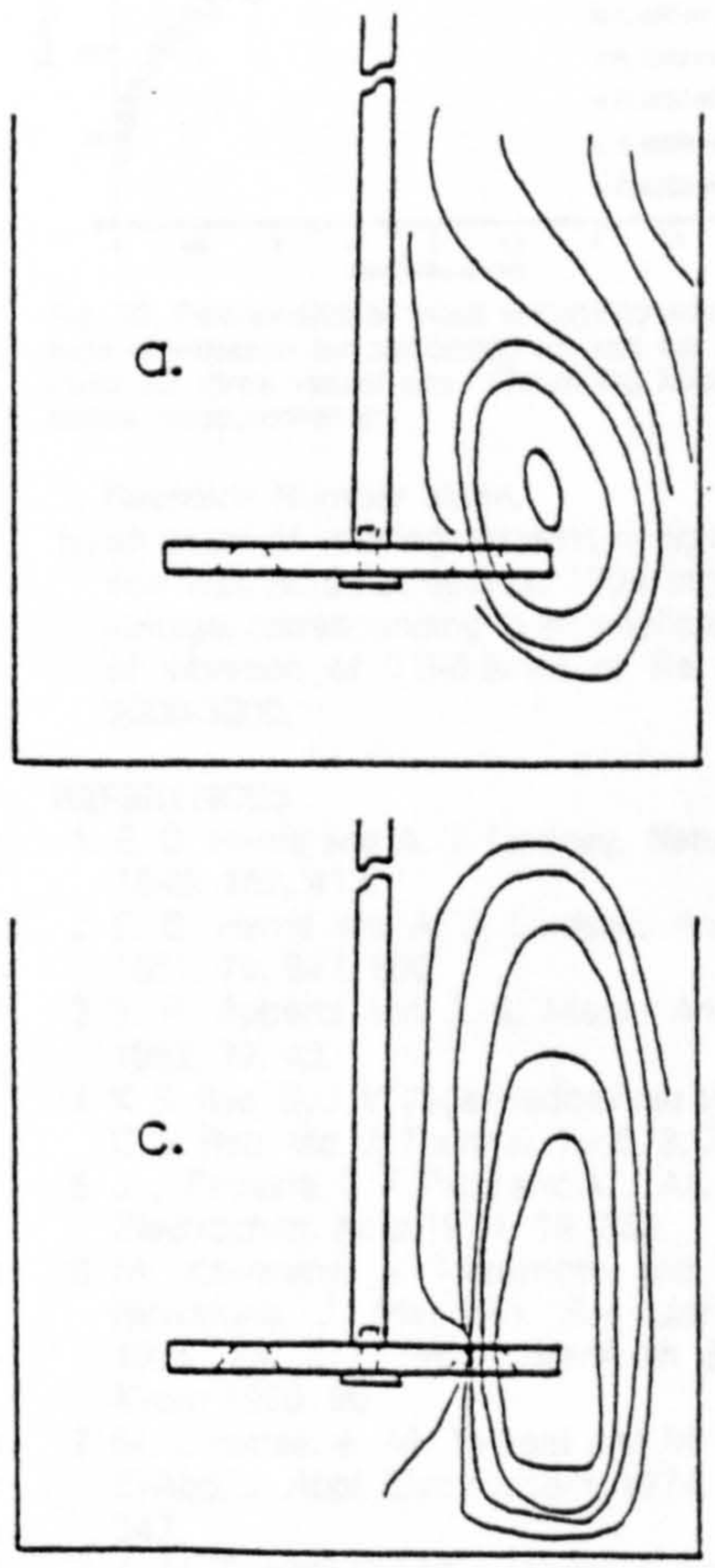

DISCUSSION

The calibration of amplitude against input power or voltage was found to be always of a paralinear form and must be considered to be a characteristic of the mechanical or inertial restraints of the motor. While a linear relation would have been ideal, the reproducibility was excellent up to the effective limit of 3.8mm. The accuracy of the two methods of measurement of amplitude should be noted. From an experimental point of view, the Travelling Microscope Vernier method was believed to be most accurate and convenient, giving results varying by only ±2%, caused primarily by focusing variations. The Chemap Indicator had a degree of convenience and was used primarily to provide a second means of calibration: its accuracy was less good partly because of the way in which it had to be used at particular amplitudes where visual coincidence occurred.

It is usual to express agitative motion in a solution by means of a Reynolds Number, defined as

$$Re = \frac{Ud}{v} \qquad \text{———} \quad 1$$

where U is the relative velocity (cm/s), d the critical diameter (cm) and v the kinematic viscosity (cm^2/s) and the whole being dimensionless. In the case of vibrational agitation the velocity $U = {}^{S}/_{t}$ where S is the distance for which the full frequency cycle applies; thus S = 2a where a is the amplitude. The time $t = {}^{1}/_{f}$ where f is the frequency, in this case 50Hz. The critical dimension for a disc has been assumed to be its diameter. Consequently we may redefine Re for a vibrating disc agitator as:

$$Re = \frac{2afd}{v} = \frac{100ad}{v} \qquad 2$$

Using this definition the experimental results have been replotted firstly for the variable viscosity fluids employed (Fig. 11) and secondly for the various bath sizes used (Fig. 12). The two methods of measurement of amplitude are now indistinguishable and the main difference is that the two solutions differ in viscosity:

Water $v = 1.002 \times 10^{-2}$ cm^2/s

Water + iron particles $v = 0.749 \times 10^{-2}$ cm^2/s

From Fig. 11 it is possible to obtain linear relationships as follows:

Water: $re = 2 \times 10^5 ({}^{a}/_{d})^{0.98}$ ——— 3a

Water + Fe Particles:

$Re = 3 \times 10^5 ({}^{a}/_{d})^{0.98}$ ——— 3b

The differences in behaviour for baths of differing size was noted initially in studies of the flow patterns generated. Purely in flow terms no difference can exist and analysis of the data obtained shows that any damping due to vessel constraint was negligible and the experimental data was absolutely predictable (Fig. 12) as would be expected if the definition of Reynolds number was correct. However this cannot be assumed to imply that the effects of agitation on an electroplating process is unaffected and this factor is consequently considered in detail in part II.

The choice of definition for the Reynolds Number was based on that given by previous authors.[4,6,8] However, other options exist through the critical dimension. No attempt was made here to prove the correctness of this definition but parallel work on the scale-up of vibro-agitation[16] suggested that a more precise definition may be

$$Re_1 = \frac{100\ a\ d_2}{\cap} \left[\frac{d_1 - d_2}{d_2}\right]$$

where d_1 is the diameter of the beaker and d_2 the diameter of the disc agitator. This expression would take account of the fact that when the gap becomes narrow eddy circulation cannot take place. The main argument of this paper is unaffected.

CONCLUSIONS

(i) the amplitude of vibration may be measured satisfactorily by either of the two methods employed;

(ii) Vibrational agitation is reproducible and systematic, and is controllable by the input voltage or power to the vibromotor;

(iii) the Reynolds Number can be defined as Re = 100 ad/v where d is the disc diameter, a its amplitude of vibration at 50Hz frequency and v is the viscosity of the solution;

(iv) perforated and flat discs induce different patterns of agitation, indicated by differing power/amplitude calibrations, but not represented in assessment by Reynolds Number alone.

(v) an onset of eddying patterns of agitation was noted at approx. 130V input voltage, corresponding to an amplitude of vibration of 0.5-0.6mm or Re = 2000-3000.

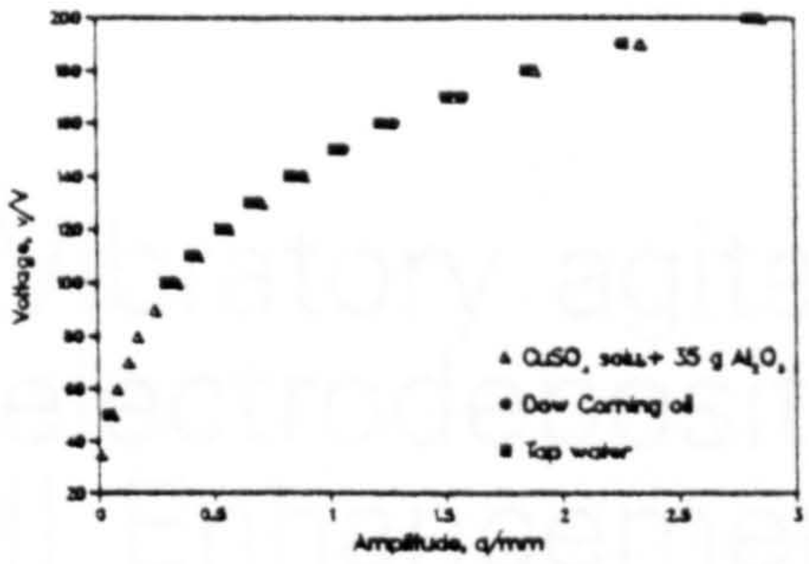

Fig. 6. Relationship of input voltage to amplitude of vibration for a perforated disc (Travelling Microscope Vernier measurement).

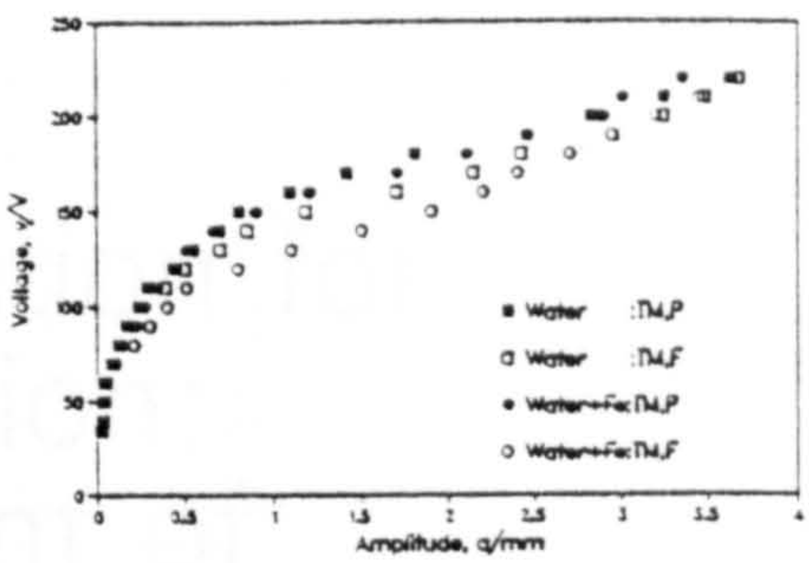

Fig. 7. Relationship of input voltage to amplitude of vibration for perforated (P) and flat (F) discs in two media (Travelling Microscope measurements).

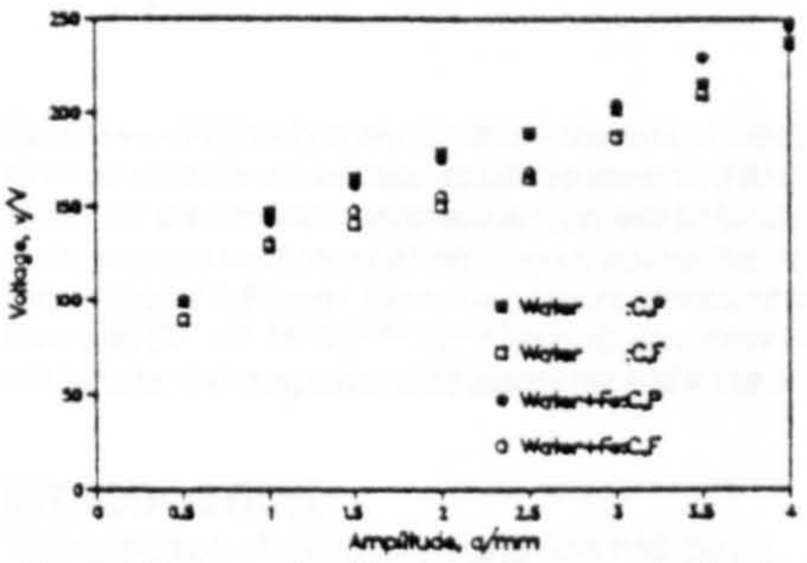

Fig. 8. Relationship of input voltage to amplitude of vibration for perforated (P) and flat (F) discs (Chemap indicator measurements).

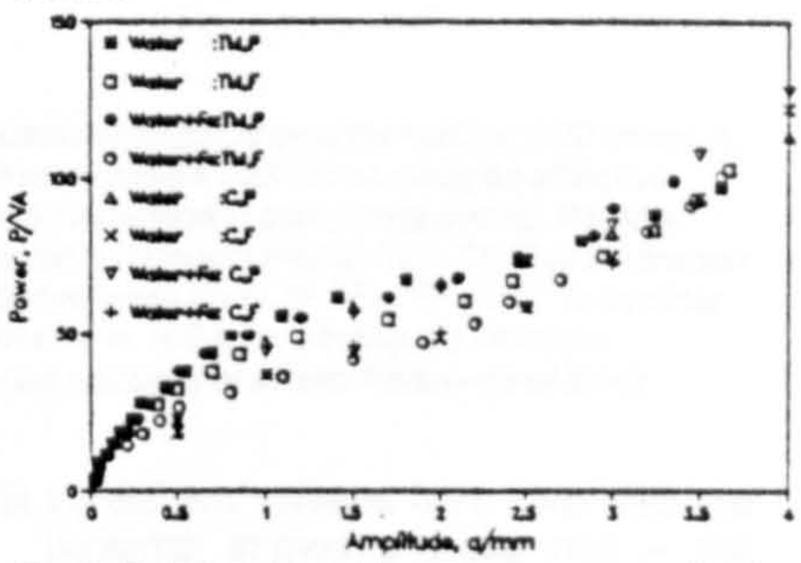

Fig. 9. Relationship of input power to amplitude of vibration for perforated (P) and flat (F) discs: Chemap (C) and Travelling Microscope (TM) measurements.

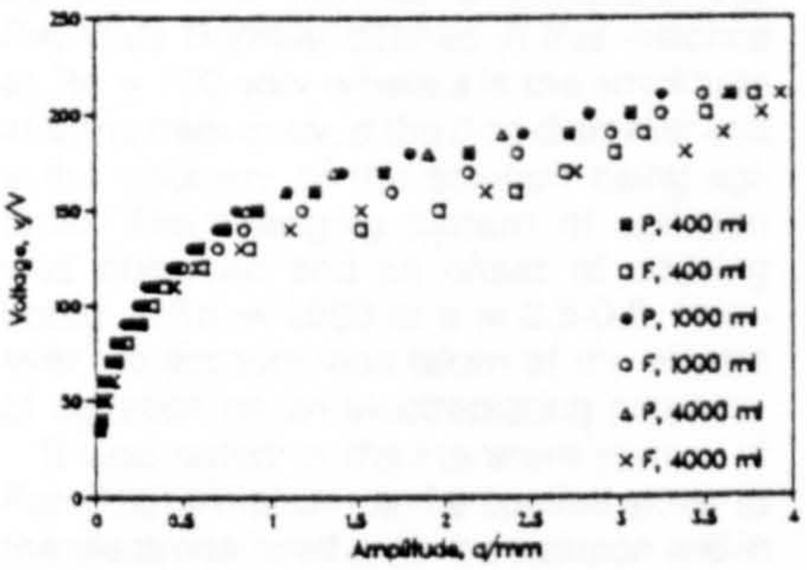

Fig. 10. Relationship of input voltage to amplitude of vibration for perforated (P) and flat (F) discs for three vessel sizes (Travelling Microscope measurements).

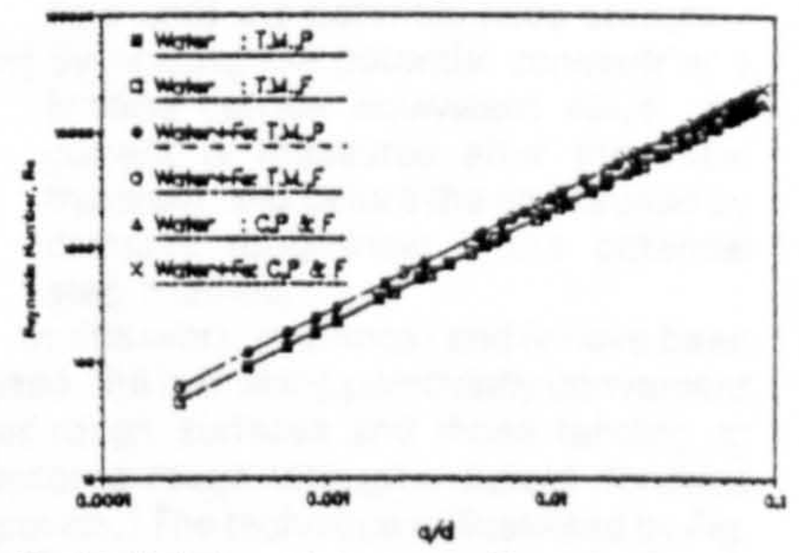

Fig. 11. Relationship between Reynolds Number and ratio of amplitude to disc diameter for perforated (P) and flat (F) discs in two media Chemap (C) and Travelling Microscope (TM) measurements.

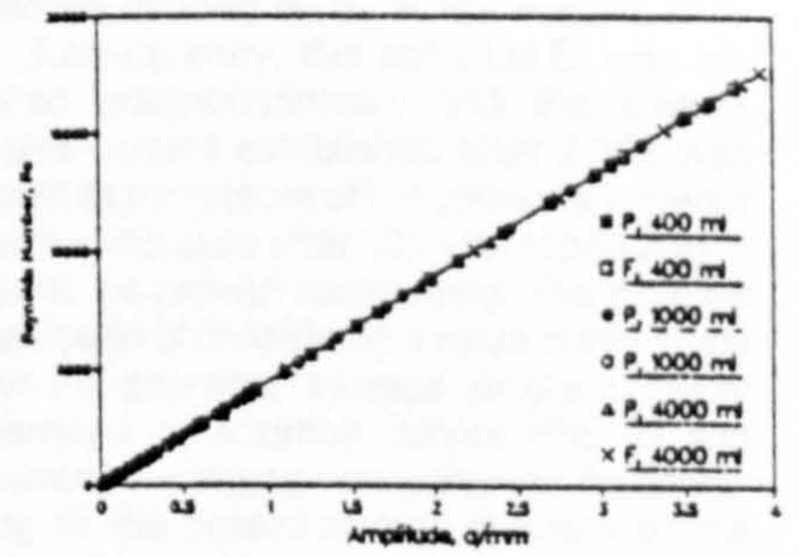

Fig. 12. Relationship between Reynolds Number and amplitude of vibration for perforated (P) and flat (F) discs for three vessel sizes.

REFERENCES

1 E. D. Harris and A. J. Lindsey, *Nature* 1948, **162,** 413.

2 E. D. Harris and A. J. Lindsey, *Anal.* 1951, **76,** 647, 650.

3 E. R. Roberts and J. S. Meek, *Anal.* 1952, **77,** 43.

4 K. S. Rao, G. J. V. Jagannadba Raju and C. V. Rao, *Ind. J. Technol.* 1965, **3,** 38.

5 J. J. Padesta, G. F. Paus and A. J. Arvia, *Electrochim. Acta* 1974, **19,** 583.

6 M. Kawasaki, S. Mizumoto and K. Nawafune, *J. Met. Fin. Soc. Japan* 1974, **25,** 272. *Proc. Interfinish 80, Kyoto* 1980, 90.

7 M. I. Ismail, A. M. Taweel and M. Z. El-Abd, *J. Appl. Electrochem.* 1974, **4,** 347.

8 A. M. Taweel and M. I. Ismail, *J. Appl. Electrochem.* 1976, **6,** 559.

9 M-B Liu, E. M. Rudnick, G. M. Cook and N. P. Yao, *J. Electrochem. Soc.* 1982, **129,** 913, 1955.

10 C. T. Walker and R. Walker, *Electrodep. Surf. Treat.* 1972, **1,** 457.

11 R. Walker and J. F. Clements, *Met. Fin. J.* 1970, **16,** 100.

12 K. Tojo, K. Miyanani and T. Yano, *J. Chem. Soc. Japan* 1975, **8,** 122, 165.

13 S. Mori, M. Yamada, S. Hiraoka, I. Yamada and E. Mizutani, *J. Chem. Eng. Japan* 1984, **10,** 648.

14 C. P. S. Johal, D. R. Gabe and D. R. Eastham. Unpublished work.

15 C. P. S. Johal, Mehrdad R. Kalantary and D. R. Gabe, (part III). *Trans. IMF* 1989.

16 Mehrdad R. Kalantary, S. A. Amadi and D. R. Gabe, *Proc. Conf. Electrochem. Eng.*, Loughborough, 1989.

Vibratory agitation for electrodeposition: II Enhancement of deposition rate

Mehrdad R. Kalantary and D. R. Gabe

Institute of Polymer Technology and Materials Engineering, Loughborough University of Technology, LE11 3TU.

SUMMARY – With vibratory agitation the rate of electrodeposition could be enhanced by 5-20 times. A laminar-turbulent transition could be identified and laminar motion was not considered effective either for electrodeposition enhancement or for particle dispersion in composite plating. Particle incorporation was most effective just above the transition which occurred at Re = 2500 or a vibration amplitude of 0.55mm. Mass transfer correlations obtained were $Sh = 29.7\ Re^{0.037}\ Sc^{0.33}$ in laminar flow and $Sh = 0.16\ Re^{0.82}\ Sc^{0.33}$ in turbulent flow where Re = 100 ad/v, a being the vibratory amplitude, d the agitator disc diameter and v the solution viscosity at a fixed frequency of 50Hz.

INTRODUCTION

The concept of vibratory agitation has been considered in Part I and quantitative measures made, initially as an amplitude of vibration and then as a dimensionless Reynolds Number defined in this instance as Re = 100 ad/v where a is the amplitude at 50Hz frequency, d the disc diameter and v the viscosity of the solution being agitated. The changing pattern of agitation was observed and an onset of eddying noted at Re ≈ 2500 or a = 0.5-0.6. However, no account was taken of the effects of agitation on an electroplating process.

It was noted in the literature review of Part I that vibration can be applied either to the electrode itself or to the solution and in this study only the latter was considered. It was also noted that the relevance of vibratory agitation was primarily to the electrodeposition of composites which will be considered in some detail.

The effectiveness of vibration as a mode of agitation will be considered in terms of the limiting current density whose value is given by

$$i_L = \frac{nFCD}{\delta(1-t)} \qquad (1)$$

where

nF is the Faradaic equivalence
C is the metal ion concentration
D its diffusion coefficient
t its transport number, and
δ the diffusion layer thickness.

The experimental conditions were given in Part I. By using a strongly acid solution $t \rightarrow 0$ and δ is the factor directly affected by the agitation. Having obtained limiting current density values, a mass transport analysis can be made, a systematic description of vibratory agitation provided, and the effectiveness of this type of agitation may be quantified.

DETERMINATION OF LIMITING CURRENTS

Cathodic limiting currents can be determined experimentally, for the purpose of mass transfer analysis, by four methods.[1-4]

(i) By sweeping potential from zero either continuously or in steps – the potentiodynamic method.
(ii) By current sweeps from zero until the potential shows a steep rise – the galvanodynamic method.
(iii) By maintaining the rate of current constant and decreasing the convective flow until the potential rises steeply.
(iv) By holding the potential constant at a limiting current equivalent value, the current is measured after the initial transient, and before the rise caused by cathodic roughening – the potential step method.

In this work, methods i and iv have been used, the last being particularly convenient for rough surfaces and those tending to become rough through incipient dendritic growth.[4] The technique is illustrated by Fig. 1. Preliminary polarization measurements were made on a smooth cathode surface to establish the limiting current value I from which an equivalent 'limiting' potential E can be defined by $E_L = (E_1 + E_2)/2$.

Subsequently, this potential E_L was applied potentiostatically and the steady-state current established after 2-10s was used as a measure of I; it generally shows a gentle increase after 60s, corresponding to dendritic growth roughening. The method has been of considerable value in this study where potential sweeps produce highly serrated polarization curves (Fig. 2) and current averaging was achieved by damping of the potentiometric recorder or the use of an analogue meter.

EXPERIMENTAL

The full experimental details were given in Part I which, combined with the two limiting current techniques, enabled a mass transport study to be made of vibrational agitation. Furthermore, because of its relevance to composite plating a specific investigation was made of copper electrodeposits containing SiC and Al_2O_3 particles.

RESULTS

Mass transport

On selecting specific rates of vibration, measured by the amplitude of vibration, limiting currents were measured on the delineated cathode surface primarily by the potential step method, but also confirmed by potential sweeps. The relationship be-

Mehrdad R. Kalantary and D. R. Gabe
Trans IMF 1989, **67**, 28

veen i_L and amplitude for copper ion eposition is shown in Fig. 3 and a clear ansition in behaviour can be noted at an mplitude of 0.5-1.5 which is better dened by using a logarithmic plot as in Fig. 4 hose validity will be discussed later. It as possible to define the critical amplide as approx 0.6mm.

In the presence of particles suspended in ne solution (3μm α – Al_2O_3 was used for hese experiments) a similar pattern of ehaviour was noted. The transition is pparent on the i_L/a graph (Fig. 5) but is nore clearly defined again on the logarithmic plot (Fig. 6). It should be noted that the particles were apparently fully fluidized below this transition value although at low amplitudes considerable time might be necessary to ensure full and uniform dispersion.

Composite structure

Scanning electron microscopy was employed to study the manner of incorporation of particles and their distribution over a vertical cathode surface held in the fluidized bed for long periods. Particles of SiC were preferred in this work because of the improved contrast obtained in the electron beam. Fig. 7a shows the distribution of SiC in a scanning electron micrograph; the X-ray micrograph shows the particle distribution unequivocally in Fig. 7b. This sample was produced by electrodeposition at 6A/dm^2 for 75 min, at 146V or a = 1.6mm vibratory agitation. Differences in the degree of particle incorporation were small but some evidence of agglomerated particle incorporation may be noted.

DISCUSSION

The origins of vibratory agitation lie in the technology of composite electrodeposition where it is one of several methods which may be used for dispersing particles in an electroplating solution. While it is difficult to state which is the best method vibration has some advantages because of the requirement to disperse the particles and transport them in a dispersed form to the growing cathode surface – thus an increase in vibratory agitation should increase the degree of incorporation. However, excessive agitation reduces incorporation as particles are swept away from the surface before incorporation can take place.

The relative characteristics of the agitative methods have been discussed elsewhere.[5] However, it is clear from this investigation that once the transition or critical amplitude (a = 0.6) is exceeded particle distribution in the bed, and consequently in the composite electrodeposit, is good. Local distribution attributable to particle agglomeration is not so satisfactory but the presence of a small amount of surfactant is helpful in this respect. Studies of the effect of current density show the classical behaviour[5] of increasing current density decreasing the degree of particle incorporation.

Fundamental analysis of the mass transport behaviour is usually based on the use of classical dimensionless correlations of the type:

$$Sh = \text{const.}\, Re^a\, Sc^b \qquad (2)$$

where the Sherwood number, Sh, expresses the rate of deposition as a mass transport coefficient, the Reynolds number, Re, describes the flow behaviour and the Schmidt number, Sc, defines the solution's physical properties. The special definition of Re in a vibratory system was discussed in Part I and Sh is primarily dependent upon i_L (see Table I); thus Fig. 6 is directly convertible to this dimensionless form, as in Fig. 8, using values of parameters obtained previously.[6-8]

$C = 0.015M$

$D = 5.84 \times 10^{-6}$ cm^2/s

$\nu = 1.0184 \times 10^{-2}$ cm^2/s

The data of Fig. 8 disregards Sc as a separate variable of course (one solution of constant D and ν was used throughout) and

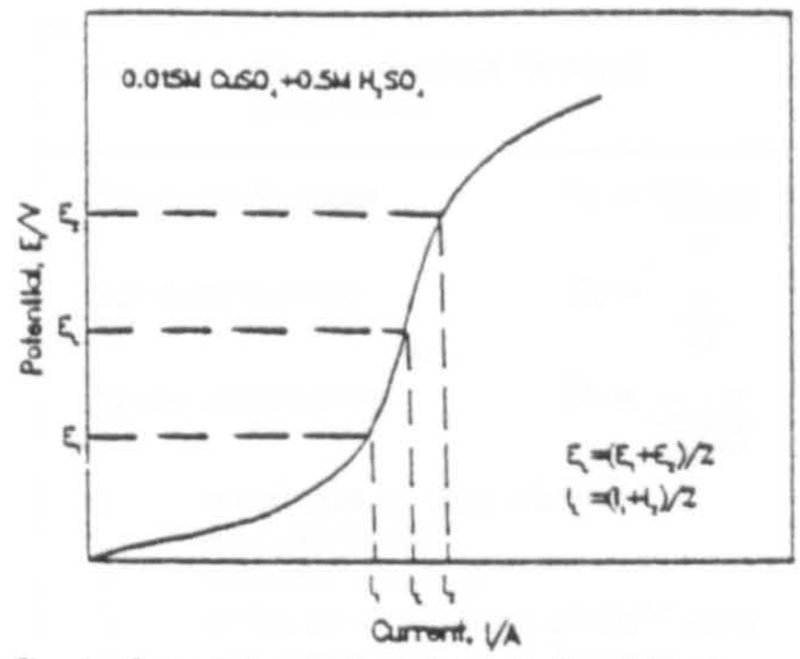

Fig. 1. Schematic polarization defining limiting currents and potentials.

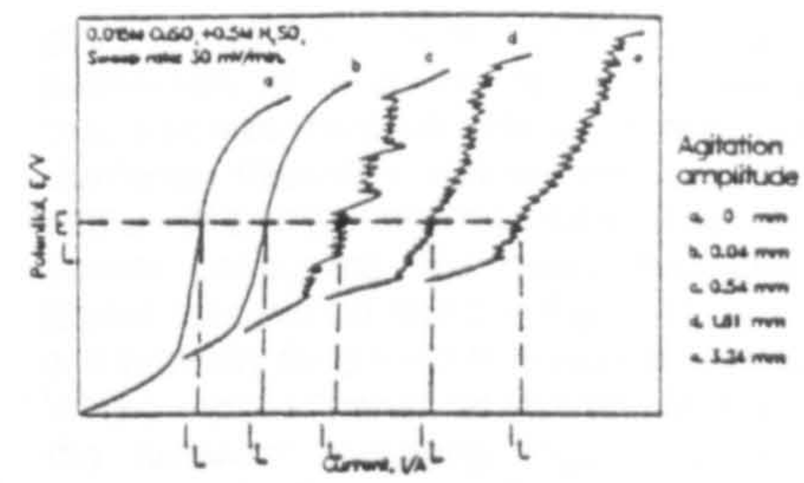

Fig. 2. Polarization curves showing limiting currents values at increasing vibratory agitation rates.

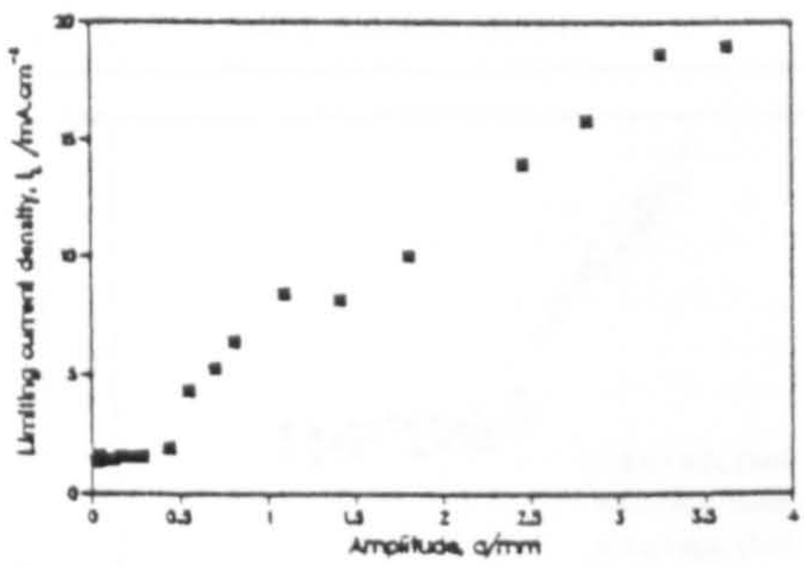

Fig. 3. Relationship between limiting current density and amplitude for a perforated disc (4.5 cm diam.) in acid copper sulphate solution.

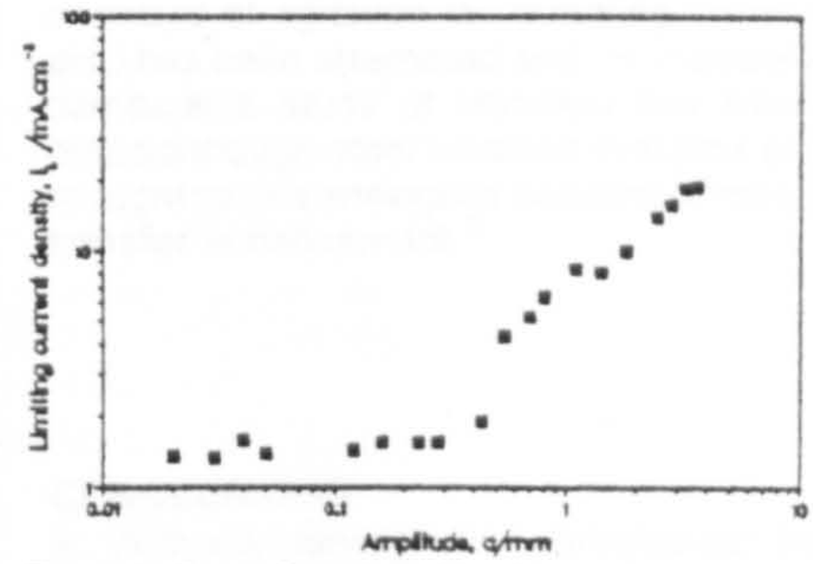

Fig. 4. As figure 3 but logarithmic plot demonstrating the laminar/turbulent transition.

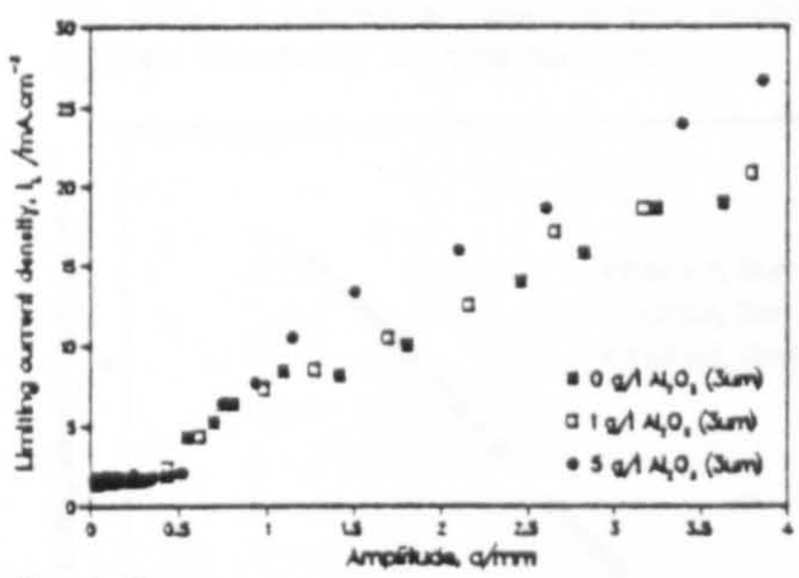

Fig. 5. Relationship between limiting current density and amplitude for perforated disc (4.5 cm diam.) in acid copper sulphate solution containing 3μm alumina particles.

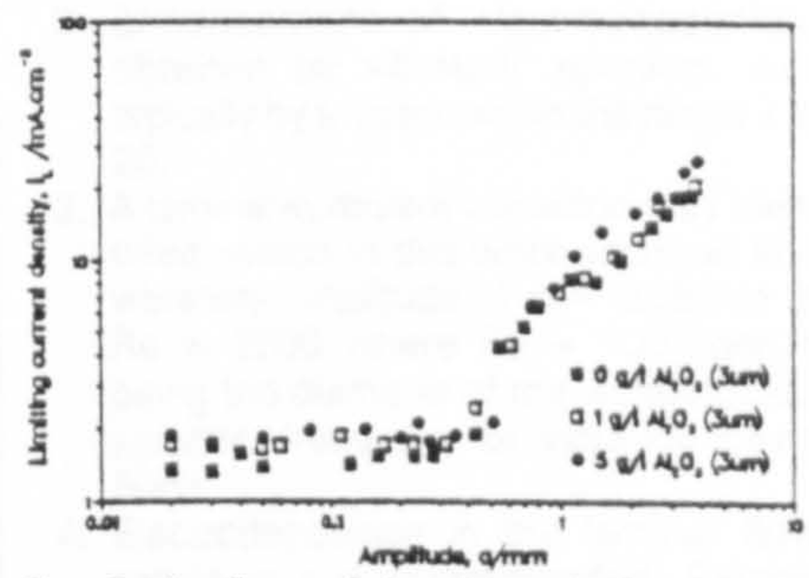

Fig. 6. As figure 5 but logarathmic plot demonstrating the laminar/turbulent transition.

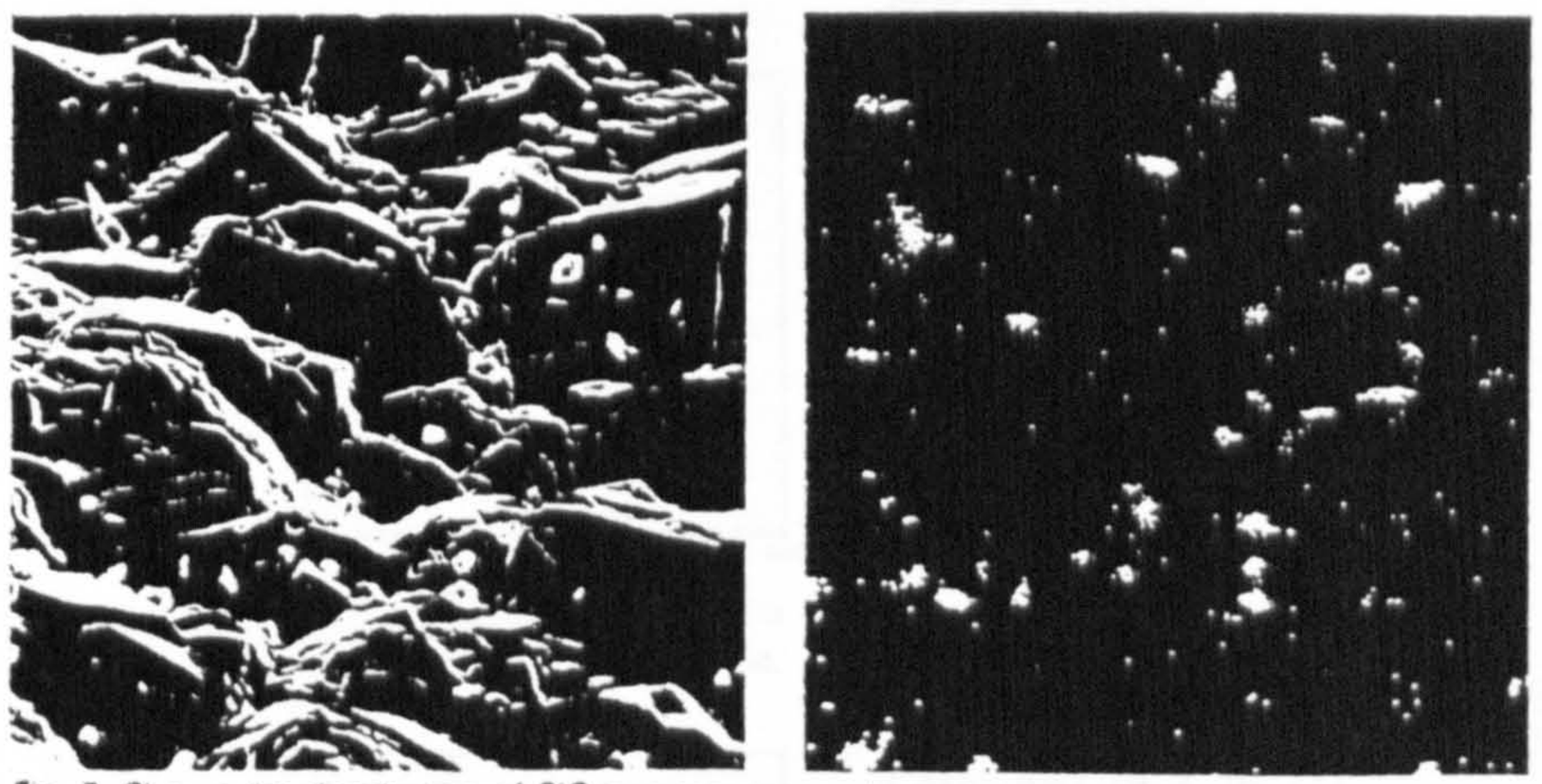

Fig. 7. Shows the distribution of SiC in a composite electrodeposit.
a. electron image b. X-ray micrograph
Plating conditions: 6A/dm^2, 75min., vibratory agitation = 146V or a = 1.6mm, magnification ×600.

so must yield a constant which includes the value for Sc. Thus two equations can be derived:

for $a < 0.45$ or $Re < 2000$,

$$Sh = 375\,Re^{0.037} \quad \text{——— 3a}$$

for $a > 0.55$ or $Re > 2500$,

$$Sh = 1.4\,Re^{0.848} \quad \text{——— 3b}$$

In the laminar flow regime (e.g. 3a) relatively little mass transfer enhancement occurs as $a = 0.02$ and the particles in a composite plating bath are probably not fluidized. In the turbulent regime substantial enhancement occurs and the agitation is highly effective. Close scrutiny of the data suggests that the index value increases as the solution becomes pseudo-viscous due to particle dispersion and with 5 g/l Al_2O_3 particles the 'best fit' value of a is 0.91.

To obtain a value for b, the power index dependence for Schmidt number, a series of solutions was prepared with glycerol added to the standard and copper sulphate solutions, to increase their viscosity, which yielded a range of Sc values from 1779 to 3057. With relatively few results in a narrow range of Sc values the data should be treated with caution (Fig. 10) but yields a relationship of the type:

$$Sh = 0.16\,Re^{0.815}\,Sc^{0.33} \quad \text{——— 4}$$

for $Re > 2500$ in the turbulent flow regime.

In the presence of suspended particles as viscosity agents there is an indication that values of a and b both rise typically to $a = 0.91$, $b = 0.24$ but these do not adequately take account of the dynamic viscosity of the solution containing fluidized alumina particles. While several studies of vibratory agitation can be found in the literature, for geometrical reasons there is no directly comparable study to this work and certainly not for particle incorporation.

From the pattern of vibratory agitation observed it may be deduced that the two regions thus described are laminar and turbulent in character although clearly of a special geometric pattern arising from the geometry of the perforated disc employed as the agitator. It is furthermore clear that for practical purposes the laminar region provides inadequate particle dispersion. The maximum rate of incorporation can be associated with the onset of turbulence at $a = 0.55$ or $Re = 2500$ and this observation has been developed elsewhere.[5]

The effectiveness of vibratory agitation in single metal electrodeposition can be defined in several ways. For this particular work the limiting current density can be converted to a diffusion layer thickness and the data reported all conforms to a single relationship (Fig. 9), which follows from eq. 1. If an agitation enhancement factor is defined as the ratio of limiting current density obtained with agitation to that obtained in still solutions, values are compared in Table 2.

Some further implications need to be clarified and will be reported later. For example, the scale-up consequences for industrial use need to be considered and the damping effects of plating electrolytes defined. Thus for a large tank more numerous and larger disc vibrators are required and the position of work being electroplated in relation to the vibrator needs to be specified (variation in position probably gave rise to the scatter in Fig. 10). From preliminary work on this aspect it seems that disc size must be defined in terms of diameter, thickness and weight, and the pattern of perforations may be critical. The power consumed has been measured (some data will be found in Fig. 9 of Part I) and typically for a full 1 litre vessel was 40 VA a.c. input at transition and 80-100 VA in the turbulent operating regime. Experiments with the same vibrator in bigger vessels required little increase in power. Comparison of flat and perforated discs would be interesting – flat discs consume less power to obtain the same amplitude of vibration. No comparison with other methods of agitation (air bubbling, jetting etc.) has been attempted and no precisely comparable study of vibration has been noted although other vibrating systems are thought to give analogous patterns of mass transfer enhancement.[2]

Table 1. Dimensionless Groups Employed.

Reynolds Number	$Re = \frac{100\,ad}{v}$
Schmidt Number	$Sc = \frac{v}{D}$
Sherwood Number	$Sh = \frac{i_L \cdot d}{zFCD}$

a amplitude of disc vibration
d disc diameter
v solution viscosity
D diffusion coefficient of Cu^{2+} ions
C concentrations of Cu^{2+} ions
z electron change in deposition
F Faraday constant
i_L limiting current density

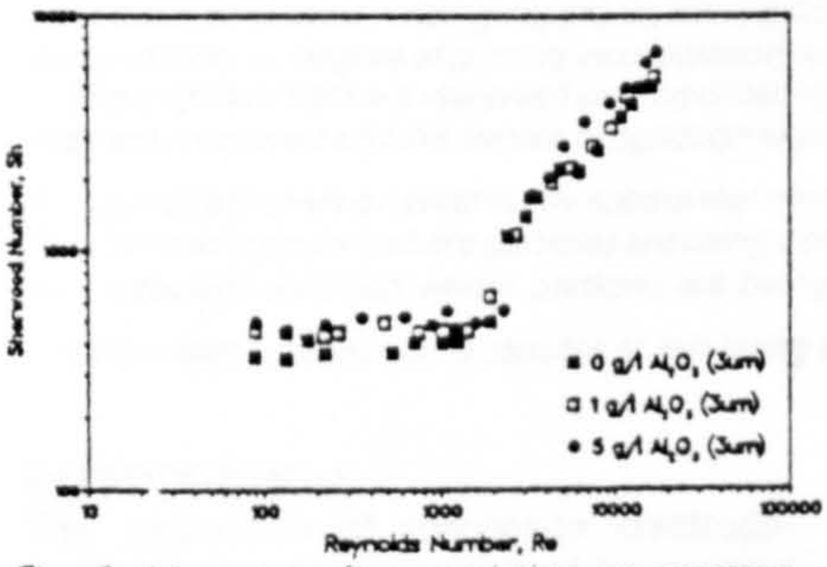

Fig. 8. Mass transfer correlation at constant Schmidt number (Sc = 1779) for vibratory agitation using a perforated disc in acid copper sulphate containing alumina particles.

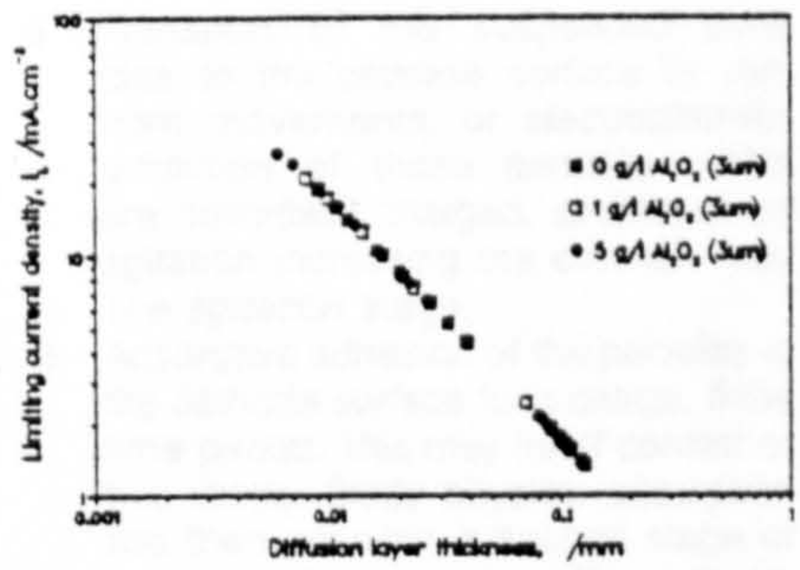

Fig. 9. Relationship between limiting current density and diffusion layer thickness in vibratory agitation electroplating.

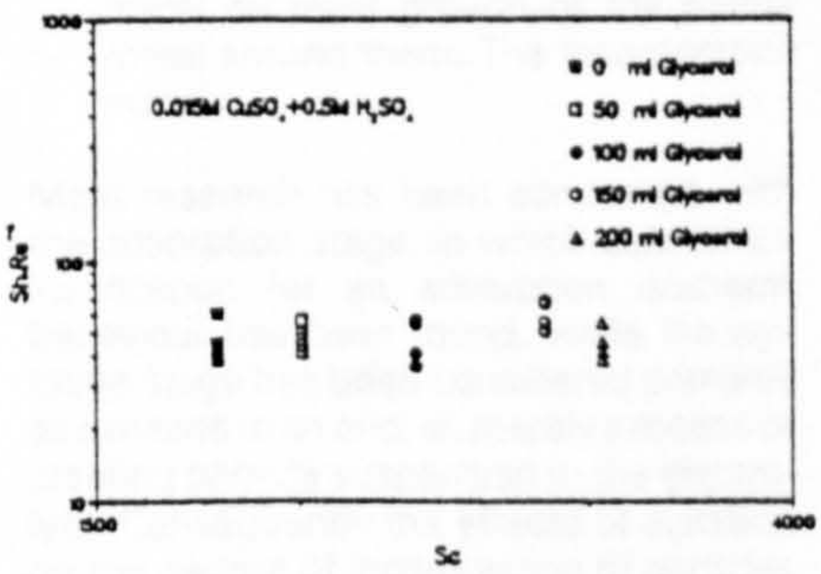

Fig. 10. Mass transfer correlation of $Sh\,Re^{-a}$ with Sc to establish dependence upon Sc, assuming $a = 0.84$.

Table 2. Enhanced Electrodeposition by Agitation.

Mode of agitation	*Enhancement factor*
Still solution	1
Natural convection	1–2
Cathode reciprocation	2–4
Air bubbling	2–4
Turbulent flow	5–50
Vibratory agitation	3–20
Ultrasound	2–10

CONCLUSIONS

1. With vibratory agitation particles can be co-deposited in an electrodeposit in a uniform manner although the absence of shear mixing action may allow particle agglomeration.
2. Enhancement of electrodeposition, obtained by vibratory agitation, was typically by a factor within the range 3 to 20.
3. A laminar-turbulent transition was identified, which in this work occurred at a vibratory amplitude of $a = 0.55$mm or $Re = 2500$ where $Re = 100\,ad/v$, d being the diameter of the vibrating disc agitator, frequency of vibration being 50Hz.
4. Electrodeposition in the laminar flow region is not recommended. Particle dispersion for composite plating is effective only in the turbulent region, maximum incorporation taking place near the transition.
5. In the laminar flow regime mass transport obeys the relationship

$$Sh = 29.7\,Re^{0.037}\,Sc^{0.33}$$

for $Re < 2000$

In the turbulent flow regime mass transport obeys the relationship

$$Sh = 0.16\,Re^{0.82}\,Sc^{0.33}$$

for the ranges $2500 \leqslant Re \leqslant 20{,}000$ and $1800 \leqslant Sc \leqslant 3200$

REFERENCES

1 A. A. Wragg, *The Chem. Eng.* 1977, 39.
2 J. S. Selman and C. W. Tobias, *Adv. Chem. Eng.* 1978, **10**, 211.
3 U. Landau, *A.I.Ch.E. Symp.* **77** (1981) 75.
4 D. R. Gabe and P. A. Makanjuola, *I. Chem.E. Symp.* **98**, (1986) 309.
5 C. P. S. Johal, Mehrdad Kalantary and D. R. Gabe, (Part III) *Trans. IMF* 1989.
6 D. J. Robinson and D. R. Gabe, *Trans. IMF*, 1970, **48**, 35; 1971, **49**, 17.
7 D. R. Gabe and F. C. Walsh, *J. Appl. Electrochem.* 1984, **14**, 555, 565.
8 D. R. Gabe and P. A. Makanjuola, *J. Appl. Electrochem.* 1987, **17**, 370.

Vibratory agitation for electrodeposition: III electrodeposition of composites

C. P. S. Johal, Mehrdad R. Kalantary and D. R. Gabe.
Institute of Polymer Technology and Materials Engineering, Loughborough University of Technology

SUMMARY – In the electrodeposition of composite coatings a variety of methods of agitation have been employed yielding apparently contradictory trends especially in relation to composite composition, ie. degree of particle incorporation within the matrix electrodeposit.

The origins of data are reviewed and the differing behaviours reconciled in terms of the agitation method employed and the degree of agitation expressed qualitatively in three stages.

i) particle dispersion prior to any substantial co-deposition being possible,
ii) laminar agitation where particles are being delivered to the cathode surface and,
iii) turbulent agitation where particles are being swept away.

Only vibratory agitation is capable of exhibiting all three stages for practical exploitation purposes.

Mehrdad R. Kalantary is a research student at Loughborough University where he completed his MSc degree in Materials Protection in 1986. He was formerly at Buckinghamshire College of Higher Education and Brunel University and his research interests are in electroplating with novel pulsing and agitation.

Dr David R. Gabe leads a research group at Loughborough University of Technology with a special interest in high speed electrodeposition. This paper forms part of the programme concerned with novel methods of agitation.

C. P. S. Johal, Mehrdad R. Kalantary and D. R. Gabe
Trans IMF 1989, **67,** 31

INTRODUCTION

The production of composite electrodeposits by the co-deposition of suspended particles during electrodeposition of the matrix metal from solution is widely believed to take place in three stages.

i) Transport of the suspended particles to the cathode surface by random movements, or electrophoretic attraction of those particles which are colloidally charged, promoted by agitation increasing the collision rate. The *agitation* stage.
ii) Adsorptive adhesion of the particles to the cathode surface for a critical, finite time period: this may itself consist of two steps, firstly physical adsorption and then possibly, a second stage of stronger chemisorption. The *adsorption* stage.
iii) Entrapment of the particles within the metal by rapid growth of the matrix metal around them. The *incorporation* stage.

Most research has been concerned with the adsorption stage, in which substantial justification for an adsorption isotherm behaviour has been found, while the agitation stage has been considered primarily as a means to an end, ie. merely a means of creating particle suspension in the electrolyte. Consequently the effects of agitation on the degree of incorporation of particles in composite plating has long been a matter of some uncertainty, partly because of a lack of good systematic data, and partly because what data exists has been obtained by widely differing experimental methods. The broad general effect was recognized many years ago by Williams and Martin[1], in an early study of electroplated fibres, who stated:

> "the degree of agitation was held between the limits set by a too violent agitation which swept the fibres off the cathode surface before they could be keyed into the deposit and by a too gentle agitation which failed to keep the fibres in suspension".

Since then only two papers have been specifically devoted to the effect of agitation[2,3] and those were for rather special cases.

Contradiction arises because agitation is used primarily to maintain particles in suspension within the solution and at least six separate methods can be identified in the literature (see Table 1). Agitation may also be used to vary rates of co-deposition although the two effects may be overlapping or interactive. Thus one study by Masuko et al[2] uses a magnetic stirrer to induce particle suspension and dispersion and then superimposes a rotating cylinder cathode to investigate the effects of rotational agitation: the rotating cylinder is a well-established turbulent flow promoter. Consequently laminar flow agitation is never available for study! Each of those agitative methods will be characterised in turn, except that simple sedimentation on to horizontal cathodes will be disregarded as a method of promoting composite deposition.

CHARACTERISTICS OF AGITATION

Plate pumping, in which a hinged baffle at the bottom of the plating tank is reciprocated by a motor-driven cam, together with solution pumping and air bubble agitation, represent eminently practical methods of agitation for industrial operation but do not lend themselves to systematic study nor reproducible control. Indeed, misleading conclusions can be drawn, as illustrated by graphical data derived from earlier work[4] (Figure 1) which suggests that at low current densities fast agitation gives greater particle incorporation while at higher current densities slower agitation does so. Without characterizing the agitation any conclusion will very deceptive when drawn from such data.

Vibratory agitation has found increasing favour as particles are maintained in suspension without swirling and gross turbulence, although the nature of the vibration transmitter is important[5-7]. For this type of application a cell-bottom plate is

Table 1. Methods of agitation in composite electroplating

Agitation Method	*References*
Plate Pumper	Kedward et al Celis and Roos 1977
Solution Pumping	Kariapper and Foster
Vibrational agitation	Celis and Roos 1978 White and Foster 1978 Johal et al Kalantary et al
Rotating disc electrode	Roos, Celis et al Kyoto Review
Rotating cylinder electrode	Bazzard and Boden Masuko and Mushiake
Magnetic rotary stirring	Sadowska-Mazur et al Johal et al
Rotary barreling	Foster et al 1965

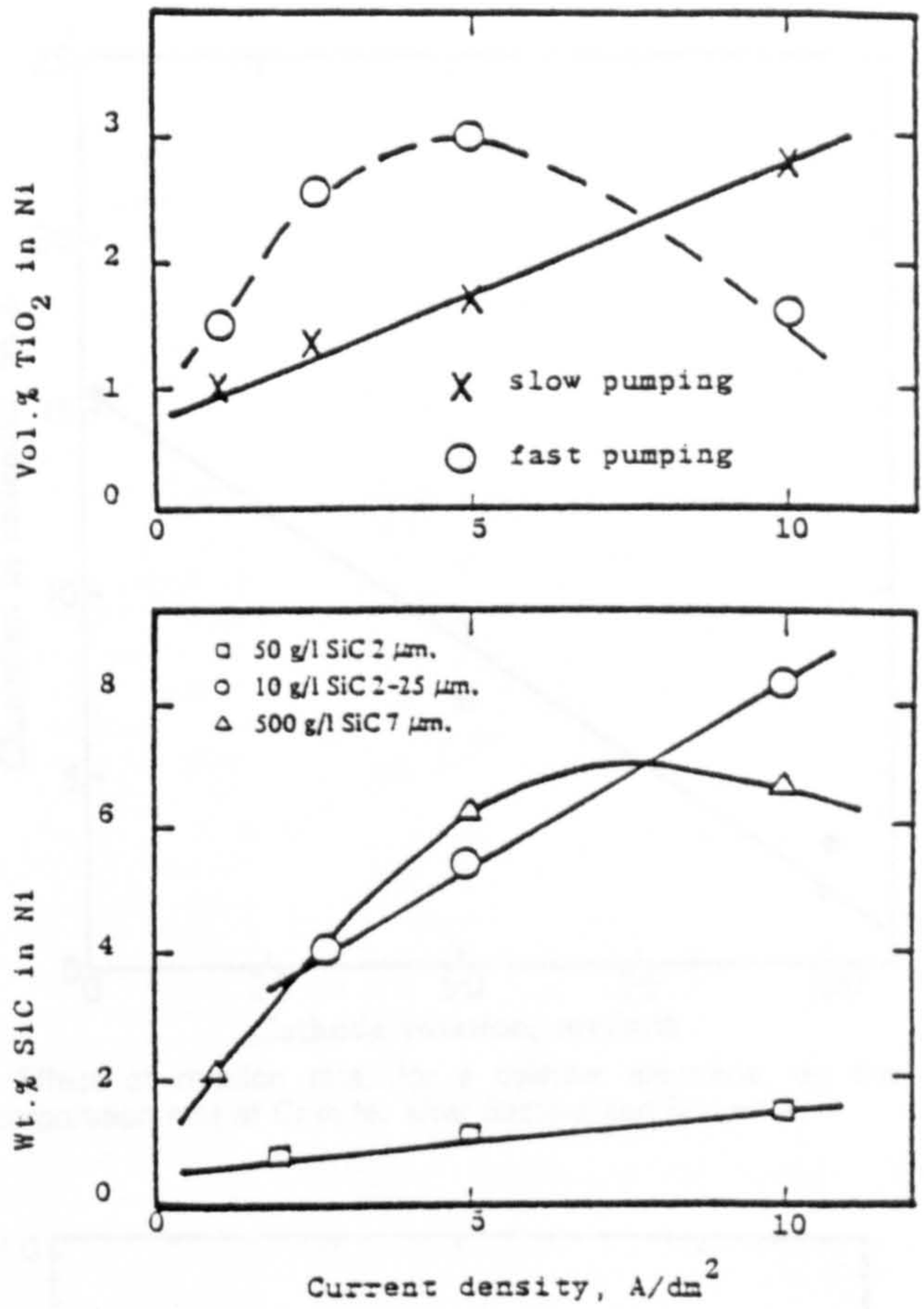

1. Effect of current density on degree of particle incorporation in composite electrodeposit from nickel sulphamate solution. TiO_2 in Ni after Kariapper and Foster[4]. SiC in Ni after Celis and Roos[9].

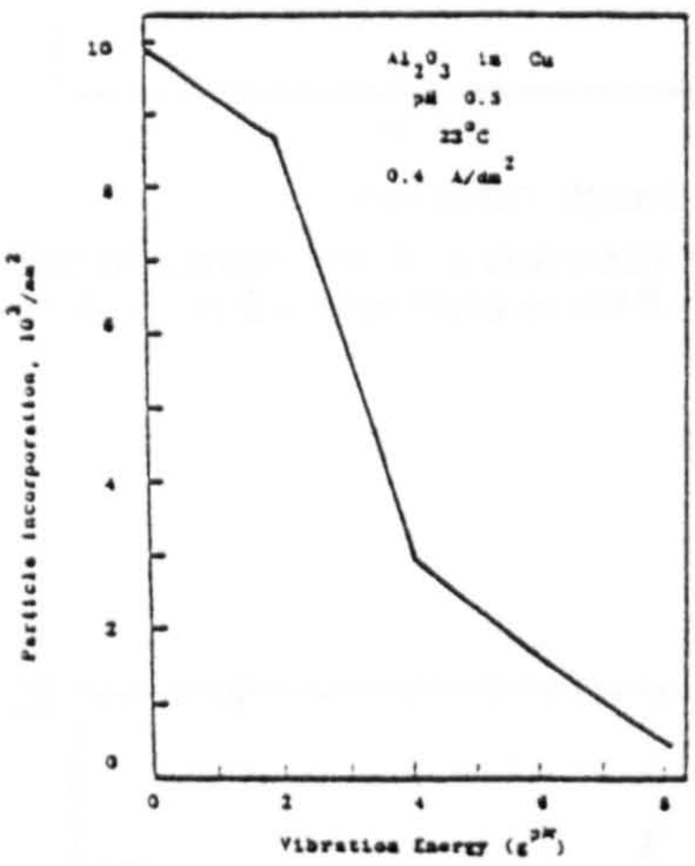

2. Effect of vibratory agitation on the absorbed incorporation of Al_2O_3 in Cu, after White and Foster[3].

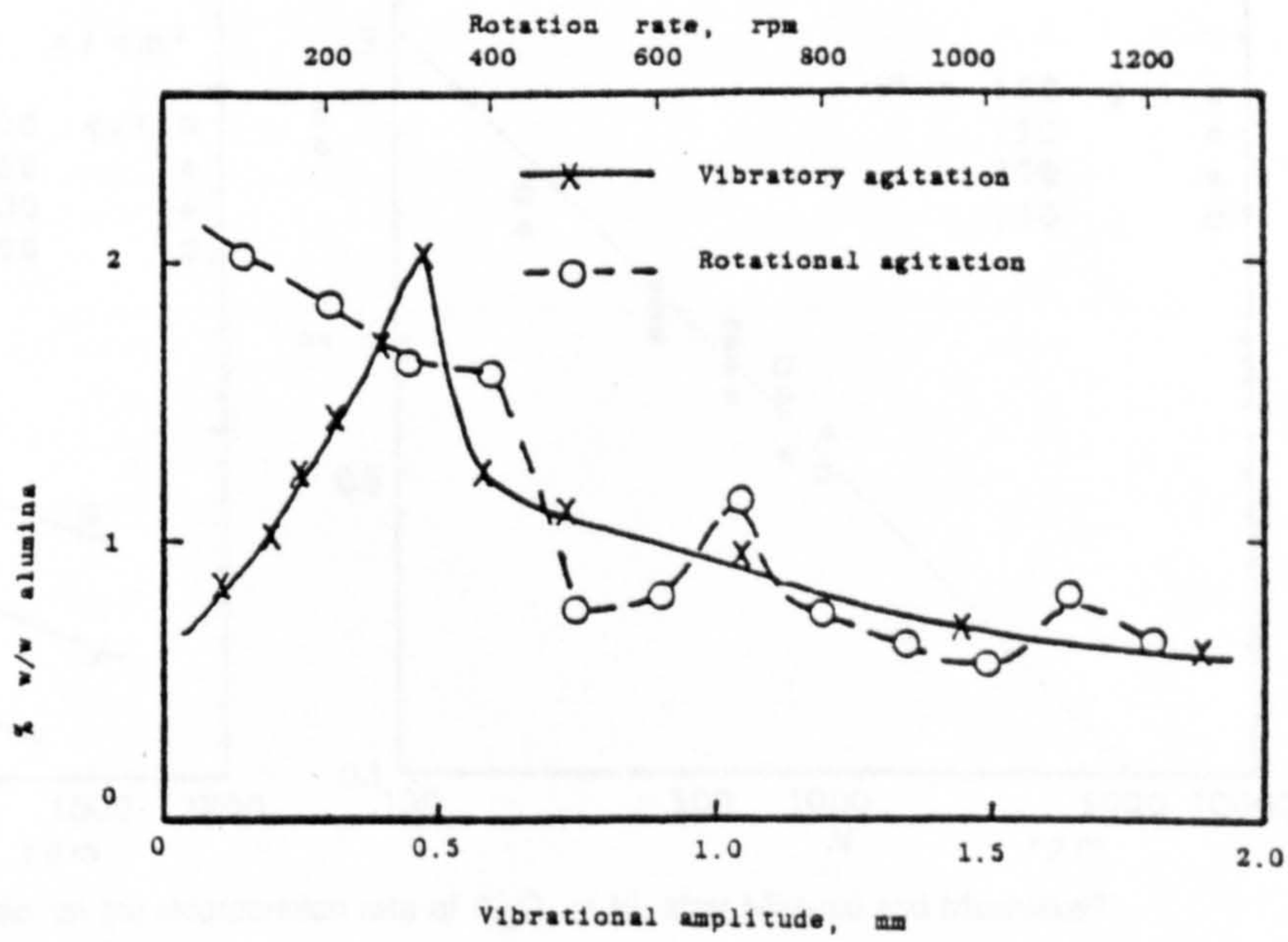

3. Effect of agitation rate on the degree of particle incorporation for Al_2O_3 in Pb, after Johal et al[6].
a) Vibratory agitation;
b) Magnetically stirred rotational agitation.

usually employed at frequencies between 20 and 50 Hz, but perforations and edge roughness can cause localized eddying. While White and Foster[3] have reported that particle incorporation decreases with the vibrational energy employed (Figure 2) more recent work[5] suggests that at very low energy or amplitude an increase occurs reaching a maximum after which it falls to approach zero at high vibrational agitation (Figure 3). Such results clearly require reconciliation.

The rotating disc system was employed by Roos, Celis et al[8,9] specifically to examine the laminar/turbulent transition for which it is peculiarly well-suited. The results obtained (Figure 4) suggest that under laminar flow conditions a constant level of particles is incorporated while in the turbulent regime a decreasing level of incorporation occurs; during the transition, flow – instability occurs, which is accompanied in this instance by an increase in incorporation. These authors suggest that agglomeration occurs in the non-laminar regions although no direct evidence is offered; rather the contrary is intuitively supposed, i.e. that agglomeration exists in the low laminar region where inadequate shear-dispersion of the sedimented particle phase is more likely.

The rotating cylinder electrode system is used primarily for turbulent flow processing but this was not apparently uppermost in the minds of the researchers who have exploited it. Both studies (Figures 5, 6) show similarity as far as a comparison is possible: Bazzard and Boden[10] (Figure 5), with a few results, show a strong reduction of co-deposition of chromium particles in nickel as cathode rotation is increased, while Masuko and Mushiake[2] (Figure 6) demonstrate a constant incorporation level at very low rotation rates (particles dispersed separately by a magnetic stirrer) decreasing with increasing rotation rate, a logarithmic relationship being possibly coincidental.

Magnetic rotary stirrers are a convenient way of stirring but lead inevitably to swirling effects[11-13]. Johal et al[6] in particular have shown that the agitative effect is quite different from that of vibration (Figure 3), and have generally discarded it as a useful technique for systematic study. Equally, barreling is an essential and successful technique for coating small components but it would, not be apt for systematic studies of agitation.

In practical terms, pumping[4], and plate

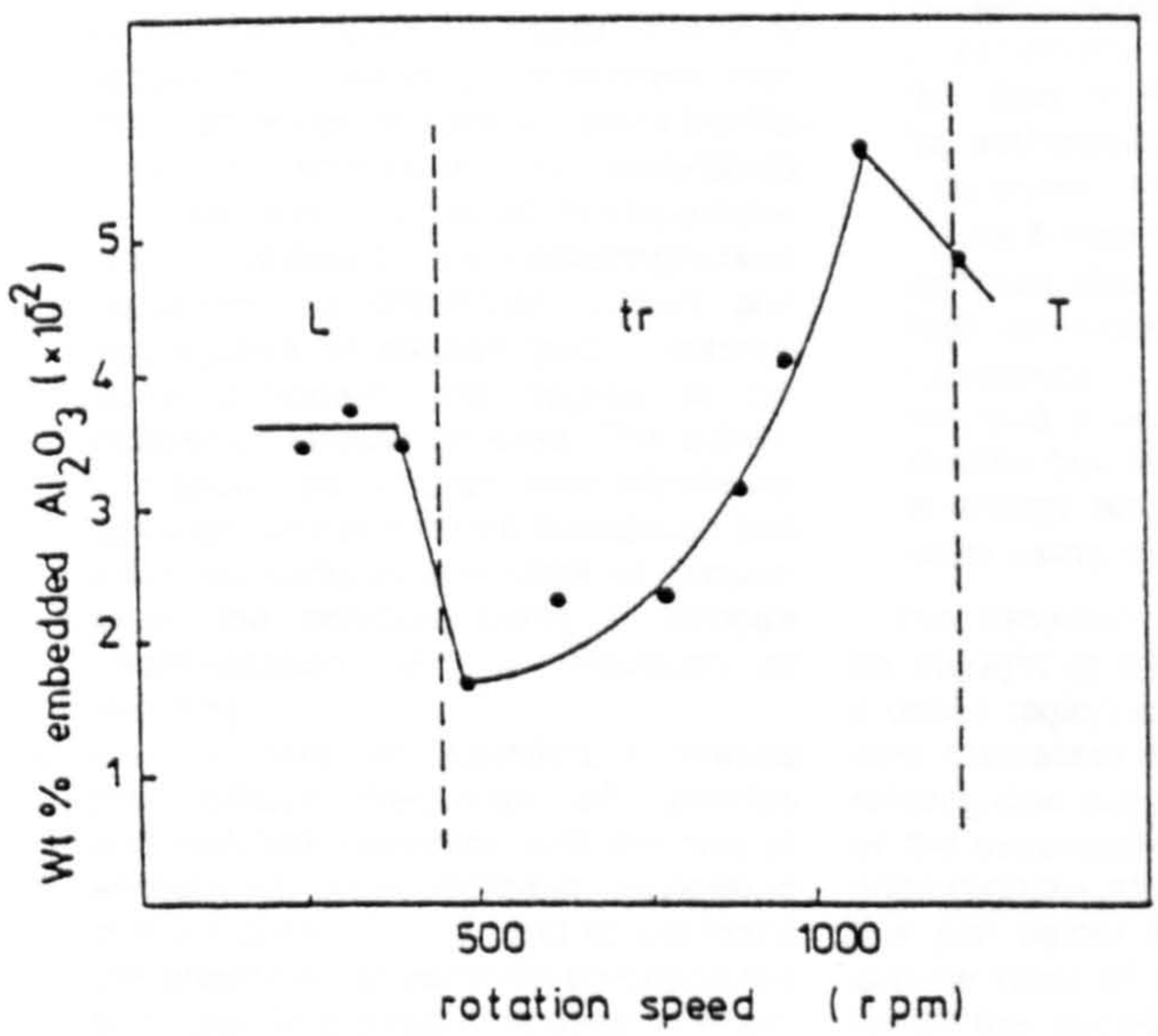

4. Effect of rotation rate, for a disc electrode, on the incorporation rate of Al_2O_3 in Cu, after Roos et al[8,9].

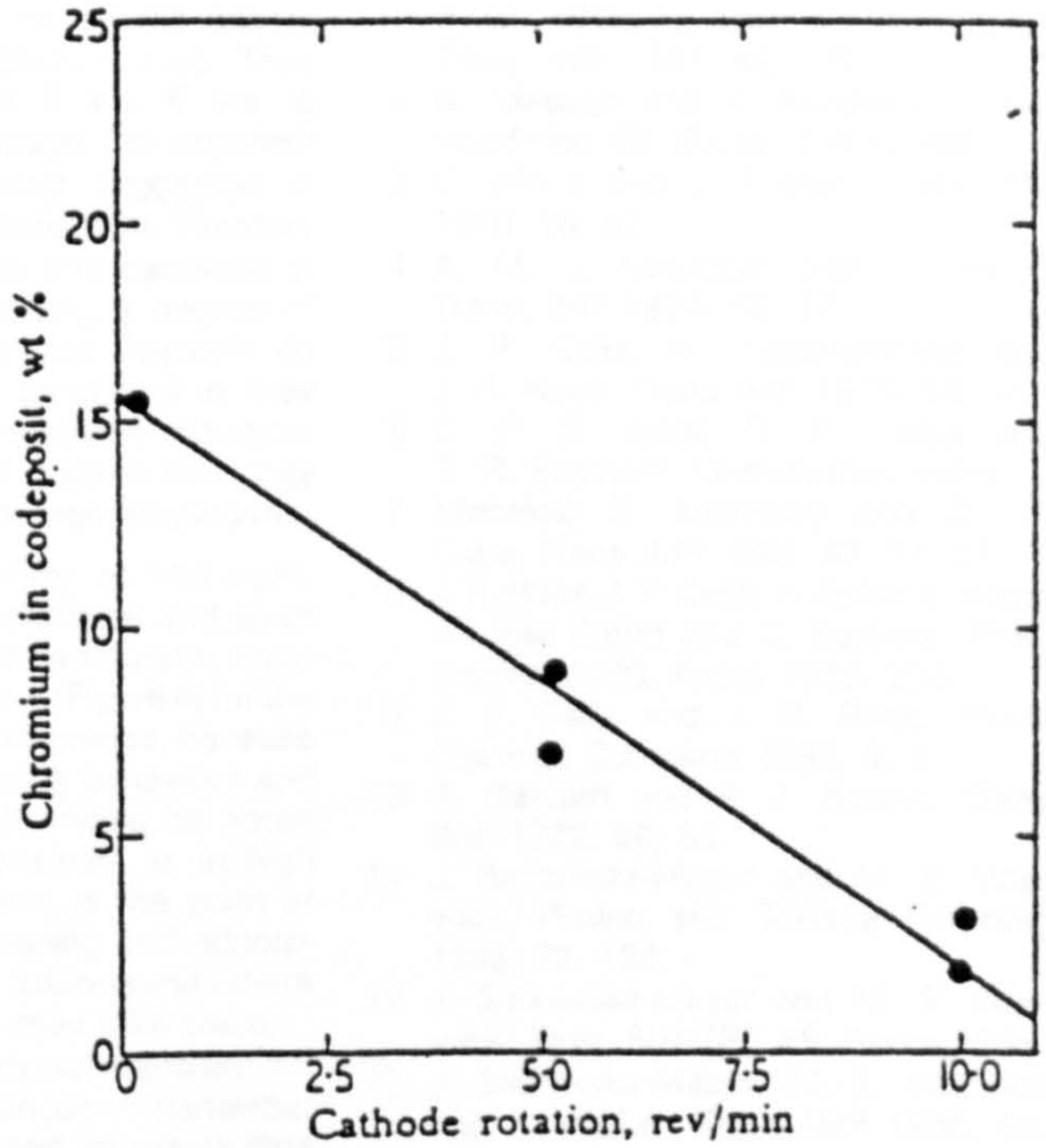

5. Effect of rotation rate, for a cylinder electrode, on the incorporation rate of Cr in Ni, after Bazzard and Boden[10].

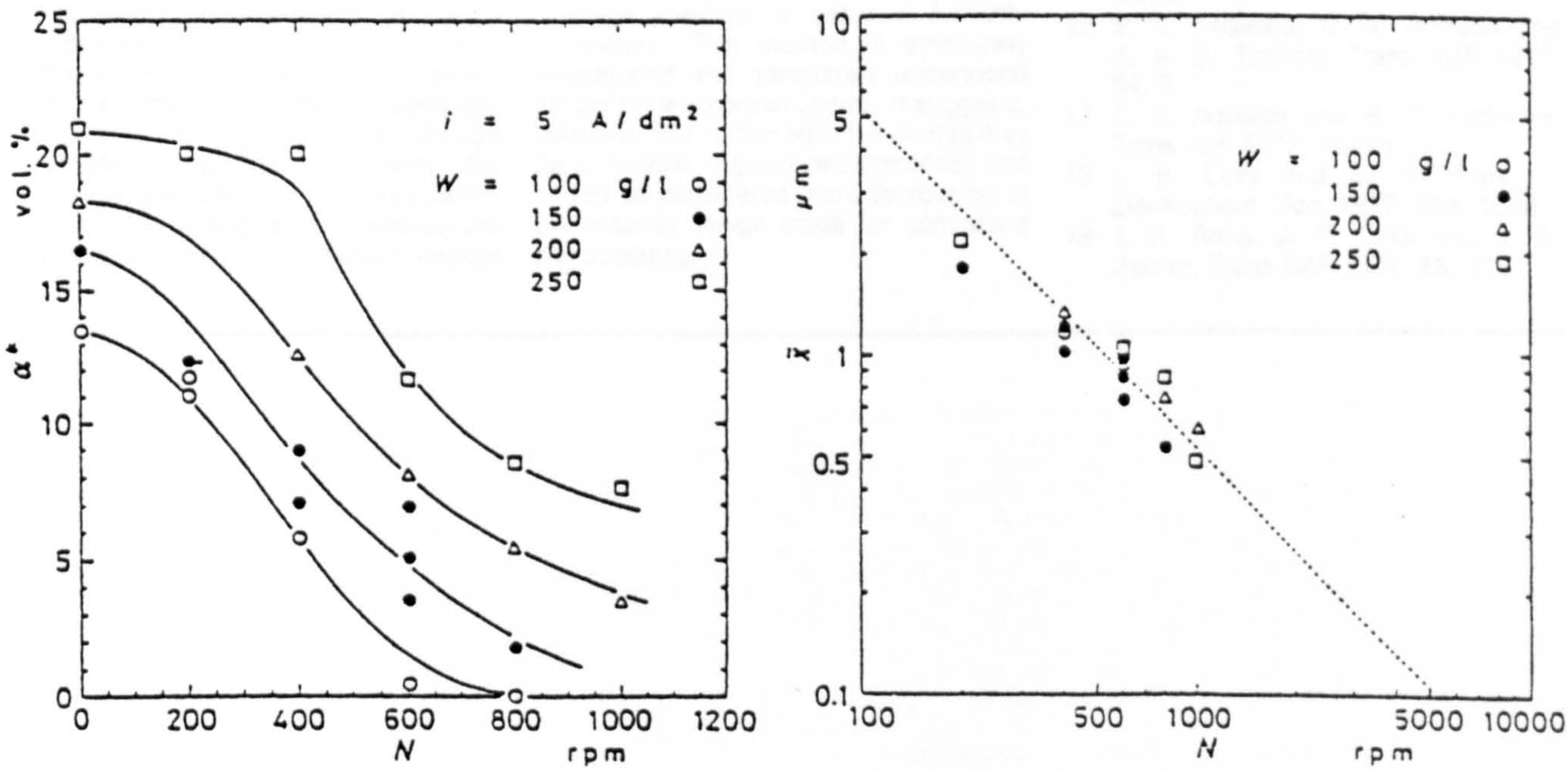

6. Effect of rotation rate, for a cylinder electrode, on the incorporation rate of Al_2O_3 in Ni, after Masuko and Mushiake[2].

pumping[15-19], have been found to be eminently convenient methods although apparently not susceptible to substantial rationalization judged from the published data.

DISCUSSION

From the foregoing review of available data it can be seen that no one technique has become a widely accepted as a means of agitation in composite electroplating, and consequently the results appear to be in substantial disarray. In this context we may neglect the sedimentation technique which may be assumed to give broadly similar results, although in practice the use of periodic disturbance must be a factor which causes variability. In practice it is little used.

The mechanism of co-deposition is widely agreed to take place in three stages of which the first is agitation dominated. Thus agitation must have two effects on co-deposition. Firstly, it ensures that particles are delivered to the growing cathode surface from suspension in solution – thus an increase in agitation rate would be expected to increase the collision frequency of particles with the cathode surface. Secondly, it may also sweep away particles which are not rapidly incorporated in the growing cathode or are unable to remain adsorbed on the surface in the presence of excessive agitative shear stresses – thus collision contact time might be involved as the second criterion. A corollary of this must be that increasing current densities should increase the rate of incorporation of particles in the electrodeposit. However, the prerequisite condition is that the particles are well dispersed in solution, a condition usually achieved by agitation. Existing theory has disregarded the mode of agitation, the relative effects of agitation energy and adsorption energy and any relationship with the current density. It is therefore proposed that the agitation stage of composite electroplating be considered in three sub-stages whose relative significance depends upon the mode of

agitation.

1. A particle dispersion stage is a prerequisite to cathodic entrapment normally achieved by agitation alone but for which surfactants or ionic adsorbants may be helpful provided co-deposition is not inhibited through electrophoretic repulsion. As dispersion occurs and aggregative or packed bed characteristics disappear, the degree of co-deposition should increase. This behaviour should be apparent with vibrational agitation, low pump rate fluidization and plate pumping at low rates of disturbance, the principle being to oppose sedimentation with a minimum of 'swirling'.
2. As the rate of agitation increases the collision frequency of particles and cathode increases and the rate of entrapment must increase. Increasing current densities will tend to decrease the proportion of particles co-deposited and could in principle be used to maintain a constant degree of incorporation. This sub-stage corresponds to laminar flow conditions.
3. As the agitation rate increases further, particle sweeping and surface desorption must also increase, resulting in, at first, no further increase in particle incorporation, and then a fall in the degree of incorporation, until at very high swirling or turbulent conditions co-deposition could fall, almost to zero. This sub-stage is clearly characteristic of the turbulent methods of agitation, especially air agitation and cathode rotation at high rates. However, the rotating disk and the rotating cylinder should be distinguished, because the former exhibits a clear laminar/turbulent transition, while the latter is virtually always turbulent in its effects except at extremely low rotation rates. Thus the data of Figures 5 and 6 are to be anticipated, although the apparent logarithmic relationship suggested in Figure 6 may be coincidental. Vibratory agitation also causes this decrease at high amplitudes implying a degree of turbulence – White and Foster[3] do not give a vibration amplitude in their studies but the considerable vibrational energy employed implies that they were using relatively high amplitudes.

The transition itself may, at first sight, be thought to be an additional and even a useful region in which to operate; however, the data of Roos et al (Figure 4) for the rotating disc suggests otherwise, because of the essentially unstable behaviour and unpredictable effects. It should be noted that just below the transition, ie. at high *laminar* rates of agitation, is the point at which the particle sweeping and adsorption energies may be in balance and where constant co-deposition may take place.

This qualitative theory substantially explains the major differences in behaviour found in the literature, and for which data should exist although not all may have been published. Unfortunately relatively few processes have alternative agitation methods in use because it is usual that a single method is adopted for other reasons. This method is empirically investigated and adequately understood for day-to-day process control. It suggests, however, that certain agitative modes may be preferable in given circumstances and should be considered more thoroughly at the process design stage for composite electroplating.

REFERENCES

1 R. V. Williams and P. W. Martin. Trans. IMF 1964, **42**, 182.
2 N. Masuko and K. Mushiake. Proc. Interfinish 80, Kyoto, 214 (1980).
3 C. White and J. Foster. Trans IMF 1978, **56**, 92.
4 A. M. J. Kariapper and J. Foster. Trans. IMF 1974, **52**, 87.
5 J. P. Celis, H. Kelchtermans and J. R. Roos. Trans IMF 1978, **56**, 41.
6 C. P. S. Johal, D. R. Gabe and D. R. Eastham. Unpublished work.
7 Mehrdad R. Kalantary and D. R. Gabe. Trans IMF 1989, **67**, 24, 27.
8 J. R. Roos, J. P. Celis, H. Kelchtermans, M. Van Camp and C. buclens. Proc. Interfinish 80, Kyoto 1980, 203.
9 J. P. Celis and J. R. Roos. Revs. Coatings Corrosion 1982, **5**, 1.
10 R. Bazzard and P. J. Boden. Trans IMF 1972, **50**, 63.
11 J. Sadowska-Mazur and M. E. Warwick. Plating and Surface Finishing 1985, **72**, 120.
12 J. Sadowska-Mazur and M. E. Warwick. Proc. SURTEC 85, Berlin 1985.
13 J. Sadowska-Mazur, M. E. Warwick and R. Walker. Trans IMF 1986, **64**, 142.
14 J. Foster, B. P. Cameron and J. A. Carew. Trans IMF 1985, **63**, 115.
15 Bristol Aerojet Ltd. Pat. Spec. 1358 (1974).
16 E. C. Kedward, C. A. Addison and A. A. B. Tennett. Trans IMF 1977, **54**, 8.
17 C. A. Addison and E. C. Kedward. Trans IMF 1977, **55**, 41.
18 J. P. Celis and J. R. Roos. J. Electrochem. Soc. 1977, **124**, 1508.
19 J. R. Roos, J. P. Celis and J. A. Helsen. Trans IMF 1977, **55**, 113.

Vibratory Agitation to Enhance Mass Transfer in Electrodeposition*

M. R. Kalantary, S. A. Amadi and D. R. Gabe

Institute of Polymer Technology and Materials Engineering, Loughborough University of Technology, Loughborough, England

ABSTRACT—A study has been carried out employing a vibratory motor, offering amplitudes of 0·4–4 mm at 50 Hz in acid copper sulphate as a model electrolyte in which α-Al_2O_3 particles are suspended for co-deposition, yielding a composite electrodeposit. Using a horizontal disc vibrator at the bottom of the container, perforated discs have been shown to give superior agitation and a laminar/turbulent transition has been identified. Incorporation of particles is a maximum at the transition. In the laminar regime $Sh \sim Re^{0\cdot037}$ and in the turbulent regime $Sh \sim Re^{0\cdot82}$.

Mass transport enhancement was measured for a variety of disc and tank diameters and enhancement factors for electrodeposition of 3–40 times were obtained. In these circumstances a modified Reynolds number Re_1 was employed $Re_1 = 100\ ad_2(d_1 - d_2)/\upsilon d_2$ and, assuming a conventional dependence upon Sc, a full correlation of the type $Sh_1 = \text{constant}\ Re_1^a\ Sc^{0\cdot33}$ was obtained where the constant took values of 10–40 and 'a' took values of 0·83–1·1 depending upon precise location within the tank of the mass transfer probe.

INTRODUCTION

Commercial electrodeposition processes are almost always operated in regions of concentration polarisation, or partial mass transfer control, partly to avoid the crystallographic preferential deposition which occurs in the region of activation polarisation control and partly to enable the process to be susceptible to rate enhancement by agitation. Although such processes are never fully mass transfer controlled, otherwise powdery or dendritic deposits would be formed and the product would be unacceptable, mass transfer analyses are generally valid because commercial processes are usually operated at fixed fractions of the limiting current densities for any given metal/solution combination—for example $0\cdot25 < i/i_L < 0\cdot65$ for acid copper deposition. However, other reasons for agitation do exist and must always be considered.

(i) To avoid stagnation, disperse products and transport reactants.
(ii) To increase electrodeposition rates by stirring of the electrode diffusion layer.
(iii) To remove heat from the surface and thereby equilibrate the deposit produced.
(iv) To incorporate particles in the deposit and thereby yield composite coatings.
(v) To modify the deposit characteristics, typically grain size, hardness and strength.

In practical terms agitation can be achieved in several ways in either the liquid phase or the solid phase. Thus solution agitation by air sparging, mechanical stirring, solution pumping or jetting is common and the cathode can be moved by slow mechanical oscillation, barrelling, rotation or vibratory agitation. Each of these is understood empirically, the criteria for improvement being related to the five reasons listed previously, but in terms of mass transfer several options exist: either use of a mass transfer parameter such as limiting current density (i_L), mass transfer coefficient (K_L), dimensionless number (Sherwood No., Sh) etc. or use of an enhancement factor (EF) relating the performance under agitative conditions such that:

$$EF = \frac{i_{L(ag)}}{i_{L(o)}} = \frac{K_{L(ag)}}{K_{L(o)}} = \frac{Sh_{(ag)}}{Sh_o} \quad \text{where } Sh = \frac{i_L d}{zFCD}$$

A further consideration is that the agitation must be economic in energy terms, and hence cost terms, but this aspect will not be considered in this paper.

Vibratory agitation has been selected for study because it has one special virtue—it is particularly effective in composite electroplating where it is necessary to maintain second phase particles in suspension in the electrolyte in such a way that they can be systematically and quantitatively incorporated in the electrodeposit. There is evidence to suggest that of several alternatives—pumping, plate pumping, rotary stirring, fluidisation—vibratory solution agitation may be best.[1]

Vibratory agitation can be applied either to the electrode itself or via an impeller plate to the solution as in ultrasonic agitation, the vibration frequency usually being less than 1000 Hz and commonly 50 Hz for convenience. Vibration is induced in the process tank either mechanically or electromechanically and can be applied either to the electrode or to the solution. Systematic studies have been reported for both vibrated electrodes,[3–6] usually in the context of electroanalysis or electrode kinetic studies in chemistry, and for enhanced mass transfer in solution.[7–12] Naturally, detailed behaviour varies from one mode of operation to another and also in the former case to whether the vibration is longitudinal or lateral and whether it is applied to a cylindrical, flat or disc-type electrode. The degree of agitation is expressed quantitatively as an amplitude of movement, a, which can be incorporated in a dimensionless Reynolds number as

$$Re = \frac{100ad}{\upsilon}$$

where d is the characteristic dimension and υ the solution viscosity. Relatively few fundamental studies have been reported for this mode of agitation and no two studies are directly comparable. For example, Kawasaki *et al*[9] used a vibrating disc electrode, vibration achieved by longitudinal shaft reciprocation, and obtained a correlation of the form:

$$Sh = 0\cdot39\ Re^{0\cdot585}\ Sc^{0\cdot33}\ (r/R)^{0\cdot235}$$

where r and R were the radii of the disc and cylindrical shaft respectively.

Fahidy[6] has reported a correlation for a similar arrangement, i.e., horizontal disc electrode vibrating longitudinally, as:

$$Sh = 0\cdot07\ Re^{0\cdot75}\ Sc^{0\cdot5}$$

Clearly different interpretations exist and a definitive quantitative description does not yet exist.

EXPERIMENTAL AND RESULTS

In this study vibration has been applied through a vertical cylindrical shaft and horizontal disc at the bottom of the container which are electrochemically inert and the agitative effect studied using mass transfer techniques just above the vibrating disc. Full experimental details will be found elsewhere[13] and only be summarised here. Vibratory agitation was provided by a Vibromixer (Chemap A.G., model E1) operating at mains frequency (50 Hz). Shaft and discs were made of 316-type stainless steel and remained inert. Flat, perforated and unperforated discs were employed (diameter of 4·5, 5, 7·5 and 10 cm), the perforated holes (9 mm diameter) being truncated to provide jet spouts of liquid. Amplitudes of vibration were varied by a Variac controller and measured by means of a travelling microscope with a mirror and indicator line illuminated by Stroboscopic lighting.

An acid copper sulphate solution (3·75 g/l $CuSO_4.5H_2O$) was used for electrodeposition, the mass transfer characteristics of which were well established. Soluble copper anodes (15 cm^2) and vertical sheet cathodes (3 cm^2) were employed with a remote junction Hg/Hg_2SO_4 reference electrode.

Limiting current values were obtained by potentiostatic step techniques and a potentiostatic step technique described previously.[14] Composite electrodeposits were obtained by using SiC (700 grit) and α-Al_2O_3(3μm) as 'model' particles.

Using flat unperforated discs, the agitation was relatively small and ineffective with fluid being diverted laterally around the edge of the disc (Figure 1a). Using perforated discs, the agitation was found to be essentially laminar up to a critical amplitude or control voltage whereupon an eddying pattern became apparent and flow was becoming markedly turbulent. The degree of agitation was clearly increased as the perforations in the disc allowed fluid to pass through and jet upwards creating large eddy-type circulation (see Figure 1b).

* This paper was presented at the International Surface Finishing Conference held in Brighton, England, in April 1989.

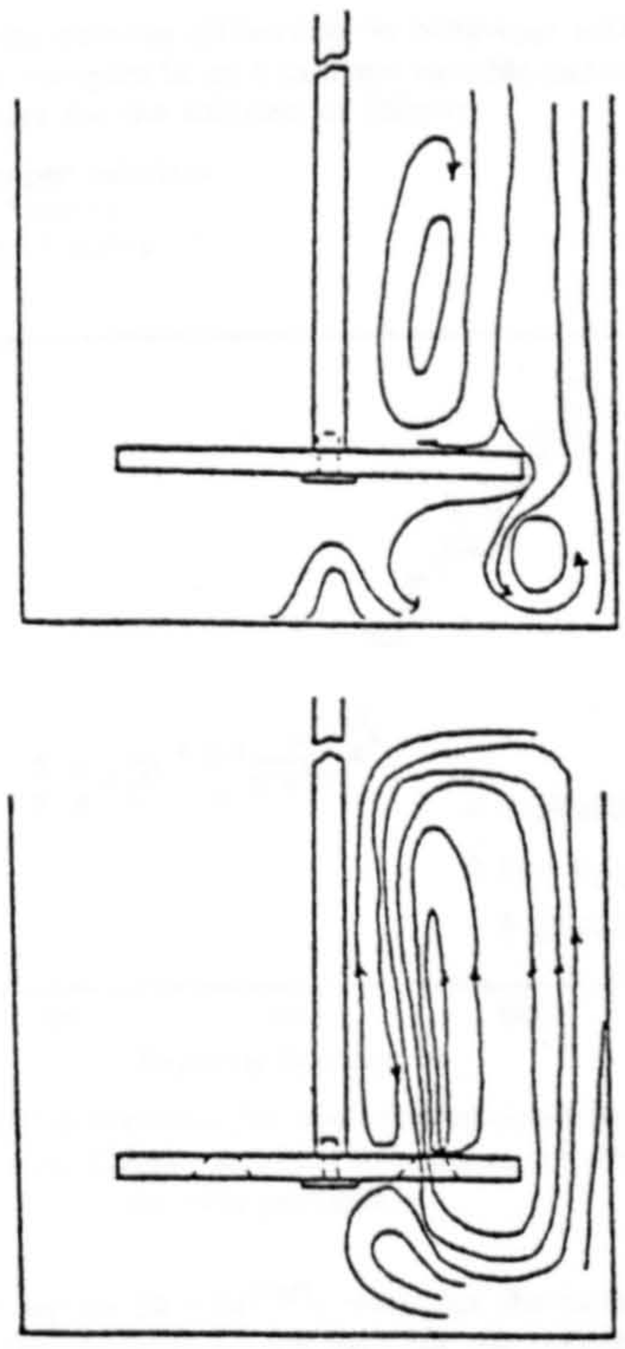

Fig. 1 *Observed patterns of vibratory agitation for a round disc in a concentric 2l beaker (a) unperforated flat disc, (b) perforated disc.*

The degree of vibration was controlled by a.c. voltage (from the variac or variable auto-transformer) which was calibrated in terms of amplitude of movement. They were not proportional but two methods of amplitude measurement with tap water, copper sulphate electrolyte and an inert oil (Dow Corning) gave the same calibration (see Figure 2). When inert particles were added to the electrolyte the calibration changed: in the case of fine low density alumina almost imperceptibly but in the case of high density iron powder quite substantially (Figure 3). It was also clear that the calibration differed for perforated and unperforated discs indicating that greater energy was required for the latter to give similar amplitudes of vibration.

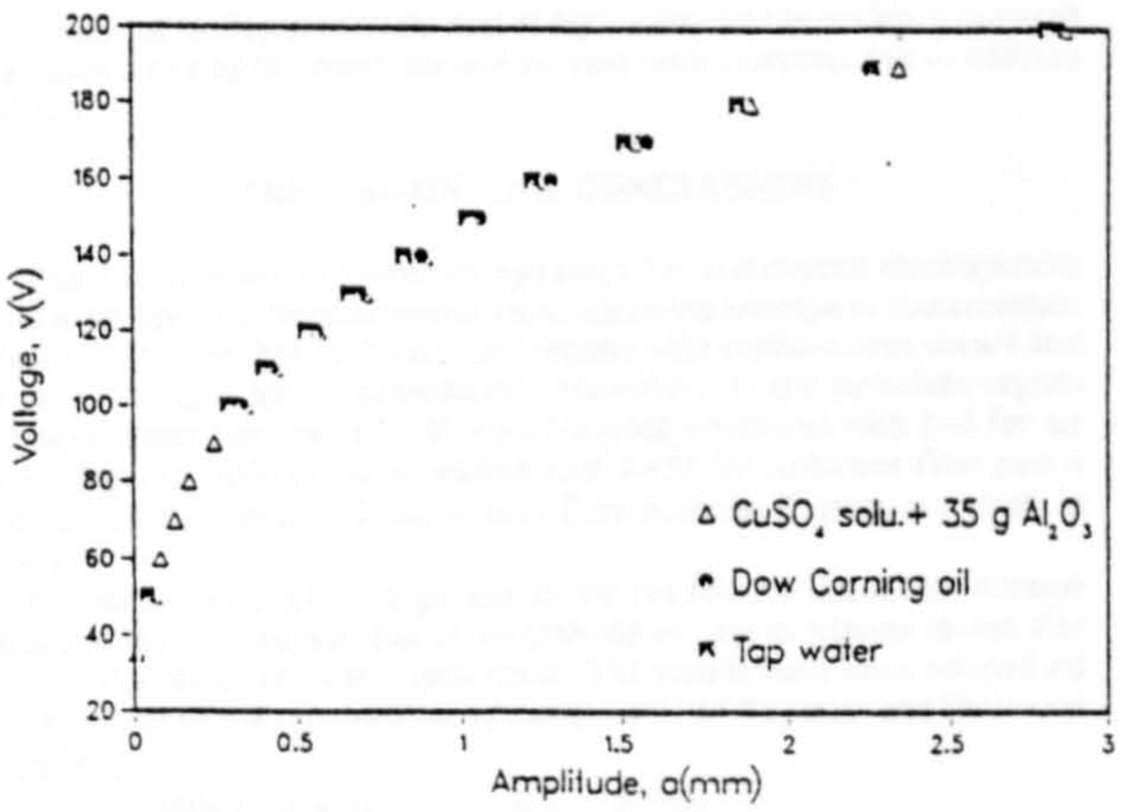

Fig. 2 *Relationship of applied voltage to vibrator motor and amplitude of vibration for the perforated disc and three different media.*

In this study the agitative motion was described by Reynolds number defined as $Re = Ud/\upsilon$ as usual where U is the relative velocity given by $U = S/t$ where S is the distance for which the full frequency cycle applies, i.e., $S = 2a$, and the time $t = 1/f$ where f is the frequency (50 Hz). The critical dimension d was taken to be the disc diameter; thus

$$Re = \frac{2afd}{\upsilon} = \frac{100ad}{\upsilon}$$

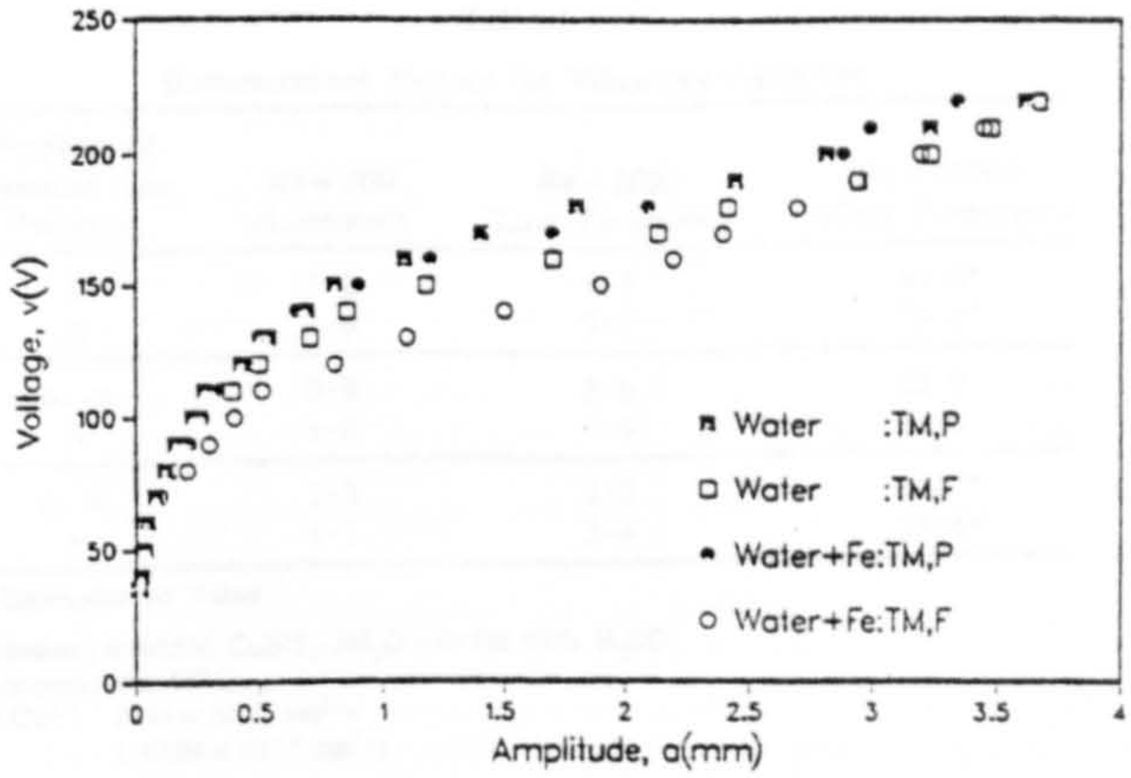

Fig. 3 *Relationship of applied vibrator voltage and amplitude of vibration for flat and perforated discs in two different media.*

Different sized discs were employed in differing plating vessel sizes and the damping effect could not be detected in flow terms, the relationship between Re and a remaining linear (Figure 4).

The limiting current technique was used to study the enhancement of mass transfer in relation to vibrational amplitude. For this purpose only perforated discs were employed and solutions with and without particles were investigated. The experimental data obtained are given in Figure 5, the data being plotted on logarithmic scales to demonstrate clearly the transition from laminar to turbulent flow at an amplitude of 0·5–0·6 mm. When plotted as a mass transfer correlation the transition remained equally

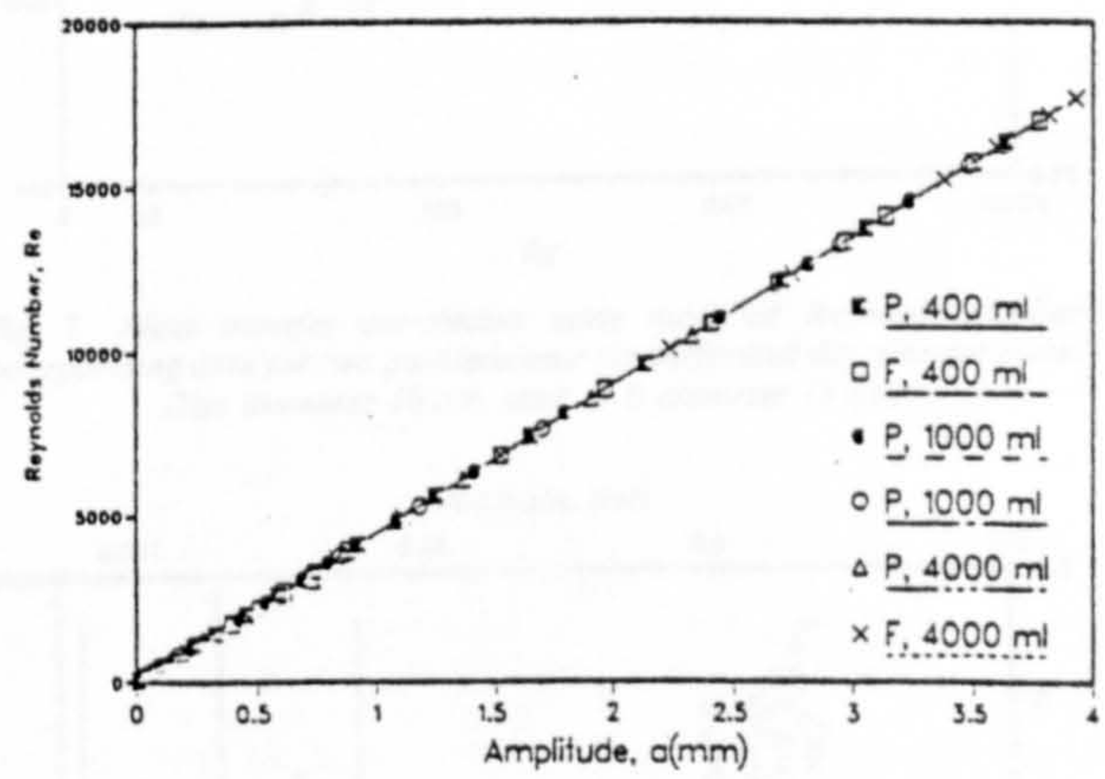

Fig. 4 *Relationship of vibration amplitude and Reynolds number for experimental conditions studied.*

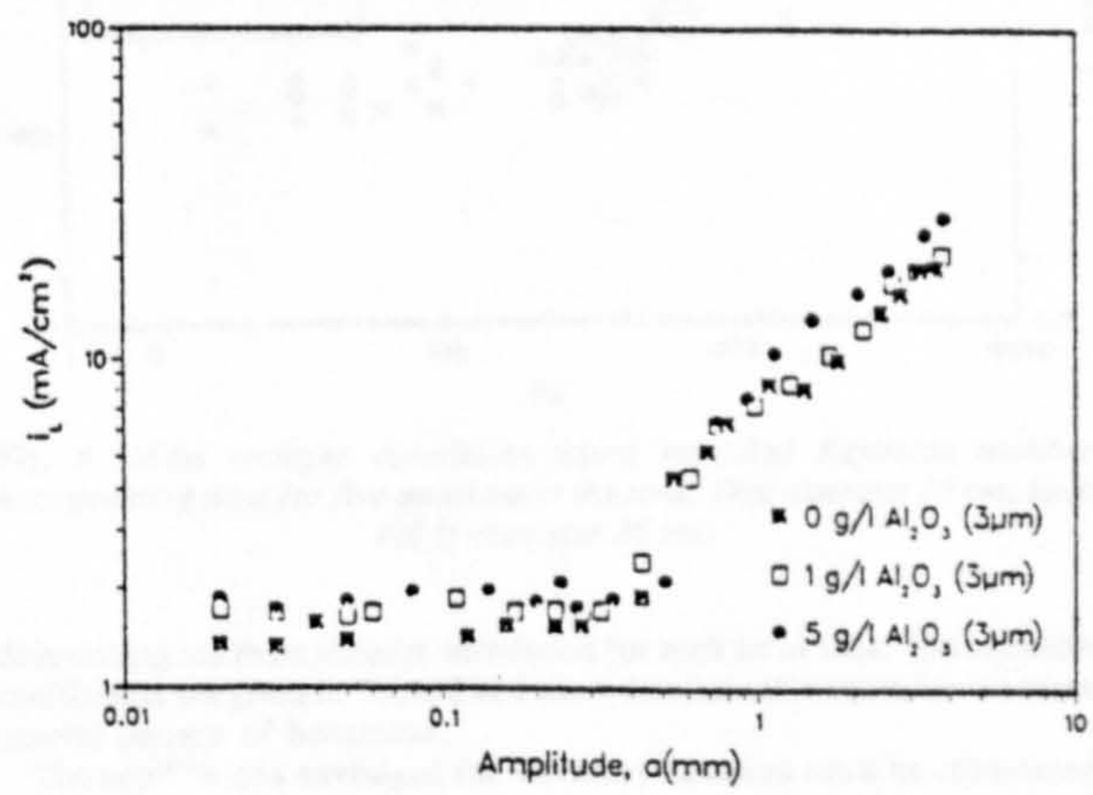

Fig. 5 *Relation of cathodic (electrodeposition) limiting current density to amplitude of vibratory agitation (laminar/turbulent transition at a = 0·45).*

clear (Figure 6) giving obvious differences in behaviour within the two regimes. These data disregard Sc as a separate variable and utilise values of physical parameters for the solution as follows:

$C = 0{\cdot}015M$ copper sulphate
$D = 5{\cdot}84 \times 10^{-6}\ cm^2/s$
$\upsilon = 1{\cdot}0184 \times 10^{-2}\ cm^2/s$

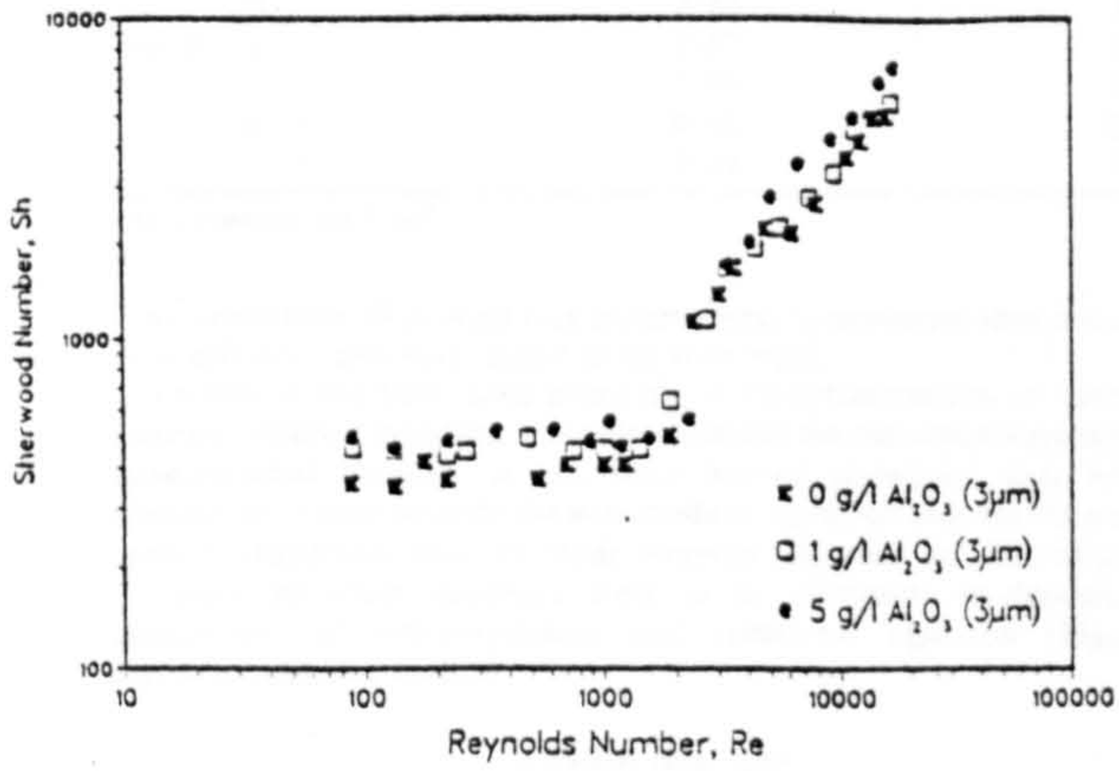

Fig. 6 *Mass transfer correlation for one solution condition (Sc = 1779) using a perforated disc. Copper sulphate solution containing suspended alumina particles.*

For the laminar regime $Sh \sim Re^{0{\cdot}037}$, while for the turbulent regime $Sh \sim Re^{0{\cdot}82}$. With the inclusion of the data for the composite deposits (containing Al_2O_3 particles) the dependence changes slightly to give $Sh \sim Re^{0{\cdot}91}$.

To obtain a full correlation, values of Sc need to be varied over at least an order of magnitude and this has not been possible. However, for $1779 < Sc < 3057$ and $2500 < Re < 20{,}000$ the correlation has been assumed to take the form:

$$Sh = 0{\cdot}164\ Re^{0{\cdot}82}\ Sc^{0{\cdot}33}$$

or

$$Sh = 1{\cdot}94\ Re^{0{\cdot}84} \text{ at } Sc = 1779$$

The effectiveness of vibratory agitation for particle incorporation is good with the microstructures revealing well-dispersed particles and a maximum incorporation rate at the onset of turbulence. This phenomenon has been discussed elsewhere but can be associated with the initial ability to disperse the particles as discrete entities and at high agitation the tendency to sweep particles away as the mean surface contact time decreases due to eddying effects.

DISCUSSION AND CONCLUSIONS

The effectiveness of vibratory agitation for commercial electroplating processes can be defined in several ways. Using the principle of Enhancement Factor it is clear that in the laminar regime little enhancement occurs and it is not a practicable proposition. However, in the turbulent regime Enhancement Factors of 3–20 were obtained compared with 2–4 for air sparging and cathode reciprocation and 5–50 for turbulent flow past a flat electrode surface. Some typical Enhancement Factors are given in Table 1.

For electroplating in a large tank or vat the relative size of the vibrator disc and the relative position of the cathode surface in relation to that disc within the tank are clearly important. The results have been normalised with respect to the relative sizes by using modified Reynolds and Sherwood numbers:

$$Re_1 = \frac{100ad_2}{\upsilon}\ \frac{d_1 - d_2}{d_2}\ ;\ Sh_1 = \frac{i_L d_2}{zFCD}\ \frac{d_1 - d_2}{d_2}$$

where d_1 is the diameter of the tank and d_2 the diameter of the agitator disc. The effect of varying mass transfer within the tank was established by using a small cathode probe and determining limiting current densities at various positions in relation to the agitator disc and at various degrees of vibratory agitation. Figures 7–8 give the data obtained and show common general patterns and some detailed differences. Positions just below or alongside the disc are less effective and those just above more effective: this behaviour is apparent from the pattern of eddy turbulence shown schematically in Figure 1. The data can be analysed numerically by determining the mass transfer correlation for each set of data. The equation coefficients are given in Table 2 and show detailed differences for the same general pattern of behaviour.

The applications envisaged for vibratory agitation must be considered in relation to process requirements and its relative efficacy when compared with other agitative systems. When compared with air agitation it is likely to be more expensive in energy terms but, as with cathode movement, it

Table 1

Enhancement Factors for Vibratory Agitation

Perforated Agitator Disc Position	*Re = 100 (Laminar)*	*Re = 1000 (Low Turbulent)*	*Re = 10000 (High Turbulent)*
Δ	1·0	5·9	64·6*
□	1·6	9·4	76·8*
Δ, ○	0·9	2·6	22·0
×	1·0	1·6	14·6
Δ, ×	1·3	4·0	39·7*
+	1·1	3·4	33·8*

* Extrapolated Value

Solution: $0{\cdot}015M\ CuSO_4.5H_2O + 0{\cdot}5M\ 98\%\ H_2SO_4$
Temperature: 18°C
$D\ Cu^{2+}$ $5{\cdot}84 \times 10^{-6}\ cm^2/s$
υ $1{\cdot}0184 \times 10^{-2}\ cm^2/s$

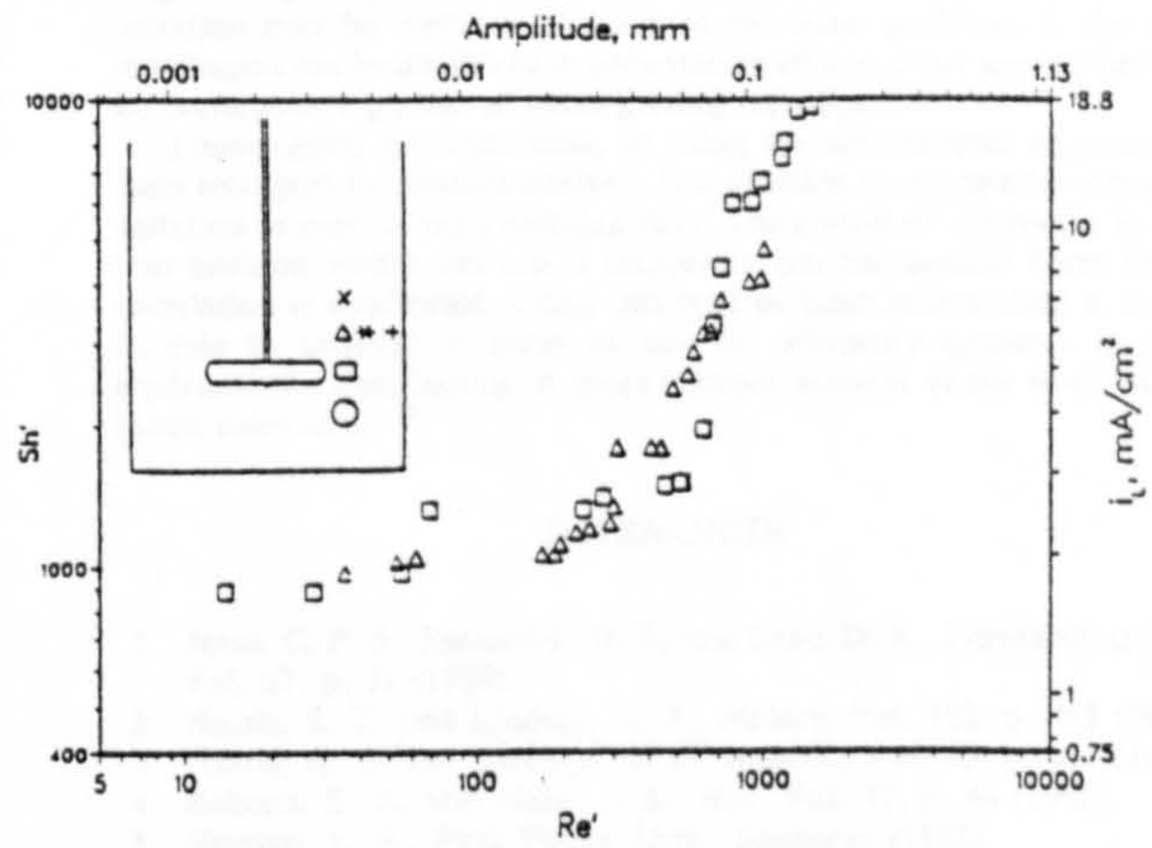

Fig. 7 *Mass transfer correlation using modified Reynolds number incorporating data for two positions near the perforated disc vibrator plate. Disc diameter 10 cm, tank (5 l) diameter 19 cm.*

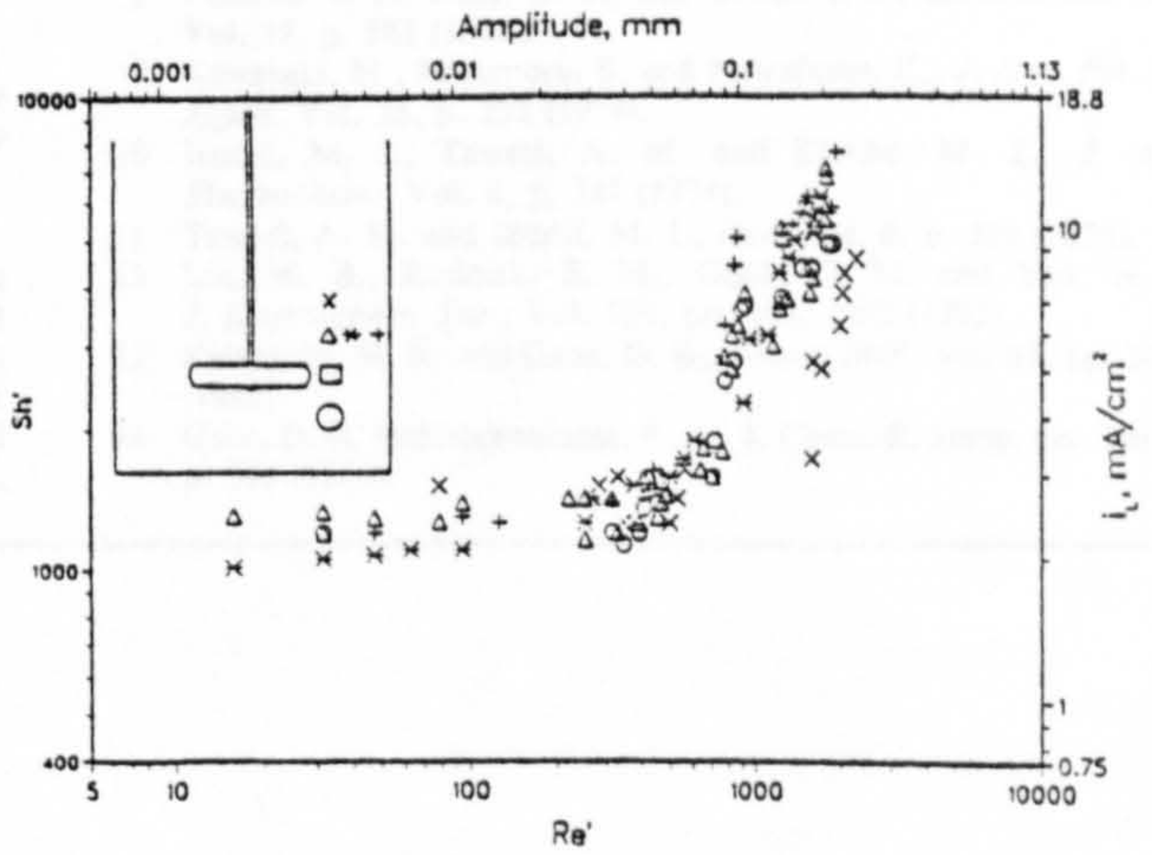

Fig. 8 *Mass transfer correlation using modified Reynolds number incorporating data for five positions in the tank. Disc diameter 10 cm, tank (25 l) diameter 26 cm.*

Table 2

Mass Transfer Correlation* Coefficients for Data of Figures 7 and 8

Data Points		*Index a*	*Constant*
Fig. 7	Δ	1·1	44·4
	□	0·86	33·7
Fig. 8	Δ ○	0·83	19·0
	×	0·86	11·8
	Δ ×	0·91	21·3
	+	0·83	16·9

*$Sh = \text{constant } Re_j^{a} . Sc^{0.33}$

is non-oxidative. If process rate enhancement is important then it is clearly very effective and must stand in its own right.

To date it has been used primarily in electrodeposition of composite coatings where it provides not only agitation but particle buoyancy in an advantageous manner. It has been argued elsewhere[1] that for this application it may provide the best mode of agitation because the particles must be dispersed, must be made buoyant and must be allowed to have adequate substrate residence time to be efficiently co-deposited. A comparison of vibro-agitation and rotational agitation (Figure 9) demonstrates this feature.

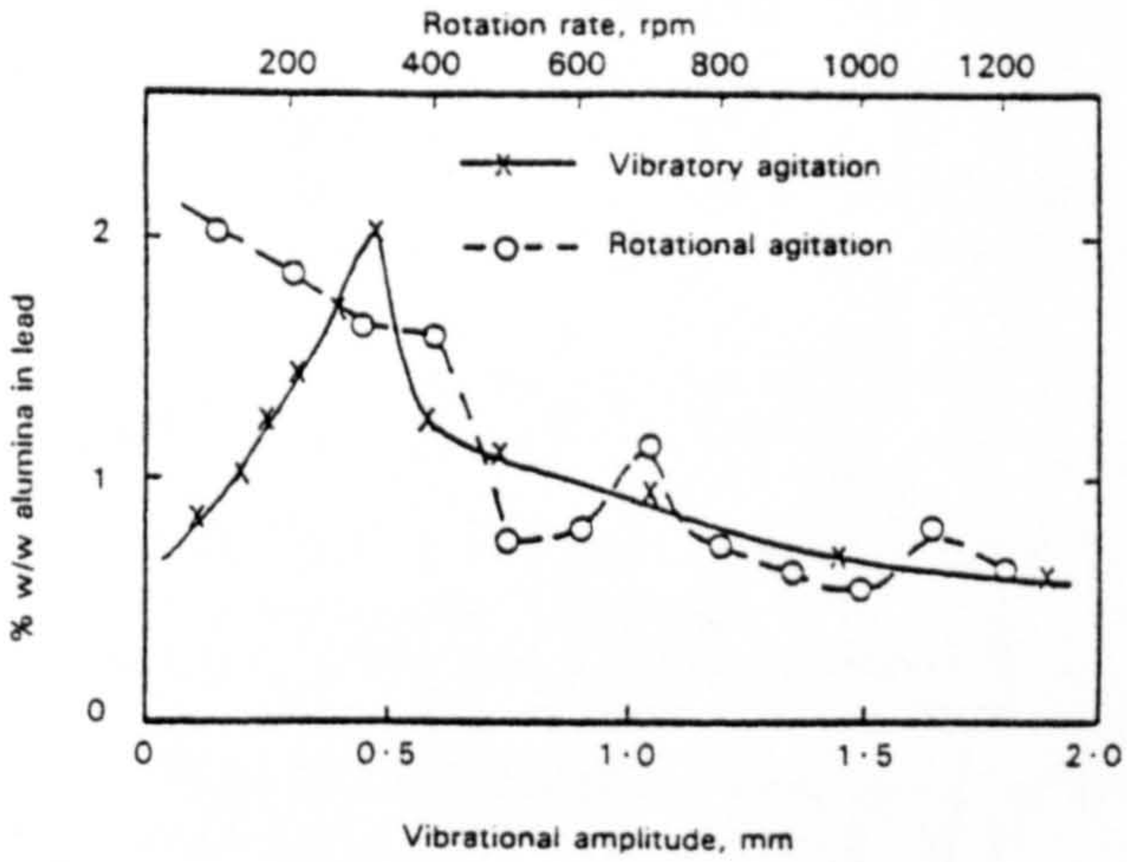

Fig. 9 *Effect of agitation rate on the degree of particle incorporation for Al_2O_3 in Pb, after Johal* et al.[1] *(a) Vibratory agitation. (b) Magnetically stirred rotational agitation.*

Vibro-agitation may also be valuable as an aid to throwing power in crevices, recesses and holes. The equalisation of deposition over an irregular surface can be achieved either by suppressing or diverting deposition on the more prominent areas (e.g., use of robbers) or by enhancing deposition in recesses by preferential agitation (e.g., jetting) or by modifying cell geometry (e.g., confirming anodes). While jetting is undoubtedly effective, it is often too effective in a highly localised sense, thus actually making it valuable for spot plating (e.g., electrical contacts): vibro agitation may provide the appropriate answer to this problem. The condition for successful recess plating must be, however, that the recess is receptive to the vibrational eddies generated by the agitator plate and it may therefore be necessary to modify conventional jigging arrangements. Thus horizontal jigging, not usually favoured with air agitation because of the danger of air bubble entrapment in the recesses, may be preferred so that the rising eddies may have maximum impact before being reflected in circulatory motion. This approach may have significant impact in both engineering/functional and electronics electrodeposition processing.

Manufacturers of printed circuit boards have two main problems of metal distribution:

(i) thickness distribution over the whole panel;
(ii) thickness distribution and continuity in through-holes.

Lack of thickness may be attributed to several factors including primary and secondary distribution patterns and also to metal ion depletion within stagnant regions such as holes, recesses and crevices. Novel methods of agitation may be useful in relation to the latter problem. If the poor distribution can be attributed to polarisation effects, other approaches may be preferable, e.g., use of pulse plating techniques.

In conclusion, it is clear that, by using the conventional approach of mass transport correlation analysis, it is possible to systematise vibratory agitation as used in electroplating cells. The scatter of the results is such that position within the cell is important but the general form of the correlation is unaffected. Using this type of basic information it is now feasible to establish a mode of use for vibratory agitators in large electroplating installations. A more detailed account of the work will be found elsewhere.[1,13]

REFERENCES

1 Johal, C. P. S., Kalantary, M. R. and Gabe, D. R., *Transactions IMF*, **Vol. 67**, p. 31 (1989).
2 Harris, E. D. and Lindsey, A. J., *Nature*, **Vol. 162**, p. 413 (1948).
3 Harris, E. D. and Lindsey, A. J., *Analyst*, **Vol. 76**, p. 647 (1951).
4 Roberts, E. R. and Meek, J. S., *ibid*, **Vol. 77**, p. 43 (1952).
5 Hoover, A. E., PhD Thesis, Univ. Michigan (1968).
6 Fahidy, T. Z., 'Principles of Electrochemical Reactor Analysis', Elsevier, Amsterdam, p. 102 (1985).
7 Rao, K. S., Raju, G. J. V. J. and Rao, C. V., *Ind. J. Technol.*, **Vol. 3**, p. 38 (1965).
8 Podesta, J. J., Paus, G. F. and Arvia, A. J., *Electrochim. Acta*, **Vol. 19**, p. 583 (1974).
9 Kawasaki, M., Mizumoto, S. and Nawafume, K., *J. Met. Fin. Soc. Japan*, **Vol. 25**, p. 272 (1974).
10 Ismail, M. I., Taweel, A. M. and El-Abd, M. Z., *J. Appl. Electrochem.*, **Vol. 4**, p. 347 (1974).
11 Taweel, A. M. and Ismail, M. I., *ibid*, **Vol. 6**, p. 559 (1976).
12 Liu, M. B., Rudnick, E. M., Cook, G. M. and Yao, N. P., *J. Electrochem. Soc.*, **Vol. 129**, pp. 913, 1955 (1982).
13 Kalantary, M. R. and Gabe, D. R., *Trans. IMF*, **Vol. 67**, pp. 24, 28 (1989).
14 Gabe, D. R. and Makanjuola, P. A., I. Chem. E. Symp. Ser. No. 98, p. 309 (1986).

APPENDIX 5

Conference paper for "Asia Pacific Interfinish 90" at Singapore, November 1990.

Pulse Plating for Printed Circuit Board Technology [133].

PULSE PLATING FOR PRINTED CIRCUIT TECHNOLOGY

Mehrdad R. Kalantary †, D. R. Gabe † and M. Goodenough*
† IPTME, Loughborough University of Technology, LE11 3TU
* LeaRonal (UK) Ltd, Buxton, SK17 9SS

Abstract

Pulse plating has been employed as a technique since the 1950s but in the last ten years, it has been recognised as being useful in certain specific applications, in particular instances of throwing power where activation polarization and solution conductivity may be the controlling factors. This is especially true for through holes in printed circuit boards (PCB).

The research has been concerned with the use of acid copper electrolyte for PCB production and the development of pulse programmes to optimise through hole plating rates. It has involved the study of cathode polarization behaviour and used the Wagner Number to rationalise the data obtained.

Introduction

Pulse plating has been of research interest since the early 50's. The reported research work has been on almost all the common metals, precious metals and some alloys and has concerned with the processing parameters and electrodeposit properties (1).

The general definition of a pulse supply is such that a constant current should be capable of being switched from one level to another. The simplest case is that of alternating switching on and off a DC supply and this represents the common pulse wave of a square wave. Other pulse waveforms include sine-wave, triangular-wave and so forth.

The main difference between DC and pulsed current is such that with DC plating, only voltage or current can be controlled but with pulse plating, three parameters, on-time, off-time and the peak current density can independently be varied (figure 1). These variations in pulse are believed by many authors to be able to create a mass transport situations, electrocrystallisation conditions and adsorption and desorption phenomena which are not otherwise possible (1,2).

The expected advantage of pulse plating can be enumerated:

a) possibility of improving the physical properties of the deposit; finer, purer and smoother deposit;
b) by applying pulse current it is possible to raise the limiting current density hence increasing the plating speed;
c) better adhesion of deposit to substrate;
d) improved plating distribution.

The use of a dimensionless group to define current distribution in a recess region was originally proposed by Wagner (3) and has subsequently been termed the Wagner Number(Wa). This recognises that the distribution of current is substantially attributed to:

a) the geometry of the recess;
b) the conductivity of the electrolyte;
c) the kinetics (or polarization) prevailing during electrodeposition.

The definition takes these factors into account and assumes 100% cathode efficiency and is given as

$$Wa = \frac{\kappa}{L}\left(\frac{d\eta}{di}\right)$$

where

κ is the electrolyte conductivity (Scm^{-1})
L is the characteristic length of the deposition process (cm)

$\left(\frac{d\eta}{di}\right)$ is the slope of the polarization curve (mV/A)

The larger the Wa the more uniform is the current distribution and subsequently the deposit distribution. When Wa→0 primary current (geometry factor) conditions prevail. Thus to raise Wa, the solution conductivity should be as high as possible and ($d\eta/di$) must also be high.

It is as a consequence of this, that solutions for use in these circumstances are formulated to maximise conductivity, ie. high acidity or support electrolyte concentration and relatively low metal ion concentration but not so low as to reduce plating rates to non-commercial levels. The Wagner Number may be derived from Tafel theory of activation polarization, the details being presented in the appendix. It is widely believed that increased throwing power can be associated with an increase in Wagner Number or Tafel slope [4].

This approach has been employed for this research programme which has been mainly concerned with developing a copper electrolyte and special pulse conditions for plating printed circuit boards having through-hole diameters as low as 0.3mm. It must be possible to plate holes having a surface to hole thickness ratio of 1:1.

The model electrolyte solution is a highly conductive acid copper sulphate with also some proprietary additives. Different agitation techniques were also used in combination with the pulse in order to increase the transport of metal ions in the through-hole PCB's.

Experimental

The experimental arrangement used, shown in figure 2, employs a pulse unit having a microprocessor controlled electronic switch which allows programming of up to 9 channels and also allows various parameters such as frequency, duty cycles and the pulse direction, either forward or reverse, to be stored.

The first part of the research was to study the characteristics of the pulse unit since the reproducibility of the data is of major importance. Various means of power sources such as Thompson 'ministat' used as potentiostat and galvanostat and also Farnell power units have been used with it. In order to study the characteristics of such power sources, polarization curves were obtained and compared to the typical polarization curve without pulsing. Polarization studies were carried out cathodically using a brass cathode with an area of $12.5cm^2$ and copper anode area of $120cm^2$. The reference electrode was mercury/mercury sulphate. The electrolyte solution consisted of 0.3M $CuSO_4.5H_2O$, 2.25M H_2SO_4 and 50ppm Cl^- and the polarization curves were taken across an ohm resistor using Advanced Bryan chart recorder.

The main part of this research work has been concerned with the effect of throwing power (ie. the ability of a solution to deposit on an uneven surface including into holes on "through-hole" PCB's) under different pulse conditions and different electrolyte solutions, the object being to optimise throwing power for through-holes.

However, other parameters which need to be emphasised on are frequency and duty cycle. The frequencies and duty cycles conditions used were 20, 500, 1000, 2000 and 5000Hz and 25, 50, 75 and 100%, respectively.

Frequency relates to the pulsation in cycles/second(Hz); duty cycle is defined as:

$$\text{Duty cycle } (\phi) = \frac{\text{time}_{on}}{\text{time}_{on} + \text{time}_{off}} \times 100\%$$

$$\underset{(Adm^{-2})}{\text{Mean current density}} = \underset{(Adm^{-2})}{\text{Peak current density}} \times \underset{(\%)}{\text{Duty cycle}}$$

The work reported here is for forward pulse only and uses the standard electrolyte. A comparison with the direct current performance is used as the criterion of behaviour.

Agitation was provided by two techniques:

a) air sparging which enhances the replenishment of metal ions around the cathode [5,6];
b) reciprocating cathode which enhances the replenishment of metal ion in and around holes [6].

Results and Discussions

Polarization curves have been obtained under series of conditions. Figure 3a Shows a typical polarization curve, that is, with increase in potential, the deposit thickness increases passing a region of ideal crystallisation yielding faceted microstructures. Continuing from that region onwards a region of levelled deposit is formed up to a stage for which the solution next to the electrolyte becomes depleted and hence the rate of consumption equals the rate of diffusion: this leads to dendritic or powder growth. After that hydrogen evolution commences and cathodic efficiency falls sharply.

However, the polarization curve (figure 3b) was obtained using potentiostatic control and a pulse unit. On this occasion the potentiostat and pulse unit were switched on with a second gap in between and consecutively. It must be noted that the pulse unit was set 'in line' and the duty cycle was fixed at 100% as direct current (DC). It can be seen that the polarization curve is substantially modified from that obtained previously.

The effect of switching can also be seen in figure 3c when both the pulse unit and the potentiostat were switched on together. It was found that when this test was repeated the polarization curves are not even reproducible. Furthermore, when the power supply was switched on a second later, the result was unsatisfactory. It was understood that the potentiostat could not be used for the study as it did not produce either an expected or a reproducible pattern. This is because it is continuously acting to correct the pulse pattern and revert to DC conditions. It was concluded that using power supply at constant current and voltage provided reproducible and acceptable polarization curves.

In PCB production the transport of metal ions as replenishment down the hole is the most important factor in obtaining an uniform deposit. Replenishment and thence deposition rate is enhanced by some means of agitation which can also affect uniformity; the use of pulse-type technique is primarily important in achieving uniformity and any rate enhancement is subordinate. The types of agitation used have been cathode reciprocation and air and reciprocation combined .

A typical polarization curve can be seen in figure 4 and that at a constant potential of typically -0.8V the limiting current density (i_L) for the still solution, reciprocating agitation and for air and reciprocating agitations i_L is about 1.5, 4.3 and 8.25Adm^{-2}, respectively. This shows that with increase in agitation the region of levelled deposit has also increased.

Figure 5 shows a typical polarization curve under different pulse conditions using air and reciprocating agitations and it can be seen that the limiting current density (i_L) has increased in some cases in comparison to the DC.

However, the main region of interest is the Tafel region. The polarization curve of figure 6 clearly shows three polarization regions: linear(a) polarization which is the first 30mV, then a region of Tafel behaviour(b) which is assumed to be the first 2-30% (or from 30-200mV) of the polarization curve, and a region of concentration polarization(c).

The Tafel slope can be calculated in two ways: the first is from the slope of a E-logi plot; it is obtained directly from the polarization curve. The second by a E-logi_C plot where i_C is a modified current density which eliminate the mass transfer component [4]. Tafel slope is calculated in mV/decade. As in associated research work the second method is preferred. A typical E-logi_C can be seen on figures 7 and 8 for solutions containing no additives and with additives, respectively. The calculated Tafel slope showed that the variations under pulsed current with or without additives are significant; in fact, the Tafel slope variations were in the range of 41.7-225.7 mV/decade, but no particular trend could be established.

In related circumstances Ibl [7] devised a method to describe qualitatively the solution characteristics, using primary and secondary current distribution. This parameter is the dimensionless Wagner Number(Wa) which relates to the uniformity of the electrodeposit and thus the throwing power of the solution.

White et al [8] and others have used the Wagner theory and studied the surface distribution and metallurgical benefits of copper deposit under pulse plating and reverse pulse plating conditions. It has been reported that the surface height uniformity on circuit board tracks decreases as plating current density increases. Furthermore, with pulse plating, enhancement in metallurgical properties tend to decrease surface height distribution. However, reverse pulse plating improves the height distribution although the magnitude of the anodic current pulse had to be limited to avoid passivation of the surface. Moreover, under reverse pulse plating, metallurgical changes such as grain size and ductility have been reported to be comparable to that of direct current with additives.

Vilambi et al [9] and Chin et al [10] have also used the Wagner theory and stated that pulsed current reduces the slope of the polarization curves and shift them to more horizontal position with decrease in duty cycle. Thus for a given average current density $(Wa)_{PC}<(Wa)_{DC}$. This implies that the current distribution is less uniform in pulse plating than with direct current plating and that more localised deposit can be obtained with pulse current. It was also reported that the extent of localisation in the cathode current distribution increased with (a) decreasing pulse duty cycles, (b) increasing average current density, and (c) decreasing anode-cathode spacing. A satisfactory agreement was reported between the theoretical current distribution and the experimental metal distribution on the cathode.

As for the use of the Wagner Number in through-hole plating studies, Yung et al [11,12,13] and Bard et al [17] have used this method with some changes to model current distribution and thus, theoretical plating uniformity in the hole. In other studies, Goodenough [5] using acid copper sulphate solution for boards of 8:1 aspect ratio, correlation is reported to be excellent using the Wagner Number theory as means of comparison for different acid concentrations, current densities, additives and temperatures. Furthermore, it was postulated that the major factor influencing deposit uniformity is the solution conductivity and the current density in attempting to obtain 1:1 surface to hole thickness ratio.

Other studies have reported using pulse current in connection with through-hole plating or PCB [14,15,18]. It has been claimed that pulse plating or pulse reverse plating decreases the effect of mass transfer boundary layer thickness and thus allows higher instantaneous plating current densities as well as better copper distribution without inducing burning of copper deposits at high current density points [15,16].

In general, parameters affecting the Wagner Number may be enumerated as:

a) electrolyte concentration or conductivity of the electrolyte
b) additives and their concentrations
c) current density
d) metal ion replenishment
e) duty cycle
f) frequency
g) temperature
h) geometry of the system

Tafel slope values obtained experimentally were used to calculate the Wagner Numbers at different current densities. A typical i-Wa relationship can be seen in figure 9. The results show that there is no particular trend but it is obvious that different pulse conditions give a different Wagner Number. Furthermore, the same trend occurs with solutions containing additives(figure 10). The combination of pulsing and additives yields a more favourable throwing power option.

To differentiate and also to characterise the changes in Wagner Number, an enhancement ratio (RWa) can be defined such that

$$R_{Wa} = \frac{\text{Pulse Wagner Number } (Wa_p)}{\text{DC Wagner Number } (Wa_{DC})}$$

Basically, RWa gives a better account in improvement for different pulse conditions in comparison to DC. Table 1 shows the RWa at $2.0 Adm^{-2}$ using both air and reciprocation for electrolyte I and II, assuming $RWa_{DC}=1$ (N.B. Electrolyte I is the solution used previously and electrolyte II a similar solution containing Lea Ronal proprietary additives optimised for DC and pulsed plating). It can be seen that for the two electrolytes used different optimum pulse frequencies and duty cycles have been obtained. This indicates that constituents of the electrolytes play an important role in pulse plating, as reported by Pearson and Dennis [16], hence the choice of electrolyte is crucial for electroplating PCB's. However, a good RWa under certain conditions for one electrolyte is not necessarily the same for another electrolyte.

Furthermore, it can be seen from table 1 that RWa can be as high as two fold, depending on the type of electrolyte and current density employed. But again depending on the particular current density the Wagner Number can be increased further (table 2), ie. with $0.5 Adm^{-2}$ the RWa increases to be as high as Five fold.

However, figure 11a and 11b show micrographs of the PCB under DC and pulse for the electrolyte I and these can be compared with the electrolyte II shown in figure 12a and 12b under the best conditions obtained. It can be seen that a marked improvement in coating distribution from pulse to DC, in terms of surface to hole thickness ratio occurs. In terms of choice of the electrolyte, microstructure studies showed that electrolyte II produces a finer deposit to that of electrolyte I which produces long columnar structure. For this reason the electrolyte II is preferred despite the fact that the RWa is lower since this grain refinement is an important factor in producing a good electrical contact surface.

Conclusions

1. Applying pulsed current does not increase the faradaic efficiency but can raise the limiting current density and thus the practical plating current affects the structure and grain size as well as surface levelling.

2. Tafel slope or Wagner Number can be increased by two fold or more depending upon the electrolyte, additives and their concentrations, duty cycle, frequency, agitation and temperature.

3. It has been shown that the RWa is a good criterion for assessing the effect of pulsed current.

4. Electrolytes containing additives improved thickness distribution and produced a fine grain deposit which is required for good electrical continuity and physical properties, although not necessarily as large as RWa value.

References

1. Puippe, J.C. and Leaman, F., Theory and Practice of Pulse Plating, Publ. AESFS (1986).
2. Kasper, C., J. Electrochem. Soc., 77 (1940) 353, 456; 78 (1940) 131, 147; 82 (1942) 153.
3. Wagner, C., J. Electrochem. Soc., 98 (1951) 116; Plating, 48 (1961) 977; Adv. Electrochem. Eng., 2 (1962).
4. Goodenough, M. and Whitlaw, K.J., Trans. I.M.F., 67 (1989) 57.
5. Uceda, D.A. and O'Keefe, J. Appl. Electrochem. Soc., 20 (1990) 327.
6. Haak, R., Ogden, C. and Tench, D., J. Appl. Electrochem. Soc., 11 (1981) 771.
7. Ibl, N., IUPAC Information Bulletin, 59 (1977).
8. White, J.R. and Galasco, R.T., Plating and Surface Finishing, (1988) 122.
9. Vilambi, N.R.K. and Chin, D.T., ibid, (1988) 67.
10. Chin, D.T., Vilambi, N.R.K. and Sunkara, M.K., ibid, (1989) 74.
11. Yung, K.E., Romankiw, L. and Alkire, R.C., Proc. Electrodeposition Technology theory and Practice, Ed. Romankiw, L.T., 87(17), 1987, 75.
12. Alkire, R.C. and Ju, J.B., J. Electrochem. Soc., 134(5) (1987) 1172.
13. Alkire, R.C. and Mirarefi, A.A., ibid, 120 (1973) 1507.
14. Ng, H.K., Tseung, A.C.C. and Hibbert, D.B., ibid, 127 (1980) 1034.
15. Pesco, A.M. and Cheh, H.Y., ibid, 131 (1984) 2259.
16. Ibl, N. and Braun, M., Chem.- Ing. - Tech., 45(4) (1973) 182.
17. Bard, A.J. and Faulkner, L.R., Electrochemical Methods - Fundamental and Applications, J. Wiley, (1980).
18. Pearson, T. and Dennis, J.K., J. Appl. Electrochem. Soc., 20 (1990) 196.
19. Albery, W.J., Electro-kinetics, Oxford (1975).

Glossary

C_O concentration of the species at the electrode surface pertaining to species O in $O+ne \Leftrightarrow R$(mol cm^{-3})

C_O^* concentration of the species of the bulk pertaining to species O in $O+ne \Leftrightarrow R$(mol cm^{-3})

C_R concentration of the species at the electrode surface pertaining to species R in $O+ne \Leftrightarrow R$(mol cm^{-3})

C_R^* concentration of the species of the bulk pertaining to species O in $O+ne \Leftrightarrow R$(mol cm^{-3})

$d\eta/di$ slope of the polarization curve(mV/A)

L characterisitc length of the deposition process(cm)

i current density(Adm^{-2})

i_C cathodic current density(Adm^{-2})

i_L limiting current density(Adm^{-2})

i_m, i_P mean and peak current density (Adm^{-2})

n,F number of electron and Faraday constant($Asmol^{-1}$)

x distance(cm)

R,T temperature(K) and gas constant(J K mol^{-1})

RWa Wagner Number enhancement ratio[$=Wa_p/Wa_{DC}$]

Wa Wagner Number

Greek letters

ϕ duty cycle(%)

κ electrolyte conductivity(Scm^{-1})

η overpotential(mV)

Appendix I

The Mathematical Derivation for the Tafel Slope has been defined by many authors [4,17,19] and it is given by:

$$i = i_o \left\{ \frac{C_o(0,t)}{C_o^*} \exp\left[\frac{-\alpha n F \eta}{RT}\right] - \frac{C_R(0,t)}{C_R^*} \exp\left[\frac{(1-\alpha) n F \eta}{RT}\right] \right\}$$

The first term describes the cathodic component current at any potential and the second gives the anodic contribution.

$$\frac{C_o(x=0)}{C_o^*} = 1 - \frac{i}{i_{L,C}} \qquad \& \qquad \frac{C_R(x=0)}{C_R^*} = 1 - \frac{i}{i_{L,A}}$$

For the cathodic reaction

$$\frac{i}{i_o} = \left(1 - \frac{i}{i_L}\right) \exp \frac{-\alpha n F \eta}{RT}$$

$$-\ln\left[\frac{1}{i} - \frac{1}{i_L}\right] = -\frac{\alpha n \eta F}{RT} + x$$

$$\ln\left[i_C\right] = -\frac{\alpha n \eta F}{RT} + x \qquad (1)$$

The slope of the Tafel region is given by:

$$\frac{d\eta}{di} = \frac{RT}{\alpha n F i} \qquad (2)$$

Equating (1) and (2) it can be seen that

$$\frac{d\eta}{di} = \frac{1}{i \ln\left[i_C\right]}$$

Equation (2) can also be written as

$$d\eta = \frac{2.303\ RT}{\alpha n F} d\log i \qquad (3)$$

Equating (2) and (3) it can be derived that

$$Wa = \frac{\kappa}{L}\left(\frac{d\eta}{di}\right)$$

where κ is the electrolyte conductivity (Scm^{-1})
L is the characteristic length of the deposition process (cm)

$\left(\frac{d\eta}{di}\right)$ is the slope of the polarization curve (mV/A)

i, i_o current density and exchange current density (Acm^{-2})
$i_{L,A}$, $i_{L,C}$ anodic and cathodic limiting current density (Acm^{-2})
α transfer coefficient

I Hz,%ϕ (RWa)	II Hz,%ϕ (RWa)
2000, 25 (1.02)	5000, 25 (1.02)
20, 75 (1.05)	5000, 75 (1.07)
500, 75 (1.18)	1000, 50 (1.09)
2000, 50 (1.30)	2000, 75 (1.10)
5000, 25 (1.42)	20, 75 (1.19)
5000, 75 (1.43)	1000, 75 (1.34)
5000, 50 (1.76)	

Table 1. Frequencies and duty cycles with their RWa values for electrolyte I and II*; Wa_p at $2.0Adm^{-2}$;

$i\ (Adm^{-2})$	I 5000Hz, 50%ϕ Wa_{DC}= 0.215	II 1000Hz, 75%ϕ Wa_{DC}= 0.253
0.5	7.07	5.38
1.0	3.53	2.68
1.5	2.35	1.79
2.0	1.76	1.34
2.5	1.41	1.08
3.0	1.18	.897

Table 2. RWa values under pulsing for the best conditions of the electrolyte I and II*; Wa_{DC} at $2.0Adm^{-2}$;

I - 0.3M $CuSO_4$, 2.25M H_2SO_4, 50 ppm Cl^-
II*- 0.3M $CuSO_4$, 2.25M H_2SO_4, 50 ppm Cl^- and a mixture of polyethylene glycol, mercaptopropayl sulphonic acid and aromatic sulphonic acid additives.
(* Lea Ronal Proprietary electrolyte)

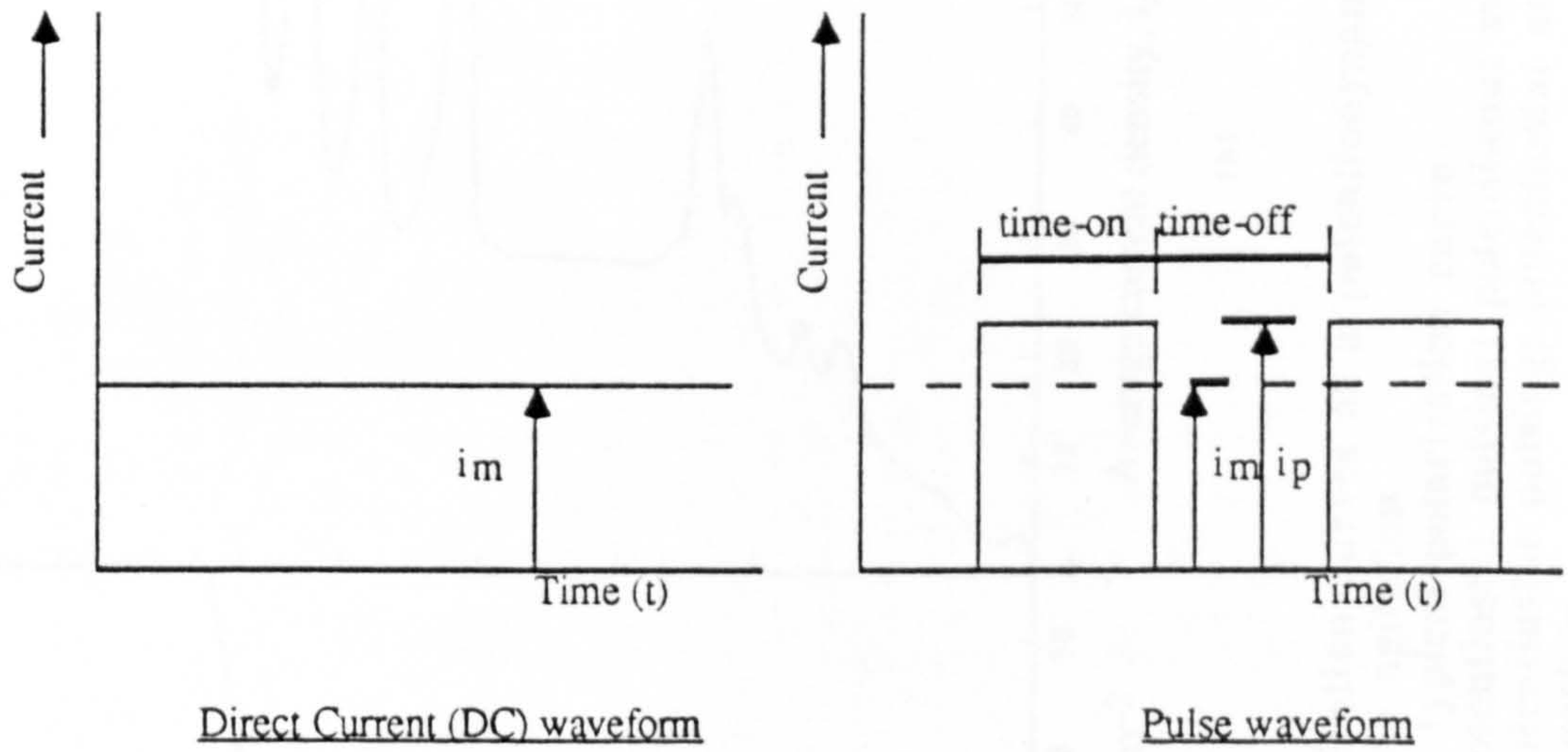

Figure 1 Typical waveforms under DC and Pulse plating conditions

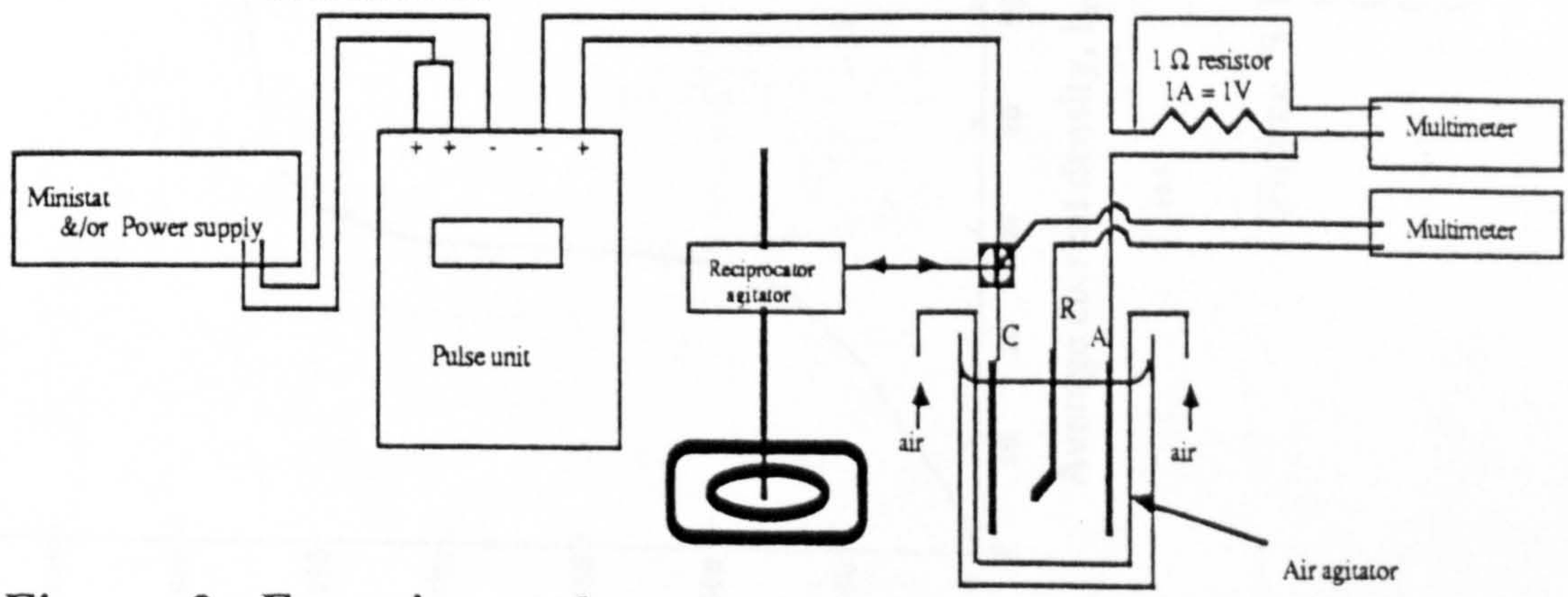

Figure 2 Experimental arrangement used for polarization studies

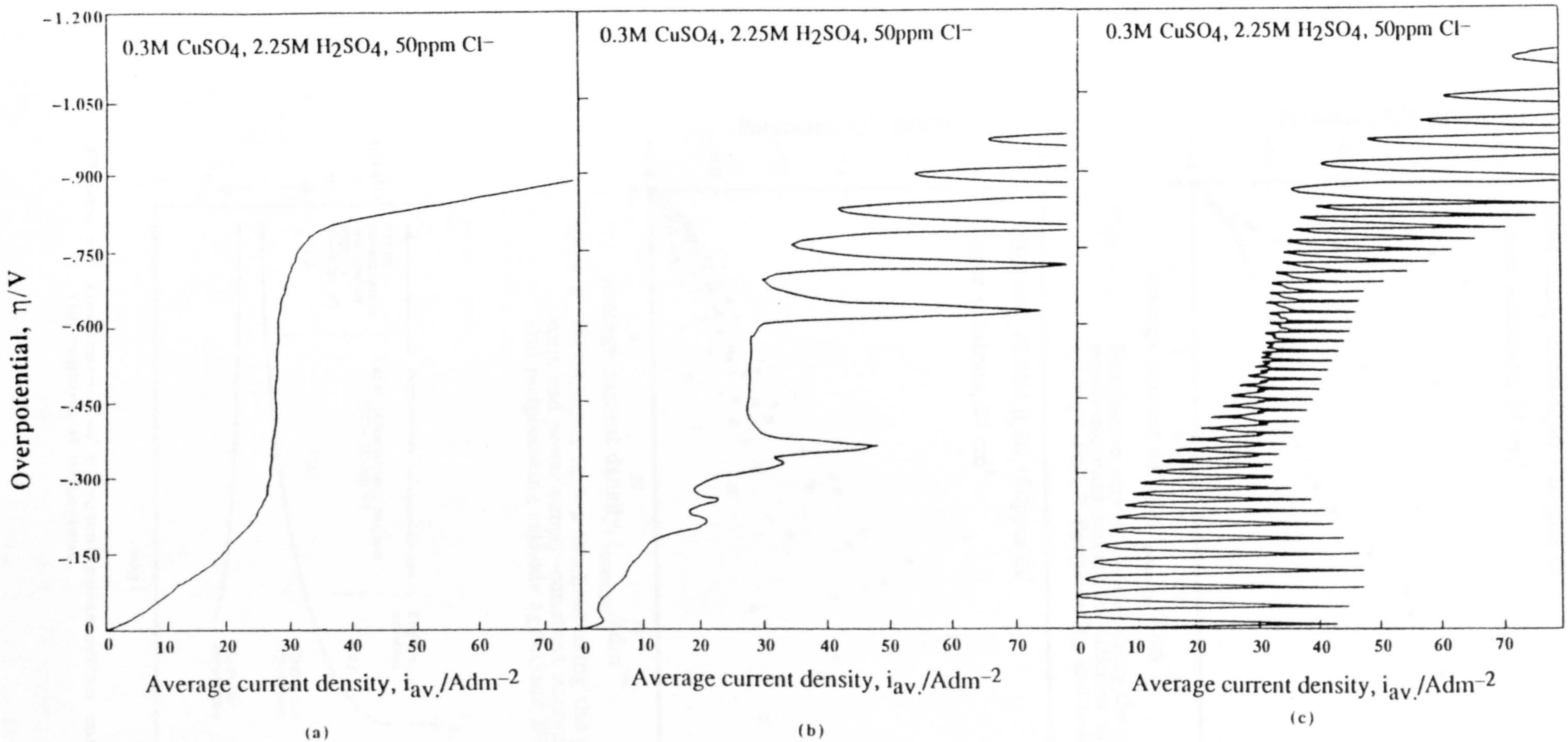

Figure 3 Polarization curves at a potentiodynamic sweep rate of 150mV/min with no agitation
(a) A typical polarization curve
(b) Potentiostat pulsing; potentiostat switched on one second later
(c) Potentiostat pulsing; potentiostat and pulse unit switched on together.

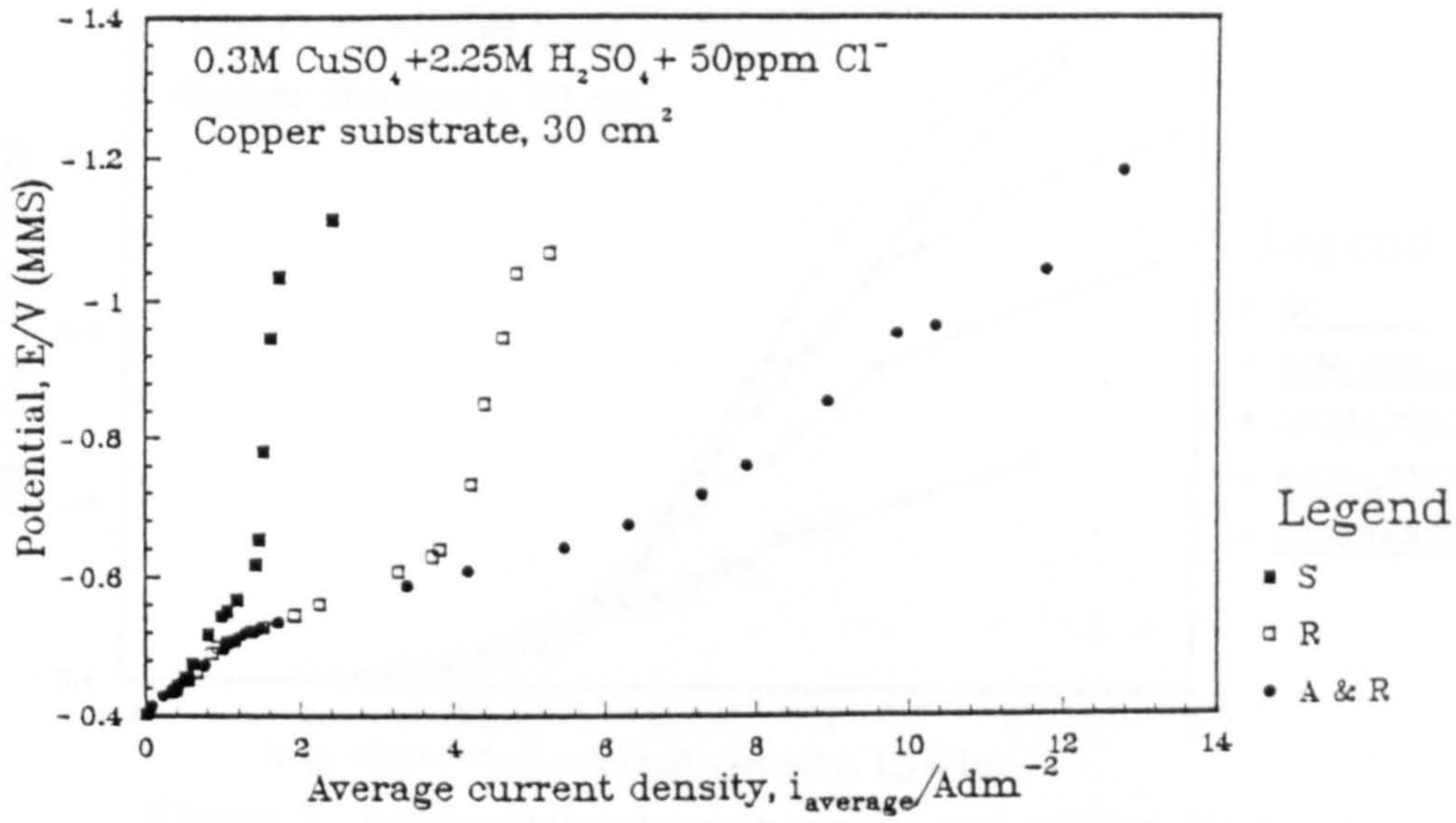

Figure 4 Polarization curves obtained using the power supply–constant current for different agitation modes, S–Still, R–Reciprocating and A–Air, DVM data.

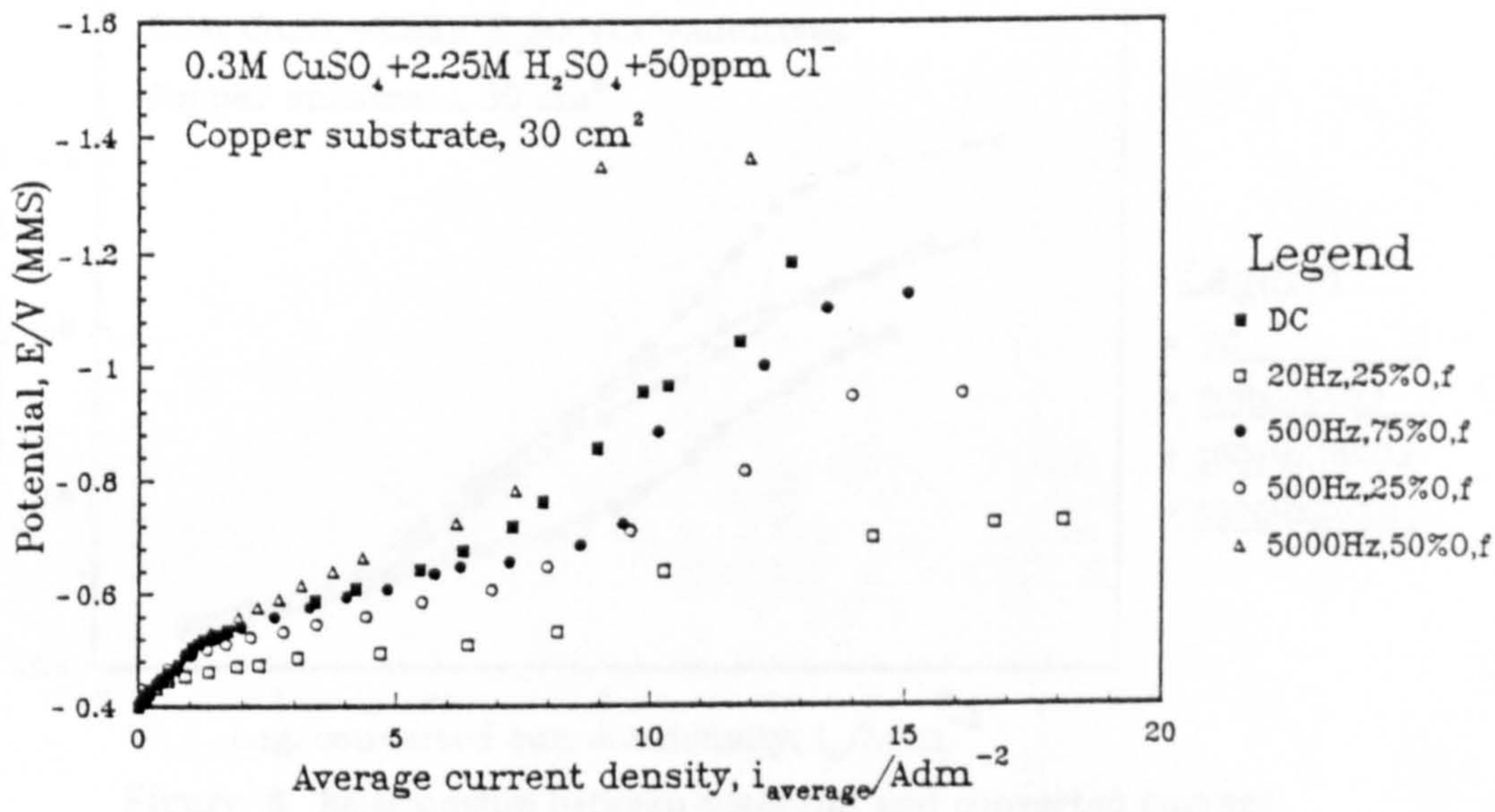

Figure 5 Polarization curves obtained using the pulse unit and power supply–constant current; air and reciprocating cathode agitations, DVM data.

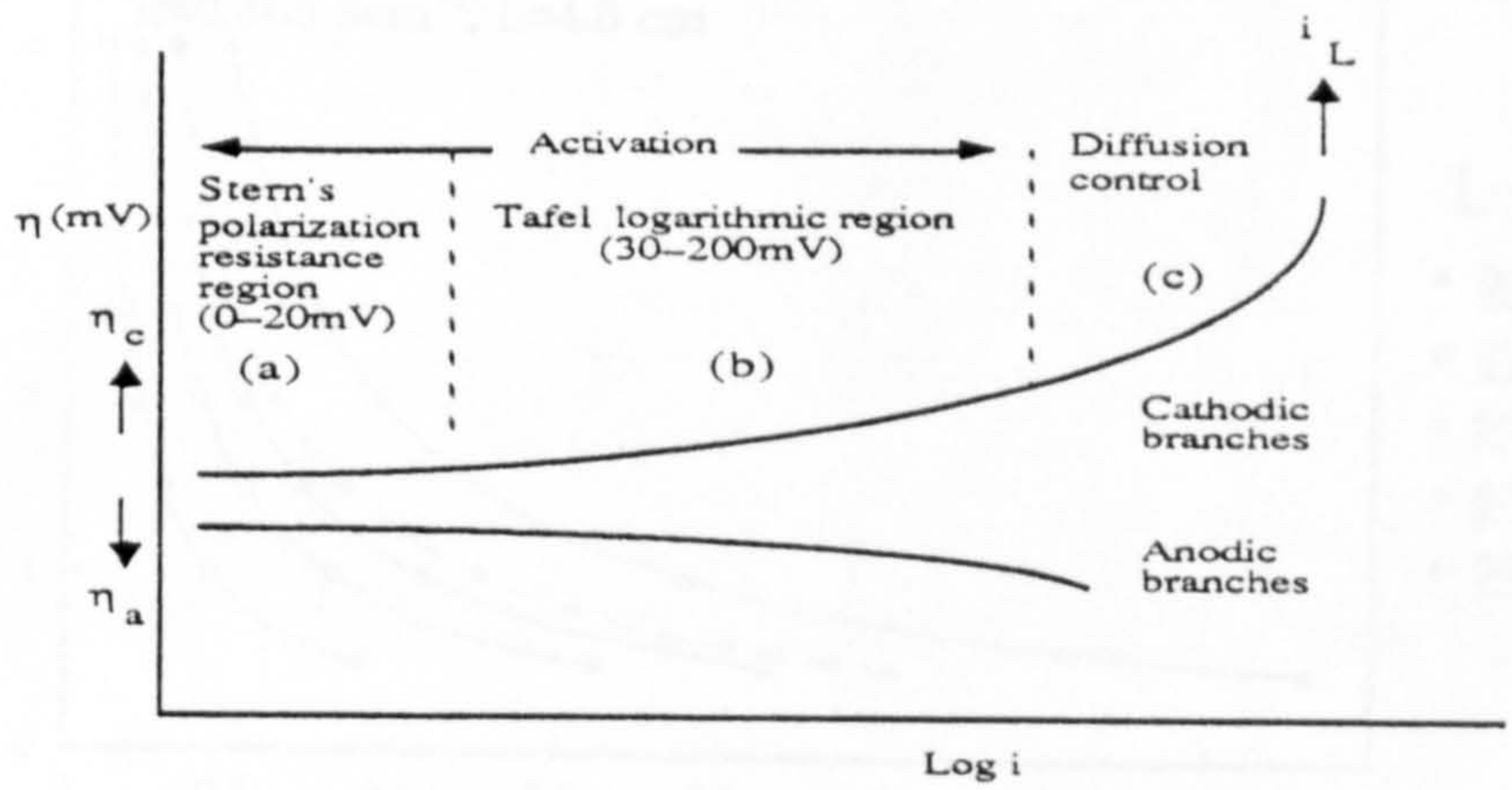

Figure 6 Illustration of a typical polarization curve showing the regions of behaviour.

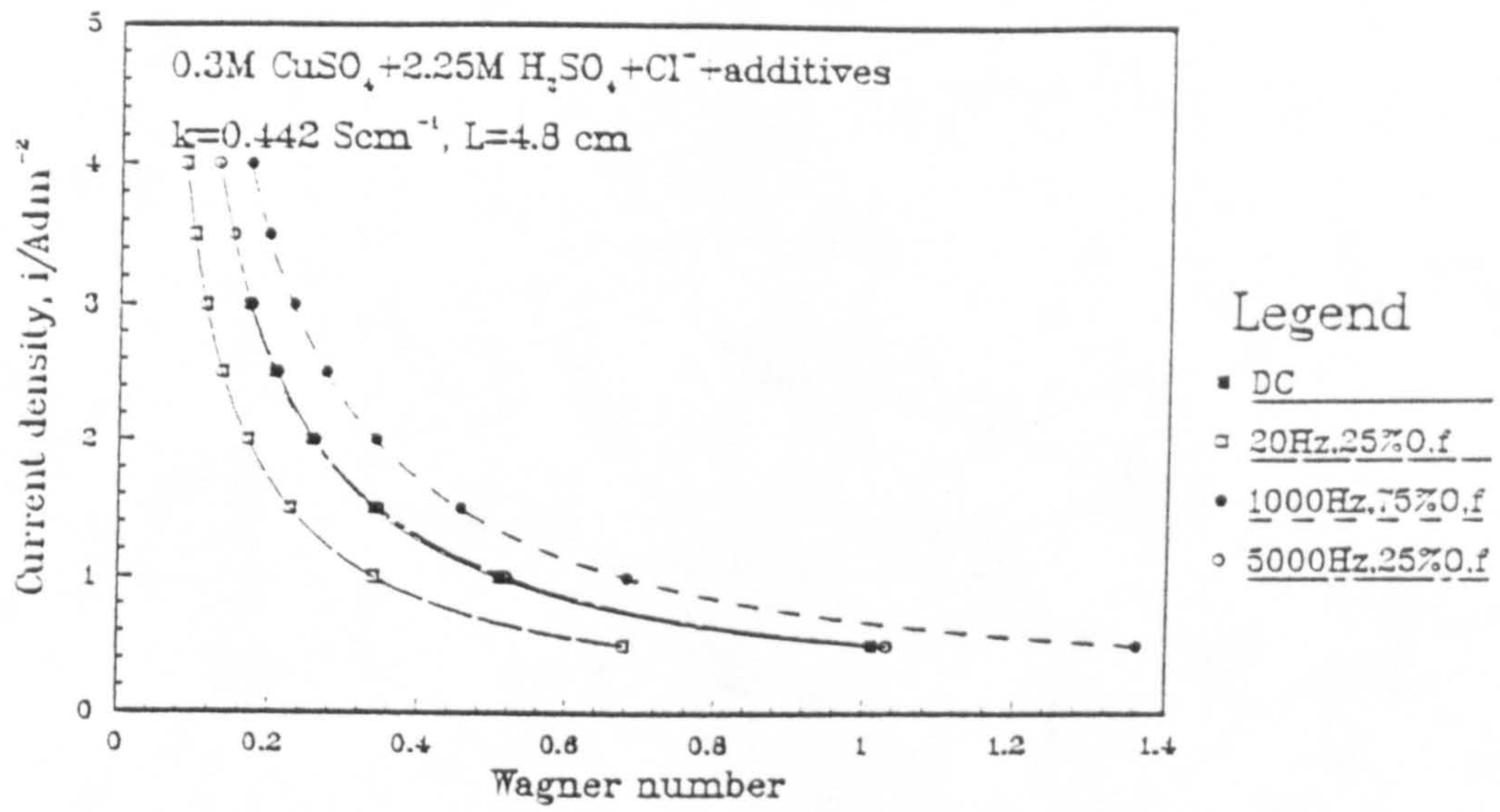

Figure 10 Relationship between current density and Wagner number under different pulse conditions.

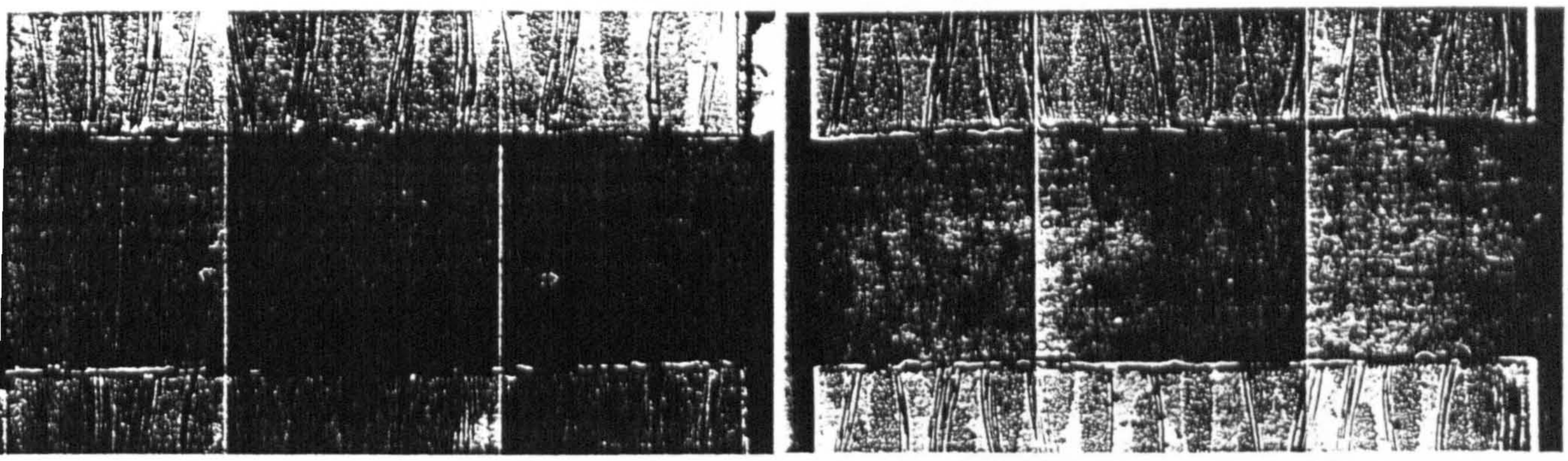

(a) (b)

Figure 11 Optical micrograph of PCB hole (diam. 0.8 mm, board thickness 2.4 mm) plated with electrolyte I under (a) DC and (b) pulse conditions.

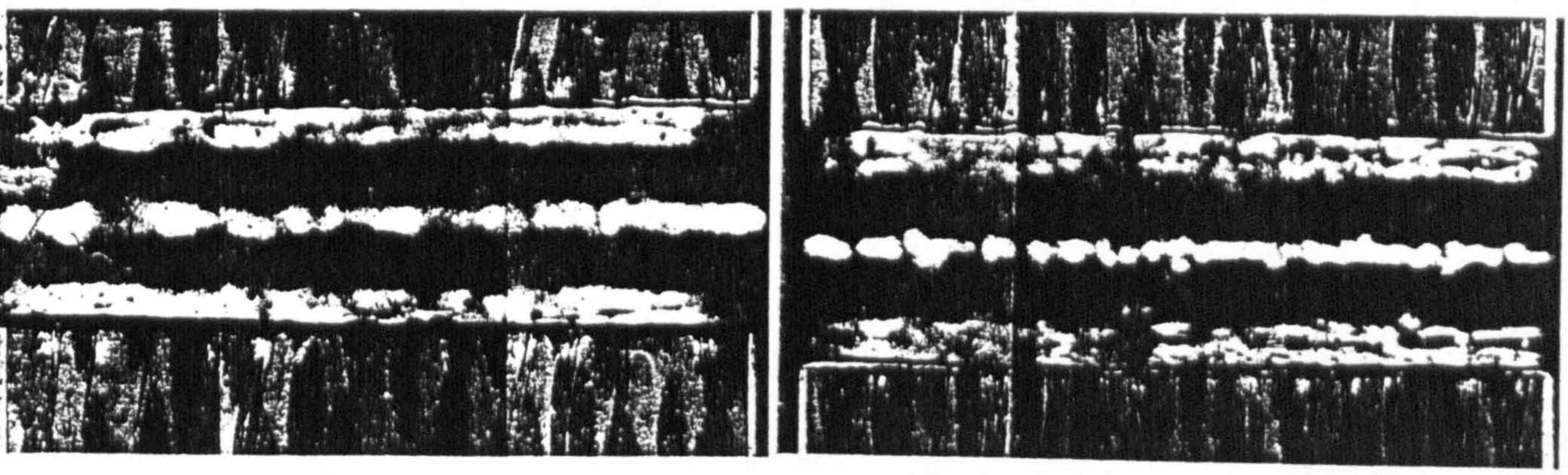

(a) (b)

Figure 12 Optical micrograph as figure 11 but using electrolyte II.